THE PERFORMANCE OF
RIPPLED FIN HEAT EXCHANGERS

BY
J.D. MALTSON

Ph.D.   1990

THE PERFORMANCE OF RIPPLED FIN HEAT EXCHANGERS

BY

JOHN DAVID MALTSON BSc

1990

Thesis submitted to the Council for National Academic Awards in partial fulfillment of the requirements for the degree of Doctor of Philosophy.

Department of Mechanical Engineering and Manufacturing Systems, Coventry Polytechnic, Coventry.

and

Covrad Heat Transfer, Canley Coventry.

April 1990

THE PERFORMANCE OF RIPPLED FIN HEAT EXCHANGERS
by
John D. Maltson

ABSTRACT

Experimental results are presented in terms of the mean Colburn j factor and friction factor for full size samples of new rippled fin heat exchangers over the Reynolds number range 500 to 7000. Heat exchangers having both three and four tube rows and fin pitches of 269 to 354 fins/m were tested. Performance evaluation studies were performed to compare the fin surfaces against previously reported data. At typical fan powers the new rippled fins were found to have a higher performance than previously reported rippled or wavy fins, but a considerably lower performance than conventional louvred fins.

The literature regarding finned tube heat exchangers and flow channels which consisted of rippled or corrugated walls was surveyed and reviewed and this highlighted the research needs in the field of rippled fin heat exchangers, in particular the lack of information regarding the fluid flow, flow friction and heat transfer characteristics in the developing flow region.

Scale models were used to measure the performance characteristics of rippled fin channels of new designs. Transient local heat transfer measurements were made in a specially designed thermal wind tunnel and the measured local Nusselt number processed into overall Colburn j factor form. Pressure drop measurements were also made locally. These heat transfer and flow friction measurements were complemented by flow visualisation studies. The Reynolds number ranges of these tests were 2000 to 8000 for flow friction and heat transfer, and 100 to 2500 for the flow visualisation work. The modelled fin pitches ranged from 345 to 533 fins/m. A discussion is presented describing the various flows visualised in relation to the local heat transfer measurements made. Complex flow patterns were observed over the range of geometric and flow parameters investigated including spanwise vortices which became unstable and shed vortices and secondary flow vortices which with increasing flow spiralled and were destroyed by turbulence. A comparative study involving heat transfer and fan power considerations was made to indicate the channel having a high performance.

Numerical, laminar and turbulent flow models of the characteristics of rippled fin channels were generated using the PHOENICS 81 computer program. The Reynolds number range in which the turbulence models were used was 8000 to 12000. A comparative performance study was made of ducts having different profile shapes and comparisons of the characteristics of one of the ducts against experimental measurements showed close agreement for flow friction in laminar and turbulent flows.

List of Figures

M indicates that the figure is produced in microfiche form and is located in a folder inside the rear cover of the thesis

List of Tables

NOMENCLATURE

A	constant
ACAL	anemometer coefficient
ANMOM	anemometer counts
A_c	minimum flow cross sectional area
A_{fi}	fin area for heat transfer
A_{fr}	frontal surface area of heat exchanger
A_g	area of fin metal for heat conduction
A_{ht}	heat transfer surface area
A_{sl}	area of solder on fin for heat conduction
A_{tun}	wind tunnel working section flow area
A_{wf}	area of water flow
A_{wh}	water sire heat transfer surface area
a_y	node spacing
cp	specific heat capacity at constant pressure
D	diameter of circular tube
Dh	hydraulic diameter
d	indicating differentiation
Fp	fan power
F_{MD}	cross flow correction factor
f	friction factor
G_c	heat exchanger mass flux
H	enthalpy (J/kg)
h	heat transfer coefficient
j	Colburn j factor
K-E	kinetic energy turbulence dissipation turbulence model
K-KL	kinetic energy turbulent length scale turbulence model

k	thermal conductivity
L	length
L_{wt}	length of heat exchanger tubes
m	mass, mass flow rate
Nu	Nusselt number
Pa	power required to accelerate fluid flow
Pd	ducting power loss
Pp	pumping power for heat exchanger core
Pr	Prandtl number
p	static pressure
pd	pressure drop
prco	nondimensional pressure
P_g	fin perimeter
P_s	spacing between the walls of a rippled duct
P_{wf}	wetted perimeter of water flow
Q	heat transfer rate
Re	Reynolds number
RH	ratio of the vertical wall spacing in a duct to the ripple pitch
RI	ratio of the ripple double amplitude to the ripple pitch
RJ	ratio of the perpendicular wall spacing in a corrugated duct to the ripple pitch
RN	number of ripples in the duct
Sc	Schmidt number
Sh	Sherwood number
St	Stanton number
T	temperature
THETA	corrugation inclination angle

Tu	turbulence intensity
t	time
th	thickness
U	overall heat transfer coefficient
v	velocity
v'	turbulent fluctuating velocity component
Wl	streamwise velocity used in PHOENICS
x,y,z	cartesian coordinates

Greek symbols

Δ	difference
η_f	fin efficiency
η_o	fin effectiveness
μ	dynamic viscosity
ρ	density
σ	ratio of the minimum flow area to frontal area
τ	shear stress
ζ	variable

Subscripts

a	air
c	liquid crystal (calibrated), or heat exchanger core
corr	correction
D	diameter
Dh	hydraulic diameter
f	fluid
fd	fully developed

g	fin
H	vertical wall spacing
i	initial, or inlet
j	monitored, liquid crystal green
LMTD	log mean temperature difference
lf	streamwise length of fin
MD	heat exchanger mean temperature difference
m	mean
max	maximum
n	new
o	outlet, old
p	perspex or cobex material
s	solid or wall surface at fluid interface
sl	solder layer
tun	tunnel
tw	tube wall
w	water
x	inlet or entry length
2H	twice the vertical wall spacing
0,1,2	referring to node numbers

CHAPTER 1

INTRODUCTION

There is considerable interest in the design of engineering machinery with regards to increased efficiency or weight reduction. These have arisen from declining fuel resources, pollution control and vehicular weight reduction.

Heat exchangers are a vital component of thermodynamic equipment where the cooling or heating of liquids by a gas (usually air) for lubrication, chemical process plant or refrigeration is required. In these situations the heat transfer rate between a liquid and a gas is governed by the gas side heat transfer coefficient. To overcome the low gas side coefficient, fins are incorporated which increase the surface area available for heat transfer. In addition the gas side heat transfer coefficient may be further increased by heat transfer enhancement techniques. Heat energy is transferred from a surface to a fluid only through a temperature gradient and enhancement techniques involve increasing this temperature gradient, by directing the cooler stream flow into the thermal boundary layer. There are ways of manipulating the flow to obtain this effect, and examples include boundary layer interruptions, vortex generators and turbulence promoters. Bergles (1969, 1973, 1979) reviewed many methods of enhancing heat transfer. In some circumstances heat transfer may be enhanced by introducing mass transfer into the system. Water may be sprayed onto the fins through the front face of the radiator and as the fins are hot the water evaporates. The evaporation process requires the enthalpy of evaporation to be supplied in addition to the forced convection heat transfer and is known as "deluge" heat/mass transfer.

Where the liquid is pressurised, the heat exchanger is generally of tubular type as the circular tubes can withstand the internal pressurisation. For low pressure liquids thin channels are preferred as they reduce the form (pressure) drag of the gas flow through the tube bundle.

The designer of thermodynamic equipment requires the knowledge of heat transfer, flow friction and fluid flow characteristics of flows in complex geometries under certain boundary conditions. These flow characteristics can be obtained by the following methods:

1   Heat transfer and flow friction measurements. These measurements are usually performed on scale models and applied to the real flow through the principle of dynamic similarity using nondimensional numbers. Measurements may be made on the full scale geometry, the size of the model permitting.

2   Theoretical analysis. In complex geometries and real flows it is usually not possible to solve the equations for the flow (three Navier Stokes Equations) which are vital to the energy equation.

3   Numerical analysis using computational techniques. The three Navier Stokes equations and the energy equation can be solved in discretised form, obtaining information at node points, using finite difference, finite element or boundary element formulations. Whilst being extremely useful for laminar flows, the computation of turbulence quantities involves the reliance upon a turbulence model and increases the number of equations to be solved.

4   Inference of the transfer characteristics from local flow vectors, measured by laser doppler anemometry or hot wire anemometry or flow visualisation techniques. These methods are very useful in

ascertaining the flow conditions prevailing allowing estimates of the transfer characteristics to be made.

1.1 Developments in Heat Transfer Technology

Over the last century, there have been many developments in heat transfer subjects, namely:

1   The use of Dimensional Analysis and the Principle of Similarity.

2   Temperature measurement and the International Temperature Scale.

3   The use of computers for the solution of the energy equation in multi-dimensional domains and arbitrary boundary conditions. Improvements to numerical techniques are continually being made and there is a considerable research effort towards turbulence models.

4   Measurement of the local velocity and turbulence quantities by laser doppler or hot wire anemometry.

1.2 The Use of Rippled Fin Heat Exchangers

The performance of a heat exchanger may be affected by environmental factors such as fouling, corrosion, flow maldistribution and vibrations. Traditionally rippled fins are commercially preferred for their fouling characteristics over interrupted (offset strip or louvred) fins although they generally do not perform as well as the latter in clean environments. However rippled fins have a considerably higher performance over plain (flat) fins which are used in low pressure drop applications.

1.3 The Aims of the Present Investigation

The main direction of the research was to investigate the performance of and understand the heat transfer and flow friction processes in a class of heat exchanger surfaces known as rippled fins. These heat exchangers are commonly used in agricultural equipment such as combined harvesters or tractors for their reduced fouling

3

characteristics from insects or fibrous matter which are more easily trapped in passages formed within louvred or strip fin surfaces.

Firstly it was required to know whether the rippled fin heat exchangers possessed a performance worthy of further study. Heat transfer and flow friction tests were to be carried out on full size heat exchangers in a thermal wind tunnel at Covrad Heat Transfer. The results of the heat exchanger tests when compared with the results of other heat exchangers would indicate whether rippled fins were worthy of further investigation.

A literature survey and review were required for the heat exchanger rippled fin tube banks and the previously studied corrugated ducts or another type of duct having high performance characteristics, using turbulence promoters or vortex generators, which could be incorporated into heat exchangers and utilised continuous plate fins.

A comprehensive series of tests was to be carried out on scale models to obtain the heat transfer, flow friction and fluid flow characteristics of the corrugated (rippled), or other type of duct. The emphasis was towards gaining as much information as possible using currently available measurement methods. This test series would include measuring the local heat transfer coefficient distribution, the pressure losses and flow visualisation using streaklines, for the flow within the duct, to gain an understanding of the principles of how the local fluid flow affected the transfer characteristics. Having gained this understanding, it was anticipated that a prediction would take place on how the performance of a rippled duct may be further improved by a variation in the geometry of the fin.

An investigation into the performance evaluation criteria was

4

needed to provide a means of comparing heat exchanger performance in a useful, but not superficial way. Performance comparisons were to be made using performance evaluation criteria which would indicate the duct of optimum geometry for the application of water coolers for agricultural vehicles or industrial applications.

1.4 Contents of the Thesis

Chapter 2 contains a literature survey and review of the relevant heat exchanger research, oriented towards both rippled (corrugated) heat exchangers and ducts.

Chapter 3 describes the experimental tests on full size heat exchanger samples. Details for the test rig, procedures, data reduction, results and comparison with other heat exchangers are reported.

Chapter 4 reviews the experimental methods available for the measurement of the local heat transfer coefficient, their advantages and disadvantages when applied to the present geometries are also discussed.

Chapter 5 reports the experimental tests on scaled ripple fin models for the flow visualisation, local heat transfer and flow friction measurements. The manufacture of the rigs and models, procedures, data reduction processes, results and comparisons are described.

Chapter 6 describes an investigation into the performance characteristics of rippled ducts by numerical methods using the PHOENICS 81 computer program. Laminar and turbulent models of the flow were found and the results obtained are presented.

Appendices 2, 3 and 4 describe numerical studies which investigated various transient conjugate heat transfer effects

relating to problems in using the transient measurement technique as applied in the present investigation and in the investigation of Tura (1986). These investigations are to the authors knowledge new and original research work and form a part of the thesis.

1.5 Rippled Duct or Channel Geometry Specification

There are many ways of specifying the geometry of a rippled duct or channel and in the literature authors have chosen systems that suit their particular type of research. In the present work the geometry of a passage was defined by two nondimensional numbers RH and RI. RH is the ratio of the vertical wall spacing to the ripple pitch and RI is the ratio of the vertical double amplitude of the wave profile to the ripple pitch. Unfortunately there is no single parameter which can be related to arbitrarily defined ripple or wave profiles. For flat sided corrugated passages additional numbers of the corrugation inclination angle and RJ, the ratio of the perpendicular wall spacing to ripple pitch have been used.

1.6 Glossary of Terms

This glossary was included to introduce some of the terms used throughout the thesis. It was not meant to define the following terms, but to provide meanings to them which may have wider or more general application in the fluid flow or heat transfer literature.

Channel

Within this thesis the term channel will be used to describe walls confining a fluid which are long in the flow direction. In a channel the flow develops from the inlet to a fully developed or in the case of a rippled channel a periodically fully developed condition.

Conjugate

This term is used in this thesis to describe heat transfer between a fluid and an adjacent wall where the conduction within the wall may be one, two or three dimensional. The term may have a wider meaning in the general heat transfer literature.

6

Duct

Term used to describe a the confining walls of a flow passage which is short in the flow direction such that the flow develops from an inlet towards the fully developed condition.

Enhancement

Enhancement is known as the increase in heat transfer that arises when a surface is modified by the addition of turbulence promoters or other intensifying device. This term has also been referred to as augmentation in the literature.

Facets

In flat sided corrugated ducts or channels the corrugated walls may be thought of as a series of flat plates known as facets. The facets are either forward facing (facing towards the inlet) or rearward (leeward) facing.

Free Shear Layer

The action of fluid particles in a plane travelling adjacent to slower fluid particles in an adjacent plane creates a shearing effect within the fluid. This action frequently occurs at wall boundaries where the fluid adjacent to the wall is constrained by viscous forces and adheres to the wall. This condition is known as the "no slip" condition and the shear layer is usually termed a boundary layer. In regions of flow unconstrained locally by a wall as is the case on the separation streamline of a recirculation zone the shear layer is known as a free shear layer.

Friction Factor

Due to the action of frictional viscous forces between fluid elements moving with different velocities, energy is required to overcome these forces and for duct flows is seen in terms of a static

pressure drop, or head loss. The friction factor is used in this thesis to present flow friction data obtained from pressure drop measurements and calculated as a ratio of a shear force to a fluid dynamic pressure force. The pressure loss of the fluid may be caused by shear forces on wall boundaries, form drag (caused by flow separation) and turbulence generation and these losses (forces) are calculated as an equivalent shear force. There are other dimensionless numbers eg. drag coefficient which could have equally been used for data presentation purposes, but for plate fin heat exchangers the friction factor has traditionally been used.

j Factor

The j factor is used to present heat or mass transfer data in a nondimensional form. The main reason for its use is that it permits the data to be used for fluids having moderately different Prandtl or Schmidt numbers. This number forms the basis of the analogy between heat and mass transfer processes due to the similarity of the transport equations in convection dominated flows.

Nusselt Number

The Nusselt number is a nondimensional group representing the local (or mean) heat transfer coefficient by a ratio of convection to conduction heat transfers. This number for duct flows is usually based on the hydraulic diameter, and for boundary layer flows on the distance of the local heat transfer coefficient from the leading edge of the model.

Out of Phase

Ducts and channels that have walls where the corrugation (or ripple) peak does not coincide with the corrugation peak or trough of

the opposing wall have out of phase walls. The case where a corrugation peak coincides with trough of the opposite wall will be known as converging-diverging, otherwise the duct or channel in question is known as corrugated or rippled.

Peak

The peak of the ripple or corrugation is the region that protrudes the furthest into the main flow channel of the duct, the highest point on the lower wall or the lowest point on the upper wall. The peak may be referred to as a point or the region in the flow closely surrounding the point. In the literature a peak has also be called a crest.

Periodically Fully Developed

In rippled ducts or channels, the flow cannot reach a fully developed flow regime due to the ripples or waves breaking up the flow every wave pitch in the flow direction. However for isothermal and incompressible flows there comes a point when the fluid motion repeats itself periodically in phase with the ripples and after this point the flow has attained fully developed periodicity. For flows with heat transfer the fluid properties vary with position forcing the flow to accelerate or decelerate, but for fin and tube type heat exchangers this effect is usually small and the effect on the flow minimal.

Plain fins

Plain fins are straight flat fins mounted on the primary heat transfer surfaces of the heat exchanger.

Reynolds number

The Reynolds number is a nondimensional number representing a ratio of momentum to viscous forces acting on a fluid element. The Reynolds number used in the present work is based on the hydraulic

9

diameter of the flow passage containing the fluid. For the presentation of the results of the rippled fin tube banks, the definition of Kays and London (1984) was used, but for the work involving rippled ducts without heat exchanger tubes, the definition chosen was that for parallel plates, twice the vertical wall spacing and irrespective of duct aspect ratio.

Ruffled fins

Kays and London (1984) measured the performance of a fin surface which was wavy in the flow direction, but the type of heat exchanger was different to their wavy fins heat exchangers and were called ruffled fins to distinguish between the two. However this type of fin could also be called rippled or wavy.

Spanwise

The spanwise direction is known as the direction perpendicular to the main flow direction in the plane of the main confining walls or plate fins.

Streamwise

The main flow direction of a fluid in a duct or channel will be referred to as the streamwise direction.

Transient

This word is used in the present document to describe a gradually changing time dependent process.

Temperature

The temperatures measured during the experiments were either "total" or "static" temperatures, but the fluid velocities present in the study were very low relative to sonic velocity and these two temperatures were assumed to be equal with negligible error.

Trough

A trough, sometimes known as a valley is the lowest region of the duct ripple or corrugation on the lower wall of the duct, or the highest region on the upper wall of the duct.

Unstable

An unstable flow is one in which the flow regime can change dramatically with only a slight variation in boundary or fluid conditions. An example occurs in fully developed pipe flow when the Reynolds number is close to the critical value at which transitional flow begins. A small perturbation in the flow will cause the flow to enter into the transitional regime, but in an unpredictable way.

Unsteady

Processes which rapidly change with time in either an orderly or chaotic fashion will be described as unsteady. An unsteady flow can also be stable and vortex shedding at a constant frequency is such a flow.

CHAPTER 2

LITERATURE SURVEY AND REVIEW

The literature regarding the fluid flow, flow friction and heat transfer of corrugated or rippled ducts, plate heat exchangers and plate fin and tube heat exchangers is reviewed in this chapter. The review is divided into three sections, associated with the type of test results reported. An additional summary of the information in sections 2.2 and 2.3 including geometry, parameter ranges and comments is presented in Table 2.1 and it is recommended that this table is read prior to sections 2.2 and 2.3.

Many references report results for the periodically fully developed region of a corrugated channel which are not generally applicable to use for the heat transfer and flow friction characteristics of a plate fin and tube heat exchanger of typical dimensions. Plate rippled fin and tube heat exchangers tend to have relatively short flow lengths where the flow is developing over a large proportion of the total length. However these studies were included in the review in order to gain as much information as possible regarding all aspects of the subject.

The literature relating to plate heat exchangers constructed from corrugated plates was also included, but these studies were largely concerned with the overall characteristics of a unit. Few studies in this area had geometries which could be applied to plate fin and tube heat exchangers as the trend was towards using herringbone patterned plates. Herringbone corrugations were typically oriented such that adjacent plates contacted at multiple locations providing considerable rigidity to a plate channel enabling large fluid pressure differences to be used in adjacent flow channels.

At the end of the chapter a section is presented, reviewing

papers of generally related topics to heat transfer, flow friction and the fluid flow characteristics of rippled ducts.

2.1 Heat Exchangers with Rippled, Wavy or Corrugated Surfaces

Norris and Spofford, (1942), have shown that the heat transfer coefficient of corrugated fins is substantially higher than that of plain fins, but lower than those of offset strip and pin fins. The results are presented on a graph of heat transfer coefficient against air mass velocity. Very limited information regarding the geometry of the corrugated fin is given in the paper. Independent values of the j factor and friction factor are not given making any comparison or performance evaluation extremely difficult.

Bohm (1955) measured the overall heat transfer performance of plate heat exchangers having horizontal waves. The pressed plates were used to investigate multiflow (mixture of parallel and counter flow) types of heat exchanger. Pressure drops were not measured or reported.

Kays and London, (1984), Presented data for six surfaces which are of significant importance to the project. The experimental results are given for the overall j factor and friction factor. Three surfaces were termed "ruffled", and had plate fins with various tube arrangement. Two surfaces had thin tubes arranged such that the fourth tube row in the flow direction repeats. This tube arrangement is known as "echelon", but the exchangers had only three rows of tubes. These heat exchangers had fin pitches of 9.1 to 11.3 fins/inch. Three surfaces of wavy plate fins mounted between flat plate channels were tested covering the fin pitch range 11.5 to 17.8 fins/inch.

Ginstling (1959) compared the heat transfer performance of various plate heat exchanger patterns. The highest heat transfer

coefficients were found for a herringbone patterned plate. A plate having horizontal corrugations had a poor heat transfer performance in comparison. The pressure drops for each plate were not mentioned.

Kays, (1960), presented data for one wavy fin surface. This surface had practically the same dimensions as the one used by Kays and London, (1984). The data was used to demonstrate the repeatability of the results of the earlier document (1964, 2nd ed.).

Yastrebenetskiy and Kovalenko (1959) and Kovalenko (1961 and 1962) measured the heat transfer and pressure drop performance of plate heat exchangers which incorporated various corrugated patterned plates. The corrugated patterns tested included both herringbone and horizontal formations. The horizontal pattern formed a flat sided corrugated channel. Measurements were taken with water as the working fluid at temperatures between 50 to 80°C. Thermistors measured the temperatures of the liquid, each being placed in copper sheaths in the inlet and exit pipes to the exchanger.

Konno (1967 and 1968) and Okada, Ono, Tomimura, Okuma, Konno and Ohtani (1970) reported the results of an investigation into the performance of various geometries of heat transfer surfaces used in plate heat exchangers. The surface patterns were formed from horizontal corrugations arranged such that the flow passage was a two dimensional corrugated channel. The corrugation profiles used were wavy rippled, rippled and flat sided corrugations. The wavy rippled surface was formed from a short wavelength wave in conjunction with a longer ripple wavelength. Heat transfer and pressure drop measurements were made on an element of a plate heat exchanger by measuring the heat transfer rate, the fluid temperatures and the plate wall temperatures. This series of experiments was summarised by Okada, Ono,

14

Tomimura, Okuma, Konno and Ohtani (1972), see Table 2.1.

Savostin and Tikhonov (1970) performed heat transfer and flow friction tests on samples of heat exchangers, which were constructed from wavy plate surfaces which had crossed corrugated patterns. The profiles forming the corrugations were primarily circular arcs, but joined by flat sections. Air and water fluids were used as the working fluids in the tests. The results were presented in tabular form, but for some of the geometries a regression equation was generated.

Zozulya, Khavin and Kalinin, (1975), took experimental measurements in bundles of oval tubes with transverse fins, for several types of finned surfaces. There are two surfaces of interest, the triangular corrugations and the cylindrical projections. It was not possible to calculate the j factor and friction factor from their dimensional results. The triangular corrugations had a slightly lower pressure drop than the cylindrical projections, but had a very similar heat transfer performance.

Hosoda, Uzuhashi and Kobayashi, (1977), made heat transfer and pressure drop measurements on a corrugated finned tube heat exchanger. Not enough information was given to use the results as design data, but a comparison was made against an offset strip fin surface indicating that corrugated fins do not perform as well as interrupted surfaces.

Hauser, Kreid and Johnson, (1981), measured the performance of a wavy plate fin on a staggered circular tube arrangement, three tube rows deep. The heat exchanger had ten fins per inch and consisted of two waves in the flow direction. Both heat transfer and pressure drop were measured, but the results uncovered inconsistencies between their

15

and the manufacturing company's own data.

Sherwin, (1981), measured the performance of circular tubes helically wound with corrugated fins. The fins in these heat exchangers had a corrugation height which varied from maximum at the tube surface to zero at the fin extremity. Due to the method of manufacture, the corrugations were all out of phase and were all at various angles to the flow. However the heat transfer coefficient was found to be insensitive to the fin pitch, but increased with the ratio of corrugation height to tube diameter. The heat exchangers consisted of one tube row only. The flow friction was calculated in terms of a simple drag coefficient which increased with the ratio of corrugation height to tube diameter, and the fin pitch.

Focke (1983) reviewed the heat transfer mechanisms that occur in plate heat exchanger passages composed of plates imprinted with herringbone corrugation patterns. The main focus of the work was towards evaluating the effect of the corrugation inclination angle on the exchanger performance.

Beecher and Fagan, (1987), measured the heat transfer coefficients in plate fin circular tube heat exchangers. Their investigation included a parametric variation of the geometric variables. The corrugated plate fins consisted of flat sided corrugations mounted in tube bundles up to six rows deep. Although pressure drop measurements were taken, they were not reported.

2.2 Rippled or Wavy Corrugated Ducts and Channels

Beloborodov and Volgin, (1971) measured the overall heat transfer and pressure drop characteristics of various channel geometries having curved confining walls. The overall heat transfer coefficient was obtained from the heat transfer rate and the mean temperature

16

difference between the two fluids. The results were regressed to equations for all cases studied. The work was related to plate heat exchangers, some of the geometrical configurations were herringbone patterned.

Sparrow and Hossfeld (1984) experimentally investigated the effect of rounding of the sharp protruding edges of a flat sided corrugated duct in the periodically fully developed region. The work was an extension to the research of Sparrow and Comb (1983). The rounded corners were formed on the peaks, but the troughs were left as sharp concave corners. Two rounded profiles were milled into the model plates of Sparrow and Comb. Flow visualisation, flow friction and heat transfer measurements were made for these plate geometries at one plate spacing. Flow visualisation revealed that the rounding reduced the size of the separated region within the trough region of a plate. It was found that the fully developed friction factor decreased considerably with the degree of roundedness, at constant Reynolds number, but the heat transfer in terms of a fully developed Nusselt number also decreased. Comparisons were made on the basis of constant, mass flow rate (Reynolds number), pressure drop and pumping power. For the constant pumping power constraint the Nusselt number was found to be relatively insensitive to the degree of rounding.

Nishimura, Ohori, Kajimoto and Kawamura (1985), Nishimura, Kajimoto, Tarumoto and Kawamura (1986), Nishimura, Kajimoto and Kawamura (1986) and Nishimura, Yoshino and Kawamura (1987) investigated the fluid flow, flow friction and heat transfer in a sinusiodal channel in the fully developed region. Out of phase walls were encompassed within the geometry range of various wall spacings

17

and wave amplitudes. They found the existence of secondary flow and spanwise vortices and the effects on the flow pattern with increasing flow rate. No data for the developing entry flow region was presented, but the fully developed flow data is useful for design and comparison purposes.

Asako, Nakamura and Faghri (1988) numerically analysed the heat transfer and flow friction in corrugated ducts with rounded corners, and compared the results against similar corrugated ducts with sharp corners from the work of Asako and Faghri (1987). The flow considered was that of fully developed laminar steady flow. In the case of the duct having a corrugation angle of 45 degrees, there is no separation visible for Reynolds numbers less than 150.0. At a Reynolds number of 174 a small separation bubble is visible which increases in size with increasing Reynolds number. At a Reynolds number of approximately 900 there was a difference in the streamline patterns for the rounded and sharp cornered channels. Both channels maintained a separated region in the trough, but the sharp cornered case also showed a separated region on the rearward facing facet. This region was formed by flow separation from the corrugation peak (corner) and reattached midway down the flat side. Another difference observed was the shape of the free shear layer bounding the separation region in the troughs. The flat sided channel exhibited a convex curvature while the rounded channel was concave. This shear layer would have influenced the way that instabilities were generated and the transition to turbulence, which was not discussed therein.

Xin and Tao (1988), numerically modelled the laminar flow in a wavy walled channel in the periodically fully developed regime. The computational flow domain was generated from a combination of two grid

18

systems, cartesian and cylindrical polar for flat and curved sections respectively. The radii forming the circular arc section both had the same centre. This arrangement gave a channel of uniform cross sectional area for a flow direction parallel or circumferencial to the wall surfaces. The Reynolds number ranged from 100 to 1000 and the prandtl number was for air having a value of 0.707. The interwall spacing and the ripple wavelength were varied parametrically. The numerical heat transfer boundary condition was that of constant wall temperature. The plotted streamlines and velocity profiles show the flow to separate and form recirculation zones. The local Nusselt number on the forward facing surface increased to a local maximum at the reattachment point, decreased slightly and then increased to a larger value at the ripple peak. On the rearward face the heat transfer coefficient decreased to the minimum in the recirculation zone within the trough. Similar trends were predicted over the Reynolds number and geometric ranges investigated.

Garg and Maji (1988) numerically modelled the fluid flow, flow friction and heat transfer in the inlet region of a sinusoidally corrugated duct. Their method of solution of the problem involved mapping the wavy flow domain onto a rectangular computational mesh by algebraic coordinate transformation. The Prandtl number of the flow was 1.0 and the Reynolds numbers investigated, based on half the ripple pitch in the flow direction were 100 and 500. This Reynolds number definition for the wall spacings investigated reverts to the more normal definition of being based on a hydraulic diameter of twice the wall spacing. Two wave amplitudes were modelled, the double amplitudes of which divided by the ripple pitch (RI) had values of 0.1

19

and 0.2 respectively. The flow was specified to be totally laminar. The flow domain was divided onto the computational mesh by 20 cells across the flow, but only two cells per ripple in the flow direction. The flow separated, causing recirculation in a wave trough at the larger wave amplitude for a Reynolds number, but this separation zone was difficult to see from the presented vector plots. At the lower Reynolds numbers and wall amplitudes no separation was found. The Nusselt number distributions showed high leading edge values which reduced to oscillate between two lower values following the geometric waviness.

Xiao, Xin and Tao (1989) numerically modelled the fully developed, laminar flow with heat transfer in an asymmetric wavy channel. The numerical method used was that of Xin and Tao (1988) and the channels investigated were composed of flat and circular arc sections arranged in an asymmetric manner. The Prandtl number of the flow was 0.707 and the heat transfer boundary condition was a constant wall temperature. The Reynolds number range of the flow was 100 to 1000. A parametric variation in the geometry was made. Their conclusion of the research was that an asymmetric channel can enhance heat transfer by a few percent over the symmetric channel of similar proportions, but the performance evaluation method used was very simplistic.

2.3 Flat Sided Corrugated Ducts and Channels

Goldstein and Sparrow, (1976a, 1976b and 1977), measured the local and overall heat transfer performance of flat sided ducts and heat exchanger elements. This work was reported in an earlier publication by Goldstein (1975). Use was made of the thick film naphthalene sublimation technique, which measured the local depression

20

of basically flat plate elements by dial indicators. Complex flow patterns of secondary flow, separation, recirculation and transition to turbulent flows were inferred from the local measurements. The pressure drop characteristics of these ducts was not measured preventing performance comparison studies using their heat transfer data.

A numerical optimisation scheme was developed by Mandel, Townsend and Parrish (1979) which was used to model the heat transfer and pressure drop in heat exchangers with flat sided corrugated fins. The corrugations were joined together with horizontal flat sections. The work was applied to mathematically optimising the performance of a plate fin heat exchanger. Unfortunately the model did not consider the following points;

1   The practical considerations of the flow around the tubes, with their associated wake regions and other flow phenomena which was reported in the work of Goldstein and Sparrow, (1976).

2   The secondary flow vortex phenomena which has been shown to exist in corrugated channels of a generally similar type of geometry by Goldstein and Sparrow, (1977).

3   Their model solved the momentum equation in one coordinate direction only, which was representative of a parabolic laminar shear layer flow with a pressure gradient. In corrugated duct geometries such as this, the ellipticity in the flow should be modelled to allow downstream disturbances to affect the flow upstream. This condition does occur in corrugated ducts where the flow separates from a sharp corrugation peak forming a region of recirculation.

Hosoda, Uzuhashi and Kobayashi, (1977), used illuminated tracer

particles in a water channel to show the flow patterns in the inlet region of a corrugated wall channel. The corrugations were made of sheet material, had straight sides and were bent at the corners, which would have had a very small radius of curvature. The flow visualisation photograph is representative of the flow in a heat exchanger having 563 fins/m (14.3fpi). The flow pattern illustrates the boundary layer growth on the walls and flow separation from a corrugation peak. Unfortunately the Reynolds number of the flow is not given and the authors do not describe the flow in detail.

O'Brien and Sparrow, (1982) performed experiments to determine the heat transfer, flow friction and fluid flow patterns for the turbulent flow in a periodically fully developed flat sided corrugated channel. The corrugation angle was 30° and the measurements were made at one wall spacing. The heat transfer measurement technique used thick copper plates heated by embedded electrical elements and the working fluid was water entering the duct at various temperatures to provide a Prandtl number variation (Pr = 4 to 8). The flow friction and flow visualisation tests used air in a plexiglass channel of similar geometry to the heat transfer plates. A photograph of a visualisation test was presented for a Reynolds number of 1.8×10^4. The flow was visualised using the oil and lampblack technique which showed that the flow separated from a corrugation peak and that flow reversal encompassed the whole of the rearward facing facet. It was noted that the flow pattern was very similar for a Reynolds number of 5000. Additional information regarding this experimental investigation was reported by O'Brien, (1981), in particular the local pressure drops were plotted in order to ascertain the periodically fully developed friction factor where the pressure gradient after the entry length

22

became linear.

Sparrow and Comb (1983) extended the work of O'Brien and Sparrow (1982) to investigate the effects of interwall spacing and inlet condition on the duct performance in the periodically fully developed flow regime. The experimental data of O'Brien and Sparrow was reworked in order to account for the conduction into the side walls. It was found that the increase in interwall spacing gave rise to an increase in the Nusselt number, but the friction factor also increased. Based upon performance comparisons of equal pumping power, pressure gradient and mass flow rate, the differences were not sufficiently great to indicate the duct of higher performance. However real heat exchanger performance evaluations were not applied to the test results and these comparisons were very artificial. The effect of inlet flow turning was investigated by placing an inlet flow section at the inlet.

Izumi, Yamashita and Oyakawa (1981), Izumi, Oyakawa, Kaga and Yamashita (1981), Izumi, Yamashita, Kaga and Miyajima (1982) and Izumi, Yamashita, Oyakawa and Mori (1983) have investigated the flow, heat transfer and flow friction characteristics of various flat sided geometries using numerical and experimental techniques. The geometries used, covered ducts with two bends at various flow bending angles and interwall spacings, and channels with many bends also with parametric geometry variation. Their investigations used air as the working fluid throughout, and encompassed both the laminar and turbulent flow regimes. The numerical models of turbulent flow used the kinetic energy - dissipation length turbulence model. The heat transfer boundary condition was specified to be constant heat flux for the experimental and numerical work.

Molki, (1986) and Molki and Yuen, (1986) measured the heat transfer and flow friction characteristics of flat sided ducts and varied the corrugation angle and wall spacing. The heat transfer measurements were made locally averaged over a facet. The work was limited to the turbulent flow regime in the Reynolds number range 4000 to 3.0×10^{4}. Flow friction results were limited to the fully developed region.

Asako and Faghri (1987) and Faghri and Asako (1987) solved the finite volume equations for laminar flow and heat transfer in flat sided corrugated wall channels. The channels were either converging and diverging or constant flow area corrugated ducts. The solutions were limited to the periodically fully developed region. The corrugated walls were specified numerically using a coordinate transformation technique. Complex fluid flow patterns in two dimensions were presented in streamline plots. The geometry was systematically varied using three corrugation angles (15, 30 and 45°) and three wall spacings. The Prandtl number was varied between 0.7 and 8. The Reynolds number range was 100 to 1500. The authors made no mention of the Reynolds number dependence on the transition to turbulent flow, which can be lower than 1500 in similar geometries.

Amano (1984, 1985a, 1985b) and Amano, Bagherlee, Smith and Niess (1987) concentrated on solving flow and energy governing equations to gain an understanding of the heat transfer and flow friction processes in corrugated channels and other related geometries, which had 90 degree bends. The numerical investigation encompassed both laminar and turbulent flows in the periodically fully developed region. Various turbulence models were used to improve the predictions based on differences between the solution and experimental data. The Reynolds-

24

stress turbulence model was found to agree with the experimental data of Izumi, Yamashita, Kaga and Miyajima (1982) and O'Brien and Sparrow (1982) for heat transfer coefficients in the periodically fully developed region. The data of O'Brien and Sparrow was taken for a channel having 120 degree flow bends. The flow friction was also shown to agree with available data.

2.4 General references

As a direct result of the literature survey and review, the survey was widened to select further information about the general field of fluid flows that were found to belong to rippled and corrugated duct flows. Literature of this nature is contained in this section, but is discussed in relation to rippled or corrugated ducts in section 2.5.

McCormack, Welker and Kelleher, (1970) experimentally measured the heat/mass transfer coefficients under the action of secondary flow vortices (Taylor-Goertler vortices) on a curved wall using naphthalene sublimation. It was found that the vortices were steady in time and did not move in the spanwise direction. Increases in the Nusselt number of between 100 to 150 percent were measured on the curved wall in the presence of the vortices, compared with the Nusselt number for a flat duct.

Kang and Chang (1982) numerically analysed the mass transfer and fluid flow in a channel with rectangular block turbulence promoters. The flow was periodically fully developed and in the laminar flow regime. The rectangular blocks were arranged either fixed to one wall or to both walls. For the two geometric configurations the fluid passed either through a channel with cavities or through a "zig-zag"

type path. The range of the non-dimensional numbers investigated were 50 to 500 for the Reynolds number and 20 to 2000 for the Schmidt number. Neither geometry would be used in a plate fin and tube heat exchanger, but the fluid flows are similar to those found in these exchangers. The results show marked flow separation behind a "block" where the fluid passes over a sharp corner. The local and overall mass transfer characteristics were presented, but in the absence of flow friction data, performance evaluations cannot be performed. The calculated streamlines were compared with streaklines obtained from flow visualisation studies. The flow streaklines photographed compared favourably with the computed streamlines at low Reynolds numbers. At higher Reynolds numbers the free shear layers bounding the separated region became unstable and the flow transitional. This instability occurred at a Reynolds number of approximately 400 in both channel geometries.

Ghaddar, Korczak, Mikic and Patera (1986) used the spectral element method to numerically model the fully developed flow in a grooved channel. The numerical method enabled transient calculations to be performed. The channel was composed of a flat plate opposite a wall having rectangular grooves. The Reynolds number (based on a normal channel in the absence of the grooves) range of interest was up to 2000 and in the absence of the grooves the flow would be totally laminar and steady. The aim of the work was to investigate the stability of the recirculation regions within the grooves and the shear layers bounding the recirculation zone. Ghaddar, Magen, Mikic and Patera (1986) modelled heat transfer convection in the grooved channel and investigated the effects of an oscillatory mass flow rate. They found considerable heat transfer enhancement as the flow

oscillatory frequency approach a critical value and excited the flow.

Nishimura, Tarumoto and Kawamura (1987) experimentally determined the fluid flow and mass transfer characteristics of wavy channels for oscillatory flow conditions. Oscillatory flows are not encountered in plate fin and tube heat exchangers, but this type of flow is used in membrane oxygenators and the authors briefly reviewed the literature in this field. The investigation dealt with the effect of the phase of the plates forming a channel of uniform, converging and diverging and intermediate phase cross sectional flow areas. The phase referred to is the phase determining the position of an adjacent plate forming either a symmetric or asymmetric channel.

Asako, Nakamura and Faghri (1987) numerically computed the laminar flow in a channel of converging diverging cross section. The authors investigated the effect of rounding the corrugation peaks (corners) on the channel performance. The heat transfer rate was found to be relatively insensitive to the rounding of the peaks, and the flow friction decreased in accordance with the rounding. The channels investigated were compared under fixed, pumping power, pressure drop and mass flow constraints.

Maubourguet-Pellerin and Pellerin (1987), numerically presented results for the fluid flow and heat transfer characteristics of a flat sided corrugated converging diverging channel, although it appears that other wavy geometries were modelled. At the low Reynolds number of 1. the flow just separated, but the recirculation zone was considerably enlarged in the troughs at a Reynolds number of 60.

Ralph (1987) numerically modelled the flow in a wavy walled circular tube using a specially developed time marching formulation to

27

produce steady flow results. Experimental pressure drop measurements were made which were compared with the numerically generated solutions. The investigation covered Reynolds numbers up to 500. based on the tube minimum diameter and mean velocity at the minimum cross section. It was found that the numerical model agreed with the experimental results up to a Reynolds number of about 300. when the flow became transitional.

2.5 Discussion of the Literature review

From the published literature reviewed it became clear that there were areas relating to corrugated and rippled ducts which had received very little attention by researchers in the field applicable to rippled plate fin and tube heat exchangers, and these are listed below;

1   Full Size Heat Exchangers

There are a few references regarding the characteristics of full size plate fin and tube heat exchangers, the most notable being that of Kays and London (1984), but there is very little data of high quality which can actually be used for design purposes. The absence of pressure drop measurements by many researchers, or the data being presented in dimensional forms make comparative performance studies either impossible or qualitative in nature. More data for rippled plate fin and tube heat exchangers using different ripple fin shapes and flow lengths is required to design more efficient systems with confidence.

2   Inlet Region Characteristics

Most investigations concentrated on either experimental measurements or numerical modelling techniques to gain information regarding the performance characteristics of rippled or corrugated

28

geometries in the fully developed flow regime. Information relating to the inlet region of a flat sided corrugated duct was reported by Goldstein and Sparrow, (1976a, 1976b and 1977). This work, was extremely important to the heat transfer literature as many fluid flow characteristics were encompassed within the geometric and flow ranges, including, the generation of secondary flow vortices in corrugated ducts, the breakdown of the vortices to turbulent flow and the characteristics of fluid flows around circular tubes in corrugated ducts. The secondary flow vortices were generated by the centrifugal forces acting on the fluid arising from the flow curvature. Molki (1986) and Molki and Yuen (1986) reported regional mass transfer measurements in the inlet region of various flat sided corrugated ducts. The measurements were made using the thick film naphthalene sublimation technique. In both of these investigations (by Molki et al) the pressure drop results were presented in terms of a friction factor representative of the periodically fully developed region and no information of the pressure drops in the inlet region were presented.

3   Ripple Profiles

Flat sided corrugated and sinusoidal wavy walled ducts and channels have been used frequently, but other profiles of a wavy nature have been shown to be important heat transfer surfaces by Sparrow and Hossfeld in the periodically fully developed region, and Beloborodov and Volgin who measured overall characteristics of a heat exchanger including the inlet region.

4   Flow and Geometric Ranges

In addition to the ripple or corrugation profile, the wall

29

spacing of the duct is extremely important to the flow characteristics and depending upon the wall profile determines the degree of flow turning or curvature fluid elements undergo when passing ripple peaks and troughs.

The flow in the periodically fully developed region of corrugated and rippled channels has received considerable attention in the past which is mainly due to the ease of numerical modelling, experimental data collection, and general application to a wide field of heat exchange apparatus covering the internal cooling passages of turbine blades, oxygenation and dialysis equipment and electronic components on circuit boards. Unfortunately some of the ducts and channels used in these devices cannot easily be formed from plate fin strip metal and used in a heat exchanger, but this literature was included in the review to gain as much information as possible of the fluid flow characteristics of arbitrary ducts and channels with enhanced heat transfer.

CHAPTER 3

EXPERIMENTAL INVESTIGATION OF THE PERFORMANCE OF RIPPLED FIN TUBE BANK HEAT EXCHANGERS

The performance characteristics of five finned tube heat exchangers were measured in a thermal wind tunnel at Covrad Heat Transfer. Three of the heat exchangers consisted of banks of tubes three tube rows deep, the other two consisted of tube banks four rows deep. The tube rows were arranged in echelon formation, for all heat exchangers, where the tube pattern repeated on the fourth row. The measurements made, the results and comparison for the heat exchangers having three tubes row were reported by Maltson, Wilcock and Davenport (see Appendix 1). An in depth description of the measurements taken and the data reduction procedure are given in this chapter.

The results of the measurements on the heat exchangers having four tube rows are reported here, together with a detailed description of the uncertainty analysis procedure. A comparison is made between the performance of the rippled fin heat exchangers having three tube rows with the louvred fin data of Tura, (1986). All the rippled fin heat exchangers and the best louvred fins of Tura are compared against the performance of the Kays and London, (1984), plain fin with thin staggered tubes, no. 9.1-0.737-S. The rippled plate fin and tube data of Kays and London was compared against their wavy plate fin data, which had a large variation in fin pitch. The results of this comparison are given.

3.1 Covrad Heat Transfer Thermal Wind Tunnel

The wind tunnel has been extensively used in previous investigations, Tura (1986), and Davenport (1983a and 1983b). The tunnel is shown in Plate 3.1, and schematically in Fig 3.1. The

31

measurements were made on samples of heat exchangers, 0.15 m by 0.15 m, the same size as the working section of the wind tunnel. The sample cores had side plates and header tanks mounted and were set up to operate as in a typical application. Care was taken to ensure that the heat exchangers were centrally positioned in the working section and sealed in place using plastercine. During installation of the exchanger into the rig, the connecting tubes carrying the liquid were closed by valves. Air was flushed from the liquid system by opening one of the valves and letting the exchanger gradually fill up with water whilst allowing the trapped air to discharge through another valve. Photographs showing a typical sample heat exchanger and how it was inserted into the tunnel are presented in Plates 3.2 a,b and c, (Plates 3.1 and 3.2 a,b, and c courtesy of Tura R.).

The tunnel operated by passing hot water through the heat exchanger tubes which was cooled by drawing in air through the fin passages. The inlet water temperature was thermostatically controlled at 80°C. The air was drawn in from the laboratory, through a damping screen, a bell mouth inlet and flow straighteners upstream of the heat exchanger.

For the present tests the water flow rate was set to a high value such that there was only a small resistance to heat transfer on the water side. The Reynolds number of the water flow was approximately 1.0×10^4 and in the turbulent flow regime which had a high heat transfer coefficient. This increased the accuracy of the heat transfer measurement on the airside by reducing the effect of the water side resistance in the overall heat transfer coefficient equation and by producing a near uniform air exit temperature from the heat exchanger.

However the water temperature difference then became very small and the uncertainty in the water temperature difference measurement increased. Typical temperature differences were 0.1 to 1.4^{o}C for the water and 45 to 20°C for the air. The water flow rate was measured by calibrated rotameters, but the uncertainty in the measurement was relatively high and could not be easily improved. In addition the rotameter fluctuated about a mean position, which had to be estimated. Energy balances between the airside and the water side heat transfer rates were not attempted here due to the above mentioned problems, but in the previous investigations of Tura, (1986), and Davenport, (1983a), energy balances of less than 4.% and 6.% were typical for similar temperature and flow rate measurement instrumentation.

3.2 Four Row Heat Exchanger Geometry

The two four row heat exchangers tested both had the same fin profile, but different fin pitches. The fins were made of copper of thickness 0.076 mm. The water tubes were made of brass of thickness 0.14 mm and coated with a thin layer of solder. The heat exchangers were assembled by placing the press formed strip plate fins into slots within a jig having the required fin pitch. The solder tubes were then inserted by hand into holes in the fins. The assembly was then baked in an oven to allow the solder on the tubes to join with the fins providing a thermal and mechanical bond. The dimensions of the fin profile and the tube layout are given in Figs. 3.2.a and 3.2.b, respectively. The geometrical dimensions of the two heat exchangers are given in Table 3.1. A photograph of the four row rippled fin is presented in Plate 3.3b. Plate 3.3a shows a four row rippled fin of profile A from Appendix 1, (see Appendix 1 description for the shape and dimensions). The two profiles viewed from the side can be seen in

33

Plates 3.4b and 3.4a respectively.

3.3 Experimental Measurements and Tolerances

The parameters which did not change during the test were measured as follows;

1   The atmospheric pressure was measured by a Fortin barometer and used in accordance with the British Standard, B.S. 2520. The height of the mercury column was read to $\pm$ 0.05 mm. The tolerance of the barometer temperature was $\pm$ 0.5°C.

2   The water volumetric flow rate was measured by one of two rotameters which had been calibrated against an accurate turbine flowmeter. The uncertainty in this measurement was estimated to be $\pm$ 2.0 in 20. Imperial (English) gallons per minute.

3   The relative humidity was measured by measuring the wet and dry bulb temperatures and reading the relative humidity from the psychrometric chart.

The above measurements were checked at the end of the experiment for variations.

The air velocity was set approximately using an analogue reading of the anemometer output and the following measurements were taken when the thermal and flow readings had stabilised and formed the basis of the heat transfer and flow friction measurements;

1   The pressure drop across the sample core was measured by an Airflow Developments inclined manometer. The pressure tappings upstream and downstream of the heat exchanger consisted of a ring of four tappings. This measurement was taken once per flow setting. The discriminations of the three manometer scales used were;

0–5 kN/m^2 $\pm$ 10.0 N/m^2

$0-1 \ kN/m^2 \ \pm \ 2.0 \ N/m^2$

$0-500 \ N/m^2 \ \pm \ 1.0 \ N/m^2$

2   The air velocity was measured by a rotating vane anemometer which was calibrated by traversing a pitot probe across the tunnel working section. The 64 point traverse was integrated to give the mean velocity. A linear regression equation was fitted to the calibration. The uncertainty in the air velocity measurement was estimated to be $\pm$ 1.% on the anemometer constant, $\pm$ 1.% on anemometer counts and $\pm$ the last digit.

3   The air temperature difference was measured by an array of nine chromel-alumel thermocouples, which were held in place by a copper wire grid of square mesh which provided an averaging mechanism for any airside temperature variations.

4   The air inlet to water inlet temperature difference was measured by a single chromel-alumel thermocouple.

5   The water temperature difference was measured by an array of four chromel-alumel thermocouples.

The output from the thermocouples was measured by a digital voltmeter which had an accuracy quoted as $\pm$ 0.1% $\pm$ the last digit. The reading was converted from millivolts to degrees Celcius by using the recommended British Standard procedure, B.S. 4937, (1973).

6   The air temperature at the inlet to the heat exchanger was measured by a mercury in glass thermometer inside the wind tunnel and was read to $\pm$ 0.5^{o}C.

The temperature differences and the tunnel velocity measurements were repeated three times for each flow setting to check that the system had stabilised.

3.4 Data Reduction Procedure

The results were calculated and are presented in a standard way (Kays and London, 1984) by reducing the data to the relevant nondimensional numbers, Reynolds number, j factor and friction factor. The reason for reducing the data to nondimensional numbers is to let the data be available to geometrically similar geometries and to other fluids at different temperatures and pressures, through the principle of Similarity. Three nondimensional numbers were required to represent the flow (mass flux), heat transfer and flow friction terms. The procedure for testing the heat exchangers was exactly the same as that adopted by Tura, (1986), with minor modifications. Where more than one measurement for a variable was taken, the mean of the readings was used in the data reduction procedure.

3.4.1 Reynolds Number

The airside Reynolds number was based on the mass velocity flux at the minimum flow cross sectional area. The hydraulic diameter was used as the representative length in the Reynolds number and was also based on the minimum flow area. The fluid properties used were evaluated at the mean air temperature through the heat exchanger. The mass flow rate of air was calculated as follows;

$$m_a = v_{a,i} \cdot \rho_{a,i} \cdot A_{fr}$$

The inlet air velocity was slightly different from the measured tunnel velocity due to the frontal area not being exactly equal to the tunnel flow area. The inlet velocity was calculated from;

$$v_{a,i} = \frac{A_{tun}}{A_{fr}} \cdot (\text{ANMOM} \cdot \text{ACAL})$$

The correction was very small as the test samples were made to

36

suit the dimensions of the tunnel. The Reynolds number was calculated
from;

$$Re_a = \frac{m_a \cdot Dh_a}{A_c \cdot \mu_{a,m}} \qquad \text{where} \qquad Dh_a = \frac{4 \cdot A_c \cdot L_{1f}}{A_{ht}}$$

The finned tube heat exchanger samples tested here had tube rows
which overlapped in the flow direction, causing a local constriction
in the flow. The minimum flow area used in the data reduction was
taken to be the area of flow between the tubes of one row only (see
Appendix 1). As the local constriction to the flow was very short in
the streamwise direction, the minimum flow area used would be more
representative of the mass flux for the total flow length. Whilst the
minimum flow area would affect the values of the nondimensional
numbers calculated, the actual performance of the heat exchanger would
not be affected.

3.4.2 j factor

The heat transfer rate from the heat exchanger to the air was
based on an airside calculation and was found from;

$$Q_a = m_a \cdot cp_{a,m} \cdot (T_{a,o} - T_{a,i})$$

The overall heat transfer coefficient was defined in the
following equation;

$$Q_a = U \cdot A_{ht} \cdot T_{MD} \qquad \text{where} \qquad T_{MD} = T_{LMTD} \cdot F_{MD}$$

T_{MD} is the mean temperature difference between the two heat exchanger
fluids evaluated for a heat exchanger in cross flow. The log mean
temperature difference was defined in the usual way for counter flow
as;

$$T_{LMTD} = \frac{(T_{w,i} - T_{a,o}) - (T_{w,o} - T_{a,i})}{\log_e \left| \frac{(T_{w,i} - T_{a,o})}{(T_{w,o} - T_{a,i})} \right|}$$

The mean temperature difference factor for cross flow was evaluated by the method of Roetzel and Nicole (1975). This was initially done to investigate the accuracy of the log mean temperature difference for counter flow applied to a heat exchanger in cross flow. The range of the cross flow factor calculated for the test results was between 0.995 and 1.0.

The airside resistance was found from the overall heat transfer equation, having a knowledge of all the other resistances acting between the two fluids.

$$\frac{1}{U} = \frac{1}{\eta_o \cdot h_a} + \frac{1}{h_w} \cdot \frac{A_{ht}}{A_{wh}} + \frac{A_{ht}}{A_{wh}} \cdot \left| \frac{th_{tw}}{k_{tw}} + \frac{th_{sl}}{k_{sl}} \right|$$

The water side heat transfer coefficient was calculated from the equations of Kern and Kraus (1972), for transitional and turbulent flow in circular tubes. The equations are also applicable to noncircular channels where the hydraulic diameter is used in place of the diameter. The mean water Reynolds number was calculated as follows;

$$Re_w = \frac{\rho_{w,m} \cdot v_{w,m} \cdot Dh_w}{\mu_{w,m}} \quad \text{and} \quad Dh_w = \frac{4 \cdot A_{wf}}{P_{wf}}$$

The equations used to calculate the mean waterside heat transfer coefficient (Kern and Kraus) and were as follows;

For $Re_w > 1.0 \times 10^4$

$$Nu_w = \frac{h_w \cdot Dh_w}{k_{w,m}} = 0.023 \cdot Re_w^{0.8} \cdot Pr_{w,m}^{1/3}$$

For $2100 < Re_w < 1.0 \times 10^4$

$$Nu_w = 0.116 \cdot \left| Re_w^{2/3} - 125 \right| \cdot Pr_{w,m}^{1/3} \cdot \left| 1 + \frac{(Dh_w)^{2/3}}{(L_{wt})} \right|$$

The water temperature difference was very small between the tube wall and the fluid, due to the high heat transfer coefficient and the corrective term for variable fluid properties was neglected.

The fin effectiveness, fin efficiency and heat transfer coefficient were calculated together by an iterative procedure. The fin effectiveness and fin efficiency were calculated assuming a rectangular fin of constant thickness. Although the geometry of the fin was not quite rectangular, due to the layout of the tubes, this solution was thought to be a good approximation. The equations used were as follows;

$$\eta_o = \left| \left(\frac{(A_{fi})}{(A_{ht})} \right) \cdot (1 - \eta_f) \right|$$

where

$$\eta_f = \frac{\tanh(\zeta \cdot b)}{(\zeta \cdot b)}$$

and

$$\zeta = \left| \frac{h_a \cdot P_g}{(k_{sl} \cdot A_{sl}) + (k_g \cdot A_g)} \right|^{0.5}$$

The conductive term in the fin efficiency equation allowed for the fin having a thin film of solder on its surfaces. This arose if the heat exchanger had been "dipped" in molten solder, to improve the fin to tube contact. From past practical experience a solder film thickness of 0.03 mm was used to calculate the cross sectional area of the solder layer. The fin efficiency equation assumed that the direction of heat conduction was parallel in the copper and solder regions. The iterative procedure used was as follows;

1   A guess for the fin effectiveness was required (0.9).

2 From the overall heat transfer coefficient equation the airside heat transfer coefficient was obtained.

3 The fin efficiency was then calculated.

4 The new fin effectiveness was calculated using the above equation.

5 Steps 2 - 4 were repeated until the required convergence for the heat transfer coefficient was obtained. The iterative process was extremely stable and convergence was usually obtained in a few iterations.

For the present three and four row heat exchangers the range of fin efficiencies calculated was from 0.80 to 0.97.

The j factor was calculated from;

$$j = St_{a,m} \cdot Pr_{a,m}^{2/3}$$

where the Stanton and Prandtl numbers were;

$$St_{a,m} = \frac{h_a \cdot A_c}{m_a \cdot cp_{a,m}} \quad \text{and} \quad Pr_{a,m} = \frac{cp_{a,m} \cdot u_{a,m}}{k_{a,m}}$$

3.4.3 Friction Factor

The measured pressure difference between the upstream and downstream pressure tappings was corrected to account for a minor loss due to the flow friction acting on the tunnel walls between the two static tapping planes. This minor loss was calculated from a regression equation which fitted measurements of the wall flow friction. These measurements were made in the absence of a heat exchanger core.

The corrected pressure drop was reduced to the friction factor using the following equation, from Kays and London, 1984.

$$pd = \frac{G_c^2}{2 \cdot \rho_{a,i}} \left| (1 + \sigma^2) \cdot \left(\frac{\rho_{a,i}}{\rho_{a,o}} - 1 \right) + f \cdot \frac{A_{ht} \cdot \rho_{a,i}}{A_c \cdot \rho_{a,m}} \right|$$

40

where

$$G_c = \frac{m_a}{A_c} \quad \text{and} \quad \sigma = \frac{A_c}{A_{fr}}$$

The equation applies to finned tube heat exchangers where the form drag acting is treated as an equivalent shear stress. The above equation eliminates the pressure loss associated with accelerating the flow due to the decrease in density (or increase in density if the heat exchanger cooled the gas) from the friction factor. However when pressure losses are being calculated this term is evaluated at the new temperatures.

The above data reduction procedure was coded into a FORTRAN computer program SWTSE, see Appendix 10. Many of the equations and algorithms were used in other programs and for consistency were placed in a subroutine libraries, see AWTSL, AWTMS and AWTNOM. AWTNOM contains a nomenclature listing for many of the variables used in SWTSE, AWTSL and AWTMS. The program SWTSE was compiled using the Harris FORTRAN77 compiler using a Harris job control program COMP which arranged access to the subroutine libraries when the executable module was created. Geometrical parameters were calculated by program SAREA.

The fluid properties were evaluated using the FORTRAN subroutines of Button and Tahmassebi, (1984). The subroutines had been compiled in Harris FORTRAN and stored as a FORTRAN library in file area 204Y008*PRLIBA. These subroutines had also been thoroughly checked by Tura, (1986). The uncertainty associated with a given property was not evaluated using the subroutines, and the Monte Carlo Simulation method was used by variation of temperature and pressure.

3.5   Four Row Heat Exchanger Results

The four row nondimensional reduced data was treated in a similar way to the three row data, by plotting all the points on large scale graphs, drawing smooth curves through the points and reading data from the curve at pertinent Reynolds numbers. All of the processed data points for the j factor and friction factor are given in Figs. 3.3 and 3.4. The resulting j factor and friction factor against Reynolds number data for these two sample heat exchanger cores from the smooth lines is presented in Table 3.2 and graphically in Figs. 3.5 and 3.6 respectively.

3.6 Uncertainty Analysis

The three nondimensional numbers calculated together with the geometry details characterise the performance of the heat exchanger. The procedures for calculating these numbers were described above. The three numbers were dependent upon a large number of measured variables and the uncertainty of a nondimensional number was dependent upon the accuracy to which the measurements were made for each variable. The Monte Carlo Simulation Method was used to assess the uncertainty of the calculated nondimensional numbers. This method was used by Obray, Wright and Baldwin, (1986), to estimate the uncertainties of the calculated nondimensional numbers from measurements on a fin tube bank. The statistical quantities were calculated from generated distributions by running through the data reduction procedure 1000 times for each data point. The 95 percent certainty intervals were obtained from the 2.5 and the 97.5 percent points in the ordered generated distributions.

The input data for each run was generated by random sampling for each measured variable to simulate an experiment. The number of

simulations (1000) was chosen based on a set of runs in which the number was varied from 50 to 1000. It was found that the distributions were quite "spiky" with numbers up to 200, but the distributions were smooth with 1000 points.

The use of the term "certainty interval" has arisen due to the fact that the distribution upon which a non dimensional number was based was simulated. The term "confidence interval" is usually used when the distribution is measured.

The computational procedure for the uncertainty analysis is described below;

1   The data specifying the heat exchanger geometry was read by the program.

2   The experimental data which did not change for a particular flow setting was then read.

3   The values previously read were then stored in a separate memory.

4   The experimental data specifying each flow setting was read. There were three sets of the following data for this setting, anemometer counts, air temperature, air inlet to water inlet and water temperature, temperature differences were measured as millivolts from thermopiles, and one pressure drop reading.

5   All the values which did not change between flow settings were set equal to their stored values.

6   The upper and lower limits to each variable read in above were found, based upon experimental tolerances.

7   A random number for each variable was obtained between its upper and lower value, based on a uniform distribution of random numbers.

8   The data reduction procedure then proceeded. This included the

fluid properties and surface geometry calculations.

9   The calculated nondimensional numbers were stored in arrays.

10   Steps 7 to 9 were repeated until 1000 sets of data had been calculated.

11   The statistical quantities were obtained from the generated distributions and written to an output file.

12   Steps 4 to 12 were repeated for the next flow setting.

The experimental tolerances used in the simulation were the discrimination of each measurement and are given in Table 3 of Appendix 1. The certainty intervals calculated for a typical four row heat exchanger test are shown in Fig. 3.7. These results represent a certainty estimate on data points in a single sample experiment. At least two separate tests were carried out on each heat exchanger sample. The performance characteristics results presented here are those that were read from smooth curves drawn through many data points. Therefore the certainty intervals presented are an overestimate of the actual interval of the calculated nondimensional numbers.

3.7   Comparison of Heat Exchanger Performance

The performance evaluation and comparison of various types of heat exchanger has now become a vital component of the selection process calculations. This section is dedicated to the performance and selection of a heat exchanger for a particular application.

3.7.1   Performance Evaluation Criteria

The performance evaluation criteria used to differentiate the performance of the heat exchangers were thoroughly reviewed by Shah, (1978). The criteria recommended by Shah were used by Maltson, Wilcock and Davenport (1989) to observe the performance characteristics of the

44

heat exchangers reported therein. It was found that the j/f ratio plotted against the Reynolds number was a misleading criteria and that the most useful criteria was the calculated heat transfer rate against fan power, with a performance ratio against the fan power for the surfaces under comparison, method of Bergles, Junkhan and Bunn (1975). The other comparison methods of, the standardised heat transfer coefficient against pumping power per unit surface area and the heat transfer rate per unit volume against the pumping power per unit volume, were not used in this study as their results can be misleading. The performance evaluation criterion of Bergles, Junkhan and Bunn was used to assess the performance of the heat exchangers tested here relative to previous data.

3.7.1.1 <u>Bergles, Junkhan and Bunn (1975) Criteria Applied to the Present Heat Exchangers</u>

This criteria calculates the performance of a system of which the heat exchanger is a part. Data for different heat exchangers is used to investigate the effect of a particular heat exchanger on the system performance. The system in which the heat exchangers were placed for the present comparison was that of hot water cooling of an agricultural tractor. The tractor moved at a low velocity and the effects of ram induced airflow considered by Davenport, Beard and Scott (1974), were negligible. The air fan was separately driven independently of the engine. The heat exchanger size was 1 m by 1 m frontal area and the flow length was that of the individual fin. The inlet water temperature was set to 80°C and the mass flow rate 5.47 kg/s which is typical of this type of heat exchanger. The mass flow rate of air was found from the Reynolds number, the heat transfer

45

coefficient from the j factor and the pressure drop from the friction factor. The inlet air temperature was specified at 20°C and a relative humidity of 45%. The water tubes considered were brass the thickness of which was 0.20 mm. A solder layer on the tube wall was included in the overall heat transfer coefficient and had a thickness of 0.03 mm. The air properties used in the nondimensional numbers were needed at the mean temperature which was calculated iteratively from an initial guess of 25°C.

The fan power was calculated from the sum of two components, the pumping power to force the air through the heat exchanger and the power required to accelerate the air from rest to the inlet frontal velocity, neglecting any ram effect. In a system there is usually another term to consider, that of the ducting power loss which can be significant, but was neglected here. The flow acceleration through the heat exchanger due to the increase in specific volume of the air was taken into account within the core pressure drop calculation. Hence;

$$Fp = Pp + Pa + Pd$$

where
$$Pp = v_{a,i} \cdot A_{fr} \cdot P_{d,c} \; , \; Pa = m_a \cdot \frac{v_{a,i}^2}{2} \; \text{ and } \; Pd = 0.$$

The above heat exchanger calculation was coded in FORTRAN in program REALEX which calculated the heat transfer rate and fan power characteristics. To quantify the performance of one heat exchanger relative to another, a performance ratio was calculated. For the following comparative study, this ratio was defined as the ratio of the heat transfer rate for the heat exchanger relative to that of a reference exchanger, with both exchangers operating at the same fan power Fp. The reference exchanger used was the plain plate fin surface 9.1-0.737-S of Kays and London (1984), which had thin rectangular

46

tubes arranged in echelon formation and three tube rows. The fan power values of the compared and reference exchangers were different and an interpolation scheme was required. This was done by fitting an equation to the heat transfer rate and fan power data of the reference exchanger and calculating the heat transfer rate of the reference surface at the same fan power as the compared exchanger. Program YRAT calculated the performance ratio from the calculated characteristics.

3.7.2 Comparison of Four Row Rippled Fins Against the Three Row data

This comparison was performed to investigate the effect of flow length on the performance of the rippled fin heat exchangers. The Kays and London ruffled fin was included in the figures.

3.7.2.1 Geometry Comparisons

The following points relate to the difference between the compared surfaces. Differences in the geometry relating to the Kays and London heat exchangers were described by Maltson, Wilcock and Davenport (1989).

1   The fin thickness of all of the rippled fins was 0.076 mm and this value was used in the Kays and London (1984) plain fin reference surface.

2   Surfaces 4 and 5 had fin pitches of 296 and 269 fins/m, whilst the three row surfaces 1, 2 and 3 had fin pitches of 353, 354 and 282 fins/m.

3   The fin length in the flow direction for the four row heat exchangers was 77.6 mm, whilst for the three row the flow length was 58.4 mm.

4   The heat transfer surface areas for the four row surfaces 4 and 5 were 49.9 and 46.2 m^2. In comparison the heat transfer surface areas

47

for the three row exchanger surfaces 1, 2 and 3 were 44.4, 44.6 and 37.6 m^2 respectively.

3.7.2.2 Performance Comparisons

The Bergles, Junkhan and Bunn criteria expressed as the heat transfer rate against fan power is shown in Fig. 3.8 with the associated performance ratio in Fig. 3.9. The four row surfaces have a higher performance than the three row, but they have larger heat transfer surface areas. Surface 5 has shown an improvement of 13 percent over surface 3, with an increase in surface area of 23 percent, for fan powers between 1000 and $1.0X10^4$ W.

3.7.3 Performance of the Louvred Fins Tested by Tura (1986)

The original data of Tura (1986), in the form of experimental measurement input computer files was reworked by the above data reduction procedure to nondimensional number form. This was necessary as the nondimensional data was published as a regression equation and it was thought that a higher accuracy would be obtained by using the original measurements. For each heat exchanger sample, two tests were performed. Instead of smoothing the data by drawing curves through the points, all of the measured data reduced to nondimensional numbers was used. The measured pressure drop was reduced to a friction factor based on Kays and London (1984) equation 2-26b. The inlet and exit pressure drop effects were not separated from the duct pressure drop and included in the friction factor.

A typical louvred plate fin with staggered tubes is shown in Plate 3.5, however the louvred fins tested by Tura were formed within triangular ducts between three inline thin rectangular tubes. The twelve heat exchangers all had a similar triangular duct geometry, but louvre angle and positioning were parametrically varied. The heat

exchanger geometry details were given in full by Tura (1986). The fin thickness used in the louvred heat exchangers was 0.06 mm and this thickness was used in the comparative study. The performance graphs which compared the different surfaces are given, Figs. 3.10 and 3.11. The louvred surfaces having louvred angles of 29° and reversal lengths of 2 and 6 mm have the highest performance.

3.7.4 Comparison of Three Row Rippled Against the Louvred Fins of Tura (1986).

The best louvred fin surface was compared with the rippled surfaces 2 and 3.

3.7.4.1 Geometry Comparison

The following differences were noted regarding the geometries of the compared surfaces. The triangular plain fin had the same fin geometry as the louvred fin.

1   The fin thicknesses were left at their earlier values of 0.060 mm and 0.076 mm for the louvred and rippled fins respectively. The fin thickness for the Kays and London fins was set to 0.076 mm.

2   The flow passage length was 50.0 mm for the louvred compared with 58.4 mm for the rippled surface and 60.2 mm for the Kays and London surfaces.

3   The fin pitches were 518 fins/m for the louvred compared with 354 for rippled surface 2. The Kays and London ruffled and plain fin surfaces had fin pitches of 366 and 358 fins/m respectively.

4   The heat transfer surface areas were 51.9 and 44.6 m^2 for the louvred and rippled surfaces respectively. The Kays and London ruffled and plain surfaces had surface areas of 46.4 and 45.6 m^2 respectively.

5   The water tube pitches in the spanwise direction were 10.1 mm for

49

the louvred fins compared with 15.2 and 14.0 mm for the rippled and Kays and London fins respectively.

3.7.4.2   Performance Comparison

The comparison was based on the performance evaluation method of Bergles, Junkhan and Bunn. The performance of each of the compared surfaces in terms of heat transfer rate and fan power were given in Figs. 3.8 and 3.10. The performance ratio graph is presented in Fig. 3.12, showing the relative performance of the louvred fin against the rippled surface 2, the Kays and London and the triangular plain fins, and the Kays and London ruffled fin. The following points were noted regarding the comparison;

1   The Kays and London Plain fin has the best performance at the low fan powers (less than 30 W).

2 The triangular plain fin has a lower performance than the Kays and London plain fin up to a fan power of 6000 W in spite of having a larger surface area, but at higher fan powers the triangular fin has a better performance.

3   At fan powers greater than 40 W the louvred surface has a considerably better performance than the other compared surfaces. At fan powers greater than 2000 W the improvement over the rippled surface was found to be 28 percent, with an increase in heat transfer surface area of 12 percent.

3.7.5   Comparison of the Wavy Fin Heat Exchangers of Kays and London with their Ruffled Plate Fin and Tube Heat Exchangers

The Kays and London surfaces compared were the three wavy plate fin heat exchangers, 11.44-3/8W, 11.5-3/8W and 17.8-3/8W and the three ruffled plate fin and tube heat exchangers, 9.29-.737-SR, 9.1-.737-S (reference surface) and 11.32-.737SR. The three wavy fin surfaces were

placed between thin flat tubes forming a one row heat exchanger.

3.7.5.1   Geometry Comparisons

The differences in geometry details of these heat exchangers are described in tabular form in Table 3.3. It was noted that there were considerable differences in the wave double amplitude and wave pitch between the surfaces in addition to the dimensional and area differences.

3.7.5.2   Performance Comparisons

The comparison was based on the Bergles, Junkhan and Bunn performance evaluation criteria as described in section 3.7.1.1. The heat transfer performance against fan power and the performance ratio graph also against the fan power are shown in Figs. 3.13 and 3.14 respectively.

The 11.32-0.737-SR surface shows an improvement of approximately 5 percent over the 9.29-.737-SR surface for most of the fan power range, although the penalty was an increase in surface area of 17.5 percent. This increase in surface area although not increasing the size of the unit would considerably increase its weight, depending upon the density of the material of the fin used.

The three wavy plate fin heat exchangers have a low performance when compared to the ruffled plate fin and tube heat exchangers. In this comparison there are the three major effects to be considered of heat transfer surface area, the log mean temperature difference and the wave geometry. Generally the three wavy plate fins have a lower performance than the plate finned tube bank heat exchangers which is mainly due to the smaller heat transfer surface areas of the former.

CHAPTER 4

EXPERIMENTAL METHODS FOR THE MEASUREMENT OF THE LOCAL HEAT

TRANSFER COEFFICIENT

4.1 Heat Transfer Methods

This chapter reviews the experimental methods available for the measurement of the local heat transfer coefficient, and outlines the advantages and disadvantages of the chosen technique when applied to measuring the coefficients in highly curved rippled ducts.

4.1.1 Transient Heat Transfer

This method involves inserting the model into a hot fluid stream and monitoring the model surface temperature with time. The local heat transfer coefficient at a particular location can only be obtained if the temperature time history at that location is known. The thermal boundary condition modelled is neither constant heat flux nor constant wall temperature as they both vary with time. The effect of the transient thermal boundary condition with regard to the accuracy of the technique has not been thoroughly investigated in developing flows, which prompted the author to research this, see Appendix 2 and further discussion on this in Chapter 7.

The models used for the testing may be either thick or thin skinned bodies, but the calculation of the heat transfer coefficients for the thin skinned body from the experimental measurements are considerably more difficult. In the thick skinned case the body is effectively infinite in wall thickness and an analytic solution may be applied to the measured times to obtain the heat transfer coefficients, provided the effects of the transient thermal boundary condition and conduction (streamwise and spanwise) effects in the wall can be neglected.

For the thin skinned case the temperature of the back wall of the model increases and the temperature profile in the wall must be simulated numerically, in addition there is natural convection heat transfer from this side of the model which must be incorporated into the simulation. In both cases there is heat conduction in the model wall in the spanwise and streamwise directions which cannot be simulated unless the heat transfer distribution is known. For thin skinned bodies the effect of streamwise conduction was considered in Appendix 3 for various conditions of imposed heat transfer coefficient variation and boundary conditions. Kidd (1987) investigated the lateral heat conduction in thin skinned models under the transient heat transfer testing of aerodynamic models. He measured the surface temperature of the rear face of the model by a thermocouple. The models were made of sheet metal and would have a high coefficient of thermal conductivity compared with that of perspex. The thin skinned case is more suitable in situations where the model is symmetrical and a similar flow exists both sides of the model. The heat transfer coefficient can be calculated with much greater confidence as the surface temperatures are the same and the temperature profile is symmetrical through the fin.

There are many methods of measurement of the surface temperature, but very few which measure a surface contour with a minimum of disturbance to the surface. The methods available for the measurement of the surface temperature were as follows:

4.1.1.1   Phase-Change Paints

Phase-change paints have the property of changing phase (solid to liquid) at a specific temperature and there may be also a slight

53

colour change. At this temperature the enthalpy of solidification must be supplied in order to melt the paint. The process is not fully reversible (due to the evaporation of liquid from the water based paint) and may only be used once, however only a thin film is required which may be applied by careful spraying. The temperature at which the change occurs must be determined by calibration, which is itself a difficult task as the calibration can only be done in a transient way, with the temperature gradually increasing. Phase-change paints were used by Metzger and Larson (1986) to measure the heat transfer distribution in a curved channel. In their situation the heat transfer coefficient varied mildly and the conduction effects within the wall were negligible. They developed the technique for thick walls to allow for an imperfect step change in fluid temperature. Jones and Russell, (1981), also used the phase change paints to measure the local heat transfer coefficients in finned, circular tube banks. The Heat transfer coefficient was calculated from the lumped parameter analysis method for thin fins. The results revealed how the local fluid flow affected the heat transfer coefficient, especially the effect of the horseshoe vortex around the cylinder.

4.1.1.2   Colour-Change Paints

Colour-change paints are similar to phase-change paints, in that at a particular temperature there is a distinct change in the colour, although the colour change is pronounced. The process of the colour change may be reversible and does not absorb the enthalpy of solidification that phase-change paints need. Colour-change paints were used by Jambunathan, Edwards and Button (1987), in an attempt to optimize the transient heat transfer technique for measuring natural convection heat transfer.

54

4.1.1.3   Liquid Crystals

Liquid crystals possess the property of transmitting light of different wavelengths at different temperatures. At the lower temperatures they appear red, and as the temperature increases they appear orange, green and blue. The colour range of temperatures can be as low as $0.5^{o}C$. Liquid crystals have advantages over the phase-change paint as they are reversible, do not require the enthalpy of the phase-change, and the calibration can be carried out with precision.

Ireland and Jones (1986) used thermochromic liquid crystals to measure the heat transfer distribution around a pedestal in a fully developed channel flow. The liquid crystals were screen printed onto the surface. In a later series of tests, microencapsulated crystals were used and calibrated the temperature against the yellow appearance. They also investigated the effect of transience on the local heat transfer coefficient. By mixing encapsulated liquid crystals, a particular colour may be observed at three separate temperatures. These three sets of experimental results were processed for the three times available at a point and the variation in heat transfer coefficient with time was obtained. Ireland and Jones, (1987), measured the response time of encapsulated crystals. It was found that the response time was a few milliseconds.

4.1.2   Heat Flux Methods

The local heat transfer coefficient may be measured by prescribing a constant wall heat flux and measuring the wall and fluid temperatures. The surface temperatures can be measured by liquid crystals, but the crystals have the disadvantage that the they can only measure temperatures accurately over small temperature ranges, in order to measure the heat transfer at numerous locations the heat flux

must be varied to keep the wall temperature constant. The boundary condition of constant heat flux may in some circumstances cause large variations in surface temperature over an area having a large variation in heat transfer coefficient. This condition is considerably different from the constant wall temperature case. This method was used by Butcher, Button, Wilcock and Wright (1985), Cooper, Field and Meyer (1975) and Simonich and Moffat (1984). Balzer and Tschudi, (1987), developed a technique for maintaining liquid crystals at a particular temperature within a compact cell, although the use of their technique was not easily adaptable for local heat transfer measurement.

4.2 Mass Transfer Methods By Analogy

4.2.1   Thick Film Naphthalene Sublimation

A thick naphthalene casting, the surface shape of which is the geometry to be studied is inserted into the flow. Naphthalene sublimes at its surface due to the concentration gradient within the flow. The boundary condition modelled is that of constant surface concentration throughout the test, the related heat transfer boundary condition is that of constant wall temperature. The mass transfer coefficient is obtained by measuring the surface recession over a time lapse. In order to obtain the surface recession locally for a test specimen the surface profiles before and after the test are required. For flat plate geometries the surface profiles may be measured by a specially designed profilometer similar to that of Button (1980) and Wilcock, (1983), or dial test indicators, Goldstein and Sparrow (1977). The time period of the test is set to limit the maximum recession to approximately 0.3 mm, depending upon the model scale, to prevent the

change in shape of the surface from seriously affecting the flow. If only the overall transfer coefficient is required then the naphthalene model need only be weighed before and after the test. The cast naphthalene surface, straight from the mould is usually smooth enough for the test, but the naphthalene has a tendency to crack on removal, due to its adherence with the metal mould.

4.2.2   Thin Film Naphthalene Sublimation

A thin film of naphthalene is applied to the model surface, the thickness of which is measured, typically 0.3 mm. The model is then placed under the required test conditions and the naphthalene surface is viewed with time. The boundary condition at the beginning of the test is that representing constant temperature, however as the test proceeds naphthalene sublimes from the surface leaving bare patches and the boundary conditions change. In this situation the concentration (thermal) boundary layer is restarted at the end of the bare patch where the remaining naphthalene layer starts. The mass transfer coefficient is obtained by timing the complete removal of naphthalene at a position. Neal (1975) developed a spraying technique using a specially designed spraying nozzle. The system was used in conjunction with a lathe for tubular geometries or a linear motion table for flat plates. However the spraying of any material onto the highly curved surfaces of the present investigation would not be deposited in a uniform manner.

The fusion of naphthalene vapour onto a rippled fin surface was attempted. A bath was designed to contain liquid naphthalene, it was produced from mild steel 10 mm thick, see Plate 4.1. Wire mesh grids were placed in the bottom to obtain a uniform temperature. The deposition of the naphthalene was a transient process, the fin surface

57

was exposed to the vapour by the use of a sliding lid. In some circumstances a layer of naphthalene was deposited, but this appeared very grainy and many crystal flakes formed in a manner perpendicular to the surface. Without considerable development the technique was unsuitable for the present application.

4.2.3   Electrochemical Techniques

Electrochemical techniques were available for the measurement of the local mass transfer coefficient. Nishimura, Ohori, Kajimoto and Kawamura (1986), measured the local mass transfer coefficient in a wavy walled duct using an electrolyte that contained potassium ferri-ferro cyanide and sodium hydroxide. The chemical reaction was diffusion controlled. The mass transfer coefficient was found by locally measuring the electric current, whilst a constant potential difference was held between the anode and cathode.

4.2.4   Mass Transfer Using Swollen Polymers

Silicon rubber when soaked in a swelling agent expands and this property may be made use of in mass transfer experiments. The test technique is very similar to that of the naphthalene thick film technique. During the test the swelling agent evaporates from the surface of the silicon rubber and into the flow. The removal of this agent in the rubber allows the rubber to shrink. The local surface recession is measured by optical methods using fringe patterns to calculate the mass transfer coefficient. The surface profile must be measured by optical methods as a mechanical profilometer would distort the rubber surface upon application. The boundary condition is that of constant surface concentration (constant wall temperature for heat transfer through an analogy). The optical methods are not as yet

available for the measurement of the highly curved surface profiles required and the technique was not considered.

Holographic methods have been used by Kapur and Macleod (1974) and Grosse-Wilde and Uhlenbusch (1978) to obtain the surface profile contours and hence the local mass transfer coefficients for various flows acting on flat plate geometries. The deviations of the surface from the flat plate were very small and these methods are not easily applied to the rippled surfaces encountered in this investigation.

4.3 Choice of Measurement Method

The above list of techniques represents the methods considered for the present measurements. Although other methods were available that could be applied to heat transfer measurement, eg. optical tomography using holographic interferometry for the measurement of three dimensional transient temperature profiles in a single phase fluid, Ostendorf, Mayinger and Mewes (1986), they would have required considerable effort in their application to the present geometries. It was initially thought that the thick film naphthalene mass transfer technique applied in a similar way to that of Wilcock (1983), or Goldstein and Sparrow (1975), would be used. However for highly curved surfaces a method of obtaining the surface recession contour was not available. The local mass transfer coefficient is obtained from knowing the surface depression in a direction perpendicular to the surface. It is possible to measure the mean mass transfer coefficient of a surface by measuring the reduction in mass of the naphthalene forming the surface, but this does not provide local information.

4.3.1 Requirements of the Measurement Technique

The main aim of the investigation was to understand the fluid flow, flow friction and heat transfer processes that take place in

59

rippled ducts. This understanding cannot be gained from the pressure drop and overall heat transfer characteristics of a full size plate fin and tube heat exchanger. The knowledge is gained from measuring the local heat (or mass) transfer coefficient and relating this to the local fluid flow. The flow friction becomes very important for comparative studies, in order to calculate the system pumping or fan powers. For the local heat (or mass) transfer coefficient measurement the following specifications were required;

1   Able to measure the local heat transfer coefficient on highly curved rippled fin surfaces.

2   Indicate spanwise variations that do occur in the presence of secondary flow vortices.

3   Model the constant temperature boundary condition as closely as possible to permit the use of the data to the design of plate fin exchangers which have spanwise variations in temperature on the fin that are accounted for by the fin efficiency calculation and generally have constant streamwise fin temperature. For water coolers of typical application the waterside heat transfer coefficient is very large and the tube metal temperature is usually very close to the water temperature.

4.3.2 Method Chosen

The measurement technique chosen to measure the local heat transfer coefficient was that of the transient heat transfer thin skinned body technique, using microencapsulated liquid crystals to measure the temperature of the fin model surface.

As soon as the decision had been made to use this technique, an experimental rig was required to provide suitable airstreams, rippled

duct geometries and various additional measurements. This work and the experimental measurements made are described in Chapter 5.

4.3.3 Advantages and Disadvantages of the Chosen Technique

1   Experience in using the technique was gained through the work of Tura (1986) at Coventry Polytechnic, although phase-change paint was used to monitor the temperature contours. It was thought feasible to investigate improving the technique by using the new microencapsulated liquid crystals.

2   A higher accuracy of absolute temperature monitoring would be obtained over the phase-change paints. Microencapsulated liquid crystals can have a complete colour range over $0.5^{\circ}C$ temperature range, giving the temperature range for a particular colour of approximately $0.1^{\circ}C$. This high temperature sensitivity would give very good definition in monitoring the local surface temperature, not obtainable with phase or colour-change paints.

3   The microencapsulated crystals were reusable and this property enabled a higher accuracy to be obtained when calibrating as the calibration may be performed for increasing, decreasing or steady temperature environments. In comparison phase-change paints may only be used once and must therefore be calibrated in a transient way or in a very slowly increasing temperature environment, and applied to the model surfaces prior to every test.

4   The effect of conjugate longitudinal conduction in the wall was found to be very small in cases of mildly varying heat transfer coefficient. For a typical fin the effect of a large variation in the heat transfer coefficient such as a step change, was found to significantly affect the coefficients close to the variation, but generally having no effect on the majority of the model surface.

CHAPTER 5

EXPERIMENTAL INVESTIGATION INTO THE FLUID FLOW, FLOW FRICTION AND
HEAT TRANSFER CHARACTERISTICS OF RIPPLED DUCTS

This chapter describes the experimental apparatus and procedures used in ascertaining the characteristics of the corrugated rippled ducts, which formed the major part of the research. The flow visualisation experiments were performed in a flow channel using water as the working fluid with dye streaklines, whilst the flow friction and local heat transfer studies were performed in a specially designed air flow rig. The local heat transfer measurements were made using the thin skinned transient technique. Heat transfer measurements were also carried out using a plain walled duct and these results were compared with well known regression equations and experimental results in similar geometries. The flat plate comparisons gave a degree of confidence in the experimental procedure and the results are presented. Comparisons of the flow friction and local heat transfer measurements with previously reported data were made in cases of similar geometry and flow.

5.1 Fluid Flow Experiments

5.1.1 Manufacture of the Models

The wavy fin rippled surfaces were produced by the vacuum forming process as follows:

1   A wooden former was made to the shape of the required fin by milling the surface with a specially made cutting tool ground to the desired profile. Warping of the former was prevented by mounting it on a metal base.

2   The wood former was covered with brass shim 0.001" thick to provide a smooth surface. Various methods of application were tried,

double sided tape was the most effective, but care had to be taken not to overheat the tape in the vacuum process as the shim would slip. Glues tended to produce creases in the shim which was thought to be due to small air bubbles captured with the application of the shim which expanded and ruptured the glue bond when the hot Cobex (vacuum formable material) was lowered on to the shim surface.

3   The material known as Cobex was vacuum formed over the former to produce the rippled fins. The heating time and rate of the fin were varied to obtain the best results of the process.

4   A jig was used to cut the fins to the required dimensions.

These fins were used in the flow visualisation, flow friction and heat transfer investigations.

A model was designed and made in perspex to hold the fins in position thus modelling heat exchanger fin passages. Several fin passages were arranged in parallel to permit the water flow to enter the central passages in a uniform manner. Removable side plates had slots milled into their sides at various fin pitches, into which the fins were placed. The model, side plates and vacuum formed fins are shown in Plate 5.1.

5.1.2 The Water Channel

A water channel shown in Plate 5.2, and schematically in Fig. 5.1 was used in the flow visualisation study to view the flow streaklines. This channel had been used by Tura, (1986) for a similar purpose. Five jets of dye were injected into the flow upstream of the model to produce the streaklines. The dye was made up by dissolving Methodone blue crystals in warm water and the mixture was left overnight to cool. The mixture was filtered to remove undissolved particles and poured into the five containers above the channel. The dye was

injected into the channel under the action of gravity and a flow reducing valves. The dye jet velocity was adjusted until the streak jets were smooth on leaving the injectors.

The mass flow rate through the model was measured by weighing the mass of water collected in a large tank over a period of time. This period was typically three minutes, timed with a stopwatch. For low mass flow rates the time period was extended up to ten minutes to give an accurate reading for the mass of water collected. The fluid properties, used in the calculation of the Reynolds numbers were evaluated at the measured water temperature and interpolated from the tables of Rogers and Mayhew (1980). The Reynolds number was based on a hydraulic diameter of twice the fin spacing and the mean water velocity through the model. The area of flow for the calculation of the mean velocity was based on the fin spacing. A venturi section was used within the water channel to reduce the area of water flow to the area through the model fin channels only and did not create disturbances to the flow. The water channel was approximately 0.30 m wide by 0.30 m deep and the venturi section reduced the width at the model inlet plane to 0.10 m. The height of the water was kept level with the top plate of the model by altering the height of the weir at the end of the channel above the weigh tank. This ensured that all the water flowed through the rippled fin channels.

5.2 Air Flow Rig

5.2.1 Description of the Rig

The air flow rig is shown schematically in Fig. 5.2 and in Plates 5.3 showing the heater, fan and expansion sections and 5.4 showing the contraction, working duct on track and the orifice plate pipes. The

various components are described individually below.

5.2.1.1 Inlet Venturi

The venturi was initially incorporated into the rig to measure the tunnel mass flow rate. Measurements through the venturi were not made for reasons described in section 5.2.2.

5.2.1.2 Heater Section

The air was electrically heated in this section by a 2 kW Eltron element, powered by an Eltron thyristor controlled power supply. The air temperature was measured downstream of the centrifugal fan in the expansion section by a resistance thermometer. The required temperature at this location was set at the control panel. The thyristor supplied the heater with the required power in order that there would be a minimum temperature difference between the set and the measured temperatures. The controlling system had been adjusted by Eltron to be stable in operation for this application. Due to thermal losses from the tunnel the controlled air temperature was higher than the tunnel exit temperature.

5.2.1.3 Centrifugal Fan

The fan was placed after the heater section, which mixed the air thoroughly to prevent layers of hot and cold air entering the tunnel. The electric motor was directly connected to the fan volute by thick metal cast vanes.

5.2.1.4 Expansion, Settling Chamber and Contraction Sections

These components originated from the work of Wilcock (1983), and were designed for minimum disturbance to the air and formed a major component in the rig. A flexible type hose of internal diameter 0.10m connected the outlet of the centrifugal fan to the expansion section. This hose was thermally insulated to prevent heat loss from the air.

65

There was a considerable temperature drop of the air, from the inlet of the expansion to the exit of the contraction. This was due to the heat loss by conduction through the wooden walls of the tunnel. Insulation was placed around the tunnel to prevent as much loss as possible, especially at the contraction section, where thermal boundary layers would affect the outlet temperature distribution.

Baffles were placed in the settling chamber section to mix the air thoroughly prior to the contraction. In the space left by a baffle for air flow, metal grids were inserted. These were found to be necessary to obtain a near uniform temperature at the exit of the contraction. As the air velocity was very low in the settling chamber the resulting increase in pressure drop and turbulence intensity were small.

5.2.1.5 Boundary Layer Bleeds Airflow Section

This flow section was required to permit the working duct to draw in an amount of air from the exit of the contraction section and to restart the boundary layer at the leading edge of the rippled duct. The excess air was turned at right angles to the duct direction (upwards and downwards), away from the duct inlet.

5.2.1.6 Working Section and Track

The rippled duct consisted of the vacuum formed rippled, or plain perspex fins housed within the working section with a wall spacing which could be varied. Attention was given to sealing the duct and associated components, by applying a film of Vaseline on mating surfaces. The wall spacing was set using slip gauges to set the distance between the metal fin supports at the four corners of the duct.

The working section was placed upon a specially made trolley which ran on an "I" section track. The digital stopwatch which displayed the time at which the photographs were taken was operated by a microswitch positioned at the end of the track such that when the trolley was fully in place the stopwatch was started. A latch was also sited on the track which prevented the trolley moving backwards down the track and out of the hot airstream, once in position. This system permitted the test section to be quickly and firmly placed in position.

5.2.1.7 Test Section Plenum Chamber

The plenum section was designed to even out the pressure field at the exit of the rippled duct. Two pipes connected the plenum chamber with the flexible hosing by a 'T' junction arrangement. A flexible pipe was used to transport the air from the plenum section to the orifice plate pipe entrance.

5.2.1.8 Orifice Plates and Pipes

The orifice plates were designed to measure the airflows which had passed through the test duct. The mass flow rates were scaled to represent those encountered in plate fin heat exchangers. Care was taken in the measuring of the orifice plate diameters and their circularity to meet the requirements of the British Standard, B.S. 1042.

The orifice plate pipes were thoroughly checked and corrected for leaks. Leaks were detected by filling the pipes with water and by holding the pipe vertical where the internal pressure at the lower end was great enough to detect the smallest of leaks. This process was repeated until no leaks remained.

The mass flow of air through the orifice plate was calculated by

the method of B.S. 1042 in a FORTRAN subroutine containing the standard iterative procedure solving both the discharge coefficient and the flow rate (see subroutine SMATHO in library AWSCD). The pressure difference between the "D and D/2" tappings was measured by a T.E.M. vertical water manometer which had a microscopic sight with a horizontal cross wire. The procedure for calculating the pressure difference across the manometer was adapted from B.S. 2520 the standard for atmospheric barometers. The construction of the T.E.M manometer was basically similar to a mercury barometer. The upstream static pressure difference relative to atmospheric, at the orifice plate was measured by an inclined Airflow Developments manometer.

5.2.1.9 Air Inlet Valve

This valve served two purposes. It was used to set the airflow through the duct, and to reduce the effort supplied by the rotary fan, by allowing ambient air to enter the system at this station. The placing of this valve after the orifice plate system had no effect on the measured air flow rate through the duct.

5.2.1.10 Rotary Fan

This fan provided the power required to drive the air through the orifice plate, the test section and connecting pipes.

5.2.1.11 Outlet Valve

A butterfly valve was sited at the exit from the fan to dampen out fluctuations in the flow by exerting a small back pressure.

5.2.2 Performance of the Air Tunnel

The requirement of the tunnel was to provide a heated airstream for the transient heat transfer measurements, and as far as possible to emulate a typical airflow upstream of an actual heat exchanger, to

enable the starting of the boundary layer at the leading edge of the fin. The scale chosen for the model size was four times full size. This was limited by the length of the vacuum forming machine, but gave excellent resolution in the heat transfer tests, and allowed the use of existing components in the rig.

The tunnel characteristics were thoroughly measured by several 84 point traverses covering velocity, turbulence intensity and temperature. The velocity and turbulence intensity profiles were measured by a hot wire anemometer and the air temperature was measured by a calibrated thermocouple.

The wire was calibrated at the same temperature as the flow it was used to measure the velocity of, for at least twelve data points. A regression equation, following the recommendations of Davies and Patrick was fitted to the data. This equation was then used as an interpolation function to calculate the velocity. The three parameters were mapped, using the NAG (Nottingham Algorithm Group) computer subroutines in conjunction with the GINO (Graphical INput and Output) FORTRAN library to produce contour graphs. The traverses were made at two temperatures, lab temperature and $50^{o}C$, the temperature traverse was made at the higher temperature only. The velocity and turbulence intensity contours at the laboratory temperature are presented in Figs. 5.3 and 5.4. The velocity, turbulence intensity and temperature contours taken with the tunnel providing a hot air stream are presented in Figs. 5.5 to 5.7 respectively. The boundary layers which formed on the upper and lower walls of the contraction section are clearly visible, but these did not interfere with the inlet air to the working duct due to their removal by the boundary layer bleed section. The boundary layers on the side walls are not so clear, but the

measurements indicate that they are relatively small. Other velocity and turbulence intensity maps were obtained at lower velocities, but these were not pertinent to the present investigation as explained below.

During the heat transfer and flow friction tests the tunnel air velocity was limited to the maximum velocity. The reason for this limitation was that the electric motor ran extremely hot at the lower air velocities (1. to 2. m/s). The heat transfer loss through the tunnel walls was such that the air inlet temperature to the expansion section had to be approximately $85^{\circ}C$ to get $50^{\circ}C$ at the exit. Due to conduction through metal supports connecting the fan with the motor, the motor temperature increased during the day to an unacceptable level. The use of high air velocity thus protected the motor windings.

The tunnel contraction exit air velocity during all tests was 5.3 m/s and exhibited a turbulence intensity of 2%. The air was drawn into the corrugated ducts at a different velocity to the tunnel velocity, and the excess air was forced away from the duct entrance in the boundary layer bleed section. However this condition gave a varying turbulence intensity to the air entering the duct, which was calculated as follows;

$$v' = Tu_{tun} \cdot v_{tun}$$

then the turbulence intensity at the channel inlet was calculated from;

$$Tu_i = v'/v_i$$

Values of turbulence intensities calculated at the entrance of the rippled and plain ducts are presented with the heat transfer results.

5.2.3 Performance of the Working Duct and Orifice Plates

A hot wire traverse was made across the exit of the working duct at various Reynolds numbers to measure the uniformity of the centreline velocity. The duct consisted of plain flat walls and the wall spacing was 0.0112 m. The hot wire position was within the exit channel formed by the metal supports and in line with the pressure tappings. This exit channel had a reduced flow area due to the metal supports holding the duct walls in place. For each flow, the centreline velocity was found to be uniform over a large proportion of the duct with an acceptable level of nonuniformity for the present tests. This traverse data is presented in Fig. 5.8 and shows the boundary layers which had grown from the exit of the contraction section, on the side walls of the working duct.

The calculated mass flow rates for each orifice plate were checked against a velocity traverse mass flow rate measurements taken in a circular pipe. Three traverses were performed for each orifice plate, but the smallest orifice plate was only used for very low Reynolds numbers of less than 1000. The pipe diameter was 18.9mm and the pitot probe was traversed across this pipe by a micrometer screw gauge arrangement. The velocity traverse was integrated to give the mass flow rates for the two halves of the pipe and the average taken for the comparison. As the flow was fully developed in the pipe there was little maldistribution. The results of this comparison are presented in Table 5.1. This independent comparison of the mass flow rates measured by the orifice plates shows that they could be used with a high degree of confidence.

71

5.3 Experimental Measurements and Data Reduction

5.3.1 Reynolds number and Flow Friction

The airflow through the duct was measured by the orifice plate at the start and end of every test. The Reynolds number was based on the mean mass flow rate and temperature of the two measurements. The duct width in the spanwise direction was 0.2 m and was used to calculate the area of flow.

Hence;

$$Re = \frac{\rho_a \cdot v_m \cdot Dh}{\mu_a}$$

where $Dh = 2.0 \cdot p_s$ and $v_m = \frac{m_a}{\rho_a \cdot (0.2 \cdot p_s)}$

The definition of the Reynolds number used to reduce the data for the flow visualisation measurements was as above, but the velocity was calculated as the mean velocity through several rippled duct channels.

Overall friction factor and local pressure drop measurements were made on the rippled ducts. Pressure tappings were mounted on the fins, with a spacing equal to the ripple pitch. The first tapping on the fin was 3mm from the front edge, which was 11mm from the leading edge of the duct for each fin. The fins were prepared in pairs, one fin had the pressure tapping mounted on the underside of the top fin in the duct while the other had the tappings on the top surface of the lower wall of the duct as shown in Plate 5.5.

Pressure differences were measured between the duct pressure tappings and the duct exit channel, by the Combist (Combustion Instruments manometer) or inclined Airflow Developments manometers. The inclined manometer was calibrated against the Combist and T.E.M. manometers. All three manometers can be seen in Plate 5.6. As the scale constant could be adjusted, a scale multiplier was evaluated

72

from the calibration. The local pressure tappings were sampled through two Norgren valves which had up to ten input channels, for both upper and lower rippled fins.

The pressure differences measured were corrected for a slight flow contraction, which occurred at the exit of the duct where the fins were held in place by metal supports, using the frictionless Bernouli equation as follows;

The two metal supports were each 1.5 mm thick and the exit velocity was;

$$v_o = \frac{\dot{m}_a}{\rho_a \cdot (0.2 \cdot (p_s - 0.003))}$$

hence the pressure correction was

$$p_{corr} = 0.5 \cdot \rho_a \cdot (v_o^2 - v_m^2)$$

The overall friction factor for a fin surface was calculated as an equivalent shear stress based on the measured pressure difference corrected as above between the duct inlet (first pressure tappings) and the support plates at the exit and the curvilinear surface area of the duct walls. There were two pressure tappings, one on each duct wall and the pressure difference was based on their average value. This pressure drop was corrected as above for the exit flow contraction and the friction factor was calculated as follows;

$$f = \frac{pd \cdot (p_s \cdot 0.2)}{2.0 \cdot L_{1f} \cdot 0.2} \cdot \frac{2.0}{\rho_a \cdot v_m^2}$$

The local pressure drop measurements were not reduced to friction factors, but were nondimensionalised as follows;

$$prco = \frac{2.0 \cdot pd}{\rho_a \cdot v_m^2}$$

A typical set of raw measurements are shown in Appendix 5.

FORTRAN program T1DFF was used to reduce the experimental friction data to nondimensional numbers.

5.3.2   Local Heat Transfer Measurements

The technique used to measure the local heat transfer coefficient was that of the transient thin skin technique. The local surface temperature, at a particular temperature and time, of the rippled fins forming the walls of a duct was measured by microencapsulated liquid crystals, type TCA 75A supplied by BDH Chemicals.

5.3.2.1   Calibration of the Thermocouples

The temperature was required at various stations in the rig to specify the boundary conditions to the test and thermocouples were used for these measurements. The thermocouples were calibrated against a Harwell calibrated platinum film resistor. The Harwell calibration used is given in Appendix 6. The calibrations were performed in an insulated and stirred water bath. The temperature was controlled by a simple thermostat which gave a variation in temperature of approximately 1.$^{\circ}$C. The temperature was held constant at a particular temperature by manually switching the heater on and off. An equation was fitted to the thermocouple output against the platinum film resistance thermometer output for each thermocouple. The platinum film resistance output was fitted against the Harwell temperature using a regression equation. The MINITAB program was used to calculate the regression constants.

5.3.2.2   Calibration of the Liquid Crystals

The liquid crystals were calibrated by measuring the temperature at which the crystals appeared green. This was performed by spraying the crystals onto a copper block which already had a thin coating of

74

matt black paint. A calibrated thermocouple was attached to the copper block to measure the temperature. The block was inserted into a low temperature oven and allowed to settle at approximately 41°C. The oven had an inner glass door through which the crystals were viewed without disturbing the air inside. The outer insulating door was opened periodically for viewing purposes. By varying the oven temperature very gradually the green temperature range could be closely observed. The calibration was performed before and after the series of transient tests to check for a variation in the green temperature with time. The two calibrated temperatures measured were 41.43 and 41.37°C. For the data reduction the mean of these temperatures 41.40°C was used.

5.3.2.3 Application of the Liquid Crystals to the Fin Models

The fins were sprayed with a thin layer of matt black paint using a small airbrush. The thickness of the paint was measured at random locations and found to be 0.005 inch. (0.00013m). This thickness was added to the thickness of the fin in the subsequent analysis. The paint used was made by Humbrol, who would not release the thermodynamic, transport or material properties of the paint. The paint was necessary to provide a contrast which enabled the colours to be viewed clearly, also the surface finish of the paint was microscopically rough which aided the mechanical bond between the paint and the liquid crystals sprayed on to the paint. The prepared fins used in the test series are shown in Plate 5.7. It should be noted that the liquid crystals were on the upper surface of both fins 1 and 2 and therefore internal to the rippled duct on fin 2, but external to the rippled duct on fin 1.

5.3.2.4 Test Procedure and Measurements Taken

The tunnel was turned on at 9 am, to allow for a six hour warm up period. This was consistent with the way the velocity and temperature profile measurements at the tunnel contraction exit were taken, to allow the tunnel walls to warm up and to stabilise the tunnel exit air

temperature.

The test section was set up with the required fin spacing, fin type and the required orifice plate was mounted in the pipe.

The atmospheric pressure was measured using a fortin barometer just prior to testing.

The required air mass flow rate was set within the duct and allowed to settle for approximately ten minutes. The air drawn through the duct was at the laboratory temperature.

The following measurements were made of the initial conditions prior to the insertion of the duct into the hot airstream;

1   The upstream pressure at the orifice plate and the pressure drop across the orifice plate were measured.

2   The temperatures were measured at the following points by calibrated thermocouples.

i   Tunnel centreline exit.

ii   Orifice plate.

iii Water manometer (T.E.M.)

iv   At four locations within the working section. These were placed, two on the underside of the upper perspex plate and two on the upper wall of the lower perspex plate. These were needed to calculate the air temperature difference required for the natural heat transfer coefficients on the rear of the rippled or plain duct walls.

v   The initial fin temperature. This was measured by resting a thermocouple on to the surface of the fin and waiting until a steady output was obtained.

The working section was then quickly inserted into the hot airstream. Two measurements were made and repeated during a transient

test, the time and the positions of the liquid crystal green appearance. These were both made photographically using a camera with a motor wind unit. The digital readout of the stopwatch was placed at an adjacent position to the fins in view by the camera. Typical photographs showing the transient progression are presented in Plate 5.8 and a set of measurements made for the flow and thermal conditions is given in Appendix 7.

The method of calculating the local heat transfer coefficients is described in Appendix 8 and the properties and constants used in the data reduction procedures are given in Appendix 9.

5.4 Rippled Duct Geometries Used in the Fluid Flow, Flow Friction and Heat Transfer Investigations

The fin profiles used in the investigation are shown in Fig. 5.9. Although there are slight differences in their shapes, profiles 1 and 4 were basically the same as respective fins A and B of Appendix 1. The geometry details for the ducts used in this investigation are given in Table 5.2 and for each type of measurement are described below;

5.4.1 Fluid Flow

Profiles 1, 2 and 3 were used in the flow visualisation experiments and six fin spacings covering the range, for full scale heat exchangers, of 280 to 727 fins/m (7.1 to 18.5 fins/inch). The fin spacing for an actual test was multiplied by the scale factor of four in keeping with geometric similarity.

5.4.2 Flow Friction and Heat Transfer

Four profiles (1 to 4) were used in the flow friction and heat transfer tests. Profile 4 which had a surface similar to heat exchanger fin surface B which had been shown to have a high

77

performance, see Appendix 1. Three fin spacings were used from 345 to 533 fins/m for full scale heat exchangers (8.8 to 13.5 fins/inch).

Local heat transfer measurements were made in the four rippled ducts at a smaller wall spacing representing 727 fins/m (18.5 fins/inch) which are described and reported in Chapter 7.

5.5 Experimental Results of the Rippled Duct Tests

Local and overall nondimensional numbers are presented for the flow friction and heat transfer in rippled ducts covering forty conditions of geometry and flow. The geometric variations were the four rippled fins and three wall spacings. The Reynolds numbers identifying the flows were 2000, 5000, and 8000, but at the smallest spacing (533 fins/m) an additional Reynolds number of 1600 was included. These parameter variations provided coverage of the range of interest and to a large extent the practicality of this type of heat exchanger in real systems.

5.5.1 Fluid Flow in Rippled Ducts

The flow visualisation study revealed highly complex flow phenomena to exist within the inlet region of a rippled duct. The Reynolds number ranged from 250 to 2500 approximately. The flow patterns were characterised and the results of this characterisation are presented in Table 5.3. Flows ranged between laminar and turbulent through various intermediate stages of separation and recirculation, secondary flow, vortex shedding and spiralling and transition to turbulent flow described in Table 5.3. At low Reynolds numbers the flows were laminar and with increasing flow rate unsteady effects developed. The positions of a particular flow pattern that occurred towards the end of a ripple pitch were found to move upstream at

78

higher Reynolds number and smaller interwall spacing. A definite change in the laminar flow pattern was noted for each profile as the wall spacing reduced in that three dimensional flow effects which were not seen at larger spacings, dominated the flows at closer spacings.

Unsteady vortex shedding flows were viewed and stored using a video camera and an Ariflex 16mm camera which was set at 24 frames/s. A selection of flows are presented in Plates 5.9 to 5.14, which were taken using the 16 mm camera. The photographic sequences are presented for the three profiles used, two wall spacings and one Reynolds number (1800 approx.). The sequences begin at the top left, proceeds downwards and then at the top of the next column to the right.

Plates 5.9 to 5.11 show the flows in rippled ducts formed by profiles 1,2 and 3 respectively at a wall spacing of 0.01055 m. All three flows were found to exhibit a similar flow behaviour for almost the same number of ripples downstream of the inlet. However it must be remembered that the ripple pitch in the flow direction is very different between profiles, see Fig. 5.9 and hence a particular ripple is a different length downstream for a different profile. The following points were noted regarding these three flows;

1   From the inlet the flow separates and forms separation zones in the initial ripple troughs. The shapes of these zones are determined by the ripple profiles.

2   In each case the flow becomes unsteady at the end of the second ripple (in the fourth trough).

3   Pronounced vortex shedding takes place at the end of the third ripple. For profiles 1, 2 and 3 these points were approximately 10, 13.5 and 5.5 cm downstream of the inlet, read from the scale.

4   Shortly after the vortex shedding, mixing takes place and the

79

transition to turbulent flow ensues dispersing the dyestreaks and making it impossible to distinguish local flow behaviour.

Plates 5.12 to 5.14 show flows in rippled ducts formed by profiles 1,2 and 3 respectively at a wall spacing of .00725 m. The three flows at this spacing are not as consistent as at the spacing of 0.01055 m and differences in flow patterns exist between rippled ducts, as listed below;

1   In the initial troughs of the ducts the separation zones seen earlier are now reduced in size for profiles 1 and 2, but profile 3 is slightly larger.

2   For profiles 1 and 3 the flow becomes unsteady at the end of the second ripple with vortex shedding from that position. Profile 2 also becomes slightly unsteady, but exhibits three dimensionality. The unsteady nature of the flow for profile 2 contains a mixture of both spanwise and secondary flow vortices.

5.5.1.1   Comparison of the Fluid Flow Results with Previously Reported Experimental Data

Nishimura, Kajimoto, Tarumoto and Kawamura (1986), presented fully developed flow visualisation results which are compared with the present results in this section. Their corrugated duct was composed of sinusoidal wavy plates having the following geometry specification, RI=0.25 and RH=0.464 in comparison with RI=0.222 and RH=0.445 for profile 3 which was formed from circular arcs. The data for both investigations was acquired at discrete Reynolds numbers, but the Reynolds numbers at which changes in the flows occurred were not recorded. At a Reynolds numbers of 480 for Nishimura and 472 of the present, both data sets show a laminar steady recirculation region in

80

a trough. At a Reynolds number of 700 Nishimura's data shows an unstable recirculation region, this unsteady motion was seen to exist at a Reynolds number of 635 for profile 3. The change in the flow pattern from laminar steady flow to the unsteady motion was reported by Nishimura, Kajimoto and Kawamura (1986) to be also 700. Nishimura et al. presents two other flow visualisation photographs at Reynolds numbers of 1120 and 2460 and the results of these tests are also consistent with the present measurements. Nishimura et al. by the use of the hydrogen bubble technique investigated the effect of three dimensionality in the flow, by taking photographs at another angle, and found at transitional and turbulent Reynolds numbers that very small longitudinal vortex structures were present near the separation and reattachment points. Three dimensional effects of this nature could not be easily determined by the present experimental technique using thin dye streaklines.

Nishimura, Yoshino and Kawamura (1987) demonstrated through flow visualisation photographs the occurrence of streamwise vortices in narrow wavy channels, RH=0.143 and RI=0.25. The wall spacing is lower than the closest wall spacing used for profile 3 (RH=0.207) which had the nearest RI for comparison, RI=0.222. However the Reynolds number at which streamwise vortices were seen was 320, in comparison with 300 (approximately) for profile 3. The unsteady spiralling motions were seen to exit in the channel of Nishimura and for the present work with profile 3 at Reynolds numbers of 500 and 418 respectively.

5.5.2 Flow Friction in Rippled Ducts

The overall friction factors are presented with the overall j factors, see section 5.5.3.3.1, the data reduction procedure for the overall and the local measurements was given in section 5.3.1.

The nondimensional wall surface pressures were plotted against the axial coordinates (not curvilinear lengths) of the fin from the leading edge of the duct. The surface pressures recorded were the local flow static pressures acting adjacent to the wall mounted pressure tappings. These measurements will be compared against the equivalent local pressures numerically modelled using the PHOENICS program in Chapter 6. The results are plotted in two parts representing the two walls of the duct, the underside of the upper wall termed 1, and the top surface of the lower wall termed 2, see Fig. 5.10. Local flow friction results are presented in Figs. 5.11 to 5.22 for profiles 1 to 4 and three wall spacings. Observations regarding the local flow friction results are reported below;

1   In all cases the wall pressure at fin 1 is lower than fin 2 which is due to the fact that the fin 1 tappings are at the top of the peaks and fin 2 tappings are at the bottom of the troughs. For the inlet flows the trough tappings are in recirculation regions and generally the flow is moving quickly and attached at the peak tappings. At positions which were seen to be in the transitional and turbulent flow regime also show this difference and is indicative of lower fluid velocities in the troughs.

2   The pressure readings show steeper gradients in the region of the duct inlet where shear layers form and the mainstream flow accelerates to compensate.

3   At some distance down a rippled duct the wall readings show a linear decrease in pressure with ripple pitch. From this point the flow has reached the fully developed region. This observation is less pronounced for profile 2 which only had 5 ripples, but can clearly be

seen in the results of profiles 1, 3 and 4.

4   Profile 3 has the highest pressure drops and profile 2 the lowest. The flow friction in a rippled duct is composed of both skin friction and form drag. The form drag component will increase with the number of ripples in the duct, profiles 3 and 2 have the highest and lowest numbers of ripples respectively indicating that the form drag constitutes a significant proportion of the pressure drop.

5   The pressure gradient changes direction at the duct exit where some flow redevelopment takes place in order to enter the flow channel leading to the plenum chamber, formed by the metal fin supports.

Further comments relating to these flow friction results can be found in section 5.5.3.3.1.

5.5.2.1 <u>Comparison of the Flow Friction Measurements with Previously Reported Data</u>

There is very little published data regarding the local pressures measured on the walls of rippled/corrugated ducts. The following comparisons are made with the available data from similar geometries in order to place the present measurements in perspective with the previously reported data through the use of nondimensional numbers. Large differences between data sets may indicate that the choice of nondimensional numbers to represent the flow was incorrectly made, but this is unlikely for the present duct flows. For example, it is known from the flow visualisation study that vortex shedding phenomena plays a considerable part in the generation of turbulence in the inlet region of ripple duct geometries and therefore the Strouhol number may be of high significance in the nondimensional representation of such flows.

Nishimura, Kajimoto and Kawamura (1986) presented friction factor

83

data for the periodically fully developed region which is compared with the friction factor calculated for the pressure gradient at a ripple near the exit of the duct formed using the profile 3 walls. The pressure tappings of Nishimura et al. were placed at the lowest point of the troughs on one wall of the sinusoidal duct. Differences in geometry between Nishimura et al. and the present geometry were RI=0.25 and RH=0.464 against RI=0.222 and RH=0.473. The data of Nishimura et al. shows a near constant friction factor of 0.132 at Reynolds numbers between 2000 and 1.0×10^4 (Re_H=1000–5000). He presented a friction factor based on the following equation;

$$f = \frac{2 \cdot \Delta p}{\rho \, v_m^2} \cdot \frac{H}{4 \cdot L}$$

For comparison purposes their friction factor was multiplied by the factor L/L_{1f} to base the friction factor on the curvilinear length on one ripple. The friction factor was calculated to be 0.116. In comparison the friction factors for ripple profile 3 were calculated to be 0.0913, 0.0999 and 0.0955 for the Reynolds numbers 2021, 4950 and 7897 respectively using the same equation. The increased ripple amplitude and slightly closer wall spacing of Nishimura et al. brought about an increase in the friction factor.

O'Brien (1981), presented local pressure drop data for a flat sided corrugated duct in the developing inlet region. The data was used to indicate the periodically fully developed condition on which the friction factor was based at Reynolds numbers of 2155, 5450, 15820 and 24880. The pressure tappings were located at the mid points of the flat corrugations in comparison with the peaks and troughs of the present measurements. This data represents the only available

84

information regarding local pressure drops in corrugated ducts, but because of the differences in geometry and the positioning of the pressure tappings, no numerical comparison is made.

5.5.3 Heat Transfer in Plain and Rippled Ducts

The transient heat transfer test technique was used to measure the local heat transfer coefficient and through a numerical trapezoidal integration procedure the overall j factor. The thermal boundary conditions which were formed by the limiting temperatures to the transience are given in Table 5.4, for both plain and rippled wall ducts. These temperatures consist of, the initial fin wall temperature, hot tunnel exit temperature and the temperature difference ratio;

$$\frac{(T_j - T_i)}{(T_{tun} - T_i)}$$

This temperature difference ratio varied between 0.599 and 0.689 for all of the heat transfer tests.

5.5.3.1 Plain Fin Test Results

The plain fins used were made from sheet perspex approximately 2mm thick. Six tests were performed covering the Reynolds number range of 2000 to 8000. These tests were treated in the same manner as the rippled fin tests. The Results are presented graphically in Figs. 5.23 to 5.28, as the local Nusselt number Nu_{Dh} (see section 5.5.3.3.1) against position from the leading edge. These results show high Nusselt numbers near the leading edge decreasing with distance down the duct.

5.5.3.2 Comparison of Plain Fin Test Results with Circular Tube Regression Equations and Experimental Data for Flat Plates and Ducts

The local data was compared against equations representing the

local heat transfer coefficient as a Nusselt number for both thermally and hydrodynamically developing flow conditions. The comparison was performed by calculating a ratio of the measured local Nusselt number to the calculated Nusselt number, given similarity of geometry and dynamic similarity of the flow conditions. The terms which modify the coefficient to take account of variable fluid properties that occur when heat is transferred across large temperature gradients were not included. In many of the equations below, the diameter was substituted by the hydraulic diameter in keeping with dimensional analysis. The equations used were as follows;

1   The Pohlhausen laminar boundary layer solution (Simonson, 1984).

$$Nu_x = 0.332 \cdot Re_x^{0.5} \cdot Pr^{1/3}$$

2   Laminar flow in the entrance region of a circular tube, Kern and Kraus (1972). This equation was modified to represent the local heat transfer coefficient. Previously it had been used to calculate the mean heat transfer coefficient between the inlet coordinates of 0.0 and x.

$$Nu_x = 1.86 \cdot Re_D^{1/3} \cdot Pr^{1/3} \cdot (D/x)^{1/3} \cdot (1 - (1/3))$$

3   For transitional flow in the entrance region of a circular tube, From Kern and Kraus, (1972), based on the work of Hausen the equation is;

$$Nu_x = 0.116 \, (Re_D^{2/3} - 125.0) \, Pr^{1/3} \left(1 + \left| \frac{1}{3} \cdot \left(\frac{D}{x}\right)^{2/3} \right| \right)$$

4   Colburn equation for a circular tube modified for the inlet length variation, Sucec (1985), McAdams (1954), and should strictly be used above a Reynolds number of 1.0×10^4 as follows;

$$Nu_x = 0.023 \cdot Re_D^{0.8} \cdot Pr^{1/3} \cdot (1 + (D/x)^{0.7})$$

5   The E.S.D.U. (1968), equation for turbulent circular tube flow was derived from experimental measurements. The equation for fully developed flow was modified for a sharp leading edge entry and constant wall temperature boundary condition.

$$\zeta = -3.796 - (0.205 \, . \, \log_e(Re_D)) - (0.505 \, . \, \log_e(Pr))$$

$$Nu_x = Re_D \, . \, Pr \, . \, \exp(\zeta) \, . \, (1.124 + (3.93 \, . \, \exp(-x/D)))$$

6   Gnielinski, (1983), modified an equation developed by Petukov and Popov which related to fully developed flow, to account for the entry length variation in the heat transfer coefficient.

$$f = (1.82 \, . \, \log_{10}(Re_D) - 1.64)^{-2}$$

$$Nu_x = \frac{(f/8) \, . \, (Re_D - 1000) \, . \, Pr}{1 + (12.7 \, . \, (f/8)^{0.5} \, . \, (Pr^{2/3} - 1))} \, . \, (1 + (D/x)^{2/3})$$

7   Sugawara, Sato, Komatsu, and Osaka, (1953, 1988), investigated the effect of turbulence intensity on the local heat transfer coefficient on flat plates. The regression equation was generated from transient thermal test results.   The fluid used for the tests was air and therefore no Prandtl number relationship was needed.   The regression equation for zero leading edge turbulence was;

$$Nu_x = 0.425 \, . \, Re_x^{0.5}$$

8   The regression equation of Sukomel, Velichko, Abrosimov and Gutsev, (1975), generated from heat transfer tests on flat rectangular ducts.   The fluid used for the their tests was also air. Over the Reynolds numbers of interest their equation was;

$$Nu_x = 0.209 \, . \, Re_x^{0.58}$$

Graphs of the above comparison ratios for equations 1 to 8 are presented in Figs. 5.29 to 5.36 respectively. A scale value of 1.0 would mean equal heat transfer coefficients between the compared Nusselt numbers. These comparisons show that the measured heat

transfer coefficients are generally higher at the leading edge and lower near the duct exit than the previously reported data. As the inlet flow exhibits a considerable degree of turbulence, the comparisons against heat transfer in laminar flows (comparisons 1 and 2) are questionable. The transitional and turbulent flow heat transfer comparisons show a high degree of scatter in the plotted ratios, but following the similar trends as the laminar cases. However for comparisons 3, 5, 6 and 7 a large quantity of measurement data lies in the region of a ratio value of 1.0 giving confidence in the measurement technique. These results are further discussed in section 7.3.

5.5.3.3 Rippled Fin Heat Transfer Test Results

5.5.3.3.1 Local Heat Transfer

The results are given in two parts representing the two walls of the duct, as was the case with the flow friction surface pressures, the underside of the upper wall termed 1, and the top surface of the lower wall termed 2, see Fig. 5.10. The local heat transfer coefficient was calculated in terms of a Nusselt number as follows;

$$ Nu_{Dh} = \frac{h_s \cdot Dh}{k_a} \qquad \text{where} \qquad Dh = 2.0 \cdot P_s $$

Graphs of the local Nusselt numbers plotted against the curvilinear length of fin from the leading edge of the duct are presented in Figs. 5.37 to 5.76 for the two fin walls. These figures present new knowledge relating to the heat transfer in developing flows of rippled ducts and the pertinent points are listed below;

1   The coefficients fluctuate with the ripple pitch and are high at ripple peaks and low in the troughs.

2   The inlet flow development from the leading edge of the fin is shown in many figures showing an initially high coefficient decreasing towards the first ripple. This effect is most pronounced for profile 2 which had a longer flat section before the first ripple.

3   The fluctuating coefficients tend to increase down the duct as flow develops to transition, but falls away towards the duct exit. The increase is due to the transitional flow behaviour, but the decrease further downstream may be due to transient effects in the temperature of the hot air.

4   In some plots, eg. Fig. 5.56, fin 1 has slightly lower Nusselt numbers than fin 2, which may be due to radiation effects being neglected from the data reduction procedure or incorrect natural heat transfer coefficients assumed for the non duct surfaces of the rippled duct walls.

5   Profiles 1 and 4 at all fin spacings produce asymmetrical ducts and definite signs of this are seen in the heat transfer coefficient distributions between fins 1 and 2.

Further discussion relating the fluid flows to the local heat transfer coefficients is given in section 7.4.3.

5.5.3.3.2 <u>Overall Heat Transfer j Factor Calculation from Local Measurements</u>

The overall j factor for each duct was calculated by integrating the local heat transfer coefficient (local Nusselt number) with respect to the curvilinear surface area. The integration was done numerically using trapezoidal elements by program TlDAVE. The j factor was calculated from the mean Nusselt number as follows;

$$j = St . Pr^{2/3} = \left(\frac{Nu_m}{Re . Pr}\right) . Pr^{2/3}$$

5.5.3.3 Presentation of the Mean Characteristics

Linear interpolation or extrapolation of the heat transfer and flow friction data was performed to obtain results between tests at the same Reynolds numbers. The processed results of the Reynolds number, friction factor and j factor are given in Table 5.5. The nondimensional numbers are also presented graphically against the Reynolds numbers for each wall spacing, the friction factor in Figs. 5.77 to 5.79, and the j factor in Figs. 5.80-5.82.

The friction factors generally decrease with increasing Reynolds number and decrease with decreasing wall spacing. For a particular Reynolds number, the fluid velocity in the smaller wall spacing case is higher affecting the comparison.

At the wall spacing of 7.1 mm there is a definite increase in the friction factor for all ripple profiles between the Reynolds numbers of 1600 and 2000. The flow visualisation results show earlier transition to turbulence at the higher Reynolds number and hence increased friction.

The j factors show similar trends to the friction factors, in that they generally decrease with increasing Reynolds number and decrease with decreasing wall spacing. Profile 3 at the three wall spacings has the highest j factors and profiles 2 and 4 have the lowest. At the lower Reynolds number of 1600 for the wall spacing of 7.1 mm the j factor does not seem as sensitive to the Reynolds number as the friction factor. Apart from profile 2, which shows a slight drop in the j factor at the Reynolds number of 1600, compared with 2000 the other profiles have higher j factors at the lower Reynolds number.

5.5.3.4 Comparison of the Local Heat Transfer Coefficient with Previously Reported Data

The local mass transfer coefficient was measured by Nishimura, Kajimoto, Tarumoto and Kawamura (1986) for a similar geometry to profile 3 at the fin spacing of .0112 m. Nishimura used a sine wave profile and limited the measurements locally to one wave cycle at the sixth wave downstream, whereas the present measurements encompassed many ripple pitches from the inlet. The data was reported in the form of the local Sherwood number at Reynolds numbers of 7094, 3210 and 586 (3547, 1605 and 293 using the wall spacing as the hydraulic diameter reported). By the analogy between heat and mass transfer the measured Nusselt number in the present work was compared with the mass transfer Sherwood number.

5.5.3.4.1 Geometry Comparison

1   Nishimura et al. used a sine wave profile compared with profile 3 which was composed of circular arcs, see Fig. 5.9.

2   The nondimensional wall spacings RH were 0.464 and 0.473 for the geometries of Nishimura and profile 3 respectively. The dimensional wall spacings were 13. mm for Nishimura and 11.2 mm for profile 3.

3 The nondimensional double ripple (wave) amplitudes were RI=0.250 for Nishimura and 0.222 for profile 3.

5.5.3.4.2 Heat/Mass Transfer Coefficient Comparisons

1   The Schmidt number for the liquid used by Nishimura was 1570 compared with a Prandtl number of 0.7 for gaseous air used for profile 3.

2   The measurement technique used by Nishimura was the diffusion limited electrochemical method compared with the transient heat transfer method used for profile 3.

3   The local transfer coefficients are plotted as $Sh/Sc^{1/3}$ or $Nu/Pr^{1/3}$ in Fig. 5.83 with the Reynolds number as parameter, against the nondimensional projected coordinate position x/L (x is not the curvilinear length along the wave). Qualitively the shape of the curves of the coefficients against position are similar. From the wave peak (x/L = 0) the coefficients decrease to x/L between 0.2 to 0.3 Then rise to a maximum at x/L between 0.7 to 0.9 and then fall back to near the starting value at x/L = 1.0. One difference to note is the inflection in the curve of the transfer coefficient of Nishimura at a x/L value of 0.4 for all Reynolds numbers 586, 3210 and 7094, which is not present in the curves of profile 3.

4   The transfer coefficients of Nishimura for a lower Reynolds number (3210 and 7094) are higher for the sine wave than for profile 3 (4993 and 8004).

To enable the effect of the Reynolds number to be eliminated from the comparison the y axis of Fig. 5.83 was divided by the Reynolds number to the power of 0.61 and the data was replotted in Fig. 5.84. For data which fits an equation of the form;

$$Nu = A \cdot Re^n \cdot Pr^{1/3}$$

plotting $Nu/(Re^n \cdot Pr^{1/3})$ will indicate the constant A. The power of n, of 0.61 was obtained from Fig.3 of Nishimura, Kajimoto, Tarumoto and Kawamura (1986) where the cycle averaged Sherwood number divided by $Sc^{1/3}$ was plotted against the Reynolds number. The local fluid flow may vary with the Reynolds number and affect the local transfer coefficient in a nonlinear way eg. by flow separation and recirculation, without affecting the cycle averaged value significantly. Therefore Fig. 5.84 must be viewed in qualitative

terms.

For Reynolds numbers greater than 3000. the power 0.61 in the nondimensional equation has generally linearized the data although there is a considerable difference in the value of A between the two data sets. The largest difference occurs at a $x/L=0.8$ where A for the present data has a value approaching 0.6, whereas Nishimura et al. data shows a value of approximately 0.85, but this difference may be caused by the fluids having considerable differences in Prandtl number.

5.6 Experimental Uncertainty Analysis

The Monte Carlo Simulation method was used to determine the certainty intervals of the Reynolds number and the friction factor. The procedure coded into the data reduction program T1DFFSA was exactly the same as that given in section 3.6. The experimental tolerances for each measured variable are given in Table 5.6. Graphs of the 95 percent certainty interval estimates are given for the friction factor and the Reynolds number in Figs. 5.85 and 5.86 respectively indicating that the measurements and instrumentation were of a high standard.

It was not feasible to use the method for the local heat transfer coefficient, because the data reduction procedure required a large quantity of computational effort and for a distribution size of 1000 points, even for one test would have been excessive on the quickest machine at Coventry Polytechnic (Sequent Balance 22000 system h, 1988).

5.7 Comparative Performance of Rippled Fin Heat Exchangers

The comparison of heat exchanger performance based upon the experimental data of the transient heat transfer and flow friction test measurements of the four profiles at the three fin spacings is

described below. The j factor, friction factor and Reynolds number data for the twelve geometric configurations were applied to plate fin and tube heat exchanger banks with inline thin rectangular tubes.

5.7.1 Heat Exchanger Comparisons Performed

The four comparative methods recommended by Shah (1978) were applied to the heat exchangers in a similar manner to Appendix 1. The friction factor was based on measured pressure drops within the duct only and entrance and exit loss coefficients were required for the full pressure drop. The pressure drop was calculated using the equation of Kays and London 2-26a with the entrance and exit loss coefficients from the multiple square duct inlet and exit graph, Kays (1950). The comparison methods used were as follows;

1   j/f ratio against Reynolds number.

2   The standardised heat transfer coefficient against the pumping power per unit surface area.

3   The standardised heat transfer per unit volume against the pumping power per unit volume.

4   The heat transfer rate against the fan power required, method of Bergles, Junkhan and Bunn (1975). With this method a performance ratio was also calculated using the Kays and London plain fin heat exchanger as the reference surface.

5.7.1.1 Geometric Configuration of the Rippled Duct Heat Exchangers

Rippled fin heat exchangers which used geometrically similar ducts to the rippled ducts tested were sized at 1. m by 1. m. The four profiles and the three fin pitches used earlier gave twelve heat exchangers for comparison. The geometric parameters which were common to all heat exchangers are presented in Table 5.7 and the details

94

particular to each heat exchanger are given in Table 5.8. The heat transfer surface area of an exchanger increases with a decrease in the interwall fin spacing for a constant frontal area.

5.7.1.2   Flow Conditions used in the Bergles, Junkhan and Bunn Comparison

A water mass flow rate of 5.468 kg/s, typical for a 1m by 1m sized heat exchanger of three tube rows was used for each unit. The water inlet temperature was set at 80.0^{o}C. The air inlet temperature was 20.0^{o}C and having a relative humidity of 45 percent.

5.7.2   Heat Exchanger Comparison Results

From the work carried out by Maltson, Wilcock and Davenport, (1989) the most accurate comparative method was the criteria of Bergles, Junkhan and Bunn. The j/f ratio against Reynolds number was found to be unreliable and the standardised heat transfer against standardised pumping power methods do not consider the realities of the system in which the heat exchangers are placed. However the graphs of all the evaluation methods above were produced for completeness in Figs. 5.87 to 5.91. Due to the significant differences in the experimental methods used in obtaining performance data between the Kays and London plain fin and the rippled ducts, the relative performance between the plain fin and the rippled ducts must be viewed with caution.

The results of the Bergles performance comparison and the performance ratio graphs, show that Profile 4 has the highest performance over the fan power and fin pitch ranges, although at the low fan powers, the performance of profile 4 is generally low. Profile 3, although having a low performance at the 348 fin s/m pitch has a high performance at 540 fins/m. There is very little difference in

95

performance between profile 1 and profile 4 at the 540 fins/m pitch.

In a situation where the fan power (efficiency) was not as important as the size or weight of an exchanger, profile 3 at all three fin pitches has the highest j factors, see section 5.5.3.3.3 and hence heat transfer coefficients. Therefore for a particular heat transfer rate, profile 3 would produce the heat exchanger of minimum size and weight, but would need a higher fan power to do it.

CHAPTER 6

NUMERICAL INVESTIGATION INTO THE FLUID FLOW, FLOW FRICTION AND HEAT TRANSFER OF VARIOUS RIPPLED DUCT GEOMETRIES

A numerical investigation was carried out using the commercially available PHOENICS program to model the heat transfer, fluid flow and flow friction characteristics of rippled ducts. Attention was focussed on the inlet region flow which is representative of plate fin heat exchangers about which very little was known for rippled ducts. This investigation centered around the comparative effect of a variation in the ripple shape upon the performance of a duct. The results of the numerical models are presented and the fluid flow and flow friction characteristics are compared with experimental data where possible. Additional turbulent flow runs using optional features of the PHOENICS code are also presented.

The PHOENICS program is a general purpose program which solves heat transfer, mass transfer combined with fluid flow problems. The local fluid flow vectors were calculated by a Navier-Stokes finite difference / finite volume semi-implicit solver. The program permitted the solution of parabolic, hyperbolic and elliptic types of mathematical equations, but only elliptic type flows were pertinent to the present investigation. An elliptic flow is one in which downstream characteristics affect the flow upstream, as in the case of a recirculation zone. Laminar and turbulent flows were both investigated.

The version of the code used was PHOENICS 81 without the available body fitted coordinate coding. The program was written in FORTRAN and was implemented on the Harris computer system "C" at Coventry Polytechnic. The subroutine library containing the EARTH

modules was compiled with the double precision option available in the Harris FORTRAN77 compiler.

6.1 Laminar Flow Models

Four laminar flow solutions were generated to investigate the effect of wall profile shape on the comparative performance of the duct, while a fifth solution investigated the effect of inlet and exit free flow sections to the duct. These five cases were described by Maltson and Wilcock (1987), see Appendix 11. Additional information regarding the work and a description of the application of the boundary conditions within the numerical models are given below.

6.1.1   Geometries

The rippled duct geometries used represented curved fins, but this was only possible using a fine cartesian grid and small steps in the wall surface composed of rectangular cells. The four rippled wall profiles are shown in Fig. 6.1 and are different to the profiles used in Chapter 5. Fig. 6.1 profiles 1 and 2 are of a similar form to Appendix 1 fins A and B respectively. The geometries given in Fig. 6.1 also show the flow domains at the wall spacing of 11.2 mm. The FORTRAN coding used to generate these wall surfaces is given in Appendix 11, in programs SATELLITE 1 and 2. The solution domain was divided into a mesh of 60 by 230 cells, (60 in the cross stream X direction and 230 in the streamwise flow direction Z. Four X cells formed the fin wall and 56 X cells within the fluid. The fifth case had 242 cells in the flow direction, 6 cells upstream and downstream to allow the fluid to find it's own way into and out of the duct. This affected the flow by forcing the fluid to stagnate at the leading blunt edge and to shear at the exit allowing a small wake to develop.

The cell dimensions were 0.20 mm in the cross stream X direction and 1.0 mm in the Z direction. The length of a cell in the Y direction was set to a large value for numerical reasons, but the flows modelled were two dimensional.

The four ducts comprised 6 cells forming a flat plate inlet section which preceded the rippled section. In all cases there were seven ripples each of 31 Z cells which occupied Z cells 7 to 224. 6 Z cells created a flat wall exit channel. These flat inlet and exit channels were included to represent a typical plate fin which is normally "hemmed" at it's edges to provide rigidity to the thin metal. The geometry of the fifth case was exactly the same as profile 1, but had the additional 12 Z cells which contained only fluid, no blocked cells representing the fin walls.

Use was made of the XCYCLE=.TRUE. boundary condition. This condition permitted flow to leave or enter the solution domain through the outside face of the last X cell. This flow was then forced to enter or leave, respectively the solution domain through the outside face of the first X cell at the same Z slab. This condition was permitted at all Z slabs. By specifying the grid in this manner the cells underneath a peak in the lower wall and over a peak in the upper wall were then available to carry the flow.

The present grids were chosen based upon the maximum executable program size which the Harris computer could process, bearing in mind the number of variables solved. Over one ripple pitch the PHOENICS grid density was 60 X cells by 31 Z cells, other recent investigations of this type had grid sizes of 30 by 22 used by Amano (1987), 16 by 52 used by Xin and Tao (1988) and 18 by 34 used by Asako, Nakamura and Faghri (1988). Many of these workers were only interested in the

periodically fully developed region and modelled one pitch having cyclic inlet and outlet boundary conditions.

6.1.2   Boundary Conditions

The flow was specified at the inlet plane to the flow domain as having a uniform velocity profile. For the fifth case a reduction in the inlet velocity was calculated to allow for the flow contraction of the four fin wall blocked cells on entering and leaving that duct, to keep the duct Reynolds number constant.

The uniform static pressure datum was put on the exit plane. The position of this pressure condition was forced to occur in this case on a plane other than the inlet plane where the flow condition was allocated.

The heat transfer boundary condition was specified using fluid enthalpies for the working fluid at the inlet and the fluid at the wall surface to provide a temperature (enthalpy) difference. The fluid was incompressible and the temperature was linearly related to the enthalpy. The laminar wall function for the enthalpy was not used as this was calculated from the Reynolds Analogy, which is more useful for shear flows, whereas the present flows had recirculation and pressure (form) drag. The grid distribution across the duct was very fine, 56 cells in the flow and the enthalpy in an adjacent horizontal surface wall cell was specified to have the wall enthalpy. Flow friction at the wall was provided for by a using laminar wall function. This was applied to the horizontal faces, but not the vertical surfaces. However the flow in the horizontal flow direction was brought to rest at a vertical face of the fin wall which was blocked. The application of these boundary conditions on the stepped

100

wall are shown in fig. 6.2a.

The above boundary conditions were programmed as FORTRAN statements in the SATELLITE program. During execution of the SATELLITE program, all the information specifying the model, (geometry, cell porosities, boundary conditions, solution control parameters etc.) was transferred to data files which were subsequently read by the EARTH modules when the program GROUND was executed. Due to limitations of the PHOENICS 81 version the boundary conditions could only be applied to the wall surface over one Z slab. Consequently these boundary conditions had to be moved for each Z slab within the EARTH modules by FORTRAN instructions in the GROUND program which called EARTH subroutines. The lines of FORTRAN coding programmed into the SATELLITE and GROUND programs was included in the conference proceedings, see Appendix 11.

6.1.3   Flow Conditions and Fluid Properties

The flow was specified to be incompressible and temperature independent, having a density of 998. kg/m3 and dynamic viscosity of 0.0010422 kg/m s. The Prandtl number was 6.09 for the four cases and 0.707 for the one case which was used for the comparison with measured data. A summary of information regarding the geometries and flows, both laminar and turbulent modelled is given in Table 6.1.

6.1.4   Data Reduction Procedure

The mean inlet pressure and the bulk mean exit enthalpy were found by numerical integration from their local values. The pressure was area weighted and the enthalpy was area and mass flux weighted during the integration procedure to find the bulk mean values on the planes. Program GRPAB was written to perform the integration as a "post PHOENICS process". The friction factor was calculated from the

pressure difference (bulk mean inlet − set exit datum plane value) using the following equation;

$$f = \frac{2 \cdot (p_{i,m} - 0.0)}{\rho \cdot v_m^2} \cdot \frac{A_c}{A_{ht}}$$

The area A_c was based on a duct width of 1.0 m and the area A_{ht} was the area of the horizontal faces of the walls, equivalent to both sides of a flat plate. Maltson and Wilcock (1987), (Appendix 11) used a different data reduction procedure in that an equivalent curvilinear length of fin formed the basis of the heat transfer surface area, but this was an artificial area to represent the surface.

The j factor was calculated from the heat transfer rate and the log mean temperature difference, although the log mean temperature difference is not strictly correct it is sufficiently accurate for this situation in which the data is used comparatively. The reason for this lack of accuracy is due to the fact that the bulk temperature of the fluid as it proceeds from the inlet to the exit of the duct does not follow the logarithmic curve. A logarithmic profile is obtained only if the heat transfer coefficient is a constant all the way down a plain walled duct. In the case of a developing flow with the effects of separation, recirculation and turbulence generation and dissipation the heat transfer coefficient continuously varies from inlet to exit and the temperature does not follow the logarithmic profile. As the wall temperature was specified as constant, the log mean temperature difference equation was the same for both counter or parallel flow definitions and the j factor was calculated from the following sequence of equations;

The heat transfer rate Q

$$Q = \rho \cdot A_c \cdot v_i \cdot (H_o - H_i)$$

The heat transfer coefficient was evaluated;

$$h = \frac{Q}{A_{ht} \cdot T_{LMTD}}$$

and the j factor from;

$$j = \frac{h}{\rho \cdot v_m \cdot cp} \cdot Pr^{2/3}$$

6.1.5 Laminar Flow Results

The laminar flow data was reworked with the above data reduction procedure (see section 6.1.4) and the results are presented in dimensional and nondimensional forms in Tables 6.2 and 6.3 respectively. The different data reduction procedure would not affect the comparison of the profile 1 solution (case 5) with experimental dimensional pressure drop data or the relative comparison of the performance of the four profiles which were reported in Appendix 11.

Velocity vector plots of the whole flow domain for the geometries investigated and the Reynolds number of 536 are presented in Figs. 6.M.1 to 6.M.5. In these figures, the blocked cells to represent the duct walls were drawn as rectangles and the plot was repeated in the X direction to see the effect of the cyclic boundary condition within the flow. The velocity vector scale in Figs. 6.M.1 to 6.M.4 is, a velocity vector of an absolute length (in the vector direction) of one cell length in the flow direction Z is equivalent to a velocity of 0.050 m/s. For Fig. 6.M.5, although the flow represented the same Reynolds number of 536, was generated using air properties and had a different velocity. Based on the cell length as before the vector length is equivalent to 1.0 m/s.

These figures show the development of the flow from the inlet boundary to a near fully developed flow condition. Similar trends were noted in each duct as follows;

1   There was very little or no flow separation in the first trough to the duct.

2   A definite small flow separation region was found in the second trough to the duct in all geometries.

3   Larger flow separation and recirculation regions exist in subsequent troughs in all of the geometries.

6.1.6   Comparison with Previously Reported Data and the Experimental Results of the Present Investigation

The flow vectors for the one laminar case which used air fluid properties agreed very closely with the flow visualised streaklines at a Reynolds number of 536. This comparison was fully described in Appendix 11, and the conclusion was that the program was accurately modelling what was happening to the flow in a rippled duct of similar geometry.

The pressure drop for this case was closely predicted, but friction factors based on total surface area did not agree. The surface area of the stepped wall was considerably greater than that of a smooth curved wall and as a result the friction factor for the prediction was lower. This problem would not have arisen if the Body Fitted Coordinate option had been available.

The averaged local heat transfer coefficient was compared with the PHOENICS prediction in Appendix 11, but at the time the measurement technique was under development and some areas of the duct were absent from the test. The problem of the surface area used to

104

base the data reduction procedures on as with the flow friction results was also present in the heat transfer comparison.

6.2 Turbulent Flow Models

The computer program incorporated two turbulence models, the two equation turbulent kinetic energy and dissipation rate model (KE-EP) and the constant turbulent "eddy" viscosity model. Both models used wall functions to calculate the shear stress at the wall surface based on an empirical laminar sublayer thickness relationship evaluated in the wall adjacent cell.

The turbulent flows modelled were representative of the upper flow velocity range of a typical heat exchanger unit. The reason for modelling this range was that at the lower Reynolds numbers of 2000 to 2500, the flows were visualised to be highly unsteady and exhibited vortex shedding type phenomena. The turbulence models available would not be able to simulate these effects in sufficient detail and higher Reynolds numbers were used where the program would reasonably be expected to model the time mean flow. A comparative investigation used the two equation model of turbulence, the KE - EP model, but a few additional runs were performed two of which used the zero equation uniform turbulent viscosity model for comparison.

6.2.1   Geometries Investigated

6.2.1.1   Comparative investigation

Four ripple shapes were used in the turbulent flow comparative investigation, these were the same as those used in the laminar flow comparative modelling work, see section 6.1.1 and Fig 6.1. The nondimensional fin spacing used for the four profiles was RH=0.361, all the profiles had the same ripple pitch (0.031 m). These geometries were set up in PHOENICS using the same SATELLITE and GROUND coding as

in Appendix 11, (SATELLITE and GROUND 1).

The absence of the body fitted coordinates meant that the mesh used had to be relatively fine such that the curved walls were specified as a "staircase" of rectangular cells.

6.2.1.2 Additional Geometries

Further runs were performed for one of the profiles, (profile 2 in Fig. 6.1) at a different fin spacing, RH=0.281 and Dh=0.0174 m. This smaller wall spacing was the same as one used in the experimental investigation, see Chapter 5, permitting the effect of fin spacing found from the PHOENICS predictions to be compared against the experimental results of profile 4 in Fig. 5.9. The grid specifying the wall was left unchanged, but the cells in the cross stream X direction were reduced in width to reduce the wall spacing and keeping the number of cells in the cross stream X direction constant. The flow domain and wall geometries are shown in Fig. 6.3. The wall thickness was not changed and kept as four X cells each 0.2 mm wide giving a total wall thickness of 0.80 mm.

The SATELLITE program used to set up the geometry for the closer wall spacing model is presented in Appendix 10, program C2TFSA. The GROUND program was exactly the same as GROUND 1 of Appendix 11 as the number of cells and their topology were unchanged.

6.2.2 Boundary Conditions

6.2.2.1 Comparative Investigation

The flow was specified to have a uniform velocity across the inlet plane of the duct. For the interwall spacing of 0.0112 m, (RH=0.361) the three Reynolds numbers 8000, 1.0×10^4 and 1.2×10^4 had mean (or inlet) velocities of 0.3729, 0.4662 and 0.5594 m/s

106

respectively.

The static pressure was set to a uniform value of zero over the exit plane, to provide the pressure datum.

The KE and EP quantities were set to zero across the inlet plane and on the horizontal wall surfaces. This ensured that any turbulence within the flows was generated within the flow domain. These settings provided the boundary conditions for the flow friction.

The enthalpy of the fluid at inlet was 8.390×10^4 J/kg and set at the wall surface to 1.2570×10^5 J/kg. The PHOENICS wall function available was used for the heat transfer (enthalpy) and was that calculated locally from the Reynolds Analogy using the local friction coefficient.

The placing of the above boundary conditions on the stepped wall are shown in Fig 6.2b. The vertical faces of the steps were left unspecified and were therefore adiabatic and isentropic frictionless surfaces.

These boundary conditions were programmed in SATELLITE program C2TFSA (for profile 2), but were exactly the same for the other profiles and wall spacings. The GROUND program for the closer wall spacing model was also the same as the GROUND 1 code in Appendix 11 as the cell topology was equivalent, only the sizes were different.

6.2.2.2   Additional Runs

For the smaller spacing (RH=0.281), the three Reynolds numbers investigated, 6213, 8000 and 1.0×10^4 had mean velocities of 0.3729, 0.4801 and 0.6002 m/s. The flows modelled are summarised in Table 6.1.

An internal switch was available within the code to correct for the staircase wall surface boundary which relaxed the fluid momentum at the wall steps. The internal switch was activated by setting

LOGIC(92)=.FALSE. in the GROUND program. This was only possible via a communication from R.B. Lightfoot (1987), and was certainly not mentioned in the user manual, Rosten, Spalding and Tatchell (1983). No technical information relating to this switch was offered, but comparisons for several cases were made and are reported in this chapter.

No difference occurred in the SATELLITE program and the only difference in the GROUND coding was the inclusion of the line;

    LOGIC(92)=.FALSE.

for the relevent cases and was inserted after the declaration statements but before the first line of numerical calculation code.

The boundary conditions for these additional runs for the pressure, turbulence quantities and enthalpy were the same as for the comparative investigation. No additional boundary conditions were required for the specification of the constant turbulent viscosity.

6.2.3   Flow Conditions and Fluid Properties

6.2.3.1   Comparative Investigation

Water was used as the fluid in the model with the following density and dynamic viscosity properties;

$\rho = 998.$ kg/m^3 , $\mu = 0.0010422$ kg/ms

The Prandtl number was used as a parameter for part of the investigation and three values were used, 0.707, 1.0 and 6.09. Having specified the dynamic viscosity the program only required the Prandtl number to calculate the ratio of k/cp used in the energy equation. The thermal conductivity was not therefore explicitly specified. The turbulent Prandtl number which is used in the transport equation for the enthalpy H1 was left at the default value of 1.0.

108

The fluid dynamic viscosity in turbulent flow was calculated as the sum of the laminar and turbulent viscosities. The turbulent dynamic viscosity component was evaluated from the kinetic turbulent energy and dissipation rate variables (KE and EP).

6.2.3.2 Additional Runs

Two runs used the constant turbulent "eddy" viscosity model and this was set upon recommendation to 100. times the laminar value for these initial trials. This turbulent model did not require the solution of any additional equations (eg. KE and EP equations) and is known as a "zero equation" model. This model was invoked by setting;

IEMU1=1 and EMUT=100.0*EMUL

EMUL was the laminar flow dynamic viscosity. The effect of the LOGIC(92) parameter was also found for this turbulent model.

6.2.4 Turbulent Flow Results

The results of the PHOENICS generated solutions found to all the flows in rippled ducts investigated are given in Table 6.2 as the mean pressure on the inlet plane and the bulk mean enthalpy on the exit plane. The nondimensional numbers calculated for all of the turbulent solutions obtained are presented in Table 6.3.

6.2.4.1 Comparative Investigation

Flow vectors, pressure contours, enthalpy contours and contours of turbulence quantities (KE and EP) for the region Z cells 150 to 190 (or 200), the nondimensional wall spacing of RH=0.361 and a Reynolds number of 8000 are presented in Figs. 6.4a,b to 6.7a,b for the four profiles 1 to 4 respectively. The scale for the velocity vectors in these plots was, a flow vector of absolute length in the vector direction equal to a cell length in the flow direction Z is equivalent to a velocity of 0.667 m/s. These results were generated with the

109

LOGIC(92) parameter left unspecified and therefore at the default value =.TRUE. The Prandtl number used for the enthalpy plots was 6.09.

Flow vector plots of the whole solution domain for Reynolds numbers of 8000, $1.0X10^4$ and $1.2X10^4$ are presented in Figs. 6.M.6 (profile 1) to 6.M.9 (profile 4), 6.M.10 to 6.M.13 (profiles 1 to 4) and 6.M.14 to 6.M.17 (profiles 1 to 4) respectively. In these plots the velocity vector scales (for the vector length of 1 mm, 1 Z cell length) for the Reynolds numbers 8000 was 0.667 m/s in all four plots, $1.0X10^4$ was 1.0 m/s in all four plots (Figs. 6.M.10 to 6.M.13) and $1.2X10^4$ was 1.176 m/s for profiles 1, 2 and 4 (Figs. 6.M.14, 6.M.15 and 6.M.17) and 1.0 m/s for profile 3 (Fig. 6.M.16).

These results show that the turbulent flow in all the duct shapes does not readily separate and form recirculation regions as in the laminar models. Although in the initial troughs of the duct, small regions of very slow velocities were seen to exist.

The friction factor and j factor for each of the comparative runs are plotted in Figs. 6.8 and 6.9 respectively. The j factor plot was produced using data relating to a Prandtl number of 6.09. For the Reynolds numbers $1.0X10^4$ and $1.2X10^4$ the effect of a prandtl number variation was found and these results are given in Figs. 6.10 and 6.11.

A comparative performance evaluation study for these results is presented in section 6.3.

6.2.4.2   <u>Additional</u> <u>Run</u> <u>Results</u>

Vector and contour plots are presented for some of the additional cases in which the LOGIC(92) parameter was set to .FALSE. and these are presented in this section. Unfortunately no plots were prepared

110

for the runs which used the constant turbulent viscosity model of turbulence. The velocity scales quoted in this section are defined as in the previous section for a vector length equal to 1 cell length in the flow direction Z (or 1.0 mm, before scaling of the plot for presentation). The velocity scale was presented in this way as, comparing the absolute length of a vector with the cell length can be performed easily on the actual plot at the Z location in question and avoids problems that may arise from photocopying and reproduction. Graphical results are presented for three flow solutions as follows;

1   Plots for profile 2, Reynolds number 8000, Prandtl number 1.0 RH=0.361 are given in Figs. 6.12a to 6.12d, and a velocity vector plot of the whole field is given in Fig. 6.M.18a to e. The velocity vector scale was 0.667 m/s in Figs. 6.12a to 6.12d and 6.M.18.

2   Plots for profile 2, Reynolds number 8000, Prandtl number 1.0, RH=0.281 are given in Figs. 6.13a to 6.13b and the velocity vector scale in these figures was 1.0 m/s.

3   Plots for profile 2, Reynolds number 1.0×10^4, Prandtl number 6.09, RH=0.281 are given in Figs. 6.14a to 6.14b and a velocity vector plot of the whole solution field is presented in Fig. 6.M.19a to e. The velocity vector scale in Figures 6.14a to b and 6.M.19a to e was 1.0 m/s.

The dimensional and nondimensional results of these additional runs are presented with the laminar data in Tables 6.2 to 6.4.

For the two additional cases run for profile 2 at the wall spacing of RH=0.361, the KE-EP turbulence model and LOGIC(92)=.FALSE., in comparison with the cases in the comparative section there is a significant change in the pressure drops calculated. The relaxation of the fluid momentum at the steps in the wall surface has permitted the

111

fluid velocity in the adjacent wall cells to be higher which in turn has reduced the effective shear stresses within the fluid in the near wall cells. The reduction in fluid friction, through the Reynolds analogy also reduced the heat transfer coefficient, as seen by the reduction in the j factor from 1.852E-2 to 1.615E-2 at the Reynolds number of 8000 and Prandtl number of 6.09.

6.2.5 Comparison with Previously Reported Data and the Experimental Results of the Present Investigation

6.2.5.1 Comparison of Fluid Flow Characteristics

The flow visualisation studies were limited by the water mass flow rate in the water channel to a Reynolds number of approximately 2500. The difference in Reynolds number of 2500 to 8000 between the flow visualisation and numerical works is too great for practical comparisons to be made.

Flow visualisation studies at higher Reynolds numbers were made by Sparrow and Hossfeld in a flat sided corrugated wall duct having curved peaks. There are significant geometric differences between any of the four profiles modelled and their curved walls, but their results taken at a Reynolds number of 3.0×10^4 show that the flow separates from the curved corrugation peak and reattaches just after the bottom of the trough. It was noted though that at lower Reynolds numbers definitive visualisation patterns could not be obtained by the technique, but a reduction in the size of the separation did occur with an increase in the rounding of the peaks.

6.2.5.2 Comparison of Flow Friction Characteristics

For profile 2 (Fig. 6.1), two additional runs were performed with the LOGIC(92) parameter set to .FALSE. and the results of these runs

112

were compared with the measurements. The local pressures measured and computed corresponding to the same positions within the duct were nondimensionalised by the following equation;

$$prco = \frac{2 \cdot pd}{\rho \cdot v_m^2}$$

The mean velocity was based on the flow rate crossing a vertical plane between the two wall surfaces and the pressure datum was set on the exit plane. A change in the predicted pressure drop was caused purely by the setting of LOGIC(92). With the value left at the default of TRUE, the pressure drops predicted were greater than the measured values and the predicted values with LOGIC(92)=.FALSE. by a factor of approximately 3, see Tables 6.2 and 6.3, due to the momentum relaxation at the wall.

The two comparisons for modelled profile 2 were made against experimental profile 4 of Fig. 5.9 at the fin spacings of 11.2 mm and 8.7 mm. The experimental nondimensional wall spacings were RH=0.350 and 0.272 in comparison to the RH=0.361 and 0.281 for the numerical solutions, due to the slightly shorter ripple pitch of the Cobex fins. The Reynolds numbers were 8000 for both the numerical computations, 7839 and 7983 were the respective experimental Reynolds numbers for the wall spacings 11.2 mm and 8.7 mm. The comparisons are given in Figs. 6.15 and 6.16. These comparisons show that the actual values and the trends in the data were generally modelled by the PHOENICS program at both fin spacings. The largest differences between the measured and predicted data occur in the developing region after the first ripple.

The overall friction factors for the two cases concerned are compared with experimentally measured friction factors. At the wall spacings of 0.0112 m and 0.0087 m the experimentally measured factors

113

were respectively 0.06876 and 0.05731, compared with 0.07153 and 0.06583 for the measured. The experimental friction factor being based on the curvilinear length of fin was expected to be slightly lower than a value calculated for the axial length as in the PHOENICS modelled factors. However in the absence of information relating to the momentum relaxation at the wall, this comparison was considered adequate.

6.2.5.3 Comparison of the Computed j Factor with the Experimentally Measured Value of Chapter 5

A comparison is made for the j factors of the cases considered in the flow friction comparison. The duct walls were composed of profile 2 walls from Fig. 6.1 and 6.3 and profile 4 walls from Fig. 5.9, for the numerical and experimental geometries. These cases are for a Reynolds number of 8000, Prandtl number 0.707, the momentum wall relaxation activated by LOGIC(92)=.FALSE. and the two wall spacings of 11.2 and 8.7 mm. The j factors computed and measured at the wall spacing of 11.2 mm were 0.0130 and 0.00786 respectively and at the spacing of 8.7 mm were 0.0119 and 0.0687 respectively. This comparison shows that the PHOENICS prediction using the Reynolds analogy for the heat transfer coefficients gives much higher j factors than those experimentally measured even in cases where the pressure drops predicted compare very well with the measured.

6.3 Comparative Performance of Rippled Wall Ducts Using the PHOENICS Generated Data

6.3.1 Performance Evaluation Criteria

From the generated results, two criteria were found to be very easily applied and these are described below. The comparisons

114

performed can only be viewed in comparative terms due to the approximations and assumptions made in the solution of the particular numerical models.

1   Highest heat transfer rate.

The highest heat transfer rate criteria as applied here is independent of the pumping power expended. For a particular heat exchanger duty and flow velocity this criteria will indicate the unit of the smallest size. This criteria should not be used when pumping power or pressure drop considerations will affect the final heat exchanger selection.

2   Highest ratio of heat transfer rate to pumping power.

When the pumping power is a major factor in heat exchanger choice, then this criteria gives the heat exchanger of highest efficiency, but the size of compared units for a given duty may vary considerably.

6.3.2   Performance Comparison Results

At the wall spacing of 11.2 mm (RH=0.361) the highest heat transfer rate was achieved by profile 3 at a Reynolds number of 536, and by profile 4 at the turbulent Reynolds numbers 8000 to 1.2×10^4. The profile having the highest heat transfer to pumping power ratio was profile 2 at the Reynolds number 536 and profile 1 at Reynolds numbers of 8000 to 1.2×10^4.

115

DISCUSSION

7.1 Introduction

This chapter contains discussions which relate to the three main parts of the investigation, the overall performance characteristics of rippled fin tube banks, the local fluid flow, flow friction and heat transfer coefficients in rippled ducts and the numerical models developed of rippled duct flows. The experimental techniques, data reduction procedures were included in the discussion where necessary.

The results of the present investigation are discussed in relation to numerical and experimental data previously reported. The comparisons made with numerical work previously presented either justify or dismiss the simplifying assumptions and computed results reported by authors when solving mathematical equations without any experimental verification.

7.2 Heat Exchanger Rippled Fin Tube Banks

7.2.1 Performance Evaluation Criteria

The performance evaluation criteria relevent to the comparison of plate fin and tube heat exchangers was briefly reviewed. It was found, through comparing the characteristics of the three row heat exchanger data using the performance evaluation methods recommended by Shah (1978), that the criteria of Bergles, Junkhan and Bunn (1975), gave the most useful results. This method utilises a heat exchanger design program to evaluate the performance of a heat exchanger within a system. The performance criteria is then based on the performance of the system or a particular parameter. In this method real effects such as log mean temperature difference, total fan power, the liquid tube internal heat transfer and fluid property variations, neglected in the

other methods are included in the evaluation to give greater accuracy.

7.2.2 Effect of Fin Length on the Performance of Rippled Fin Heat Exchangers

The effect of the flow length through a rippled fin heat exchanger was found by comparing the performance of three and four row ripple fin heat exchangers whose characteristics were measured and reported, three row surface 3 in Appendix 1 (Maltson, Wilcock and Davenport, 1989) and four row surface 5 in Chapter 3. It must be noted that fins having other rippled profiles to the one used here will behave in a different manner to those compared here. Surfaces 3 and 5 had fin pitches of 282 and 296 fins/m, and the two surfaces were of the same ripple profile.

The Bergles, Junkhan and Bunn (1975), performance characteristics of the heat exchangers were plotted in Fig. 3.8 and the performance ratio graph in Fig. 3.9. The geometric and performance comparison between these surfaces were described in section 3.7.2. It was found that an increase in surface area of the four row surface 5 of 23 percent brought about an increase in the heat transfer performance of approximately 13 percent for the same fan power, over the three row unit at fan powers greater than 1000 W. For the four tube row heat exchanger the water to air temperature difference over the last tube row was low which reduced the log mean temperature difference from 43.2 to 40.6 K at a fan power of 2.3 kW. At this fan power the additional flow length increased the core pressure drop from 235.4 N/m^2 for the three row to 249.3 N/m^2 for the four row surface.

Comparing the nondimensional numbers for the two heat exchangers, for surface 3 see Table 2 of Appendix 1, and for surface 5 see Table

3.2. It can be seen that there is very little difference in the j factor between the two surfaces over the Reynolds number range 1000 to 3000, but at Reynolds numbers greater than 3000, surface 3 has slightly higher j factors. There is a much larger difference in the friction factor between the two surfaces. At a Reynolds number of 1000 surface 5 has a friction factor just below that of surface 3, but as the Reynolds number increases the difference between the two surfaces also increases.

Comparing the heat exchangers transferring the same quantity of heat, the three row surface would require a considerable increase in fan power. In Fig. 3.8, consider the four row unit surface 5 operating at a fan power of 890. W and transferring 199.6 kW of heat, the three row exchanger would have to operate with a fan power of 1365. W for a heat transfer rate of 196.9 kW, an increase in fan power of the order of 50 percent. The three row exchanger at the higher fan power requires a higher core velocity, 8.7m/s compared with 8.4 m/s for the four row, to increase, the heat transfer coefficient (from 131. W/m^2K to 147. W/m^2K) and log mean temperature difference (from 39.6K for the four row to 42.8K). At the higher velocity the core pressure drop and the inlet air accelerational power increased the fan power to a higher level than the four row.

7.2.3   Effect of Fin Profile on the Performance of Fin Tube Heat Exchangers

The effect of the profile shape was investigated in Chapter 3 and Appendix 1, and found to be one of the main factors determining the performance of a heat exchanger. Geometric and performance comparisons were made in Chapter 3 between two basically similar profiles, A and B, see Appendix 1 (surfaces 1 and 2), the Kays and London ruffled fin

and the plain fin.

Based on the Bergles, Junkhan and Bunn performance ratio graph, Fig. 3.9 profile B is marginally superior over profile A at high fan powers, but these two profile shapes were very similar in ripple amplitude and pitch. The Kays and London ruffled fin had a significantly different ripple shape, a shorter ripple pitch and smaller wave double amplitude, which brought about a corresponding reduction in the performance. The plain fin data was useful in that it could be considered as a ripple fin of infinitesimally small amplitude.

With data for only a small number of rippled fins it is very difficult to make conclusions regarding the effect of ripple shape on the performance of rippled fin heat exchangers. However it is thought that the increase in ripple amplitude of profiles A and B, over the Kays and London ruffled fin, at the fin pitch of 353 fins/m, was the geometric variation responsible for the increase in performance.

7.2.3.1   Comparison of Rippled With Louvred Fins

The louvred fins were shown in Chapter 3 to have a considerably higher performance over rippled fins which was due to the following points;

1   Predominantly shear flow through the louvred fins reduced pressure losses through the exchanger, in comparison with rippled fin tube banks which have a high form drag component.

2   Boundary layer leading edge shear flow that occurs on a flat plate was repeated at every louvre. The heat transfer coefficient is very high near the leading edge of a flat plate, giving a high mean coefficient for the louvred surface as a whole.

3   The triangular supporting duct permitted a high surface area density and created a very compact surface.

7.2.4   Effect of Fin Spacing on the Performance of Rippled Fin Tube Heat Exchangers

Rippled fin heat exchangers having the same ripple profile, but with different fin spacings were compared in Chapter 3. The comparisons made between such heat exchangers are discussed below;

1   The performance of the three row surfaces 2 and 3 are given in Fig. 3.9, for the typical application described in Chapter 3. The increase in surface area of surface 2 over surface 3 was 19 percent as the fin density was decreased from 354 fins/m for surface 2 to 282 fins/m for surface 3. The increase in fin density of surface 2 brought about an increase in heat transfer performance over surface 3 of approximately 10 percent at fan powers greater than 1 kW, but decreased at fan powers less than this.

2   The Kays and London surfaces 9.29-.737-SR and 11.32-.737-SR utilised the same ruffled fin profile ,but had fin pitches of 336 and 446 fins/m. The increase in surface area of the 11.32 case was 18 percent which resulted in an increase in the heat transfer rate of approximately 6 percent over the 9.29 surface for a wide fan power range.

3   The Kays and London plate fin surfaces 11.44-3/8-W and 17.8-3/8-W both had wavy plate fins of two wave cycles and fin pitches of 450 and 701 fins/m respectively. The increase in the surface area was 46 percent and this resulted in an increase in performance of 26 percent, which decreased at the highest fan powers.

By increasing the fin density for a heat exchanger of 1.0 m^2 frontal area, the performance has been found to increase. The main

reason for the increase is the larger heat transfer surface area involved, but the weight of the heat exchanger increases by the additional fins. The increase in performance for a heat exchanger having a higher fin density over the lower fin density exchanger is less than the increase in surface area, as a percentage, in all of the cases investigated.

A comparison of data between heat exchangers of different fin pitches using nondimensional numbers was performed. Heat exchangers of the present investigation surfaces 2 and 3, the Kays and London ruffled fins at 9.29 and 11.32 fins per inch and the Kays and London wavy plate fins 11.44-3/8W and 17.8-3/8W were included in the comparison. The effect of an increase in the fin density was found to decrease the j factor for all types of rippled or wavy fins. For an increase in the fin density the friction factor in the case of surfaces 2 and 3 decreased at high Reynolds numbers, but surface 2 had a higher friction factor than surface 3 in the Reynolds number range 500 to 2000. In the case of the two ruffled and two wavy Kays and London fins, the increase in fin density reduced the friction factor.

Further discussion on the effect of fin (wall) spacing is given with regards to the local fluid flow, flow friction and heat transfer of rippled duct characteristics in section 7.4.

7.3   Discussion on the Measurements and Data Reduction of the Local Heat Transfer Coefficients of Plain and Rippled Fins

7.3.1   Local Nusselt Numbers and Overall j Factors

The transient heat transfer measurement technique, by the nature of the test increasing the wall temperature above the constant wall temperature boundary condition with time introduced an uncertainty

121

into the plain wall test results. This uncertainty had not been considered in the earlier works of Tura (1986) or Jones and Russell (1981), but was dealt with for laminar and turbulent flat plate flow in Appendix 2. For the present rippled fin tests transition to turbulent flow occurred and the effect of the nonuniform wall temperature assumed to be small. To some extent the tests were also made in a partially steady state manner due to the effect of heat transfer loss from the external surfaces of the fins by natural convection and counteracting the problem described in Appendix 2.

However this problem occurred with the laminar flow heat transfer coefficient measurements of Tura (1986) who found considerable discrepancy (up to 20 percent differences in the the local Nusselt number) in flat plate measurements with the Pohlhausen equation using the transient test technique.

The temperature used to calculate the local heat transfer coefficient from a transient test, was the inlet air temperature to the working duct. However during a test the air temperature downstream of the leading edge was lower than this value as heat was transferred from the air to the fins. The temperature at this position would be lowest at the time of insertion into the hot airstream and increase with time to a temperature approaching the tunnel temperature. It would have been extremely difficult to measure the bulk temperature at any location and any time, which would have been needed for the data reduction analysis. Using the inlet temperature in the data reduction meant that the simulated temperature differences, between the fin wall and the air, were larger than they were in the test. This had the

122

effect of decreasing the local Nusselt number calculated.

Transient effects may also have affected the natural heat transfer coefficients on the external surfaces of the rippled and plain fin walls which were calculated for plain flat walls in steady conditions and used to approximate transient natural coefficients in the data reduction procedure.

The effect of radiation exchange to and from the test surfaces is a very difficult problem to analyse because during the heat transfer experiments two lamps were used to illuminate the ripple or plain fins in the test section. As far as was possible the lamps were positioned such that the incident light was first reflected off the adjacent wall. However the effect of radiation to and from the fin surface to the surroundings was not included in the data reduction procedure because the fin temperature at any location would be radiating to other locations within view which would be at different temperatures, through complicated view factors. Fin 1 which was exposed to the lower temperature surroundings more than fin 2, for the symmetrical profiles 2 and 3 exhibited lower peak Nusselt numbers and a simple radiation term in the data reduction procedure would have provided an additional heat loss, increasing the fin 1 Nusselt number and reduced this deficit.

A simple radiation heat transfer coefficient for the external duct surfaces is

$$q = \varepsilon \cdot \sigma \cdot (T_c^4 - T_a^4)$$

and translates to a heat transfer coefficient of approximately $5 W/m^2 K$ at the end of a transient test, but would be considerably less than this for a large proportion of the transience. Typical local convective heat transfer coefficients for the rippled surface ranged between 10 and 200 $W/m^2 K$. Therefore the simple radiation model would have increased the lower measured heat transfer coefficients slightly, but for the higher values the radiation effects would be negligible.

7.3.2   Discussion on the Local Plain Fin Heat Transfer Measurements

Generally the results show that the measured local heat transfer coefficients for the plain ducts tested had higher coefficients at the duct inlet than were predicted by many well established regression equations.

123

The contributing factors to these heat transfer coefficient distributions were as follows;

1   High turbulence intensity at the inlet of the duct. At the largest wall spacing the turbulence intensity was relatively high, at 6% for a Reynolds number of 2000, but this decreased to 2% at 8000.

It was found by Sugawara, Sato, Komatsu and Osaka (1953) that an increase in turbulence intensity had marked influence on the heat transfer coefficient for a flat plate under zero pressure gradient and Reynolds numbers based on the length from the leading edge of 4.0×10^4 to 3.5×10^5.

Junkhan and Serovy (1967), measured and reviewed the available data to date, 1967, and found conflicting results with the work of Sugawara, Sato, Komatsu and Osaka. The main difference was that for Reynolds numbers in the range 4.0×10^4 to 1.0×10^5 and the zero pressure gradient case, no appreciable increase in the heat transfer coefficient with an increase in turbulence intensity was found and their measured data agreed very closely with the laminar Pohlhausen equation. This Reynolds number range covers most of the data points taken in the present measurements, but these were taken in a relatively narrow channel compared with a flat plate.

2   The wind tunnel air velocity at the contraction exit was generally higher than the velocity in the working rippled duct. The air impinged on the rear of the fin at the leading edge and was turned through a right angle, see Fig 5.10. In the impingement region the rear wall of the fin was subject to increased heat transfer coefficients and this heat energy was conducted to the working duct side wall. This effect was not accounted for in the data reduction procedure and therefore heat transfer coefficients close to the

leading edge have larger uncertainties associated with them.

3   At the boundary layer bleed airflow section there was an air layer under large shear stress. The air entering the working duct had a different velocity to the tunnel contraction exit velocity. Excess air was forced away from the duct inlet, but this air had a higher velocity and the shear layer occurred immediately at the leading edge of the fin. Higher turbulence intensities may have been generated in this region affecting the heat transfer results by forcing a turbulent boundary layer to develop from the leading edge, but confirmatory measurements were not taken.

7.3.3   Discussion on the Local Rippled Fin Heat Transfer Measurements and Techniques

Conduction within the rippled fin wall in the longitudinal direction would have been present during the transient tests. The effects of conduction were considered in Chapter 4 and Appendix 3 where it was found that, for heat transfer distributions typical of rippled ducts used here, some modification of the distribution does take place, but the effect is limited to localised areas.

The heat transfer coefficient was calculated for a rippled duct wall neglecting the effect of curvature of the surface. The data reduction procedure could have accounted for this by using an annular element with nodes in the radial direction across the thin wall and calculating the local heat transfer coefficient at every surface position. However the wall was very thin and this assumption was thought to be valid. If a plate having the surface profile machined onto it's surface had been used, then this assumption would not necessarily be valid and the local surface curvature would have to be

125

considered in the data reduction. The limiting factor here would be the transient temperature profiles within the wall.

7.4   Discussion on the Local Rippled Fin Characteristics

7.4.1   Local Fluid Flows

The fluid flow characteristics, from the flow visualisation experiments reported in section 5.5.1 are discussed in relation to visualisation measurements from other geometries found in the literature. An attempt has been made to characterise the flows into regimes particular to a geometry and flow condition (Reynolds number).

The flow visualisation study has shown that highly complex flow fields exist in rippled ducts. Unfortunately the measurements were limited to Reynolds numbers of less than 2500 and the practical range extends beyond this value to Reynolds numbers of around 1.0×10^4. Although much needed information regarding flow patterns at the lower Reynolds numbers has been obtained, which can be extrapolated into the near, medium flow range. In addition to the flow patterns visualised, the local flow friction and heat transfer measurements made on the rippled wall surfaces provide further qualitative information about the flow patterns.

There are distinct flow regimes present in the flow field which change with variation in geometry and Reynolds number. These flow regimes are described below;

1   Laminar Flow Separation and Recirculation

At a certain Reynolds number (separation Reynolds number) for a particular duct, the laminar flow separated from a ripple peak (or the region near the peak) and the separation streamline bounded a recirculation zone within the trough. This streamline was seen to

126

reattach near the mid point on the forward facing part of the next ripple. Below this Reynolds number the flow remained attached to the surface throughout the duct. For a rippled duct and flow, the size of the separation zone varied and the reattachment point moved accordingly.

Although data for this laminar regime is scarce from the present measurements, the results indicate that the separation Reynolds number decreases as the wall spacing decreases, but at a certain wall spacing, instead of the flow separating to exhibit a generally two dimensional spanwise vortex pattern, three dimensional streamwise vortices were generated.

2   Unstable Shear Layers, Unsteadiness and Vortex Shedding

In a similar way to the onset of separation and recirculation that occurs in rippled ducts and channels, the free shear layer bounding a spanwise recirculation zone becomes unstable with increasing fluid velocity and marks the onset of transition to turbulent flow. The present tests have shown that the parameters defining the criteria at which this fluid flow manifests itself are dependent upon the geometry of the confining walls and the Reynolds number.

The instability was visualised to begin with a slight oscillation of the reattachment point on the wall surface. As the flow velocity increases this oscillation becomes more pronounced. At the reattachment point when the separation streakline moved downwards the fluid velocity in the recirculation zone increased. This in turn lifted the separation streakline slightly near the separation point. This rocking motion subsequently could not be maintained and a vortex

127

shedding flow dominated. Nishimura, Kajimoto and Kawamura (1986) visualised the unstable shear layers in a sinusoidal wall corrugated duct in the periodically fully developed region. The wall double amplitude was RI=0.25 and the wall spacing RH=0.464. In this geometry the Reynolds number at which the unsteadiness appeared was about 700.

Goldstein and Sparrow (1977) did not encounter the spanwise recirculation vortices in the ripple troughs in flat sided corrugated wall ducts at the wall spacing of RH=0.178 and a corrugation height of RI=0.358. The flow was dominated by secondary flow vortices where the vortex axis was oriented in the main flow direction.

Kang and Chang (1982) found through flow visualisation experiments the Reynolds number at which the instability of the free shear layer bounding a recirculation zone occurs. The geometry was that of a plain wall channel with rectangular blocks placed alternatively on opposite walls. Considering a block and the portion of plain wall between blocks on the same wall to be the equivalent ripple pitch, the "zig zag" channel had nondimensional geometry values of RH=0.05 and RI=0.05. The size of the separation zone formed on the leeward face of the block grew in size from a Reynolds number of 40 to 220 (20 to 110, by his definition, based on the mean velocity of the fluid in the absence of the blocks and the plain wall spacing). At a Reynolds number of 820 (410) the shear layer had become unstable.

3 Secondary Flow Vortices and Their Instability in Rippled Ducts

The most striking phenomenon to be seen from the flow visualisation study was the generation of secondary flow vortices first seen for profile 2 (Fig. 5.9) at a fin spacing of 7.25 mm (RH=0.189) and a Reynolds number of 818. This flow pattern was not seen to exist for any of the profiles at larger wall spacings, or

profiles 1 (RH=0.227) and 3 (RH=0.306) at the 7.25 mm wall spacing. As the wall spacing reduced, over the range tested, the secondary flow vortices became more pronounced. The appearance of the streamwise vortices for profile 2 at the 7.25 mm wall spacing was unexpected as this geometry offers the mildest curvature to the flow. The flows in the other two geometries formed by profiles 1 and 3 exhibited large spanwise vortices and instead of the flow following the curvature of the walls, the main flow followed the curved walls over the attached regions and the free shear layers of the recirculation zones. Hence the effective curvature of the main flow over a ripple cycle was considerably reduced. At the wall spacing of 7.25 mm and RH=0.306 for profile 3 as the flow increased the spanwise vortices became unstable and considerable three dimensionality did occur at Reynolds numbers between 764 to 1056, but this was difficult to interpret.

From the local mass transfer measurements of Goldstein and Sparrow (1977) the fluid flow patterns which exist in the entrance region (first two ripples) of a flat sided corrugated duct were inferred. The mass transfer variations that occurred in the spanwise direction indicated the presence of secondary flow vortices at Reynolds numbers of 370 to 3080. At the 3080 Reynolds number the spanwise variations in mass transfer coefficient occurred over the first corrugation cycle and on subsequent facets the coefficient became more uniform which inferred that the onset of turbulent flow had destroyed the secondary flow vortices.

Nishimura, Yoshino and Kawamura (1987), visualised secondary flow vortices in a sinusoidal channel having geometrical parameters of RH=0.143 and RI=0.25 at Reynolds numbers (Re_{2H}) of between 200 to 500.

At Reynolds numbers up to 320 the flow was steady, but at a Reynolds number of 500 the secondary flow vortices had become unstable. Additional views of the flourescein and rhodamine B streaklines were photographed to prove that the flow streaklines did actually move in the spanwise direction. Their geometry was similar to the geometry of profile 3 at a fin spacing of RH=0.127 and wall amplitude of RI=0.222. The secondary flow vortices were visualised for this geometry to be steady at a Reynolds number of 551, but at a Reynolds number of 696 the flow had become unstable. The unsteadiness was visualised as a spiralling of the secondary flow vortices.

4   Turbulent Flow

Information gained from the flow visualisation study in fully turbulent flows was limited to the interpretation of streaklines, which were dispersed by the development of upstream unstable and transitional flows. Turbulent flow phenomena, vortices, separation, reattachment and recirculation could not be identified. Further discussion on the turbulent flows simulated numerically using the PHOENICS program can be found in section 7.6.5.

7.4.2   Local Flow Friction

Data relating to the local wall pressure at points on every ripple was presented in Chapter 5. This data for rippled ducts represents new and reasonably accurate data which is available for use in design and research. For performance comparison purposes, these flow friction studies are of equal importance as heat transfer.

7.4.3   Effect of Fluid Flows on the Local Heat Transfer Coefficient

To aid in the understanding of the results presented in Chapter 5, of the local fluid flows and heat transfer coefficients, Figures 7.1 to 7.12 are presented of the local heat transfer coefficient

130

plotted against the linear axial coordinate. Included on the graphs for direct comparison are fluid flow streaklines from a near Reynolds number flow, sketched within the rippled ducts drawn at the same scale as the heat transfer plot. The figures given concentrate on comparing the effect of a variation in the duct geometry, the wall profile, profiles 1 to 4 from Fig. 5.9 and interwall spacings 11.2, 7.1 and 4.9 mm, on the local heat transfer coefficient. The fluid flows were not visualised for profile 4, but the heat transfer coefficient distributions were included for comparison.

The heat transfer results presented in Figs. 7.9 to 7.12 at the 4.9 mm spacing for the four profiles were treated in a different manner to those presented in Chapter 5 in that the contours were not digitised because of spanwise variations in the heat transfer coefficient. The plots were prepared by projecting the colour liquid crystal contours from slide photographs onto paper and copying the green contours directly. The heat transfer coefficient data reduction procedure was based on the mean fin wall thickness as before in Appendix 8, but the resulting Nusselt number at any time and position was not scaled by the local fin wall thickness, as the coordinates of this point were not available. From the line contour plots drawn and the Nusselt numbers calculated, colour contour plots were prepared. In these drawings, where there was a large gradient in the Nusselt number with position, all the contours could not be represented accurately and some averaging took place.

These comparisons are discussed in three parts as follows;

1   11.2 mm Wall Spacing

The four heat transfer data sets all show many similar trends in

131

the variation of the coefficient with position over a ripple pitch. At the inlet of the ducts the laminar boundary layer flow exists, but is completely disturbed by the first ripple. The flow behaviour in each duct is also very similar. Laminar separation zones characterised the flow at the first ripple and vortices were shed in the third ripple trough.

Flow separation regions are apparent in the inlet region and the heat transfer coefficient varies accordingly, but sharp changes in the heat transfer distribution at separation and reattachment points are not evident although at reattachment an inflexion in the distribution is visible which becomes more pronounced further downstream in the presence of unsteady flow phenomena. An explanation for this is that as the main flow approaches a ripple peak, the wall shear layer accelerates and masks the effect of reattachment. The main flow also accelerates due to the fact that the flow is separated in the trough underneath reducing the area of flow. Similarly as the main flow tries to go around the ripple peak bend, the wall shear layer flow is decelerating and the Nusselt number is already decreasing to the point separation after which a further decrease takes place.

2   7.1 mm Wall Spacing

The heat transfer coefficient distributions shown in Figs. 7.5 to 7.8 exhibit marked differences over those at the 11.2 mm spacing. Due to the walls being closer together and the vortices shed from behind a ripple affected the flow on both walls of the duct. This effect is most pronounced in Figs. 7.5 and 7.8, where a second peak in the Nusselt number distribution occurs in the ripple trough where vortex shedding takes place and increases the time mean thermal gradients by entrainment of the main flow into the wall shear layer.

132

The flow in the duct formed by profile 2 had become partially three dimensional, but this was not noted in the photographs of the isotherms.

3   4.9 mm Wall Spacing

All four duct flows at this wall spacing show development through three dimensional flows exhibiting strong secondary flow vortices. The impingement of these vortices on the walls produced "spots" of high heat transfer coefficient. The onset of turbulent flow in these ducts destroyed the vortices and the flow, by inference of the Nusselt number contours, became two dimensional.

At the higher Reynolds number of 8000, no fluid flow visualisation studies were performed, but information from the local flow friction measurements and the PHOENICS generated flow solutions were used to propose a flow pattern for the rippled duct formed by profile 4 of Fig 5.9 (PHOENICS profile 2 Fig. 6.1 and 6.3) at the wall spacings of 11.2 and 8.7 mm, described in section 7.6.5. The flow field, downstream of the developing entrance flow was proposed to be attached at both ripple peak and trough positions. The PHOENICS flow prediction had a high velocity at the peak and low in the trough. Therefore the heat transfer Nusselt number distributions of Figs. 5.48 and 5.60 may be caused by accelerating and decelerating flows at the wall surface. Interestingly there is a difference in the shape of the distributions between the fin 1 Nusselt numbers of Figs. 5.48 and 5.60. At the wall spacing of 8.7 mm there is a distinct peak in the distribution which reduces before increasing to the higher peak. The smaller peak occurs before the first protruding corner between the concavely curved and flat sections. The major peak occurs at the first

protruding corner between these sections and the distribution decreases sharply on the underneath of the flat section. Figures 5.48 and 5.60 tend to suggest that the flow does not accelerate smoothly underneath the curved sections and that there is an impingement of the flow at the position of the smaller peak in Fig. 5.60 and at the point of inflexion in Fig. 5.48. A possible flow to cause this effect is one which has vortex shedding from the fin 1 peaks which "scrub" the forward facing concave section before the next peak.

7.5 Discussion on the Mean Rippled Fin Characteristics and Application of the Results in the Design of Real Systems

7.5.1 Flow Friction

The pressure tappings at the entrance to the rippled ducts were positioned quite closely to the rippled sections of the walls and at this position the pressure profile across the channel may have been affected by the downstream ripples. The overall friction factor was calculated from the average of the two values on opposite walls. Measured differences between these first pressure tappings were generally well below 10 percent of the overall pressure drop for the duct. One data set shows larger differences though, Profile 2 at the wall spacing of 8.7 mm and Reynolds number 2021, but apart from the local flow effects no reason could be proposed for these differences.

The overall friction factor for the rippled ducts measured was based on the pressure loss within the rippled duct alone. In order to calculate the fan power for a real system the following terms must be included;

1   The flow acceleration of the gas within the system. For the case considered in Chapter 5 of the tractor cooling system, the air was

accelerated from rest to the inlet velocity of the exchanger.

2   Entrance and exit losses at the leading and trailing faces of the exchanger. For fin tube heat exchangers, flow losses are generated as the flow accelerates locally at the inlet and exit of the fins and tubes. If the present measurements are used for design purposes, it is recommended that inline thin flat tubes or single thin channels are used. Staggering the tube arrangement as was the case with the heat exchangers measured in Chapter 3 may interfere with the characteristics.

3   The pressure drop through the heat exchanger core should be based on the Kays and London (1984) 2-26a equation which includes a term for the gas acceleration through the core due to the density variation.

4   A ducting loss term. As the gas travels to and from the heat exchanger and fan components additional surfaces are encountered which apply friction forces on the gas.

The flow friction measurements on the plate fin and tube heat exchangers reported in Chapter 3 were based on Kays and London (1984) equation 2-26b for the friction factor in which the entrance and exit losses were included in the friction factor. The four terms detailed above are evaluated as before, but terms 2 and 3 are combined in the core pressure drop term.

7.5.2   Heat Transfer

For the comparison of the proposed heat exchangers in Chapter 5, use was made of the averaged local heat transfer coefficients in rippled ducts. The local data was reduced using the inlet heated air temperature (tunnel contraction exit temperature) to the local Nusselt number and overall j factor and no account was taken of the transient thermal loss of heat from the air to the fin. For design purposes, a

135

better approximation for a comparison may be to use the inlet air temperature and the mean water temperature in the heat transfer rate equation as follows;

$$Q = U \cdot A_{ht} \cdot (T_{w,m} - T_{a,i})$$

This equation would replace the log mean temperature difference form and would have the effect of increasing the calculated heat transfer rates from all the compared heat exchangers.

The problems associated with the local heat transfer measurements will be also present in the overall results which were integrated from the local coefficients. These problems could be overcome by testing a full scale sample of the designed plate rippled fin and tube heat exchanger to check on its performance characteristics.

The j factors from the investigation of Chapter 5 are representative of the fins alone and effects of side walls (tube walls) were not included. For the comparison of the proposed heat exchangers in Chapter 5 it was assumed that the side walls had the same j factor as the fins. For design purposes the gas side j factor for the fins should be area weighted with a j factor for the tube walls.

The overall j factor for the sample cores measured in Chapter 3 represented the gas side heat transfer for both the fins and tubes.

A comparison was made between the integrated liquid crystal transient heat transfer tests and the overall heat transfer tests on full scale heat exchangers. This comparison is tabulated below;

Heat Transfer j factors

	liquid crystal results		full scale results	
Reynolds number	profile 1	profile 4	surface 1	surface 2
2000	0.0101	0.00808	0.0131	0.0129
5000	0.0089	0.00807	0.0094	0.0097

The presence of the tubes in the full scale measurements at Reynolds numbers in this range will tend to increase the j factors over the rippled ducts without tubes. The reason for this are as follows;

There will be a complex flow at the intersection of the tubes and fins, typically a horseshoe vortex system enhancing the heat transfer coefficient locally.

The main flow will accelerate due to the boundary layers on the tube walls leading to higher heat transfer coefficients.

Wakes formed behind the tubes will be turbulent increasing the general level of turbulence in the passage also enhancing the heat transfer.

Bearing the above in mind it was expected that the full scale j factors would be higher than the liquid crystal results and this is shown in the comparison, giving considerable confidence to the liquid crystal transient heat transfer measurements.

7.6 Discussion on the Numerical Simulations Performed

The aim of the numerical modelling investigation was to gain as much comparative information as possible regarding the fluid flow, flow friction and heat transfer characteristics for the inlet region of various rippled duct geometries, with application to plate fin heat exchangers. Comparisons of the numerically generated results with

experimental data were made to assess the accuracy of the mathematical model.

7.6.1   Laminar Flow

The program and numerical model was found to accurately predict the fluid flow and pressure drop in the inlet region of a rippled duct. The parameter LOGIC(92) was left at its default value, but in the laminar flow the fluid viscosity dominated the flow friction and the velocity was very low at the walls. Therefore the momentum relaxation on the stepped wall cells would have made a very small difference to the pressure drop. Some flow visualisation studies were performed in conjunction with the numerical investigations for the four wall profiles. For the three profiles for which the flow visualisation was not performed there were assumptions made that the flow was steady and two dimensional.

7.6.2   Previous Rippled and Corrugated Duct Laminar Flow Numerical Models

Many authors numerically investigated periodically fully developed flows in wavy or corrugated channels that were believed to be laminar and two dimensional in the Reynolds number range 500 to 2000, but in the absence of flow visualisation studies the flows may in reality have been unsteady to a certain degree or exhibit areas of three dimensionality. Investigations carried out in the Reynolds number and geometry ranges in question which may have suffered from the above problems are detailed below;

1   Asako, Nakamura and Faghri (1988) numerically modelled the periodically fully developed flow in a corrugated channel with rounded corners. The geometries they investigated had wide variations in corrugation amplitude and wall spacing. The Reynolds number range was

137

extended up to 1000, but for the geometry of RI=0.25 and RH=0.25 to 0.5 three dimensional effects may be significant at these Reynolds numbers. Nishimura, Yoshino and Kawamura (1987) in a sinusoidal wavy geometry of RI=0.25 and RH=0.143 found considerable three dimensional effects in the flow occurring at a Reynolds number of 320 which became unsteady at 500. At a wall spacing of RH=0.464 (RI=0.25) Nishimura, Kajimoto and Kawamura found from flow visualisation that increasing from a Reynolds number of about 700, an unsteady type of vortex shedding occurred. In the present experimental investigation detailed in Chapter 5, three dimensional and unsteady effects were noted to occur at low Reynolds numbers.

2   Amano (1984 b) modelled the laminar two dimensional flow around two right angled bends in the Reynolds number range 200 to 2000. The flow at the inlet was specified as a fully developed laminar channel flow, which then separated from the corners. The corners created a disturbance to the flow which may have been strong enough for a real flow to become unsteady or transitional especially at a Reynolds number of 2000. The wide geometry variation produced bends to be investigated which were sufficiently narrow to cause extensive flow curvature within the bend. This effective flow curvature can lead to three dimensionality of the flow in basically two dimensional channels. Three dimensional flows involving secondary flow vortices (otherwise known as Taylor-Goertler vortices) were inferred by the mass transfer data of Goldstein and Sparrow (1977) in which the flow was bent through 120 degree bends instead of the sharper 90 degrees of Amano.

3   Faghri and Asako (1987) numerically modelled laminar, steady and

138

two dimensional flow in a converging-diverging channel having flat sided corrugated walls. Although the authors noted the lack of previously reported research for their geometry their assumptions of steady laminar flow was deemed questionable by Nishimura, Yoshino and Kawamura (1987).

4   Webb and Ramadhyani (1985) modelled the fully developed flow in a channel having staggered baffles up to a Reynolds number of 2000. Although the channel was not of the type investigated here, either corrugated or rippled, the separation zones calculated may easily have become unstable, or especially in the fully developed region, turbulent.

7.6.3   Turbulent Flow

The K-E model was used to solve two additional equations for the turbulence quantities KE and EP at Reynolds numbers of 8000, $1.0X10^4$ and $1.2X10^4$. It is generally accepted, Pletcher (1988), that the K-E model of turbulence does not perform well in situations of flow curvature, rotation, separation and recirculation. The K-E model of turbulence should strictly be used for flows in rippled ducts, with a correction for flow curvature which accounts for the additional strain terms imposed upon the fluid elements. Leschiner and Rodi (1981) developed a correction which accounted for flow curvature. Benodekar, Goddard, Gosman and Issa used this correction for the flow over wall mounted ribs and definite improvements in the calculated flow parameters were found in comparison with experimental measurements. Whilst it would have been possible to incorporate this correction within the PHOENICS program, writing subroutines within the main program GROUND was beyond the scope of this investigation.

The zero equation eddy viscosity model of turbulence was used to

model the flow in a rippled duct. This model was expected to provide only qualitative results due to the turbulent viscosity being specified as a constant whereas in reality the turbulence is generated and dissipated locally within the flow.

7.6.4 Boundary Conditions Used in the Models

The flow was bounded by the staircase walls and the imposed boundary conditions for the flow friction and enthalpy were significant approximations and the turbulent flows solved and reported here must be viewed in comparative terms.

A Body Fitted Coordinates grid ought to have been used and was available commercially from CHAM Ltd within the 84 version 1.4, but financial constraints prevented the 81 code from being updated at Coventry Polytechnic.

The use of the LOGIC(92) switch lowered the flow friction by a factor of approximately three and brought the computed friction factors in line with those experimentally measured.

7.6.5 Discussion of the Numerically Generated Turbulent Flow Results

Two flow friction results for PHOENICS profile 2 (Figs. 6.1 and 6.3) were compared with experimental measurements of vacuum formed profile 4 (Fig. 5.9) in Figs. 6.15 and 6.16 for the Reynolds number of 8000. The comparison showed differences of the local wall pressure between the measured and simulated in the developing region after the first ripple, but downstream where both streams tend towards the periodically fully developed region, the PHOENICS results and the measurements agreed quite closely. These PHOENICS flow solutions were obtained with the LOGIC(92) parameter set to FALSE to activate a stepped wall momentum relaxation switch. The calculated (time mean)

flow fields shown in Figs. 6.12 and 6.13 which do not show separated flow regions, may be representing the flow present in the air flow rippled duct. The high velocity attached flow at the ripple peaks adjacent to the pressure tappings are believed to be accurate, and as the pressure difference between the two pressure tappings at the ripple peak and the trough opposite has effectively been experimentally verified, then the time mean flow in the ripple troughs may be very similar to the low velocity attached flows predicted. Therefore this comparison indicates that within the ripple trough region of this profile, separated flow with recirculation does not occur. The heat transfer distributions for the profile 4 (Fig. 5.9) fins indicate a modification to this flow as described above.

Sparrow and Hossfeld (1984) also noted that the higher the degree of rounding of the peaks of a corrugated duct reduced the size of the separation zones.

The j factor calculated from the numerical models which were used for the flow friction comparison were found to be considerably higher than the measured values for similar ripple wall profiles. The flow friction prediction compared well with the measured values and these cases would provide the optimum cases for comparison as the heat transfer boundary conditions were based on the wall friction through the Reynolds analogy. For rippled ducts a considerable portion of the flow friction occurs as form drag in addition to wall shear friction. The Reynolds analogy was developed through flat plate shear friction without form drag effects and the rippled wall heat transfer coefficients should be calculated using just the shear flow friction.

7.7 Measurement Uncertainty of the Presented Results

As far as possible measurements were taken using equipment which

141

provided accurate measurement data. Uncertainty analysis simulations were performed where feasible using the Monte Carlo method and the results of these simulations were presented with the calculated data. Although every type of measurement uncertainty of every instrument used could not be included in the analysis, the Monte Carlo simulations performed can be regarded as good estimates of the actual measurement uncertainty.

7.8 Postulation of High Performance Heat Transfer Surface of General Application

Previously reported information on the growth of secondary flow vortices and the knowledge gained from the flow visualisation studies at close wall spacings, for the profiles considered in the present research, indicated that the curvature, especially on the concave walls brought about the increase in heat transfer. The profiles used in the experimental research see Fig. 5.9, whilst having a considerable degree of concave curvature, the turning of the flow in the concave sense was activated by a proportion of the convex curve, by fluid impingement near the ripple peaks. This impingement also carries with it form drag components which decrease the performance of the duct.

To overcome this problem, a fin profile was designed to make the maximum use of the concave wall turning and the fin profile was given in Fig. 6.1 profile 4. For the numerical analysis performed with this profile at the large wall spacing no secondary flow vortices were anticipated, but flow visualisation for this profile was not performed to check this. However at a closer wall spacing (14-18 say fins/inch) this fin profile would be expected to produce significant secondary

142

flow and with this flow, enhancement in heat transfer. The pressure drop and hence fan (or pumping) power must also be considered which are vital for performance comparison studies.

CHAPTER 8
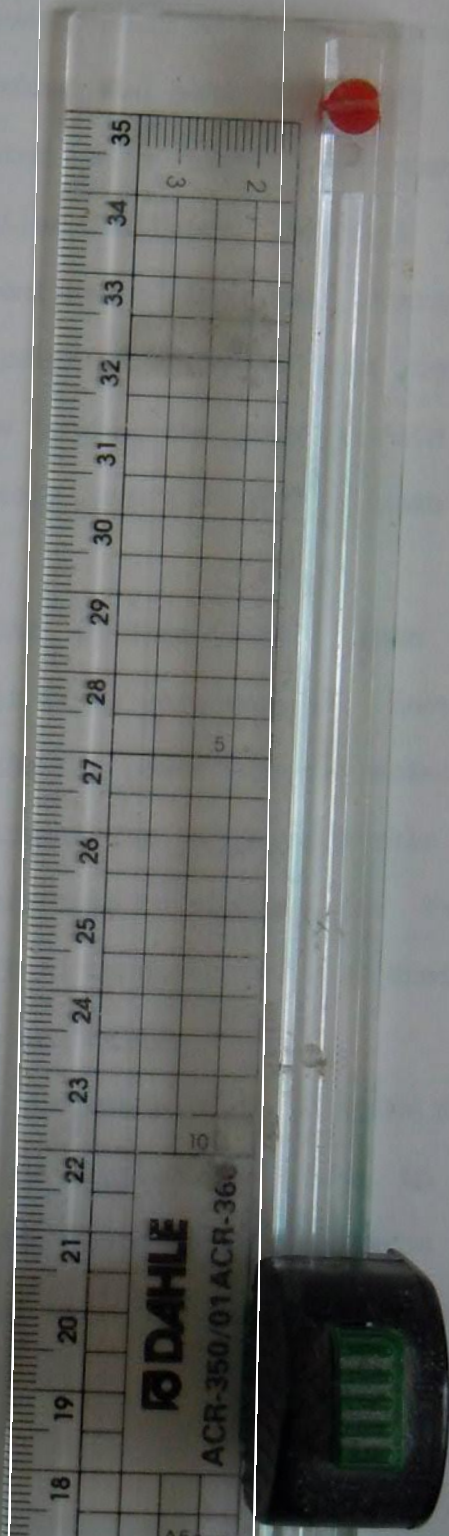
CONCLUSIONS AND RECOMMENDATIONS

8.1 Conclusions

The overall heat transfer and pressure drop measurements made on three and four row sample heat exchangers in the Covrad wind tunnel enabled their performance characteristics to be evaluated relative to previously reported data of ruffled, plain and louvred fins. The conclusions relating to the full scale heat exchanger tests were, that the most accurate performance evaluation method for this type of heat exchanger was that of Bergles Junkhan and bunn (1975) and that the three tube row rippled fins tested had a higher performance than previously reported data for similar fin types. The four row heat exchangers permitted a more efficient use of fan power relative to the three row, but due to the degredation of the log mean temperature difference with the increased flow length, the proportionate increase in heat transfer rate was considerably less than the increase in heat transfer surface area.

The louvred heat exchanger data of Tura (1986), when compared with the ruffled, rippled and plain fins, were shown to have higher performance characteristics over the fan power range associated with industrial and agricultural equipment by a considerable margin. Louvred fins should be used in preference to rippled fins for clean environment situations where the fluid temperatures are similar and assumptions made for the comparison are valid.

Flow visualisation experiments were made to investigate the flow development in the entrance region of rippled wall ducts. An attempt has been made to characterise the wide range of flow patterns found in order to present the extensive visual data in a consistent manner. The

144

existence of spanwise and streamwise vortices was proven and in addition the mechanisms for the flow development and the processes of transition to turbulence were found. The streamwise vortices exist when the fluid undergoes curvature and centrifugal forces generate the secondary flow. These were seen in both the flow visualisation and heat transfer measurements. The spanwise vortices, as the Reynolds number increases become unstable and shed vortices.

While it was known that spanwise vortex shedding and streamwise vortex spiralling flows existed in wavy walled ducts, this investigation is the first to the authors knowledge that shows the development of these flows in rippled ducts in the entry length region.

For the laminar, transitional and turbulent developing flows visualised in rippled ducts, the accompanying local flow friction and heat transfer measurements made, represents new and modern data which is currently in absence within the available literature. Problems relating to the experimental techniques were described and discussed for future reference and development.

Local pressure drop measurements were made which may be used for design or comparative purposes. Extreme care and attention was given to the experimental measurements, data reduction and procedures used in obtaining these results. The results of these measurements are consistent with the flow visualisation measurements.

The local heat transfer measurement technique used by Tura (1986), the phase-change paint transient technique was developed as far as possible to measure the heat transfer coefficient using micro encapsulated liquid crystals. The problems investigated here, namely the streamwise wall conduction and the transient measurement technique problems show that;
1 The lower the temperature difference ratio used in the measurements,

as defined in section 5.5.3 then the smaller the effect the conduction has on the final results.

2   The transient heat transfer test technique can be used with confidence in the turbulent flow regime where the heat transfer coefficient is insensitive to the nonuniform wall temperature experienced during a test, but should be used with caution in laminar flows where quantitative data is required, but will still give useful qualitative information.

The rippled duct formed by profile 4 of Fig. 5.9 was found to give a high performance relative to the others used here. Unfortunately flow visualisation studies were not undertaken for this ripple type. Profile 3 at the wall spacings used, was found to offer the duct of highest heat transfer coefficient and hence the smallest heat exchanger irrespective of fan power.

The conclusion of the numerical research using PHOENICS (81) was that numerical flow and heat transfer must be accompanied by some form of experimental research in order to verify the use of the model under specified conditions. This was shown to be true for the present work where approximating steps in the wall geometry were used to represent a curved boundary. The differences in the pressure drops predicted between two numerical models where one had a momentum relaxation condition applied at the steps, but which were otherwise identical were very large. The separation and recirculation patterns found from flow visualisation measurements at the duct inlet region were not seen in the PHOENICS results.

The certainty intervals at the 95 percent level were calculated using the Monte Carlo simulation approach and were also reported for experimental data presented in Chapters 3 and 5. These numerically

146

generated certainty intervals confirmed that the associated measurements were taken to a high degree of accuracy, commensurate with current engineering practice.

8.2 Recommendations for Future Research

For laminar flows it is recommended that a measurement technique which can accurately model the situation of the uniform wall temperature boundary condition, is used to measure the overall mass transfer coefficient of the duct geometries for the purposes of a comparative study. Many experimentalists investigating the heat transfer characteristics of confined flows of various geometries have used the thick film mass transfer technique and a considerable data base of mass transfer experiments which relate to heat transfer investigations is readily available for the comparison of data from tests on new geometries. However the transient heat transfer method does give useful qualitative information in laminar flows. For turbulent flows this method approximates the uniform wall temperature boundary condition and may be used with confidence.

Boundary fitted coordinate grids for numerical flow and heat transfer modelling are available (eg. PHOENICS '84 1.4, FLUENT, STAR-CD etc.) and should be used to model curved geometries. The actual curvature of the body surface was not modelled exactly here, but as a series of rectangular cells forming a stepped wall. In boundary fitted coordinate systems nodes can be placed at the pertinent points on a curved wall to permit the curvature to be accurately modelled.

No grid refinement runs were performed to check on the grid independence, but the results were used for relative performance

comparisons and to see how well the flow and heat transfer processes were modelled with a high density grid. The grid over one ripple pitch was of a similar density to other investigations which had only one ripple pitch, see section 6.1.1. Future work should encompass grid independence studies which are important in obtaining the correct solutions from finite difference numerical procedures.

Investigations into the effect of a variation in the values of the turbulence quantities (KE and EP) on the inlet boundary would also be useful in ascertaining whether the level of turbulence in the duct is affected and how this relates to heat transfer. In the present investigation these were set to zero on the inlet plane, but the experimental measurements reported in Chapter 5 were made using air which had various degrees of turbulence at the duct inlet.

It has been shown by Irwin and Smith (1975), Launder Priddin and Sharma (1977) and Gibson (1978) that Reynolds stress turbulence models can model with reasonable accuracy flows with streamline curvature. However all turbulence models require the specification of the turbulent Prandtl number for the energy equation. For flows with streamline curvature and heat transfer Gibson and Servat-Djoo (1989) recommend using an assumed turbulent Prandtl number distribution which relates the thermal fluxes to the Reynolds stresses within the flow field.

There is at present a complete lack of experimental data regarding the local fluid flow vectors in corrugated and rippled ducts or channels in the turbulent flow range of Reynolds numbers from about 3000 to 1.0×10^4. It is recommended that future work be concentrated on obtaining local fluid flows over the inlet and fully developed regions. Flow visualisation studies that would give an indication of

148

the local flow field at the higher Reynolds numbers 3000 to 1.0×10^4, and the type of flow development would also be extremely valuable in this area of research. This need was noted by Amano (1987) who had no Reynolds stress measurements to compare with computed values and in his case advantages of the Reynolds stress turbulence model over the standard K-E model were limited to comparing variables of pressure drop and heat transfer against experimental data.

REFERENCES

Amano R. R., 1984, Laminar Heat Transfer in a Channel with Two Right-Angled Bends., J HEAT TRANSFER TRANS ASME, vol. 106, pp. 591-596.

Amano R. S., 1985 a, A Numerical Study of Laminar and Turbulent Heat Transfer in a Periodically Corrugated Wall Channel., J HEAT TRANSFER TRANS ASME, vol. 107, pp. 564-569.

Amano R. S., 1985 b, A Numerical Study of Turbulent Heat Transfer in a Channel With Bends., ASME paper no. 85-HT-20, Presented at the National Heat Transfer Conf. Denver, Colorado, 1985.

Amano R. S., Bagherlee A., Smith R. J., Niess T. G., 1987, Turbulent Heat Transfer in Corrugated-Wall Channels With and Without Fins, J HEAT TRANSFER TRANS ASME, vol. 109, pp. 62-67.

Asako Y., Faghri M., 1985, Finite-Volume Solutions for Laminar Flow and Heat Transfer in a Corrugated Duct., NATIONAL HEAT TRANSFER CONF, Denver, Colorado, pp. 43-51.

Asako Y., Faghri M., 1987, Finite-Volume Solutions for Laminar Flow and Heat Transfer in a Corrugated Duct., J HEAT TRANSFER TRANS ASME, vol. 109, pp 627-634.

Asako Y., Nakamura H., Faghri M., Heat Transfer and Pressure Drop Characteristics in a Converging-Diverging Duct with Rounded Corners, HEAT TRANSFER JAPANESE RESEARCH, vol. 16, part 5, pp. 56-69.

Asako Y., Nakamura H., Faghri M., 1988, Heat Transfer and Pressure Drop Characteristics in a Corrugated Duct with Rounded Corners. INT J HEAT MASS TRANSFER, vol. 31, no. 6, pp 1237-1244.

Balzer W., Tschudi T., 1987, Combination of Heating and Temperature Measurement in a Compact Liquid Crystal Cell., J PHYS E SCI INSTRUM, vol. 20, no. 5, pp. 568-571.

Beecher D. T., Fagan T. J., 1987, Effects of Fin Pattern on the Air-Side Heat Transfer Coefficient in plate Finned-Tube Heat Exchangers. ASHRAE Annual Meeting, Nashville, Tenessee, June 27 - July 1, pp 1961-1984.

Beloborodov V. G., Volgin B. P., 1971, Heat Transfer and Pressure Drop in Heat Transfer Equipment with Slot Channels of Varying Cross Section., INTERNATIONAL CHEMICAL ENGINEERING, vol. 11, no. 2, pp. 229-233.

Benodekar R. W., Goddard A. J. H., Gosman A. D., Issa R. I., 1983, Numerical Prediction of Turbulent Flow Over Surface Mounted Ribs, ASME paper no. 83-FE-13.

Bergles A. E., 1969, Survey and Evaluation of Techniques to Augment Heat and Mass Transfer., Progress in Heat and Mass Transfer, vol 1, pp. 331-.

Bergles A. E., 1973, Recent Developments in Convective Heat Transfer Augmentation., APPLIED MECH REV, vol. 26, pp. 675-682.

Bergles A. E., Junkhan G. H., Bunn R. L., 1975, Performance Criteria for Cooling Systems on Agricultural and Industrial Machines., SAE paper no. 751187.

Bergles A. E., 1979, Augmentation of Forced-Convection Heat Transfer, Turbulent Forced Convection in Channels and Bundles, Theory and Applications to Heat Exchangers and Nuclear Reactors, eds. Kakac S., Spalding D. B., Hemisphere Publ. Corp., vol. 2, pp. 883-909.

Bohm J., 1955, KALTETECHNIK, part 12, pp. 358-362, (in German).

Brakell J. P., Cowell T. A., 1986, An Analysis of the Uniform Naphthalene Layer Mass Transfer Analogue Method Applied to Laminar Flow Over a Flat Plate, 8th International Heat Transfer Conference, San Fransisco, Vol. 2, pp. 495-499.

British Standard 1042, 1981, Methods of Measurement of FLUID FLOW IN CLOSED CONDUITS.

British Standard 2520, 1983, Barometer Conventions and Tables, Their Application and Use.

British Standard 4937 : Part 4, 1973, Nickel-chromium / Nickel-aluminium (chromel-alumel) Thermocouples - Type K. (revised 1981).

Butcher M. R., Button B. L., Wilcock D., Wright C. C., 1985, Verification of the liquid crystal/heater technique for heat transfer measurement in confined flows., The Institute of Mechanical Engineers Conference, Developments in Measurements and Instrumentation in Engineering, pp 139-144.

Button B. L., 1980, Jet Penetration of a Cooling Film., PhD Thesis, Coventry Polytechnic.

Button B. L., Tahmassebi N., 1984, Computer Programs for Transport and Thermodynamic Properties with Uncertainties, Coventry (Lanchester) Polytechnic, Mechanical Engineering Report ME. 492.

Chinnappa J. C. V., 1970, Free Convection in Air Between a 60° Vee-Corrugated Plate and a Flat Plate. INT J HEAT MASS TRANSFER, vol. 13 pp. 117-122.

Chow J. F. C., Soda K., 1973, Laminar Flow and Blood Oxygenation in Channels with Boundary Irregularities., J APPLIED MECHANICS TRANS ASME, vol. 95, pp. 843-850.

Cooper T. E., Field R. J., Meyer J. F., 1975, Liquid Crystal Thermography and its Application to the Study of Convective Heat Transfer, J HEAT TRANSFER TRANS ASME, vol. 107, pp. 442-450.

Davenport C. J., Beard R. A., Scott P. A. J., 1974, Optimization of

Vehicle Cooling Systems., SAE paper no. 740089.

Davenport C. J., 1983a, Heat Transfer and Flow Friction Characteristics of Louvred Heat Exchanger Surfaces., in Heat Exchangers Theory and Practice, eds. Taborek J., Hewitt G. F., Afgan N., pp. 397-412.

Davenport C. J., 1983b, Correlations for Heat Transfer and Flow Friction Characteristics of Louvred Fins, AIChE Symposium Series 225, vol. 79, pp. 19-27.

Davies T. W., Patrick M. A., A Simplified Method of Improving the Accuracy of Hot-Wire Anemometry., Fluid Dynamic Measurements in the Industrial and Medical Environments, Conference papers, edited by D. J. Cockrell, Leicester Univ. Press, vol. 1, pp. 152-155.

E.S.D.U. 68007, 1968, Forced Convection Heat Transfer in Circular Tubes., Part iii, Further Data for Turbulent Flow., I.Ch.E.

Faas S. E., McEligot D. M., 1980, Convective Heat Transfer for Ship Propulsion, Report no. 1248-7, Office of Naval Research, Aerospace and Mechanical Engineering Department.

Faghri M., Asako Y., 1987, Numerical Determination of Heat Transfer and Pressure Drop Characteristics for a Converging-Diverging Flow Channel., J HEAT TRANSFER TRANS ASME, vol. 109, pp. 606-612.

Focke W. W., 1983, Turbulent Convective Transfer in Plate Heat Exchangers, INT COMM HEAT MASS TRANSFER, vol. 10, pp. 201-210.

Focke W. W., Zachariades J., Oliver I., 1985, The Effect of the Corrugation Inclination Angle on the Thermohydraulic Performance of Plate Heat Exchangers., INT J HEAT MASS TRANSFER, vol. 28, no. 8, pp. 1469-1479.

Focke W. W., Knibbe P. G., 1986, Flow Visualization in Parallel-Plate Ducts with Corrugated Walls., J FLUID MECH, vol. 165, pp. 73-77.

Garg V. K., Maji P. K., 1988, Flow and Heat Transfer in a Sinusoidally Curved Channel., International Journal of Engineering Fluid Mechanics, vol. 1, no. 3, pp. 293-319.

Ghaddar N. K., Korczak K. Z., Mikic B. B., Patera A. T., 1986, Numerical Investigation of Incompressible Flow in Grooved Channels. Part 1. Stability and Self-Sustained Oscillations., J FLUID MECH, vol. 163, pp. 99-127.

Ghaddar N. K., Magen M., Mikic B. B., Patera A. T., 1986, Numerical Investigation of Incompressible Flow in Grooved Channels. Part 2, Resonance and Oscillatory Heat Transfer Enhancement., J FLUID MECH, vol. 168, pp. 541-567.

Gibson M. M., 1978, An Algebraic Stress and Heat-Flux Model for Turbulent Shear Flow with Streamline Curvature., INT J HEAT MASS TRANSFER, vol. 21, pp. 1609-1617.

Gibson M. M., Servat-Djoo K., 1989, Effect of a Short Region of High Convex Curvature on Heat Transfer through a Turbulent Boundary Layer., INT J HEAT FLUID FLOW, vol. 10, no. 1, pp. 75-82.

Ginstling A. M., 1959, KHIMICHESKOYE MASHINOSTROYENIYE, no. 6, pp. 20-22, (in Russian).

Gnielinski V., 1983, Forced Convection in Ducts. Heat Exchanger Design Handbook, Hemisphere Publ. Corp., 2.5.1.

Goldstein L. Jr., 1975 Local Mass Transfer in Corrugated-Walled Ducts and Heat Exchanger Configurations., Ph.D. Thesis, University of Minnesota.

Goldstein L. Jr., Sparrow E. M., 1976 a, Experiments on the Transfer Characteristics of a Corrugated Fin and Tube Heat Exchanger Configuration., J HEAT TRANSFER TRANS ASME, vol. 98, pp. 26-34.

Goldstein L. Jr., Sparrow E. M., 1976 b, Mass-Transfer Experiments on Secondary-Flow Vortices in a Corrugated Wall Channel., INT J HEAT MASS TRANSFER, vol 19, pp. 1337-1339.

Goldstein L. Jr., Sparrow E. M., 1977, Heat/Mass Transfer Characteristics for Flow in a Corrugated Wall Channel., J HEAT TRANSFER TRANS ASME, vol. 99, pp. 187-195.

Grosse-Wilde H., Uhlenbusch J., 1978, Measurement of Local Mass-Transfer Coefficients by Holographic Interferometry, INT J HEAT MASS TRANSFER, vol. 21, pp. 677-682.

Hasegawa E., Nagashima F., 1986, Heat Flux Across Viscous Flow in Wavy Channels., BULL JSME, vol. 29, no. 249, pp. 854-861.

Hosoda T., Uzuhashi H., Kobayashi N., 1977, Louver Fin Type Heat Exchangers., HEAT TRANSFER JAPANESE RESEARCH, vol. 6, pp. 69-77.

Ireland P. T., Jones T. V., 1985, The Measurement of Local Heat Transfer Coefficients in Blade Cooling Geometries., Agard Conference proceedings No. 390, Heat Transfer and Cooling in Gas Turbines, Bergen, Norway, 6-10th May.

Ireland P. T., Jones T. V., 1986, Detailed Measurements of Heat Transfer On and Around a Pedastal in Fully Developed Passage Flow. Eighth Int. Heat Transfer Conf., San Fransisco, California, pp. 975-980.

Ireland P. T., Jones T. V., 1987, The Response Time of a Surface Thermometer Employing Encapsulated Thermochromic Liquid Crystals., J PHYS E SCI INSTRUM, vol. 20, no. 10, pp. 1195-1199.

Irwin H. P. A. H., Arnot Smith P., 1975, Prediction of the Effect of Streamline Curvature on Turbulence., PHYS FLUIDS, vol. 18, no. 6, pp. 624-630.

Izumi R., Yamashita H., Oyakawa K., 1981, Fluid Flow and Heat Transfer in Corrugated Wall Channels. (1st Report, Analysis in the Case Where Channels are Bent Two Times). BULL JSME, vol. 24, no. 194, pp. 1425-1432.

Izumi R., Oyakawa K., Kaga S., Yamashita H., 1981, Fluid Flow and Heat Transfer in Corrugated Wall Channels. (2nd Report, Experiments in the Case Where Channels are Bent Two Times). BULL JSME, vol. 24, no. 198, pp. 2098-2106.

Izumi R., Yamashita H., Kaga S., Miyajima N., 1982, Fluid Flow and Heat Transfer in Corrugated Wall Channels - Experimental Study for Many Bends., Proceedings of the 19th JSME Symposium on Heat Transfer, paper no. A101.

Izumi R., Yamashita H., Oyakawa K., Mori N., 1983, Fluid Flow and Heat Transfer in Corrugated Wall Channels. (3rd Report, Effects of Bending Angles in the Case Where Channels are Bent Two Times). BULL JSME, vol. 26, no. 216, pp. 1027-1035.

Izumi R., Yamashita H., Oyakawa K., 1983, Fluid Flow and Heat Transfer in Corrugated Wall Channels. (4th Report, Analysis in the Case Where Channels are Bent Many Times). BULL JSME, vol. 26, no. 217, pp. 1146-1153.

Jambunathan K., Edwards R. J., Button B. L., 1987, Convective Heat Transfer Coefficients: The Colour Change Paint Technique., APPL ENERGY, vol. 28, no. 2, pp. 137-152.

Jones T. V., Russell C. M. B., 1981, Local Heat Transfer Coefficients on Finned Tubes., ASME Winter Annual Meeting, REGENERATIVE AND RECUPERATIVE HEAT EXCHANGERS, HTD vol. 21, pp 17-25.

Junkhan G. H., Serovy G. K., 1967, Effects of Free-Stream Turbulence and Pressure Gradient on Flat-Plate Boundary-Layer Velocity Profiles and on Heat Transfer. J HEAT TRANSFER TRANS ASME, vol. 89, pp. 169-176.

Kang I. S., Chang H. N., 1982, The Effect of Turbulence Promoters on Mass Transfer - Numerical Analysis and Flow Visualization, INT J HEAT MASS TRANSFER, vol. 25 no. 8 pp 1167-1181.

Kapur D. N., Macleod N., 1974, The Determination of Local Mass-Transfer Coefficients by Holographic Interferometry, INT J HEAT MASS TRANSFER, vol. 17, pp. 1151-1162.

Kays W. M., London A. L., 1984, Compact Heat Exchangers, Third edition, McGraw-Hill.

Kays W. M., 1950, Loss Coefficients for Abrupt Changes in Flow Cross Section with Low Reynolds Number Flow in Single and Multiple Tube Systems., TRANS ASME, vol. 72, pp. 1067-1074.

Kays W. M., 1960, The Basic Heat Transfer and Flow Friction Characteristics of Six Compact High-Performance Heat Transfer

Surfaces., J ENG POWER TRANS ASME, vol. 82, pp. 27-34.

Kelly R. E., Pal D., 1978, Thermal Convection with Spatially Periodic Boundary Conditions., J FLUID MECH, vol. 86, pp. 433-456.

Kern D. Q., Kraus A. D., 1972, Extended Surface Heat Transfer. Mcgraw Hill, New York, pp. 26-29.

Kidd C. T., 1987, Lateral Heat Conduction Effects on Heat Transfer Measurements with the Thin Skin technique., ISA TRANSACTIONS, vol. 26, part 3, pp 7-18.

Konno H., 1967, Fundamental Studies on the Heat Transfer Characteristics of a Plate Type Heat Exchanger., Kagaku Kogaku, vol. 31, no. 9, pp. 872-877. National Translation centre 72-10433.

Konno H., 1968, Studies on the Heat Transfer Coefficient and Pressure Drop of Several Kinds of Plate Heat Exchangers, Kagaku Kogaku, vol. 32, no. 11, 1127-1132. National Translation Centre 72-10431.

Kovalenko L. M., 1961, KHIMICHESKOYE MASHINOSTROYENIYE, no. 2, pp. 14-16, (in Russian).

Kovalenko L. M., 1962, A Study of Convective Heat Transfer in Winding Slit Channels, TEPLOENERGETICA, no.2, pp. 77-79, Unedited rough draft translation, FTD-TT-62-1175/1+2+4.

Launder B. E., Priddin C. H., Sharma B. I., 1977, The Calculation of Turbulent Boundary Layers on Spinning and Curved Surfaces., J FLUIDS ENG TRANS ASME, vol. 99, pp. 231-239.

Leschziner M. A., Rodi W., 1981, Calculation of Annular and Twin Parallel Jets Using Various Discretization Schemes and Turbulence Model Variations., J FLUIDS ENG TRANS ASME, vol. 103, pp 352-360.

Lightfoot R. B., 1987, private communication. Staircase wall momentum relaxation switch (LOGIC(92)).

Maltson J. D., Wilcock D., 1987, Laminar Flow and Heat Transfer in Corrugated (Rippled) Ducts., PROC 2nd INT PHOENICS USER CONF, 23rd-25th November, London, published by CHAM Ltd.

Maltson J. D., Wilcock D., Davenport C. J., 1989, Comparative Performance of Rippled Fin Plate Fin and Tube Heat Exchangers., J HEAT TRANSFER TRANS ASME, vol. 111, pp. 21-28.

Mandel S. W., Townsend M. A., Parrish T. F. Jr., 1979, Optimal Fin-Side Design of Compact Tube-in-Fin Heat Exchangers with Rippled Fins. J HEAT TRANSFER TRANS ASME, vol. 101, pp. 514-520.

Maubourguet-Pellerin M. M., Pellerin F., 1987, Evaluation of Mean Heat Transfer Coefficient in Periodically Corrugated Channels. NUMER HEAT TRANSFER, vol. 11, pp. 213-227.

McAdams W. H., 1954, Heat Transmission, 3rd ed., McGraw-Hill, New York.

McCormack P. D., Welker H., Kelleher M., 1970, Taylor-Goertler

Vortices and Their Effect on Heat Transfer. J HEAT TRANSFER TRANS ASME, vol. 92, pp. 101-112.

Metzger D. E., Larson D. E., 1986, Use of Melting Point Surface Coatings for Local Convection Heat Transfer Measurements in Rectangular Channel Flows with 90-Deg Turns., J HEAT TRANSFER TRANS ASME, vol. 108, pp. 48-54.

Molki M., 1986, Heat Transfer Characteristics of Corrugated Ducts with Variable Corrugation Angle., 8th INT HEAT TRANSFER CONF, San Fransisco, California., vol. 6, pp. 2879-2884.

Molki M., Yuen C. M., 1986, Effect of Interwall Spacing on Heat Transfer and Pressure Drop in a Corrugated-Wall Duct., INT J HEAT MASS TRANSFER, vol. 29, no. 7, pp. 987-997.

Nakayama A., Koyama H., 1985, Separated Flows in Three Dimensional Ducts with Wavy Surfaces., NIPPON GAKKAI RONBUNSHU BHEN, vol. 51, part 468, pp. 2720-2727.

Neal S. B. H. C., 1975, The Development of the Thin-Film Naphthalene Mass-Transfer Analogue Technique for the Direct Measurement of Heat Transfer Coefficients., INT J HEAT MASS TRANSFER, vol. 18, pp. 559-567.

Nishimura T., Ohori Y., Kajimoto Y., Kawamura Y., 1985, Mass Transfer Characteristics in a Channel with Symmetric Wavy Wall for Steady Flow. J CHEMICAL ENGINEERING JAPAN, vol.18, no. 6, pp. 550-555.

Nishimura T., Kajimoto Y., Tarumoto A., Kawamura Y., 1986, Flow Structure and Mass Transfer for a Wavy Channel in Transitional Flow Regime., J CHEMICAL ENGINEERING JAPAN, vol. 19, no. 5, pp. 449-455.

Nishimura T., Kajimoto Y., Kawamura Y., 1986, Mass Transfer Enhancement in Channels with a Wavy Wall., J CHEMICAL ENGINEERING JAPAN, vol. 19, no. 2, pp. 142-144.

Nishimura T., Tarumoto A., Kawamura Y., 1987, Flow and Mass Transfer Characteristics in Wavy Channels for Oscillatory Flow., INT J HEAT MASS TRANSFER, vol. 30, no. 5, pp. 1007-1015.

Nishimura T., Yoshino T., Kawamura Y., 1987, Instability of Flow in a Sinusoidal Wavy Channel with Narrow Spacing., J CHEMICAL ENGINEERING JAPAN, vol. 20, no. 1, pp. 102-103.

Norris R. H., Spofford W. A., 1942, High-Performance Fins for Heat Transfer, TRANS ASME, vol. 64, pp. 489-496.

O'Brien J. E., 1981, Corrugated-Duct Heat Transfer, Pressure Drop and Flow Visualisation., Ph.D. Thesis, University of Minnesota.

O'Brien J. E., Sparrow E. M., 1982, Corrugated-Duct Heat Transfer, Pressure Drop, and Flow Visualization., J HEAT TRANSFER TRANS ASME, vol. 104, pp. 410-416.

Okada K., Ono M., Tomimura T., Konno H., Ohtani S., 1970, KAGAKU KOGAKU, vol. 34, no. 1, pp. 93-95, (in Japanese).

Okada K., Ono M., Tomimura T., Okuma T. S., Konno H., Ohtani S., 1972, Design and Heat Transfer Characteristics of New Plate Heat Exchanger., HEAT TRANSFER JAPANESE RESEARCH, vol. 1 no. 1, pp. 90-95.

Ostendorf W., Mayinger F., Mewes D., 1986, A Tomographical Method using Interferometry for the Registration of Three-Dimensional Unsteady Temperature Profiles in Laminar and Turbulent Flow., Eighth Int. Heat Transfer Conf., San Fransisco, vol. 2, pp. 519-524.

Pletcher R. H., 1988, Progress in Turbulent Forced Convection, J HEAT TRANSFER TRANS ASME, vol. 110, pp. 1129-1144.

Raithby G. D., Hollands K. G. T., 1985, Natural Convection, Handbook of Heat Transfer Fundamentals, Rohsenow, Hartnett and Ganic eds., McGraw-Hill, New York, chapter 6.

Ralph M. E., 1987, Steady Flow Structures and Pressure Drops in Wavy-Walled Tubes. J FLUIDS ENG TRANS ASME, vol. 109, pp. 225-261.

Rogers G. F. C., Mayhew Y. R., 1980, Thermodynamic and Transport Properties of Fluids - S. I. Units, 3rd ed., Oxford Basil Blackwell.

Rosten H. I., Spalding D. B., Tatchell D. G., 1983, CHAM TR/75 PHOENICS INSTRUCTION MANUAL, Concentration Heat and Momentum Limited.

Savostin A. F., Tikhonov A. M., 1970, Investigation of the Characteristics of Plate-Type Heating Surfaces, THERMAL ENGINEERING, VOL. 17, no. 9, pp. 113-117. (Translated from TEPLOENERGETIKA, vol. 17, no. 7, pp. 75-78).

Shah R. K., 1978, Compact Heat Exchanger Surface Selection Methods, Sixth International Heat Transfer Conference, Toronto, vol. 4, pp. 193-199.

Sherwin K., 1981, The Performance of Finned Tubes with Helically Wound Corrugated Fins., ASME Winter Annual Meeting, REGENERATIVE AND RECUPERATIVE HEAT EXCHANGERS, HTD vol. 21, pp 11-16.

Siegel R., Sparrow E. M., 1959, Transient Heat Transfer for Laminar Forced Convection in the Thermal Entrance Region of Flat Ducts., J HEAT TRANSFER TRANS ASME, vol. 71, pp. 29-36.

Simonich J. C., Moffat R. J., 1984, Liquid Crystal Visualization of Surface Heat Transfer on a Concavely Curved Turbulent Boundary Layer., J ENG GAS TURBINES POWER TRANS ASME, vol. 106, pp. 619-627.

Simonson J. R., 1975, Engineering Heat Transfer, Macmillan Publ. Ltd., reprinted 1984.

Sparrow E. M., Comb. J. W., 1983, Effect of Interwall Spacing and Fluid Flow Inlet Conditions on a Corrugated-Wall Heat Exchanger., INT J HEAT MASS TRANSFER, vol. 26, no. 7, pp. 993-1005.

Sparrow E. M., Hossfeld L. M., 1984, Effect of Rounding of Protruding Edges on Heat Transfer and Pressure Drop in a Duct., INT J HEAT MASS TRANSFER, vol. 27, no. 10, pp. 1715-1723.

Sucec J., 1985, Heat Transfer, William C. Brown Publishers.

Sugawara S., Sato T., Komatsu H., Osaka H., 1988, Effect of Free Stream Turbulence on Flat Plate Heat Transfer., INT J HEAT MASS TRANSFER, vol. 31, no. 1, pp. 5-12, reprinted and translated from the earlier 1953 publication.

Sukomel A. S., Velichko V. I., Abrosimov Yu. G., Gutsev D. F., 1975, An Investigation Of Heat Transfer in the Entry Section of a Rectangular Duct. THERMAL ENGINEERING, vol. 22, no. 3, pp. 99-103, (translated from TEPLOENERGETICA, pp. 81-83).

Vajravelu K., 1980, Fluid Flow and Heat Transfer in Horizontal Wavy Channels, ACTA MECH, vol. 35, pp. 245-258.

Webb B. W., Ramadhyani S., 1985, Conjugate Heat Transfer in a Channel With Staggered Ribs., INT J HEAT MASS TRANSFER, vol. 28, no. 9, pp. 1679-1687.

Wilcock D., 1983, Multijet Impingement Heat Exchanger Modules., PhD Thesis, Coventry Polytechnic.

Xiao Q., Xin R. C., Tao W. Q., 1989, Analysis of Fully Developed Laminar Flow and Heat Transfer in Asymmetric Wavy Channels, INT COMM HEAT MASS TRANSFER, vol. 16, pp. 227-236.

Xin R. C., Tao W. Q., 1988, Numerical Prediction of Laminar flow and Heat Transfer in Wavy Channels of Uniform Cross-Sectional Area., NUMER HEAT TRANSFER, vol. 14, pp. 465-481.

Yastrebenetskiy A. R., Kovalenko L. M., 1959, KHIMICHESKOYE MASHINOSTROYENIYE, no. 2, pp. 29-31.

Zozulya N. V., Khavin A. A., Kalinin B. L., 1975, Effect of Fin Deformation on Heat Transfer and Drag in Bundles of Oval Tubes with Transverse Fins., HEAT TRANSFER SOV RES, vol. 7, no. 2, pp. 95-98.

BIBLIOGRAPHY

Adarkar D. B.,, Kays W. M., 1963, Heat Transfer in Wakes, Technical Report no. 55, Dept. Mech. Eng., Stanford University.

Ashton G., Kennedy J. F., 1972, Ripples on the Underside of River Ice Covers., J HYDRAULICS DIVISION, PROC. AMERICAN SOCIETY OF CIVIL ENGINEERS, vol. 98, pp. 1603-1624.

Bacher E. V., Smith C. R., 1986, Turbulent Boundary Layer Modification by Surface Riblets., vol. 24, no. 8, pp. 1382-1385.

Balfour A., Marwick D. H., 1979, Programming in Standard FORTRAN77,

Heinemann Educational Books Ltd., reprinted 1985.

Bradshaw P., Pankhurst R. C., 1964, The Design of Low-Speed Wind Tunnels., PROG AEROSPACE SCI, vol. 5, pp. 1-69.

Button B. L., Tura R. A., Wright C. C., 1984, Investigation of the Airflow Through Louvred Rectangular Ducts using Laser Doppler Anemometry., 2nd International Symposium on Applications of Laser Anemometry to Fluid Mechanics, Lisbon, Portugal, 2nd-4th July.

Crane R. I., Sabzvari J., 1989, Heat Transfer Visualisation and Measurement in Unstable Concave Wall Laminar Boundary Layers., J TURBOMACHINERY TRANS ASME, vol. 111, no. 1, pp. 51-56.

Eckert E. R. G., Goldstein R. J., Pfender E., Ibele W. E., Patankar S. V., Ramsey J. W., Simon T. W., Decker N. A., Kuehn T. H., Lee H., Girshick S. L., 1988, Heat Transfer - A Review of 1987 Literature., INT J HEAT MASS TRANSFER, vol. 31, no. 12, pp. 2401-2488.

Garg V. K., Maji P. K., 1988, Laminar Flow and Heat Transfer in a Periodically Converging-Diverging Channel., INT J NUMER METHODS FLUIDS, vol. 8., pp. 579-597.

Gerrard J. H., 1978, The Wakes of Bluff Bodies at Low Reynolds Numbers., Philosophical Transactions of The Royal Society of London, Series A, mathematical and physical sciences, vol. 228, no. 1354, pp. 351-382.

Gibbings J. C., 1970, Thermomechanics, Pergamon Press Ltd.

Greiner M., 1986, Experimental Investigation of Resonance and Heat Transfer Enhancement in Grooved Channels., Ph.D. Thesis, Massachusetts Institute of Technology.

Karvinen R., 1988, Transient Conjugate Heat Transfer to Laminar Flow in a Tube or Channel., INT J HEAT MASS TRANSFER, vol. 31, no. 6, pp. 1326-1328.

Kurosaka M., Sundaram P., 1986, Illustrative Examples of Streaklines in unsteady vortices : Interpretational difficulties revisited., PHYS FLUIDS, vol. 29, no. 10, pp. 3474-3477.

Liang C. Y., Wen-Jei Yang, 1975, Heat Transfer and Friction Loss Performance of Perforated Heat Exchanger Surfaces., J HEAT TRANSFER TRANS ASME, vol. 97, pp. 9-15.

Lilley G. M., 1983, Vortices and Turbulence., AERONAUT J, Dec., pp. 371-393.

Martin B. W., Brown A., 1979, Factors Influencing Heat Transfer to the Pressure Surfaces of Gas Turbine Blades., INT J HEAT FLUID FLOW, vol. 1, no. 3, pp. 107-114.

Massey B. S., 1968, Mechanics of Fluids, Van Nostrand Reinhold Company Ltd., 4th ed. 1979.

Patankar S. V., 1988, Recent Developments in Computational Heat Transfer., J HEAT TRANSFER TRANS ASME, vol. 110, pp. 1037-1045.

Shah R. K., London A. L., 1971, Laminar Flow Forced Convection Heat Transfer and Flow Friction in Straight and Curved Ducts - A Summary of Analytical Solutions., Technical Report No. 75, Dept. Mech. Eng., Stanford University, California.

Shah R. K., Webb R. L., 19 , Compact and Enhanced Heat Exchangers., in Heat Exchangers Theory and Practice, eds. Taborek J., Hewitt G. F., Afgan N., Hemisphere Publ. Corp., pp. 425-468.

Shapiro A. H., 1961, Shape and Flow, The Fluid Dynamics of Drag., Heinemann Educational Books Ltd., Reprinted 1981.

Sobey I. J., 1980, On Flow through Furrowed Channels., Part 1. Calculated Flow Patterns., J FLUID MECH, vol. 96, pp. 1-26.

Sparrow E. M., 1977, Heat Transfer in Complex Duct Flows., ASME paper no. 77-HT-95.

Sparrow E. M., Cur N., 1982, Turbulent Heat Transfer in a Symmetrically or Asymmetrically Heated Flat Rectangular Duct with Flow Separation at Inlet., J HEAT TRANSFER TRANS ASME, vol. 104, pp. 82-89.

Weaver D. S., Abd-Rabbo A., 1985, A Flow Visualisation Study of a Square Array of Tubes in Water Crossflow, Trans ASME J HEAT TRANSFER, vol. 107, pp. 354-363.

Wilkie D., 1985, The Correlation of Engineering Data Reconsidered., INT J HEAT FLUID FLOW, vol. 6, no. 2, pp. 99-103.
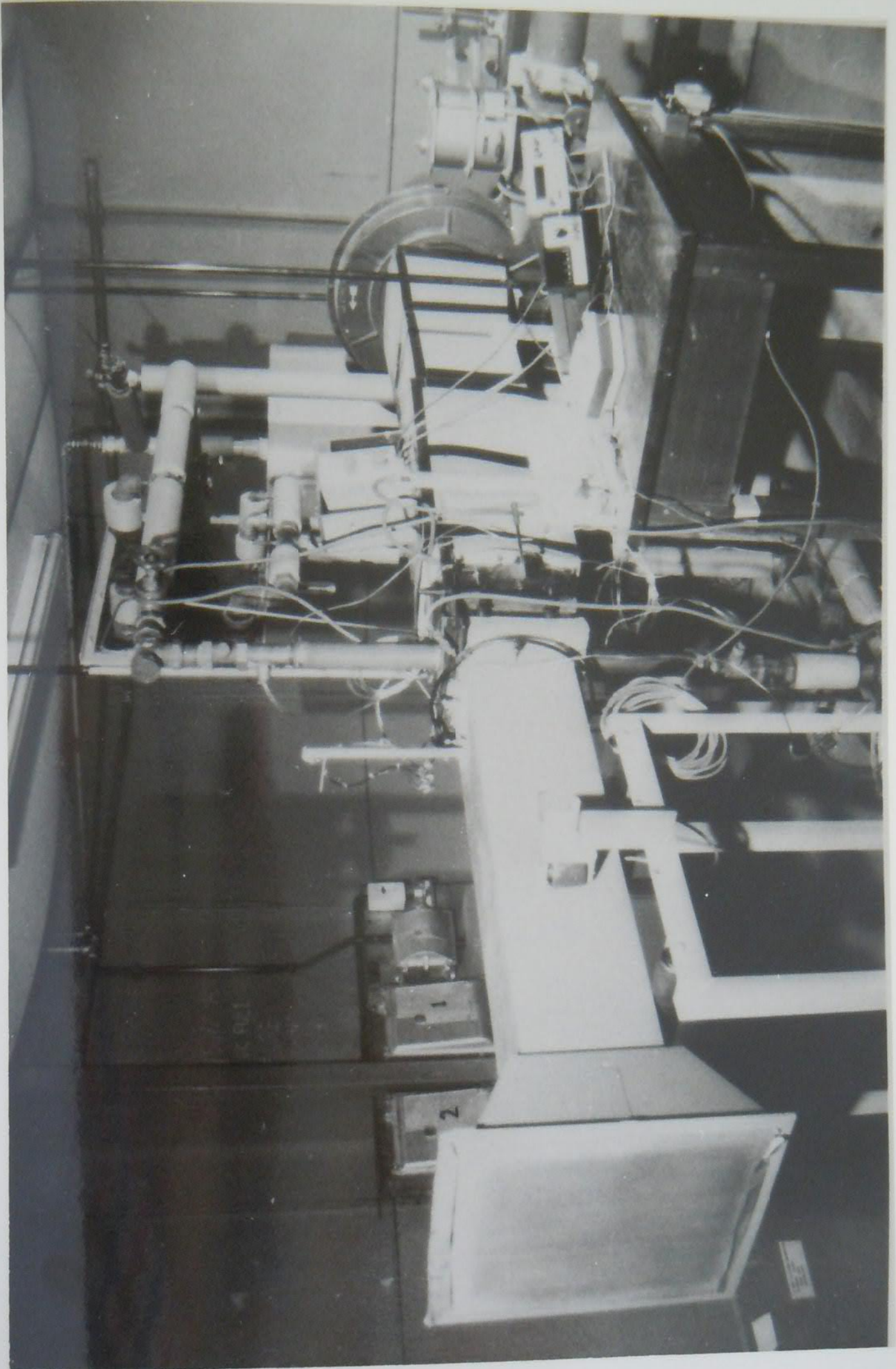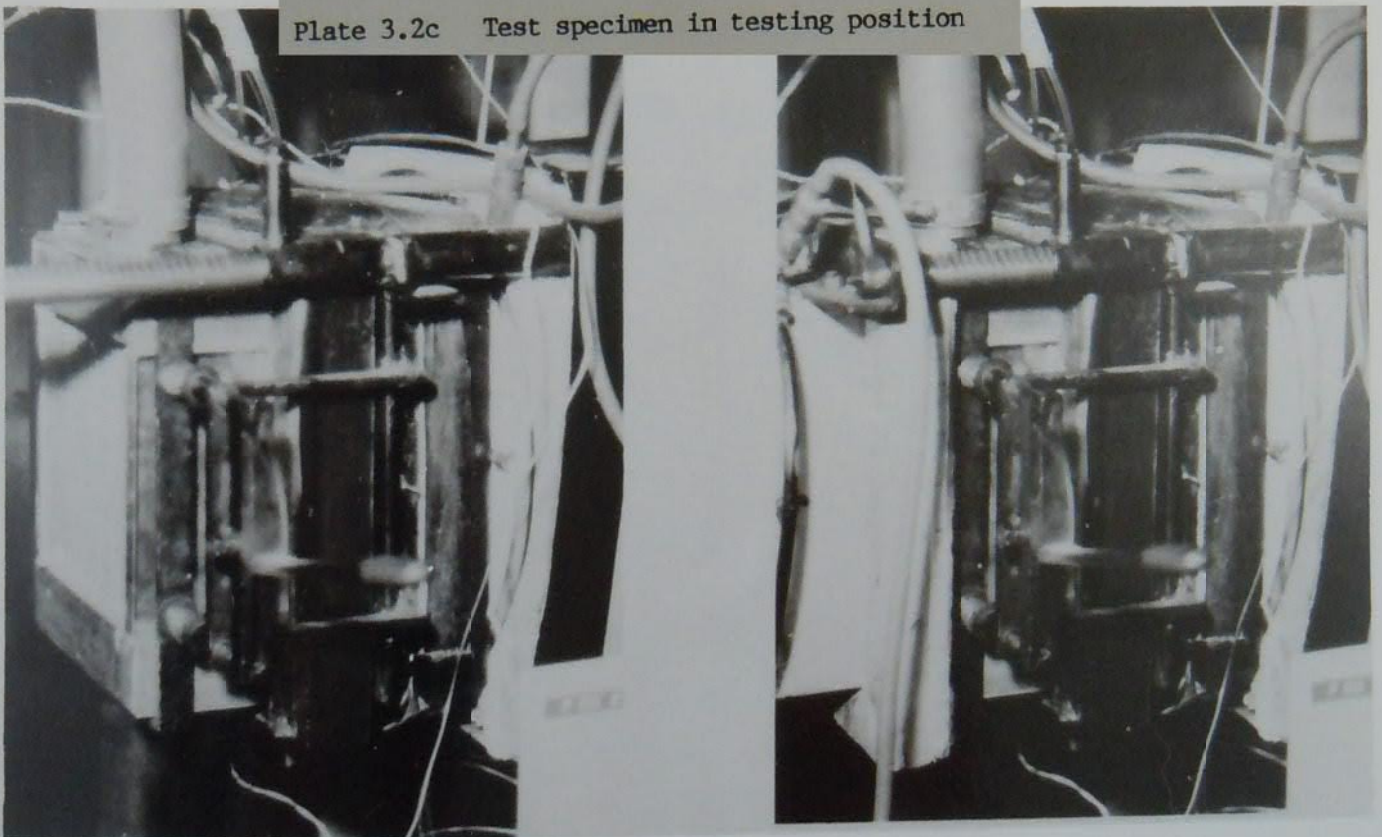
Plate 3.1   The Conrad Heat Transfer thermal wind tunnel

Plate 3.2a   Typical heat exchanger sample

Plate 3.2b   Test specimen in clamping mechanism

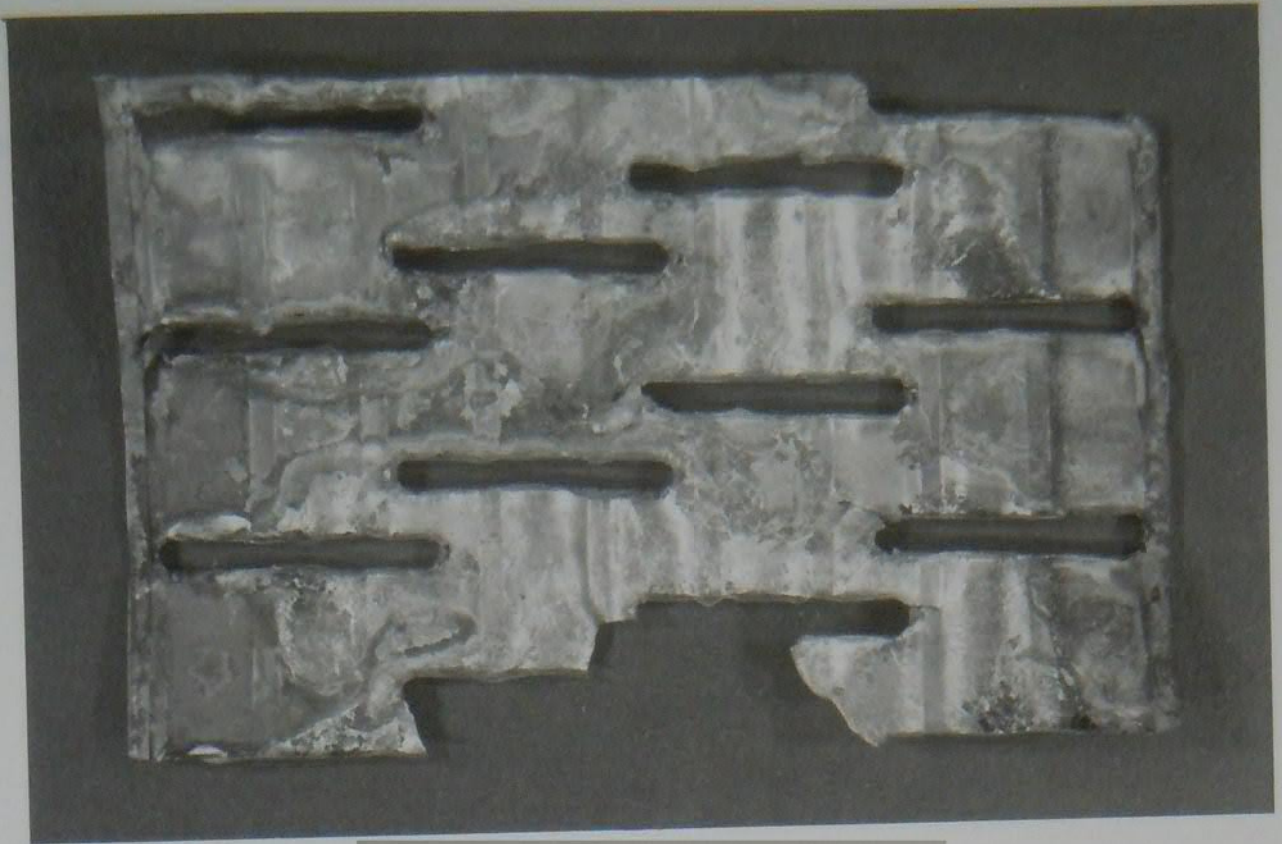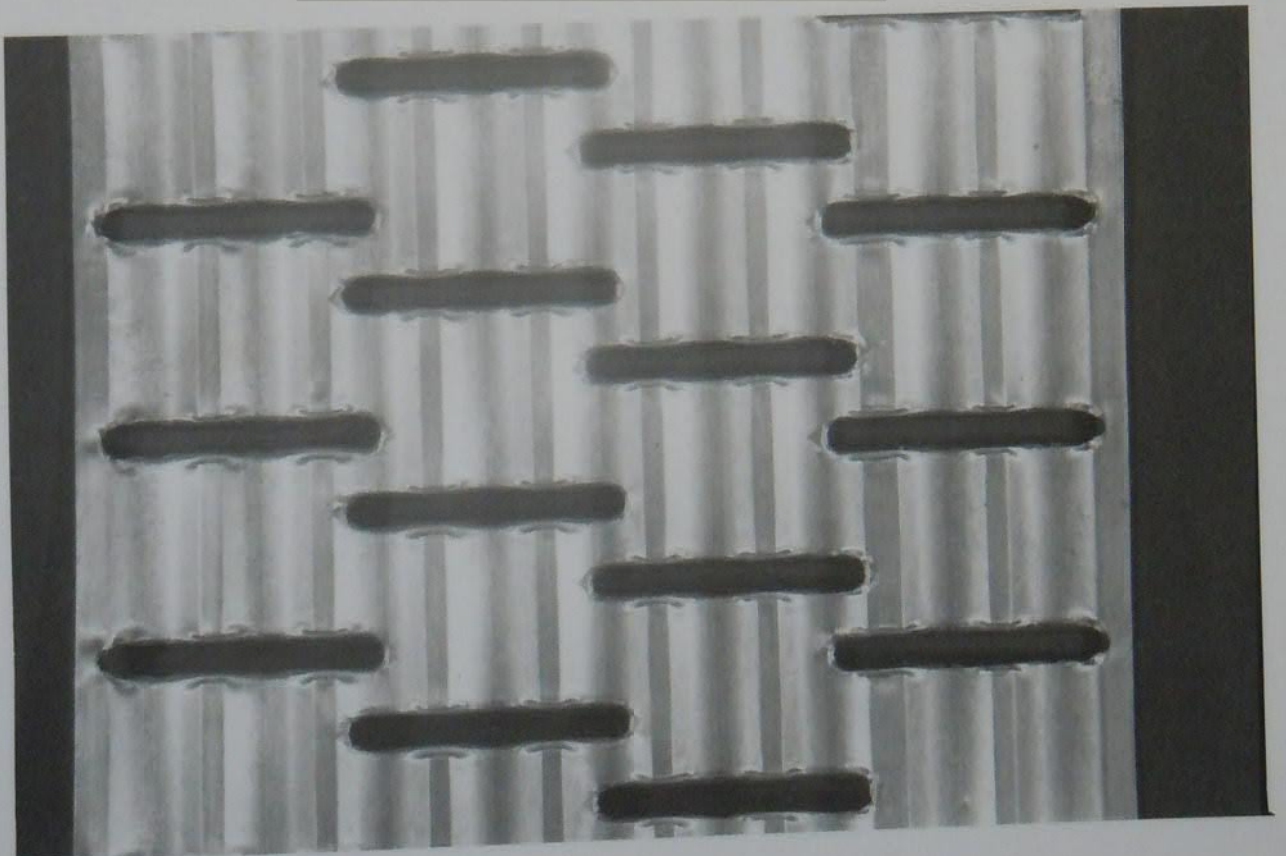Plate 3.2c   Test specimen in testing position

Plate 3.3a   Plate fin profile A
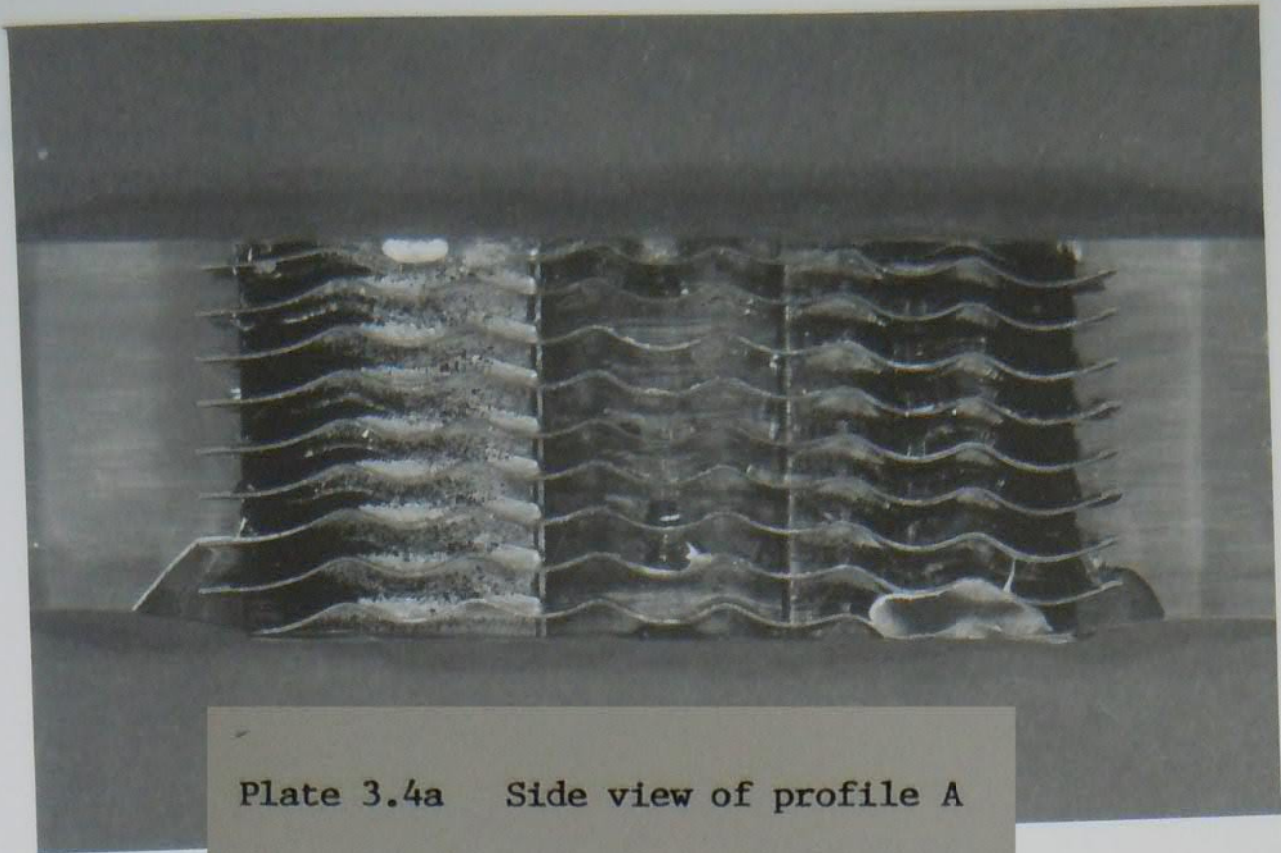
Plate 3.3b   Plate fin profile B
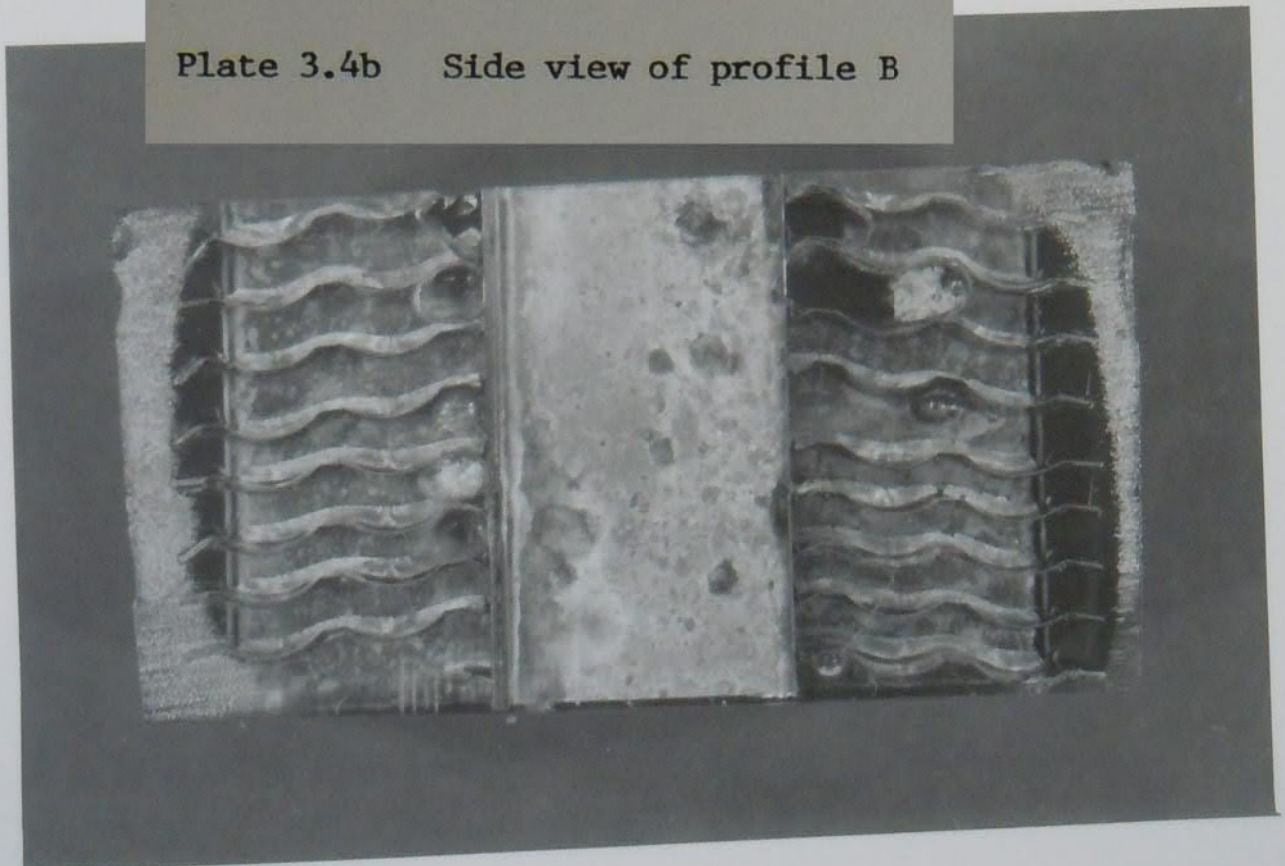
Plate 3.4a   Side view of profile A

Plate 3.4b   Side view of profile B
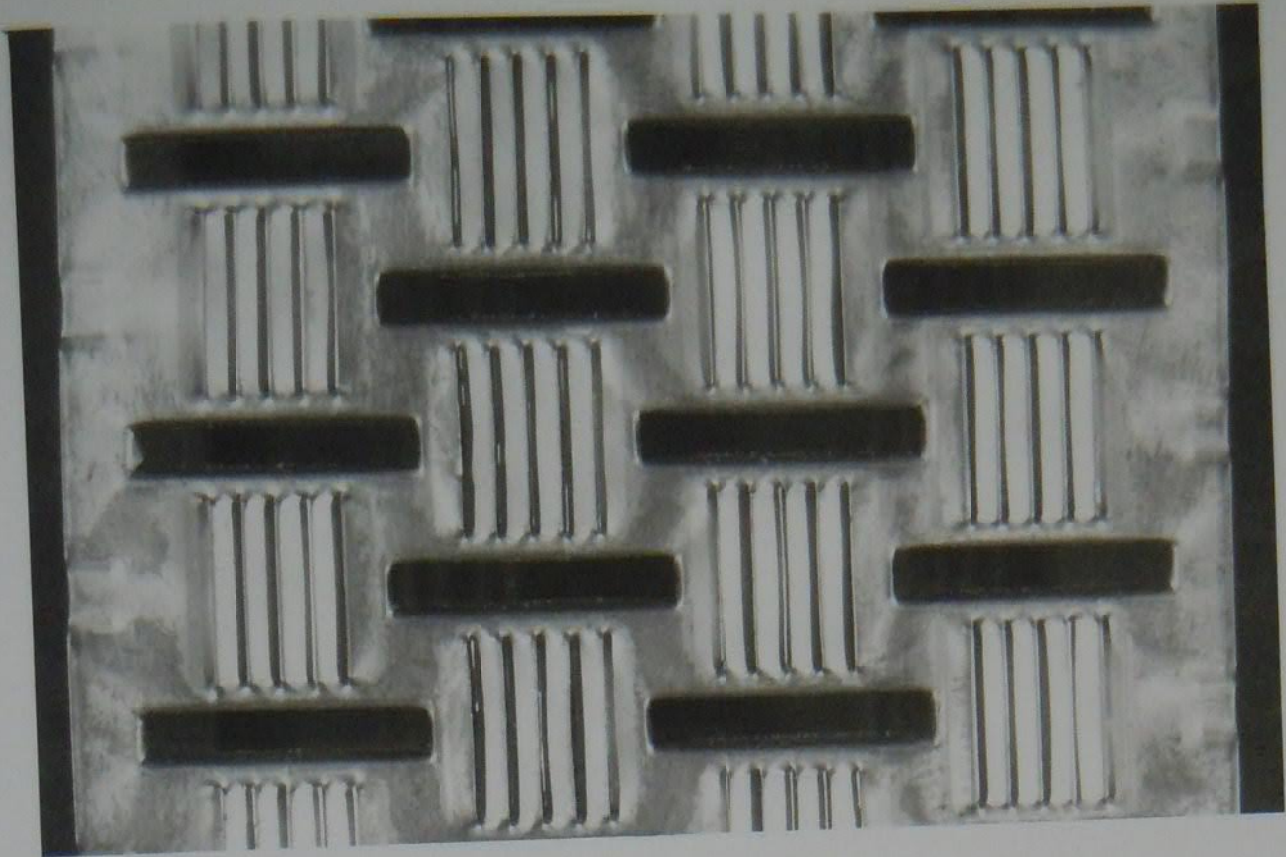
Plate 3.5   Typical louvred plate fin
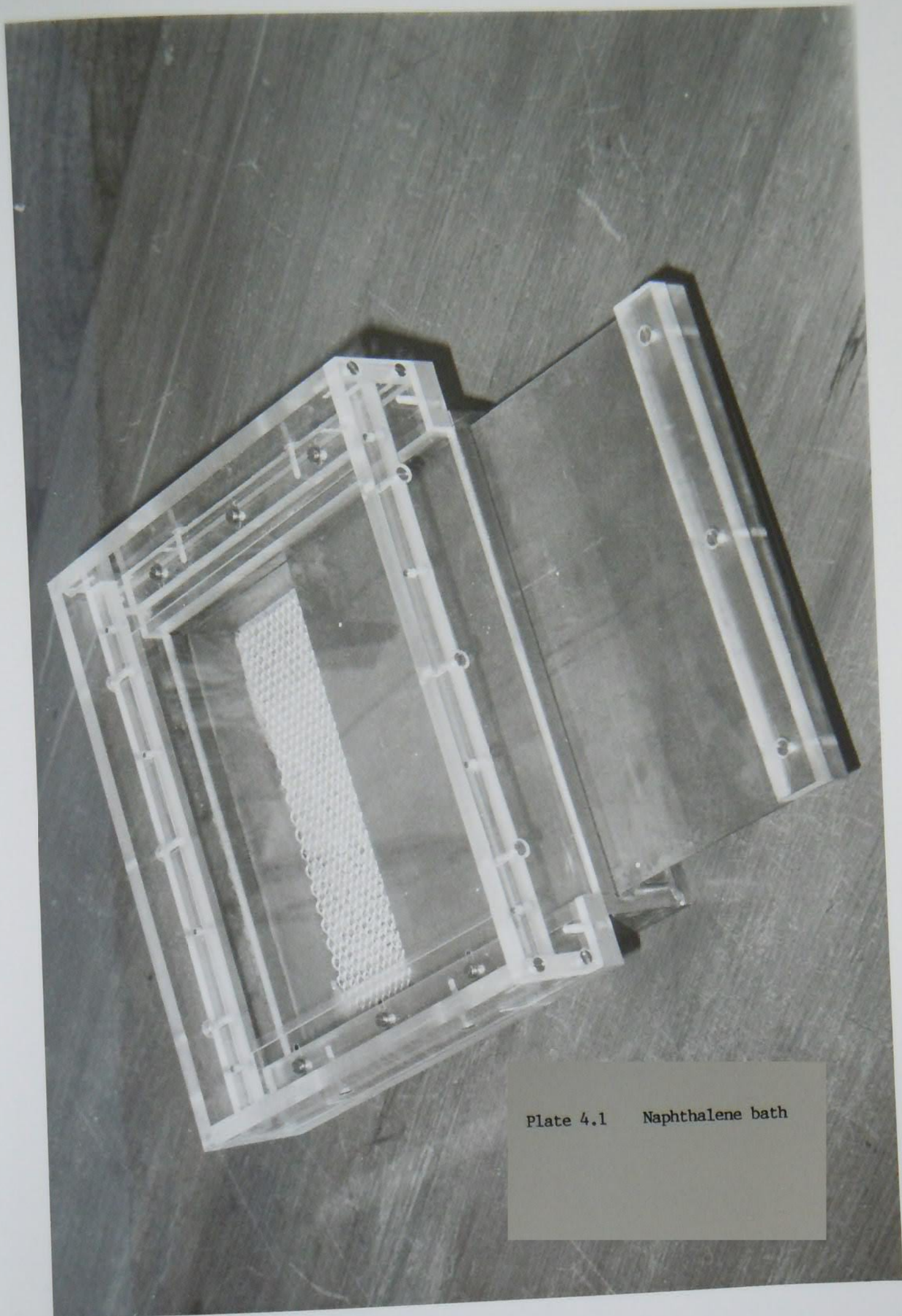
Plate 4.1   Naphthalene bath
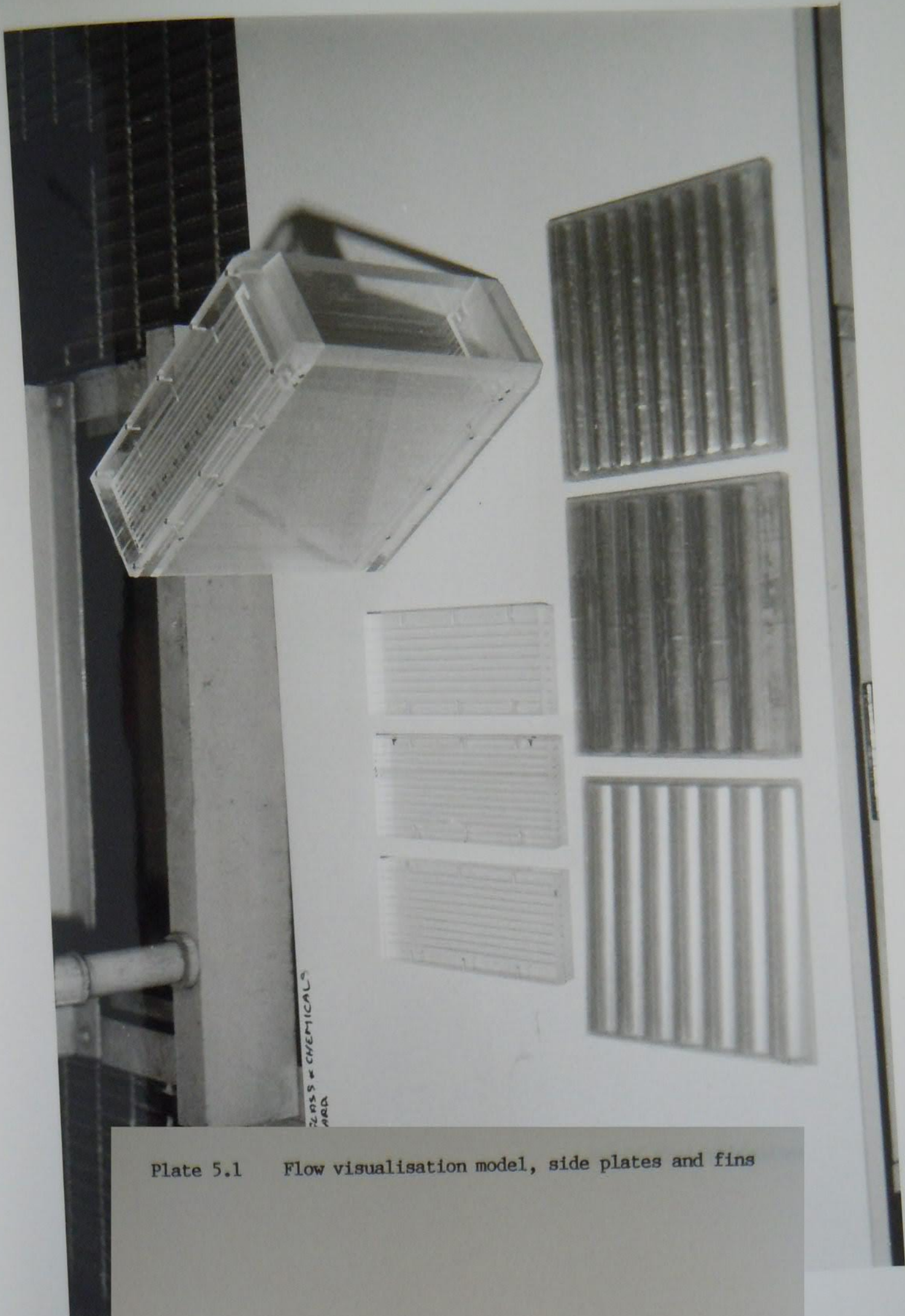
Plate 5.1   Flow visualisation model, side plates and fins

Plate 5.2   Water channel
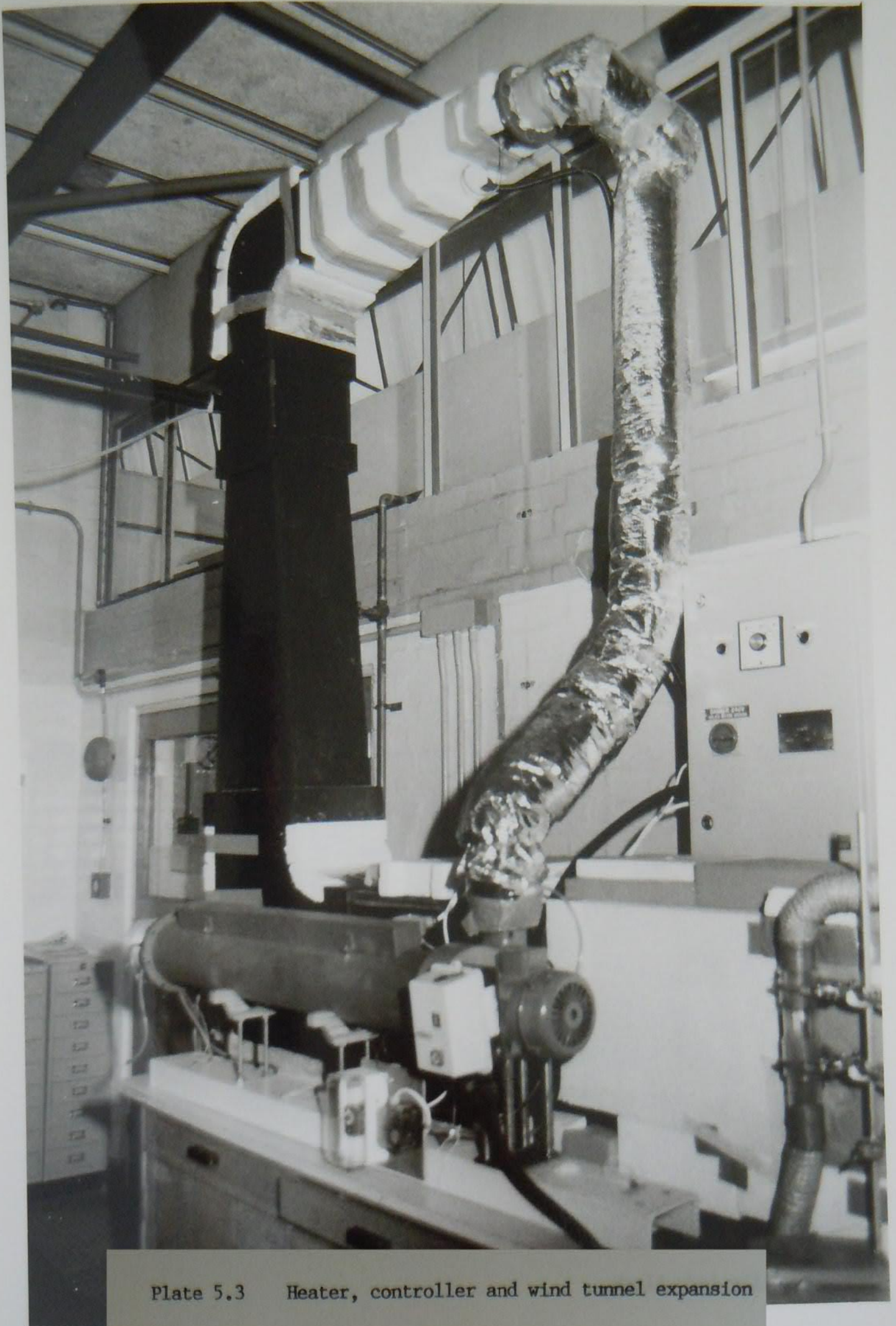
Plate 5.3   Heater, controller and wind tunnel expansion

Plate 5.4   Wind tunnel contraction and rippled duct test section
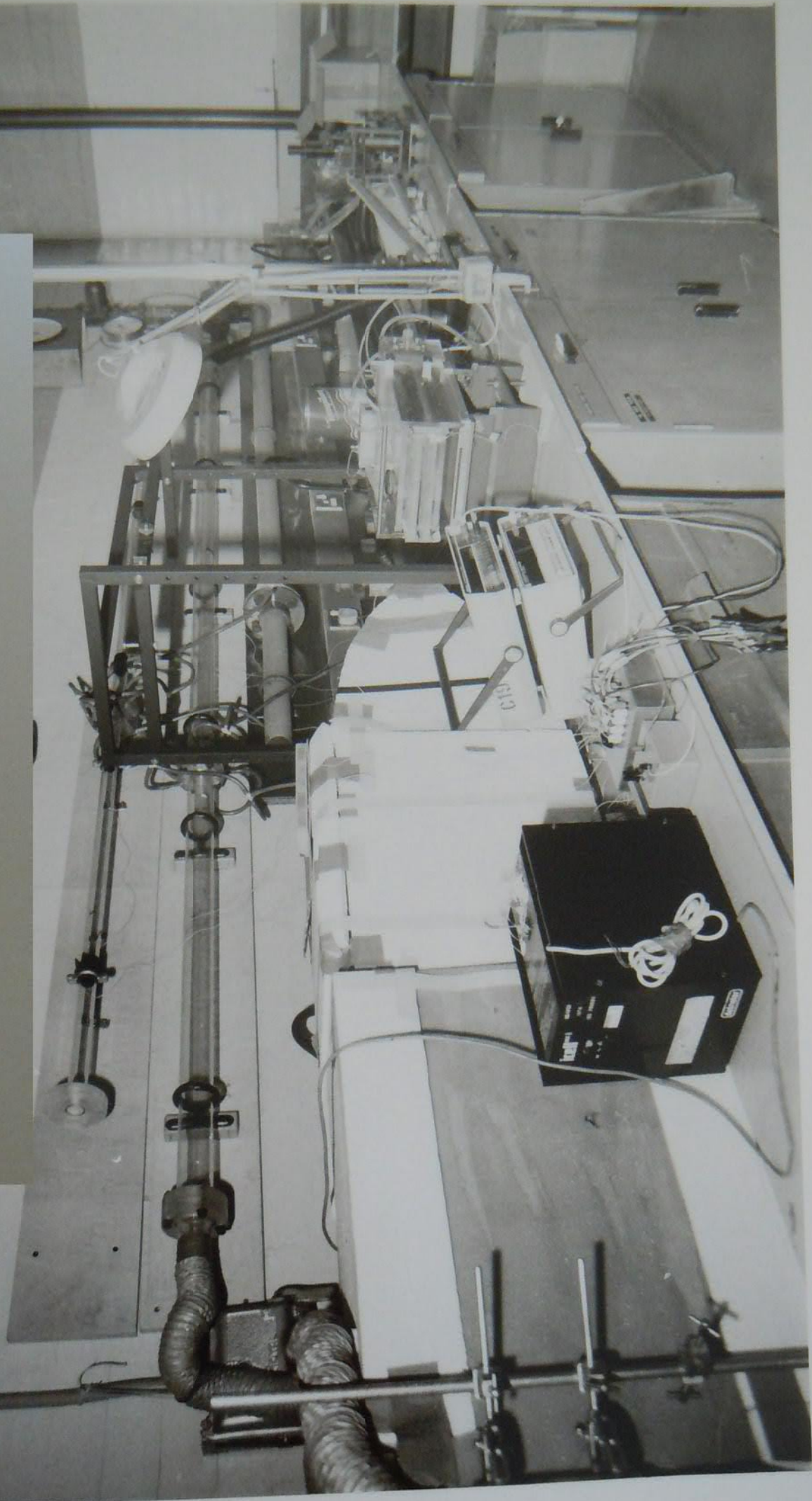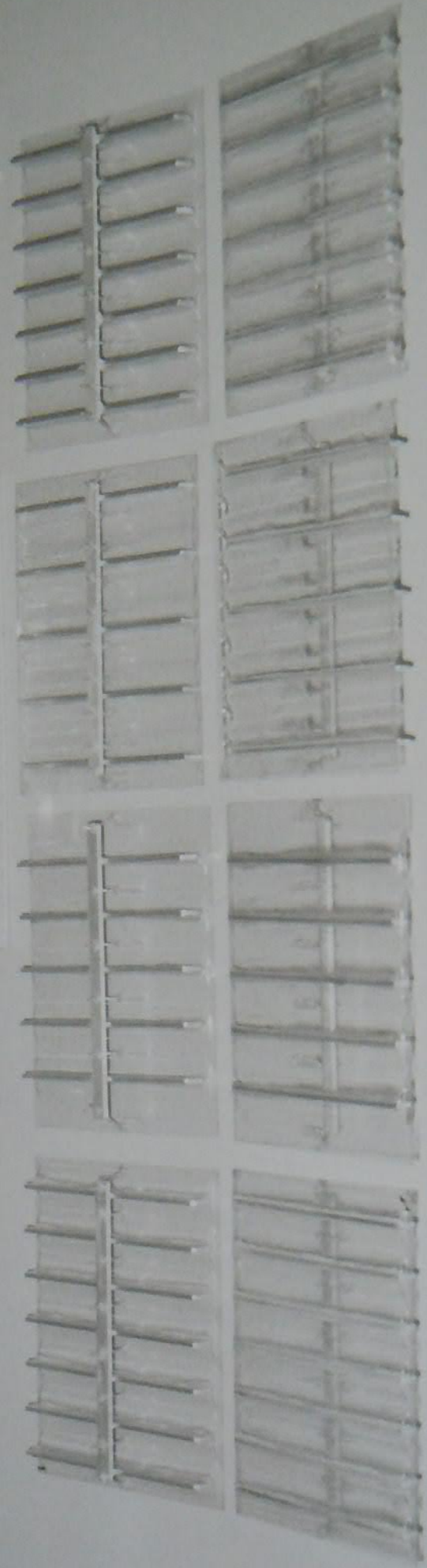
Plate 5.5   Fins with pressure tappings mounted
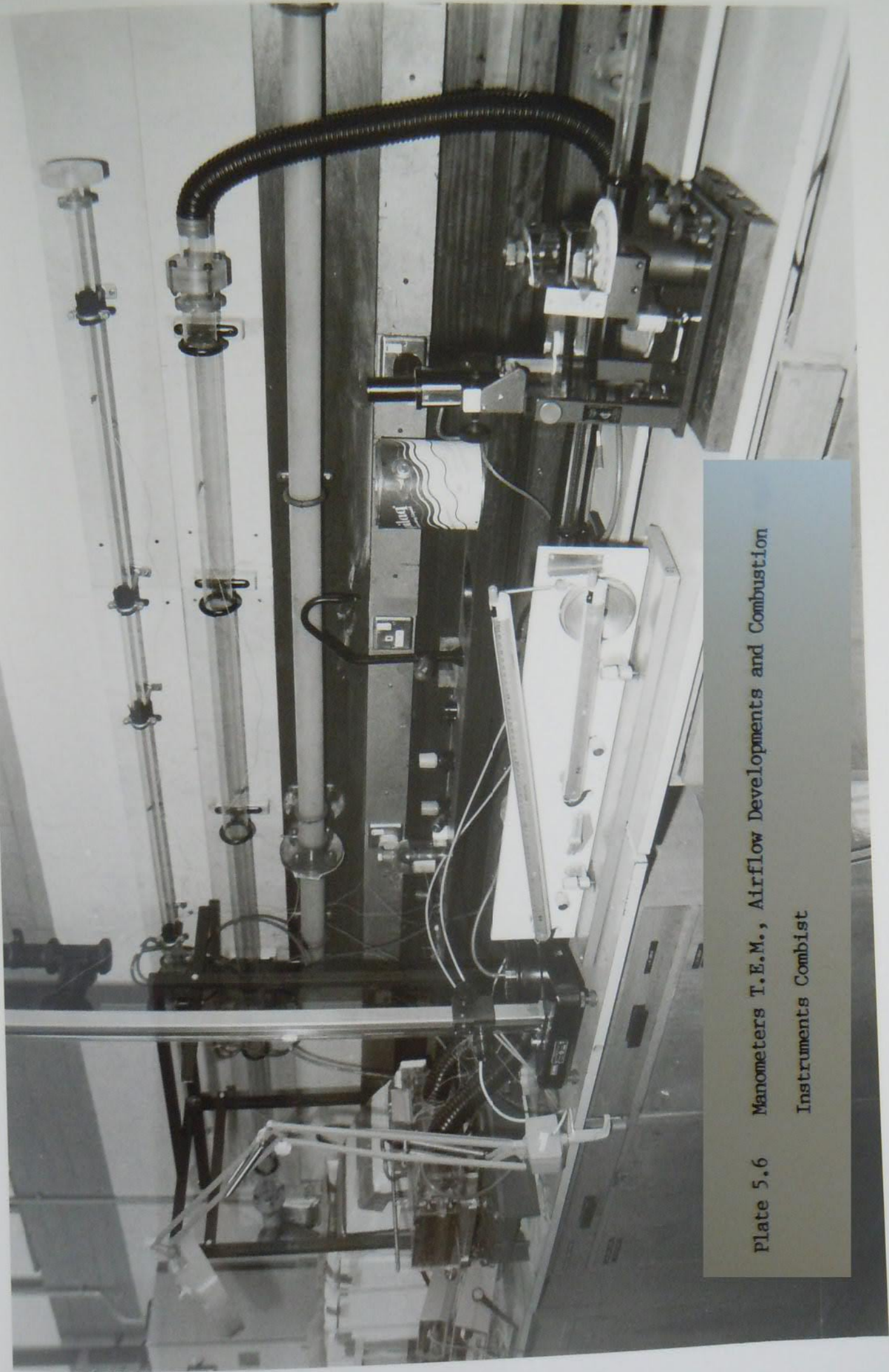
Plate 5.6   Manometers T.E.M., Airflow Developments and Combustion

Instruments Combist.
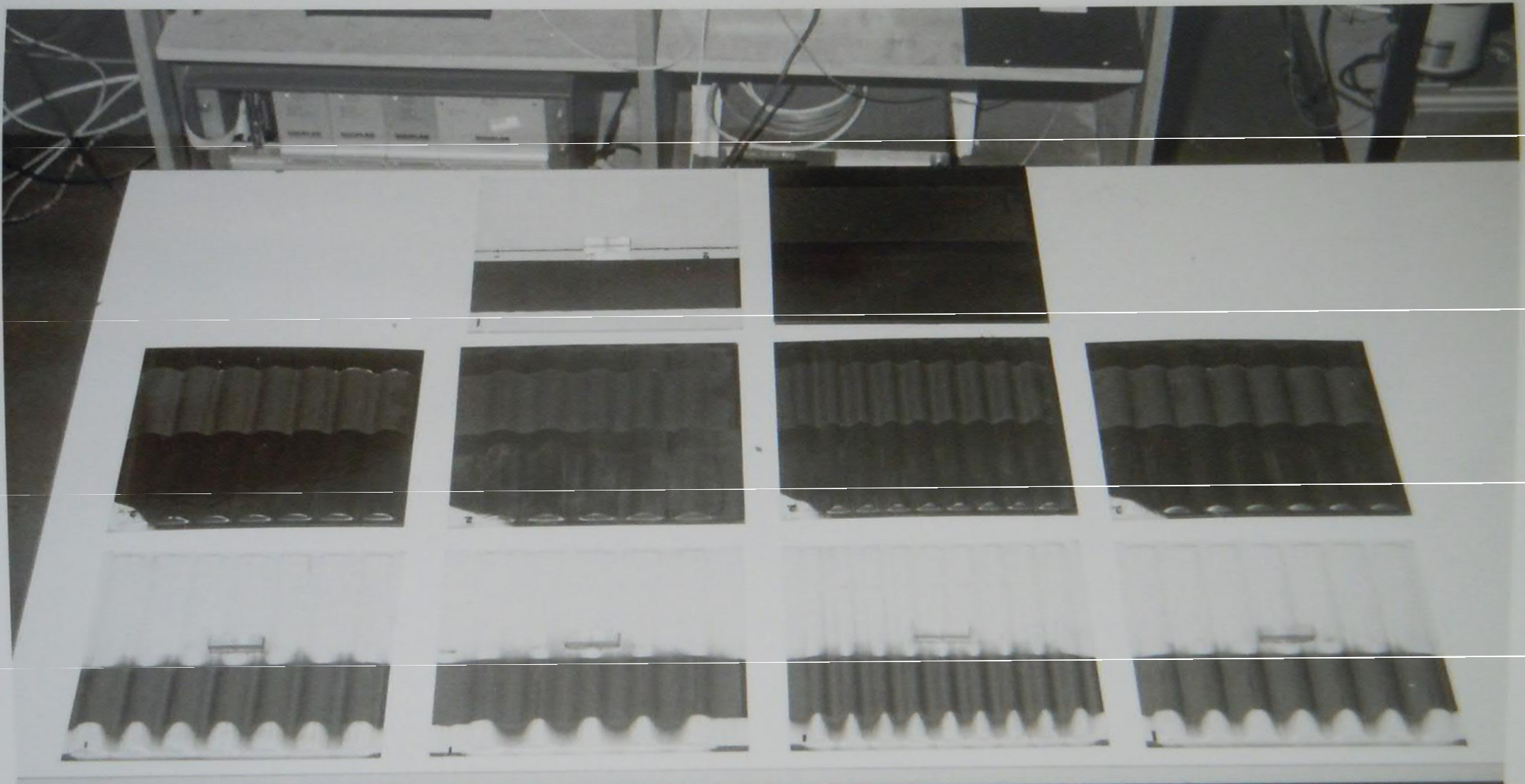
Plate 5.7   Fins with liquid crystals applied
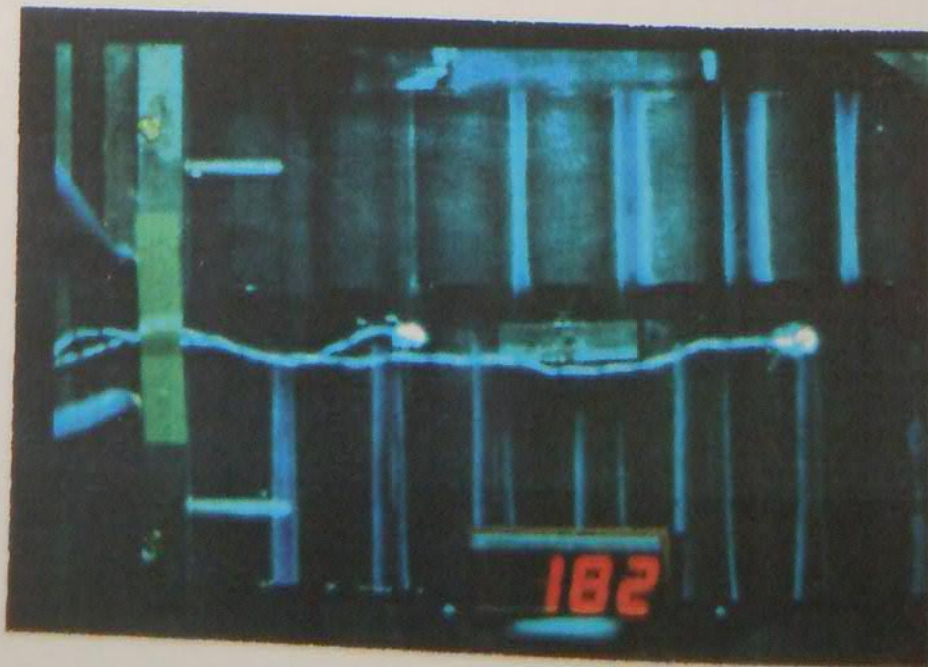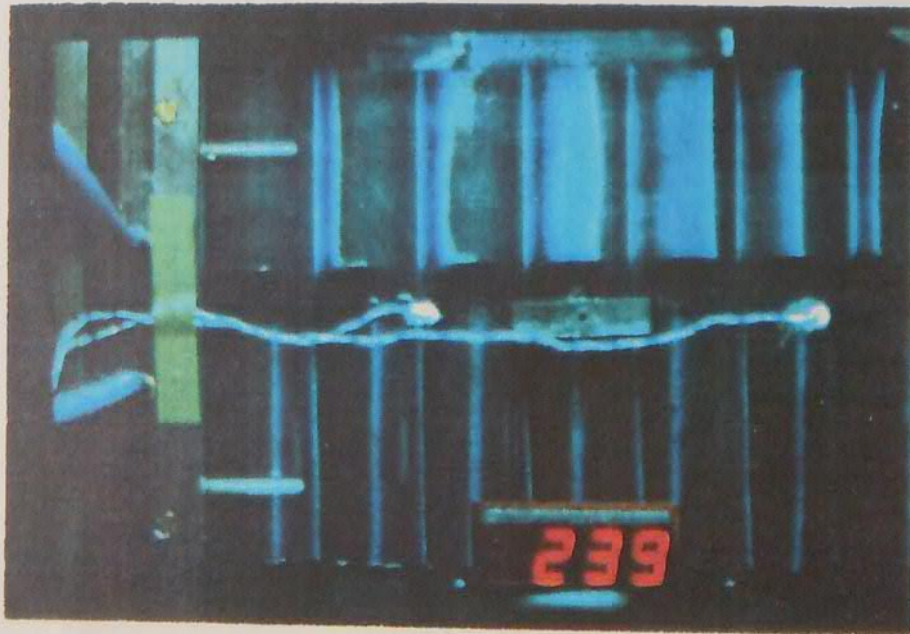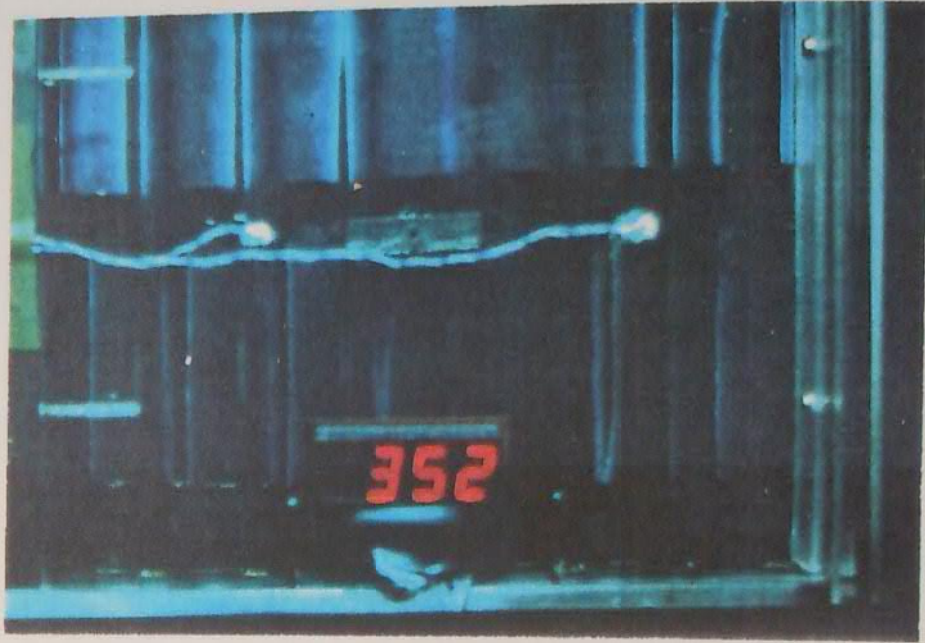
Plate 5.8   Typical transient heat transfer isotherms

Plate 5.9a   Streaklines in duct of profile 1, RH = 0.330, Re = 1876
wall spacing = 10.55 mm
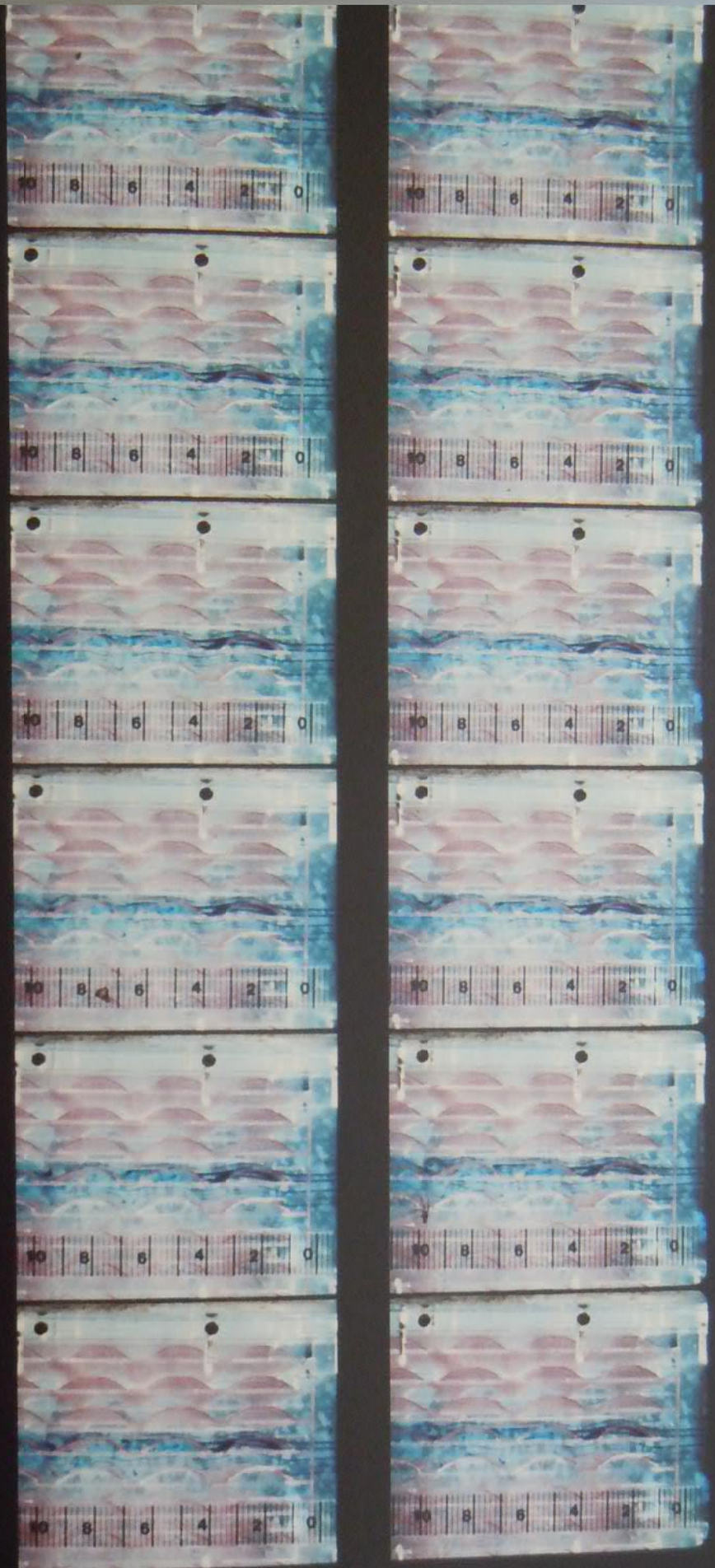
Plate 5.9b   Streaklines in duct of profile 1, RH = 0.330, Re = 1876
wall spacing = 10.55 mm
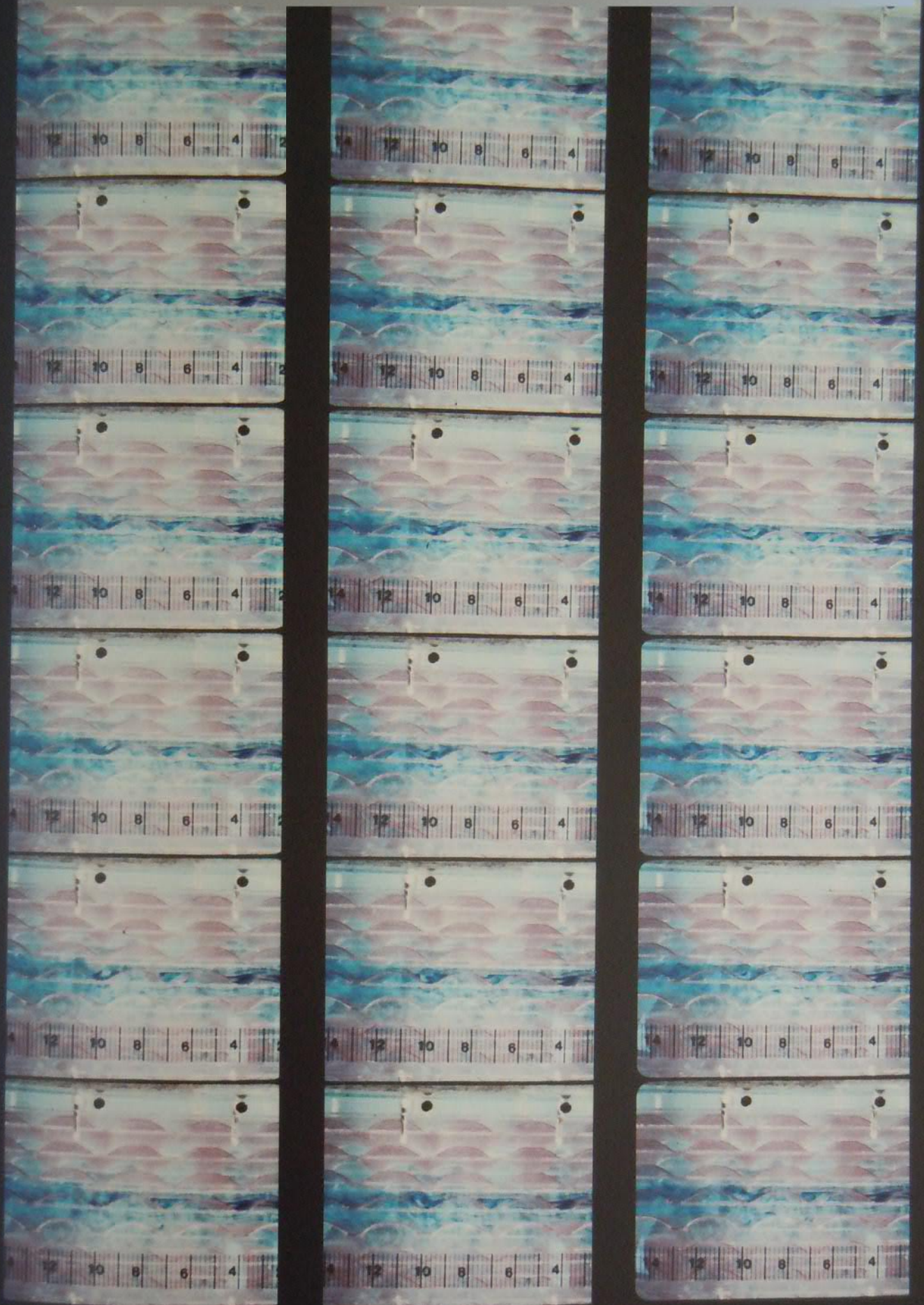
Plate 5.9c Streaklines in duct of profile 1, RH = 0.330, Re = 1876
wall spacing = 10.55 mm
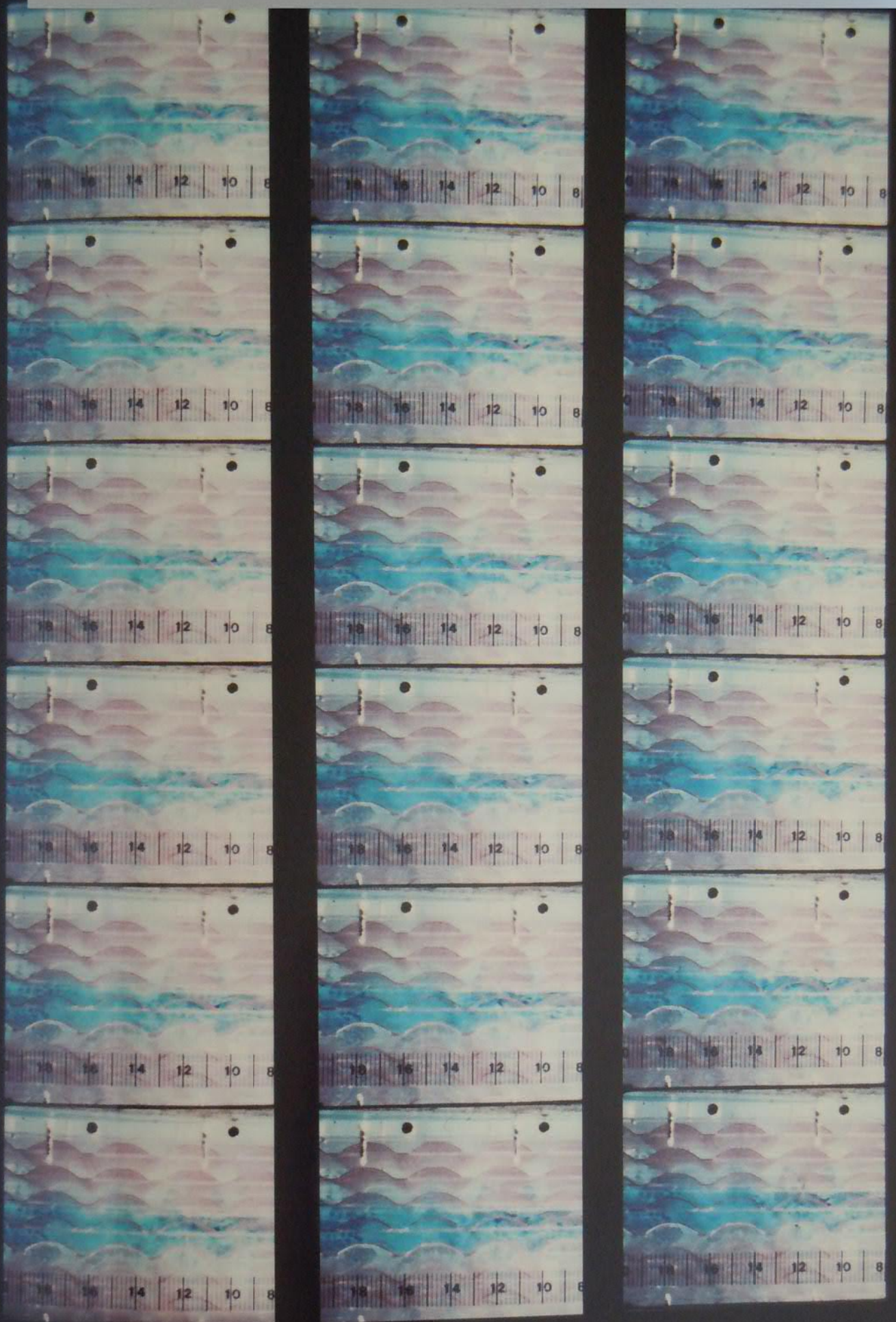
Plate 5.10a Streaklines in duct of profile 2, RH = 0.273, Re = 1826
wall spacing = 10.55 mm
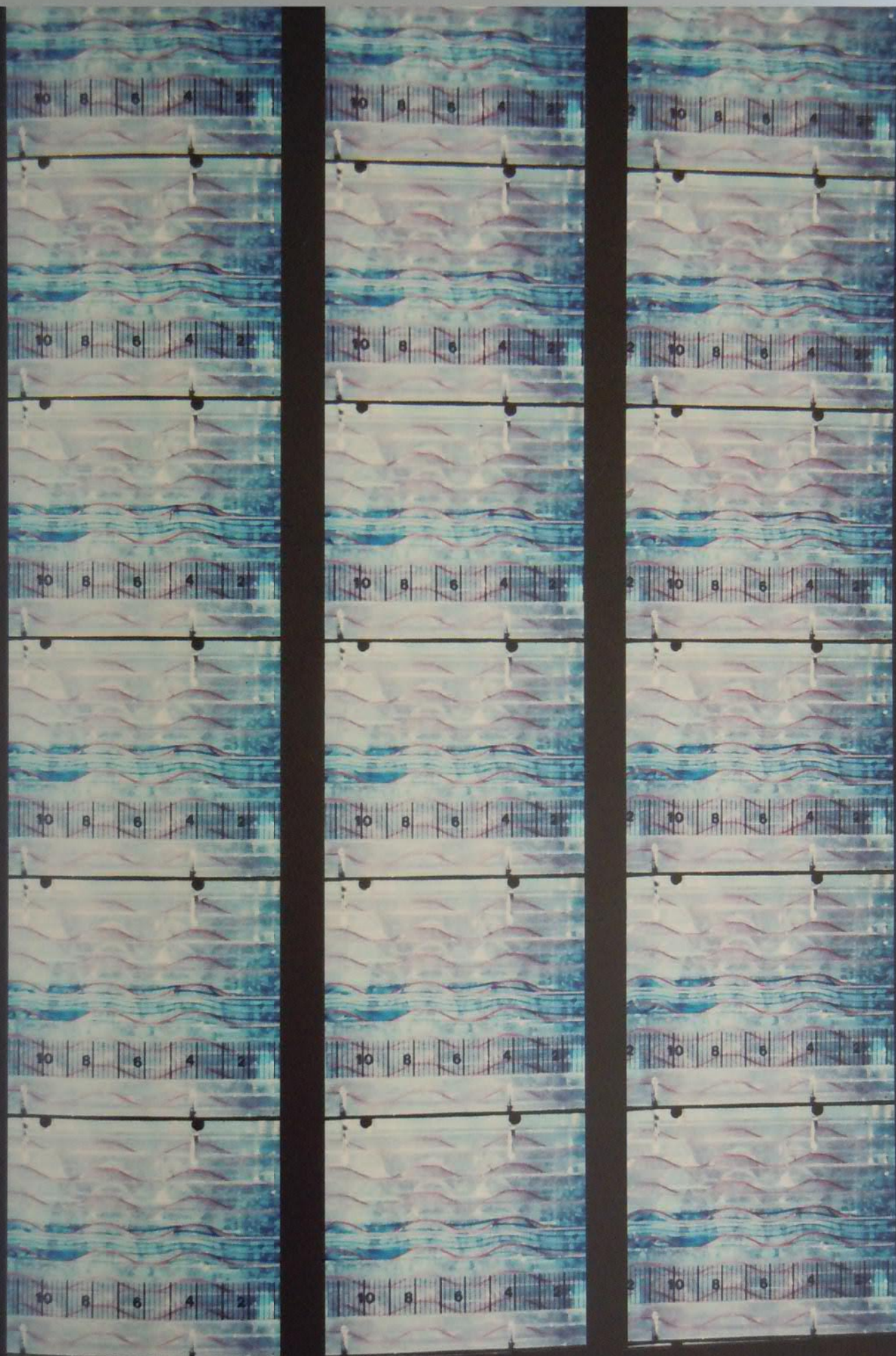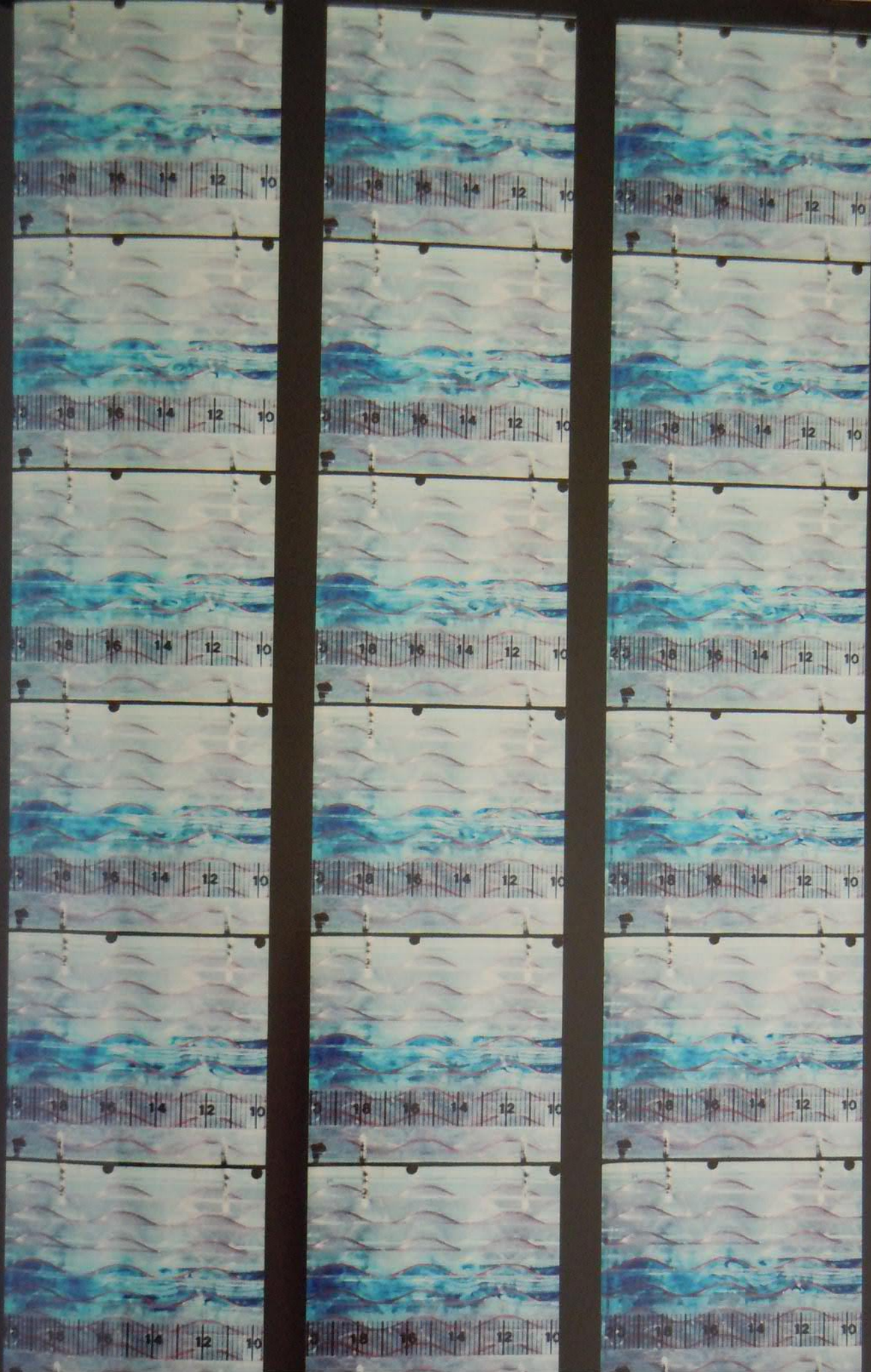
Plate 5.10b Streaklines in duct of profile 2, RH = 0.273, Re = 1826
wall spacing = 10.55 mm

Plate 5.11a Streaklines in duct of profile 3, RH = 0.445, Re = 1878
wall spacing = 10.55 mm
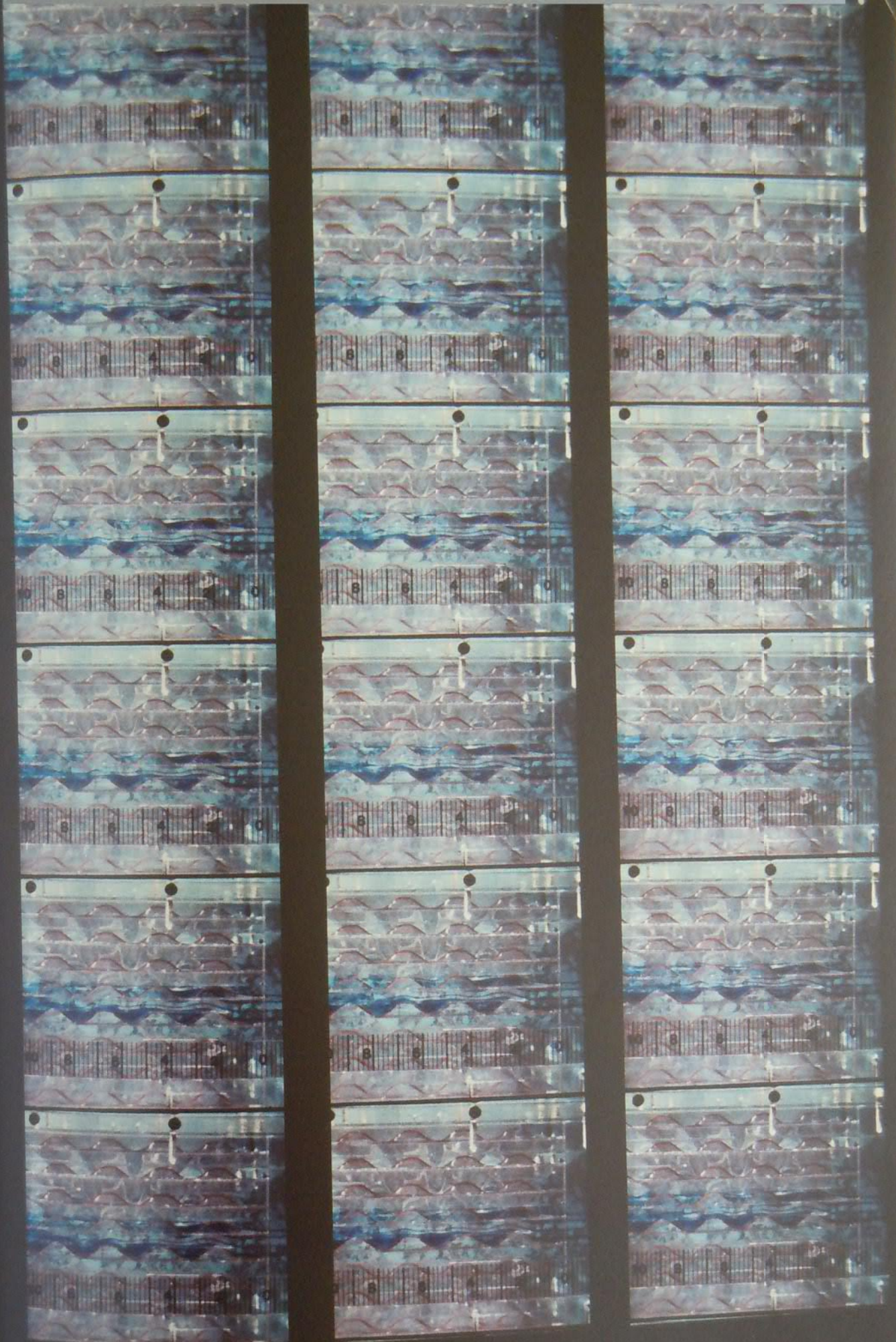
Plate 5.11b Streaklines in duct of profile 3, RH = 0.445, Re =   1878

wall spacing = 10.55 mm
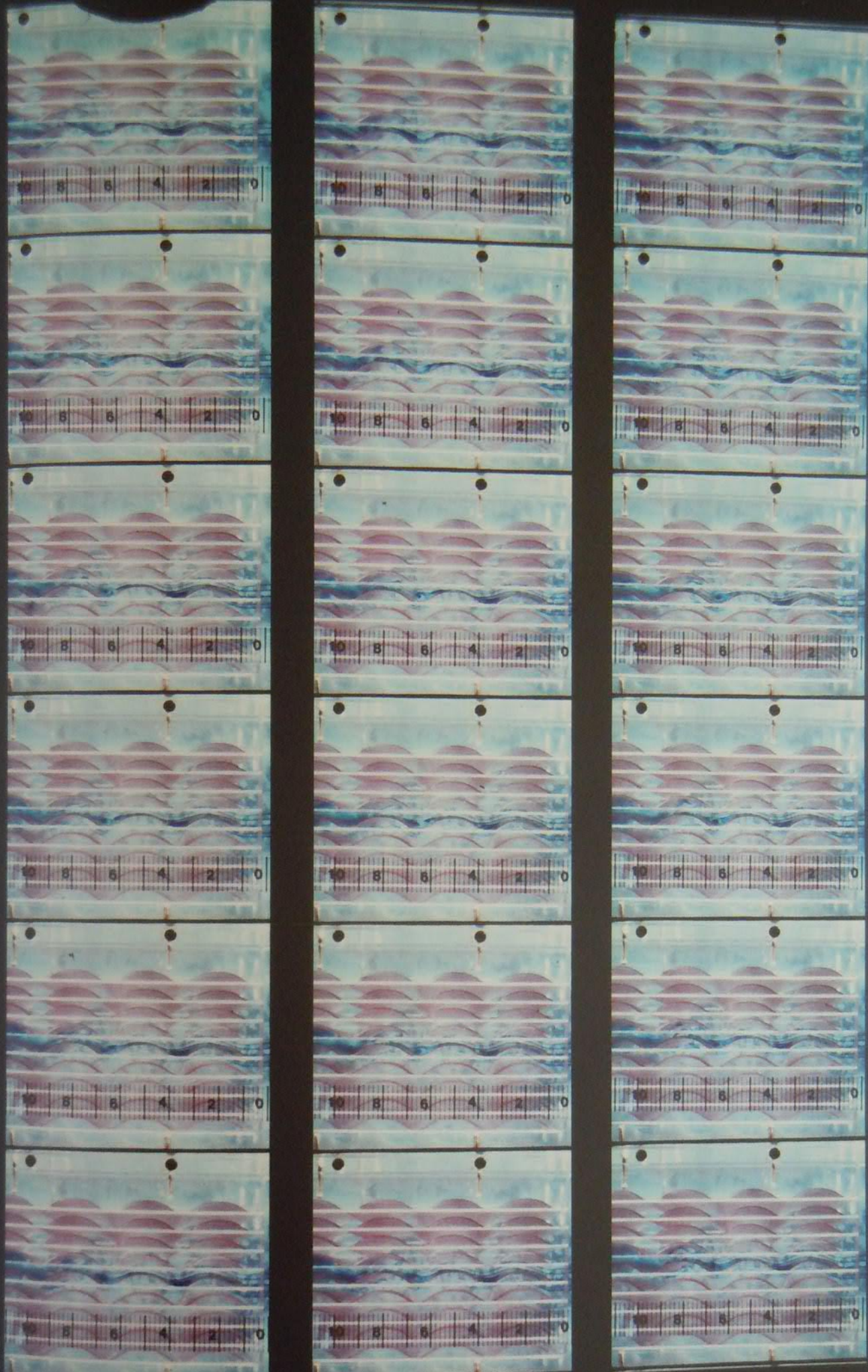
Plate 5.12a   Streaklines in duct of profile 1, RH = 0.227, Re = 1826
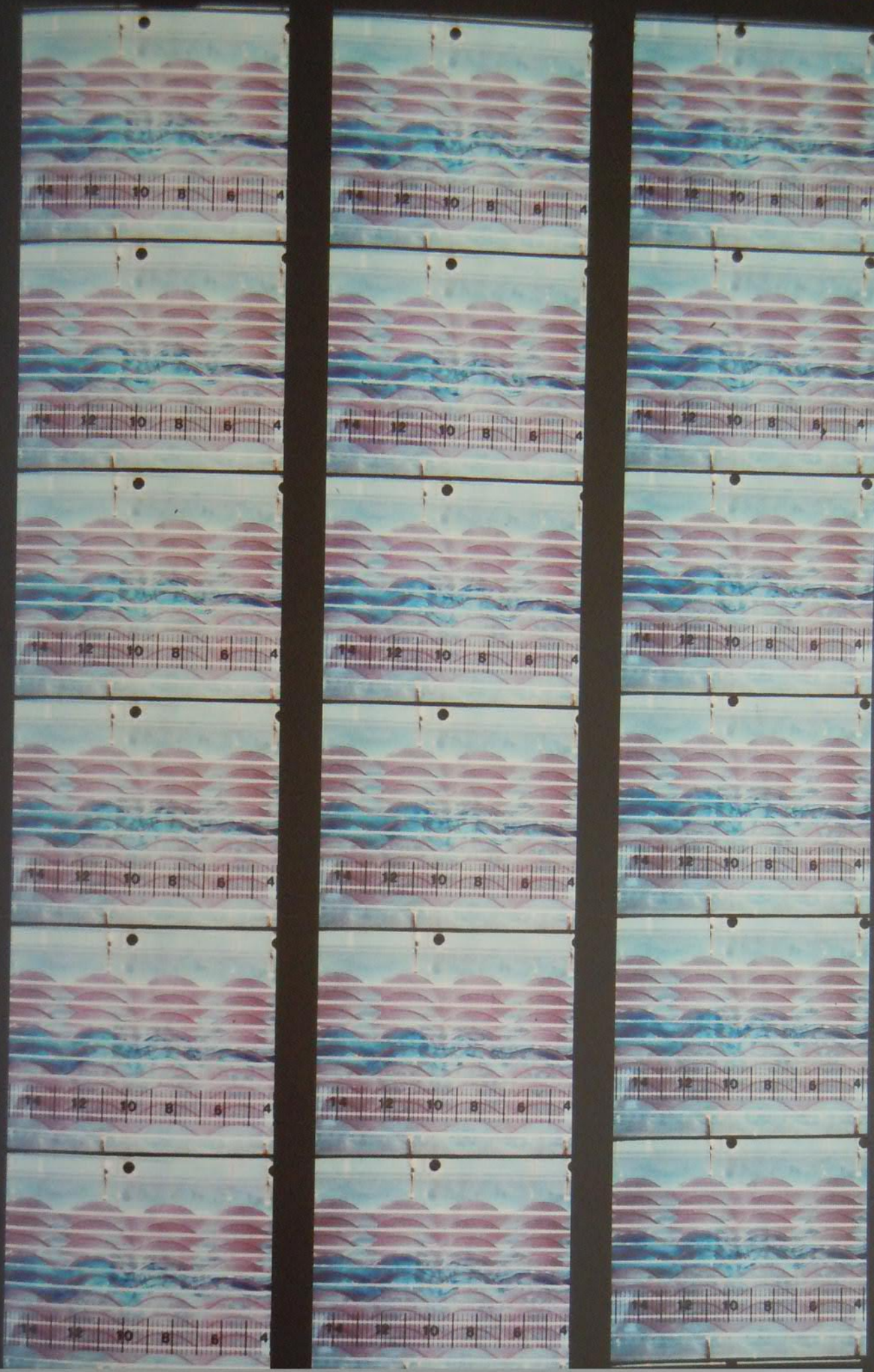
wall spacing = 7.25 mm

Plate 5.12b Streaklines in duct of profile 1, RH = 0.227, Re = 1826
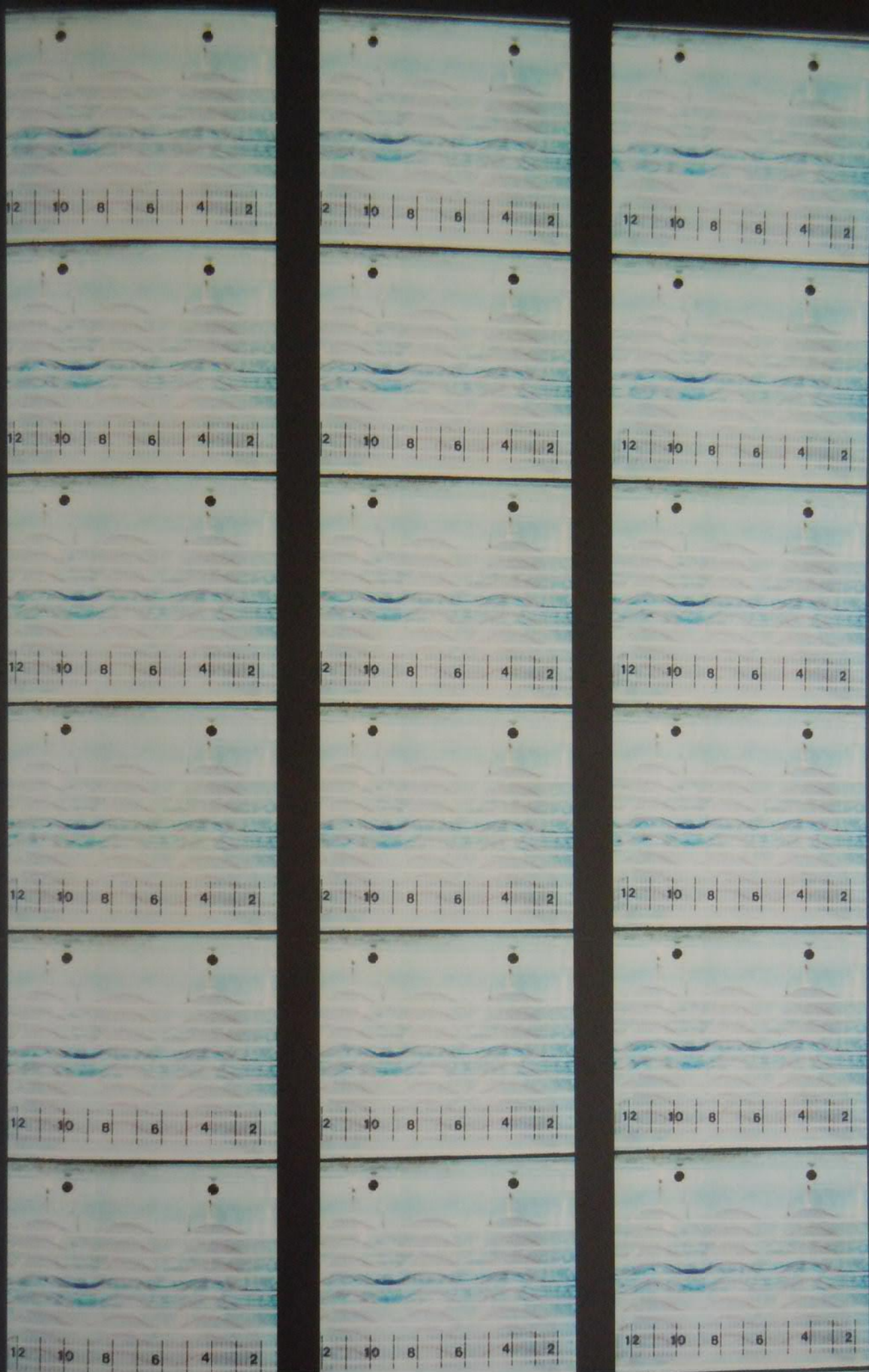
wall spacing = 7.25 mm

Plate 5.13a Streaklines in duct of profile 2, RH = 0.189, Re = 1801
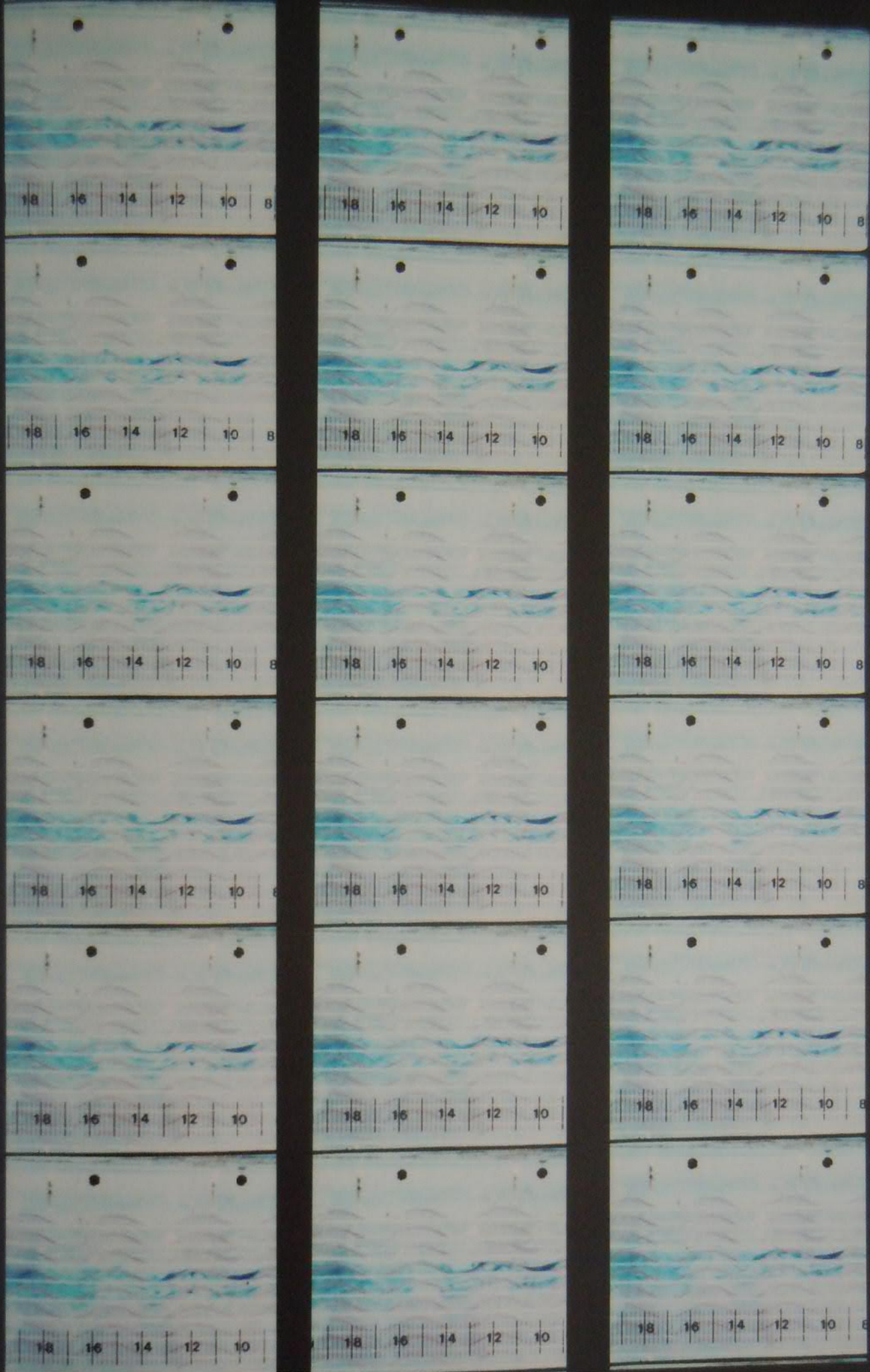
wall spacing = 7.25 mm

Plate 5.13b Streaklines in duct of profile 2, RH = 0.189, Re = 1801
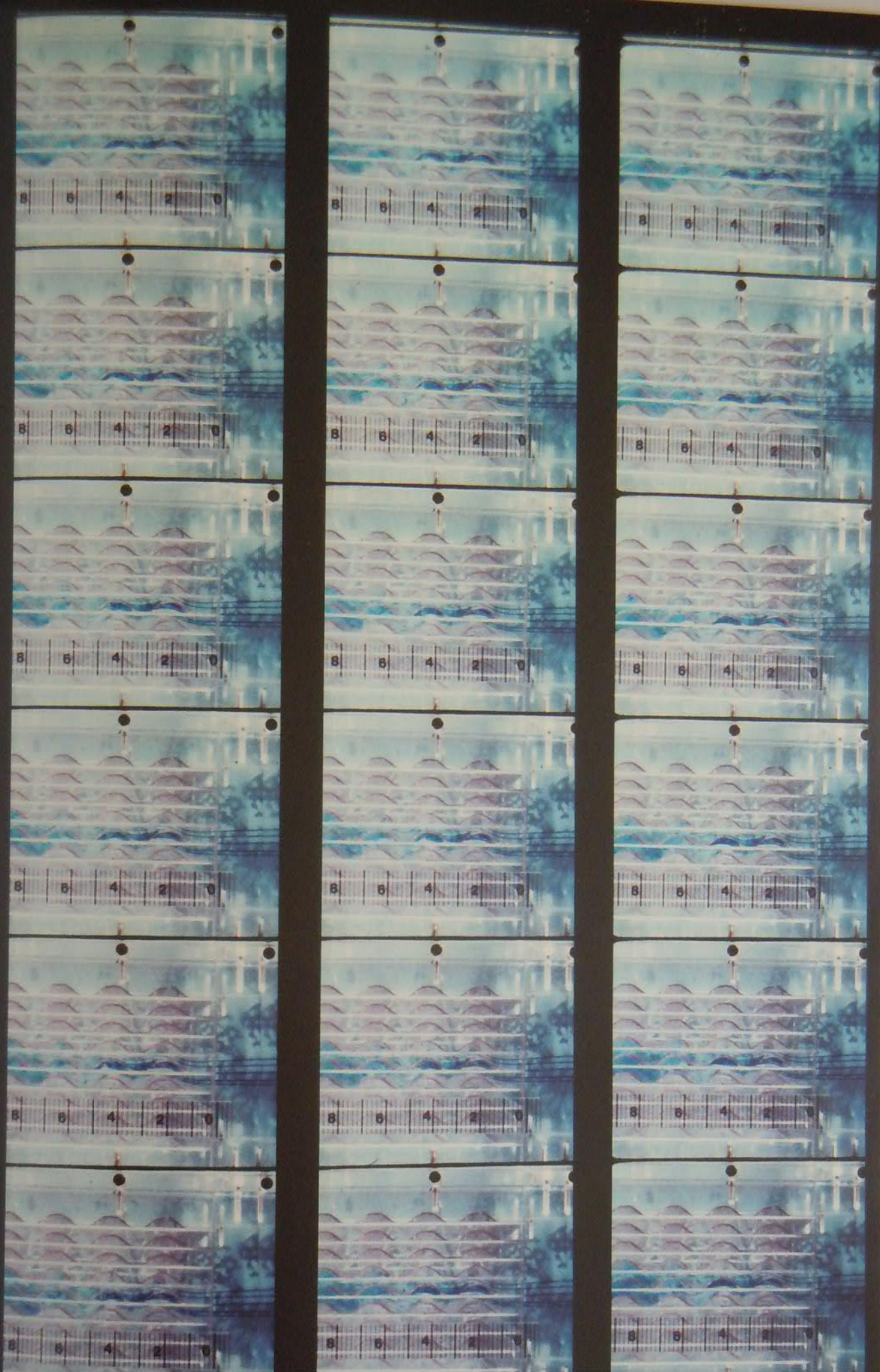
wall spacing = 7.25 mm

Plate 5.14a   Streaklines in duct of profile 3, RH = 0.306, Re =   1831

wall spacing = 7.25 mm

Plate 5.14b   Streaklines in duct of profile 3, RH = 0.306, Re =   1831

wall spacing = 7.25 mm

Plate A8.1   Slide projector, digitizer and computer arrangement

1-1   9 x 9 chromel alumel thermocouple array
2-2   chromel alumel thermocouple
3-3   4 x 4 chromel alumel thermocouple array
4   4 point pressure tapping ring
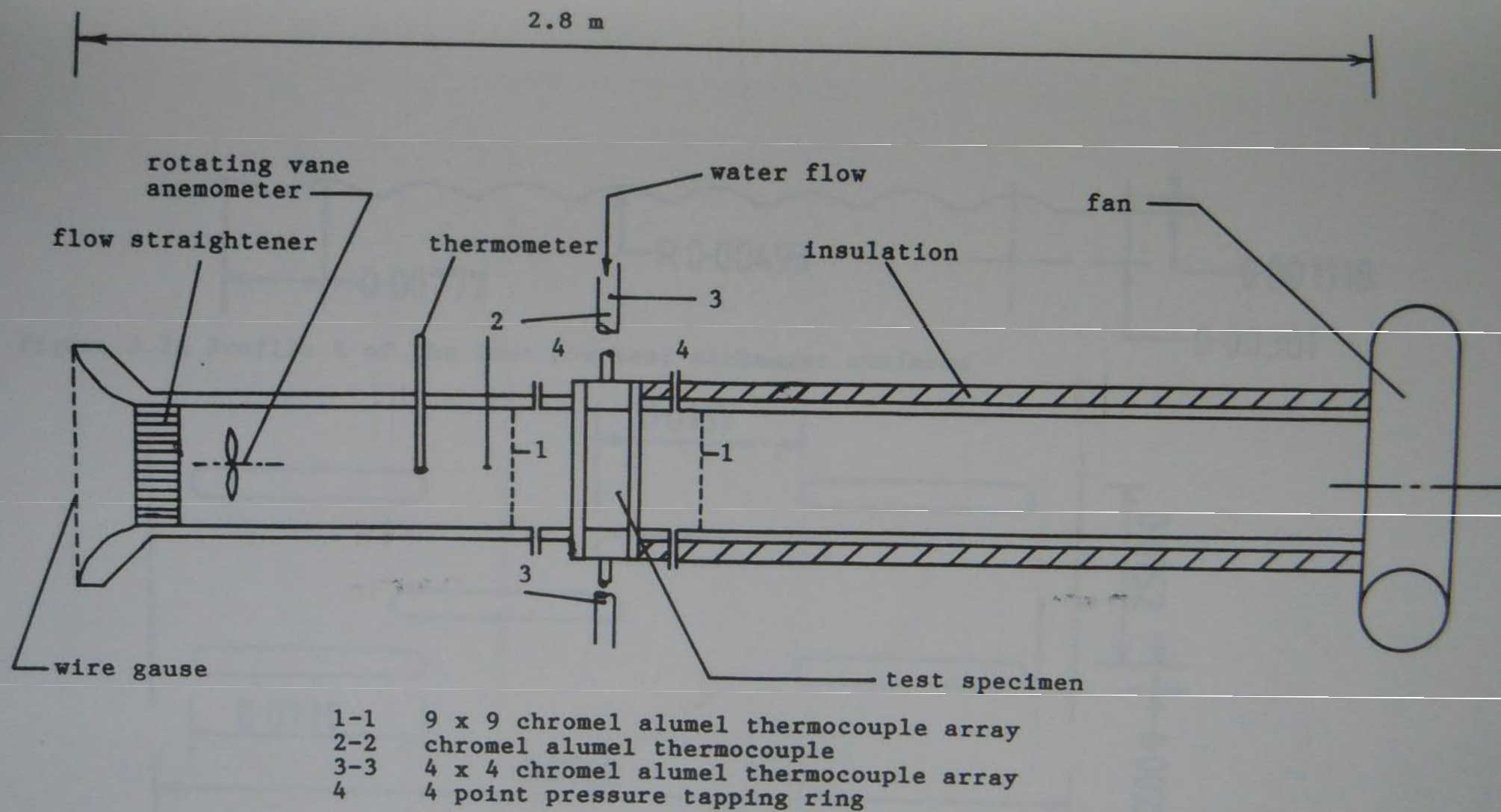
Fig. 3.1 Schematic representation of the Covrad thermal wind tunnel
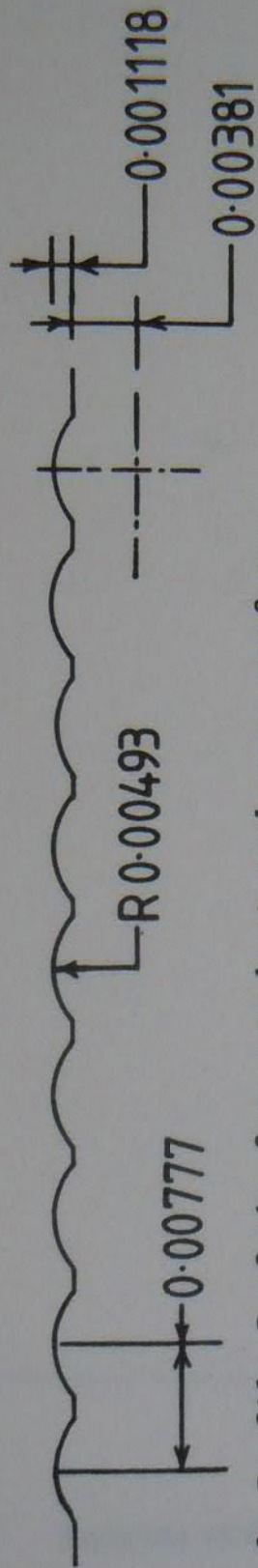
Figure 3.2a Profile B of the four row heat exchanger surfaces
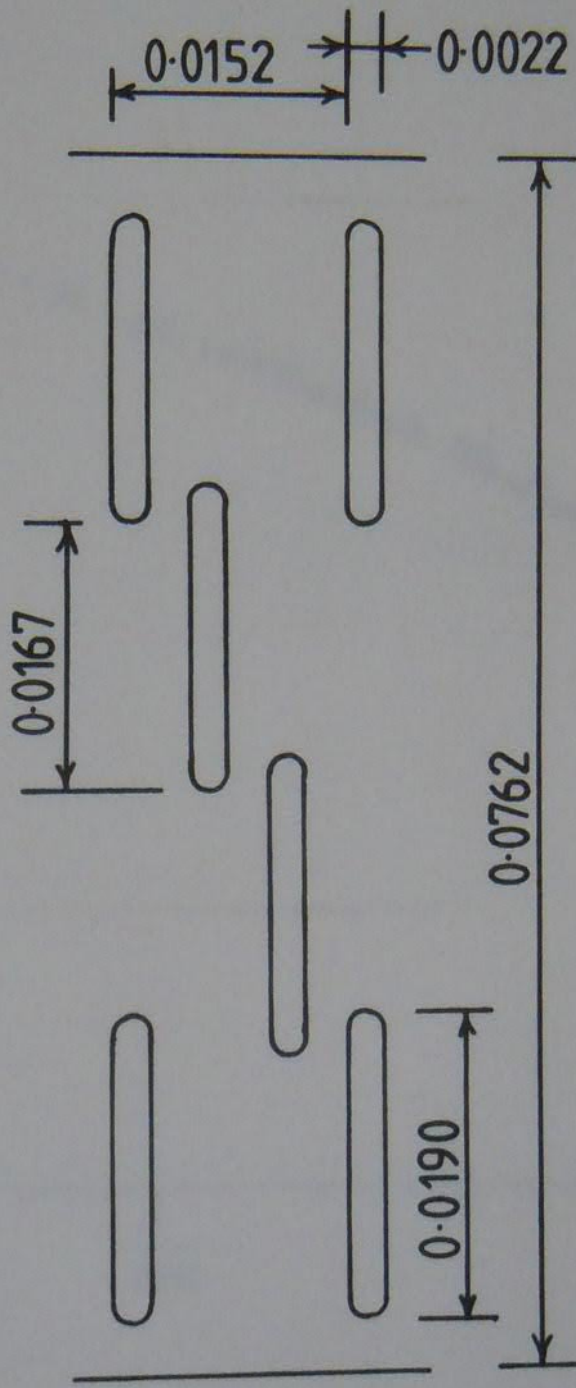
Figure 3.2b Fin dimensions and tube layout for the four row surfaces
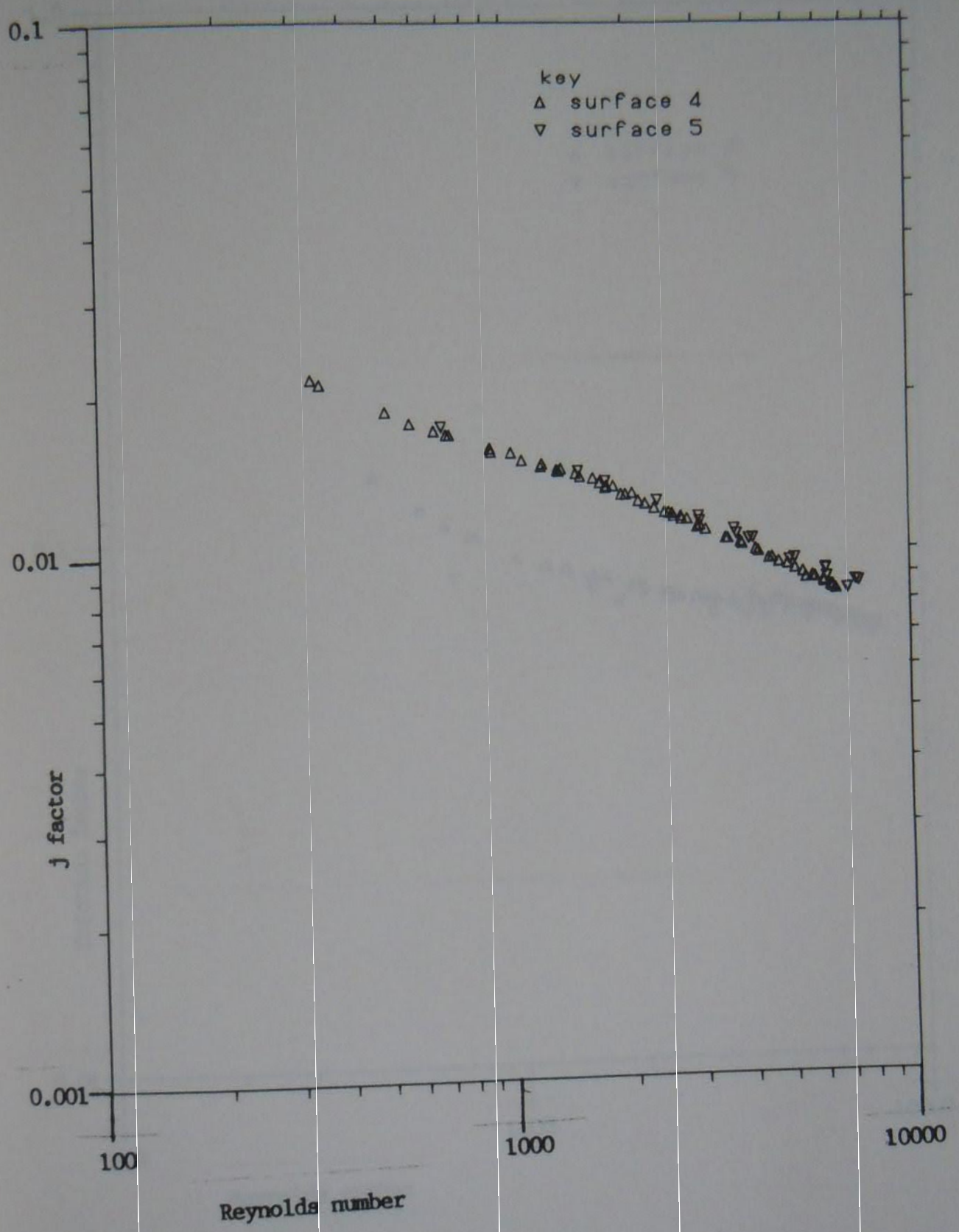
Figure 3.3 Graph of the measured j factors for the four row heat exchangers

191
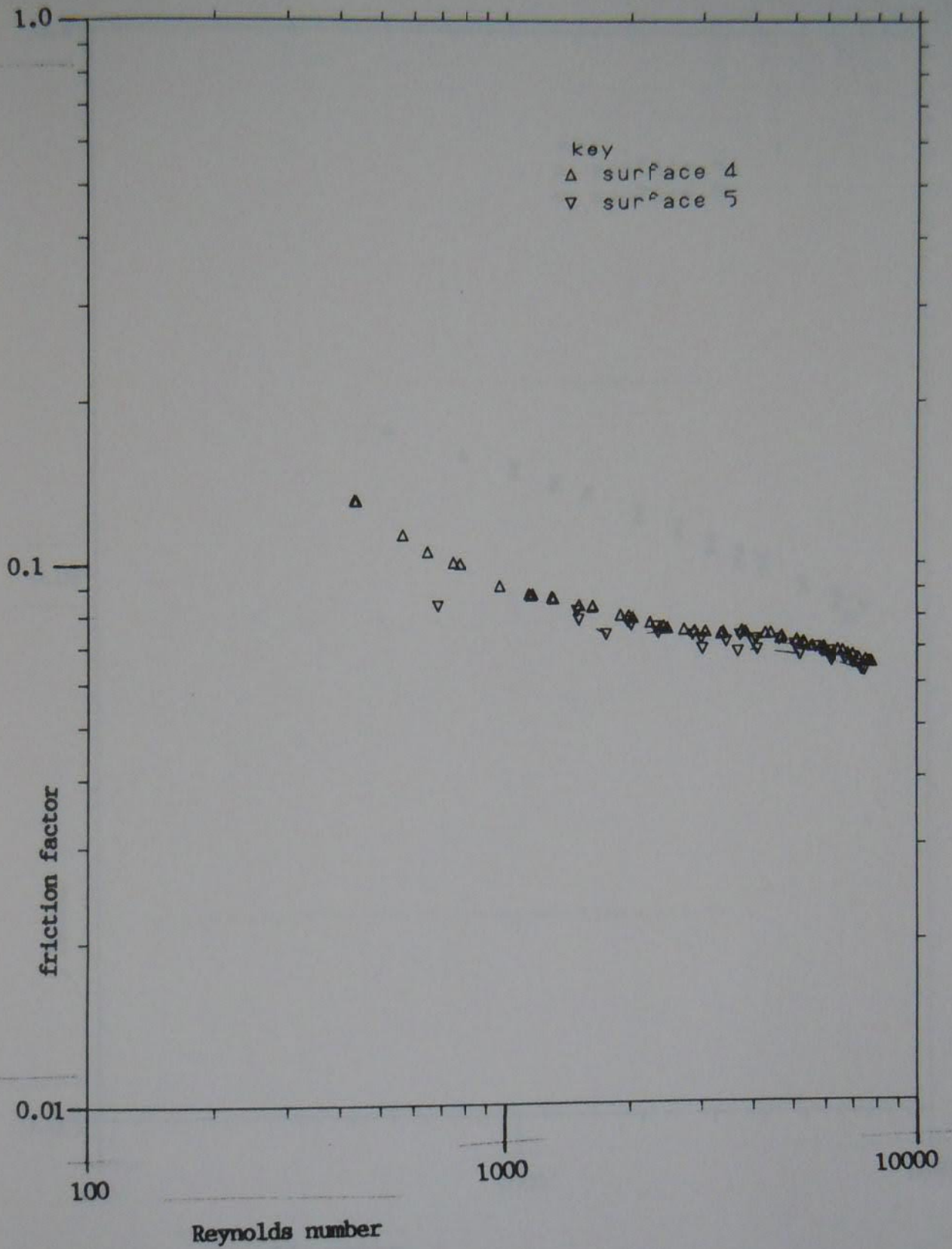
Figure 3.4 Graph of the measured friction factors for the four row heat exchangers
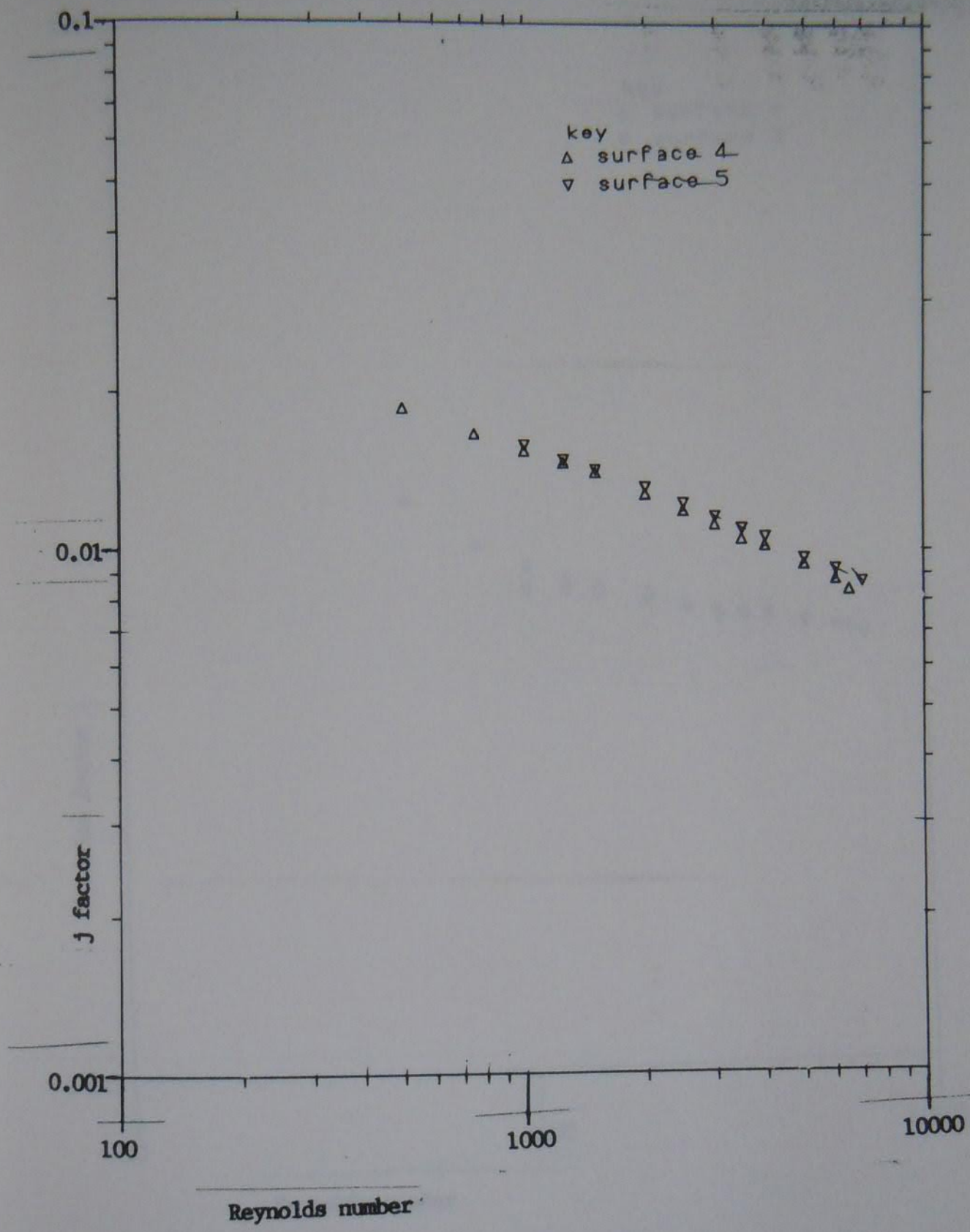
Figure 3.5   j factor results for the four row heat exchangers

193
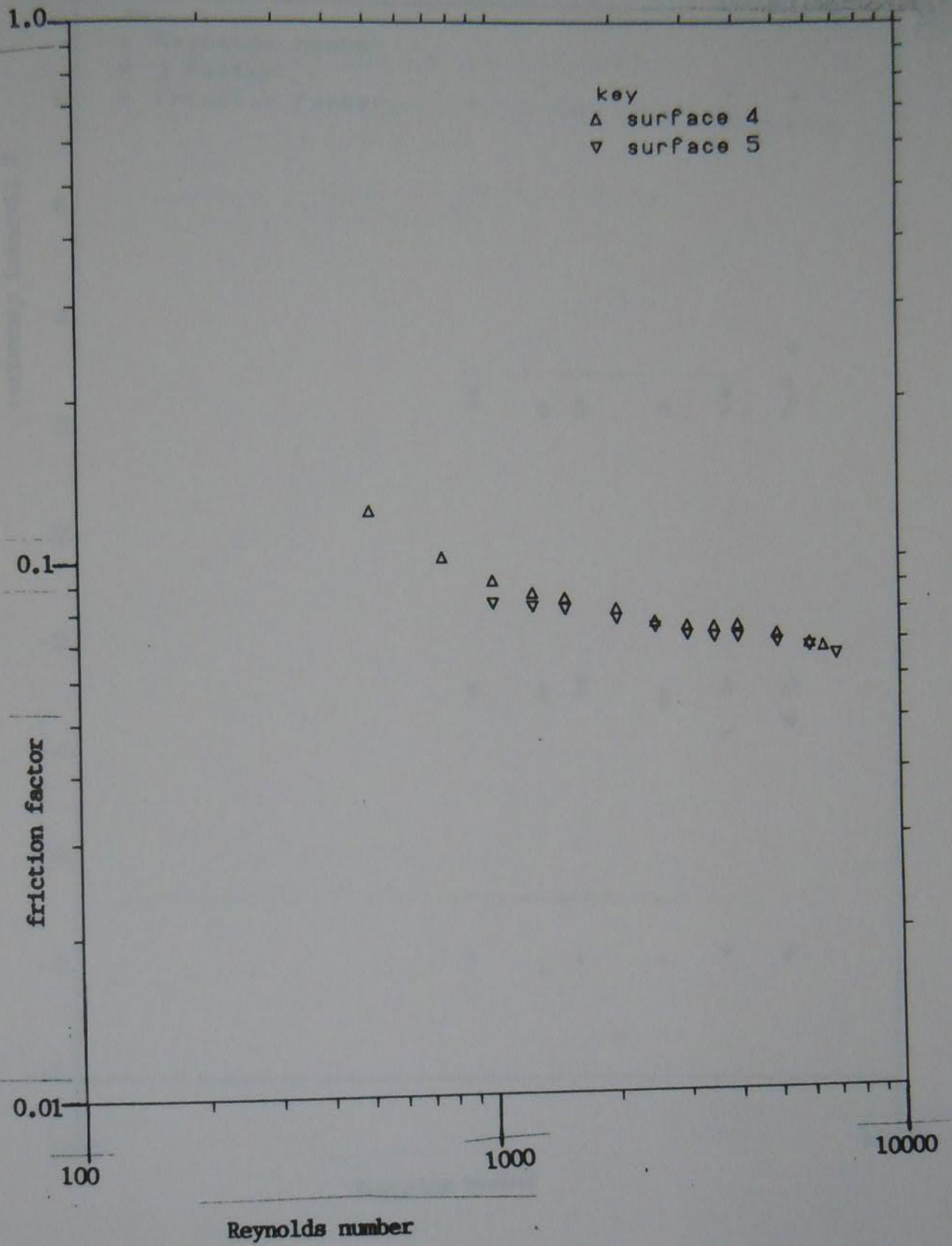
Figure 3.6 friction factor results for the four row heat exchangers

194

Figure 3.7 Graph of certainty interval against the Reynolds number for the j factor, friction factor and Reynolds number for the four row heat exchangers
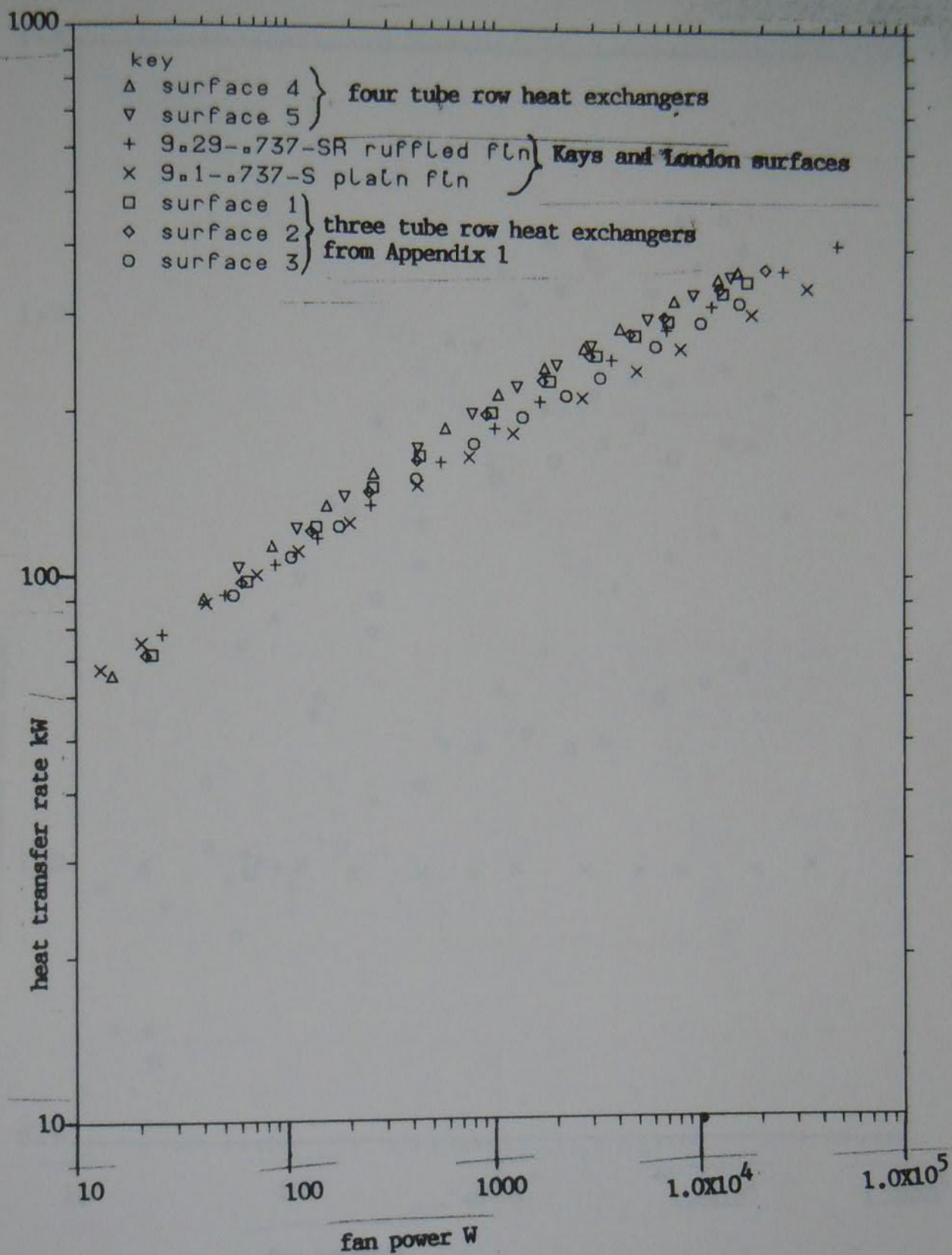
Figure 3.8 Graph showing the comparison of heat transfer rates against fan powers for the four row heat exchangers
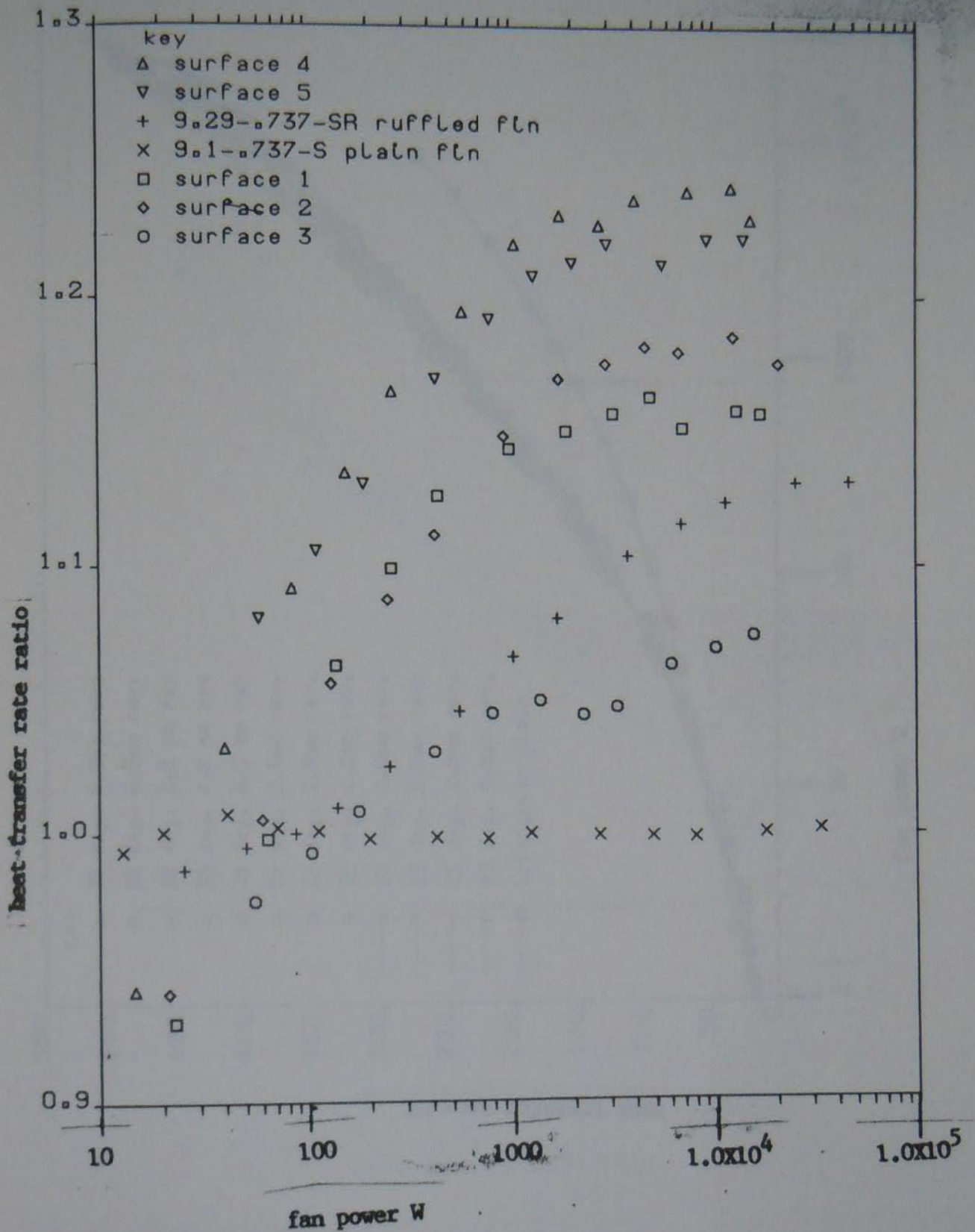
Figure 3.9 Performance ratio graph for the four row surfaces against the three row and Kays and London surfaces
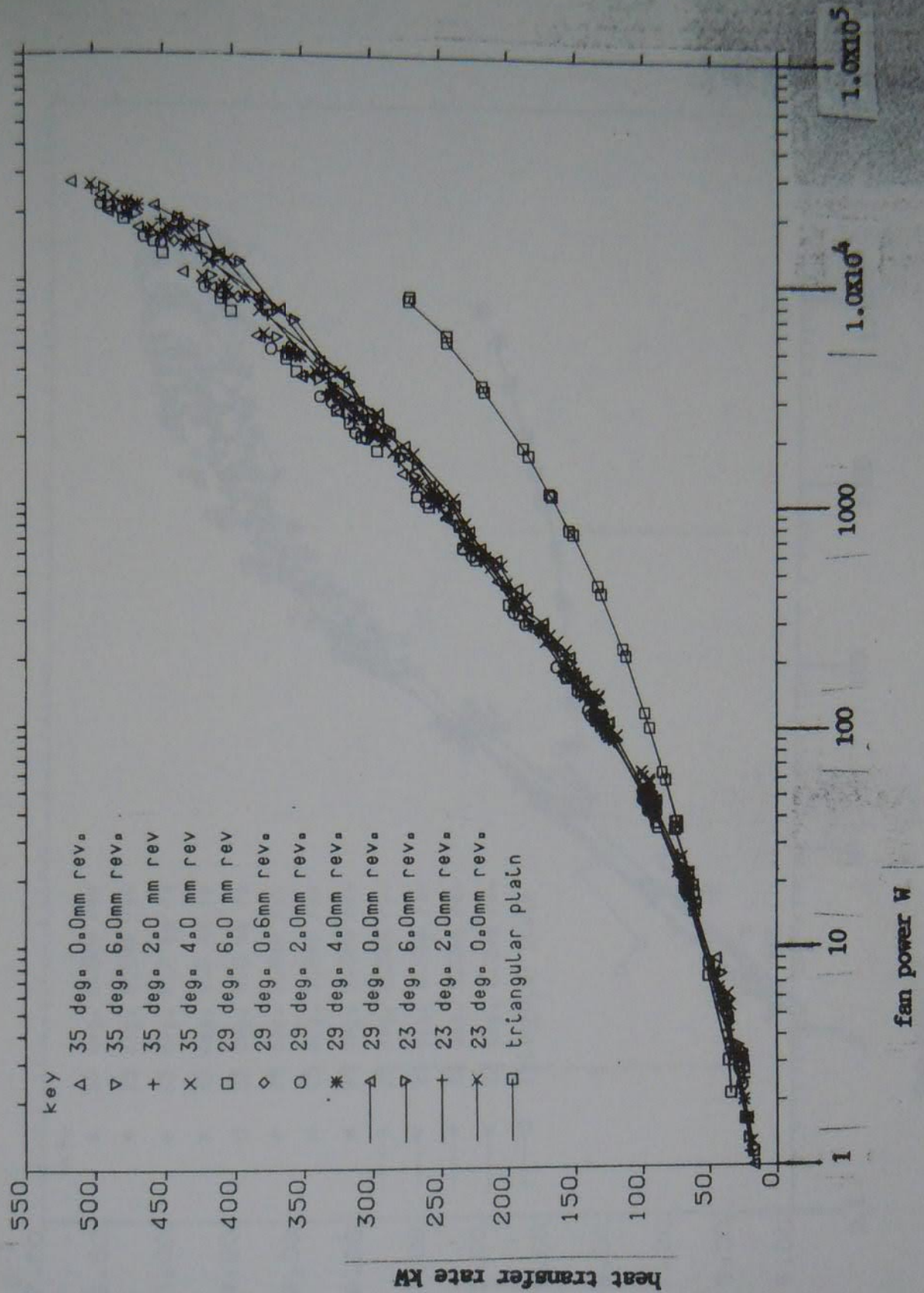
Figure 3.10 Graph showing the comparison of the louvred heat exchangers by heat transfer rate against fan power
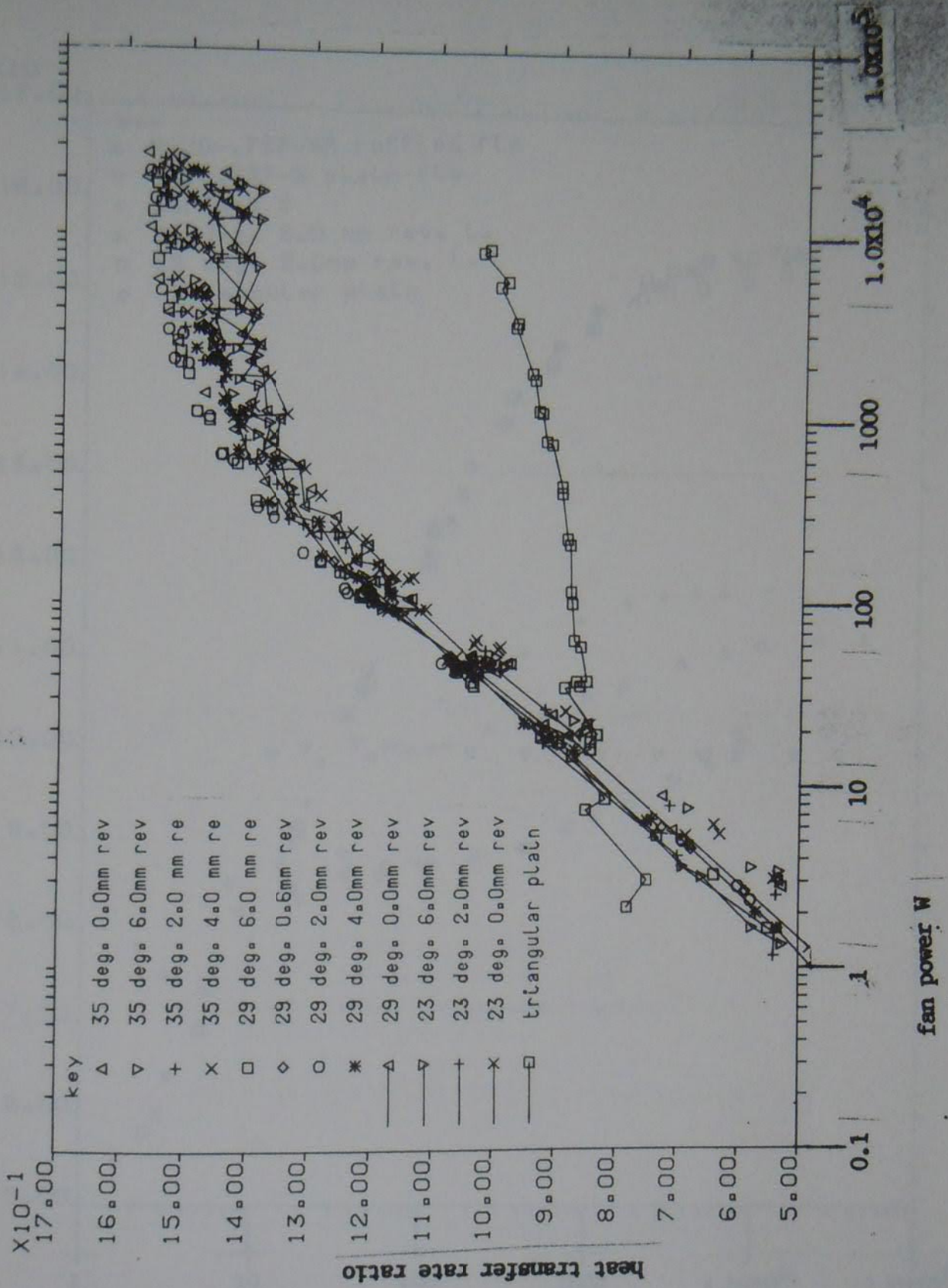
Figure 3.11 Performance ratio graph for the louvred surfaces
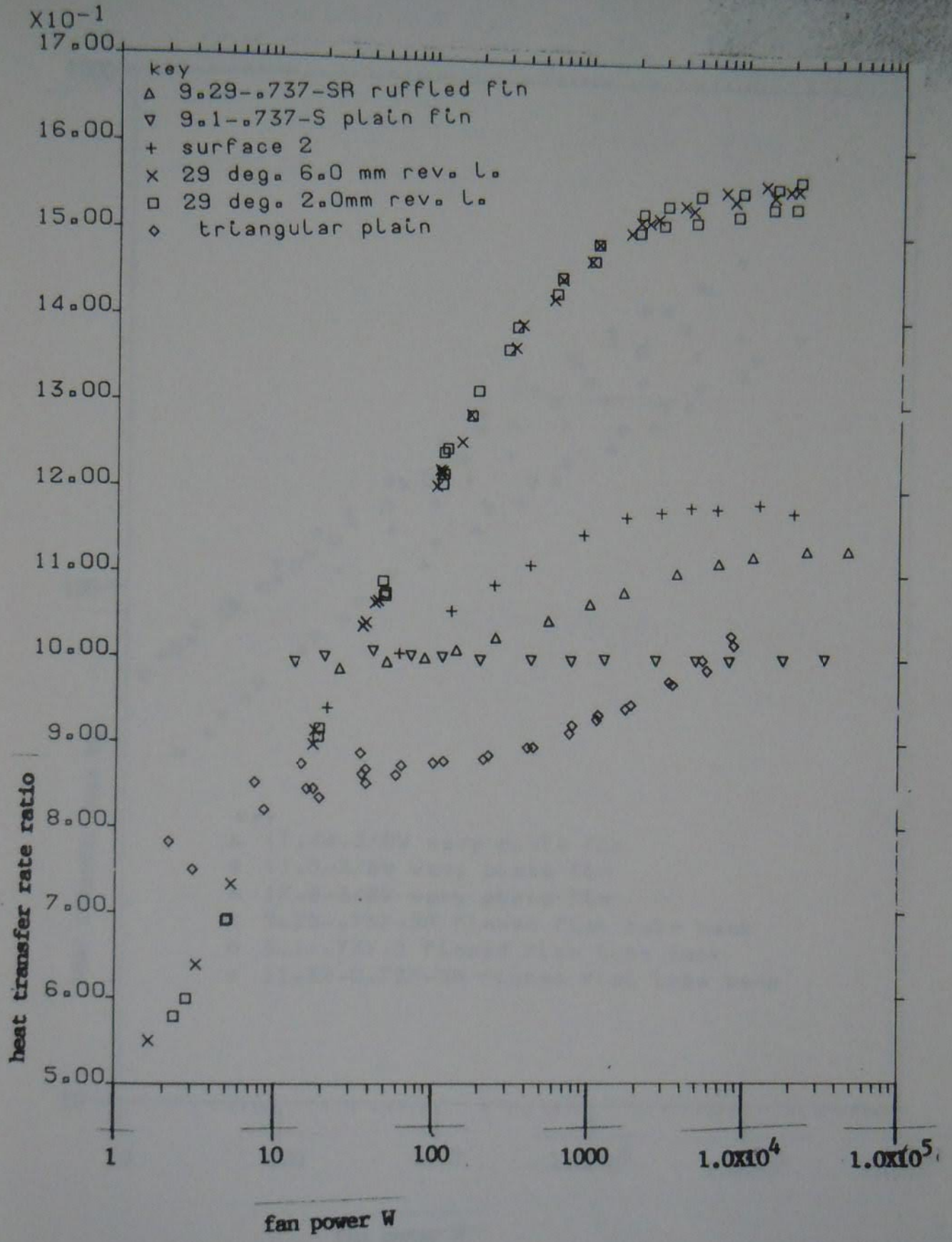
Figure 3.12 Performance ratio graph comparing various surfaces using the Kays and London Plain fin as reference
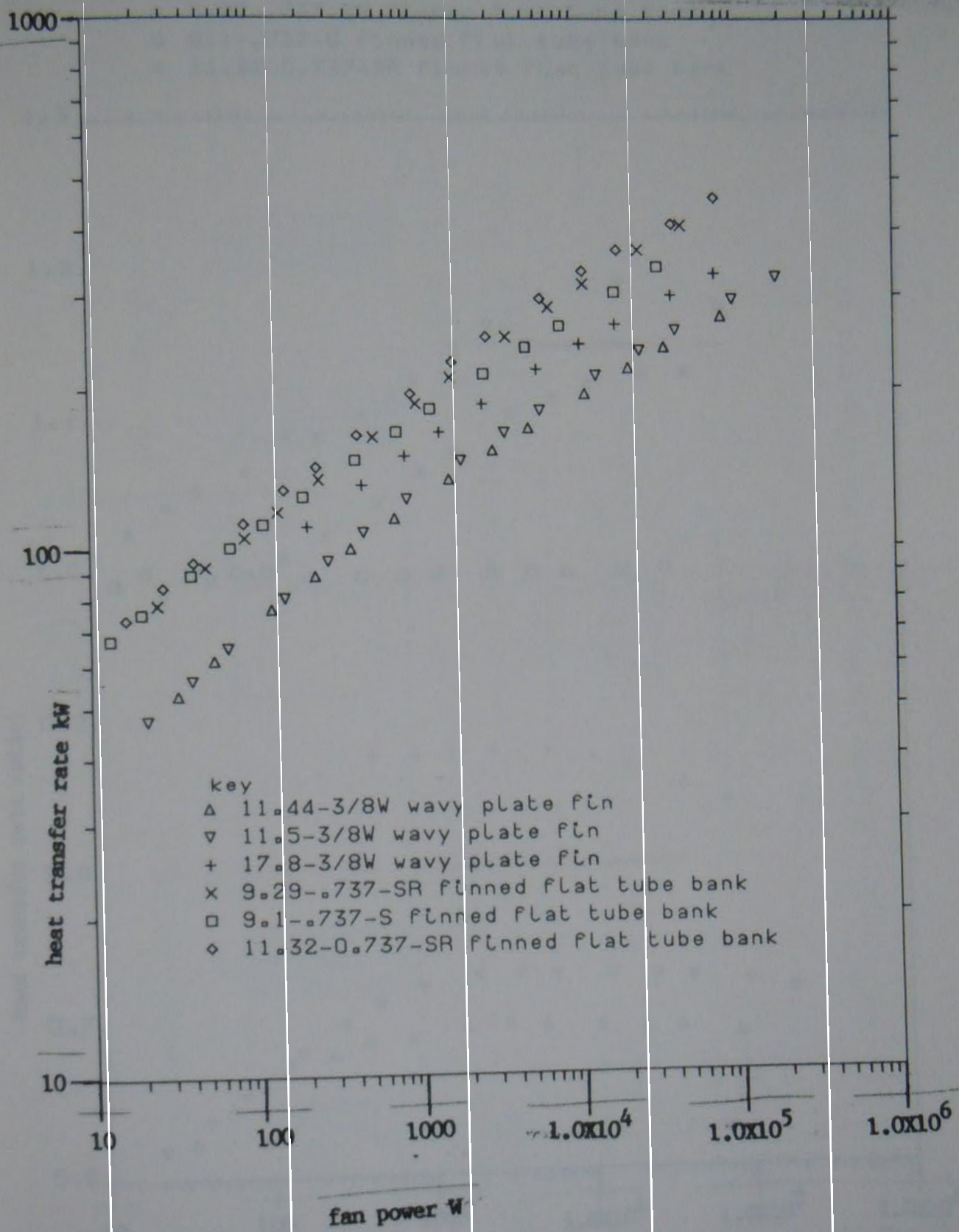
Figure 3.13 Comparison of the performance of Kays and London wavy fin surfaces with the ruffled plate fin heat exchangers

key
△ 11.44-3/8W wavy plate fin
▽ 11.5-3/8W wavy plate fin
+ 17.8-3/8W wavy plate fin
× 9.29-.737-SR finned flat tube bank
□ 9.1-.737-S finned flat tube bank
◇ 11.32-0.737-SR finned flat tube bank

heat transfer rate kW

fan power W
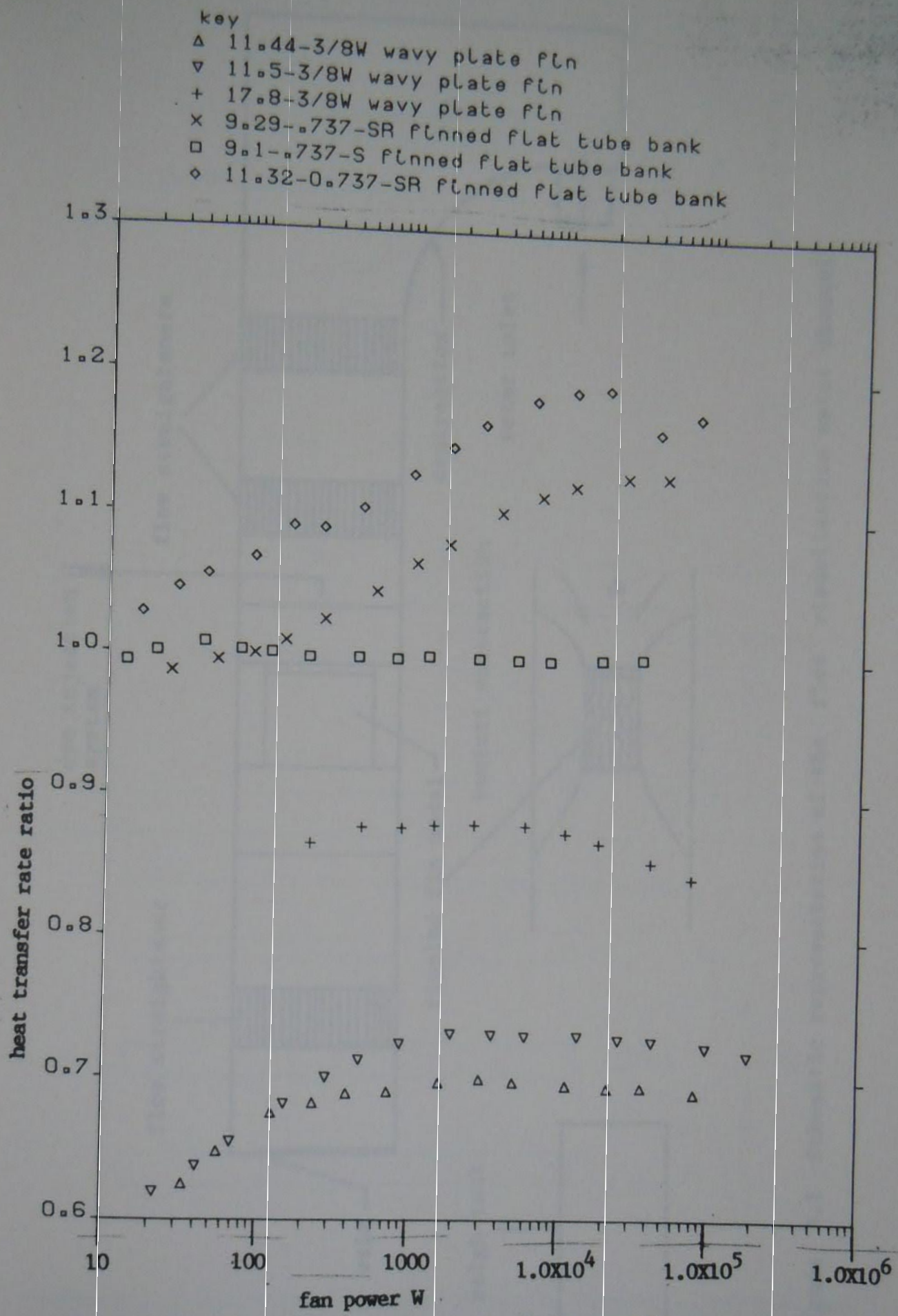
Figure 3.14 Performance ratio graph of the wavy fins in comparison with the ruffled plate fins
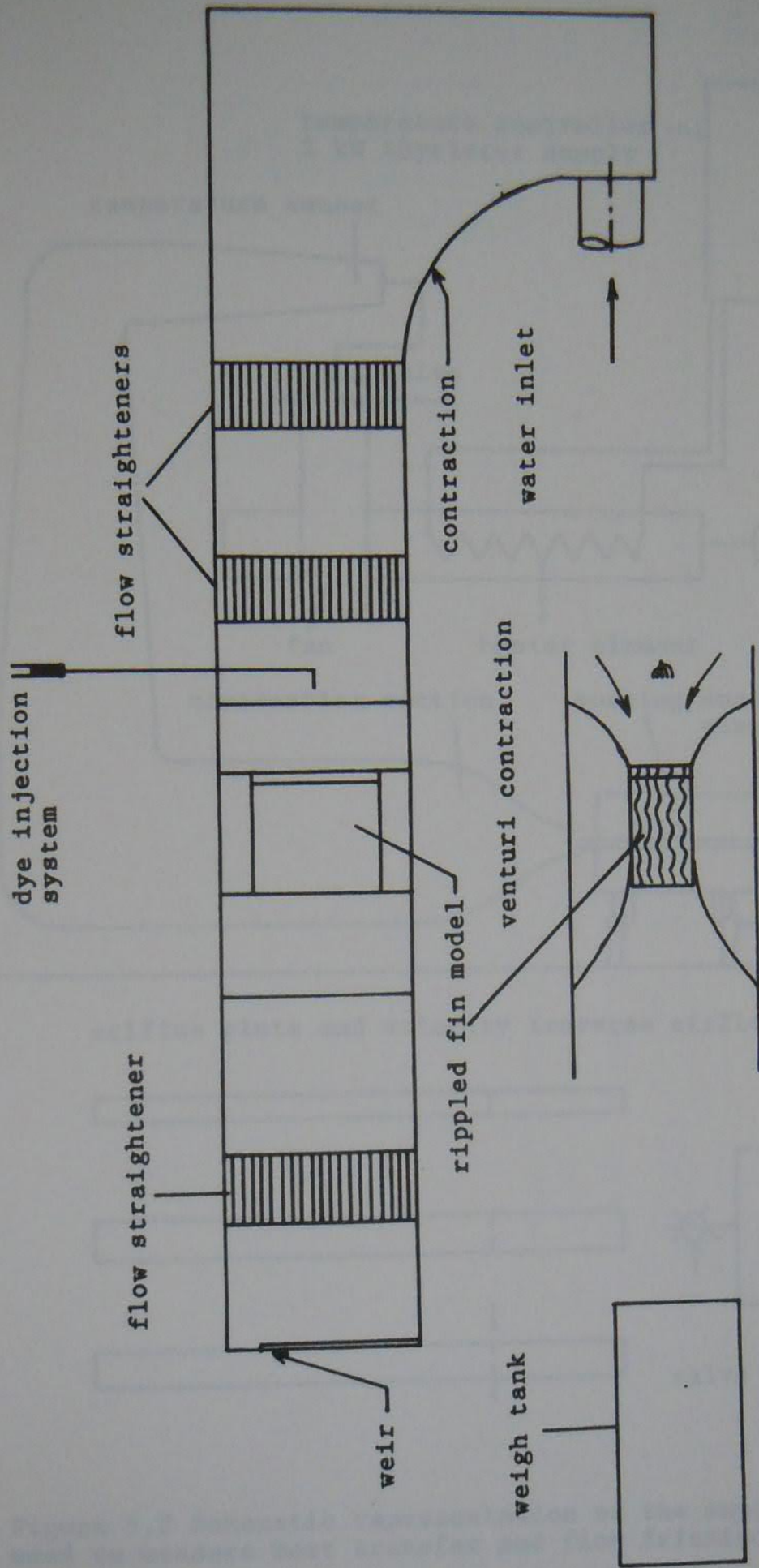
Figure 5.1 Schematic representation of the flow visualisation water channel

203
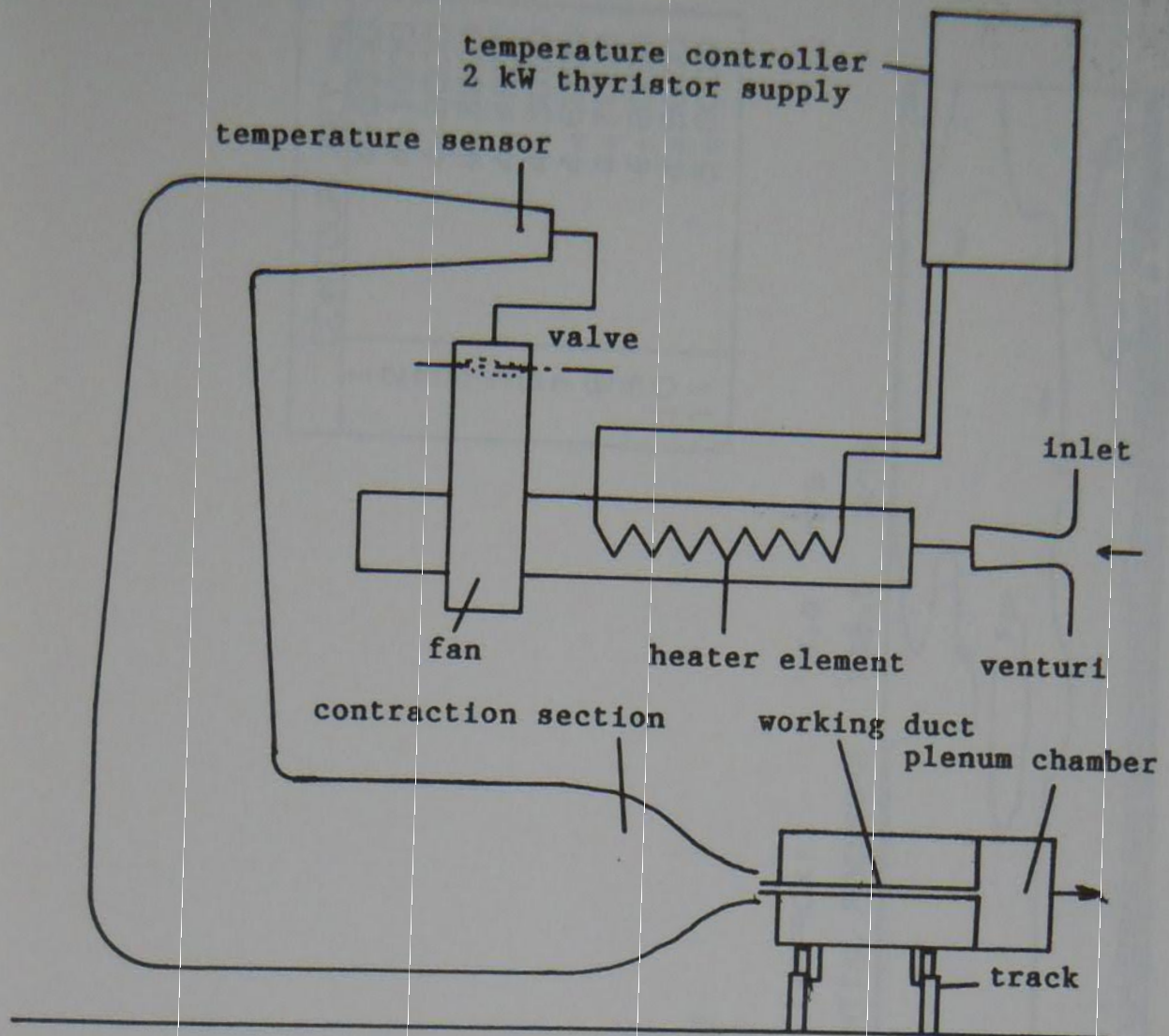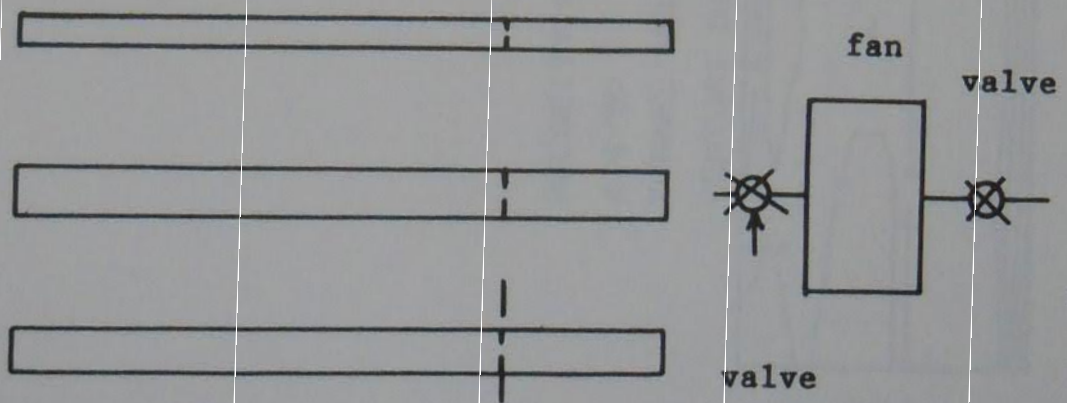
Figure 5.2 Schematic representation of the experimental rig
used to measure heat transfer and flow friction quantities

CONTOUR KEY m/s

1	4.0000
2	4.1000
3	4.2000
4	4.3000
5	4.4000
6	4.5000
7	4.6000
8	4.7000
9	4.8000
10	4.9000
11	5.0000

VELOCITY PROFILE

4/6/87

TUNNEL VELOCITY (APPROX)   5.0   M/S

VENTURI DIFFERENTIAL PRESSURE   758.5   N/M2
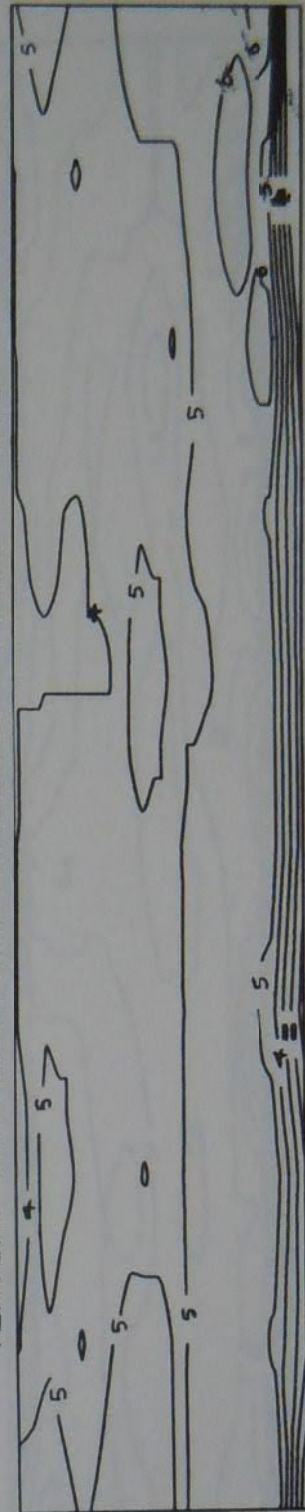
Figure 5.3   Velocity contours for the tunnel contraction at 5 m/s   and
laboratory temperature

205

CONTOUR KEY

1	0.0100
2	0.0110
3	0.0120
4	0.0130
5	0.0140
6	0.0150
7	0.0160
8	0.0170
9	0.0180
10	0.0190
11	0.0200
12	0.0210
13	0.0220
14	0.0230
15	0.0240
16	0.0250

TURBULENCE INTENSITY PROFILE

4/6/87

TUNNEL VELOCITY (APPROX)   5.0   M/S

VENTURI DIFFERENTIAL PRESSURE   758.5   N/M2

Figure 5.4 Turbulence intensity contours for the tunnel contraction at 5 m/s and laboratory temperature

CONTOUR KEY m/s

1	4.0000
2	4.0500
3	4.1000
4	4.1500
5	4.2000
6	4.2500
7	4.3000
8	4.3500
9	4.4000
10	4.4500
11	4.5000

VELOCITY PROFILE (HOT)

11/6/87

TUNNEL VELOCITY (APPROX)   4.2   M/S

VENTURI DIFFERENTIAL PRESSURE   600.0   N/M2
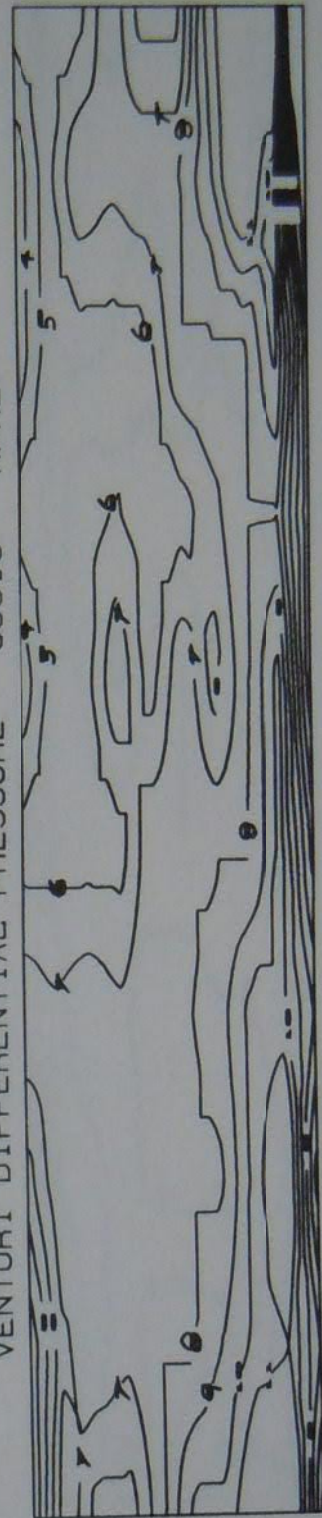
Figure 5.5 Velocity contours for the tunnel contraction at 4.2 m/s with heated air

Figure 5.6 Turbulence intensity contours for the tunnel contraction
at 4.2 m/s and heated air

CONTOUR KEY °C

1	47.0000
2	47.2000
3	47.4000
4	47.6000
5	47.8000
6	48.0000
7	48.2000
8	48.4000
9	48.6000
10	48.8000
11	49.0000
12	49.2000
13	49.4000
14	49.6000
15	49.8000
16	50.0000

TEMPERATURE PROFILE

22/6/87

TUNNEL VELOCITY (APPROX)   5.0   M/S

VENTURI DIFFERENTIAL PRESSURE   616.0   N/M2

Figure 5.7   Isotherm contours for the tunnel contraction at 5 m/s and heated air.

209
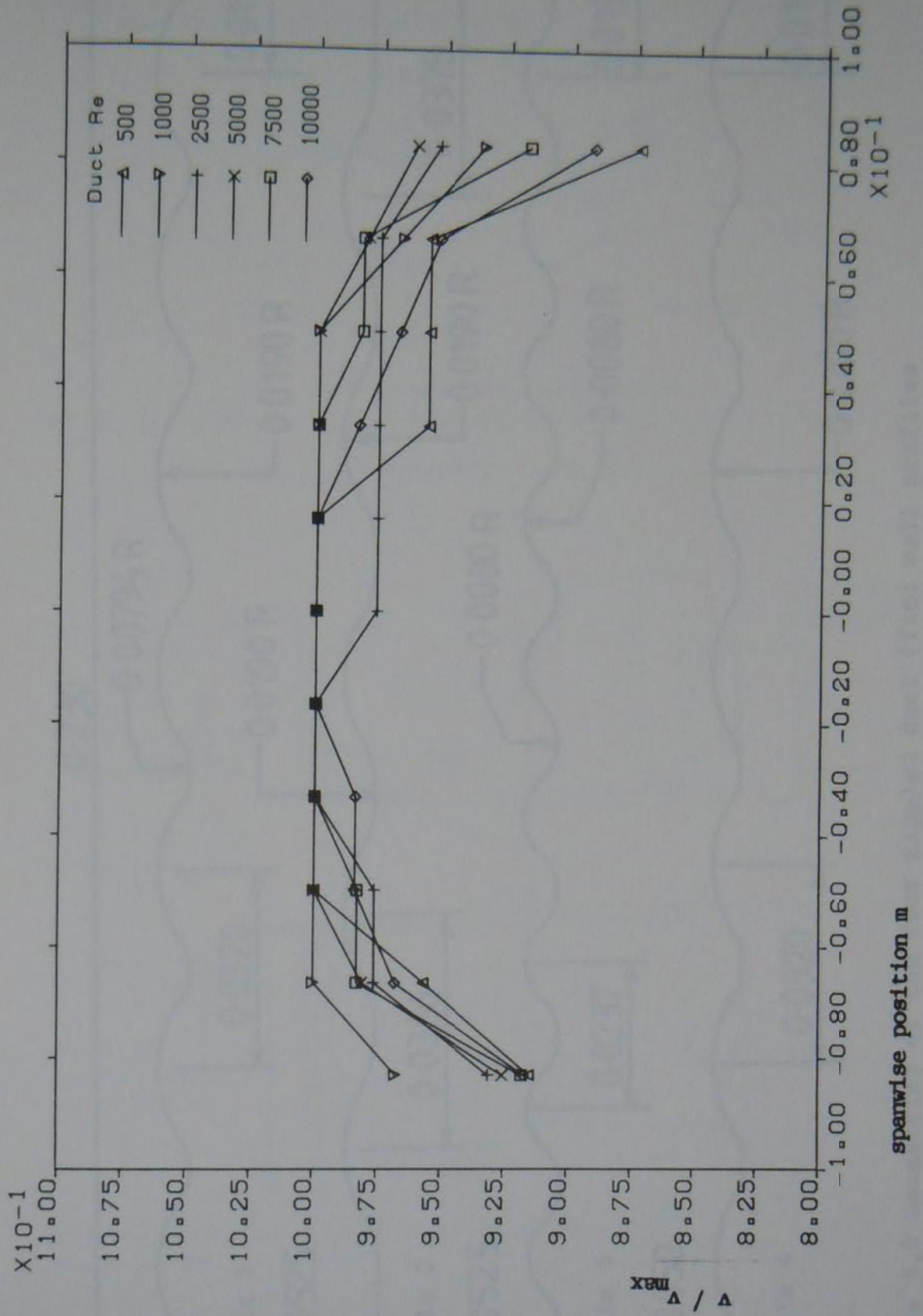
Figure 5.8 Centreline velocity profiles in the exit channel of the test duct for various Reynolds numbers
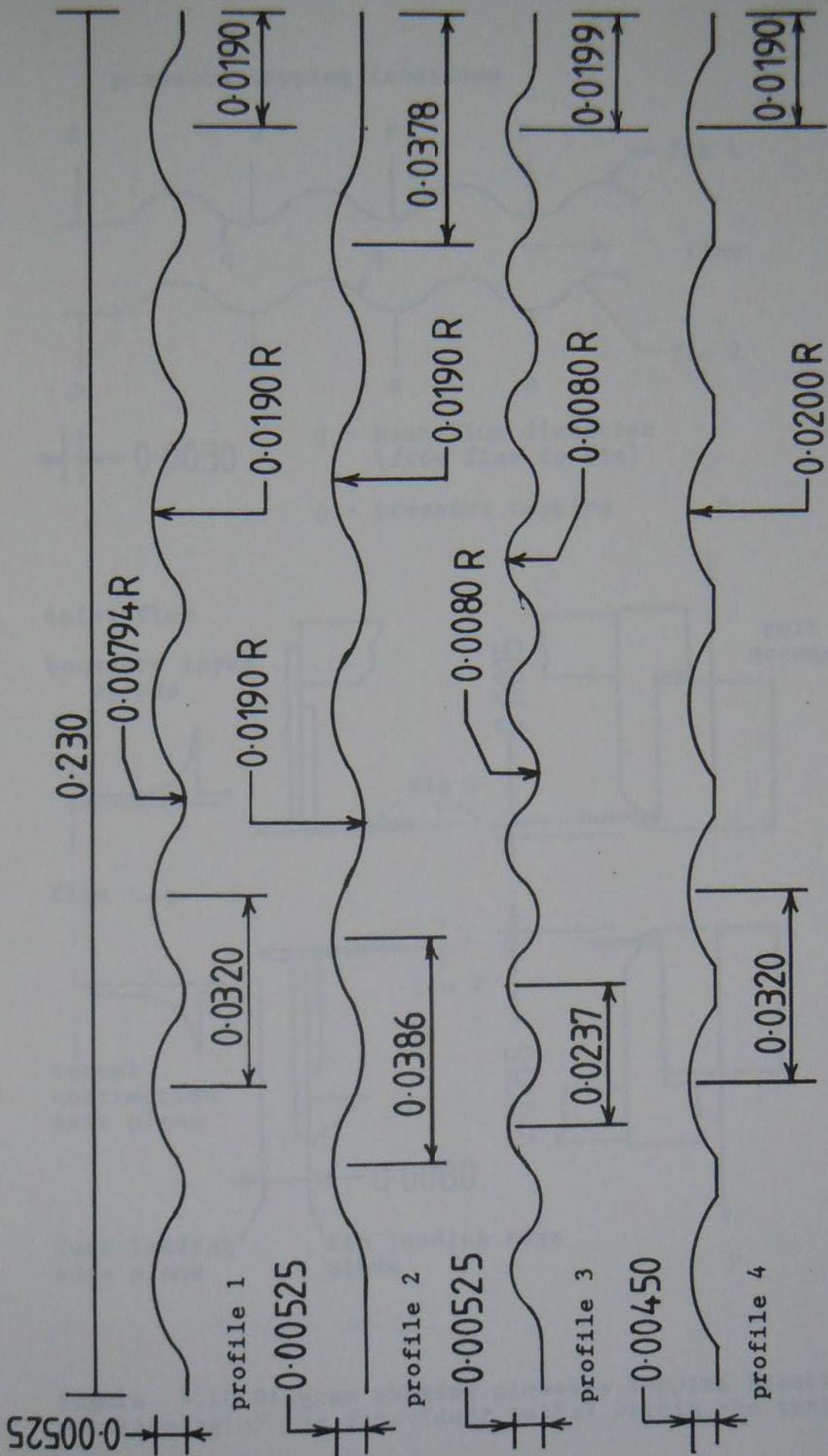
Figure 5.9 Geometries of the four rippled duct (fin) wall profiles

pressure tapping locations

0·0030

q – heat flux direction
(from flow to fin)

p – pressure tapping

inlet flow

boundary layer
bleeds

flow

tunnel
contraction
exit plane

duct leading
edge plane

fin leading edge
plane

fin 1

fin 2

0·0080

0·0015

0·0015

exit flow
arrangement

plenum
chamber
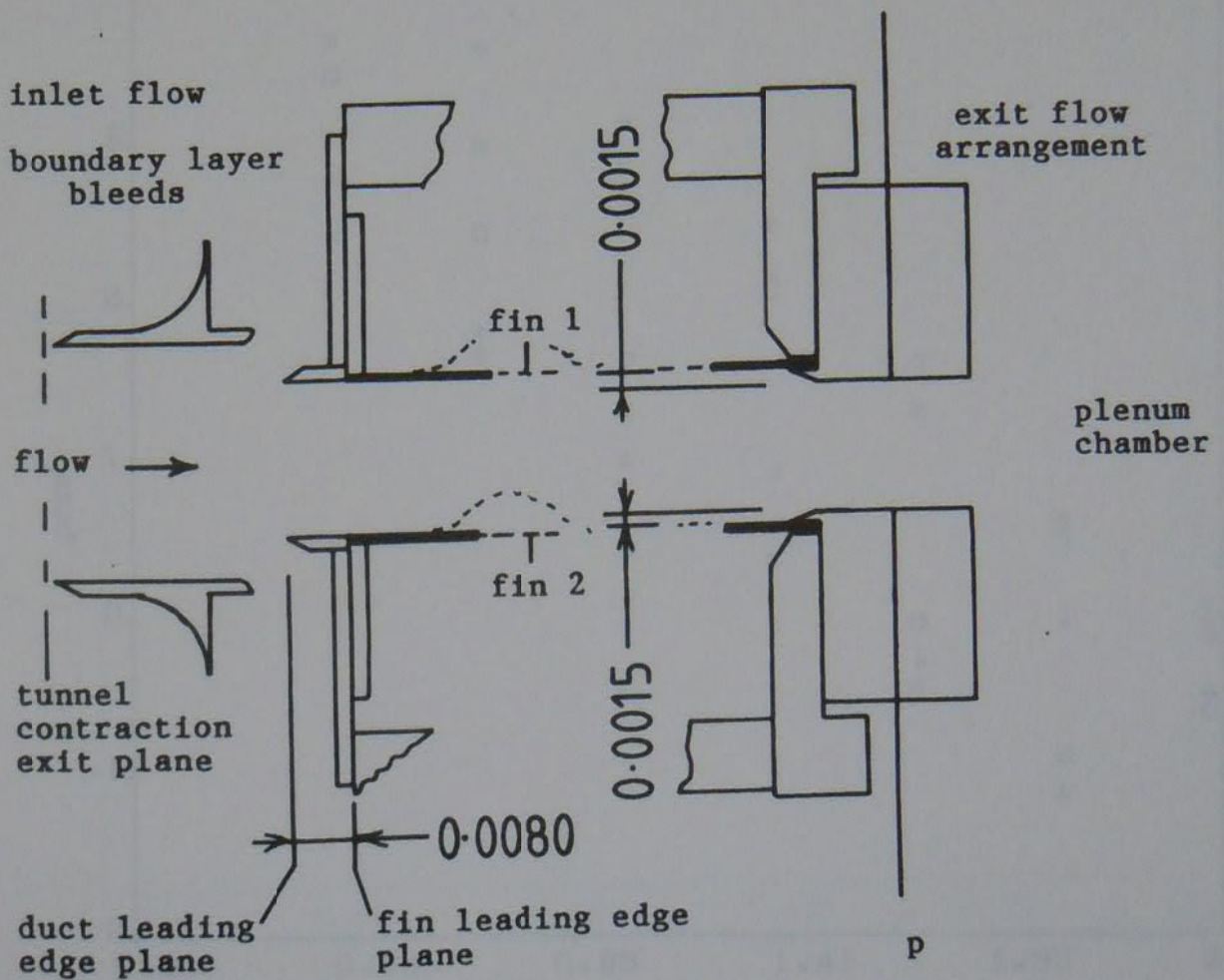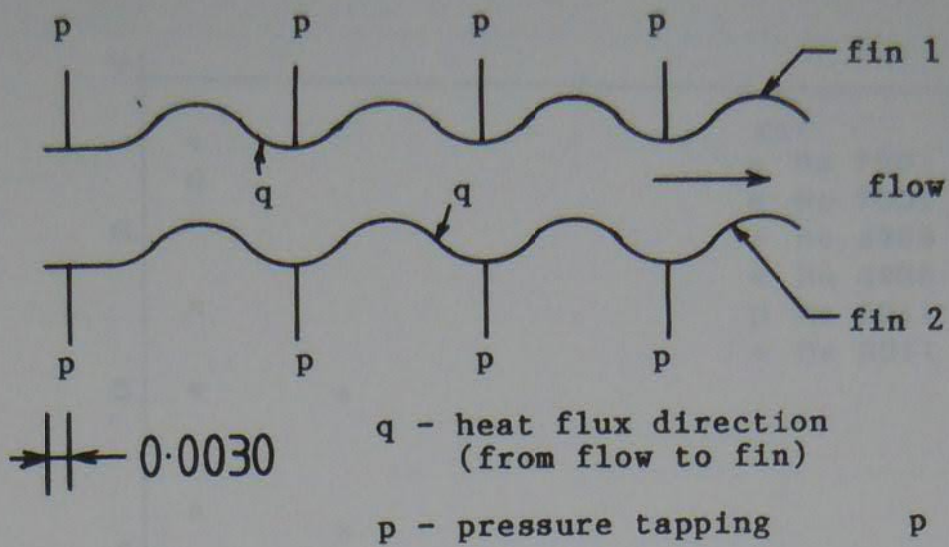
Figure 5.10 Diagram showing pressure tapping locations and positioning of the fins (duct walls) within the test section
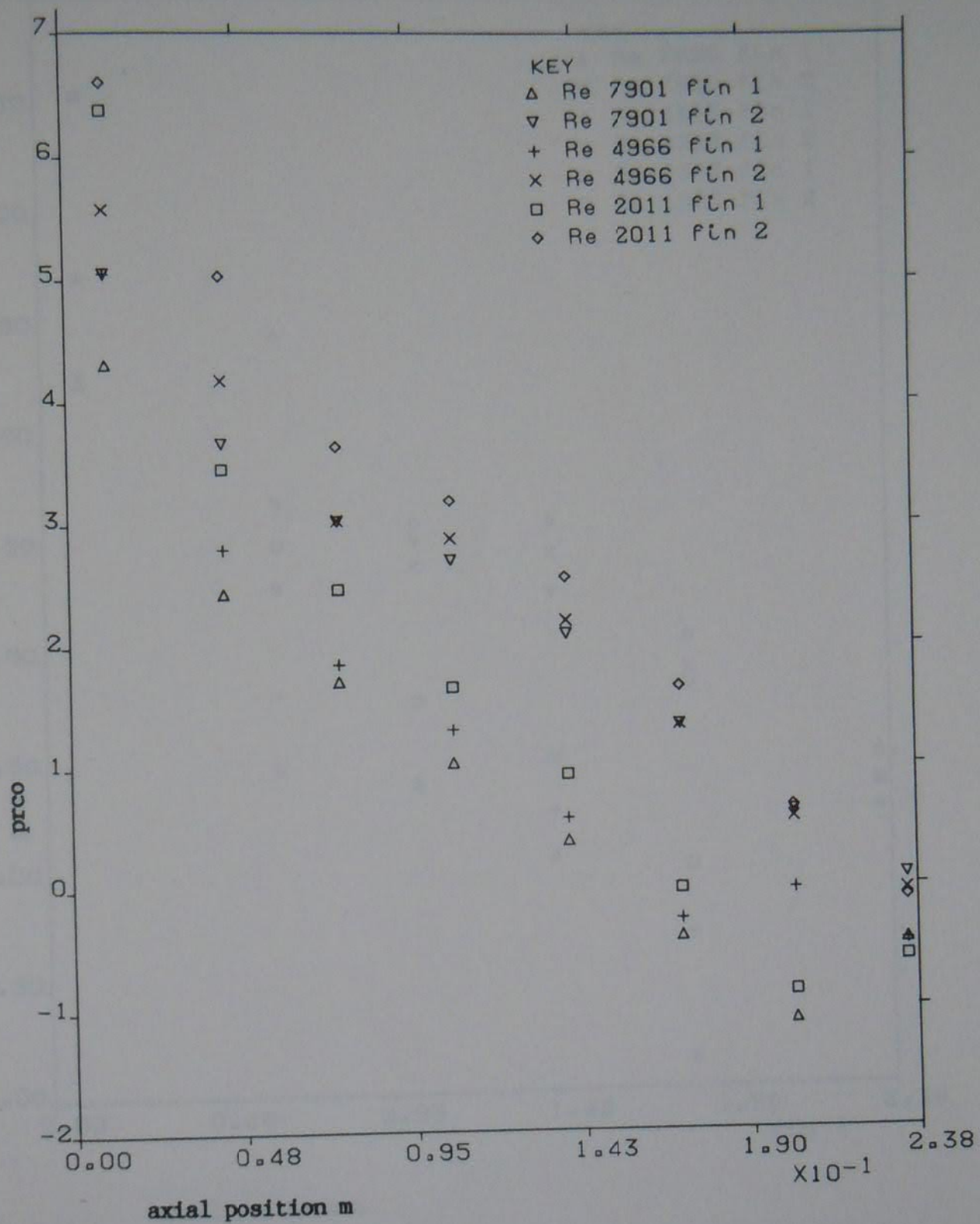
Figure 5.11 Friction data for profile 1, RH = 0.350, Dh = 0.0224 m
Re = 7901, 4965 and 2011

213
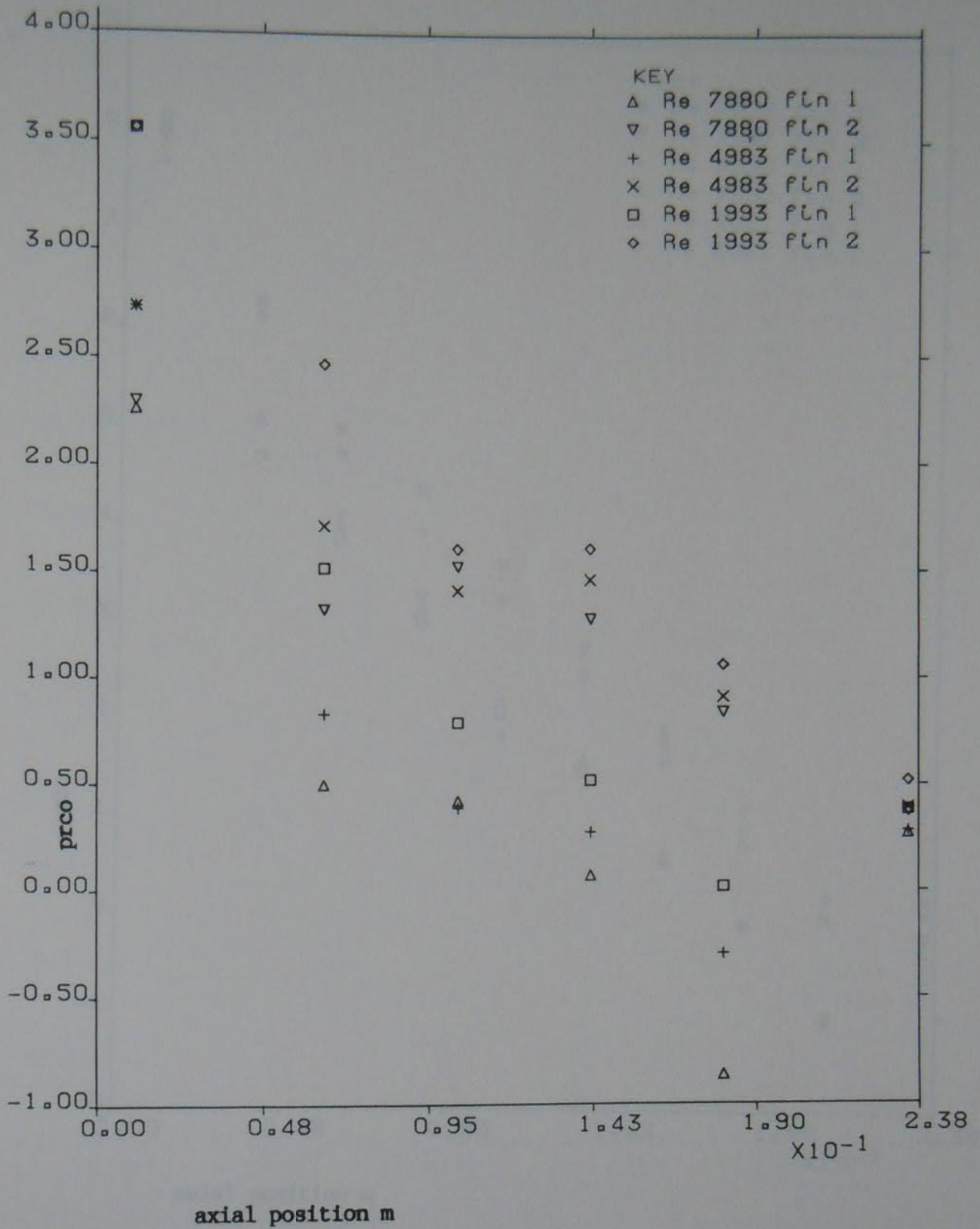
Figure 5.12 Friction data for profile 2, RH = 0.290, Dh = 0.0224 m
Re = 7880, 4983 and 1993

KEY

△   Re 7897 fln 1
▽   Re 7897 fln 2
+   Re 4950 fln 1
×   Re 4950 fln 2
□   Re 2021 fln 1
◇   Re 2021 fln 2

prco

axial position m

9

8

7

6

5

4

3

2

1

0

-1

-2

0.00   0.48   0.95   1.43   1.90   2.38

X10⁻¹
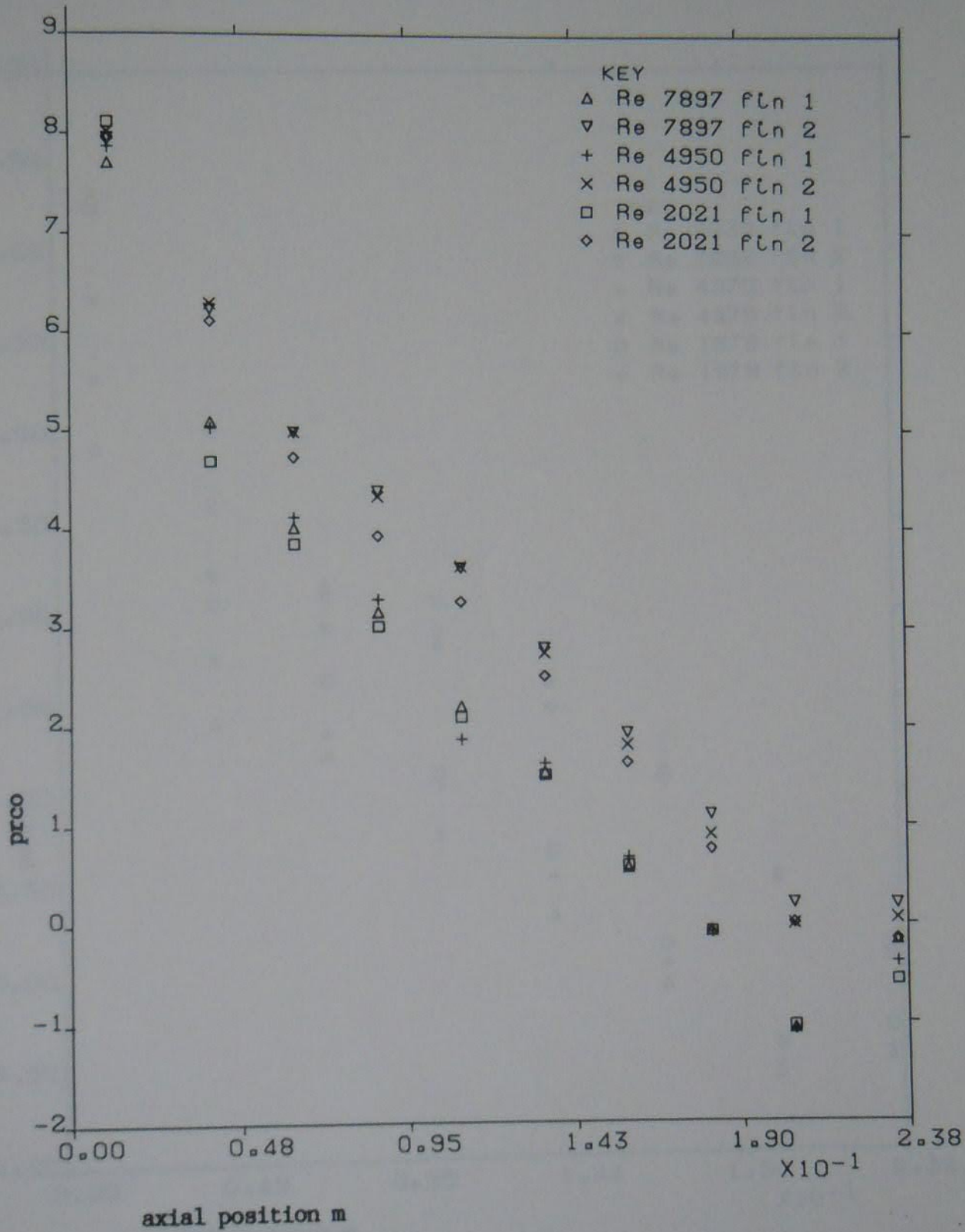
Figure 5.13 Friction data for profile 3, RH = 0.473, Dh = 0.0224 m
Re = 7897, 4950 and 2021

215
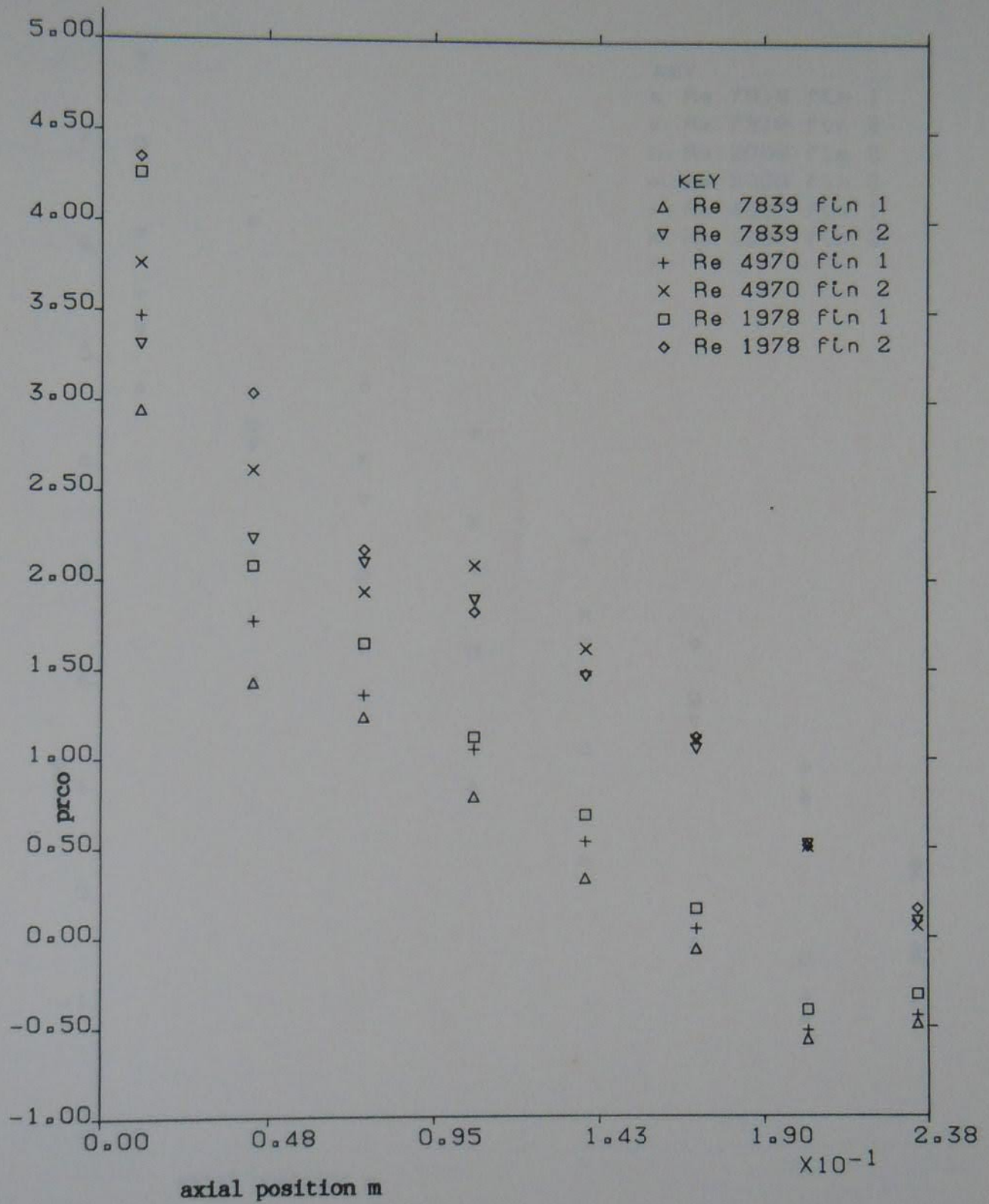
Figure 5.14 Friction data for profile 4, RH = 0.350, Dh = 0.0224 m
Re = 7839, 4970 and 1980
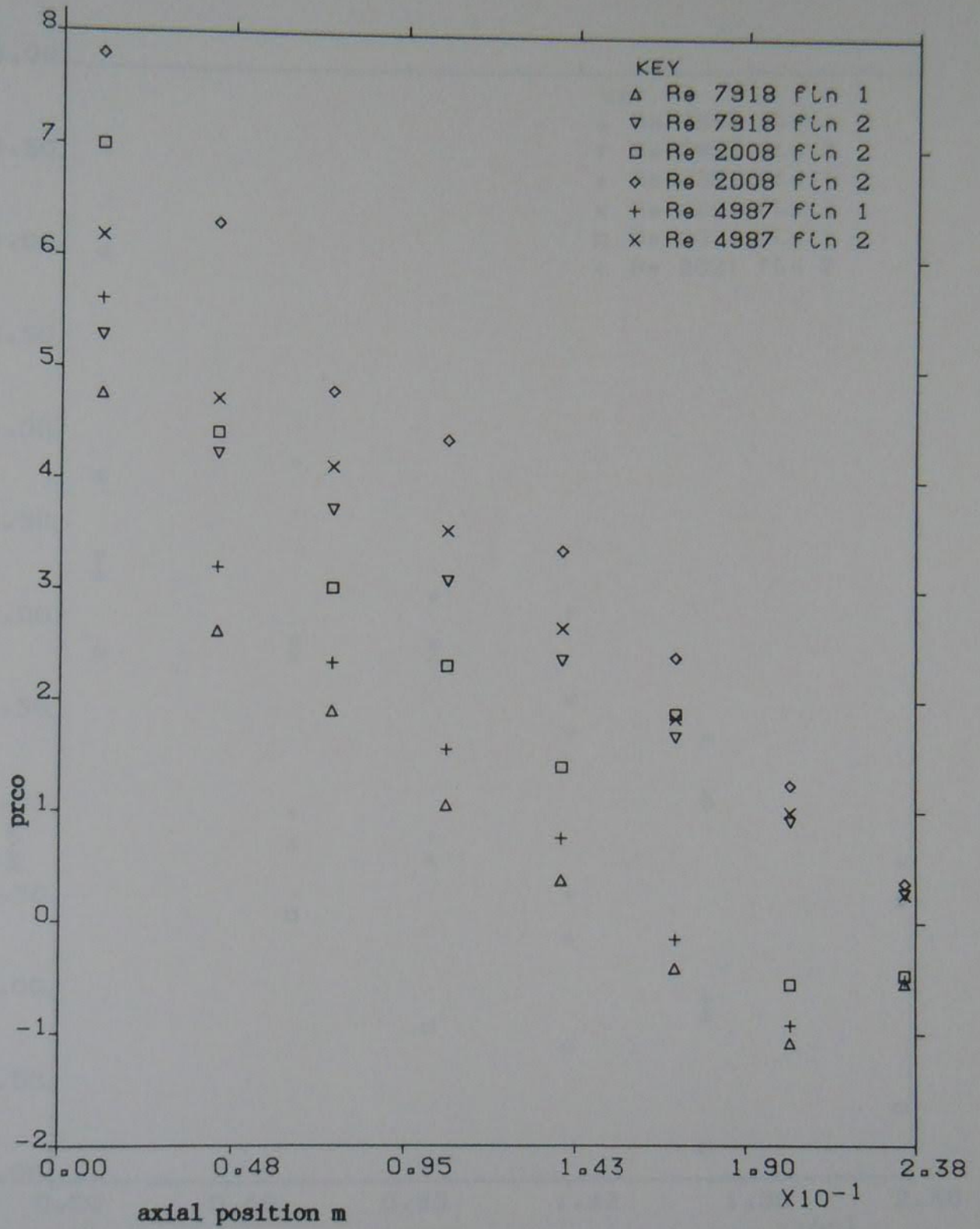
Figure 5.15 Friction data for profile 1, RH = 0.272, Dh = 0.0174 m
Re = 7918, 2008 and 4987
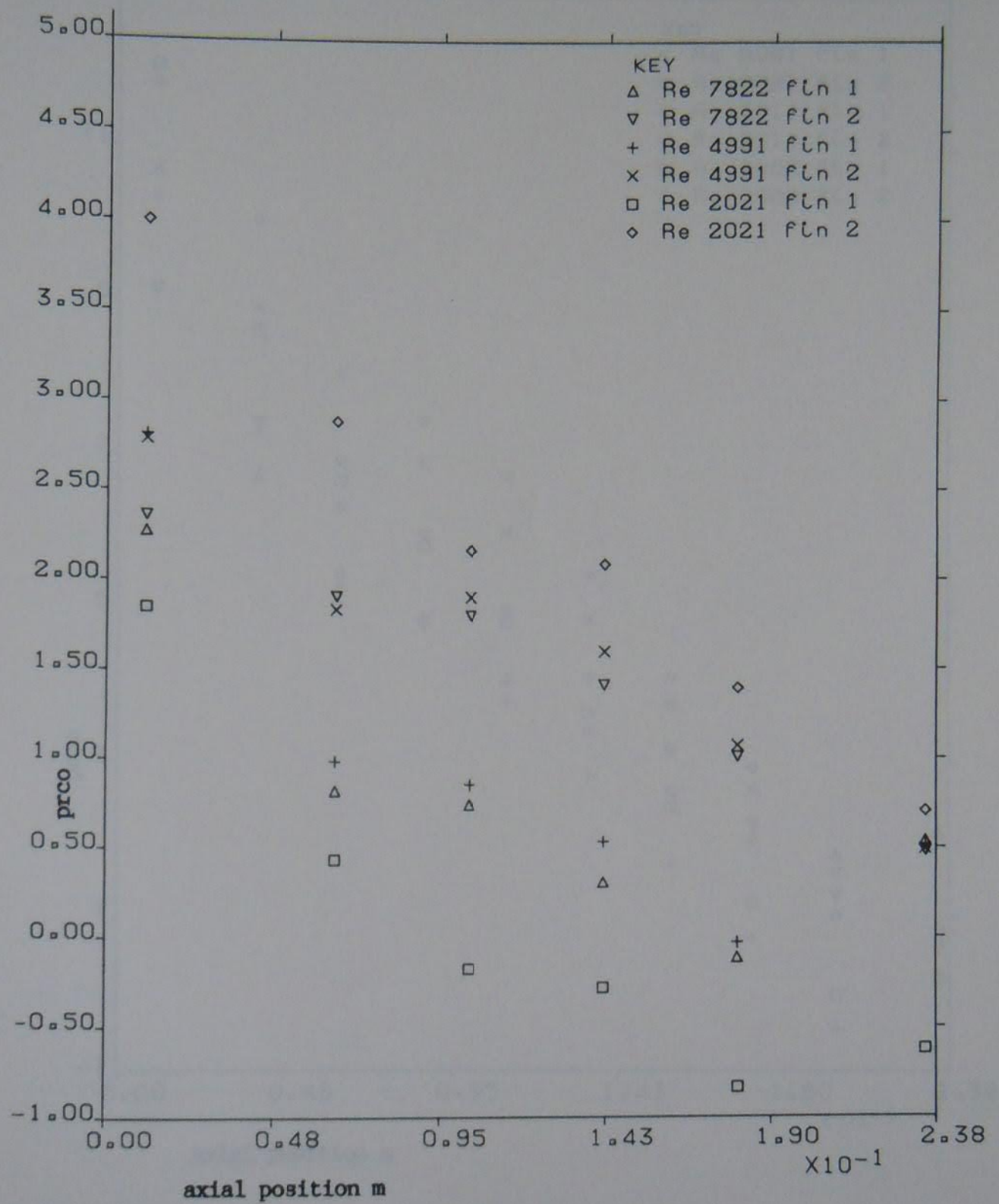
Figure 5.16 Friction data for profile 2, RH = 0.225, Dh = 0.0174 m   Re = 7822, 4991 and 2021 .mt 55
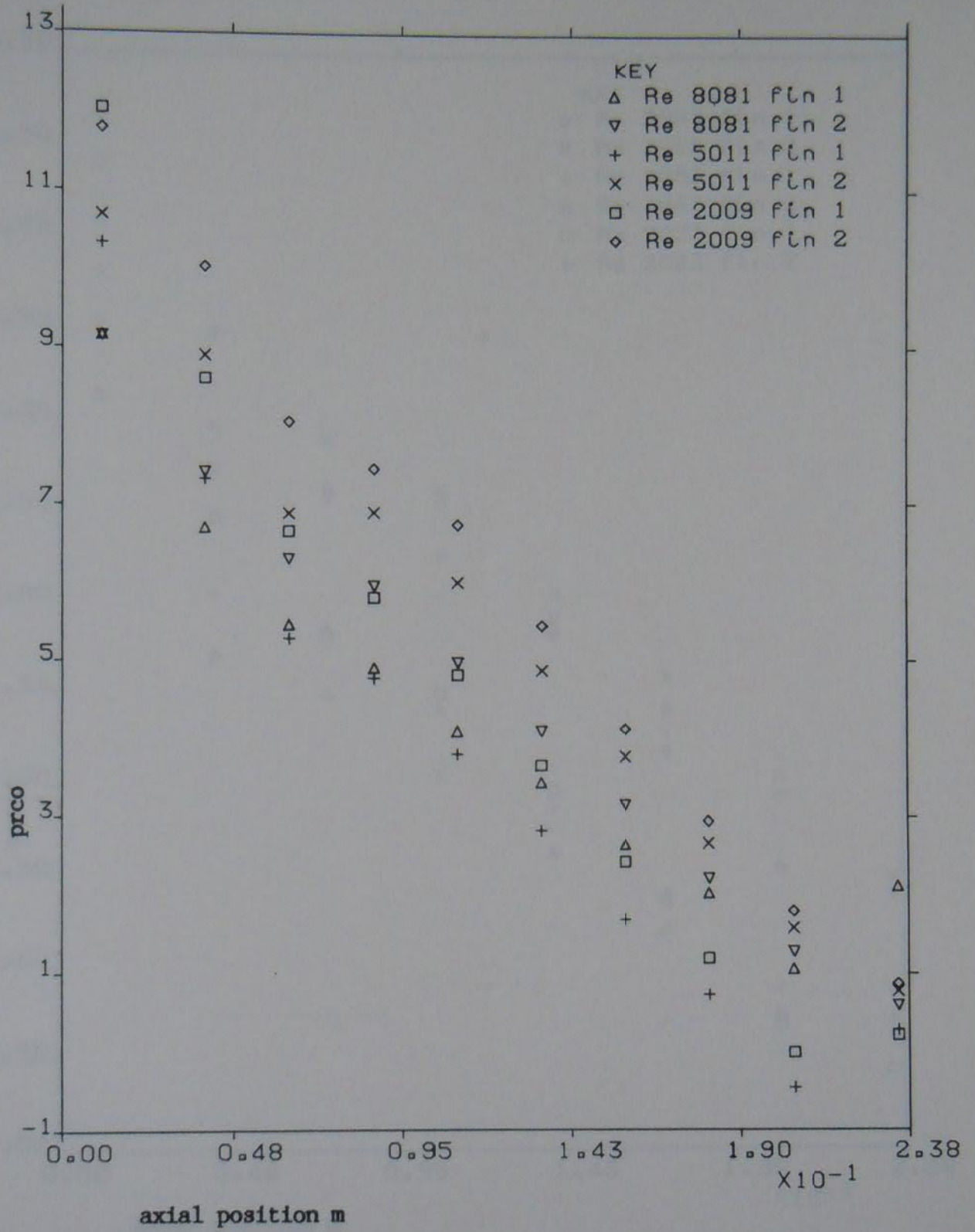
Figure 5.17 Friction data for profile 3, RH = 0.367, Dh = 0.0174 m
Re = 8081, 5011 and 2009
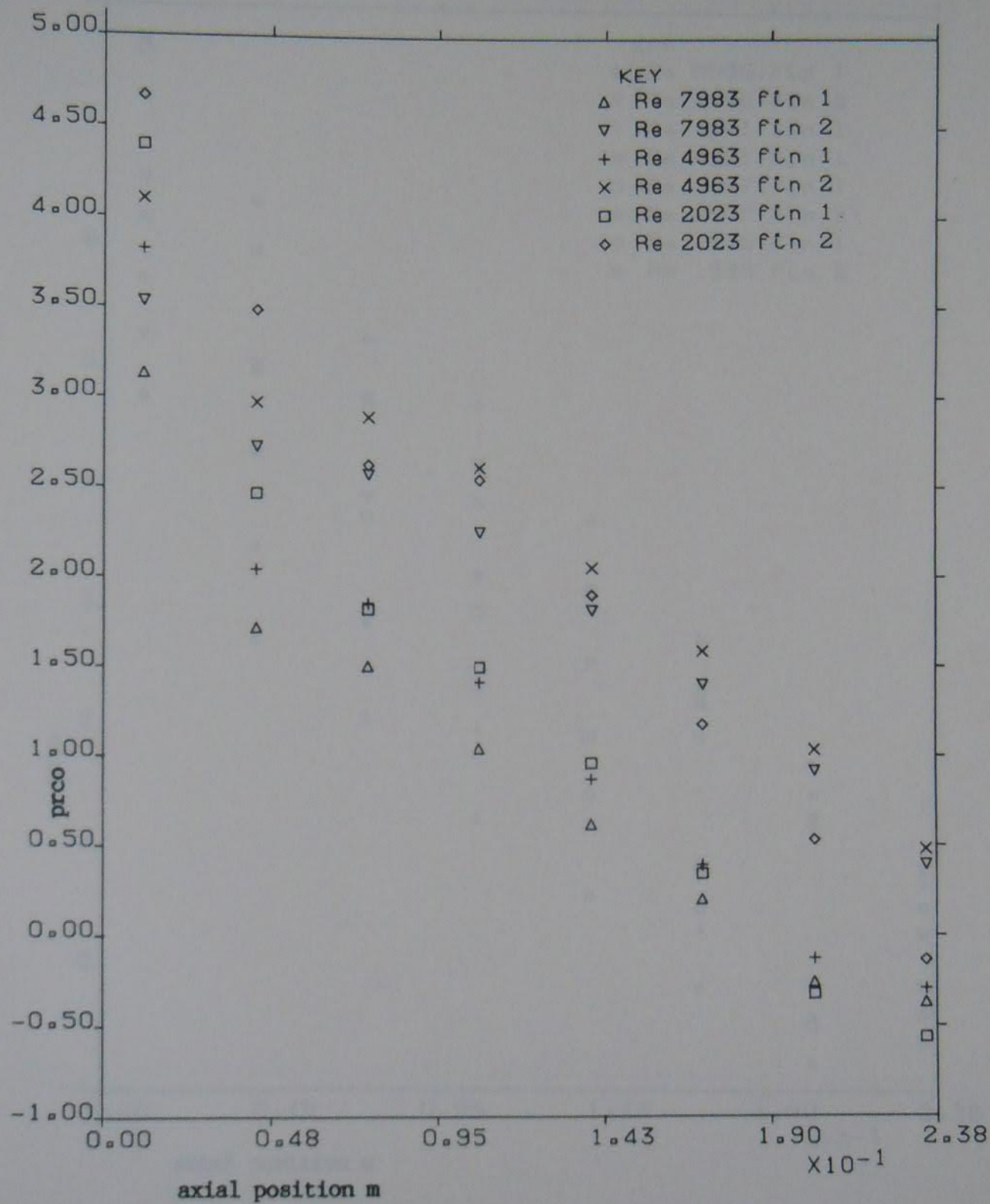
Figure 5.18 Friction data for profile 4, RH = 0.272, Dh = 0.0174 m
Re = 7983, 4963 and 2023
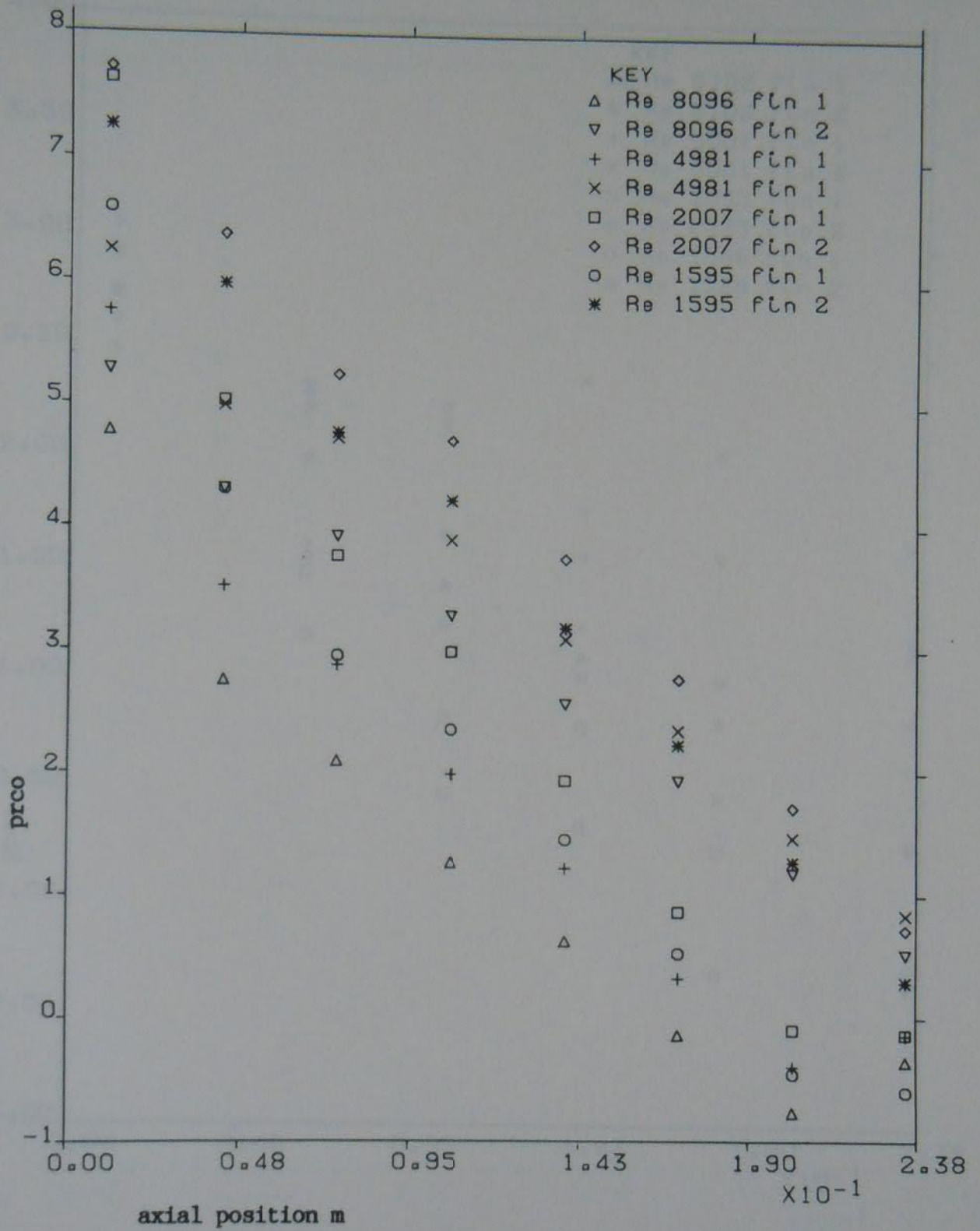
Figure 5.19 Friction data for profile 1, RH = 0.222, Dh = 0.0142 m
Re = 8096, 4981, 2008 and 1595
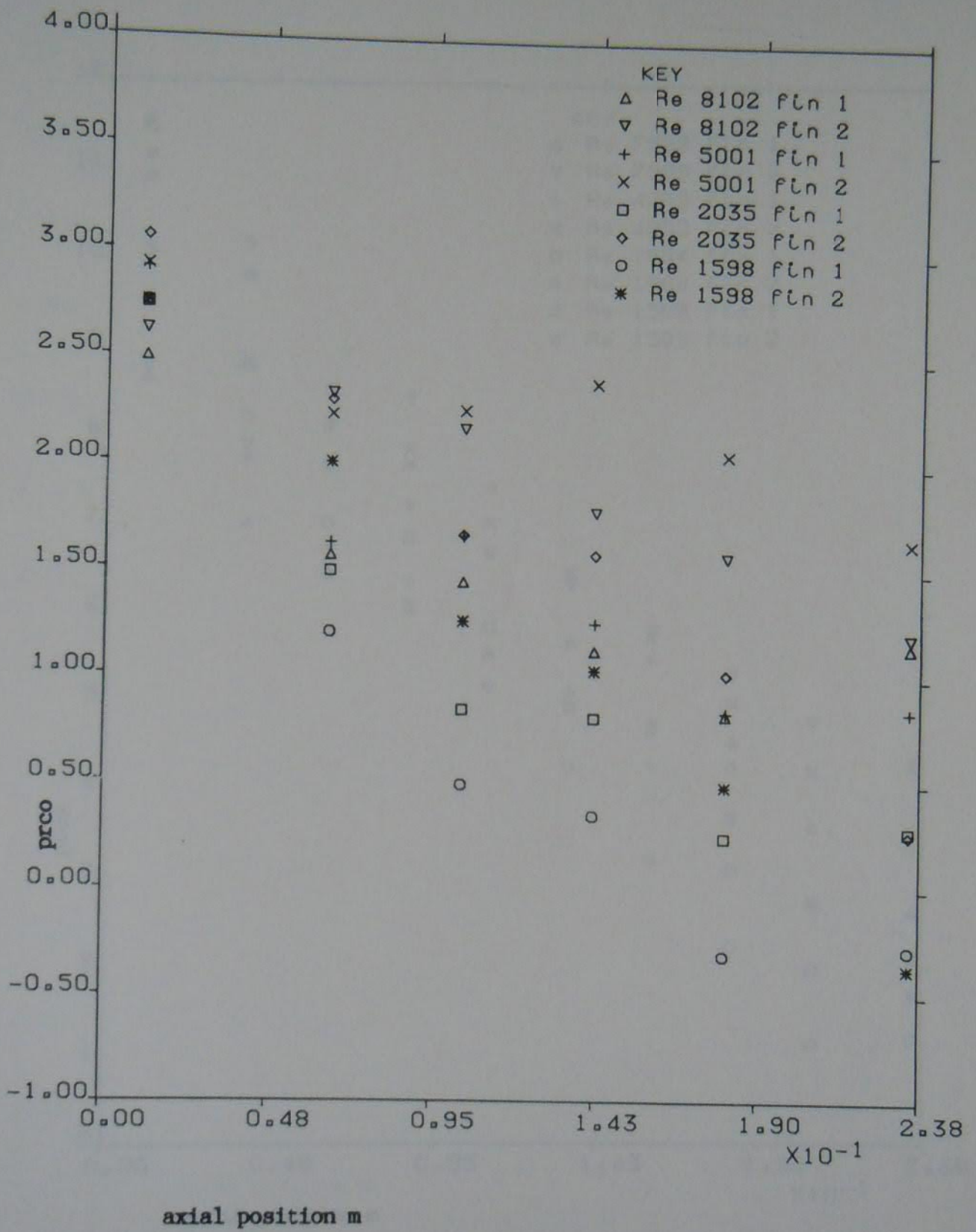
Figure 5.20 Friction data for profile 2, RH = 0.184, Dh = 0.0142 m
Re = 8102, 5001, 2035 and 1598
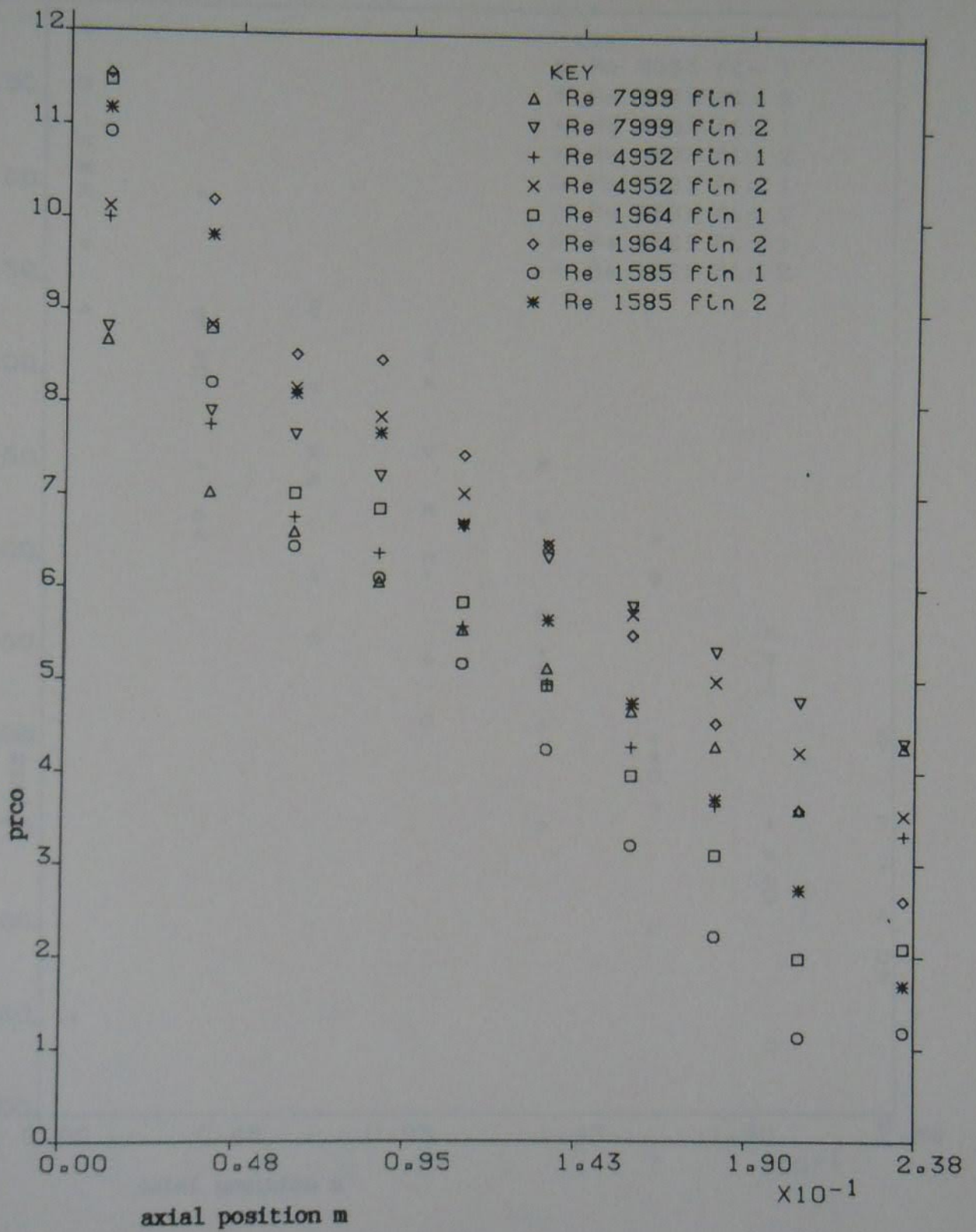
Figure 5.21 Friction data for profile 3, RH = 0.300, Dh = 0.0142 m
Re = 7999, 4952, 1964 and 1585
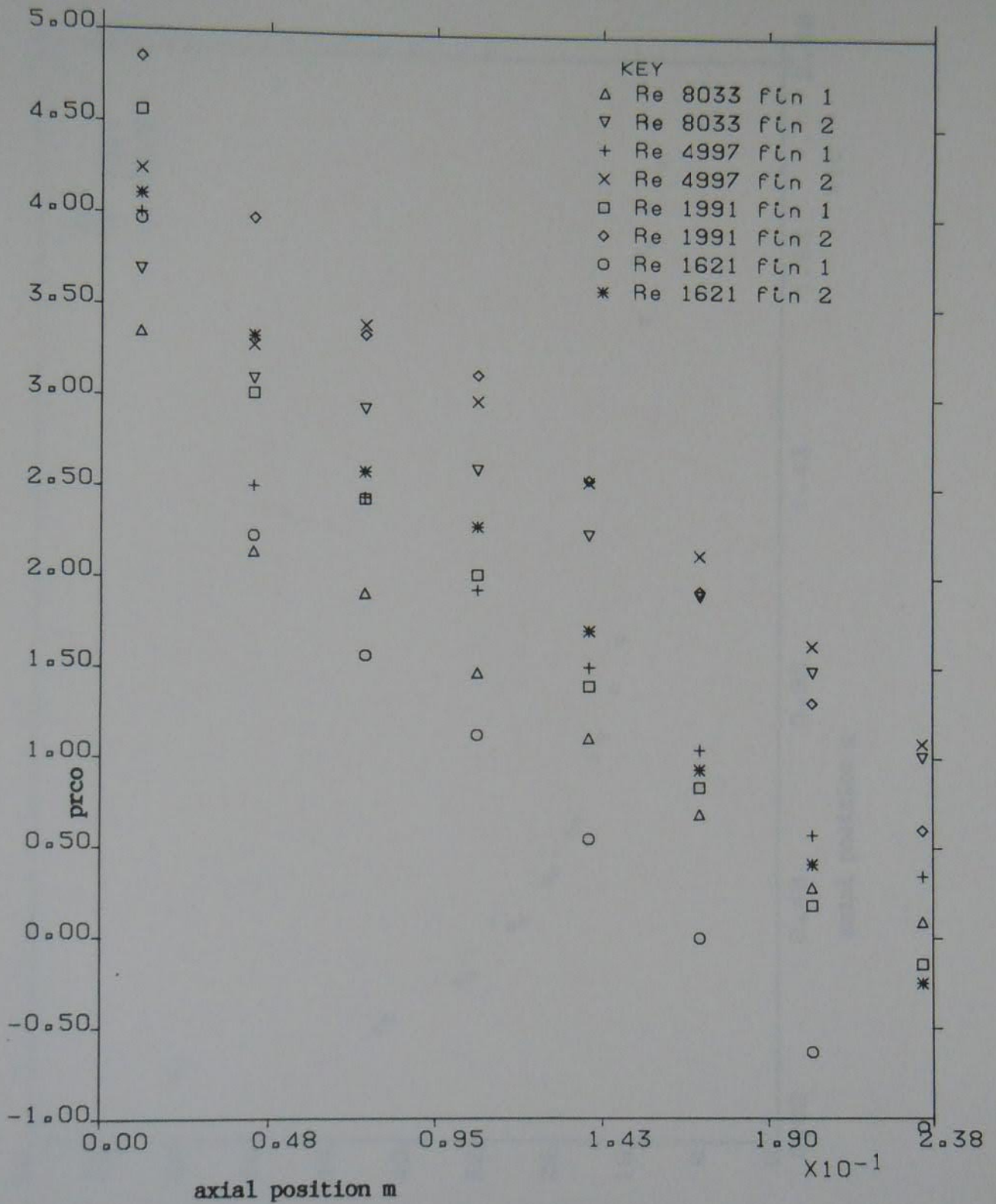
Figure 5.22 Friction data for profile 4, RH = 0.222, Dh = 0.0142 m
Re = 8033, 4997, 1991 and 1621
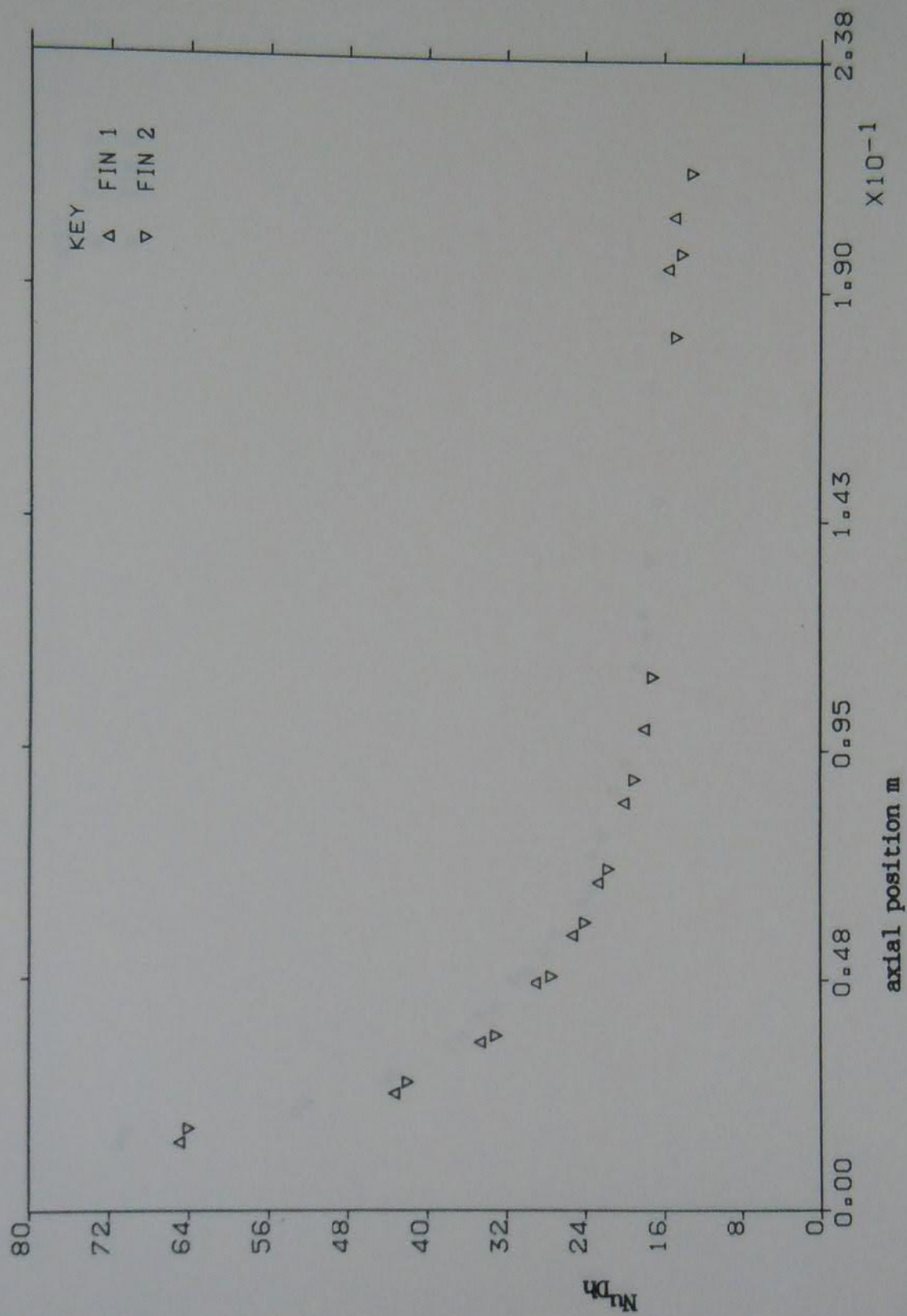
Figure 5.23 Heat transfer test data, plain fin, Dh = 0.0224 m,
Re = 7832
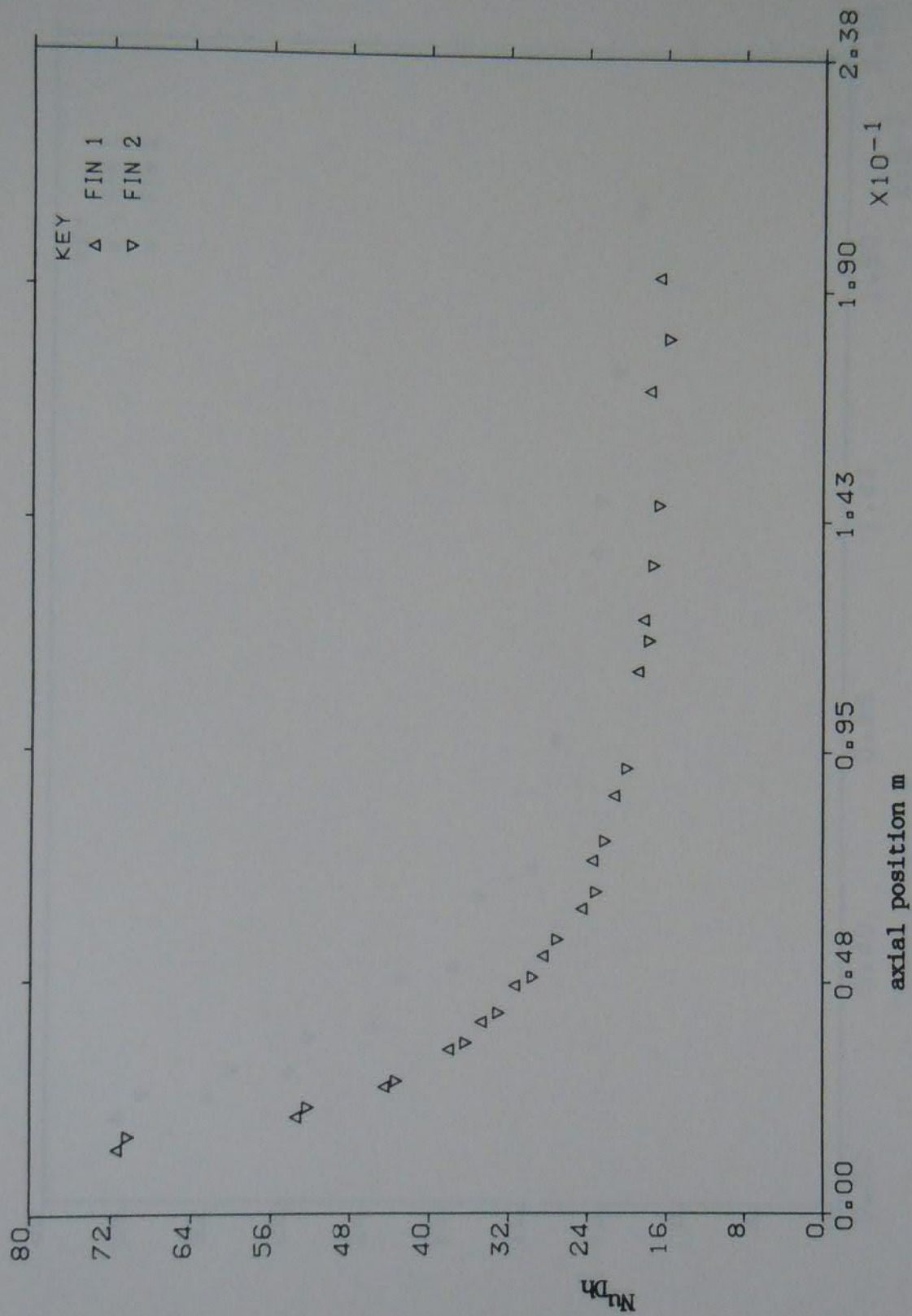
Figure 5.24 Heat transfer test data, plain fin, Dh = 0.0224 m,
Re = 7952
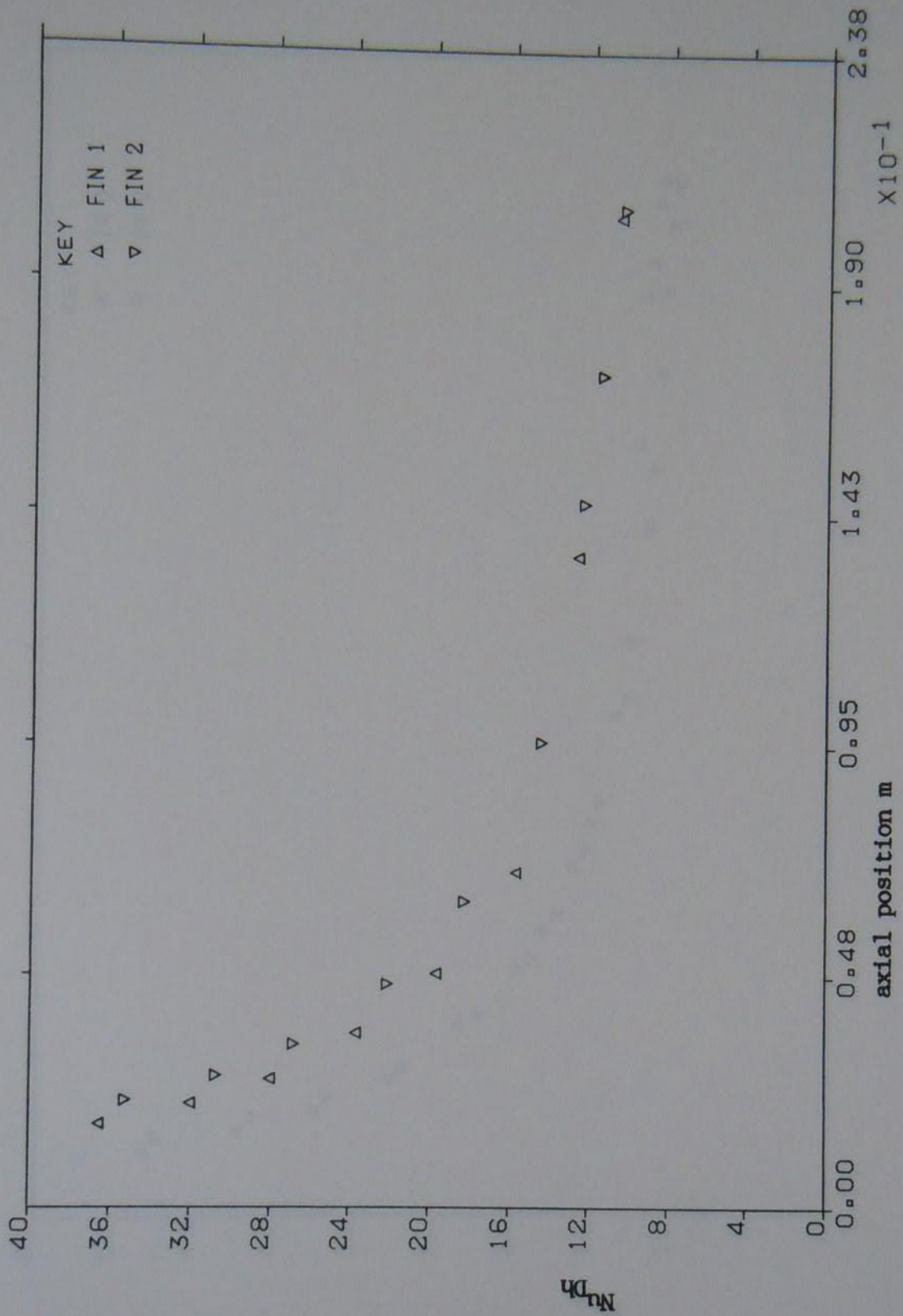
Figure 5.25 Heat transfer test data, plain fin, Dh = 0.0224 m, Re = 4973
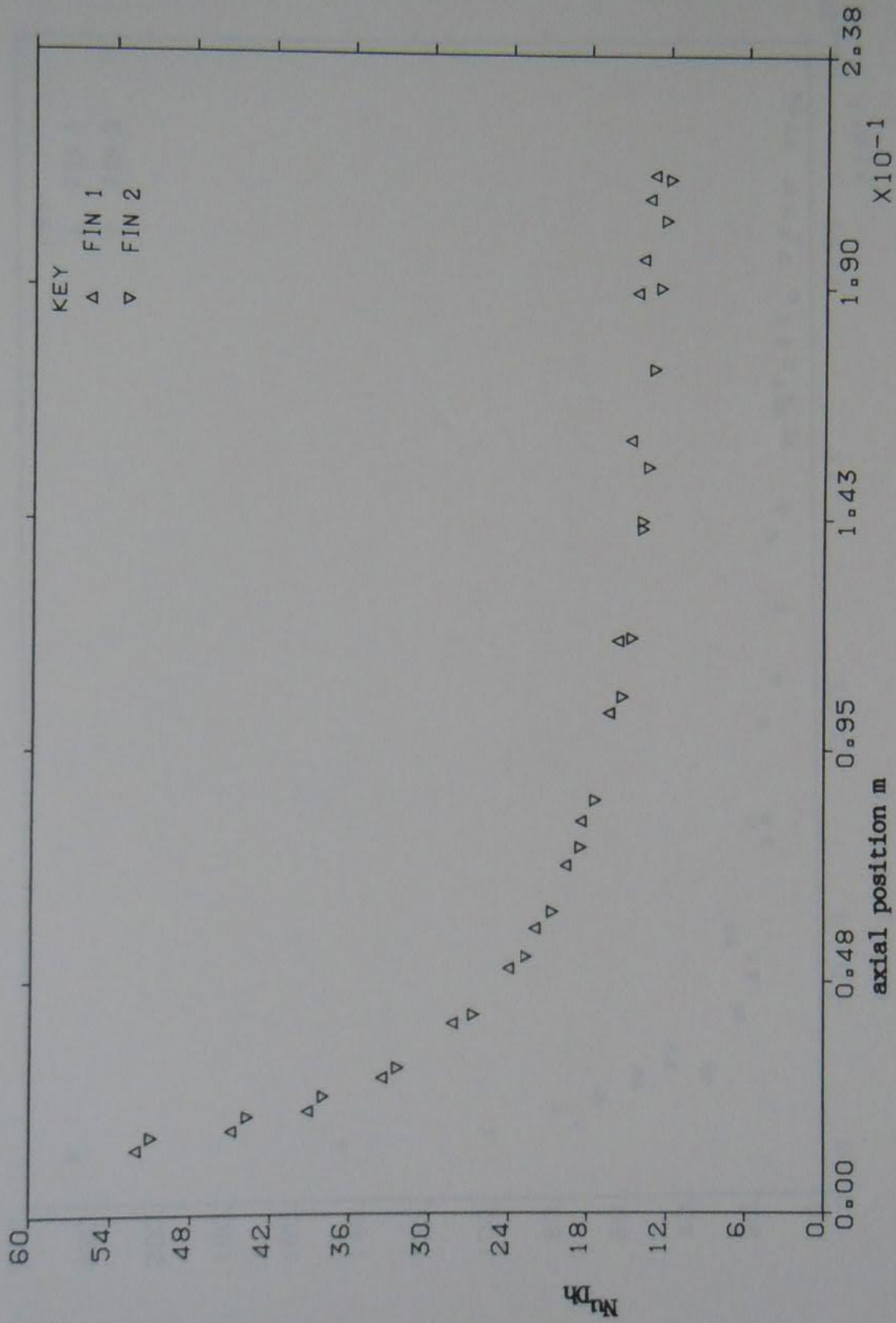
Figure 5.26 Heat transfer test data, plain fin, Dh = 0.0224 m,
Re = 6424
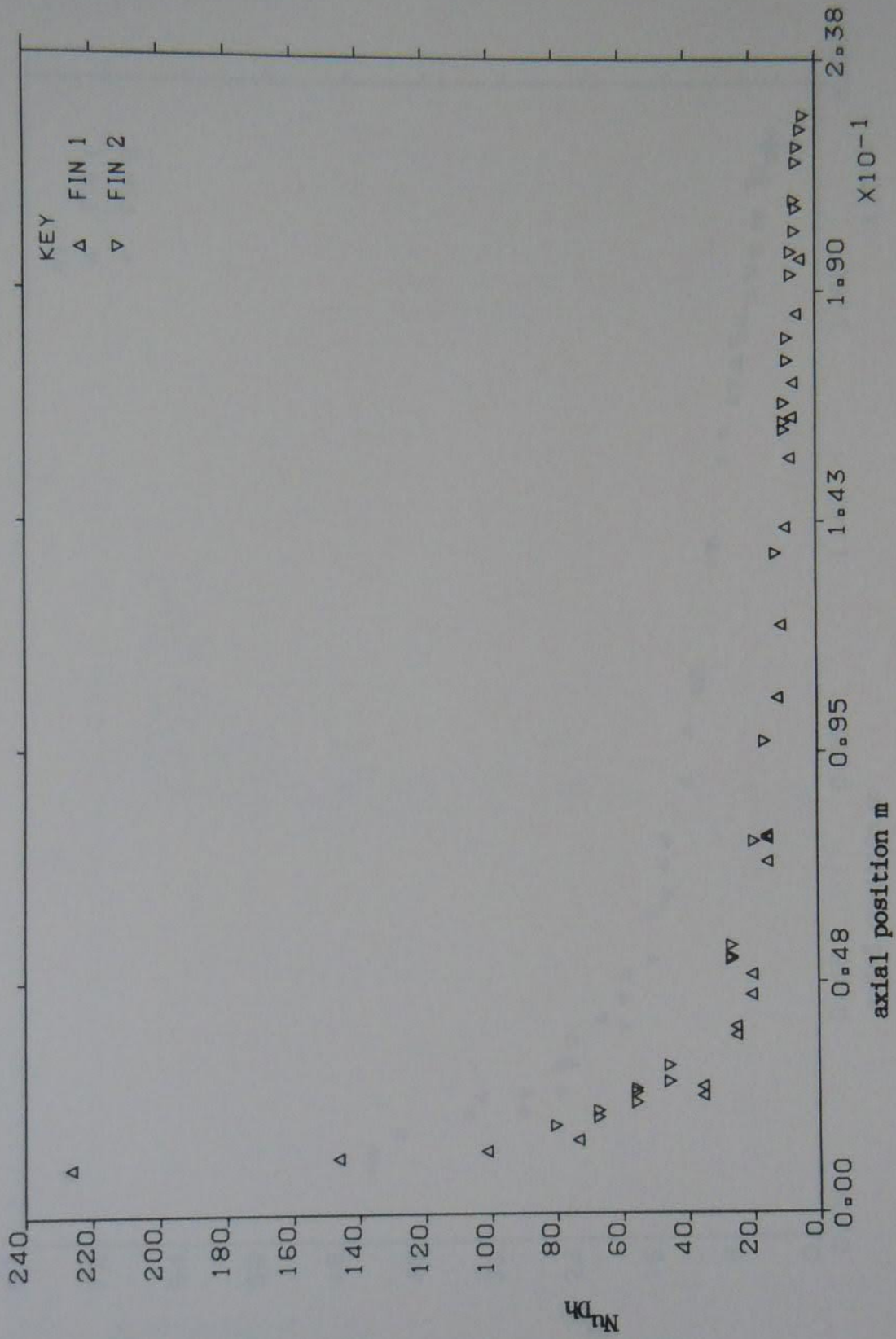
Figure 5.27 Heat transfer test data, plain fin, Dh = 0.0224 m,
Re = 2049
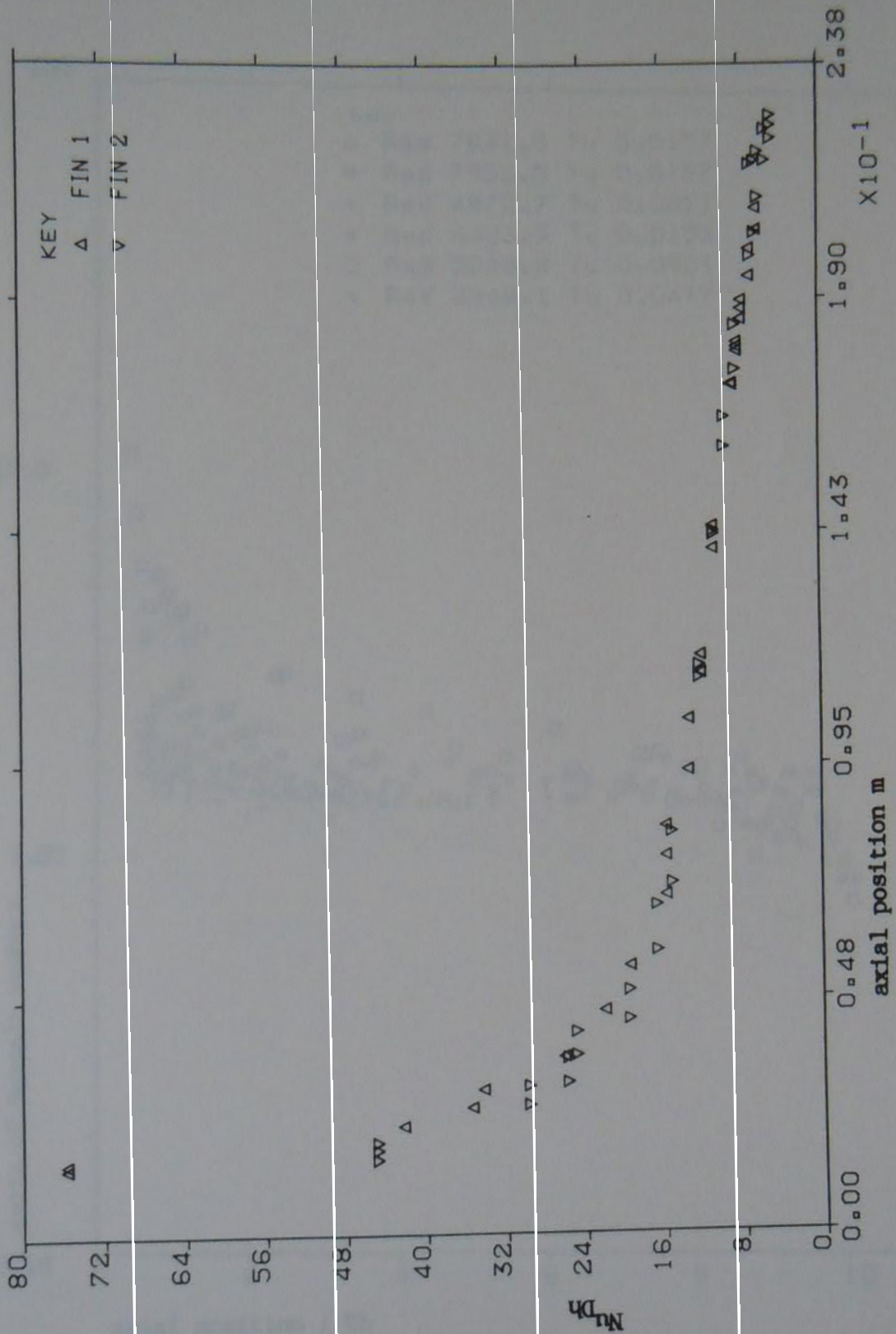
Figure 5.28 Heat transfer test data, plain fin, Dh = 0.0224 m,
Re = 2943
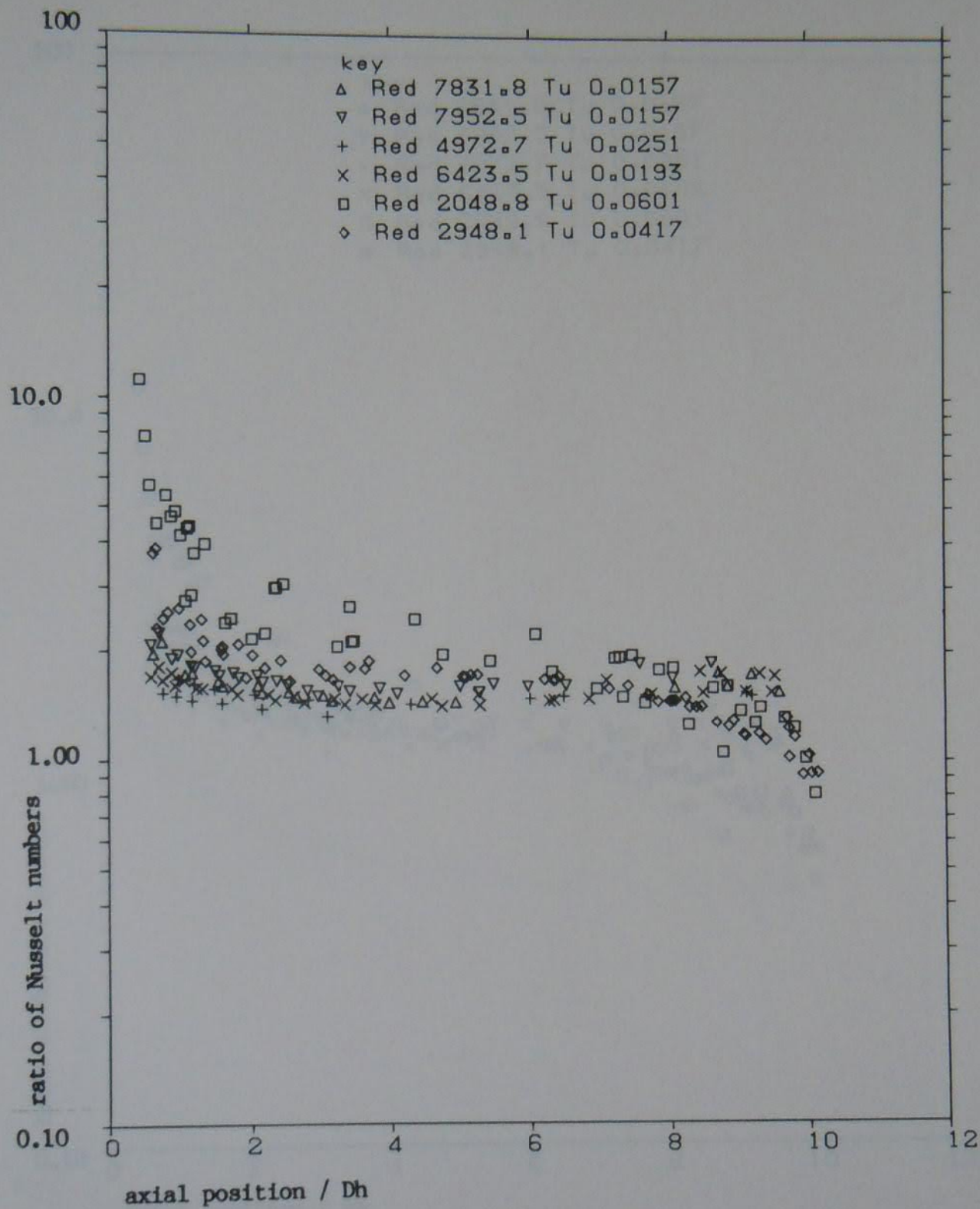
Figure 5.29 Comparison of plain fin heat transfer test data with the Pohlhausen laminar flow over a flat plate

key
△ Red 7831.8 Tu 0.0157
▽ Red 7952.5 Tu 0.0157
+ Red 4972.7 Tu 0.0251
× Red 6423.5 Tu 0.0193
□ Red 2048.8 Tu 0.0601
◇ Red 2948.1 Tu 0.0417
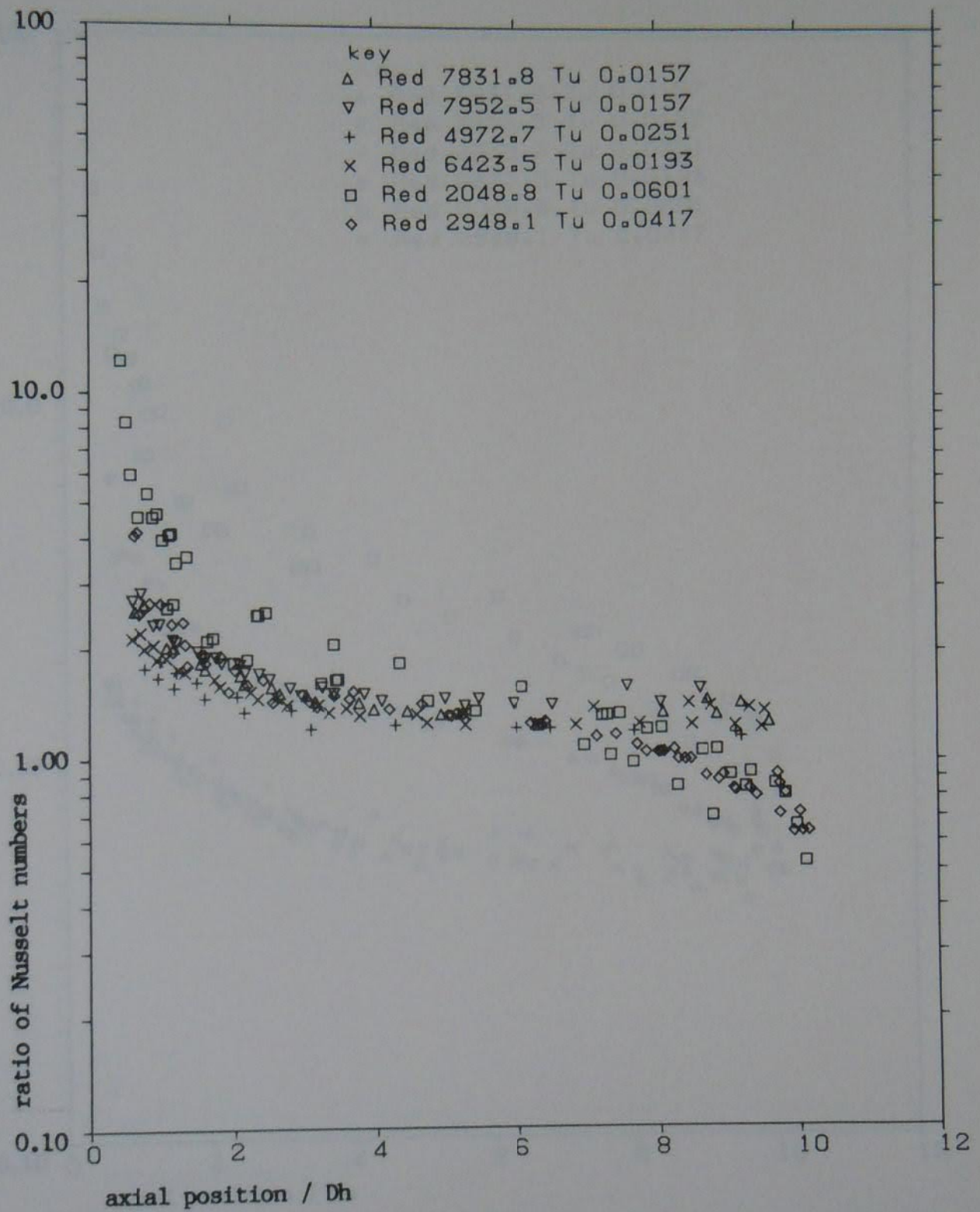
Figure 5.30 Comparison of plain fin heat transfer test data with the laminar circular tube inlet region from Kern and Kraus (1972)

key
△ Red 7831.8 Tu 0.0157
▽ Red 7952.5 Tu 0.0157
+ Red 4972.7 Tu 0.0251
× Red 6423.5 Tu 0.0193
□ Red 2048.8 Tu 0.0601
◇ Red 2948.1 Tu 0.0417
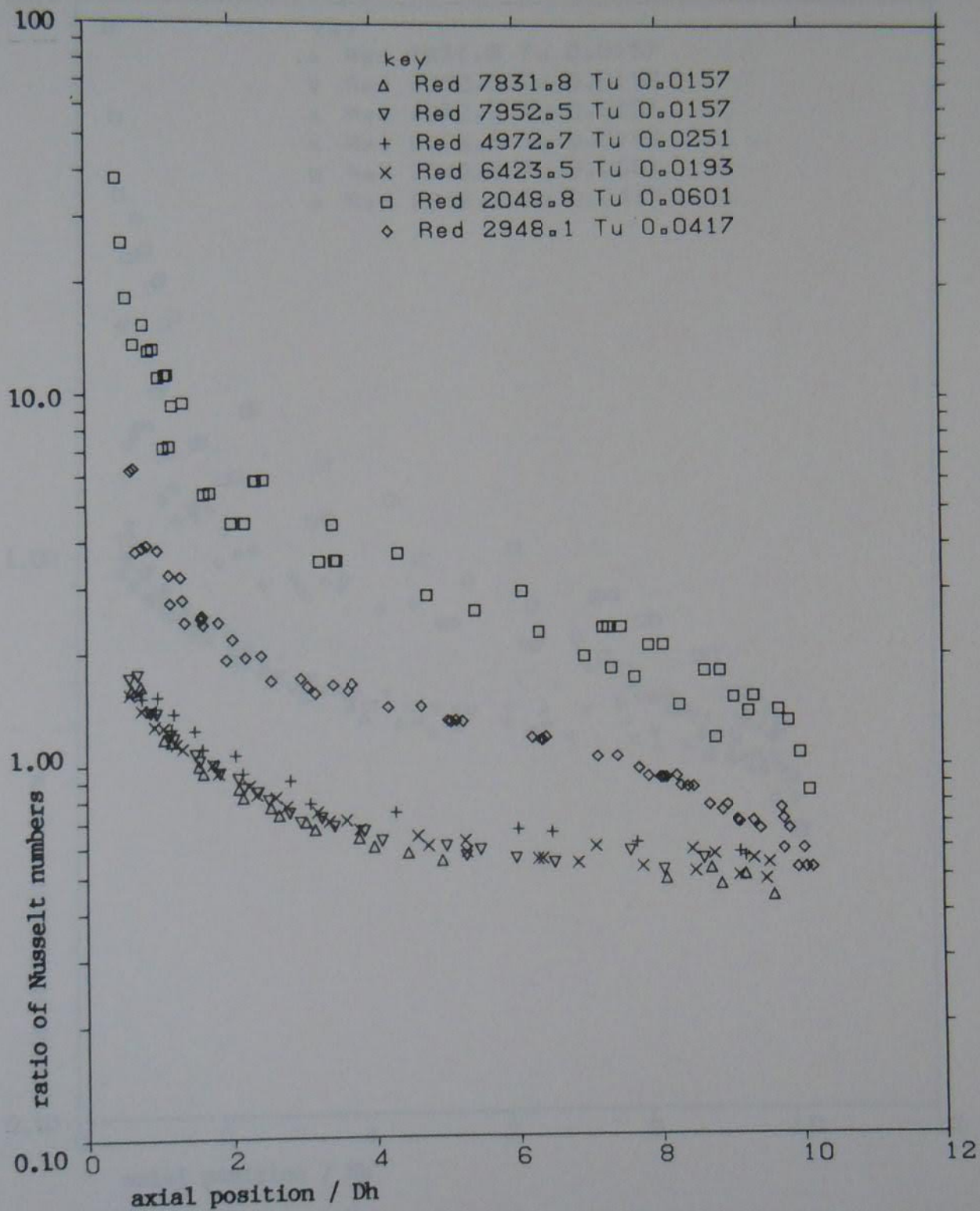
Figure 5.31 Comparison of plain fin heat transfer test data with the transitional circular tube inlet region from Kern and Kraus (1972)
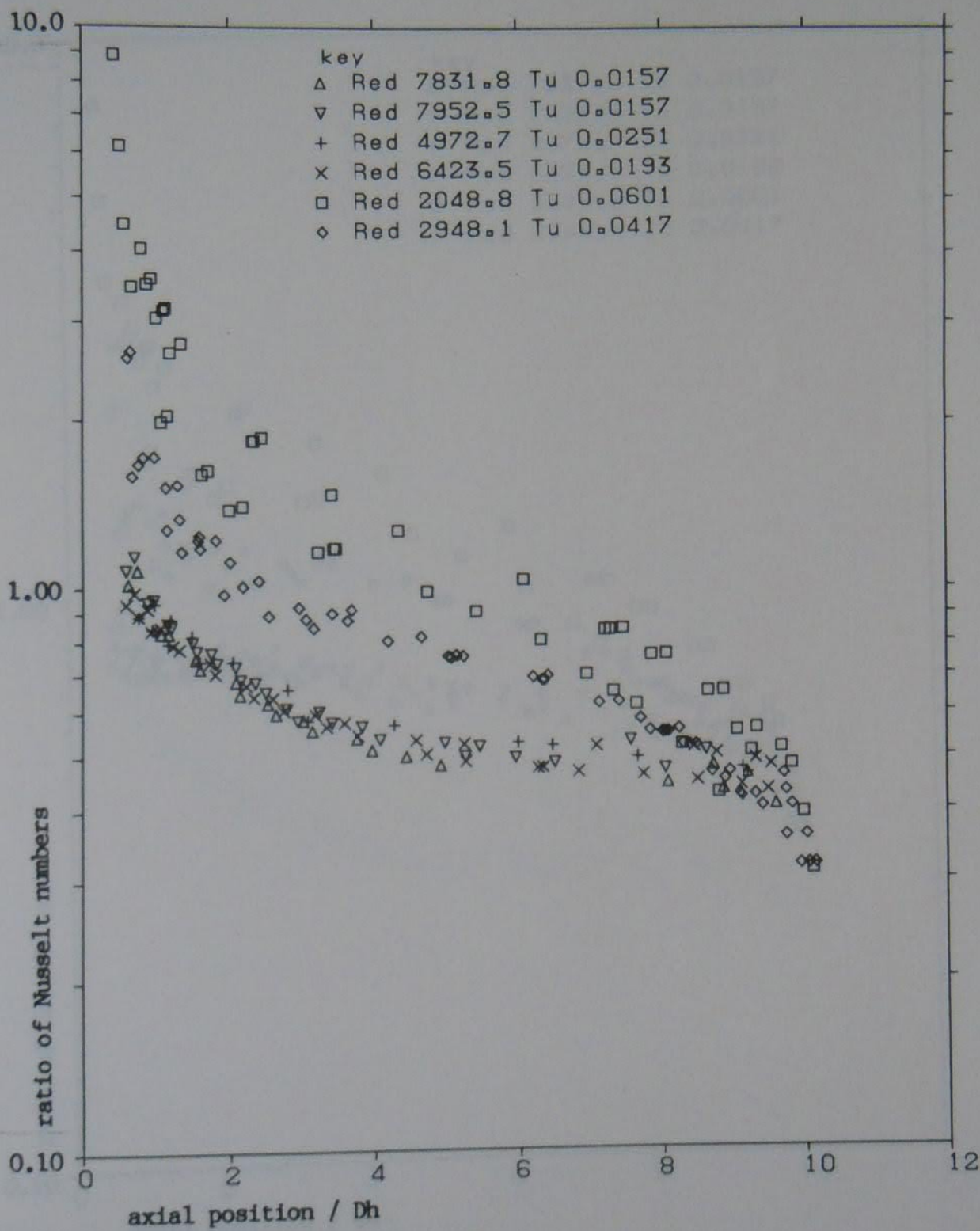
Figure 5.32 Comparison of plain fin heat transfer test data with the turbulent circular tube inlet region from McAdams (1954)

key
△ Red 7831.8 Tu 0.0157
▽ Red 7952.5 Tu 0.0157
+ Red 4972.7 Tu 0.0251
× Red 6423.5 Tu 0.0193
□ Red 2048.8 Tu 0.0601
◇ Red 2948.1 Tu 0.0417
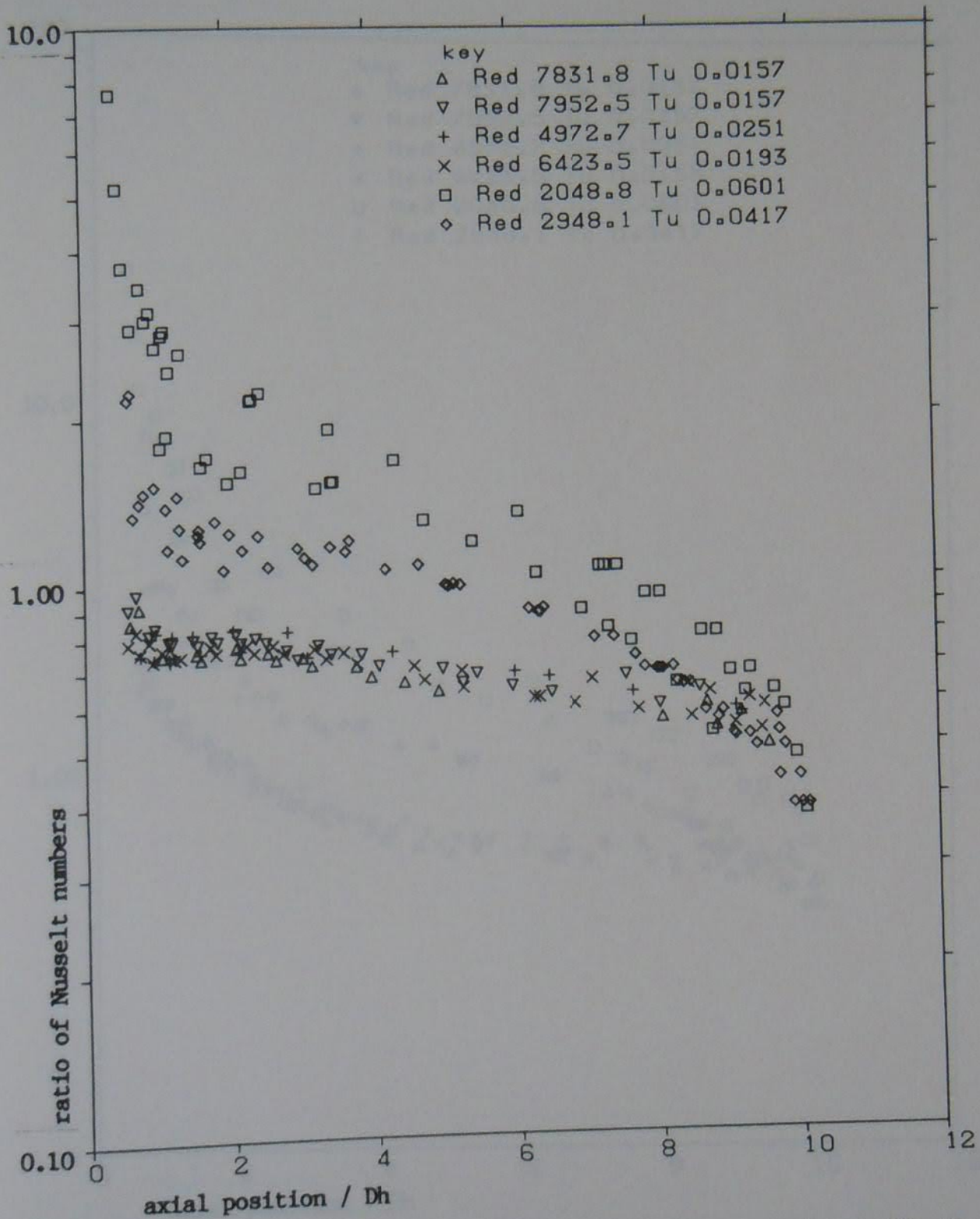
Figure 5.33 Comparison of plain fin heat transfer test data with the turbulent circular tube inlet region using the ESDU correlation with inlet modification
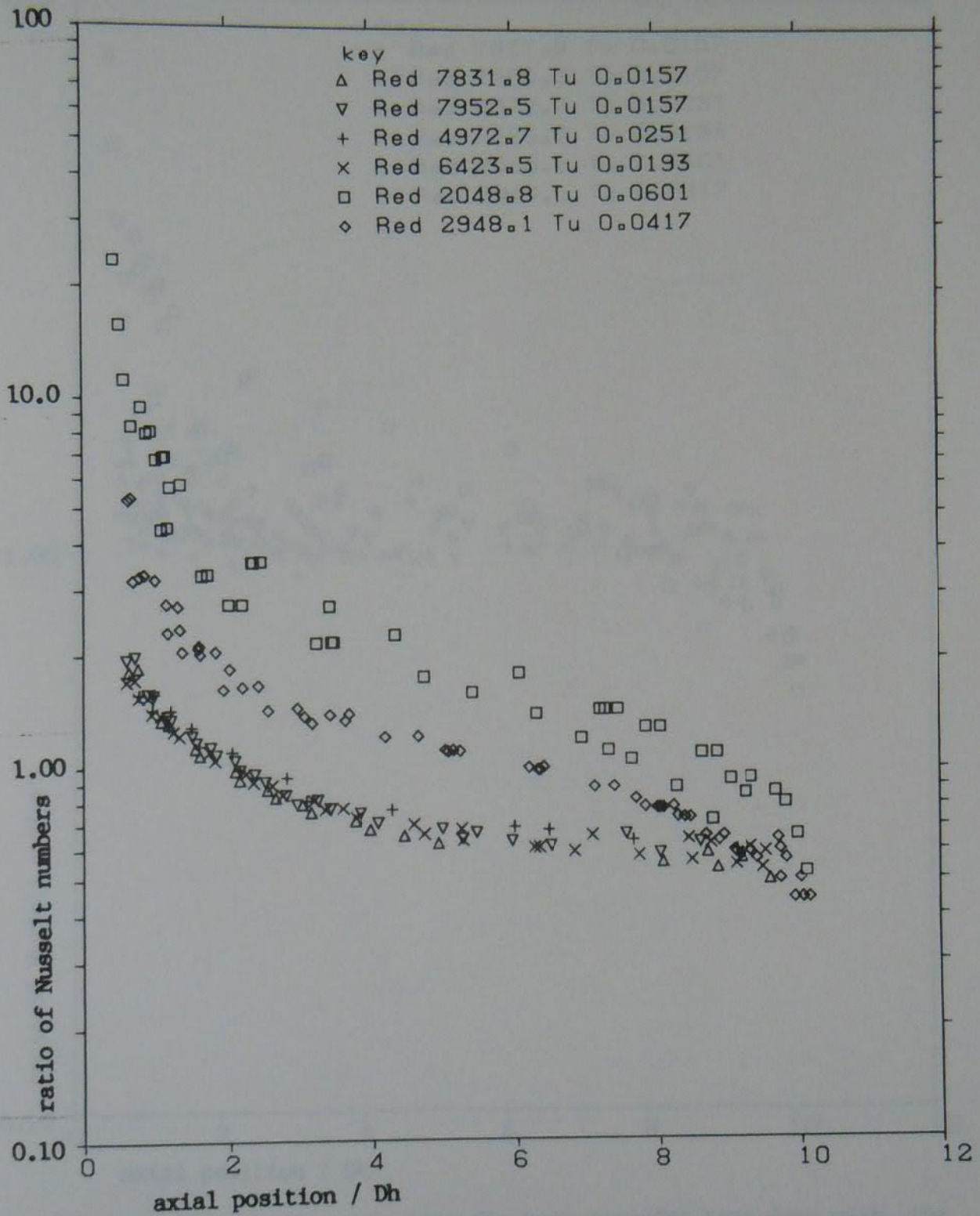
Figure 5.34 Comparison of plain fin heat transfer test data with the turbulent circular tube inlet region from Gnielinski (1983)

key
△ Red 7831.8 Tu 0.0157
▽ Red 7952.5 Tu 0.0157
+ Red 4972.7 Tu 0.0251
× Red 6423.5 Tu 0.0193
□ Red 2048.8 Tu 0.0601
◇ Red 2948.1 Tu 0.0417
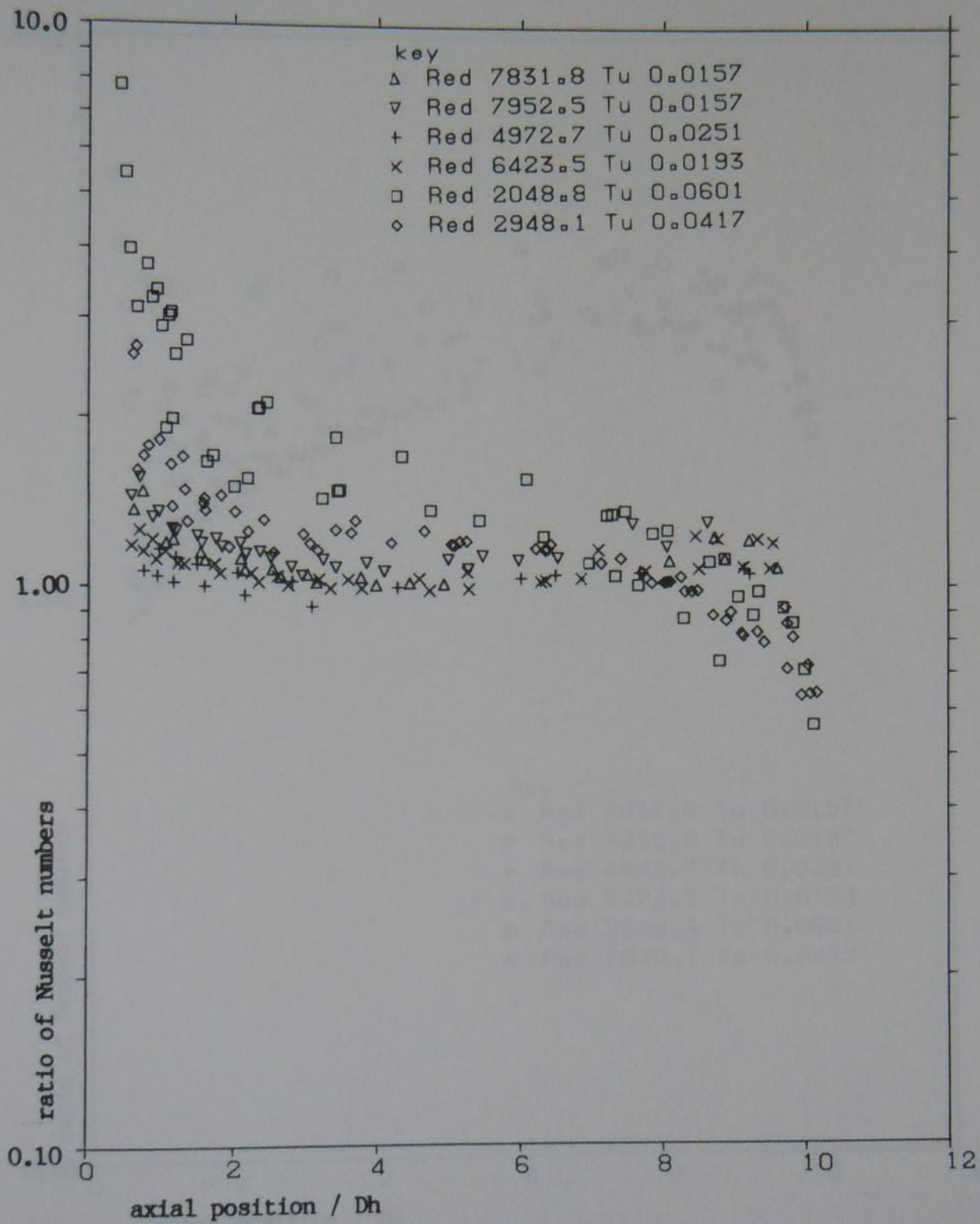
Figure 5.35 Comparison of plain fin heat transfer test data with the regression equation of Sugawara, Sato, Komatsu and Osaka (1953, 1988) for flow over a flat plate
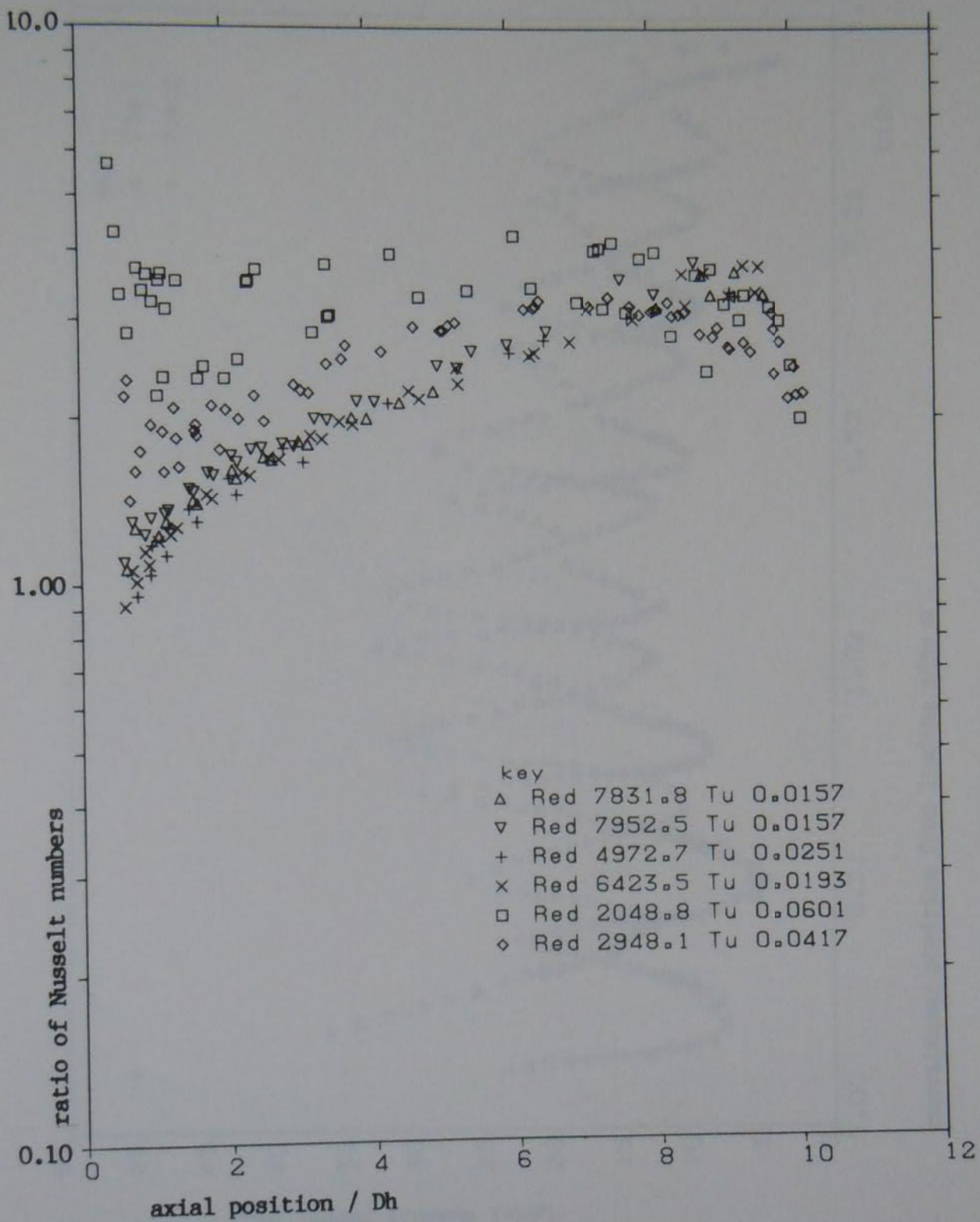
Figure 5.36 Comparison of plain fin heat transfer test data with the rectangular duct inlet region regression equation of Sukomel, Velichko, Abrosimov and Gutsev
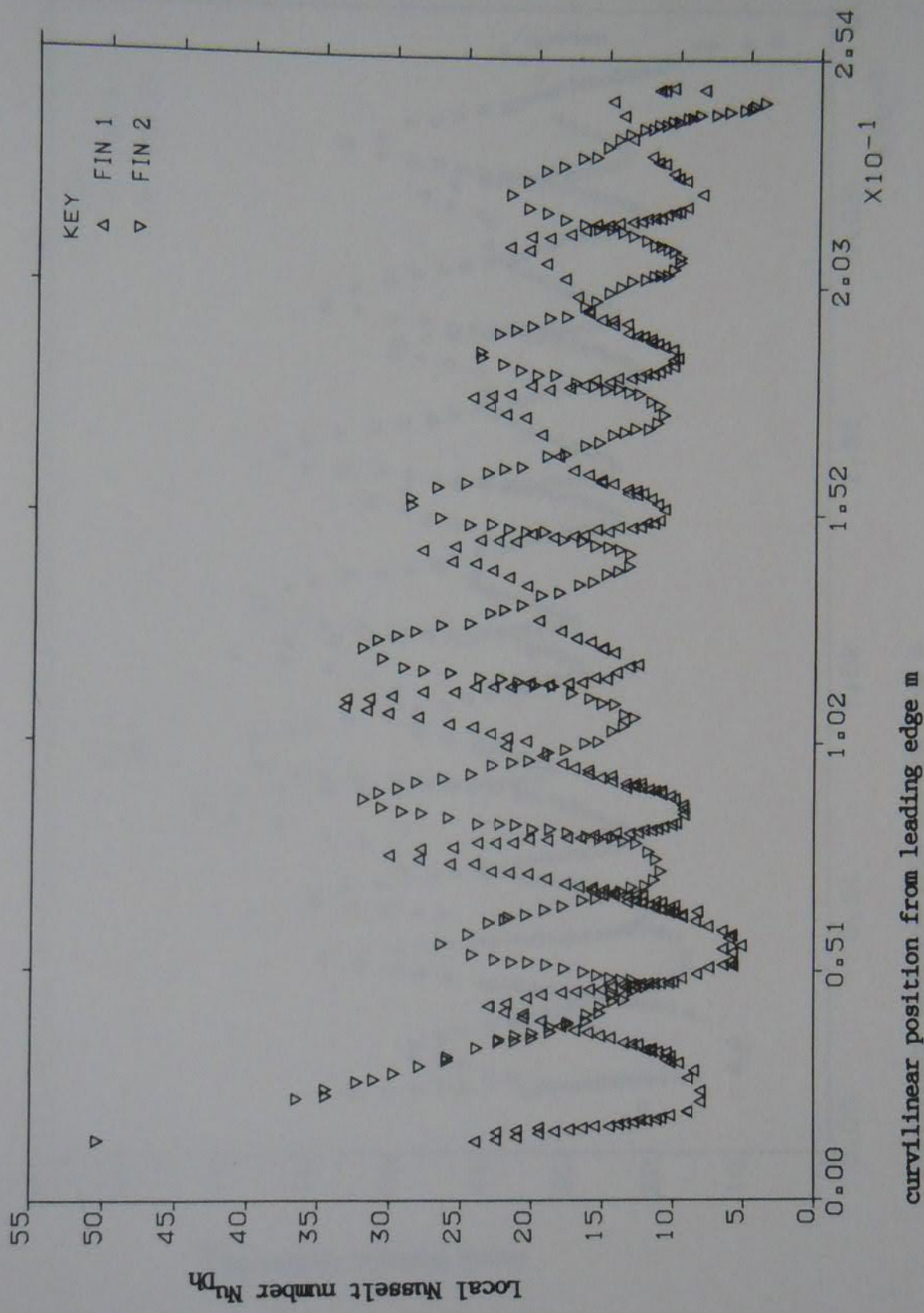
Figure 5.37 Local Nusselt number against curvilinear coordinate, profile 1, Dh = 0.0224 m, Re = 2004
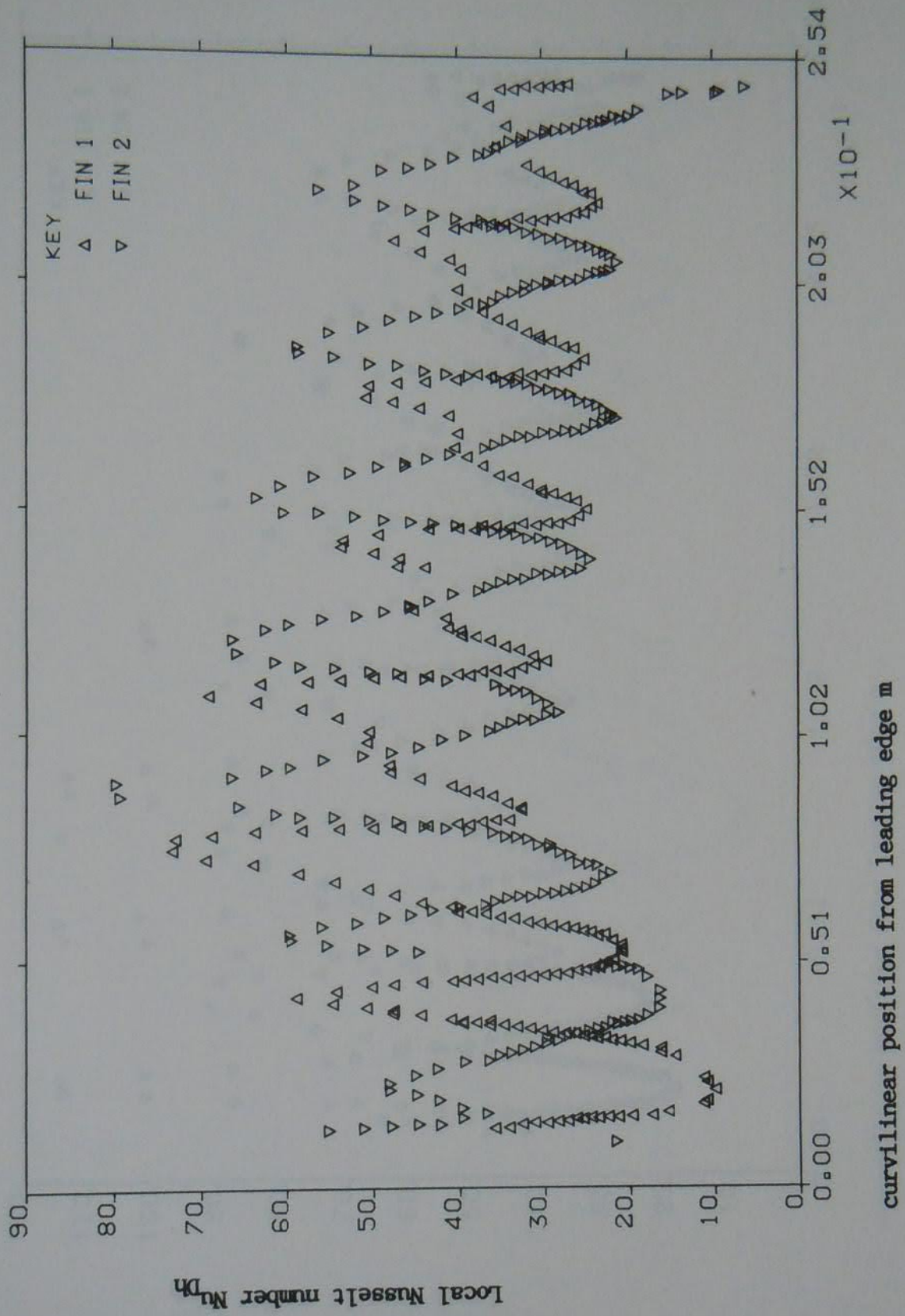
Figure 5.38 Local Nusselt number against curvilinear coordinate, profile 1, Dh = 0.0224 m, Re = 4930
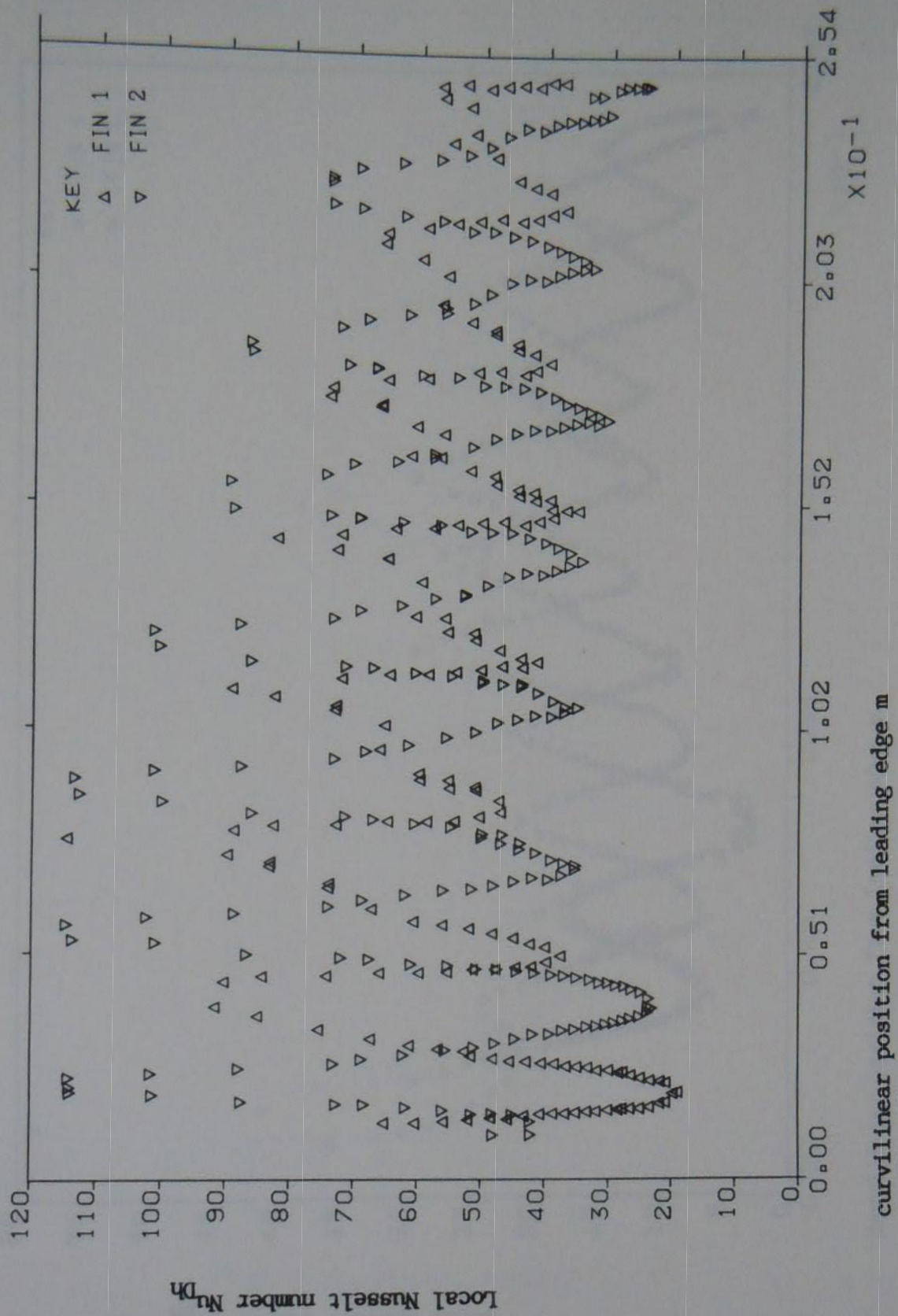
Figure 5.39 Local Nusselt number against curvilinear coordinate, profile 1, Dh = 0.0224 m, Re = 7991

241
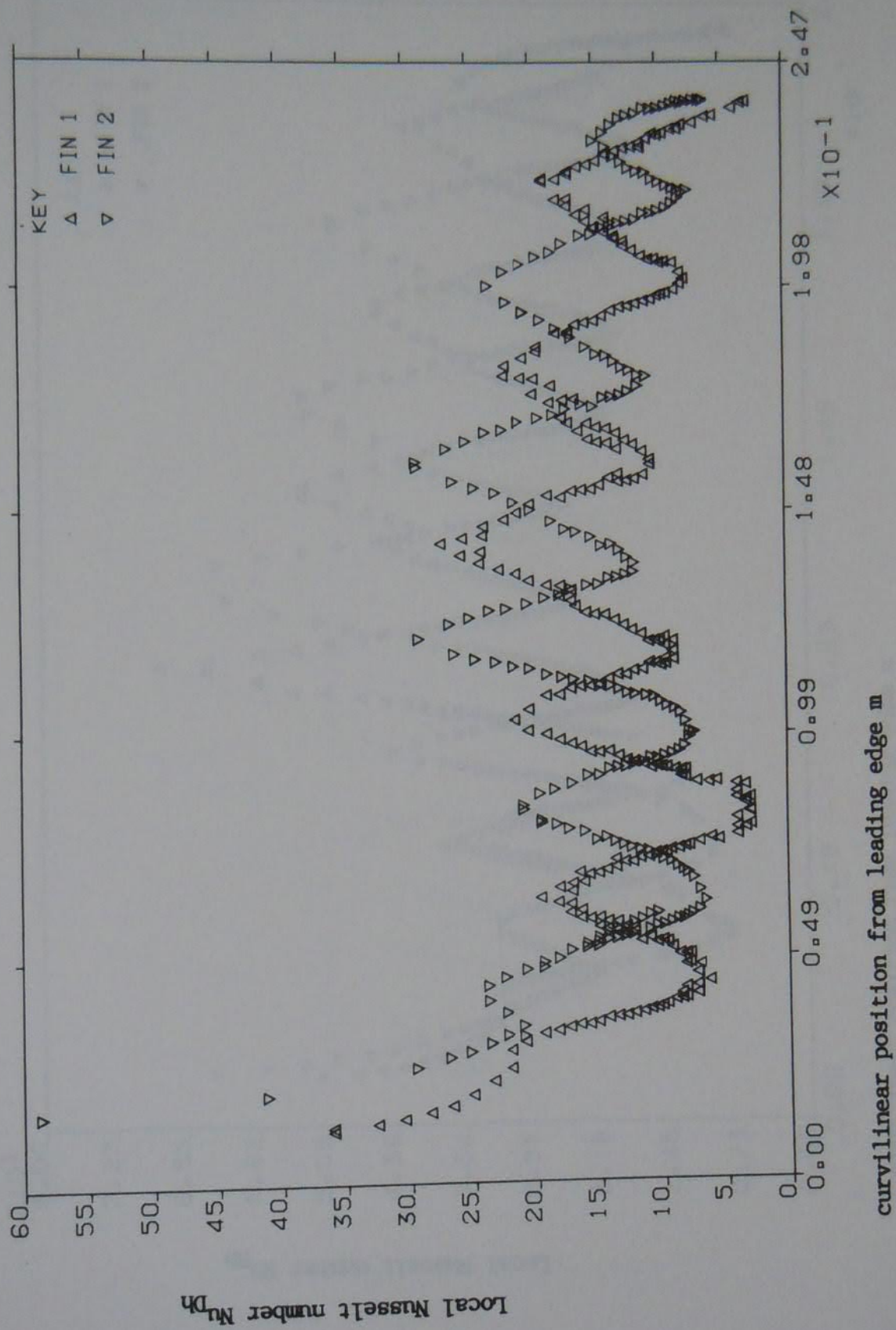
Figure 5.40 Local Nusselt number against curvilinear coordinate, profile 2, Dh = 0.0224 m, Re = 2016
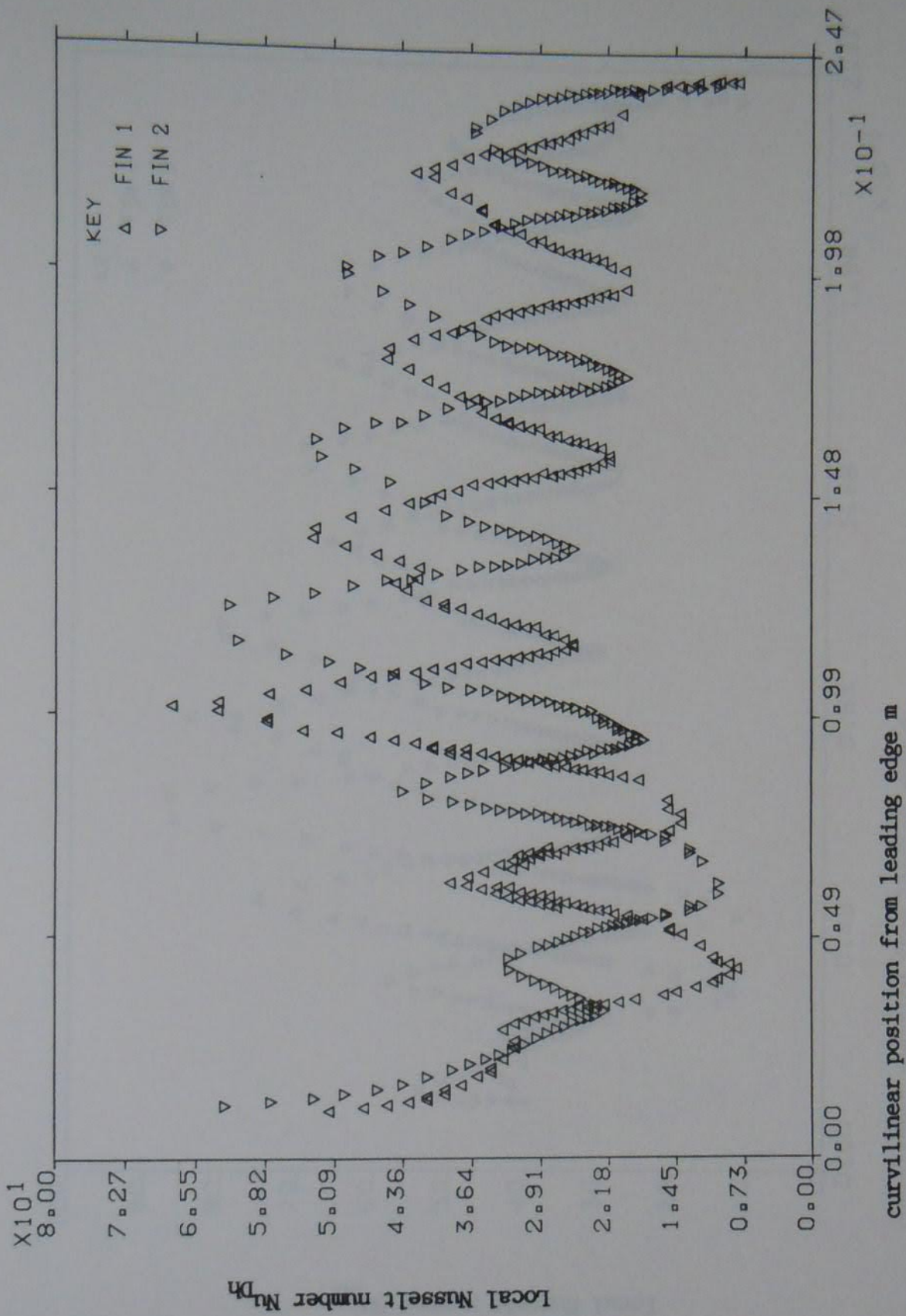
Figure 5.41 Local Nusselt number against curvilinear coordinate, profile 2, Dh = 0.0224 m, Re = 4944
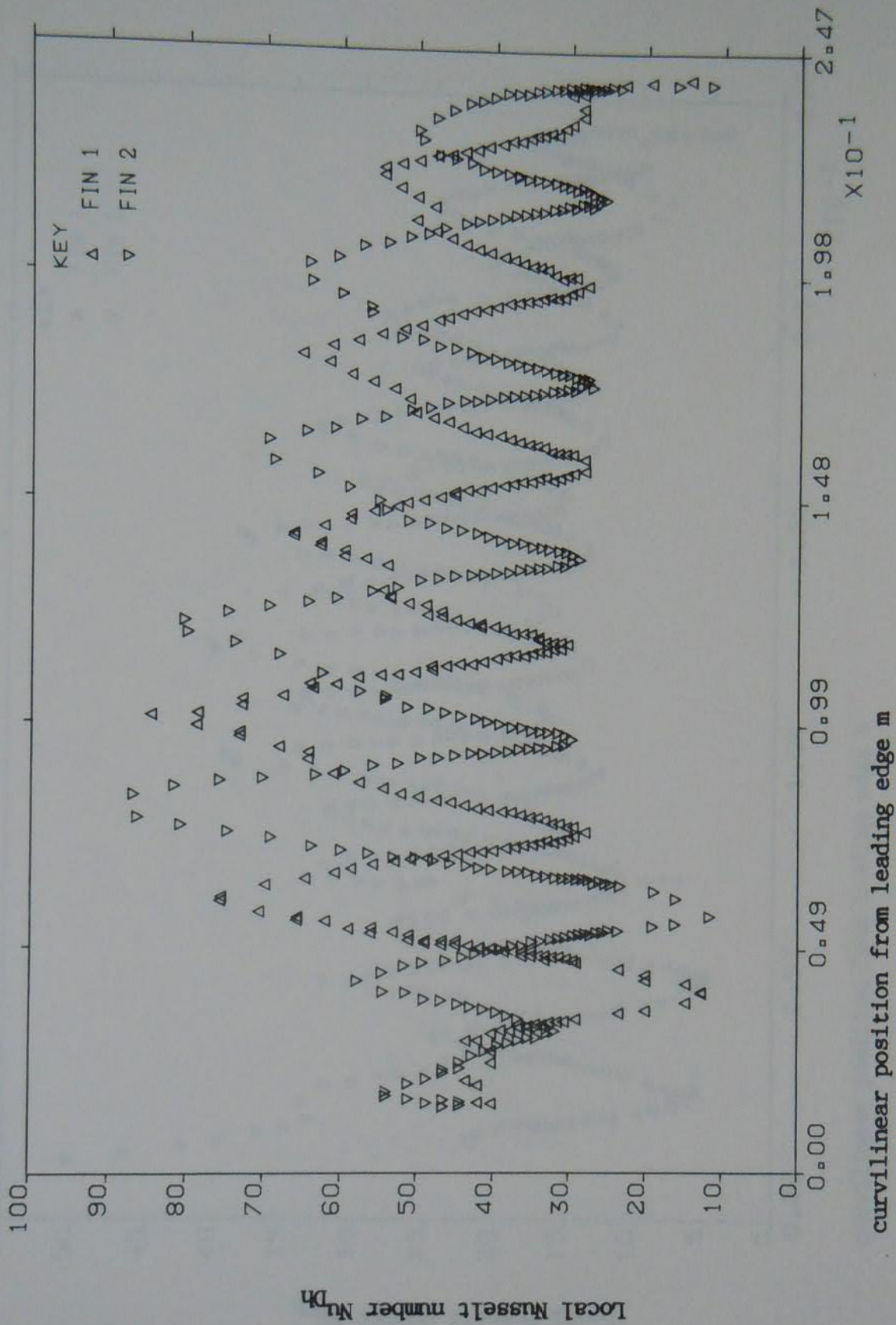
Figure 5.42 Local Nusselt number against curvilinear coordinate, profile 2, Dh = 0.0224 m, Re = 7961

244
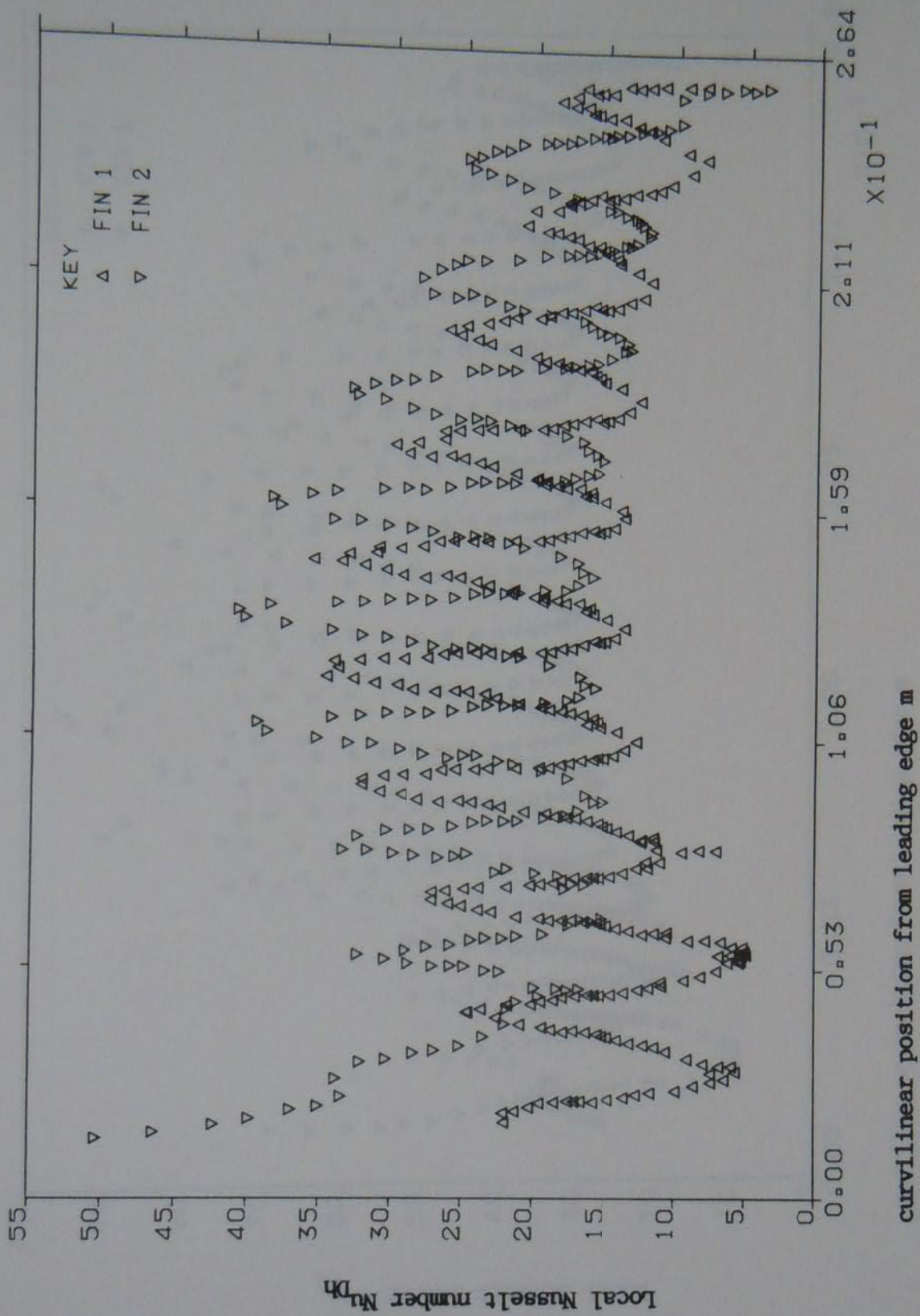
Figure 5.43 Local Nusselt number against curvilinear coordinate, profile 3, Dh = 0.0224 m, Re = 2007

245
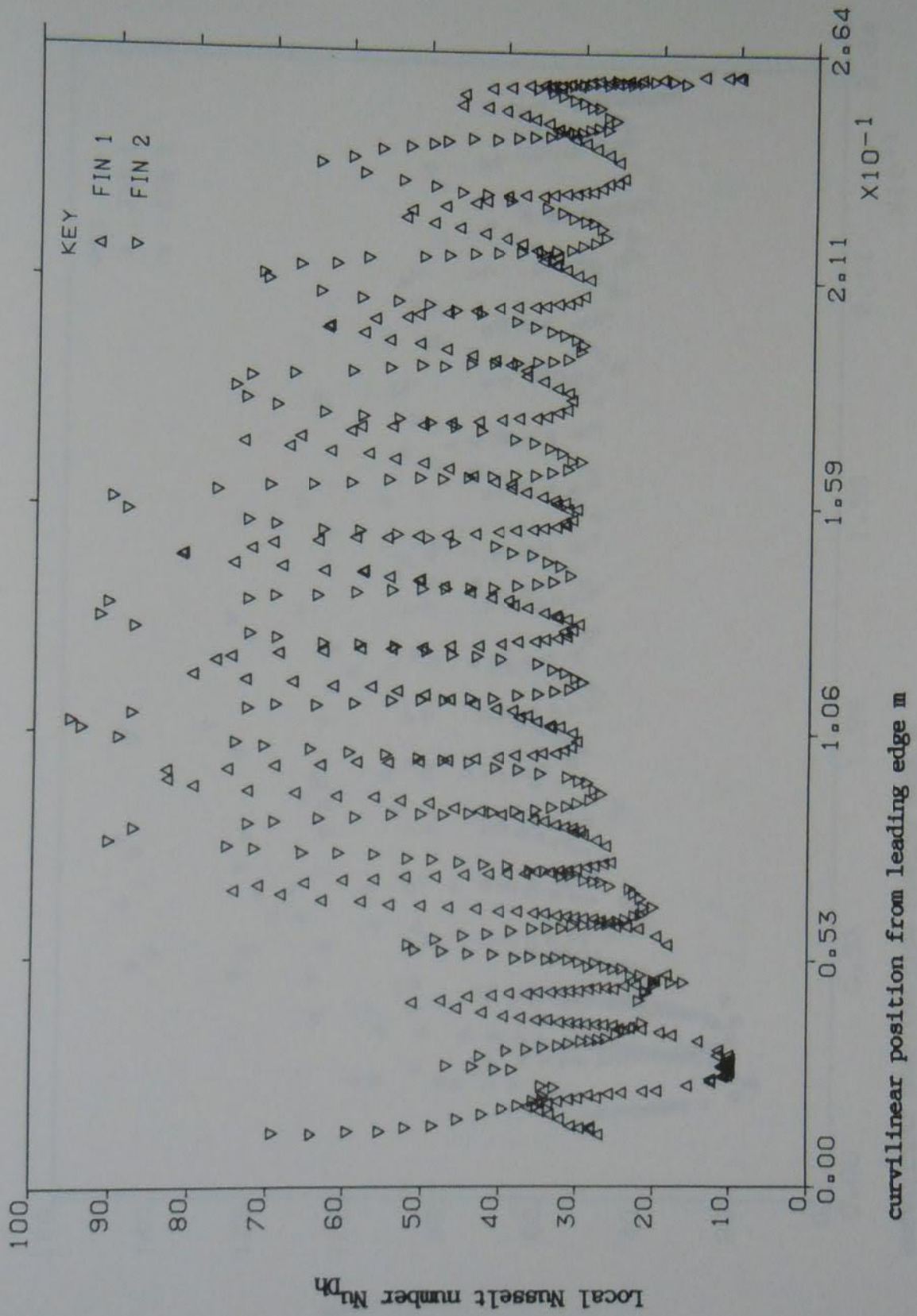
Figure 5.44 Local Nusselt number against curvilinear coordinate, profile 3, Dh = 0.0224 m, Re = 4993
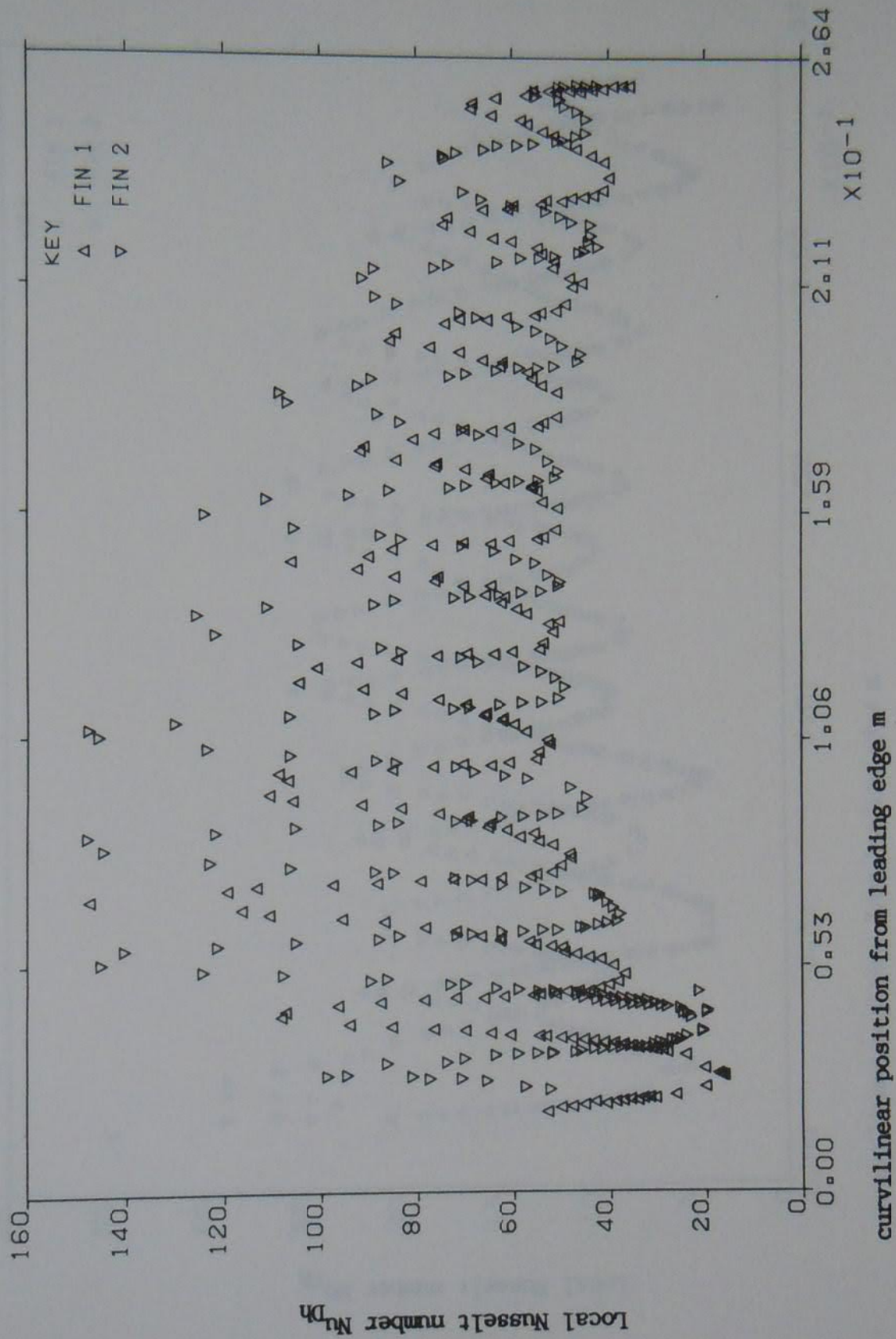
Figure 5.45 Local Nusselt number against curvilinear coordinate,
profile 3, Dh = 0.0224 m, Re = 8004
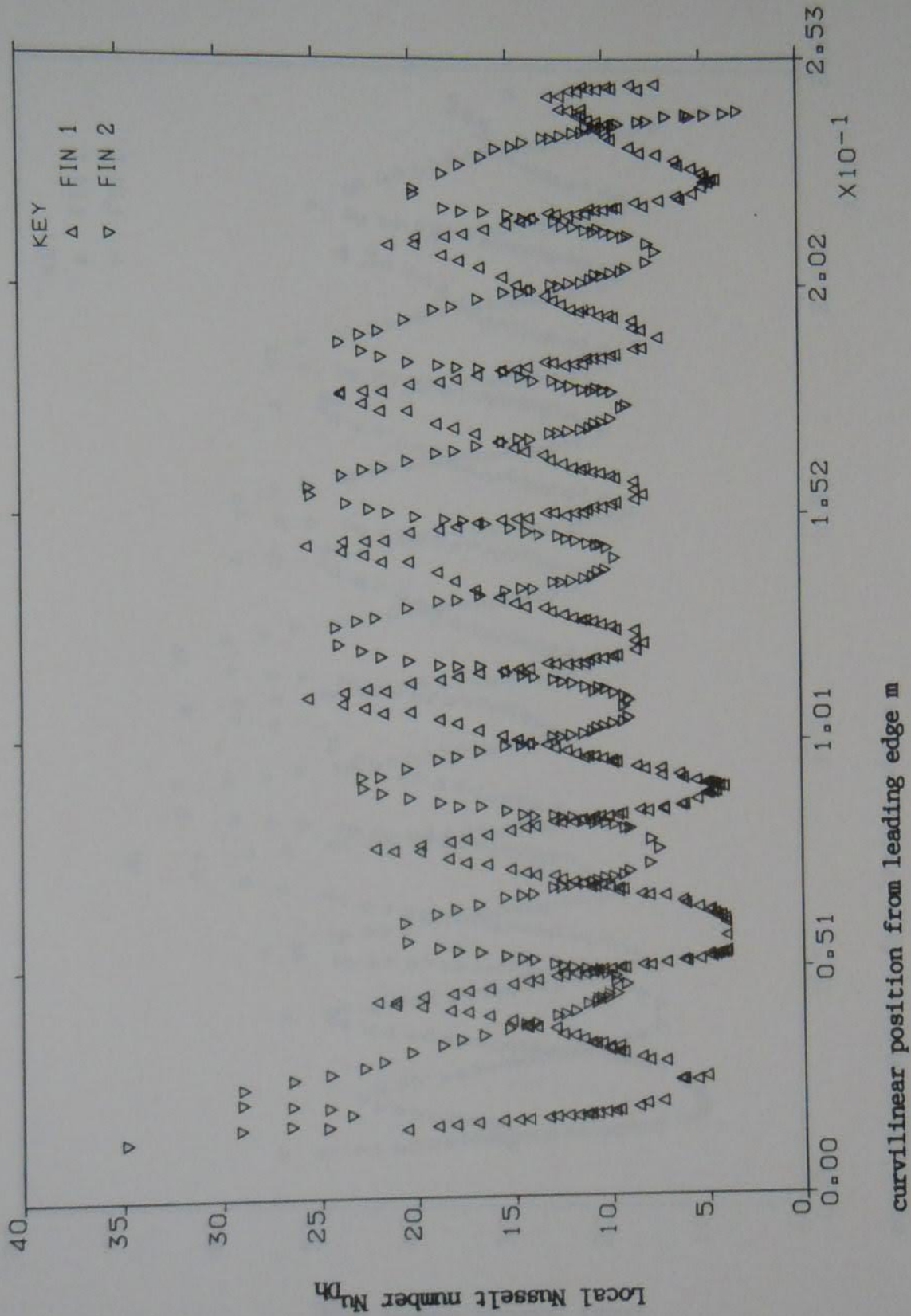
Figure 5.46 Local Nusselt number against curvilinear coordinate, profile 4, Dh = 0.0224 m, Re = 2004

248
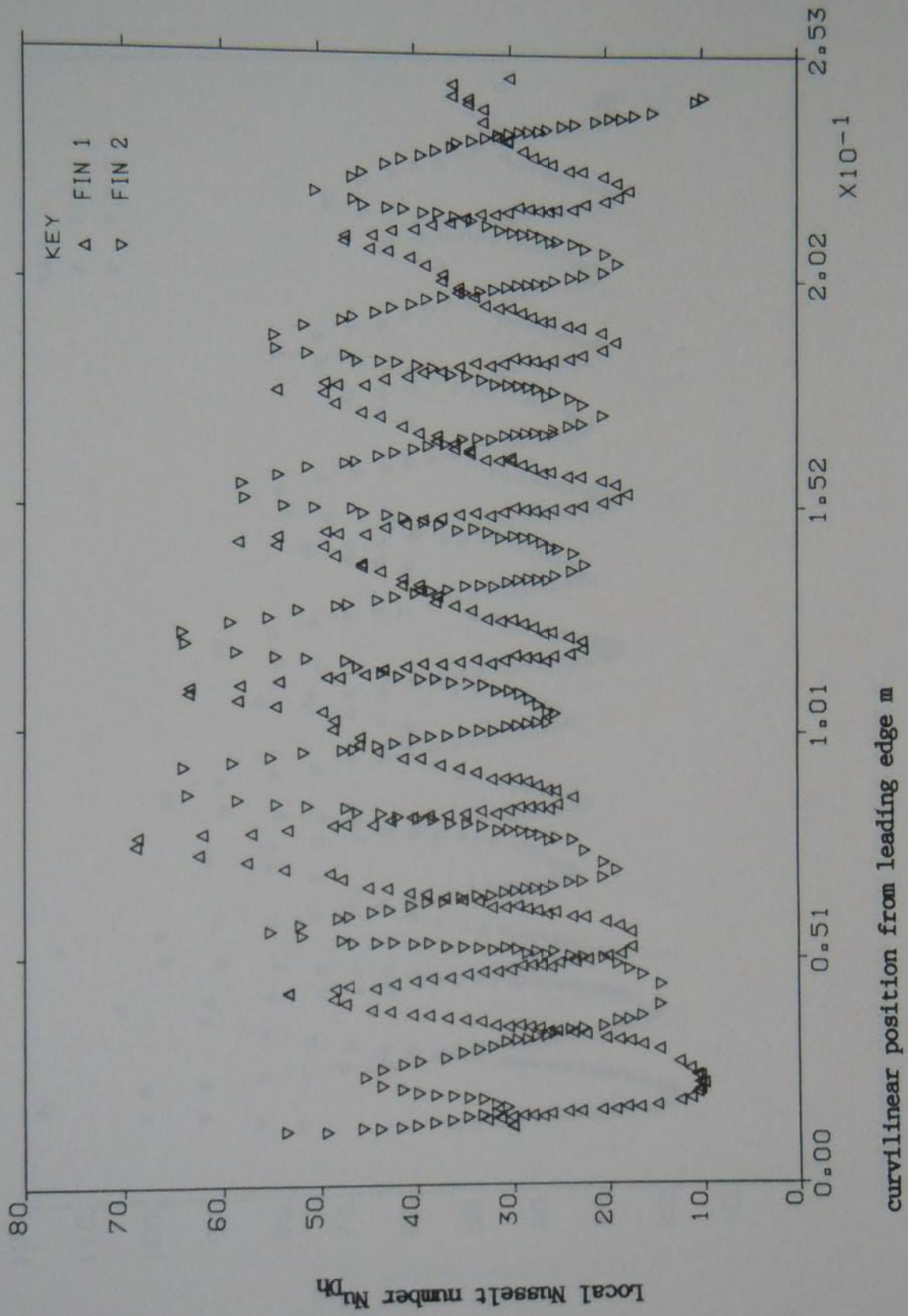
Figure 5.47 Local Nusselt number against curvilinear coordinate, profile 4, Dh = 0.0224 m, Re = 4974

249
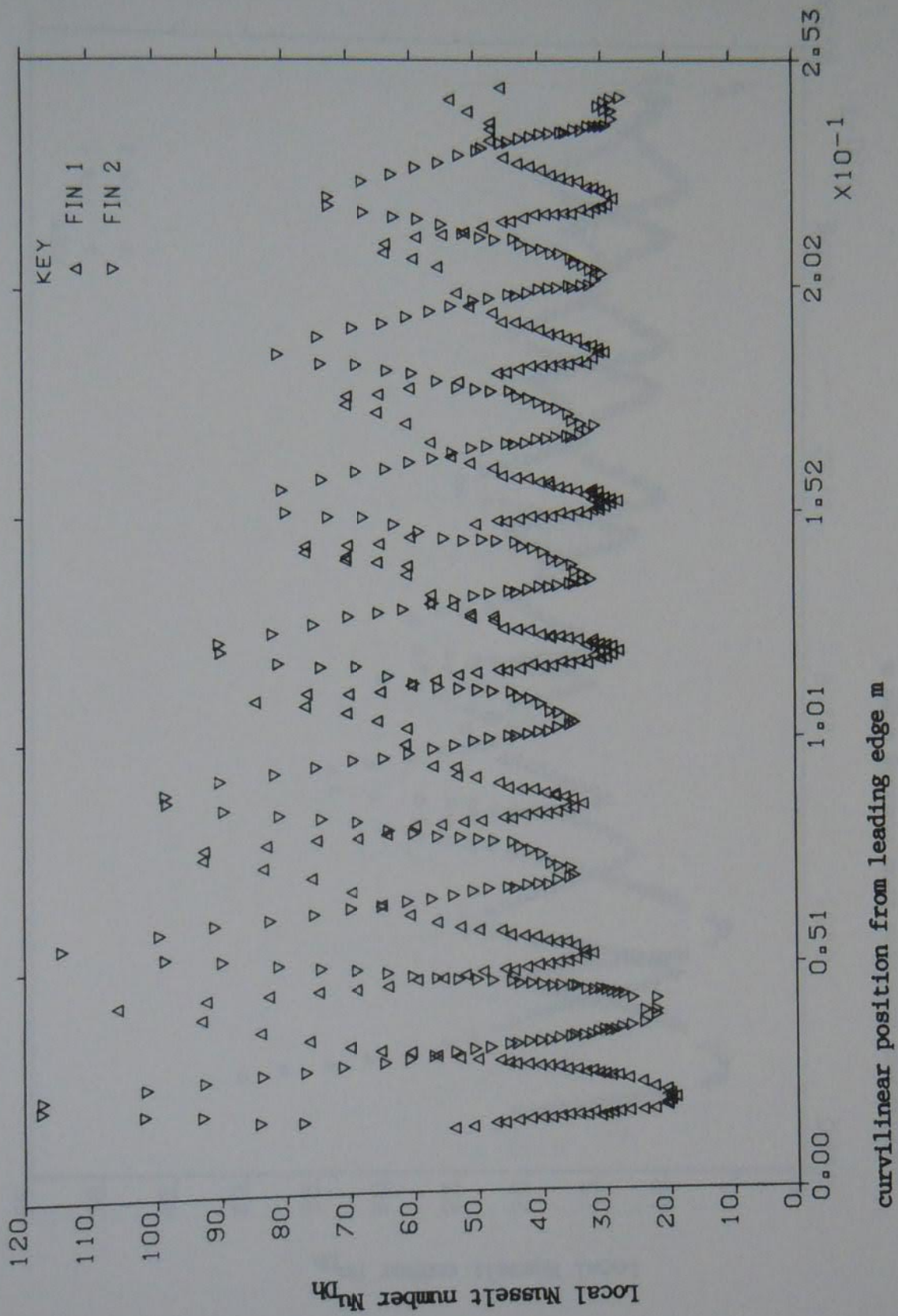
Figure 5.48 Local Nusselt number against curvilinear coordinate, profile 4, Dh = 0.0224 m, Re = 8015
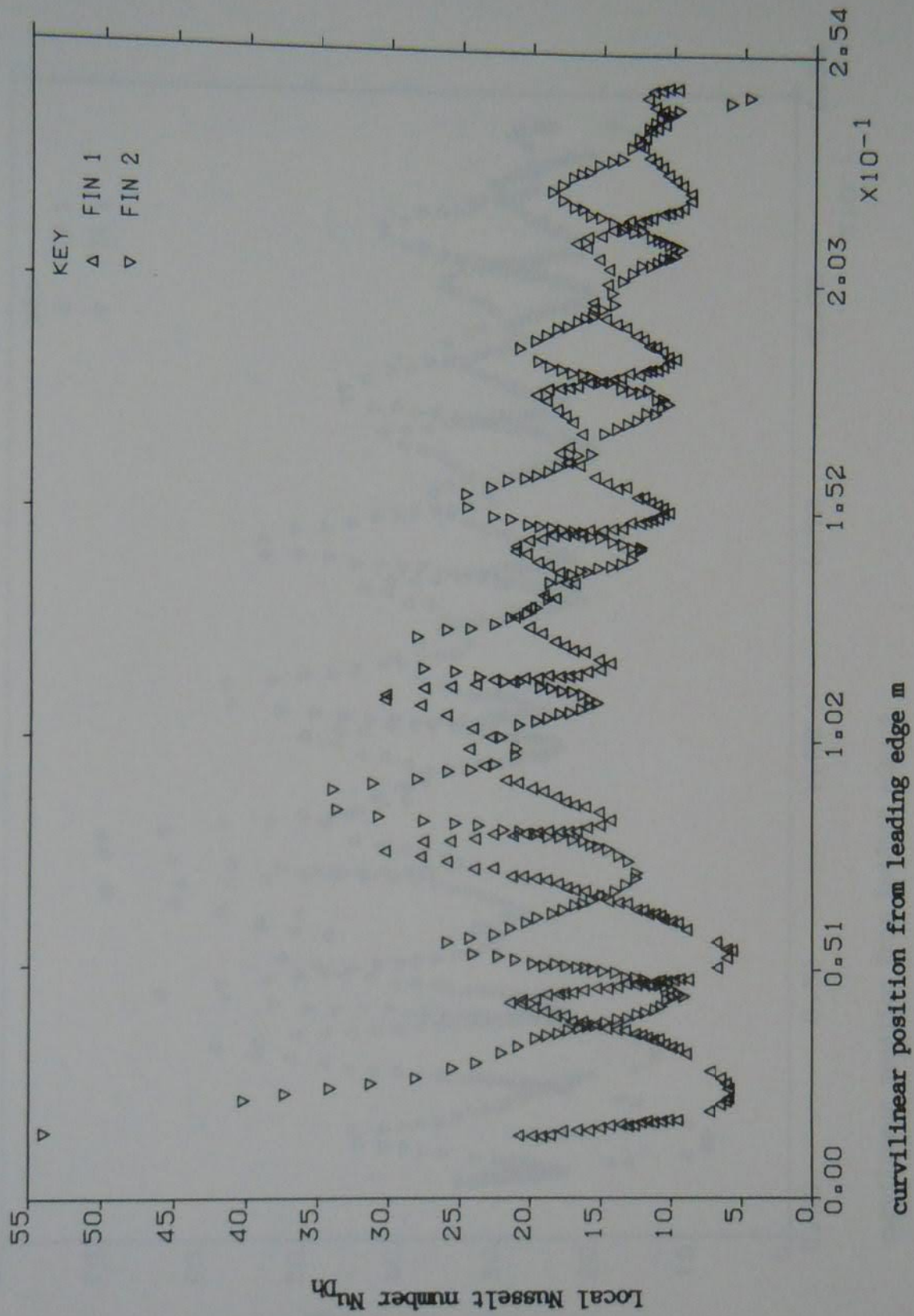
Figure 5.49 Local Nusselt number against curvilinear coordinate, profile 1, Dh = 0.0174 m, Re = 1977
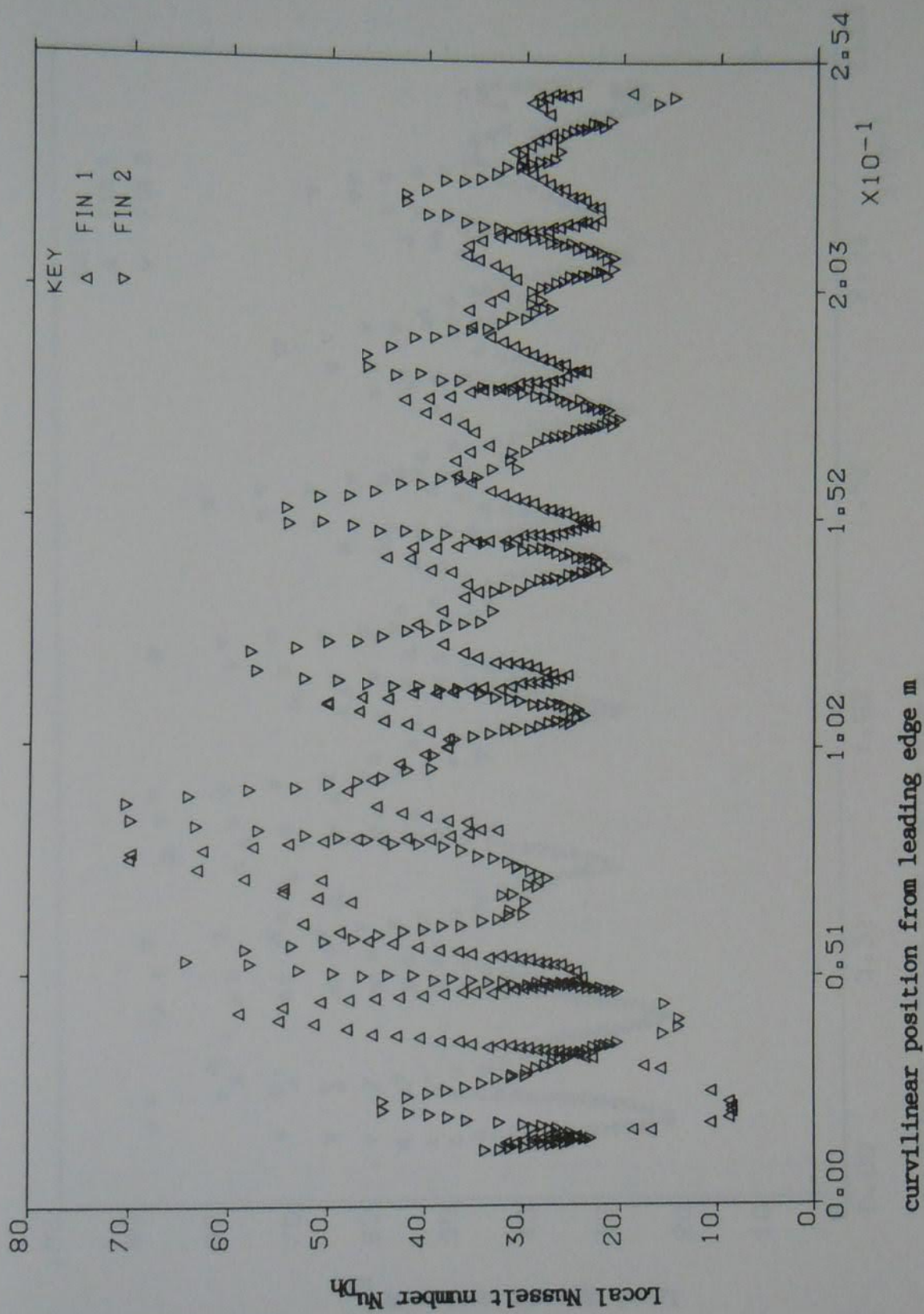
Figure 5.50 Local Nusselt number against curvilinear coordinate, profile 1, Dh = 0.0174 m, Re = 4940

252
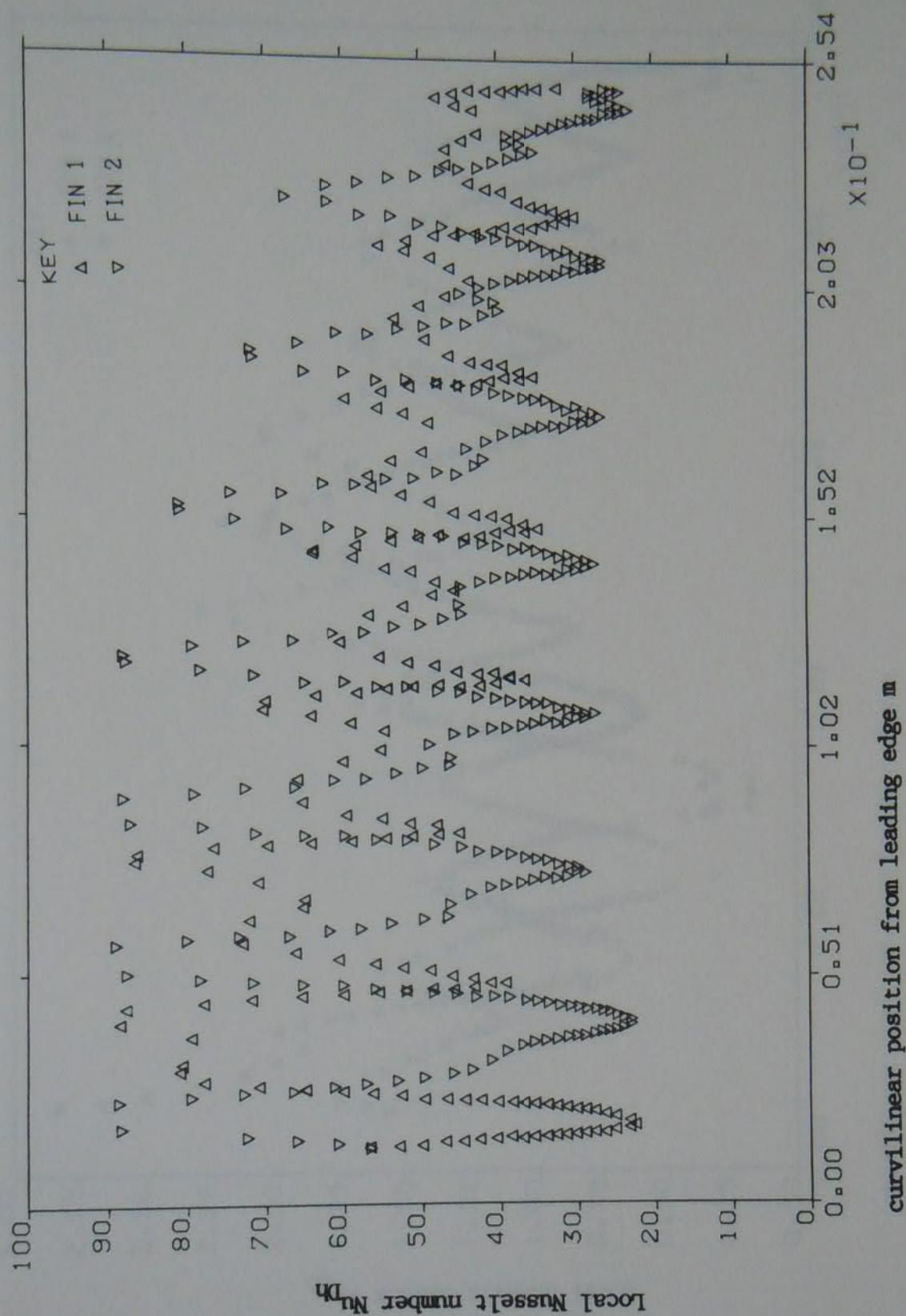
Figure 5.51 Local Nusselt number against curvilinear coordinate, profile 1, Dh = 0.0174 m, Re = 7770
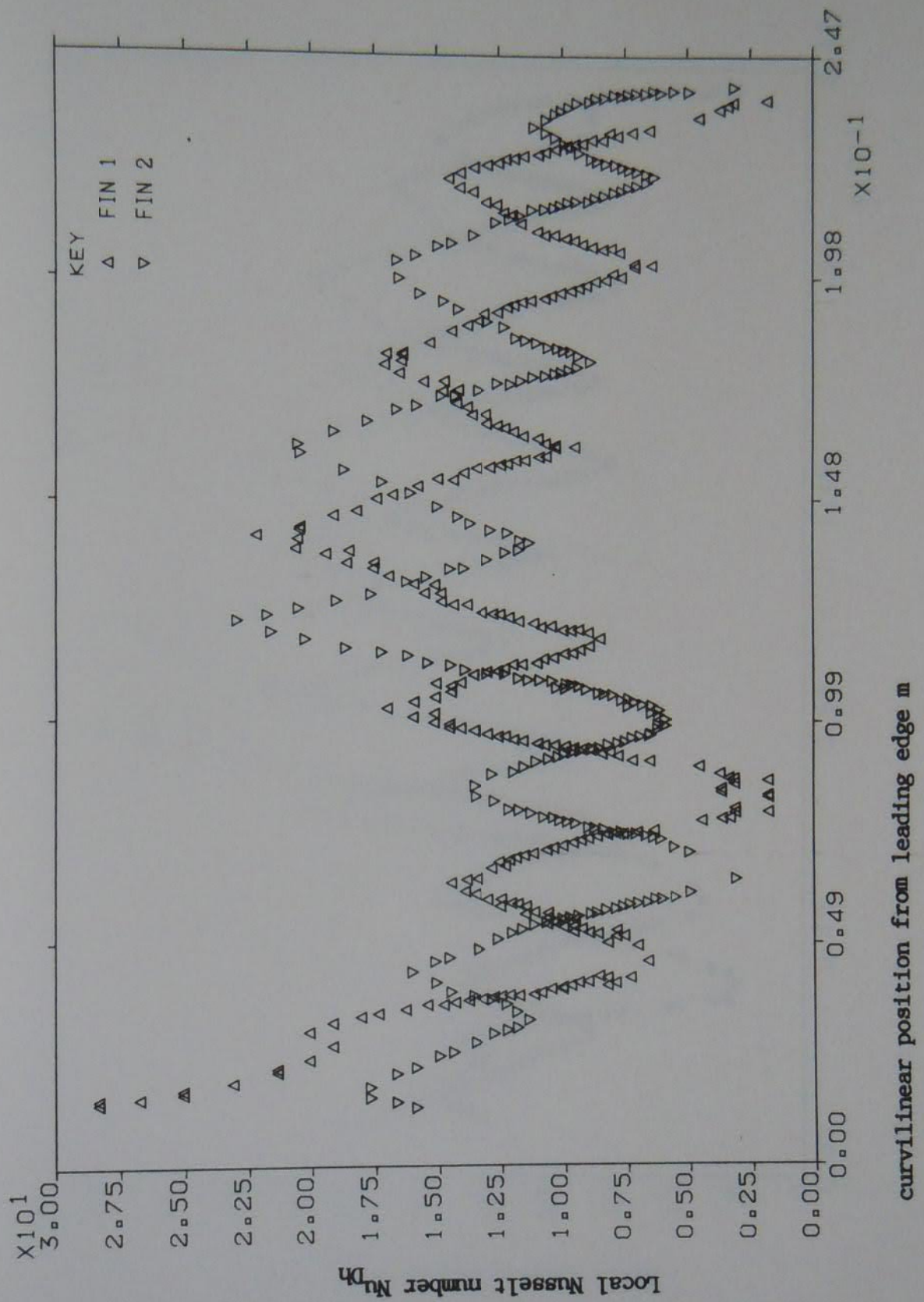
Figure 5.52 Local Nusselt number against curvilinear coordinate, profile 2, Dh = 0.0174 m, Re = 2025
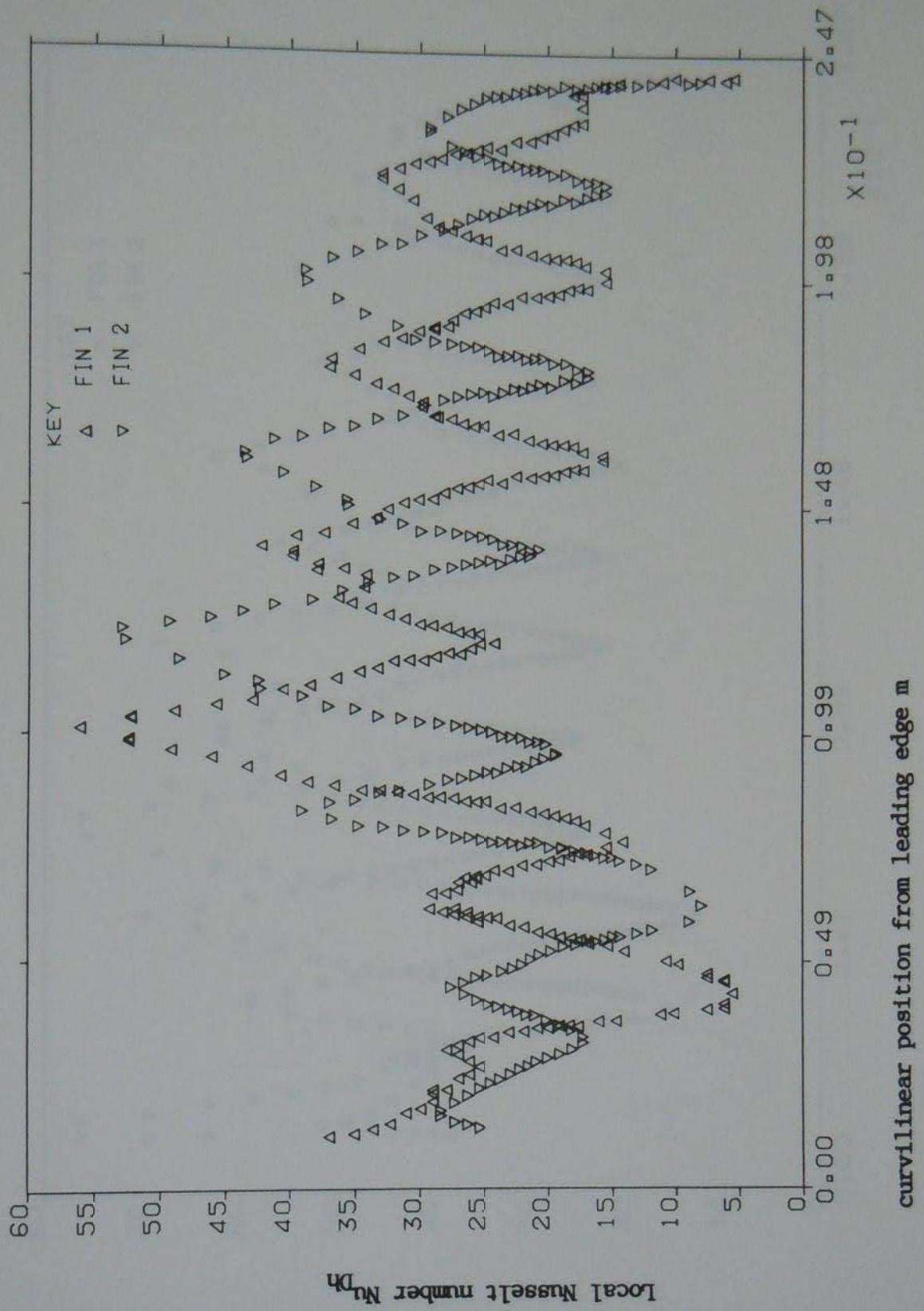
Figure 5.53 Local Nusselt number against curvilinear coordinate, profile 2, Dh = 0.0174 m, Re = 4921

255
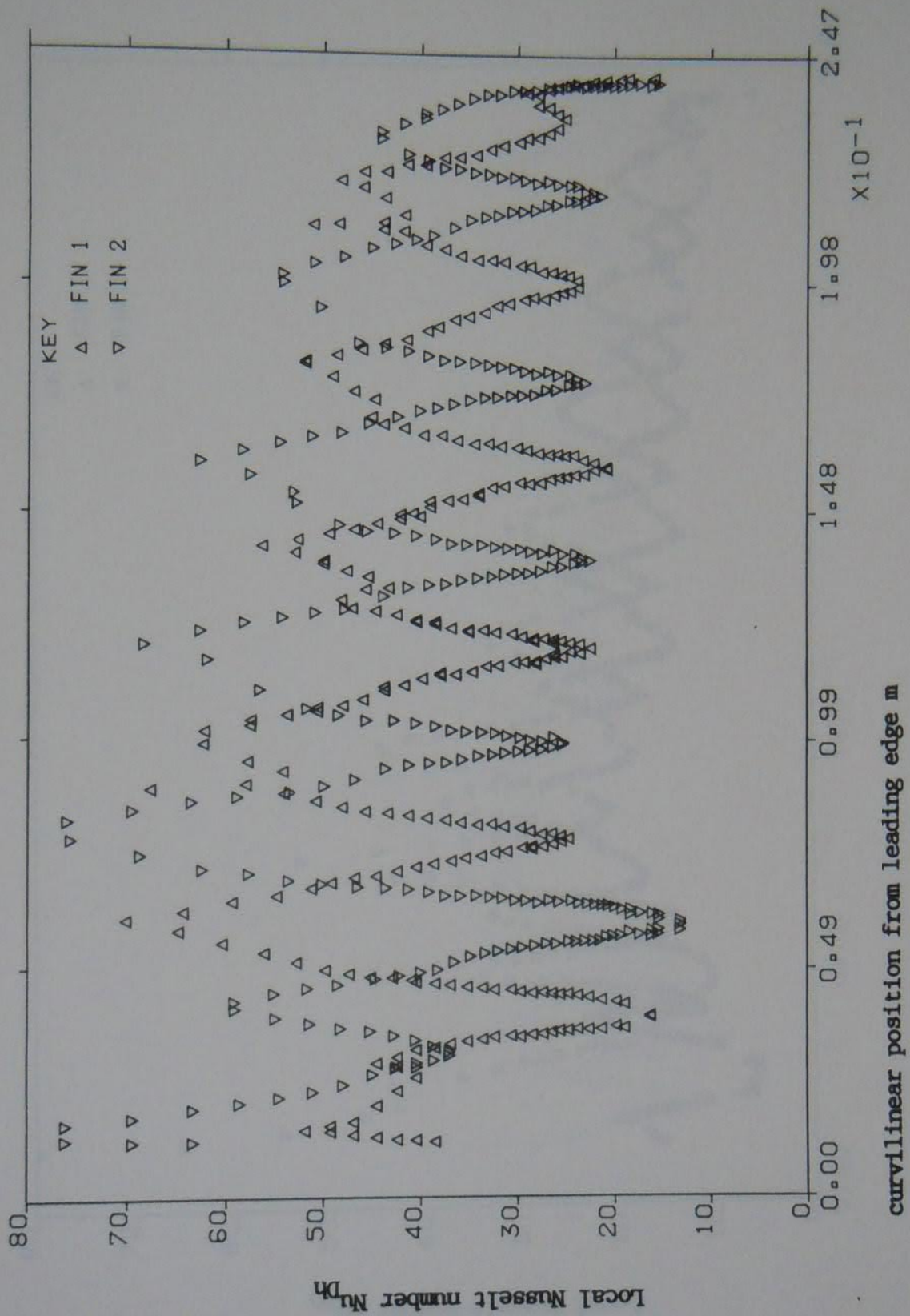
Figure 5.54 Local Nusselt number against curvilinear coordinate, profile 2, Dh = 0.0174 m, Re = 7958

256
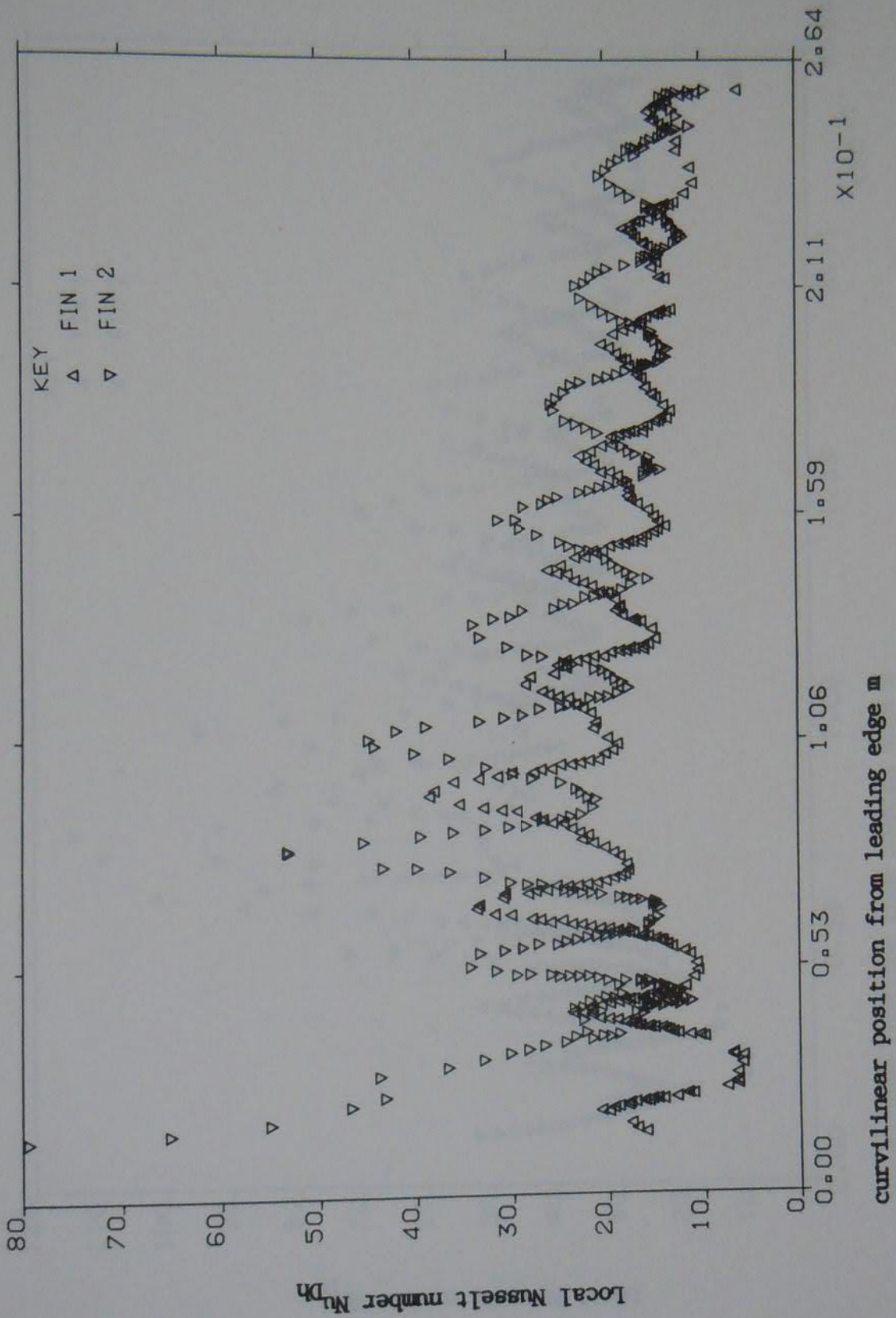
Figure 5.55 Local Nusselt number against curvilinear coordinate, profile 3, Dh = 0.0174 m, Re = 1986
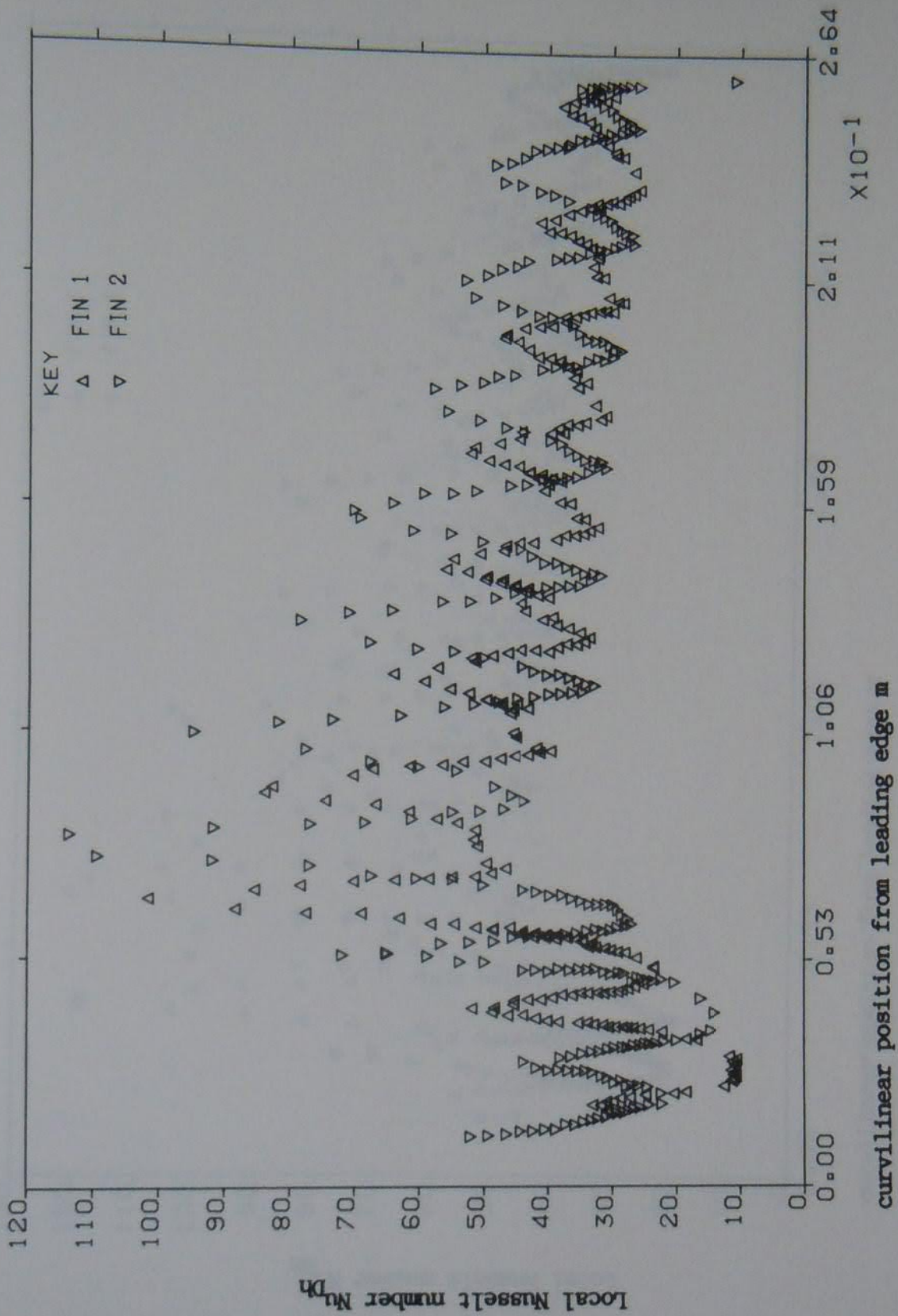
Figure 5.56 Local Nusselt number against curvilinear coordinate, profile 3, Dh = 0.0174m, Re = 4946
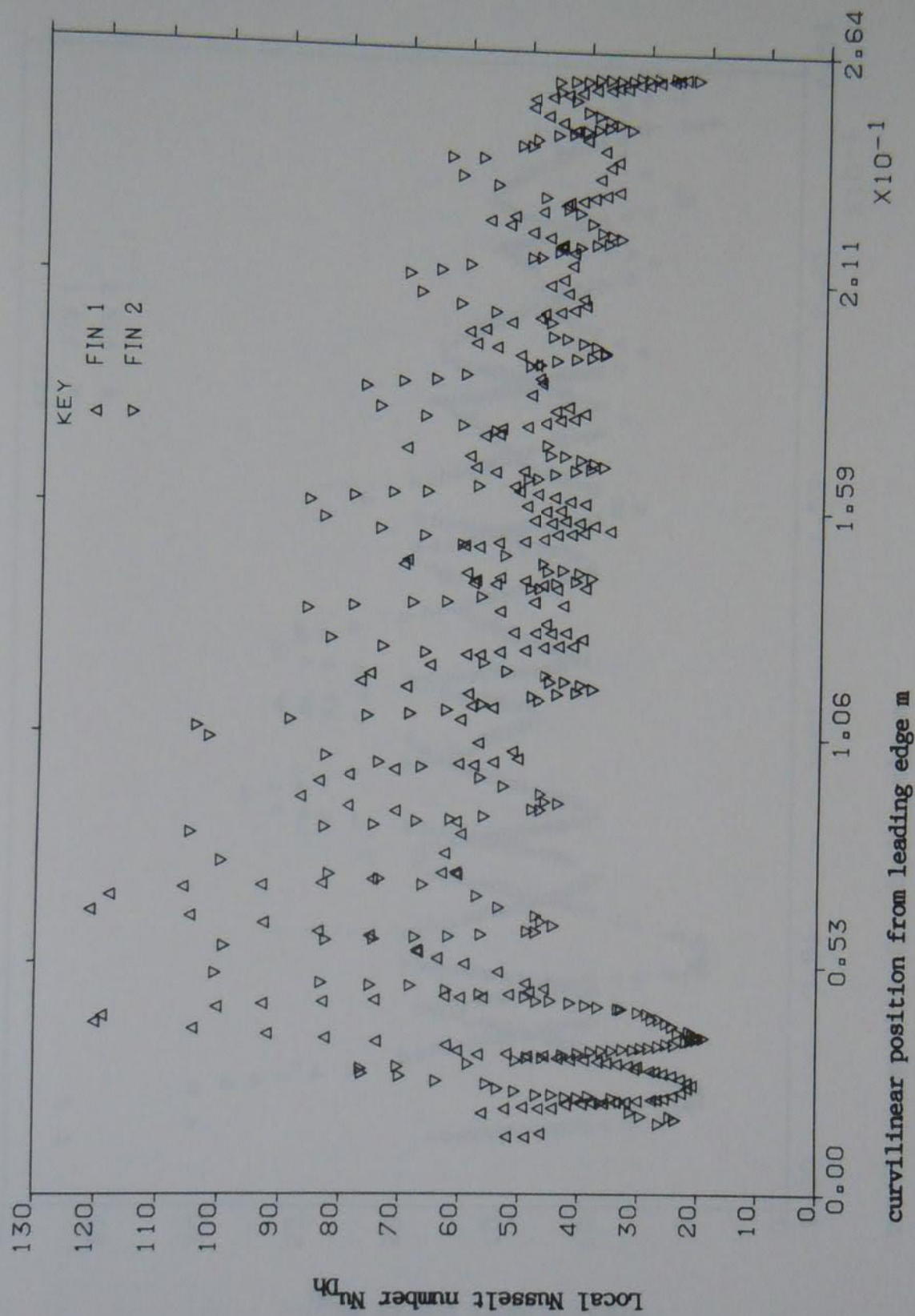
Figure 5.57 Local Nusselt number against curvilinear coordinate, profile 3, Dh = 0.0174 m, Re = 7814
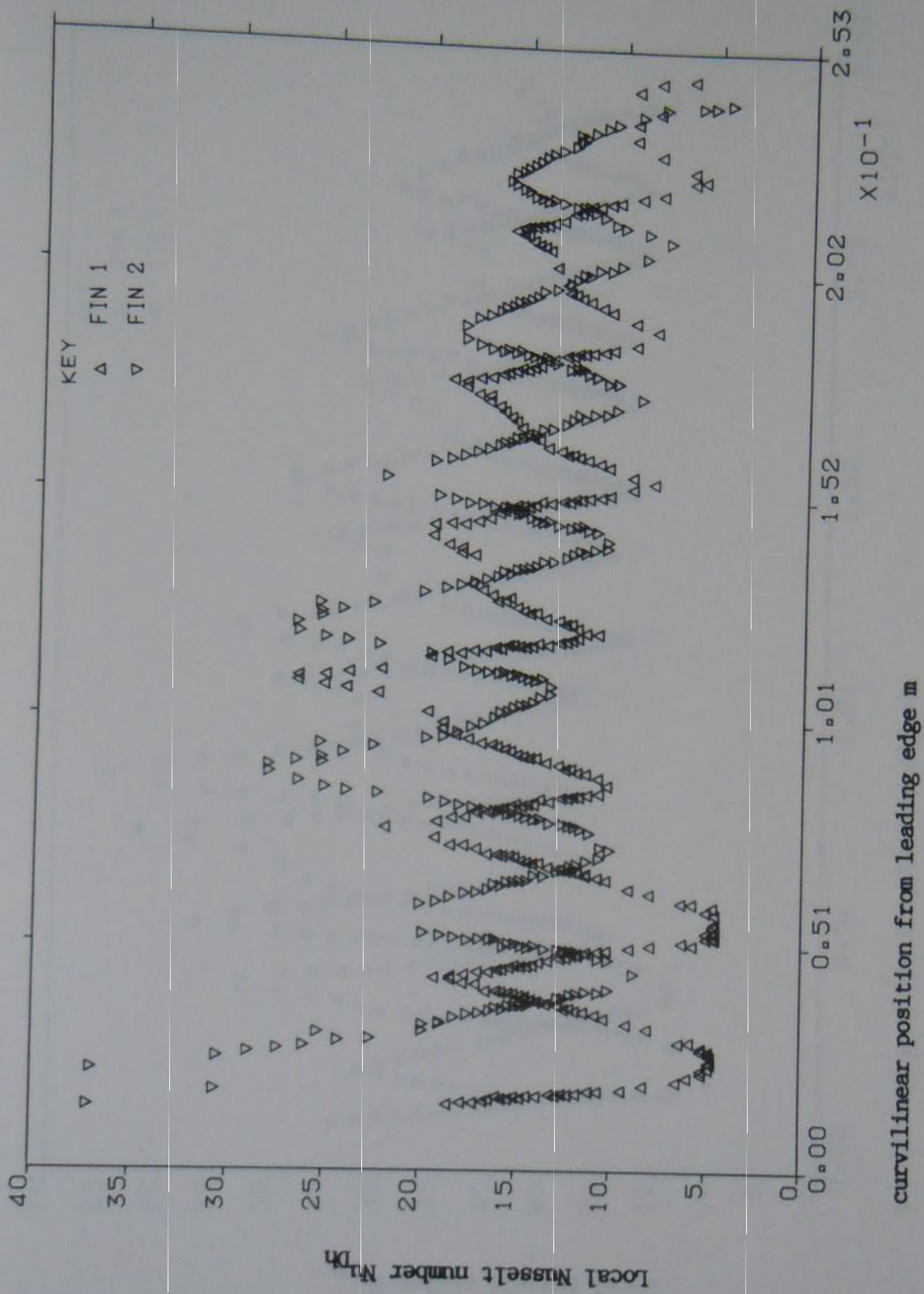
Figure 5.58 Local Nusselt number against curvilinear coordinate, profile 4, Dh = 0.0174 m, Re = 1982
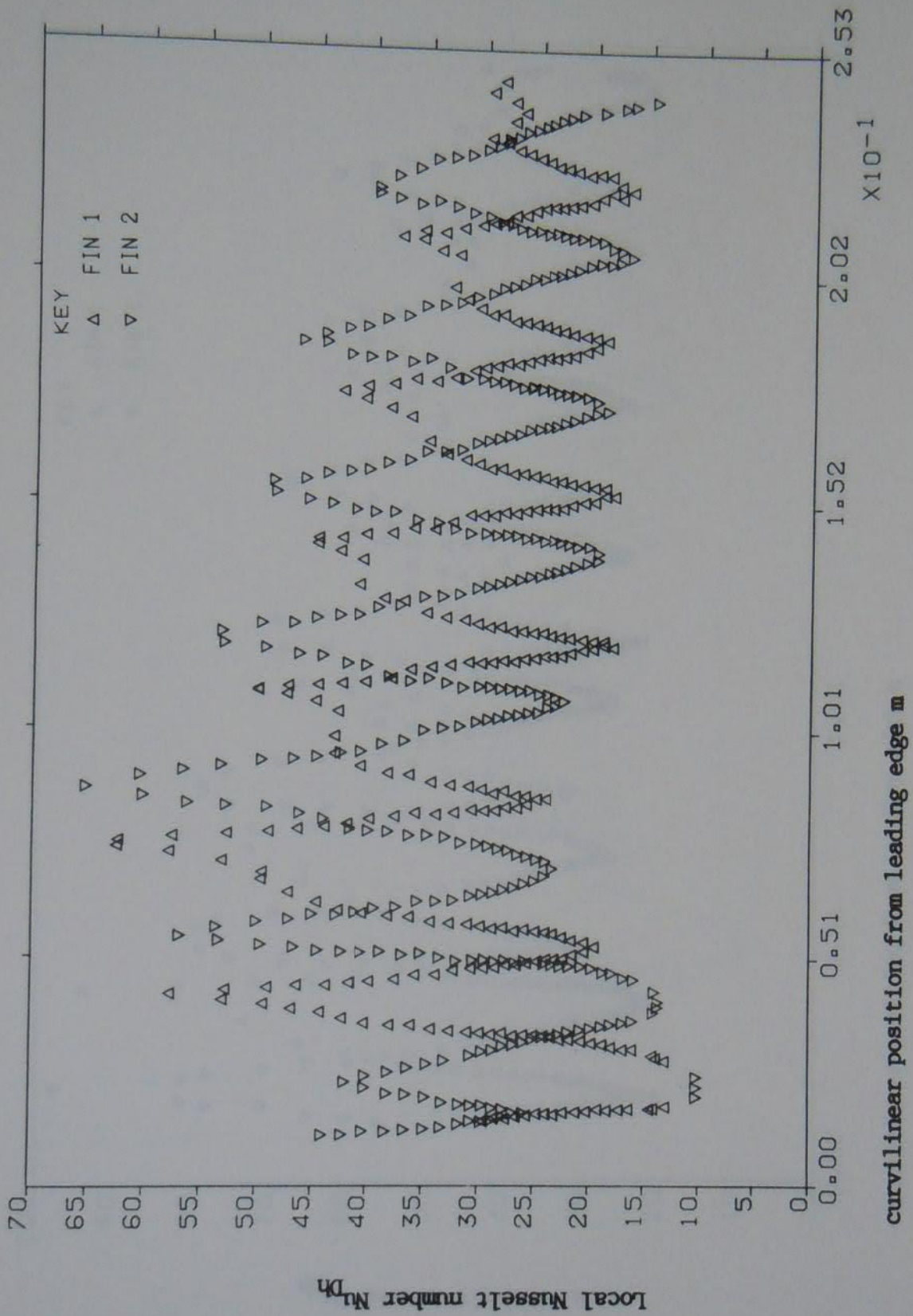
Figure 5.59 Local Nusselt number against curvilinear coordinate, profile 4, Dh = 0.0174 m, Re = 4946
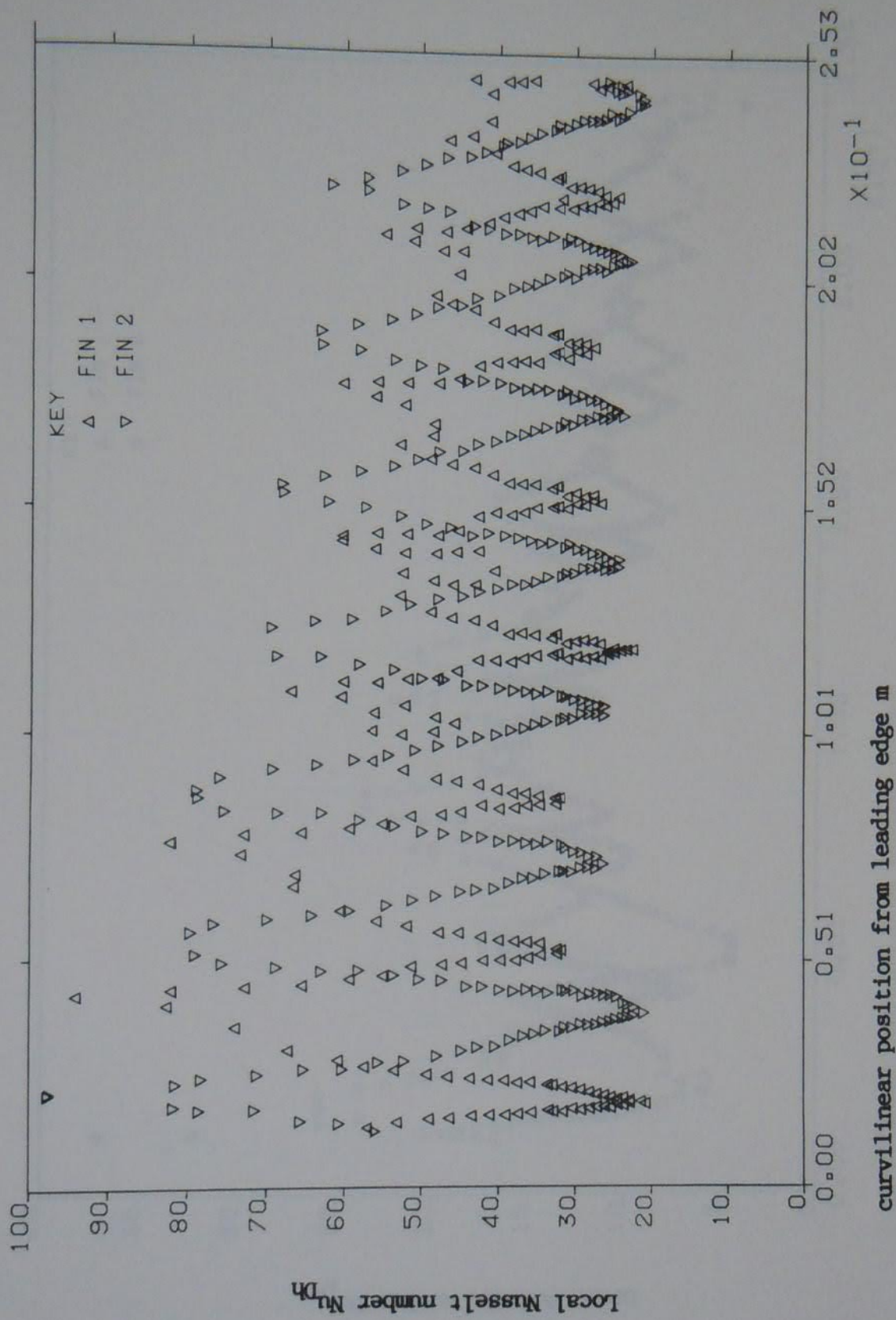
Figure 5.60 Local Nusselt number against curvilinear coordinate, profile 4, Dh = 0.0174 m, Re = 7889
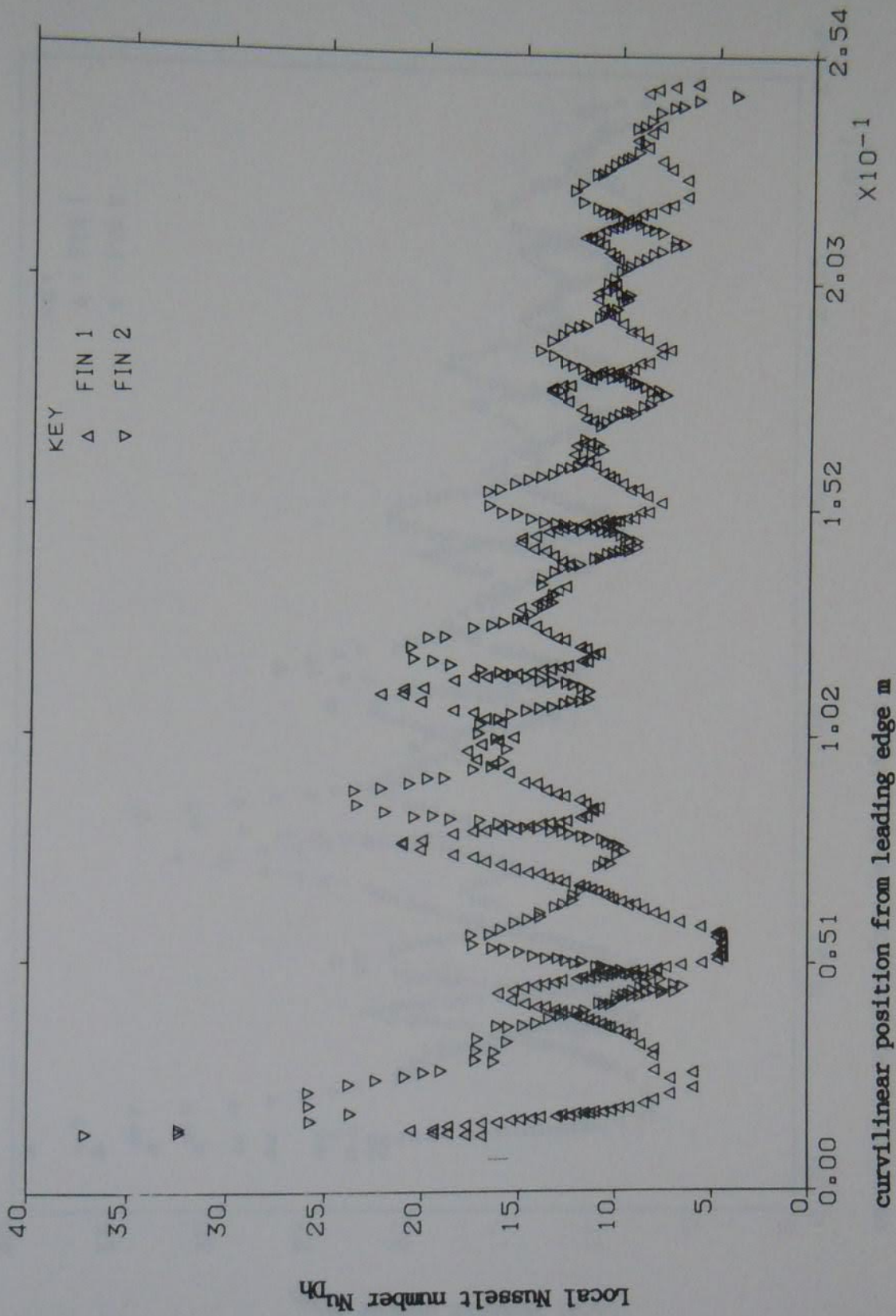
Figure 5.61 Local Nusselt number against curvilinear coordinate, profile 1, Dh = 0.0142 m, Re = 1605

263
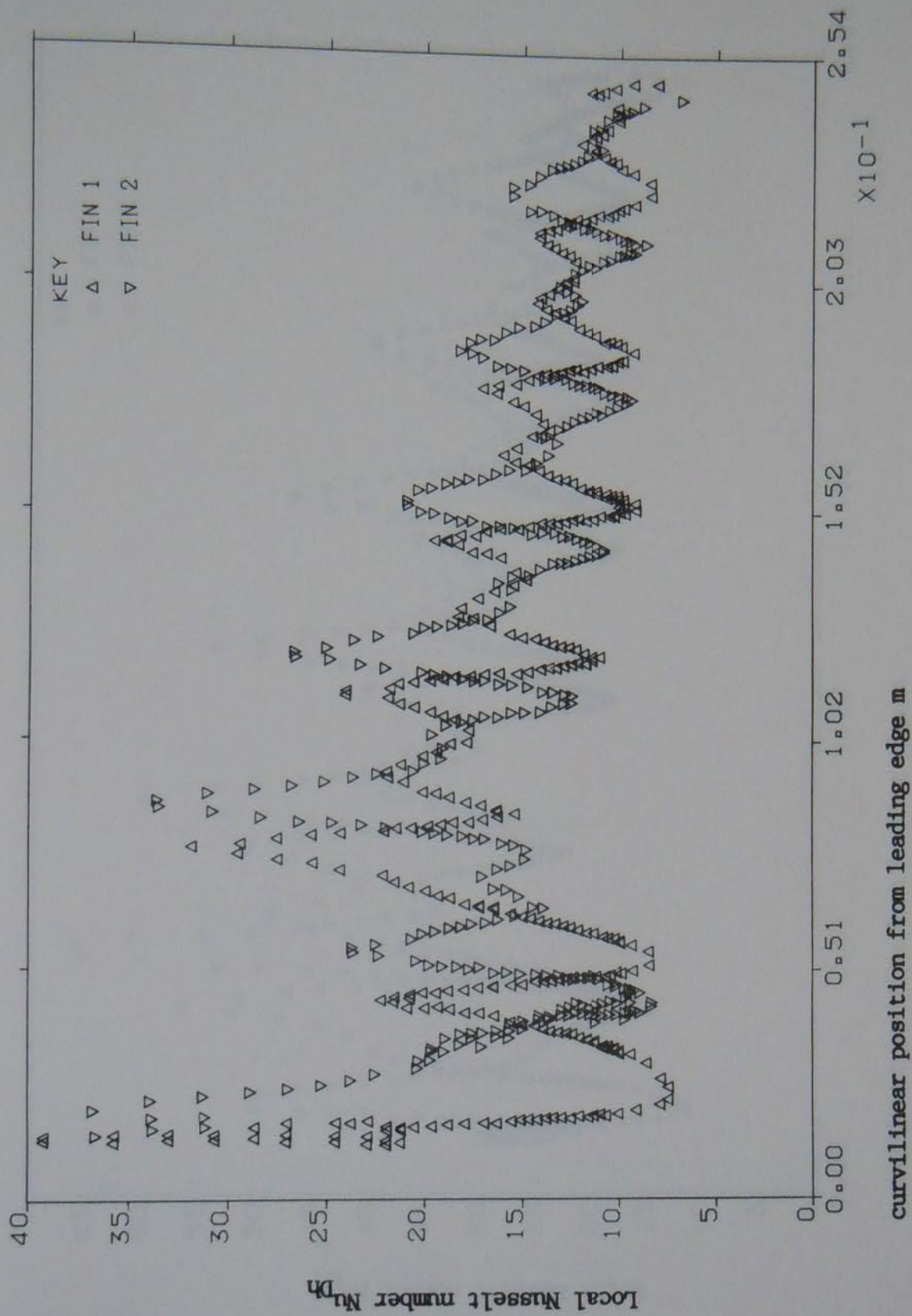
Figure 5.62 Local Nusselt number against curvilinear coordinate, profile 1, Dh = 0.0142 m, Re = 1992
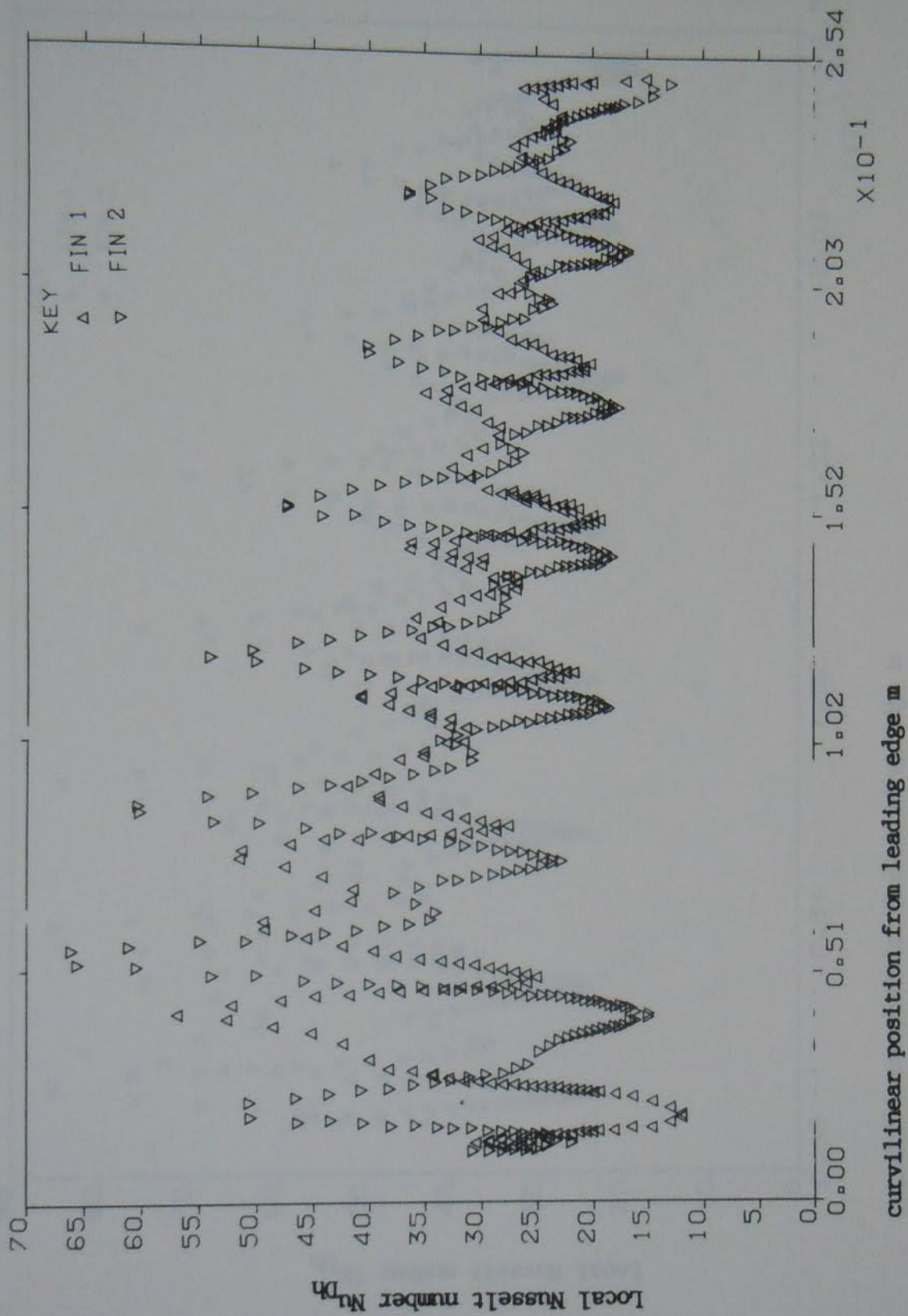
Figure 5.63 Local Nusselt number against curvilinear coordinate, profile 1, Dh = 0.0142 m, Re = 4915
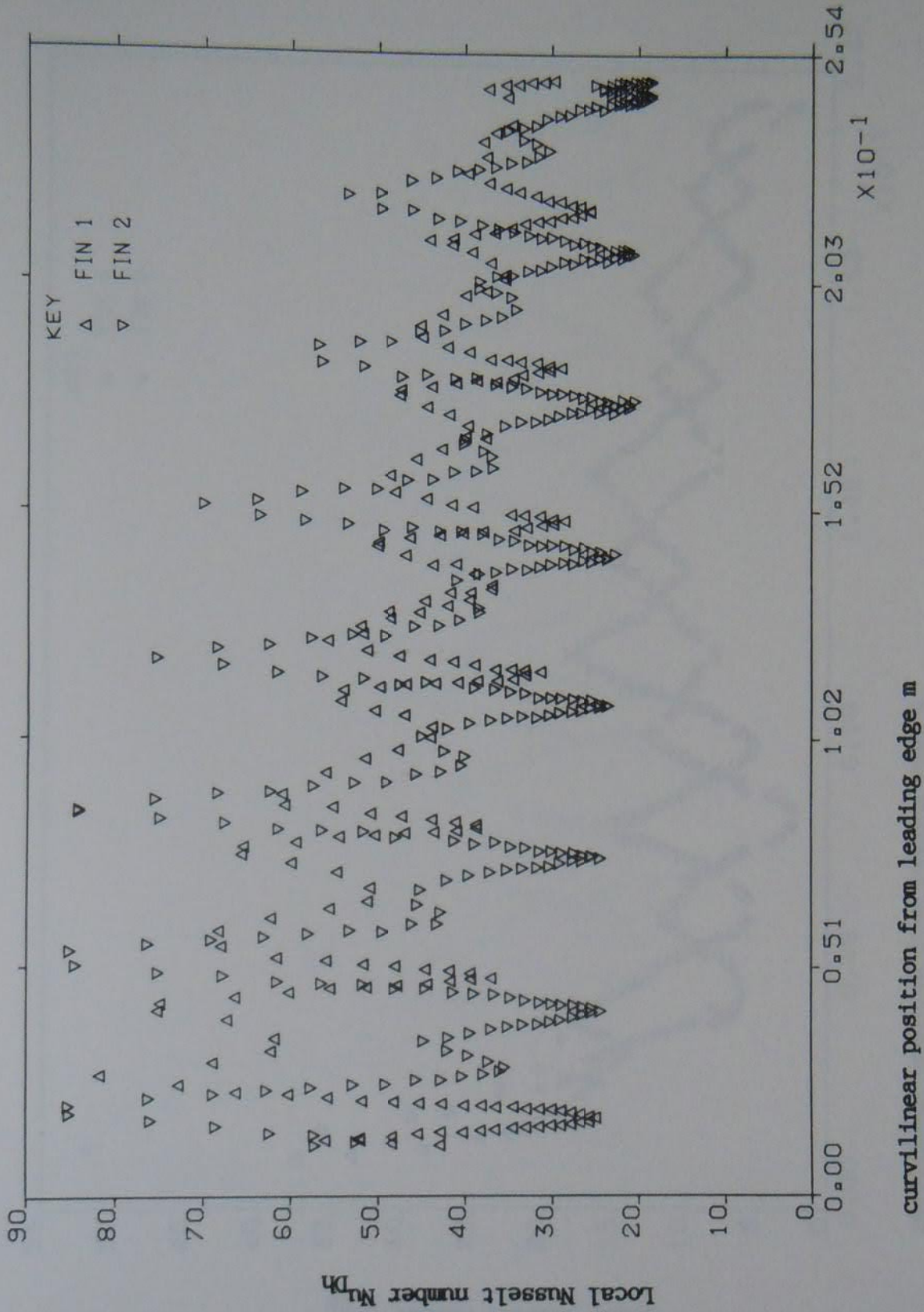
Figure 5.64 Local Nusselt number against curvilinear coordinate, profile 1, Dh = 0.0142 m, Re = 7954

266
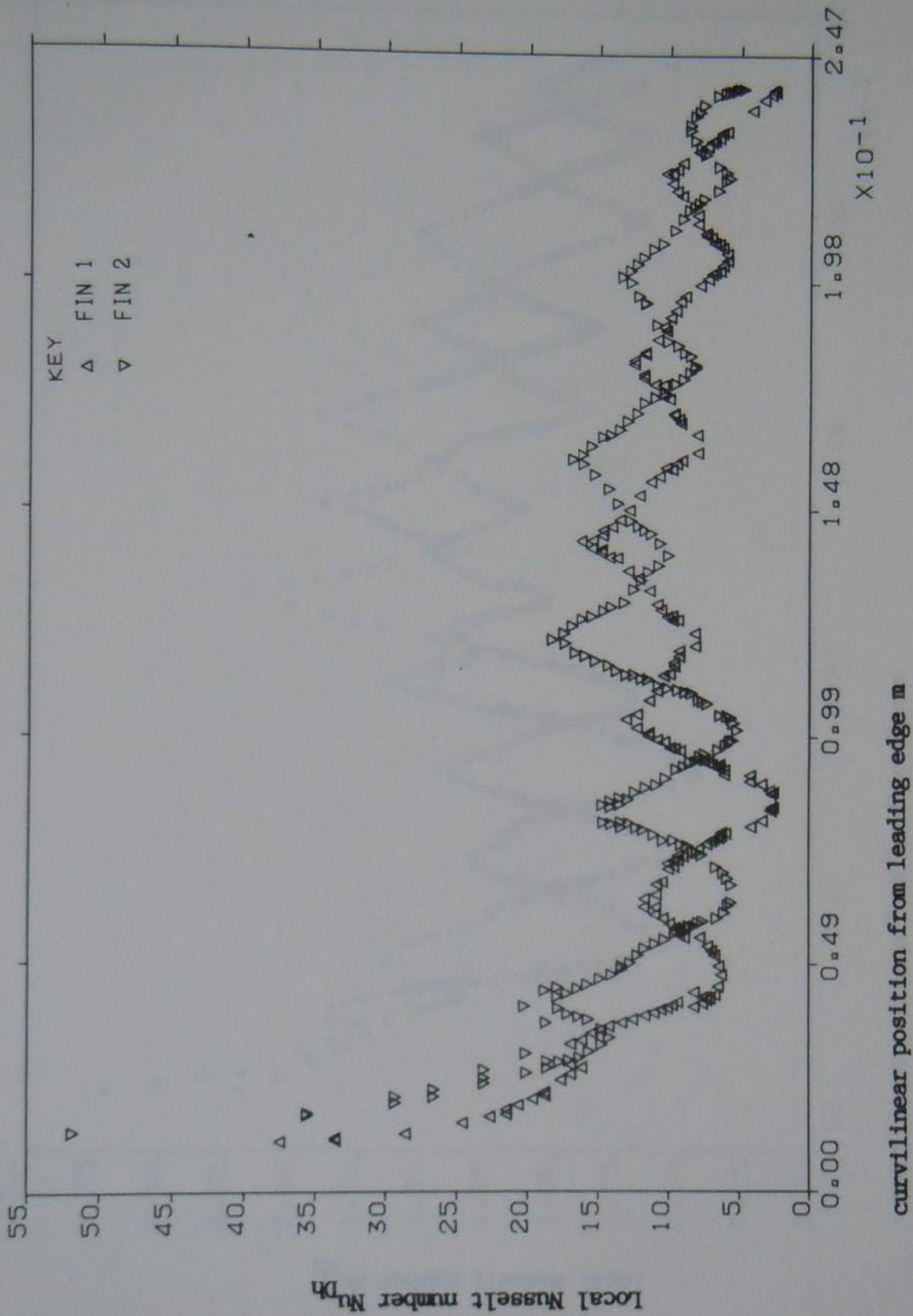
Figure 5.65 Local Nusselt number against curvilinear coordinate, profile 2, Dh = 0.0142 m, Re = 1601

267
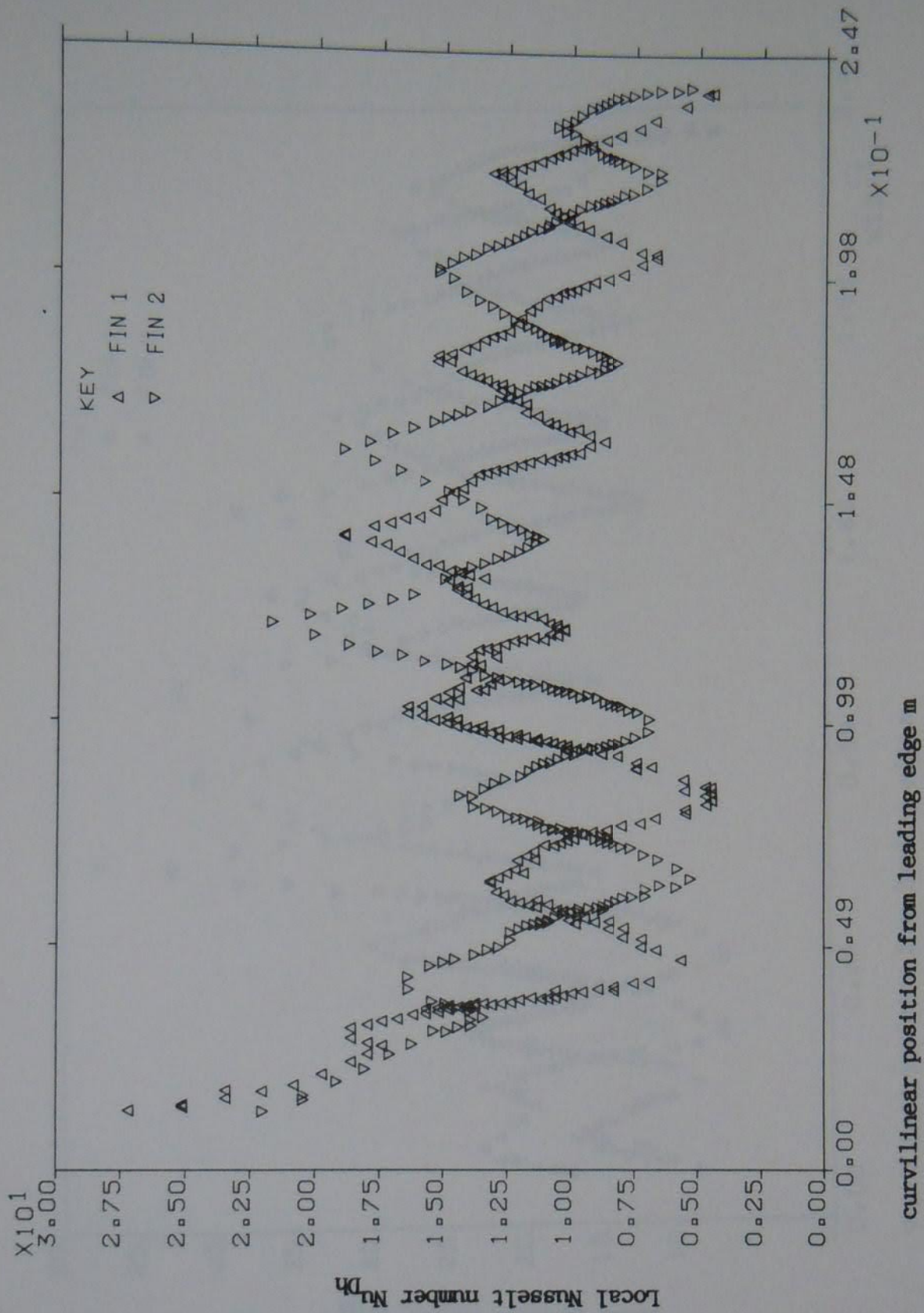
Figure 5.66 Local Nusselt number against curvilinear coordinate, profile 2, Dh = 0.0142 m, Re = 2040

268
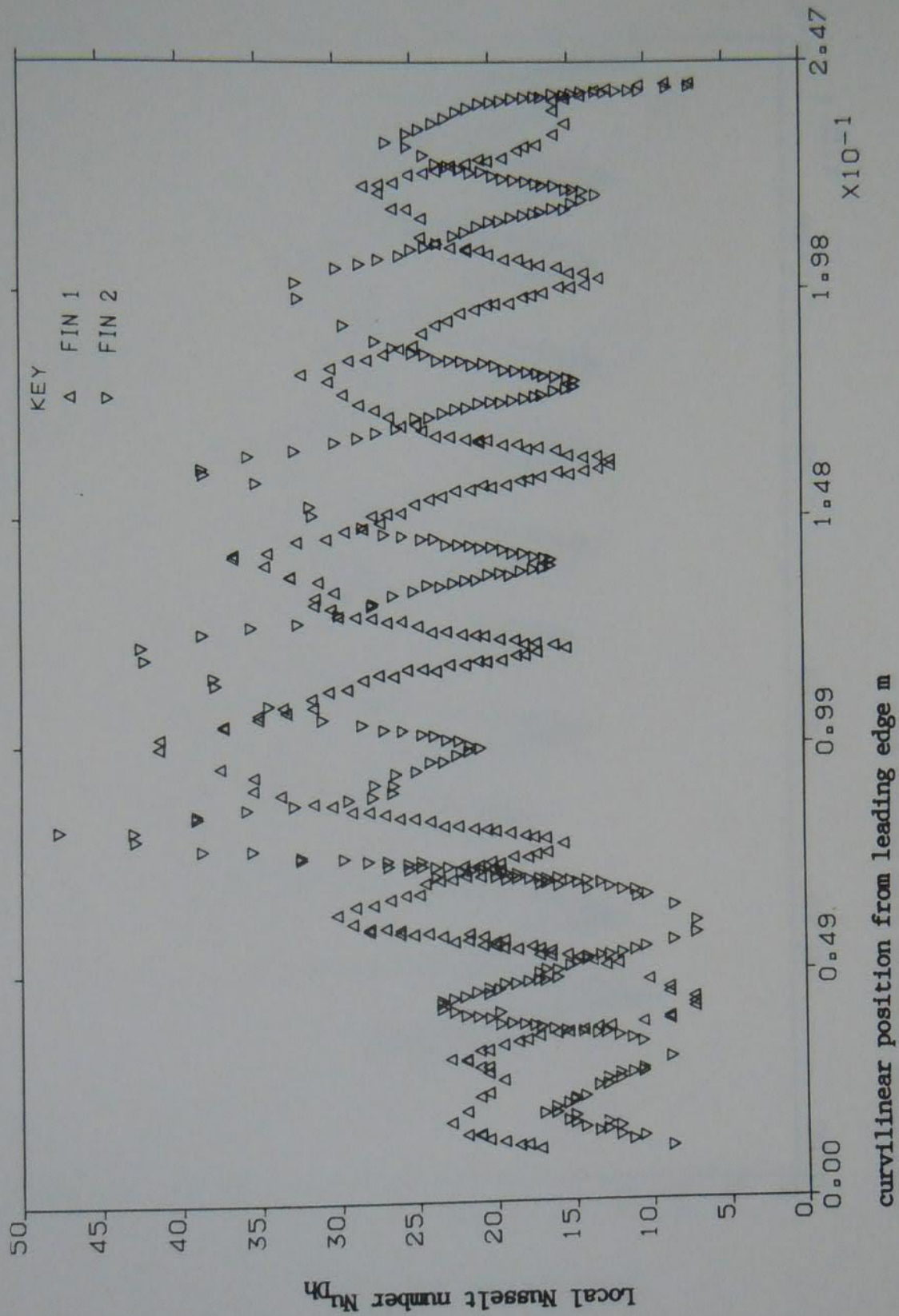
Figure 5.67 Local Nusselt number against curvilinear coordinate, profile 2, Dh = 0.0142 m, Re = 4925

Figure 5.68 Local Nusselt number against curvilinear coordinate, profile 2, Dh = 0.0142 m, Re = 7827

Figure 5.69 Local Nusselt number against curvilinear coordinate, profile 3, Dh = 0.0142 m, Re = 1607

271

Figure 5.70 Local Nusselt number against curvilinear coordinate, profile 3, Dh = 0.0142 m, Re = 2023

Figure 5.71 Local Nusselt number against curvilinear coordinate, profile 3, Dh = 0.0142 m, Re = 4905

273
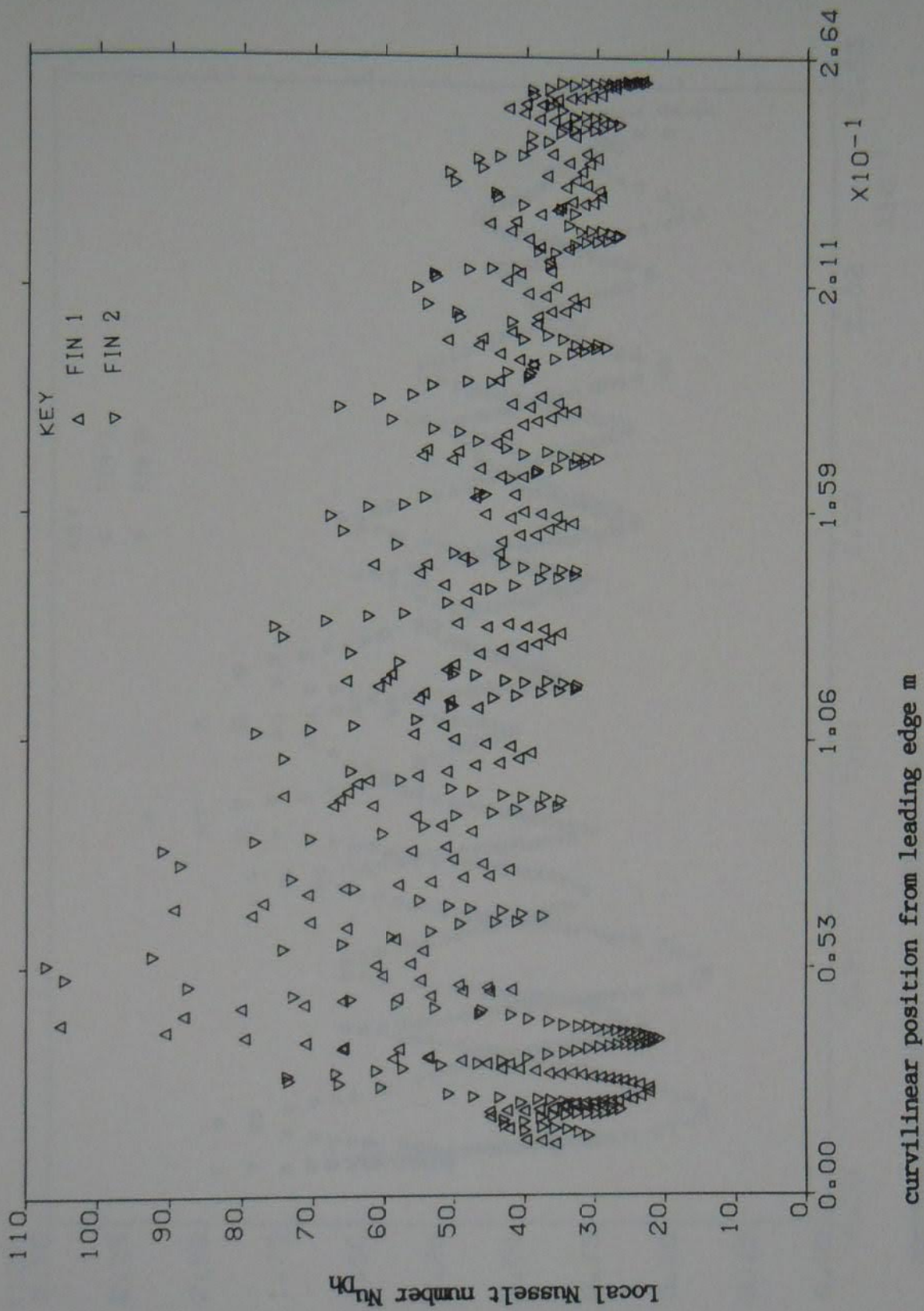
Figure 5.72 Local Nusselt number against curvilinear coordinate, profile 3, Dh = 0.0142 m, Re = 7755
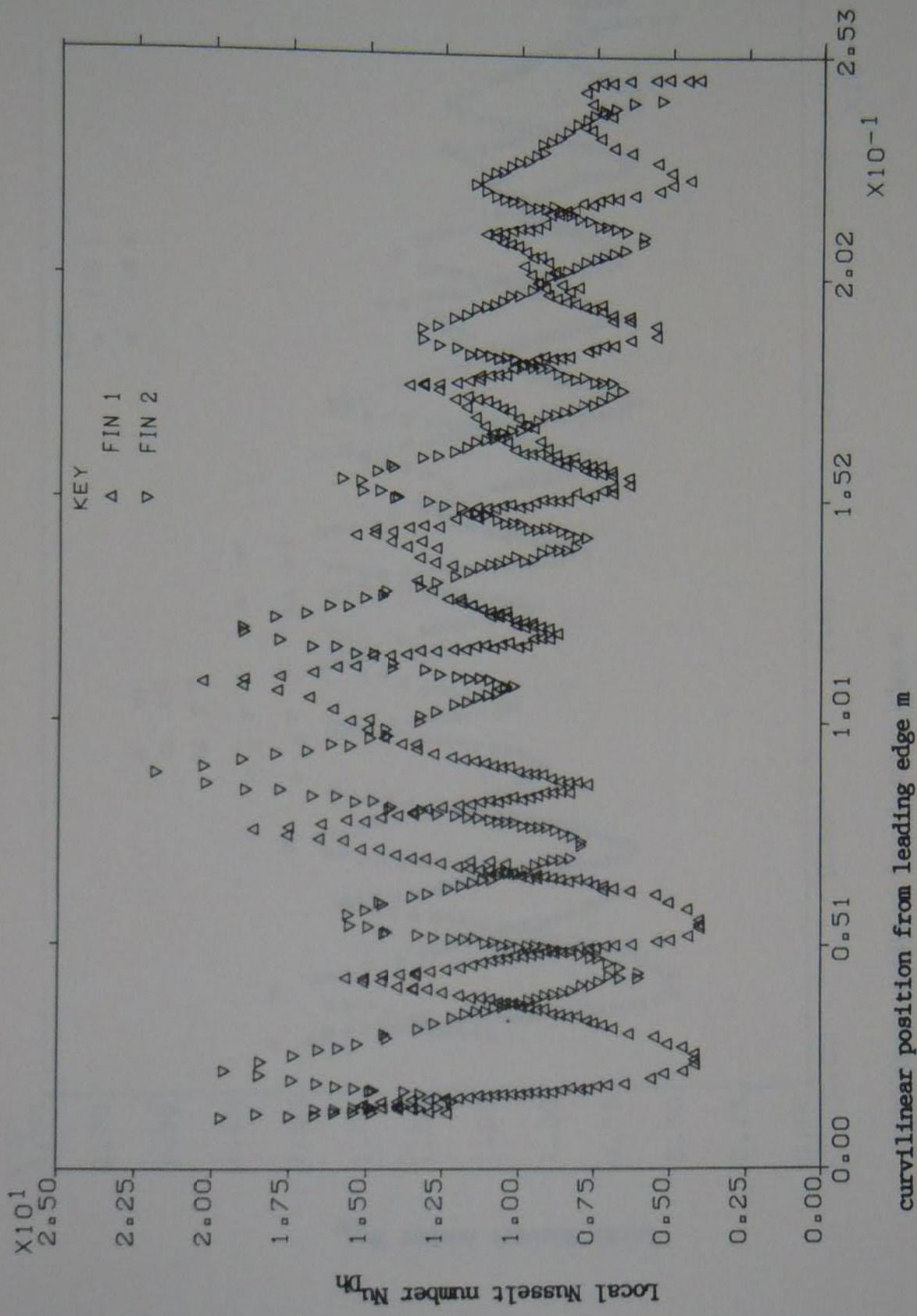
Figure 5.73 Local Nusselt number against curvilinear coordinate, profile 4, Dh = 0.0142 m, Re = 1608
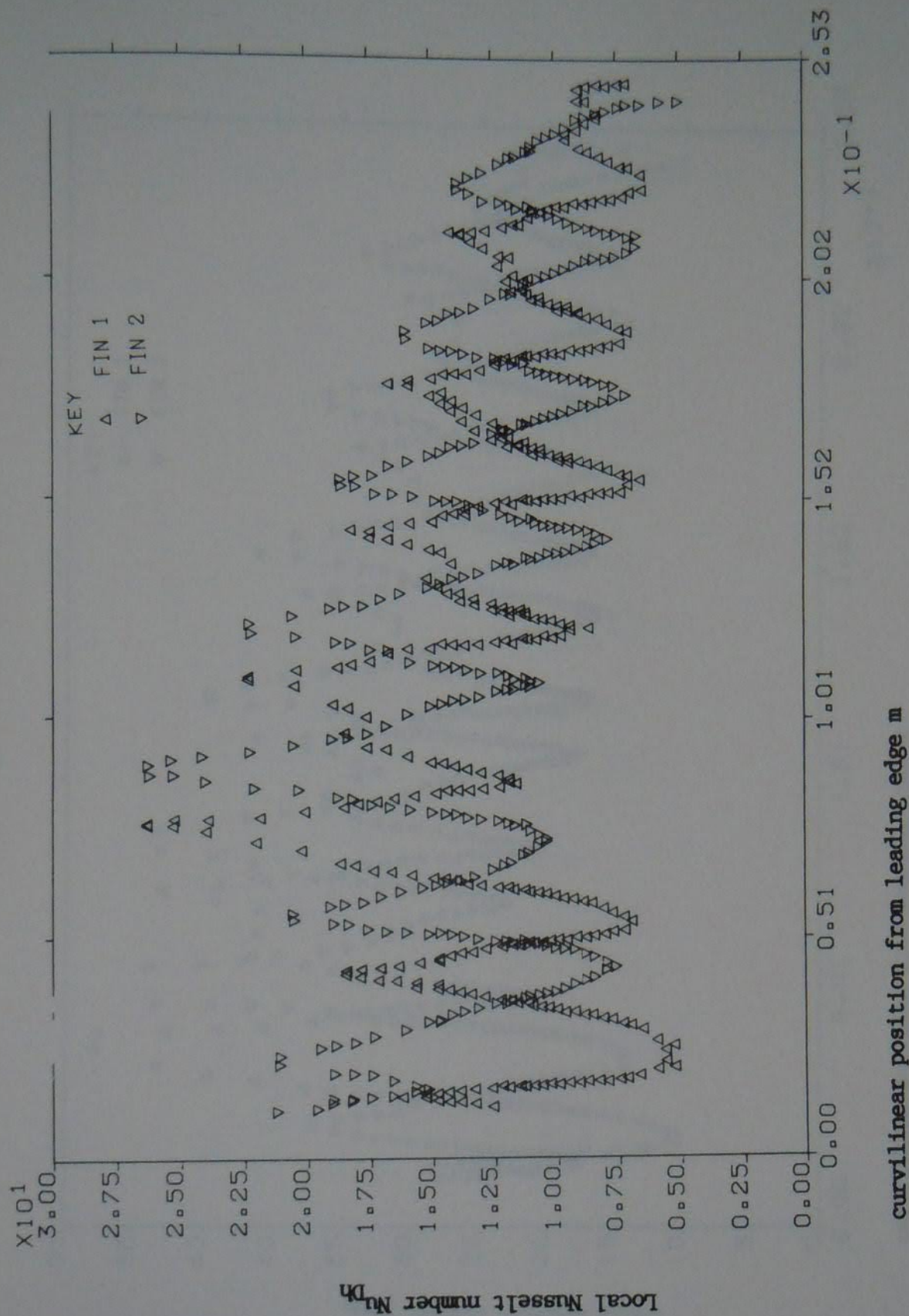
Figure 5.74 Local Nusselt number against curvilinear coordinate, profile 4, Dh = 0.0142 m, Re = 1999

276
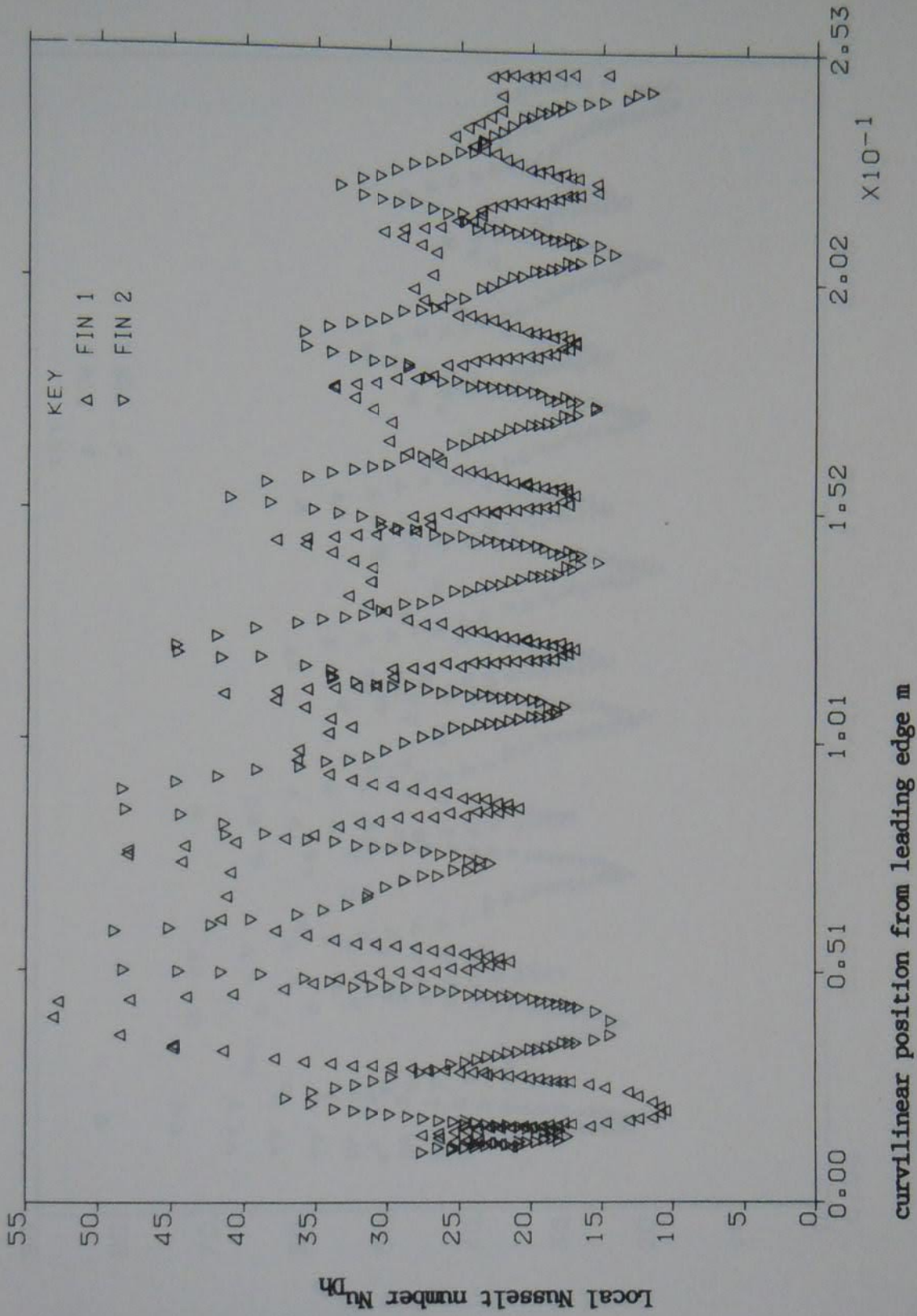
Figure 5.75 Local Nusselt number against curvilinear coordinate, profile 4, Dh = 0.0142 m, Re = 4936

277
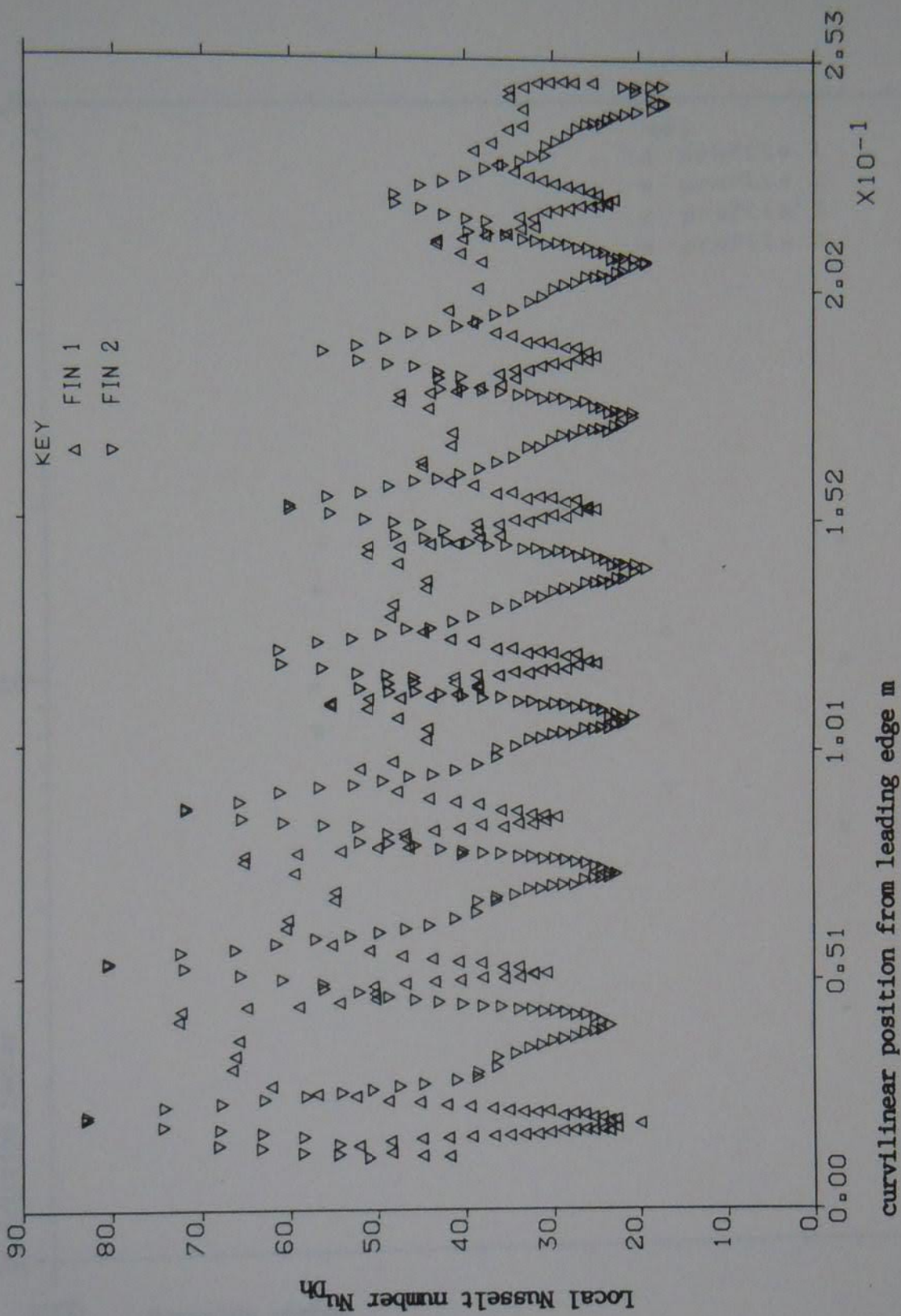
Figure 5.76 Local Nusselt number against curvilinear coordinate, profile 4, Dh = 0.0142 m, Re = 7894
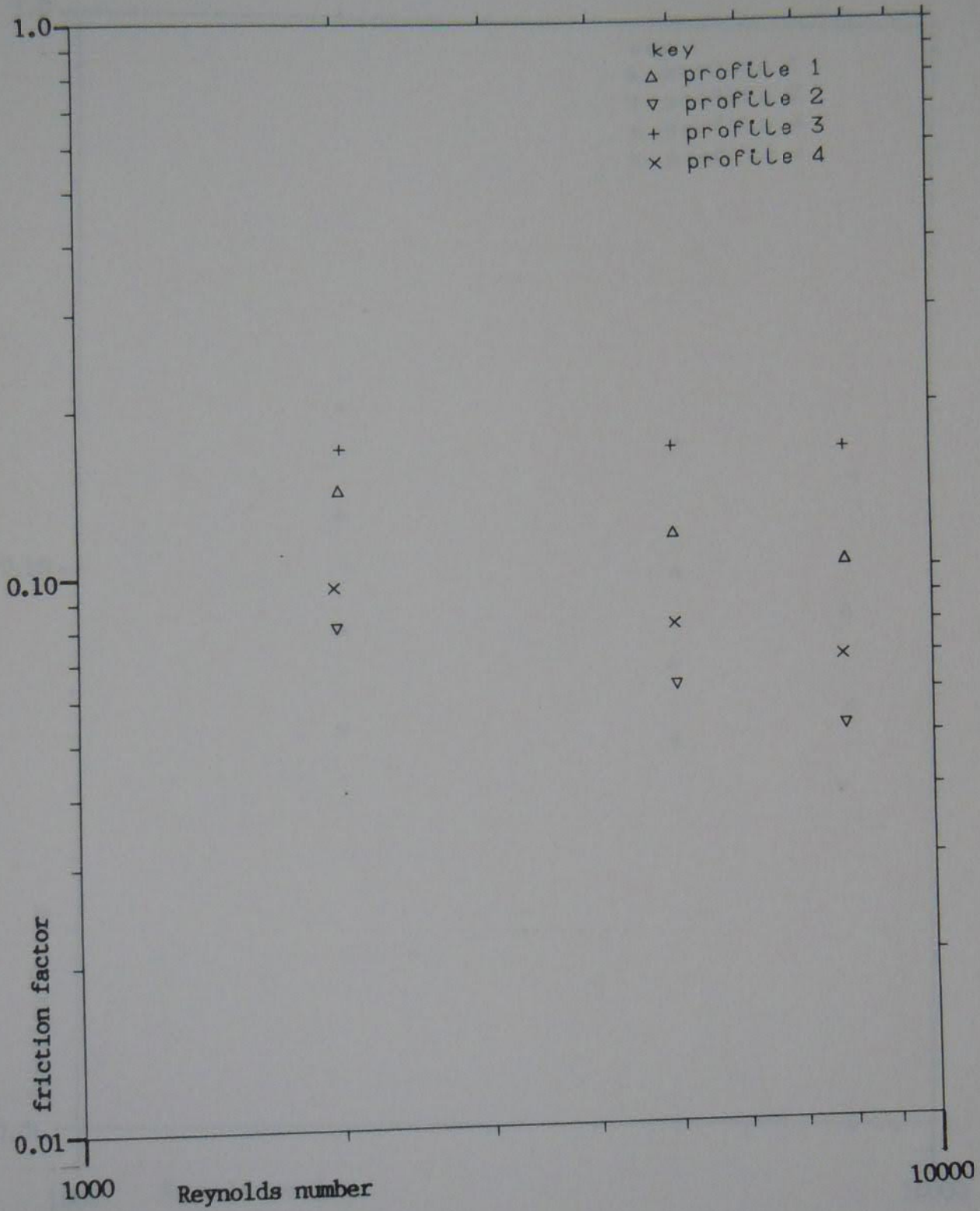
Figure 5.77 The friction factor shown against the Reynolds number for the four profiles at Dh = 0.0224 m
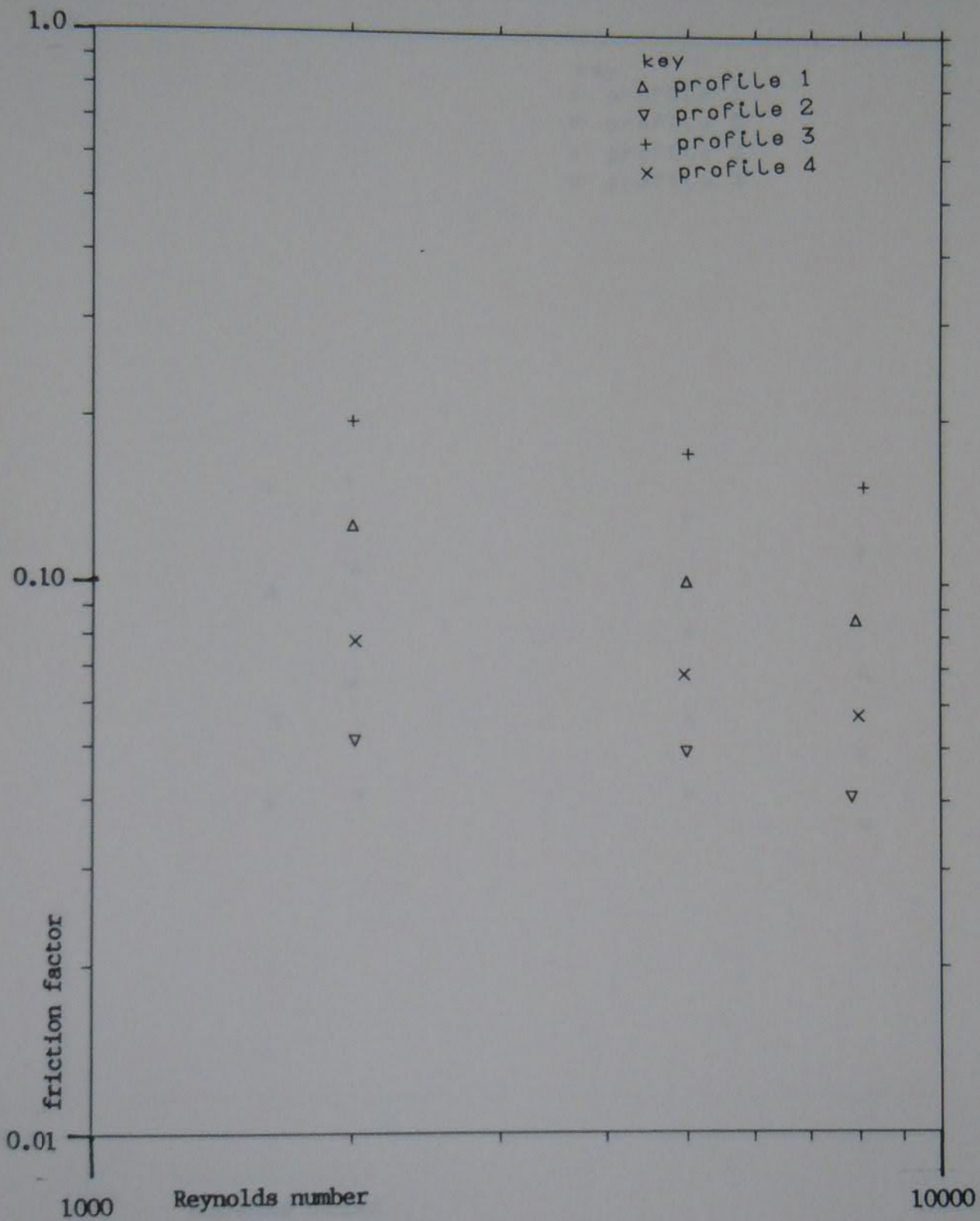
Figure 5.78 The friction factor shown against the Reynolds number for the four profiles at Dh = 0.0174 m
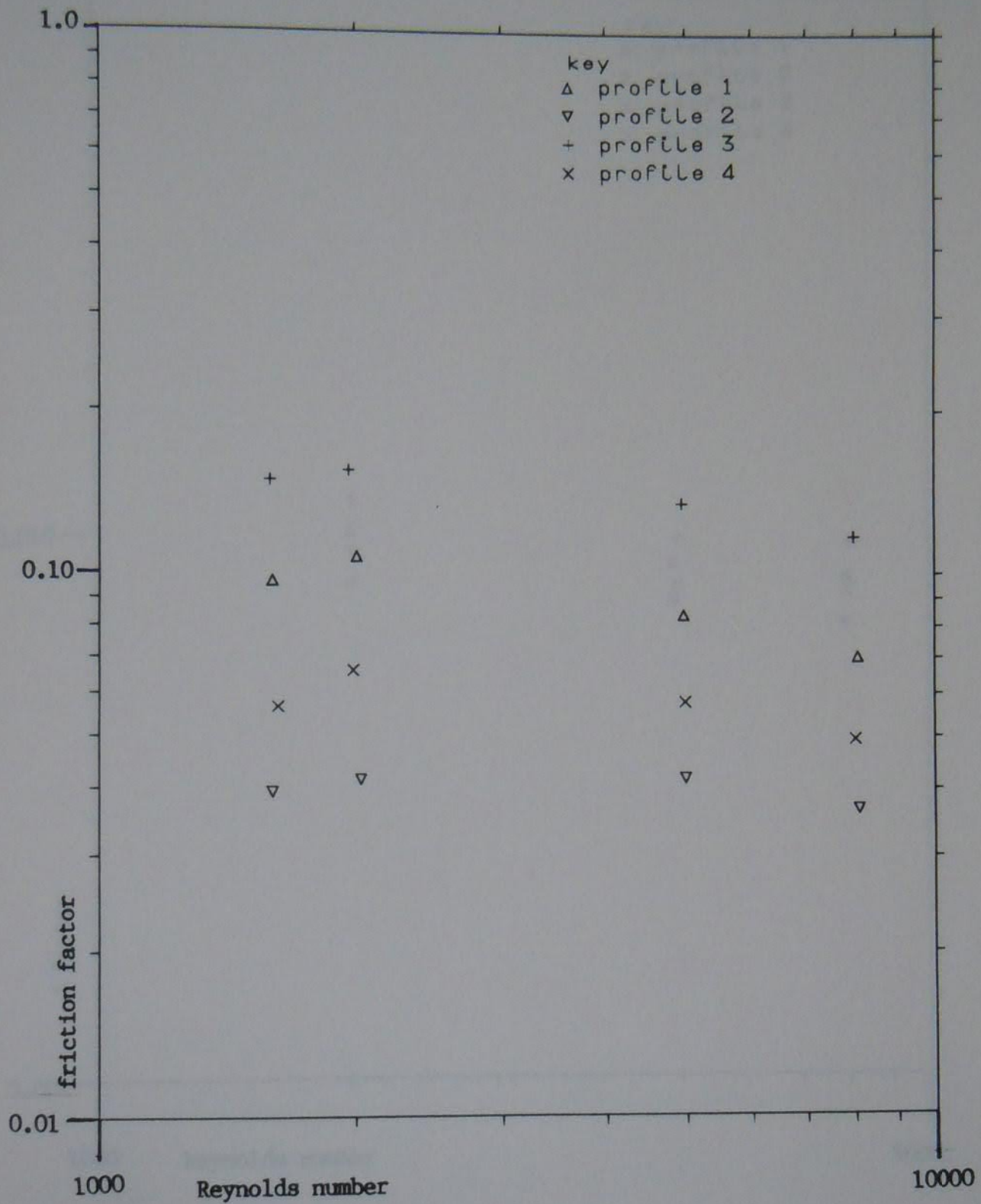
Figure 5.79 The friction factor shown against the Reynolds number for the four profiles at Dh = 0.0142 m
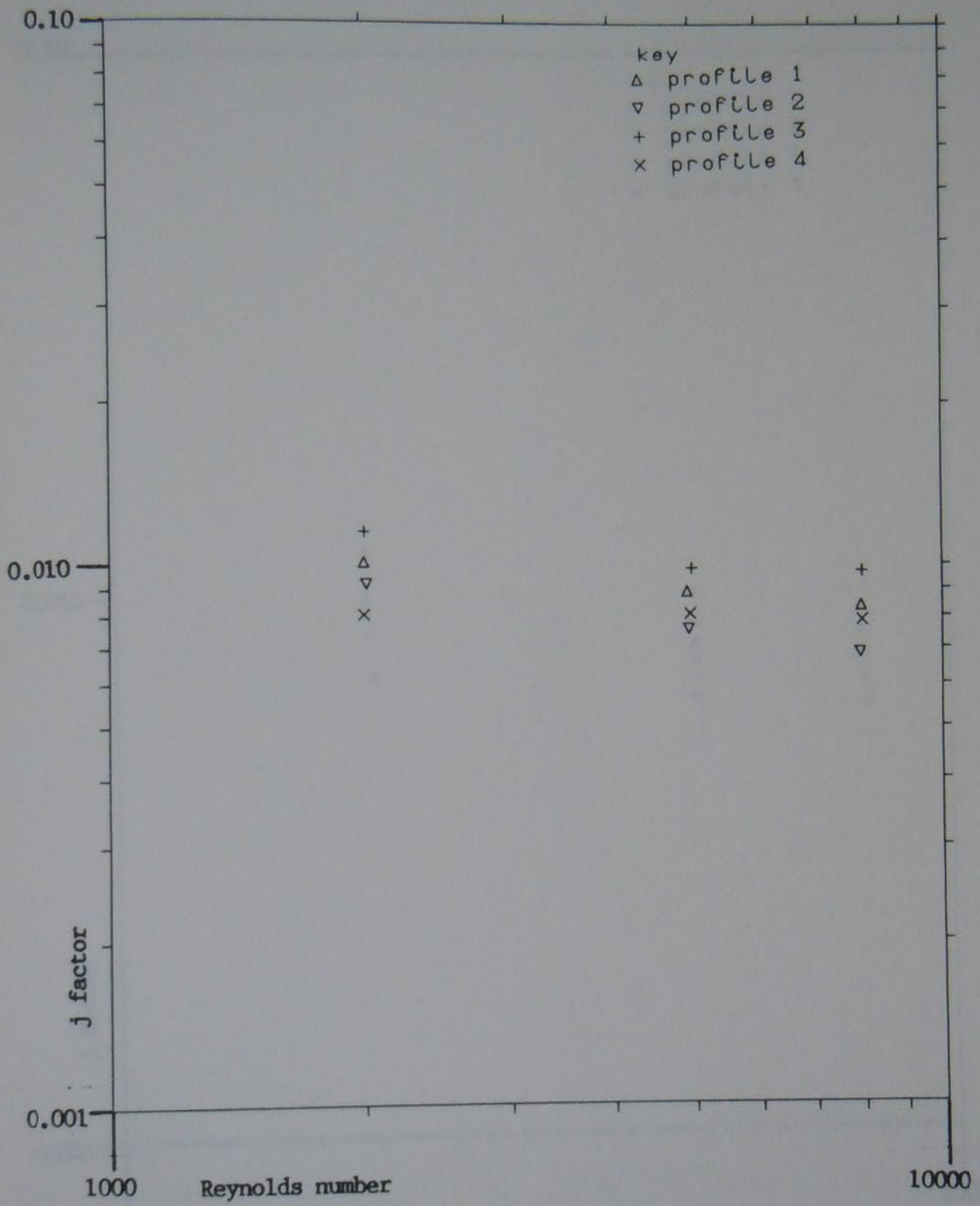
Figure 5.80 The j factor shown against the Reynolds number for the four profiles at Dh = 0.0224 m
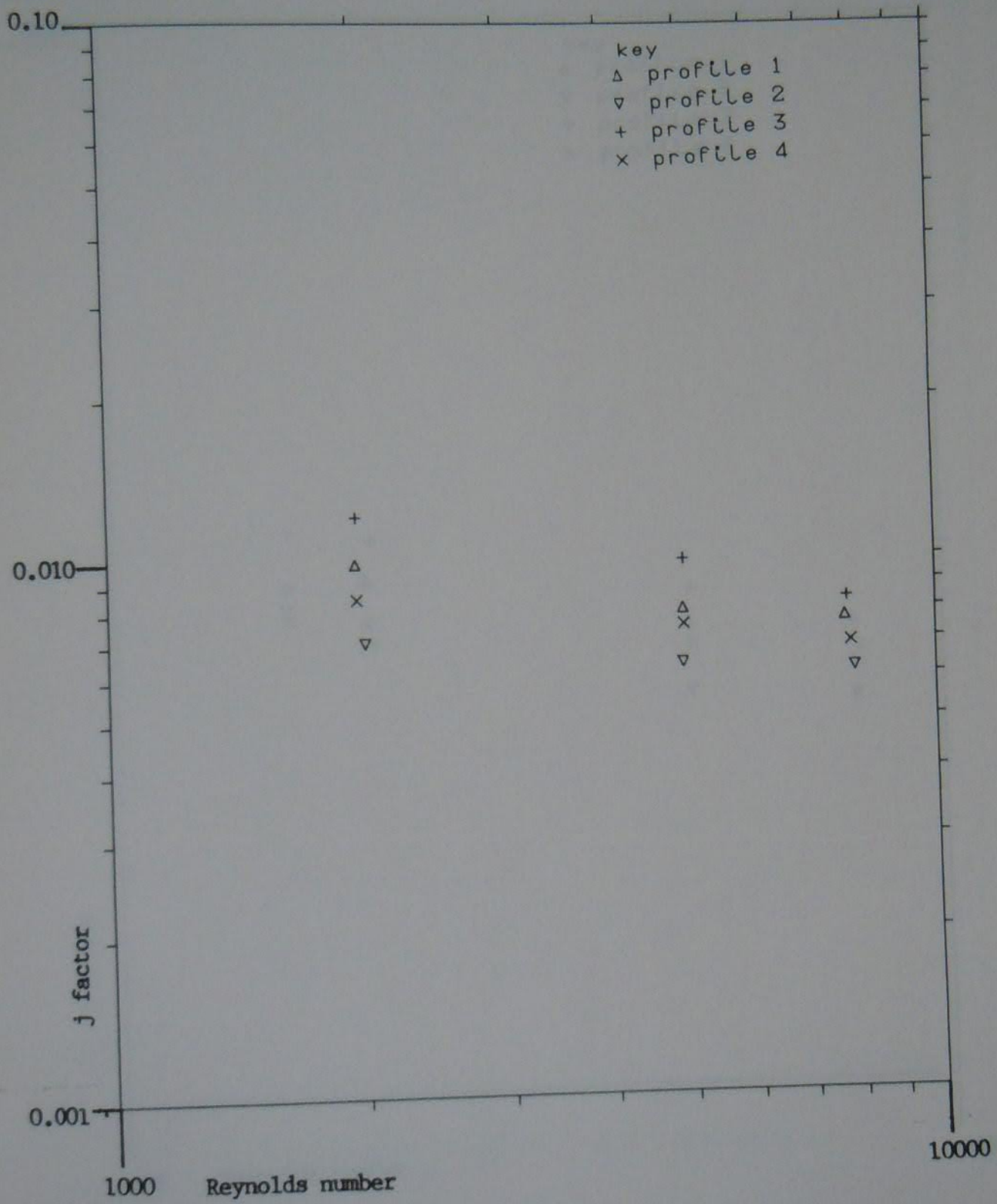
Figure 5.81 The j factor shown against the Reynolds number for the four profiles at Dh = 0.0174 m
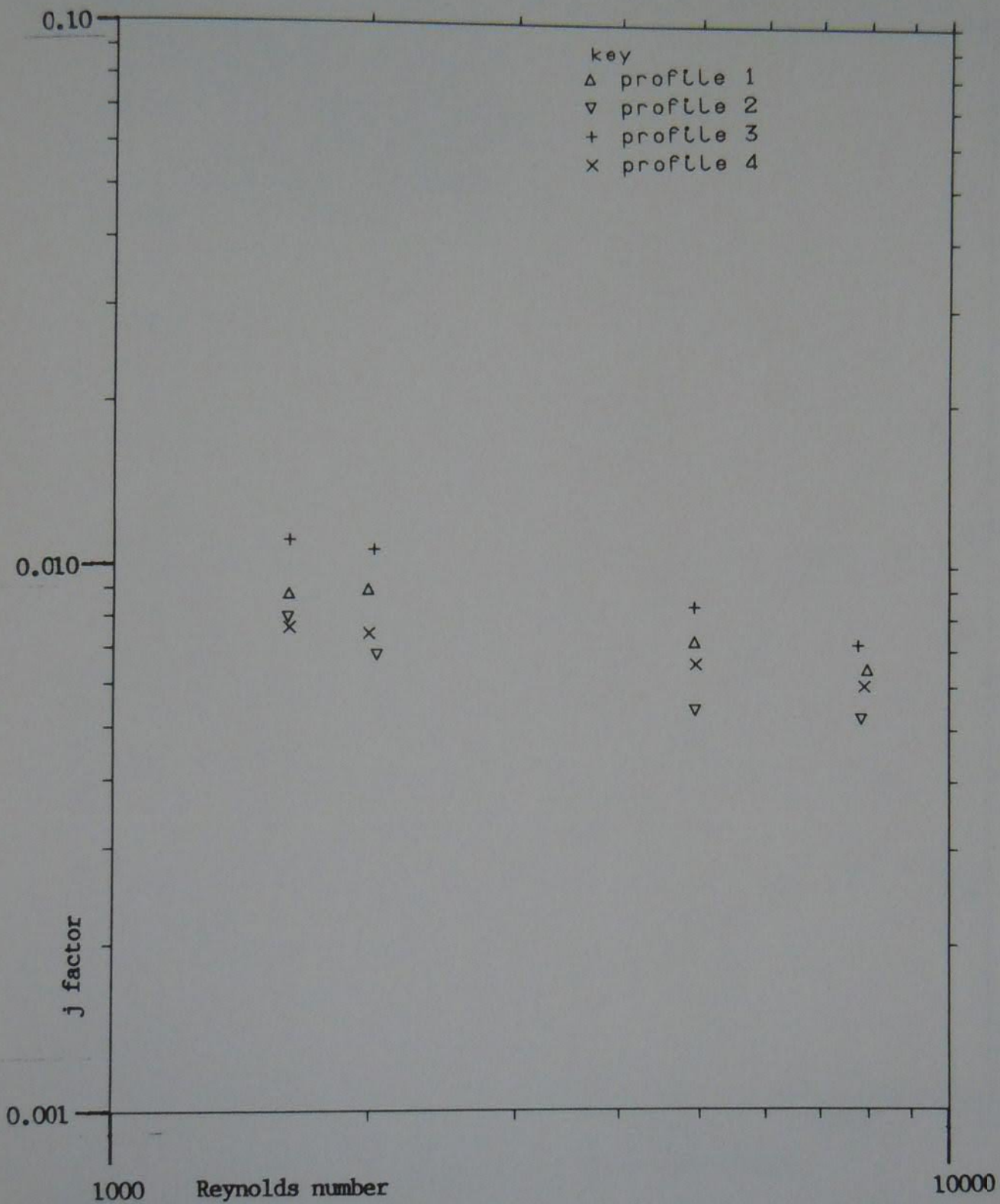
Figure 5.82 The j factor shown against the Reynolds number for the four profiles at Dh = 0.0142 m
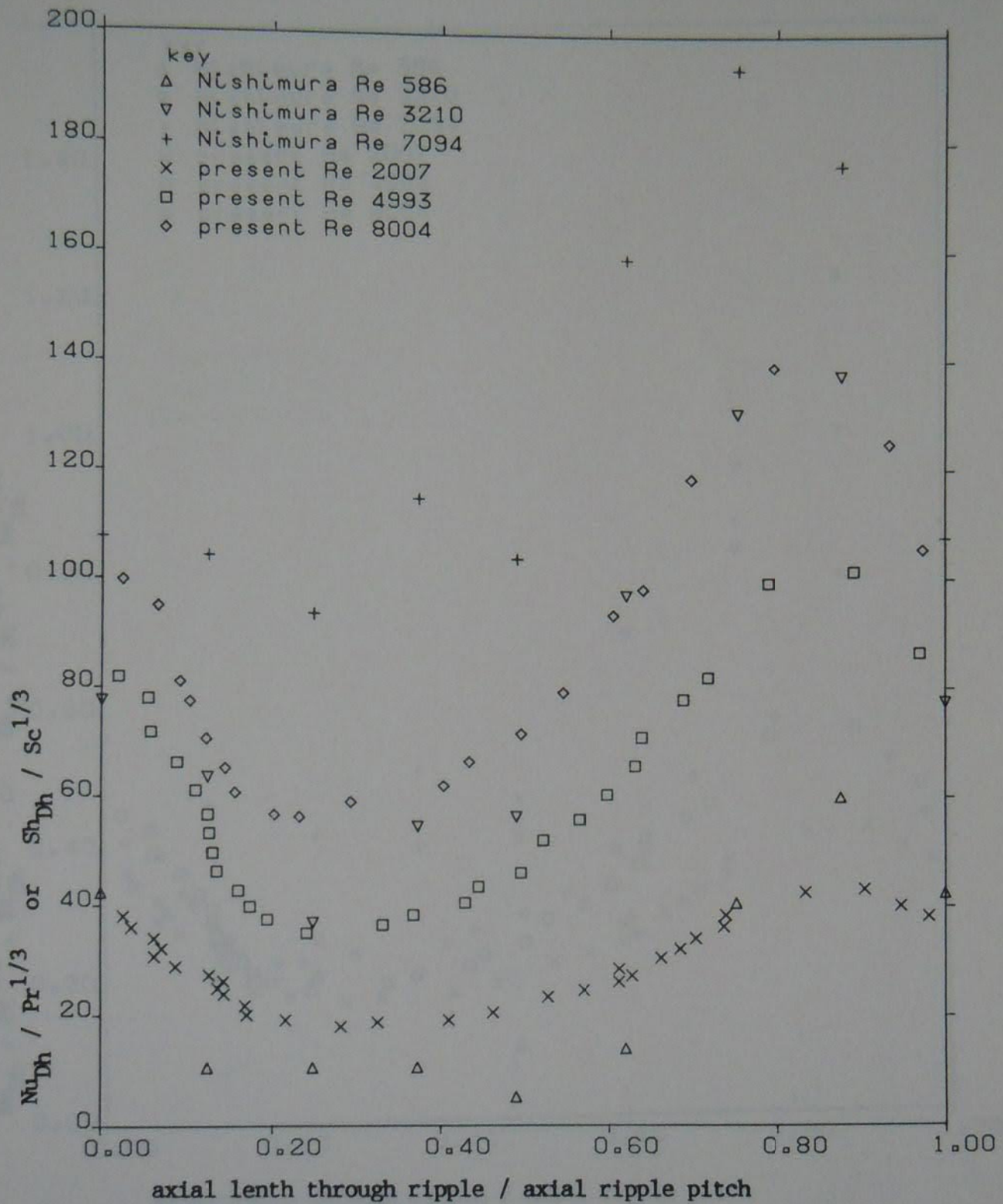
Figure 5.83 Comparison of the mass transfer coefficients with the measured heat transfer coefficient
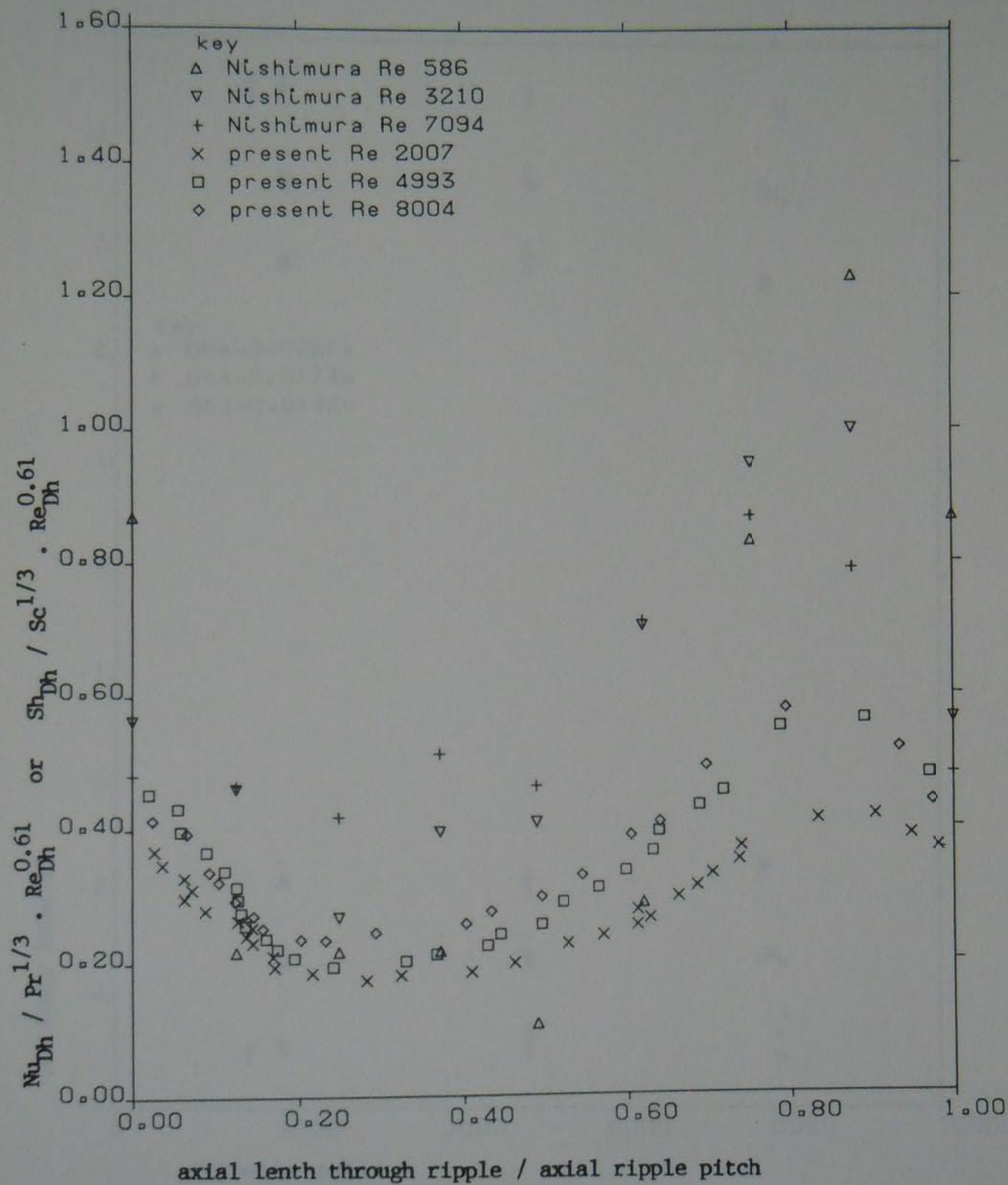
Figure 5.84 Comparison of constant values in the nondimensional relationships A = Sh / f(Re,Sc) or A = Nu / f(Re,Pr)
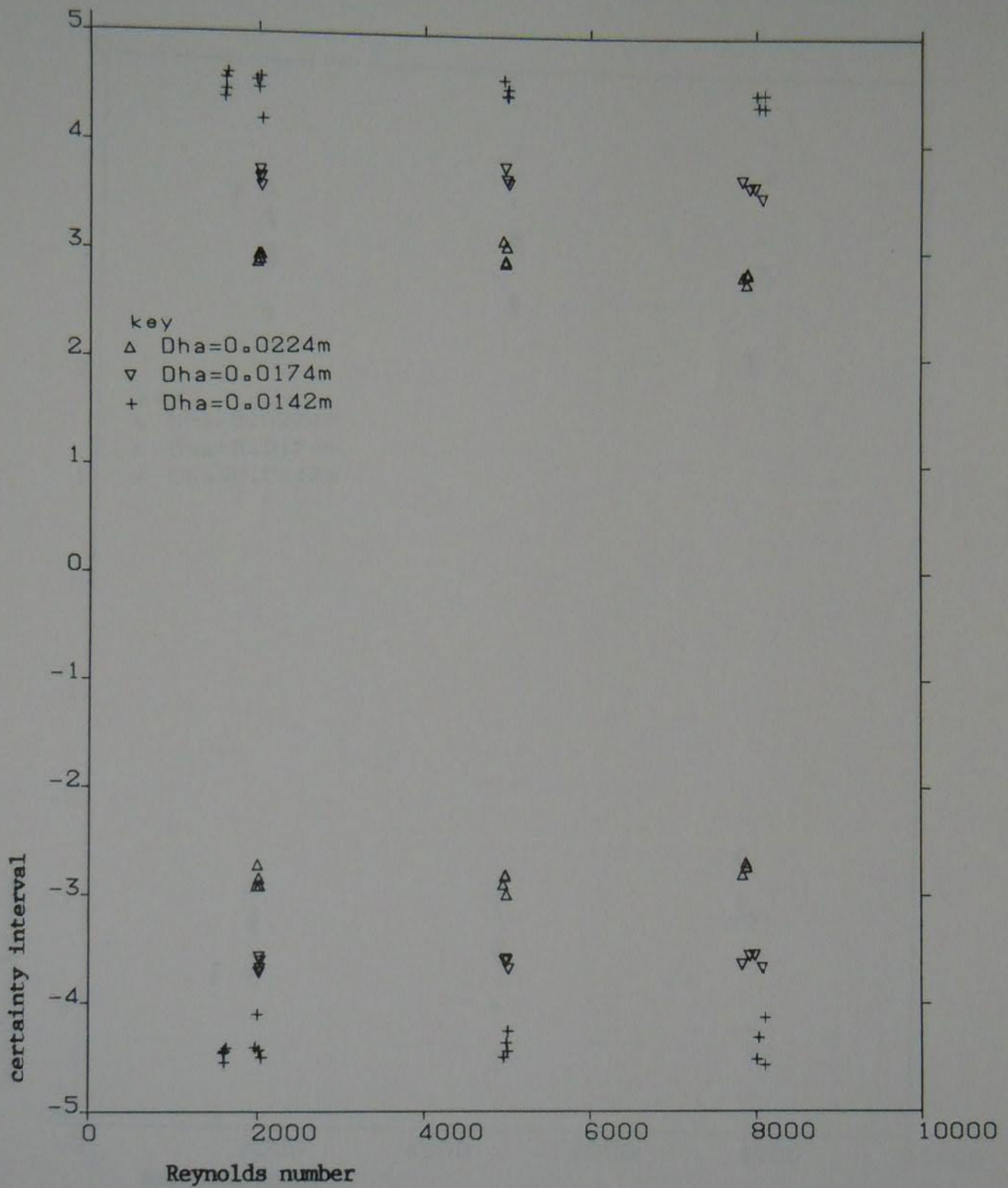
Figure 5.85 The 95 percent certainty interval for the friction factor from Monte Carlo simulation
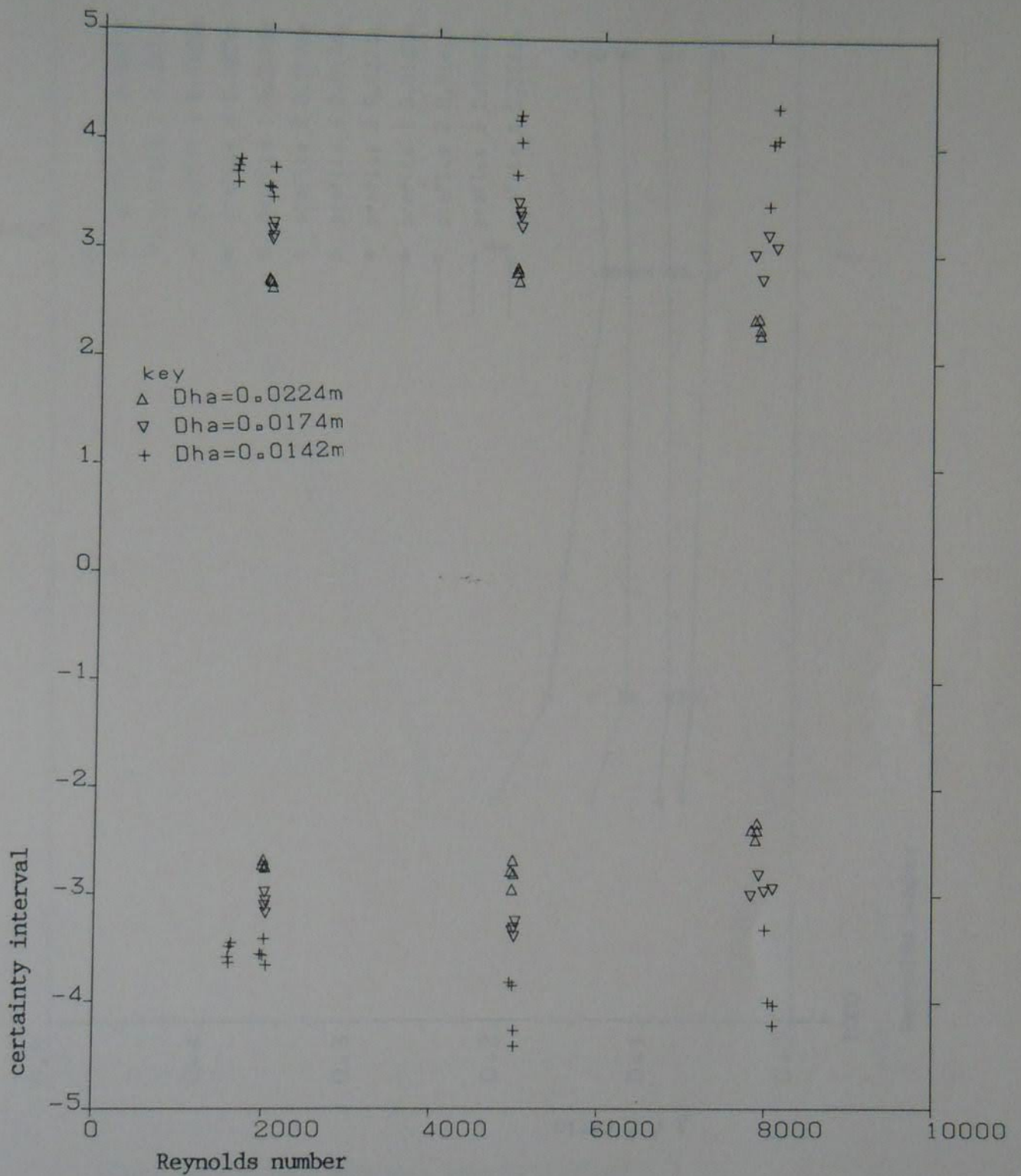
Figure 5.86 The 95 percent certainty interval for the Reynolds number from Monte Carlo simulation
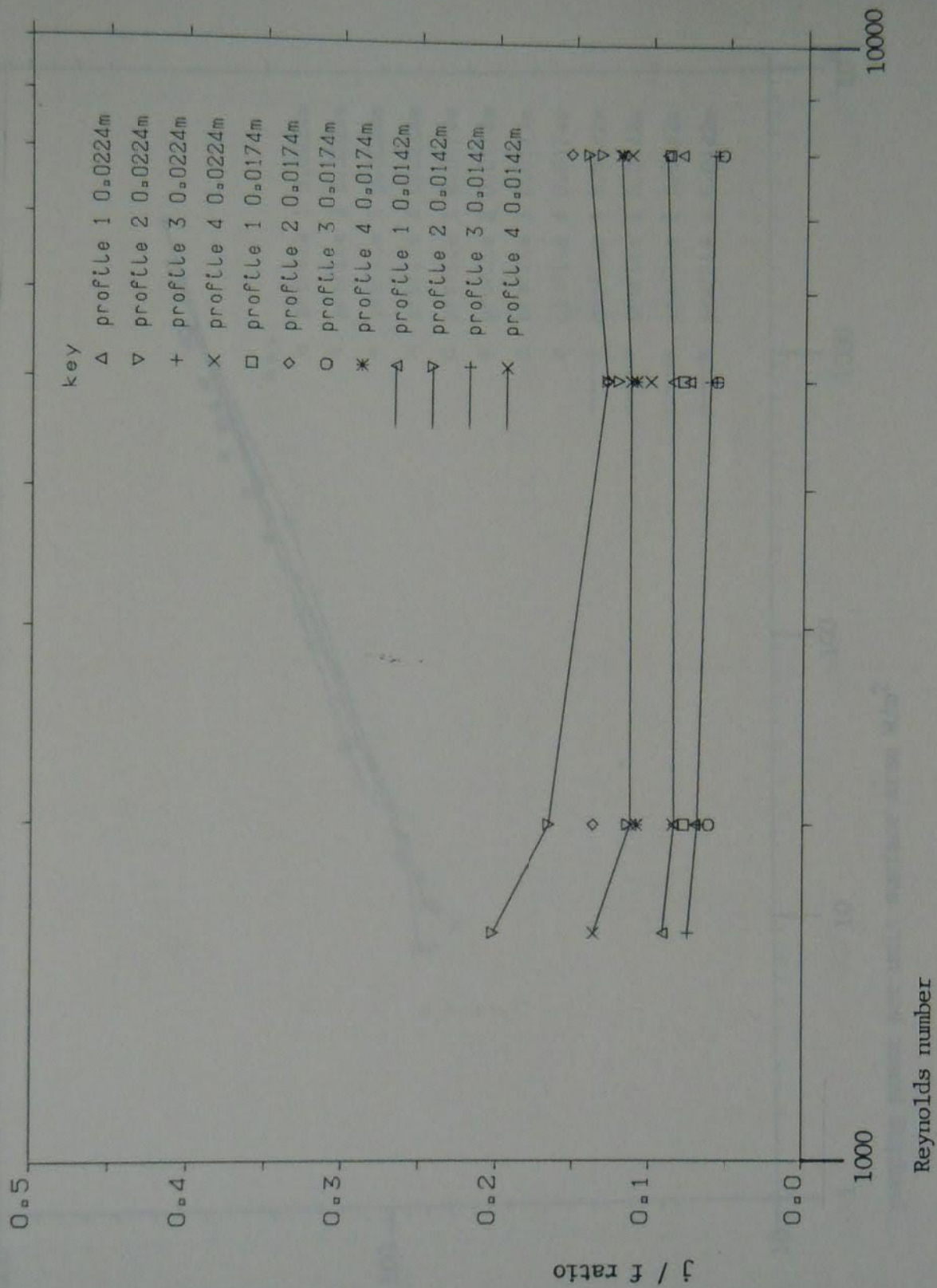
Figure 5.87 Comparison of rippled fin surfaces based on the j/f ratio
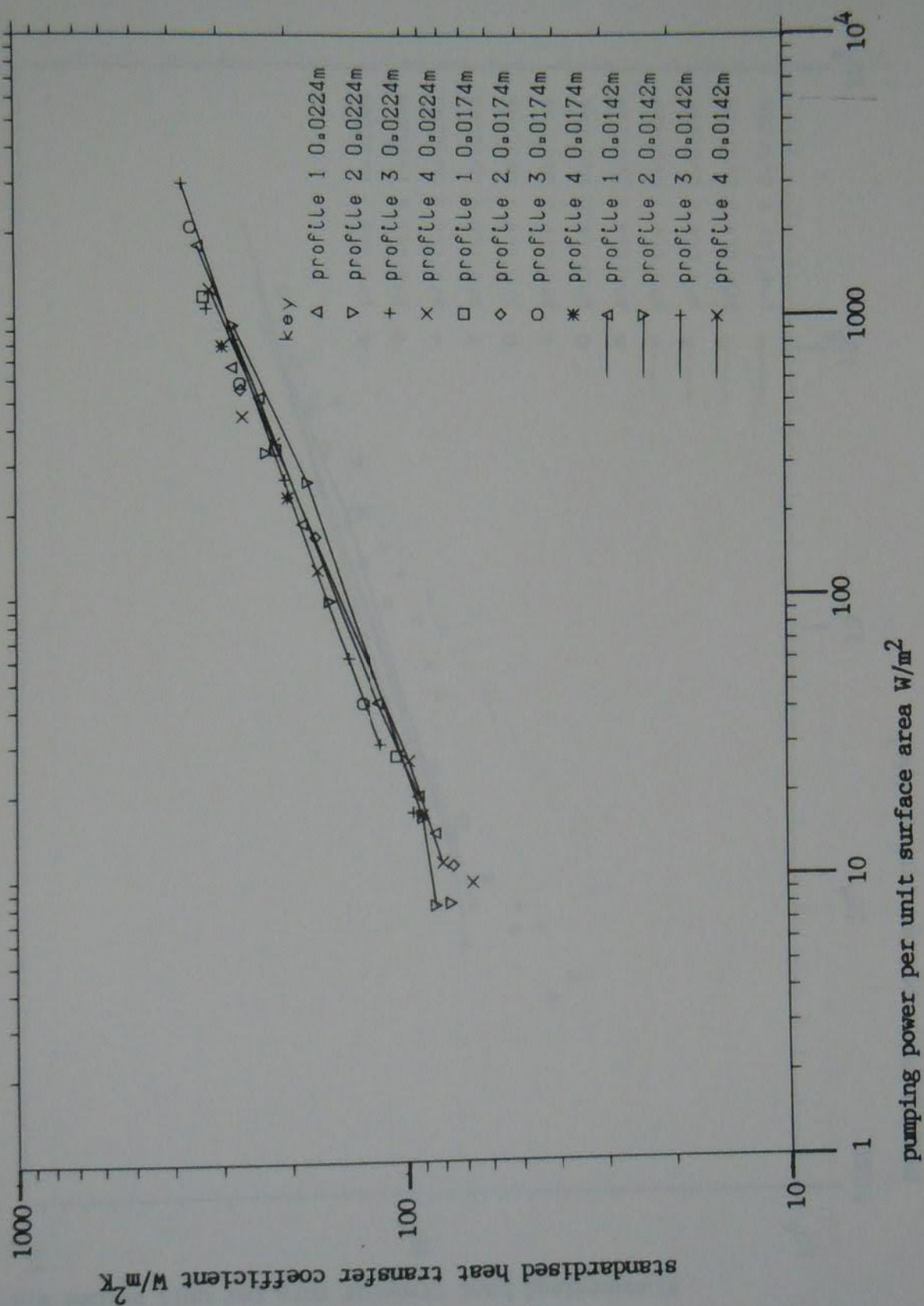
Figure 5.88 Comparison of rippled fin surfaces based on the London and Ferguson criteria

key

△ profile 1 0.0224m
▽ profile 2 0.0224m
+ profile 3 0.0224m
× profile 4 0.0224m
□ profile 1 0.0174m
◇ profile 2 0.0174m
○ profile 3 0.0174m
✱ profile 4 0.0174m
◁ profile 1 0.0142m
▽ profile 2 0.0142m
+ profile 3 0.0142m
× profile 4 0.0142m

pumping power per unit surface area W/m²

standardised heat transfer coefficient W/m²K

290

profile 1 0.0224m
profile 2 0.0224m
profile 3 0.0224m
profile 4 0.0224m
profile 1 0.0174m
profile 2 0.0174m
profile 3 0.0174m
profile 4 0.0174m
profile 1 0.0142m
profile 2 0.0142m
profile 3 0.0142m
profile 4 0.0142m

pumping power per unit volume W/m^3

standardised heat transfer rate per unit volume W/m^{3}K

Figure 5.89 Comparison of rippled fin surfaces based on the criteria of Shah

key

△	profile 1	0.0224m
▽	profile 2	0.0224m
+	profile 3	0.0224m
×	profile 4	0.0224m
□	profile 1	0.0174m
◇	profile 2	0.0174m
○	profile 3	0.0174m
✳	profile 4	0.0174m
△	profile 1	0.0142m
▽	profile 2	0.0142m
+	profile 3	0.0142m
×	profile 4	0.0142m
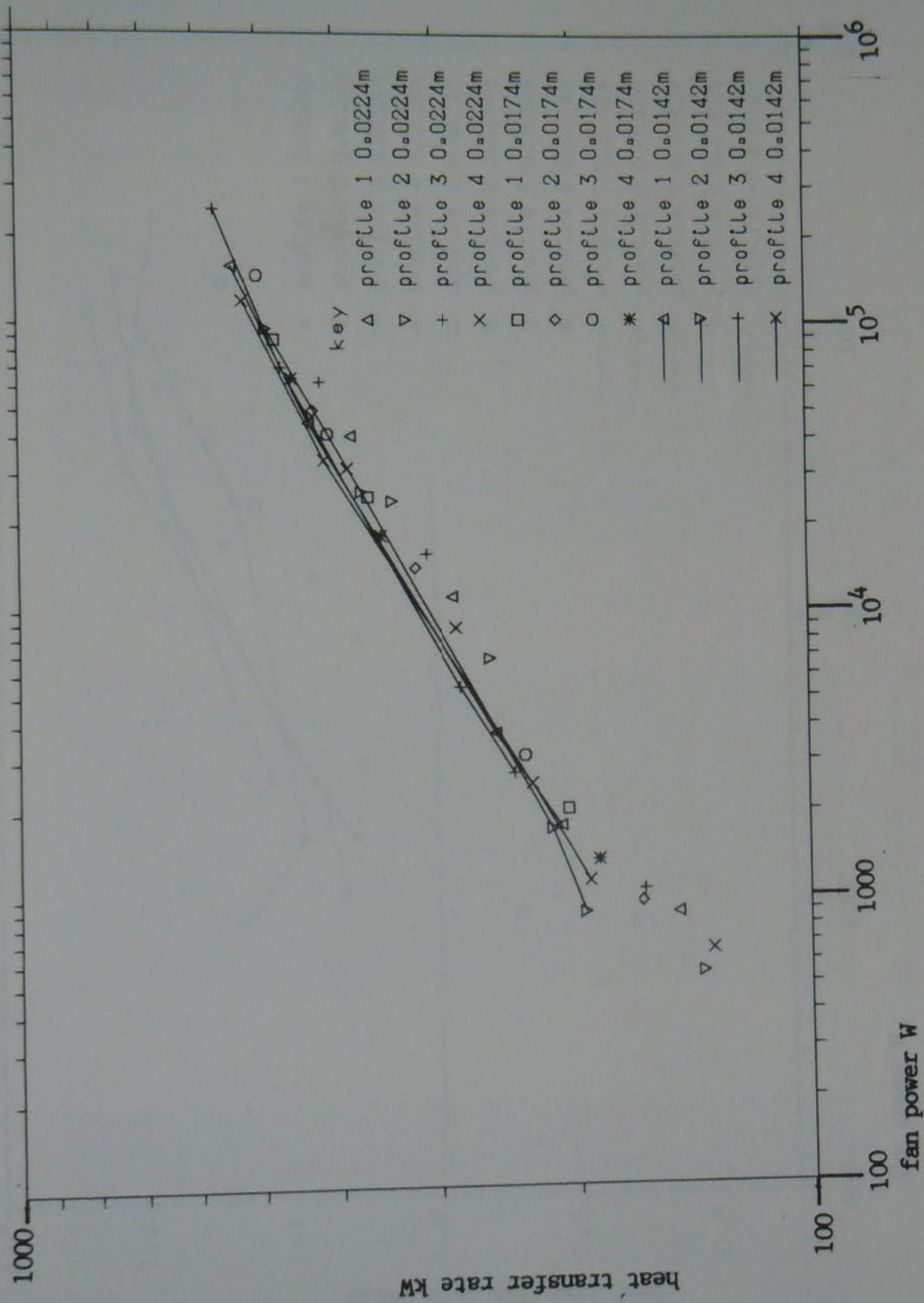
Figure 5.90 Comparison of rippled fin surfaces based on the criteria of Bergles, Junkhan and Bunn
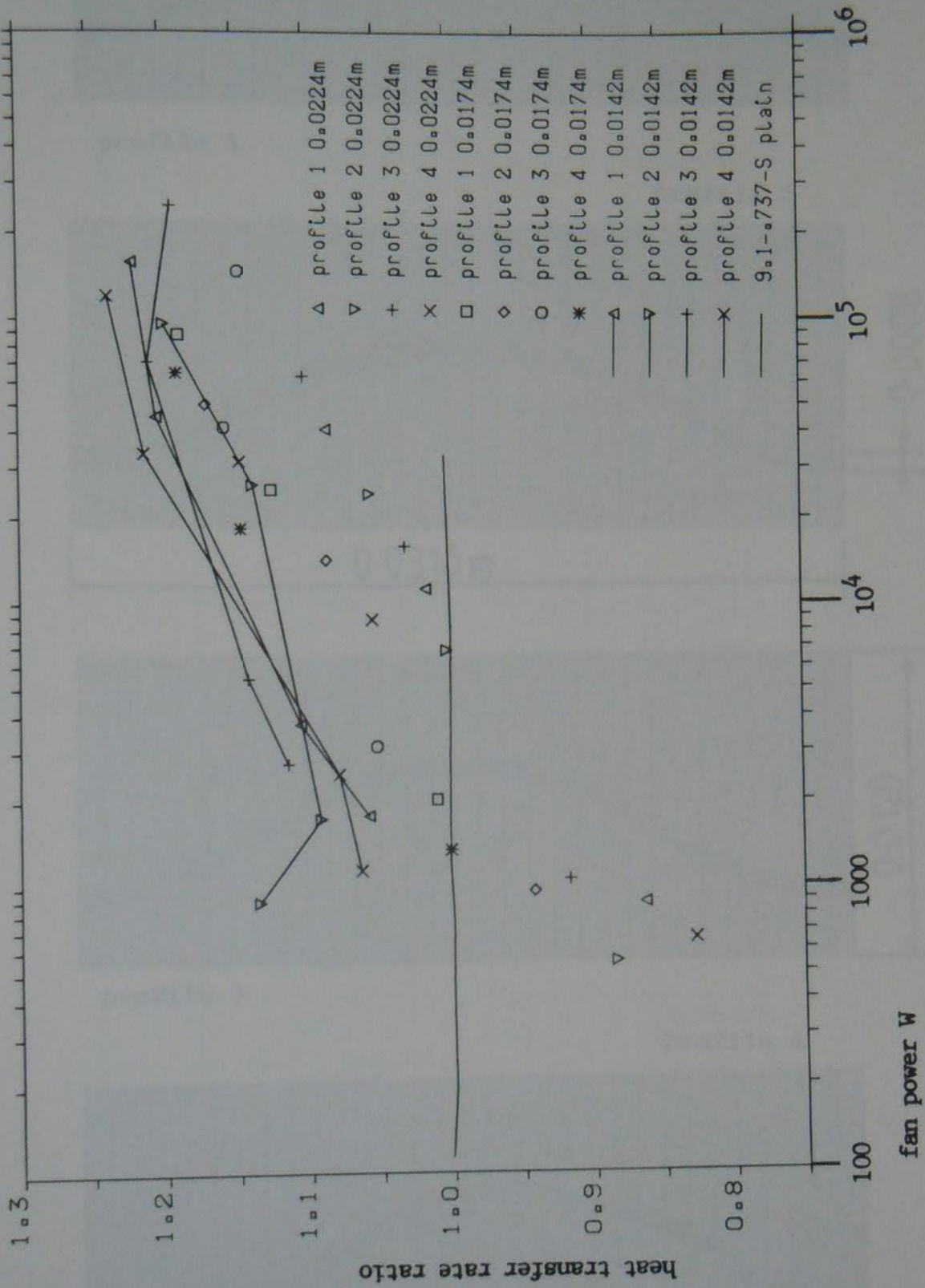
Figure 5.91 Performance ratio graph associated with the criteria of Bergles, Junkhan and Bunn for the rippled fin surfaces
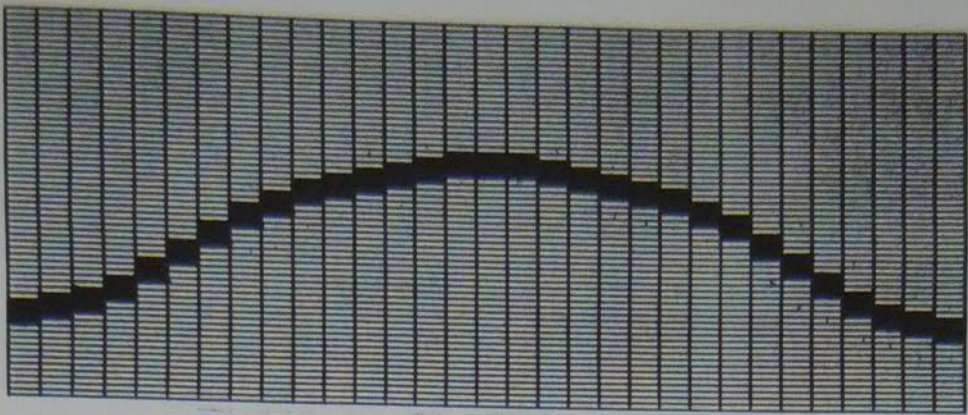
profile 1

profile 2

0.0008

0·0310 m

0·0120
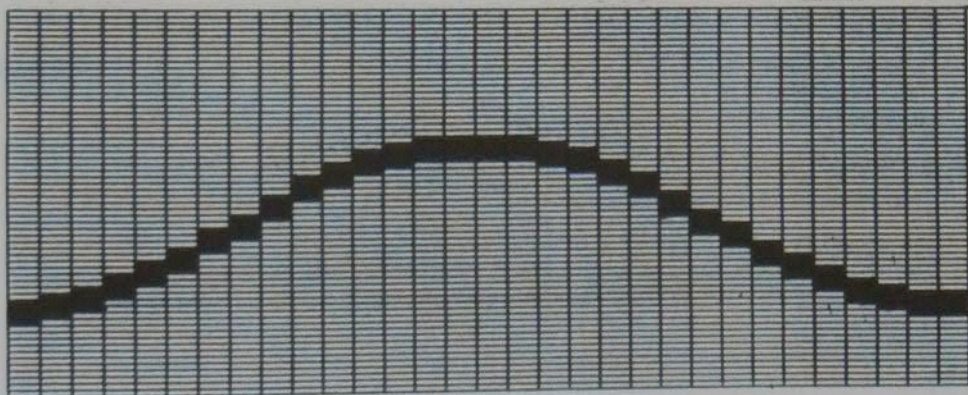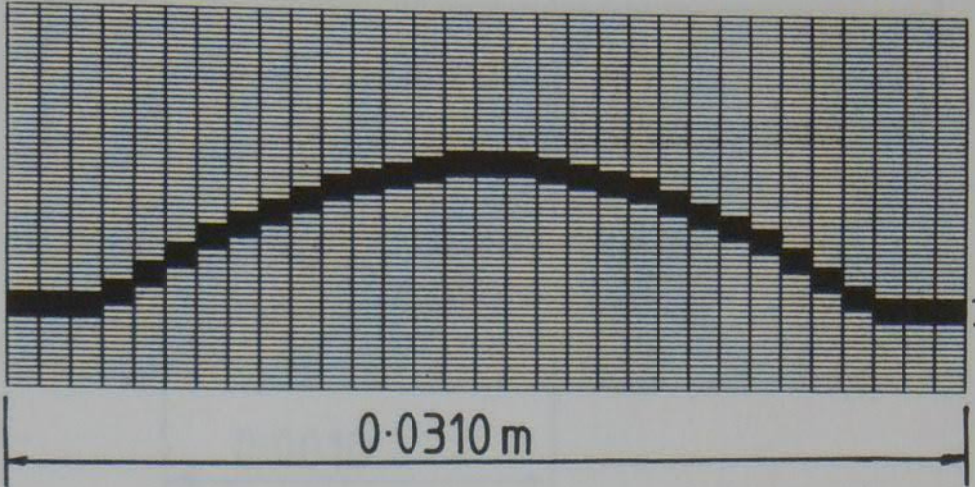
profile 3

profile 4
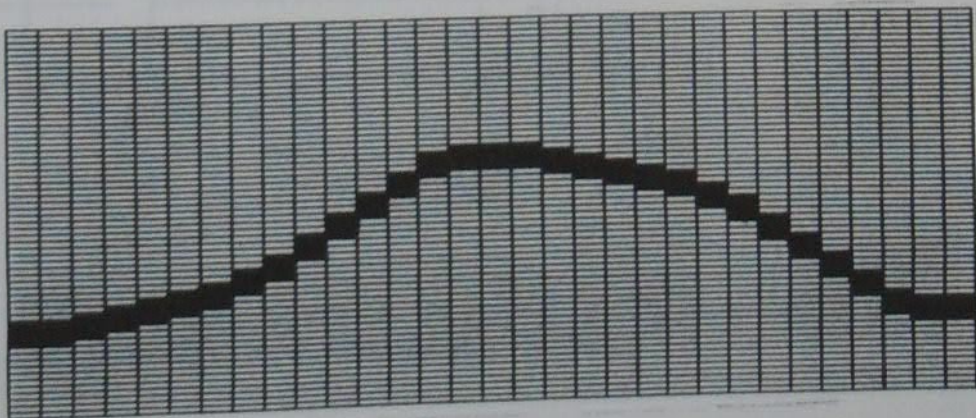
Figure 6.1 PHOENICS rippled profiles and flow domain geometries

a, laminar
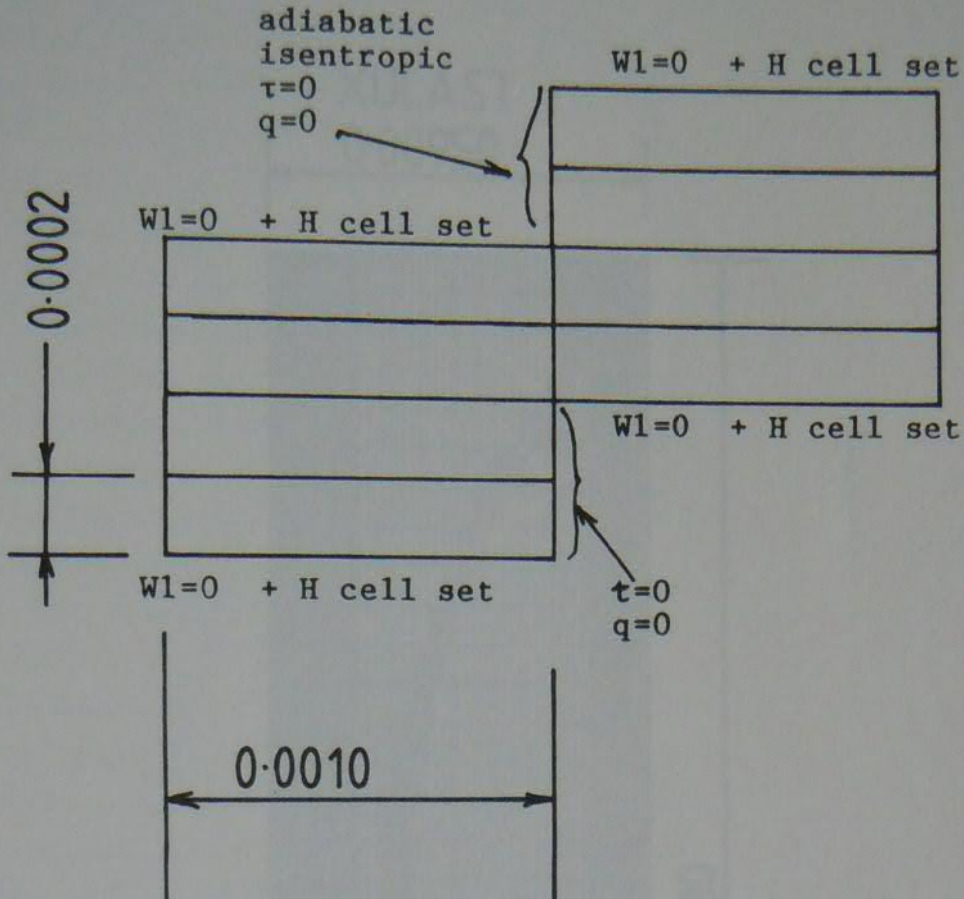
b, turbulent
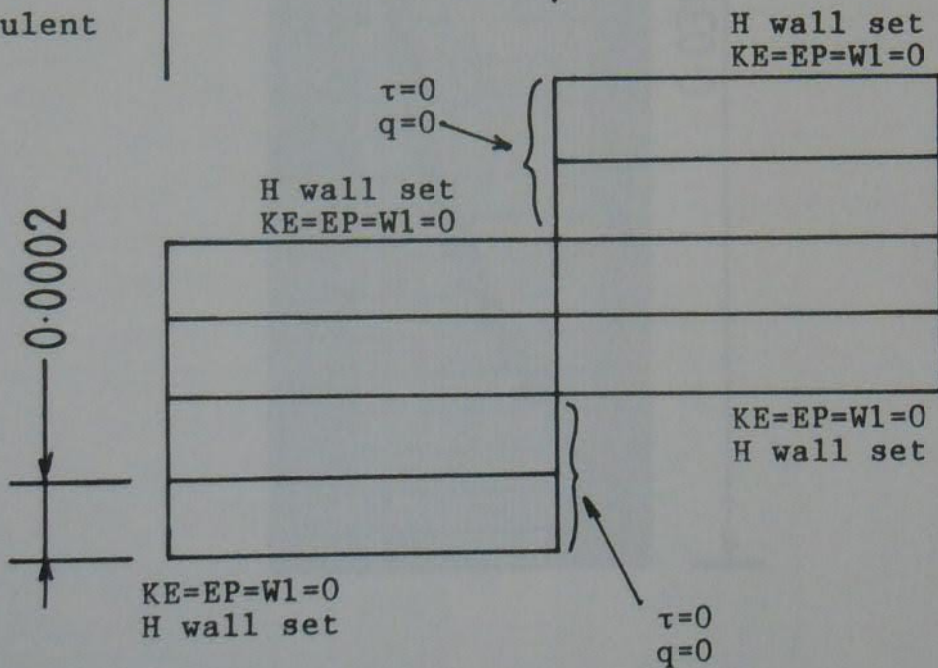
Figures 6.2 a and b Stepped wall boundary conditions for laminar and turbulent flows.

Figure 6.3 Diagram showing the PHOENICS solution domain for profile 2 (Fig. 6.1), at a wall spacing of RH=0.281.

Z = 190

Z = 200
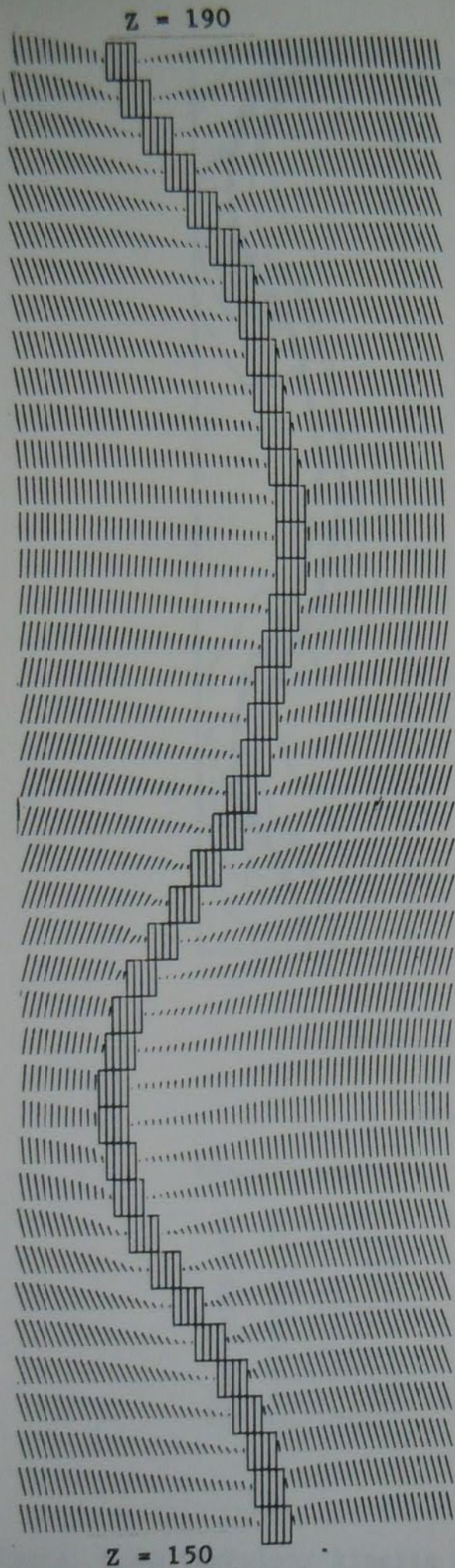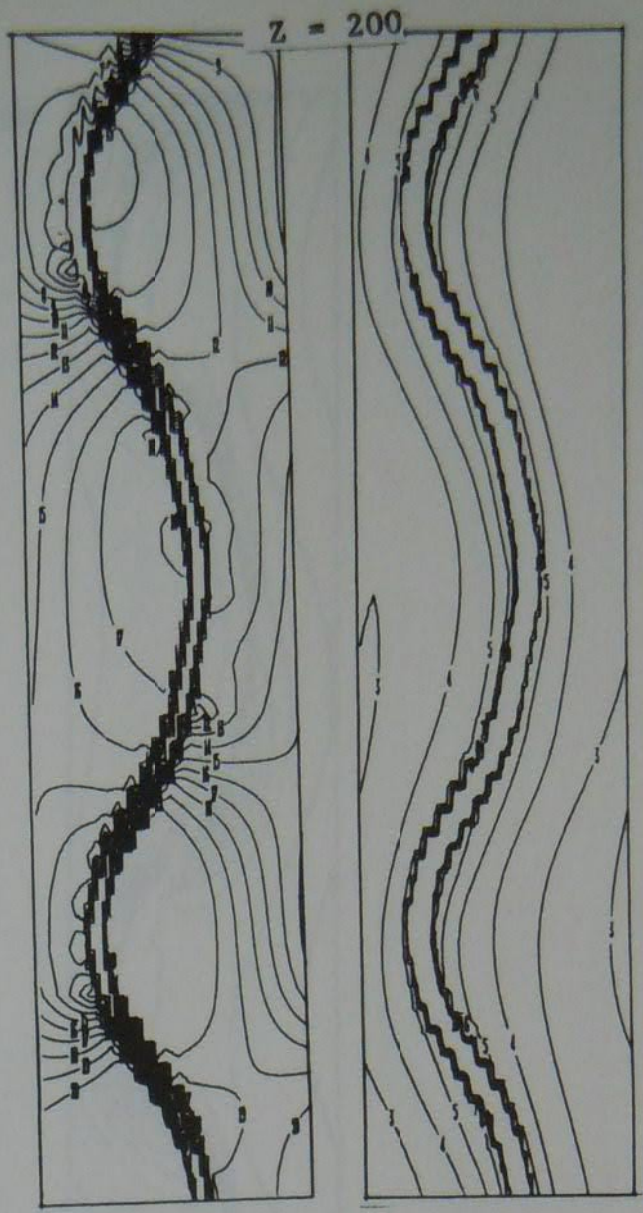
Z = 150

contours of   pressure and enthalpy

P1

contour key

	N/m^2		H1 J/kg
1	-50.073		
2	-36.100	1	83900.
3	-22.127	2	86480.
4	-8.155	3	89060.
5	5.817	4	91640.
6	19.790	5	94220.
7	33.763	6	96801.
8	47.736	7	99381.
9	61.709	8	101961.
10	75.681	9	104541.
11	89.654	10	107122.
12	103.627		
13	117.600		
14	131.573		
15	145.546		
16	159.519		
17	173.491		
18	187.464		
19	201.437		
20	215.410		

Z = 150

Figure 6.4a Velocity vectors, pressure and enthalpy contours for profile 1, Reynolds number 8000., RH=0.361

Z = 200

Z = 150
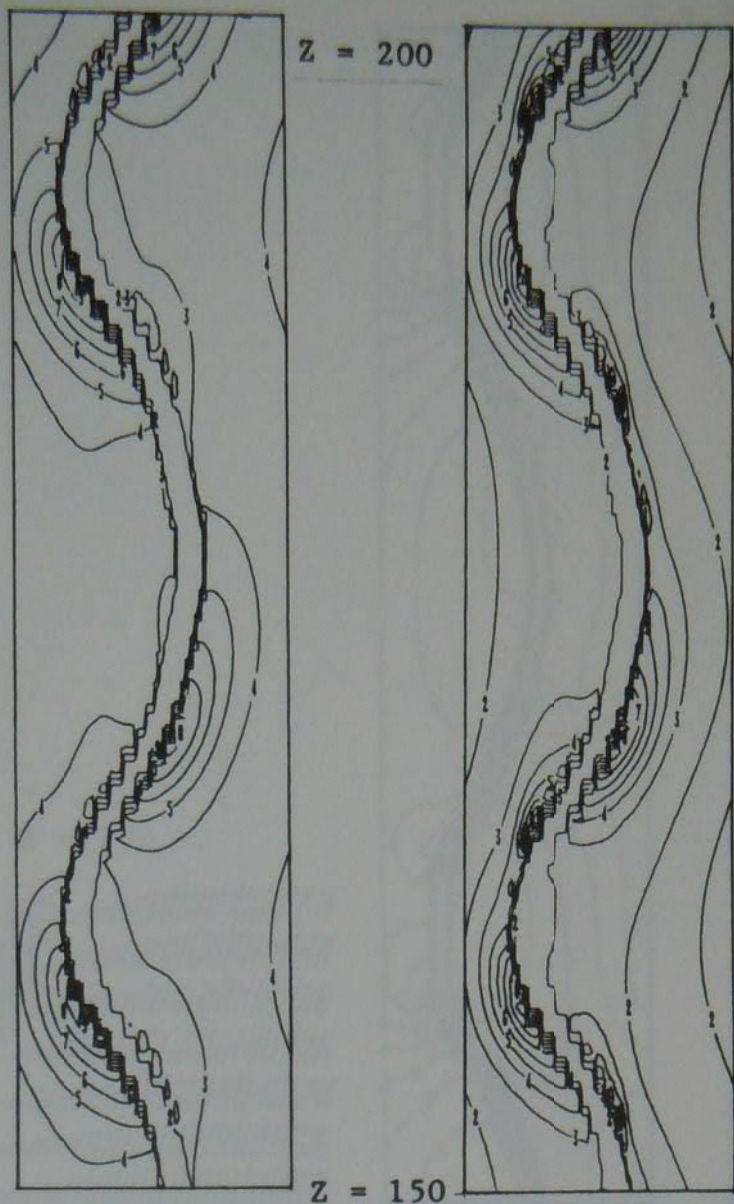
turbulence quantities

contour key

kinetic energy		dissipation rate	
1	0.00000	1	0.000
2	0.00892	2	0.451
3	0.01784	3	0.902
4	0.02676	4	1.353
5	0.03568	5	1.804
6	0.04459	6	2.256
7	0.05351	7	2.707
8	0.06243	8	3.158
9	0.07135	9	3.609
10	0.08027	10	4.061

Figure 6.4b Turbulent kinetic energy (KE) and dissipation rate (EP) contours for Profile 1, Reynolds number 8000., RH=0.361

Z = 200

Z = 170

contours of pressure and enthalpy

Z = 150

P1 N/m^2	contour key	H1 J/kg
1	-85.05	1	83900.
2	-62.20	2	86686.
3	-39.35	3	89473.
4	-16.51	4	92260.
5	6.33	5	95046.
6	29.18	6	97833.
7	52.02	7	100620.
8	74.87	8	103406.
9	97.72	9	106193.
10	120.56	10	108980.
11	143.41	11	111766.
12	166.26	12	114553.
13	189.10	13	117340.
14	211.95	14	120126.
15	234.80	15	122913.
16	257.64	16	125700.

Z = 170

Z = 150
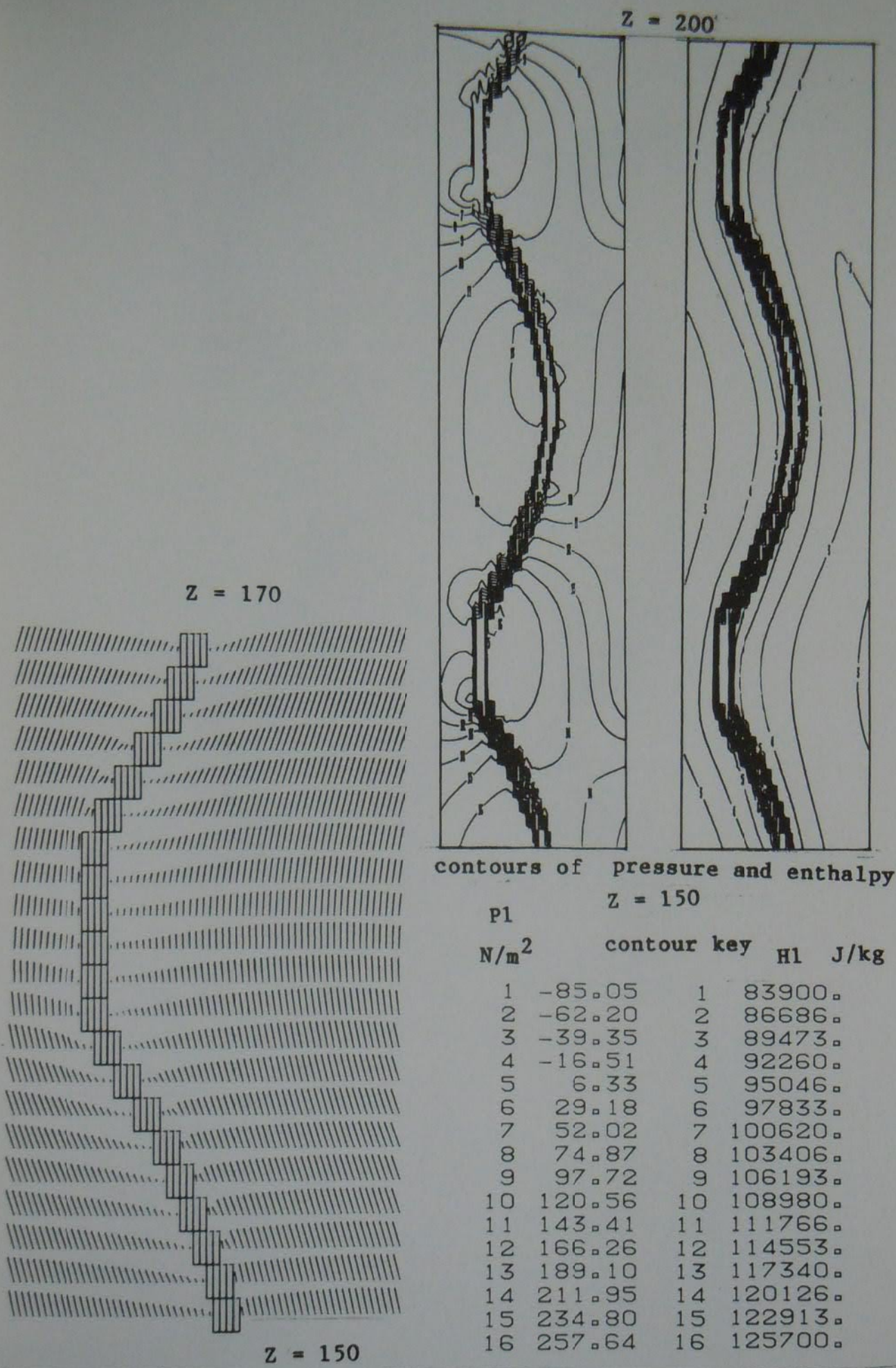
Figure 6.5a Velocity vectors, pressure and enthalpy contours for profile 2, Reynolds number 8000., RH=0.361

turbulence quantities
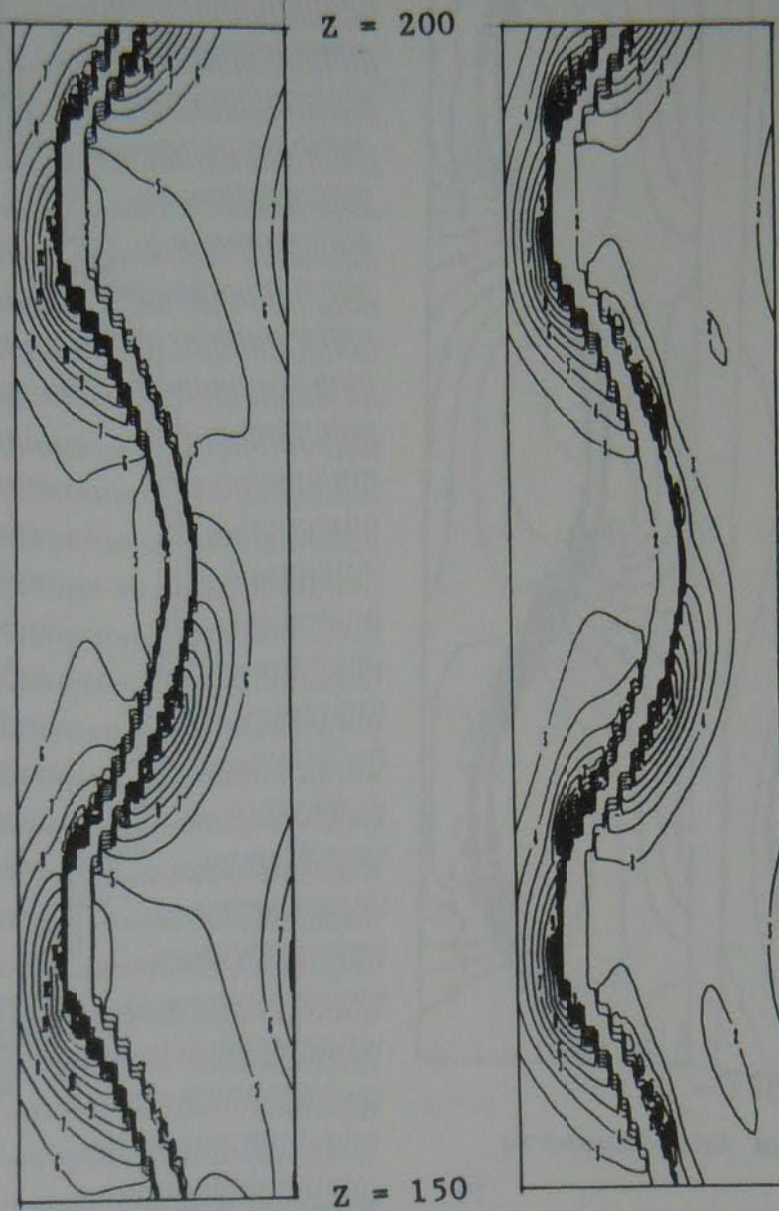
Z = 200

Z = 150

	kinetic energy	contour key		dissipation rate
1	0.00000		1	0.0000
2	0.00540		2	0.3666
3	0.01080		3	0.7332
4	0.01620		4	1.0998
5	0.02160		5	1.4664
6	0.02700		6	1.8330
7	0.03240		7	2.1996
8	0.03780		8	2.5662
9	0.04319		9	2.9328
10	0.04859		10	3.2994
11	0.05399		11	3.6660
12	0.05939		12	4.0326
13	0.06479		13	4.3992
14	0.07019		14	4.7658
15	0.07559		15	5.1324
16	0.08099		16	5.4990

Figure 6.5b Turbulent kinetic energy (KE) and dissipation rate (EP) contours for Profile 2, Reynolds number 8000., RH=0.361

Z = 190

Z = 200

Z = 150

pressure and enthalpy

P1

N/m^2 contour key

H1   J/kg

1	−42.80	
2	−27.92	
3	−13.04	
4	1.82	1 83900.
5	16.70	
6	31.58	2 86686.
7	46.46	
8	61.34	3 89473.
9	76.21	
10	91.09	4 92260.
11	105.97	
12	120.85	5 95046.
13	135.73	
14	150.61	6 97833.
15	165.48	
16	180.36	
17	195.24	
18	210.12	
19	225.00	
20	239.87	

Z = 150
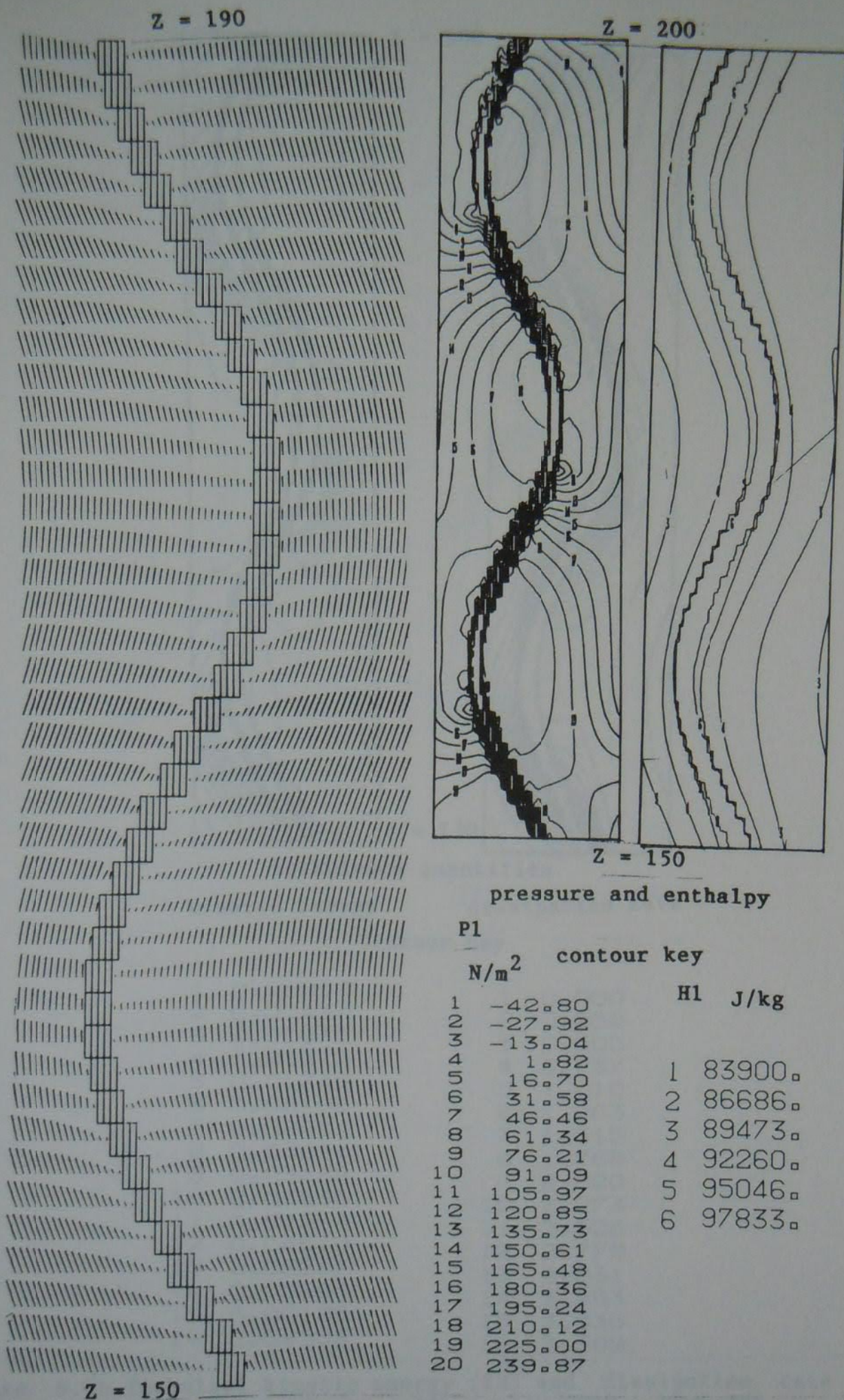
Figure 6.6a Velocity vectors, pressure and enthalpy contours for
profile 3, Reynolds number 8000., RH=0.361

Z = 200

Z = 150

turbulence quantities

kinetic energy   dissipation rate

contour key

	kinetic energy		dissipation rate
1	0.00000	1	0.000
2	0.00437	2	0.252
3	0.00875	3	0.505
4	0.01312	4	0.757
5	0.01749	5	1.010
6	0.02186	6	1.263
7	0.02624	7	1.515
8	0.03061	8	1.768
9	0.03498	9	2.020
10	0.03935	10	2.273
11	0.04373	11	2.526
12	0.04810	12	2.778
13	0.05247	13	3.031
14	0.05684	14	3.283
15	0.06122	15	3.536
16	0.06559	16	3.789

Figure 6.6b Turbulent kinetic energy (KE) and dissipation rate (EP) contours for Profile 3, Reynolds number 8000., RH=0.361

Z = 190

Z = 200

Z = 150

contours of

pressure and enthalpy

P1   contour key

N/m²

	P1 N/m²		H1 J/kg
1	-70.82		
2	-55.24		
3	-39.66		
4	-24.09	1	83900.
5	-8.51	2	86686.
6	7.06	3	89473.
7	22.63	4	92260.
8	38.21	5	95046.
9	53.79	6	97833.
10	69.36		
11	84.94		
12	100.51		
13	116.09		
14	131.67		
15	147.24		
16	162.82		
17	178.40		
18	193.97		
19	209.55		
20	225.13		

Z = 150

Figure 6.7a Velocity vectors, pressure and enthalpy contours for profile 4, Reynolds number 8000., RH=0.361

Z = 200

Z = 150
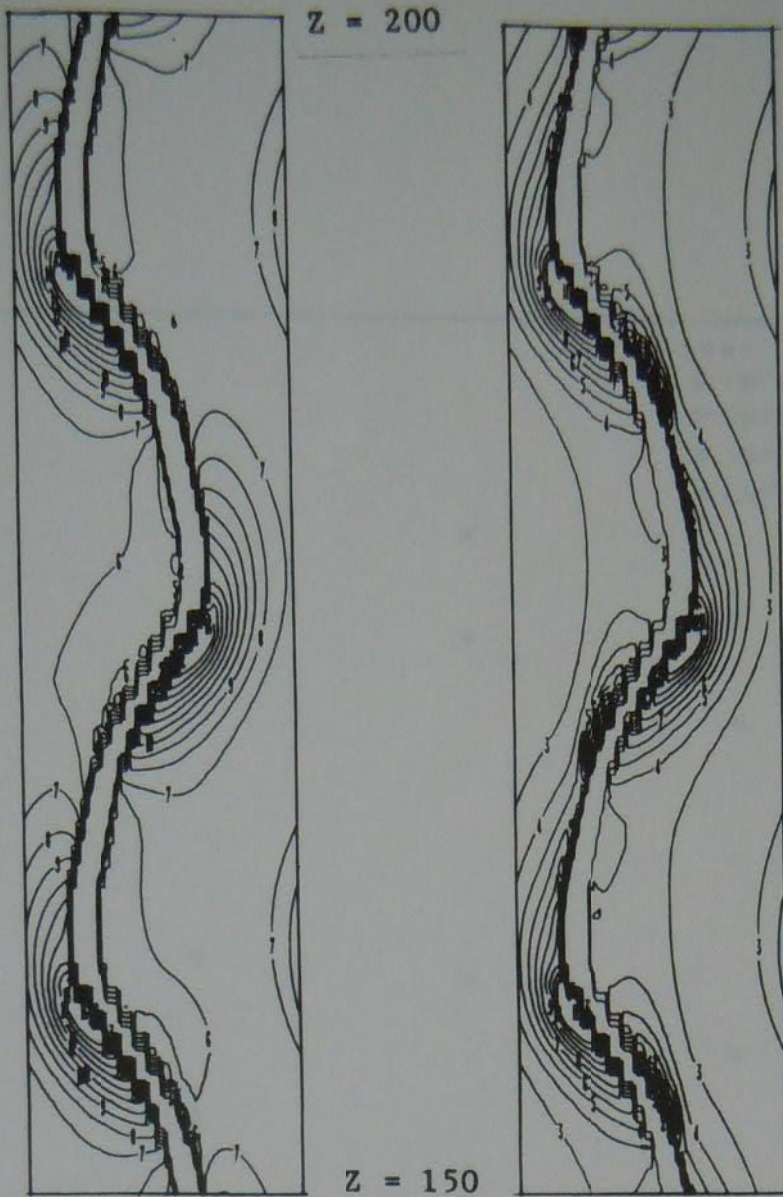
turbulence quantities

kinetic energy   dissipation rate

contour key

1	0.00000		1	0.000
2	0.00461		2	0.295
3	0.00922		3	0.590
4	0.01382		4	0.885
5	0.01843		5	1.180
6	0.02304		6	1.475
7	0.02765		7	1.770
8	0.03226		8	2.066
9	0.03686		9	2.361
10	0.04147		10	2.656
11	0.04608		11	2.951
12	0.05069		12	3.246
13	0.05530			
14	0.05990			
15	0.06451			
16	0.06912			

Figure 6.7b Turbulent kinetic energy (KE) and dissipation rate (EP) contours for Profile 4, Reynolds number 8000., RH=0.361
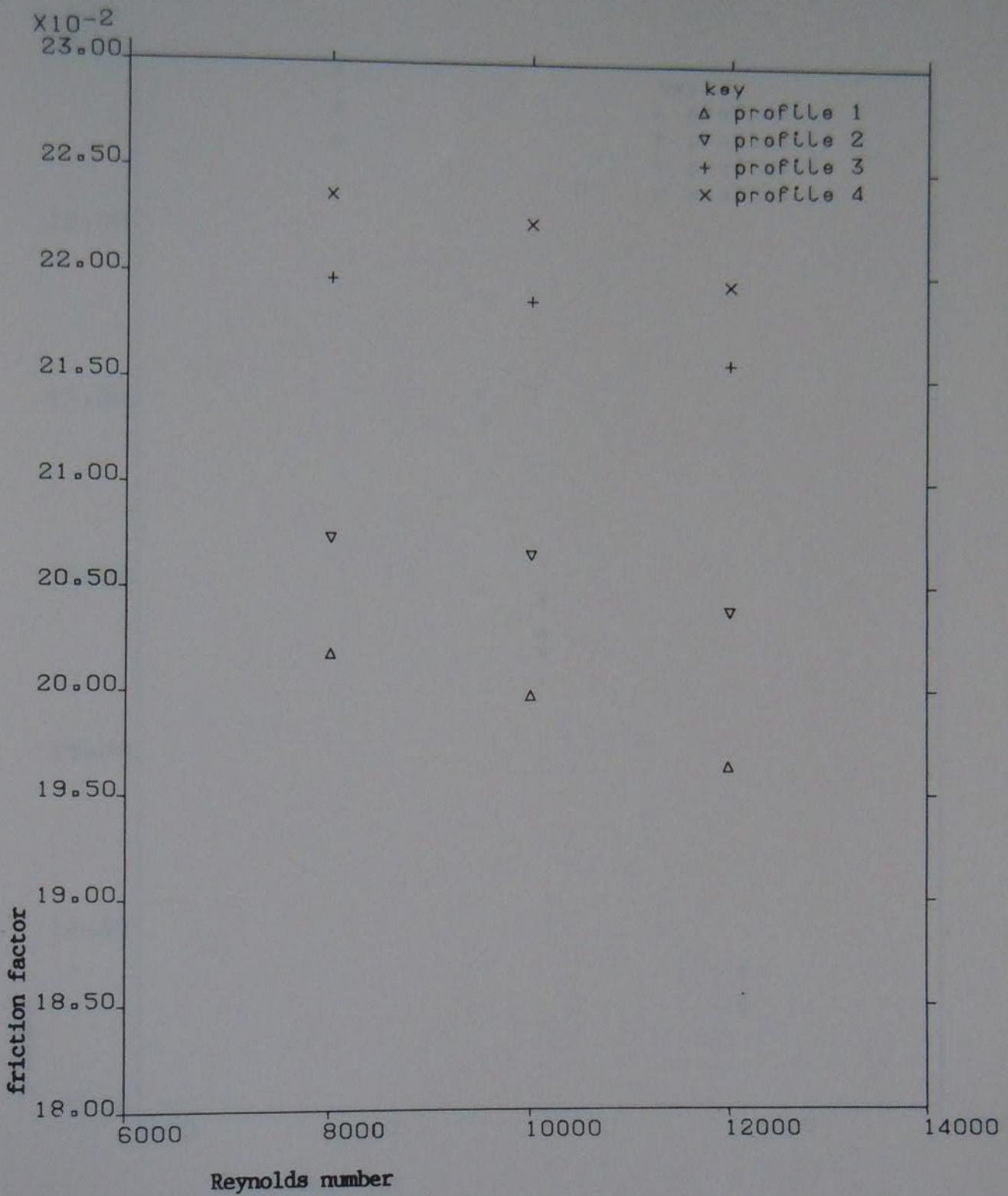
Figure 6.8 Friction factor against Reynolds number for the four
profiles at RH = 0.361, Dh = .0224 m, comparative investigation.
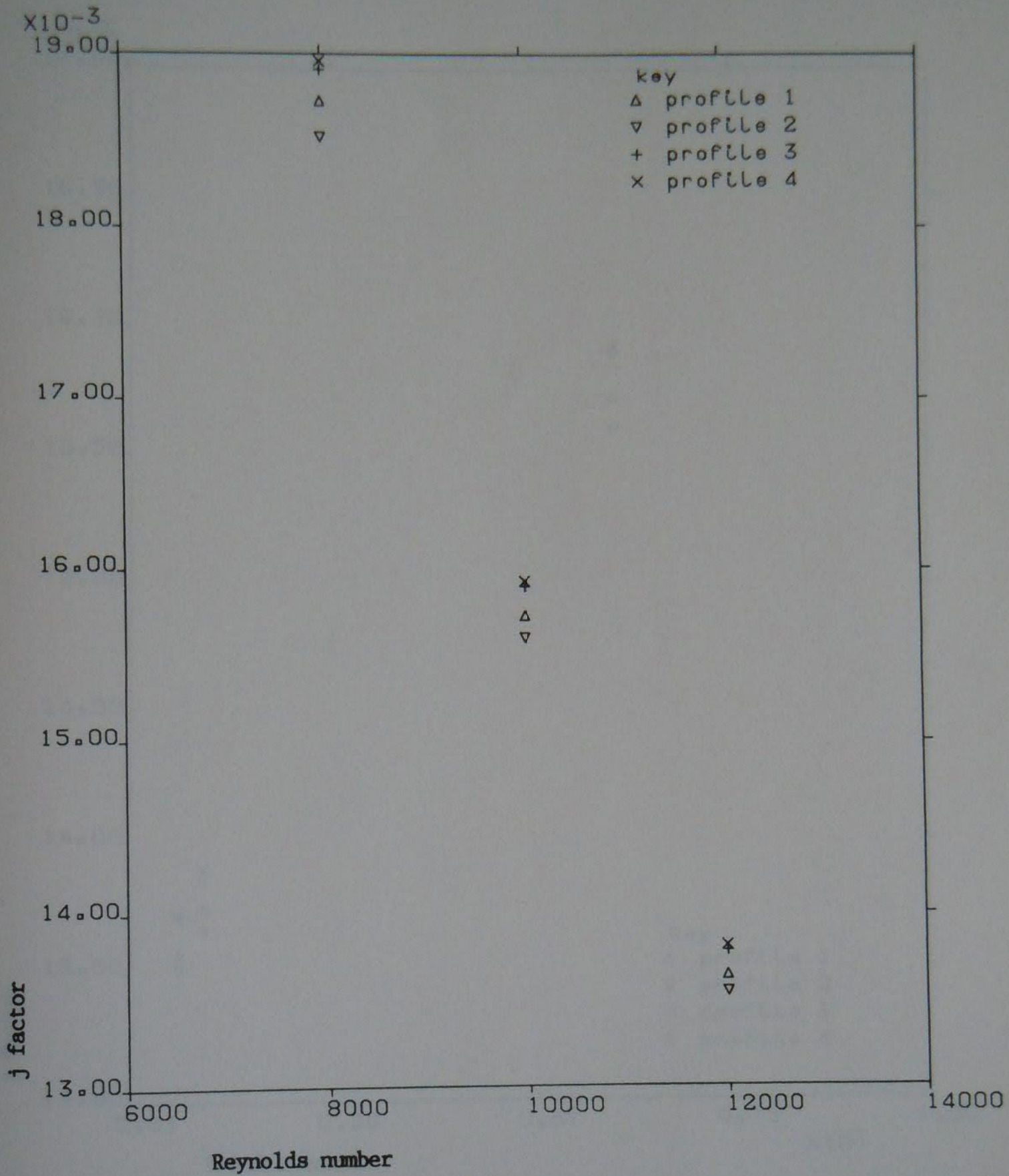
Figure 6.9 j factor against Reynolds number for the four profiles at
RH = 0.361, Dh = 0.0224 m, Prandtl number 6.09 for the comparative
investigation
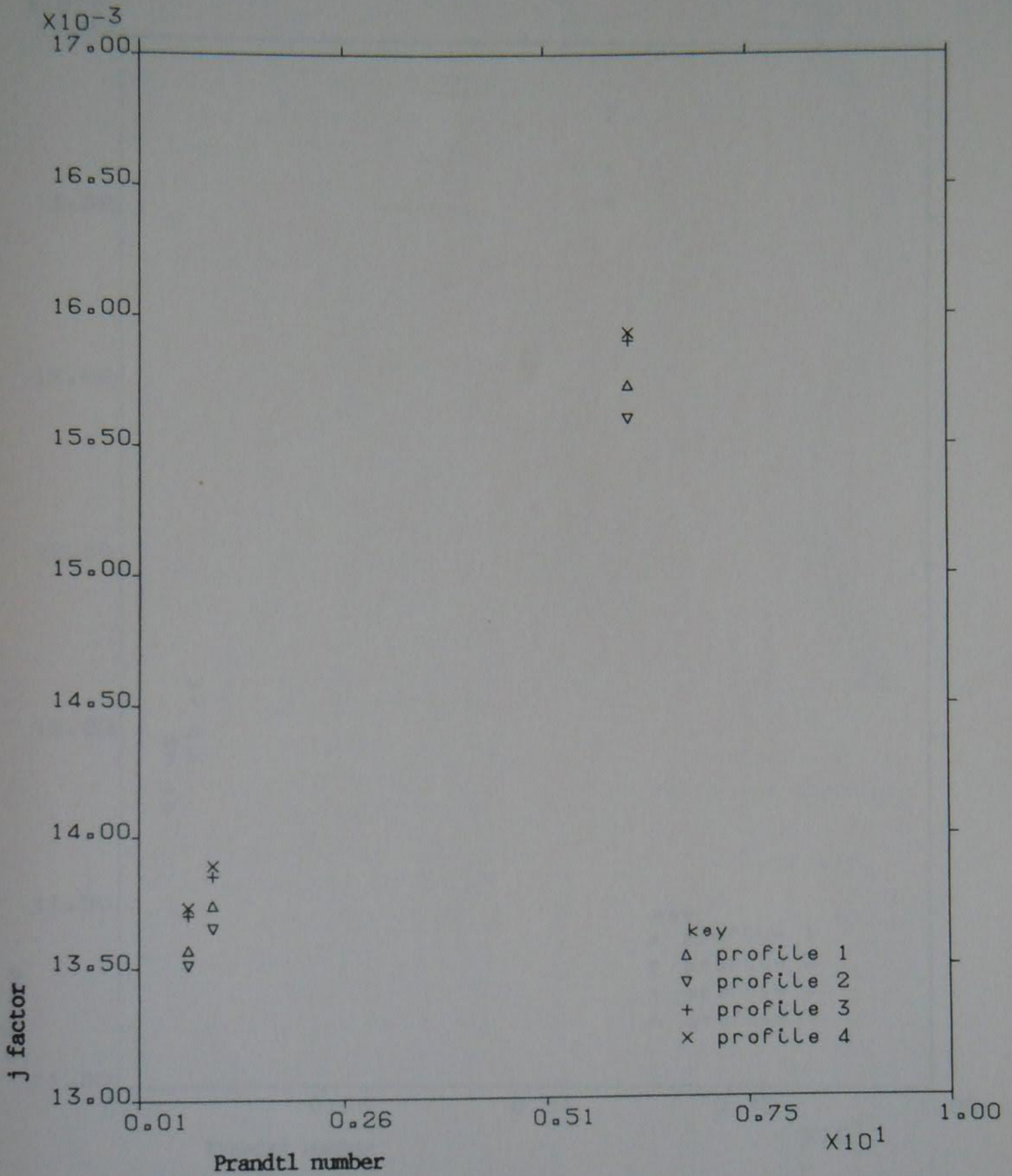
Figure 6.10 j factor against Prandtl number for the four profiles at a
Reynolds number of 10000, RH = 0.361 m comparative investigation
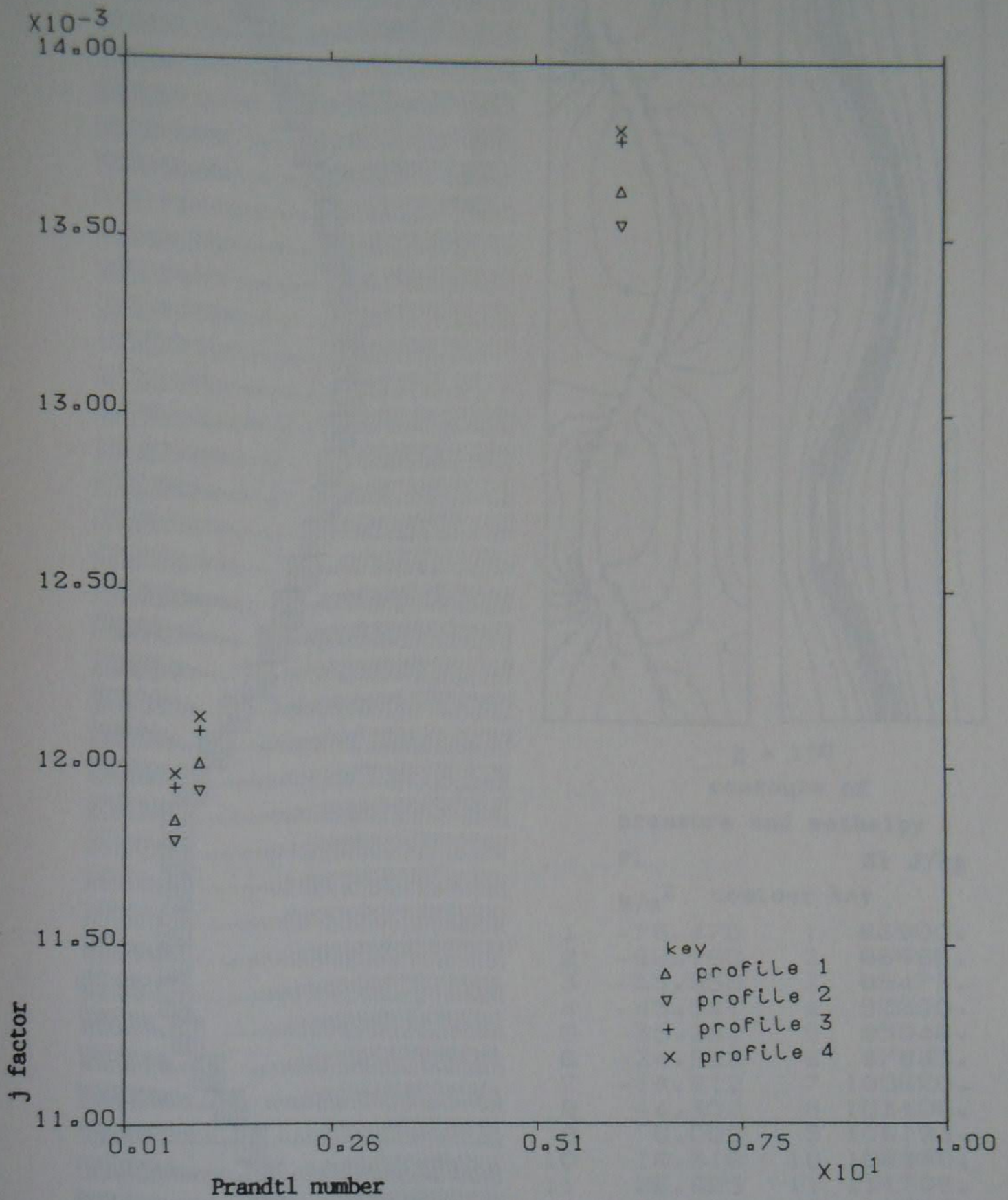
Figure 6.11 j factor against Prandtl number for the four profiles at a Reynolds number of 12000, RH = 0.361 m comparative investigation

Z = 190

Z = 200
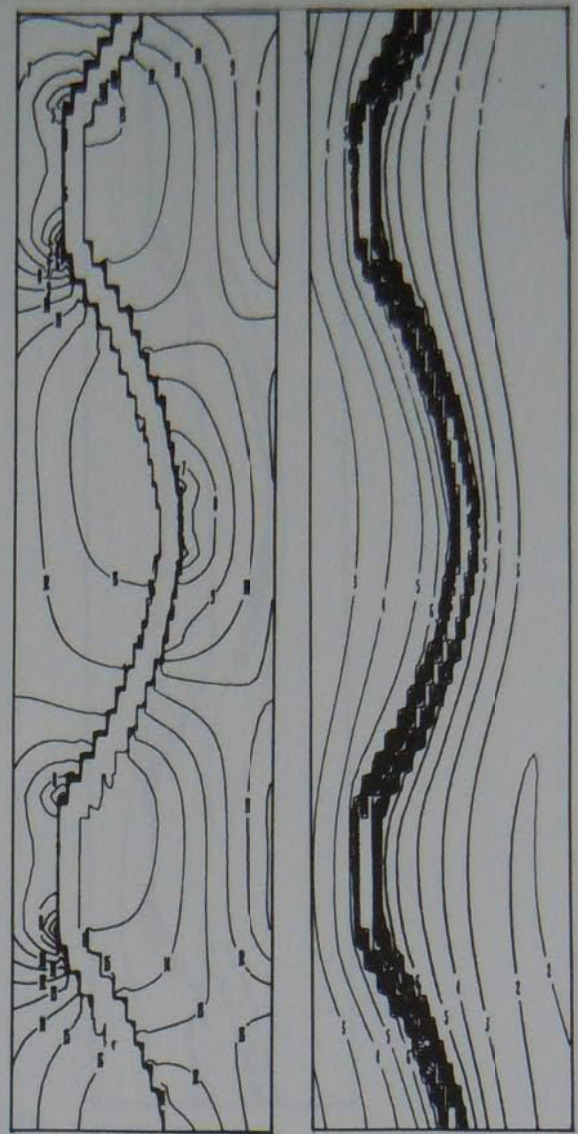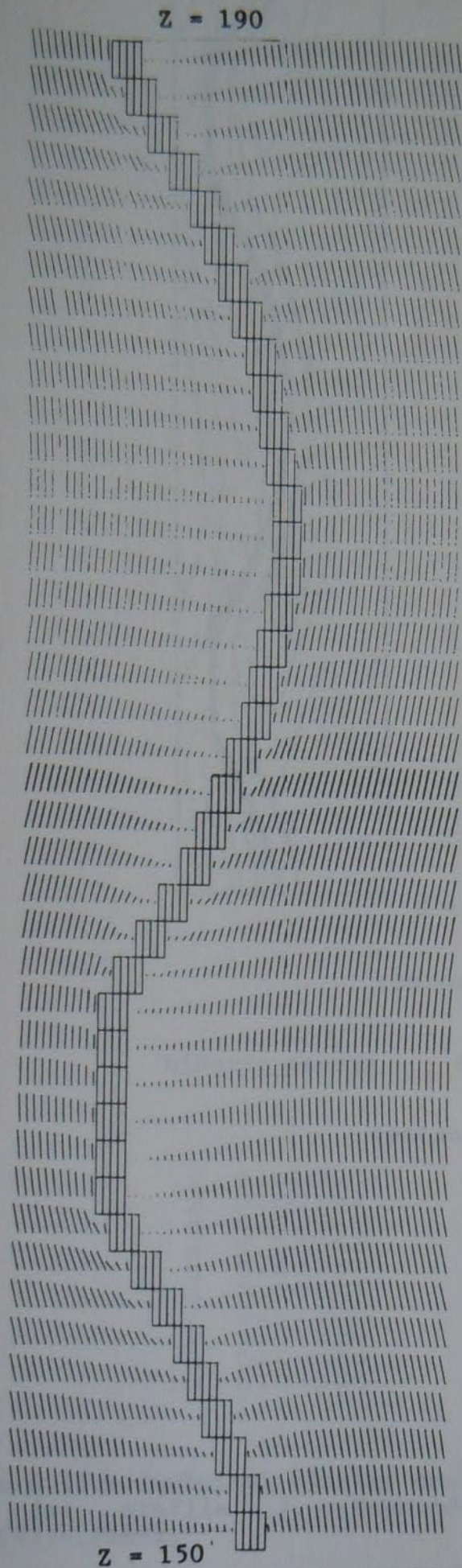
Z = 150

contours of

pressure and enthalpy

	P1 N/m^2		H1 J/kg
	contour key		
1	−76.470	1	83900.
2	−66.160	2	86686.
3	−55.850	3	89473.
4	−45.541	4	92260.
5	−35.231	5	95046.
6	−24.922	6	97833.
7	−14.612	7	100620.
8	−4.302	8	103406.
9	6.006	9	106193.
10	16.316	10	108980.
11	26.625	11	111766.
12	36.935	12	114553.
13	47.244	13	117340.
14	57.554	14	120126.
15	67.864	15	122913.
16	78.173	16	125700.

Z = 150

Figure 6.12.a Velocity vectors, pressure and enthalpy contours for profile 2, Reynolds number 8000, RH=0.361, LOGIC(92)=.FALSE.

Z = 200

Z = 150

contours of

kinetic energy   dissipation rate

contour key

	kinetic energy		dissipation rate
1	0.00000	1	0.00000
2	0.00184	2	0.26078
3	0.00368	3	0.52156
4	0.00553	4	0.78233
5	0.00737	5	1.04311
6	0.00921	6	1.30389
7	0.01105	7	1.55467
8	0.01290	8	1.82544
9	0.01474	9	2.08622
10	0.01658	10	2.34700

Figure 6.12.b Turbulent kinetic energy (KE) and dissipation rate
(EP) for profile 2, Reynolds number 8000, RH=0.361,
LOGIC(92)=.FALSE.

Z = 190

Z = 200

Z = 150

PVS 0.001

Z = 150

pressure and enthalpy
contour key

P1	N/m^2	H1	J/kg
1	−123.50	1	83900.
2	−100.96	2	86686.
3	−78.42	3	89473.
4	−55.88	4	92260.
5	−33.35	5	95046.
6	−10.81	6	97833.
7	11.72	7	100620.
8	34.25	8	103406.
9	56.79	9	106193.
10	79.33	10	108980.
11	101.87	11	111766.
12	124.40	12	114553.
13	146.94	13	117340.
14	169.48	14	120126.
15	192.01	15	122913.
16	214.55	16	125700.
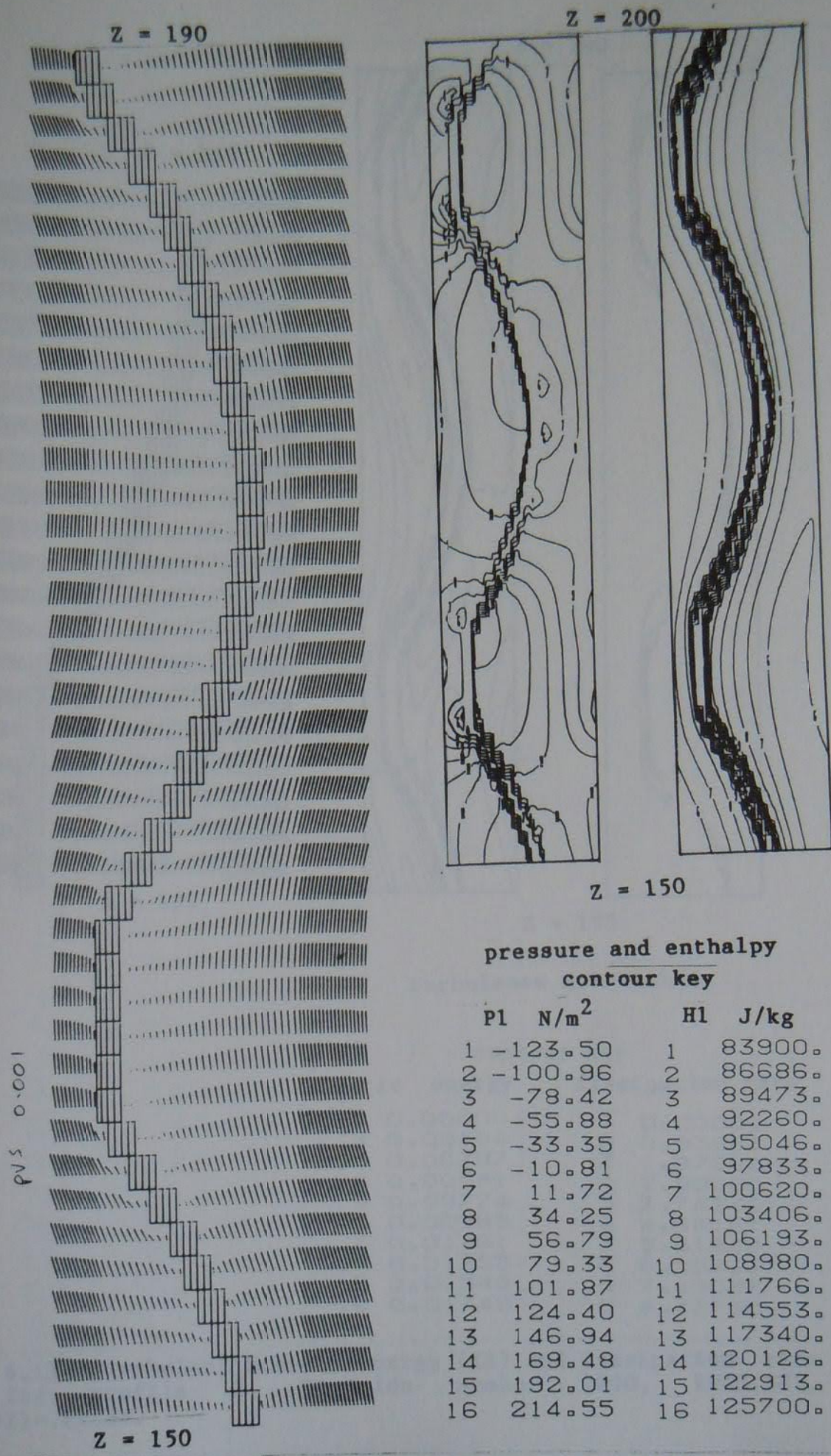
Figure 6.13.a Velocity vectors, pressure and enthalpy contours
for profile 2, Reynolds number 8000, RH=0.281, LOGIC(92)=.FALSE.

Z = 210

Z = 200
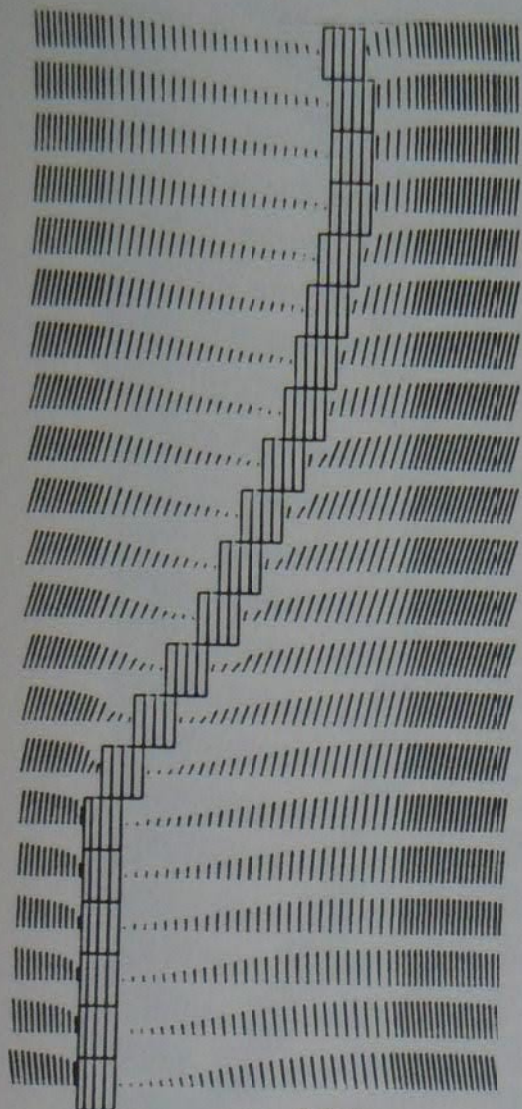
Z = 190
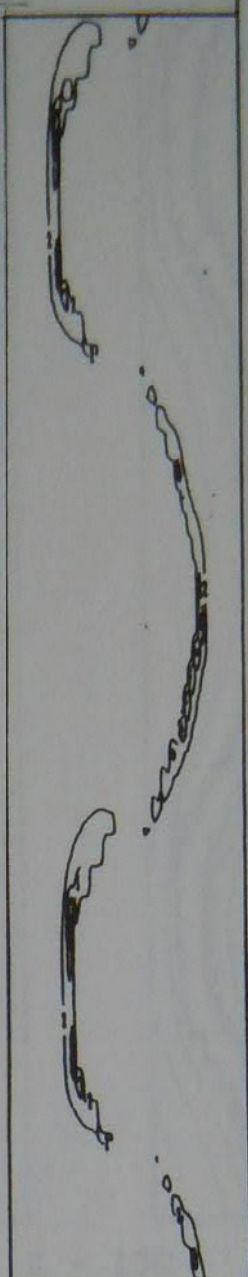
Z = 150

turbulence quantities

contour key

	kinetic energy			dissipation rate
1	0.00000		1	0.00000
2	0.00194		2	0.93633
3	0.00387		3	1.87267
4	0.00581		4	2.80900
5	0.00774		5	3.74533
6	0.00968		6	4.68167
7	0.01161		7	5.61800
8	0.01355		8	6.55433
9	0.01548		9	7.49067
10	0.01742		10	8.42700

Figure 6.13.b Turbulent kinetic energy (KE) and dissipation rate (EP) for profile 2, Reynolds number 8000, RH=0.281, LOGIC(92)=.FALSE.

Z = 190

Z = 200

Z = 150

contours of

pressure and enthalpy

P1 N/m^2 contour key

	P1 N/m^2		H1 J/kg
1	−193.200		
2	−165.756		
3	−138.313		
4	−110.870		
5	−83.427		
6	−55.984		
7	−28.541	1	83900.
8	−1.098	2	86067.
9	26.344	3	88234.
10	53.788	4	90402.
11	81.231	5	92569.
12	108.674	6	94737.
13	136.117	7	96904.
14	163.560	8	99071.
15	191.003	9	101239.
16	218.446	10	103406.

Z = 150

Figure 6.14a Velocity vectors, pressure and enthalpy contours for profile 2, Reynolds number 10000, RH=0.281, LOGIC(92)=.FALSE.

Z = 200

Z = 150

kinetic energy   dissipation rate

contour key

	kinetic energy		dissipation rate
1	0.00000	1	0.000
2	0.00168	2	0.658
3	0.00336	3	1.316
4	0.00504	4	1.974
5	0.00672	5	2.632
6	0.00840	6	3.290
7	0.01008	7	3.948
8	0.01176	8	4.606
9	0.01344	9	5.264
10	0.01512	10	5.922
11	0.01680	11	6.580
12	0.01848	12	7.238
13	0.02016	13	7.896
14	0.02184	14	8.554
15	0.02352	15	9.212
16	0.02520	16	9.870

Figure 6.14b Turbulent kinetic energy (KE) and dissipation rate (EP) for profile 2, Reynolds number 10000, RH=0.281, LOGIC(92)=.FALSE.
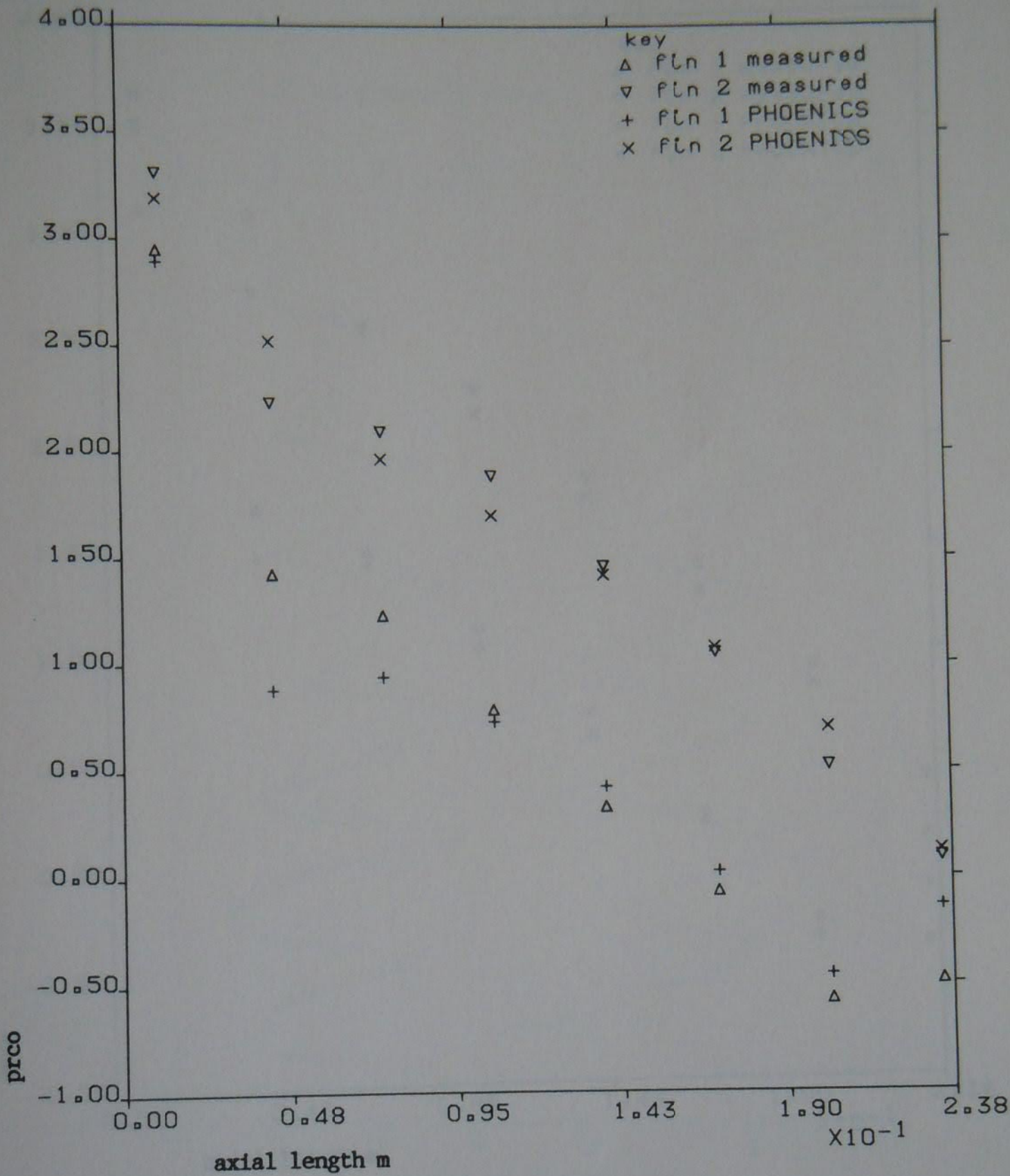
Figure 6.15 Comparison of local pressure coefficients, PHOENICS profile 2, Reynolds number 8000, Dh = 0.0224 m, LOGIC((2)=.FALSE., measured profile 4, Reynolds number 7839, Dh = 0.0224 m.
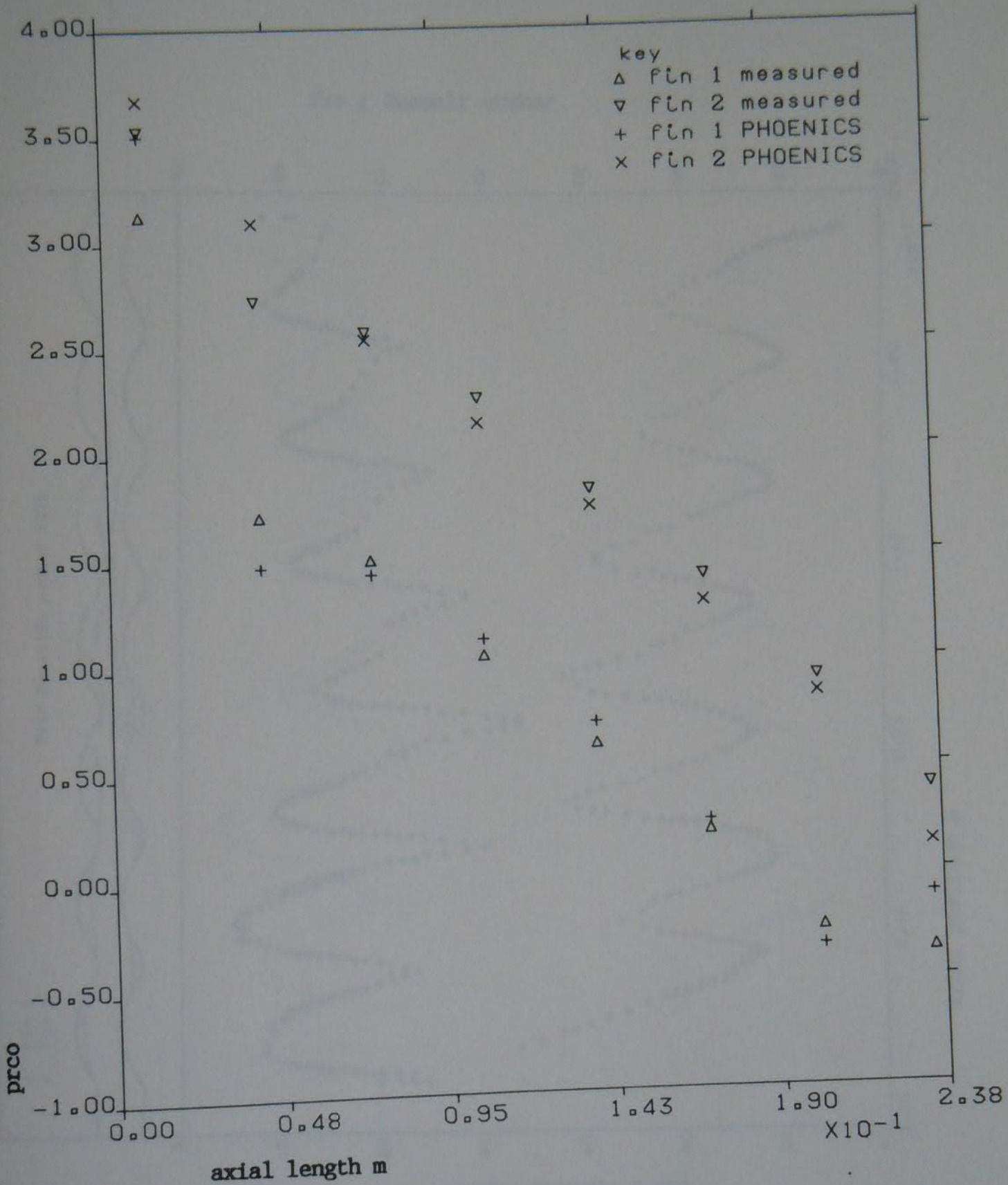
Figure 6.16 Comparison of local pressure coefficients, PHOENICS profile 2, Reynolds number 8000, Dh = 0.0174 m, LOGIC((2)=.FALSE., measured profile 4, Reynolds number 7839, Dh = 0.0174 m

fin 2 Nusselt number
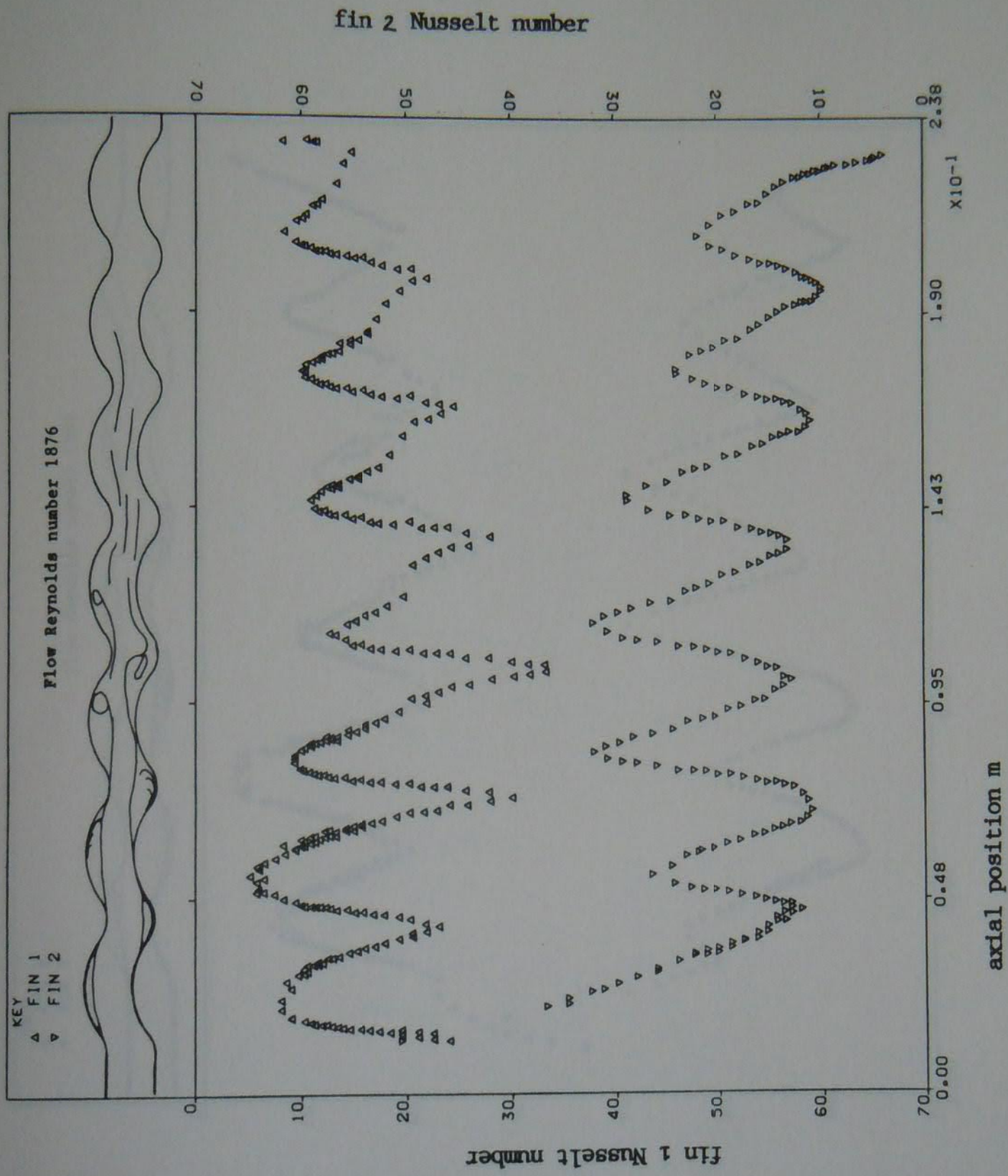
Figure 7.1   Local Nusselt number against axial coordinate, profile 1
Dh = 0.0224 m, Re = 2004

319

Figure 7.2   Local Nusselt number against axial coordinate, profile 2
Dh = 0.0224 m, Re = 2016
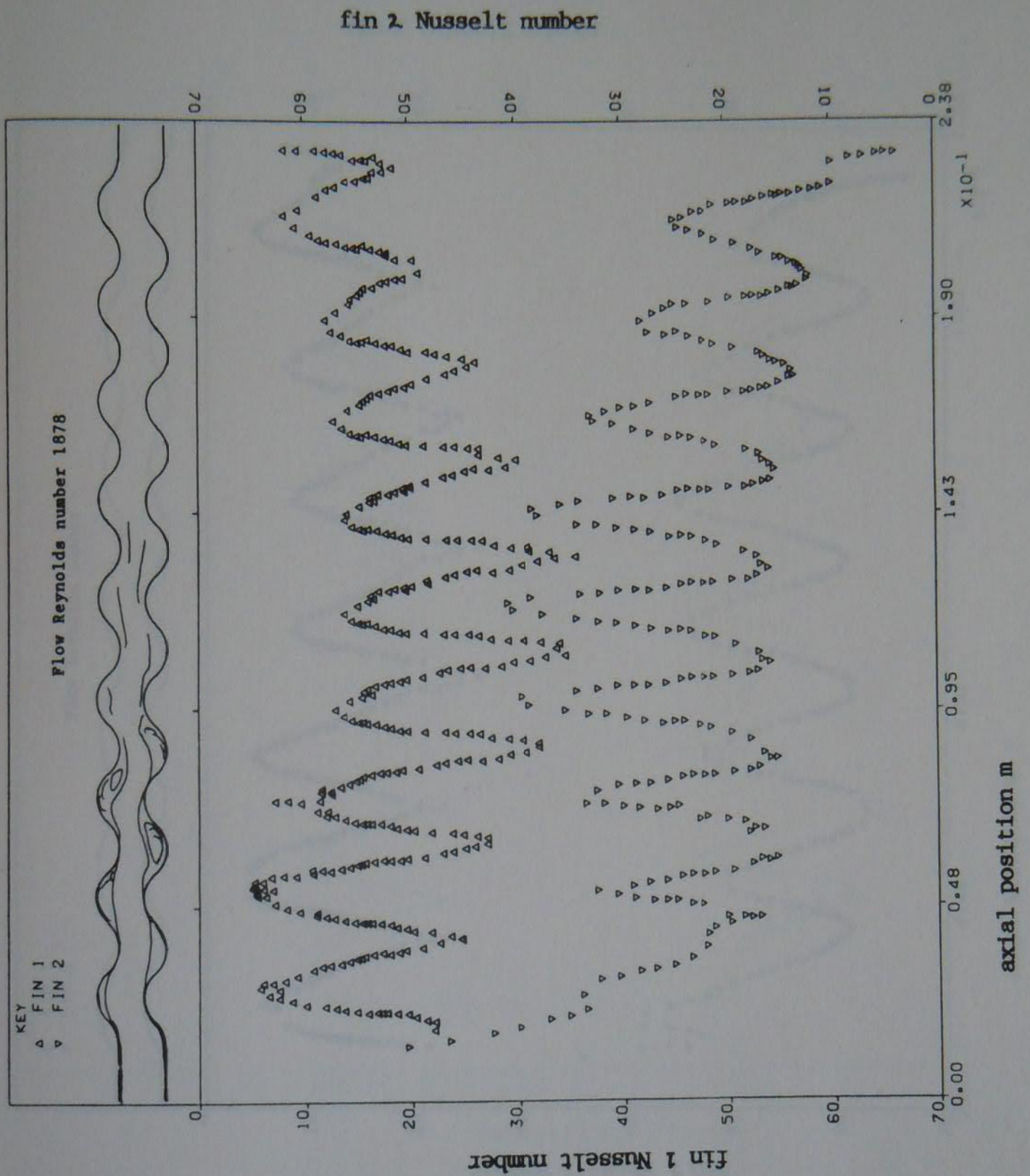
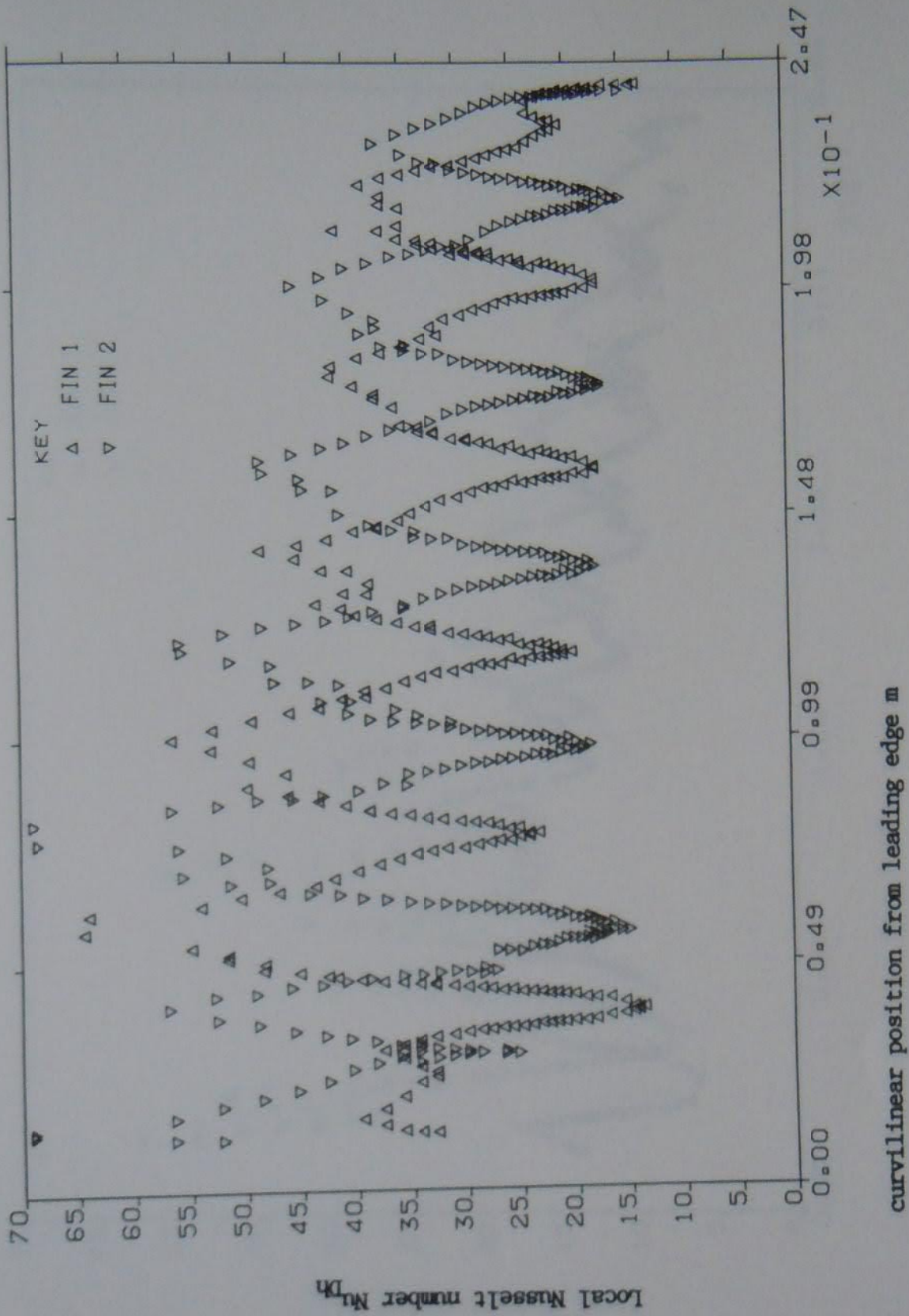Figure 7.3 Local Nusselt number against axial coordinate, profile 3
Dh = 0.0224 m, Re = 2007
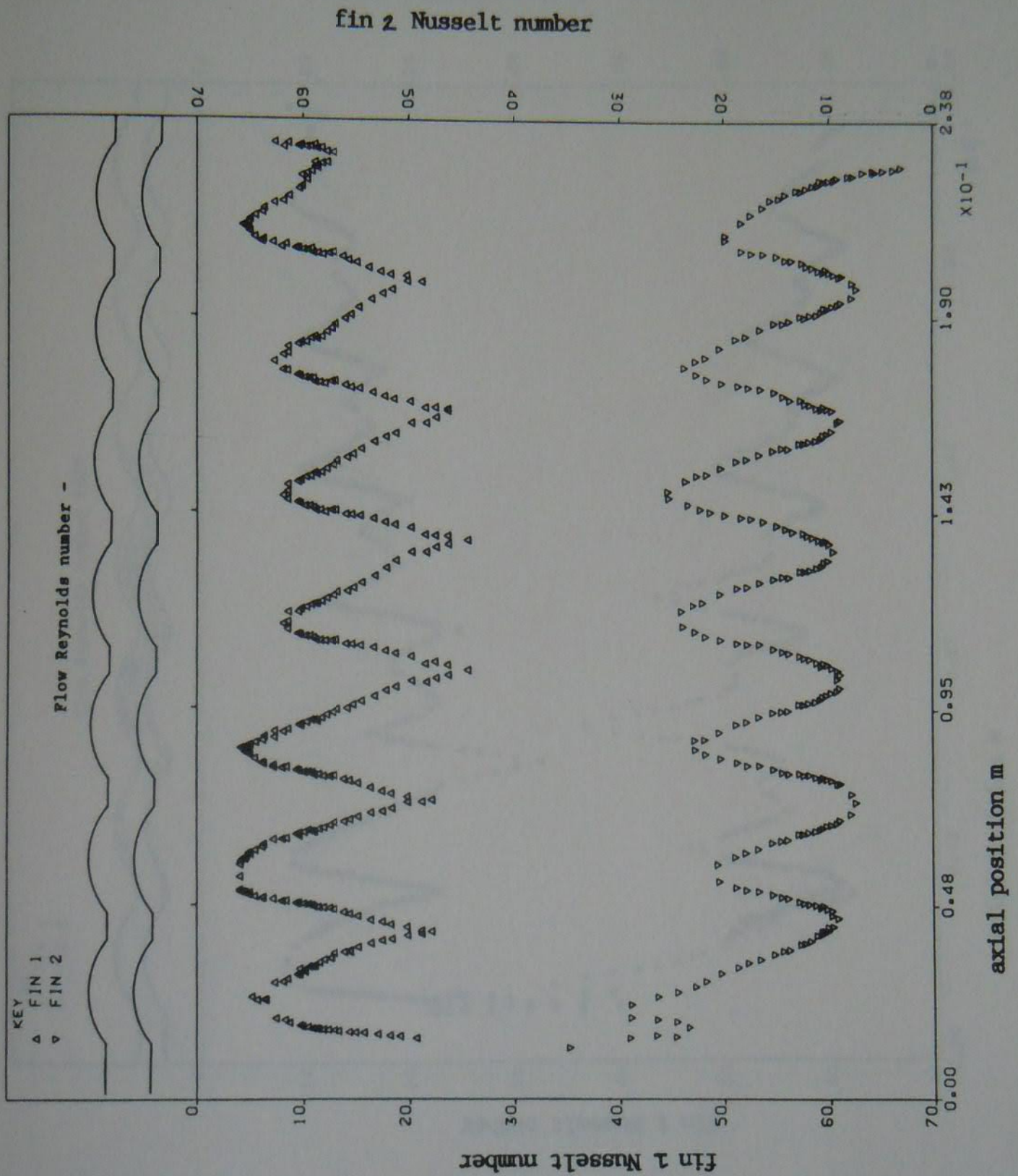
Figure 7.4   Local Nusselt number against axial coordinate, profile 4
Dh = 0.0224 m, Re = 2004

fin 2 Nusselt number
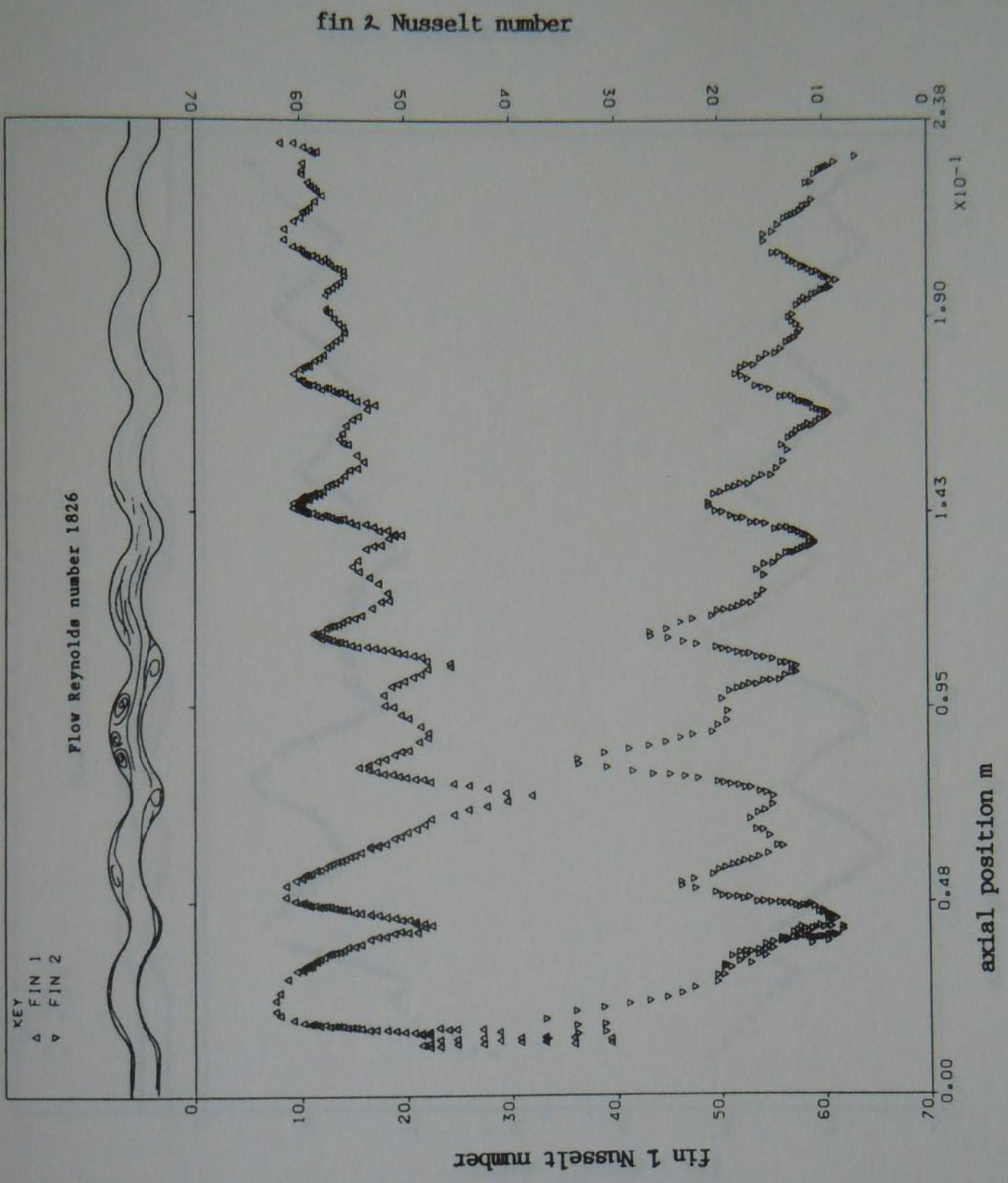
Figure 7.5 Local Nusselt number against axial coordinate, profile 1
Dh = 0.0142 m, Re = 1992

323
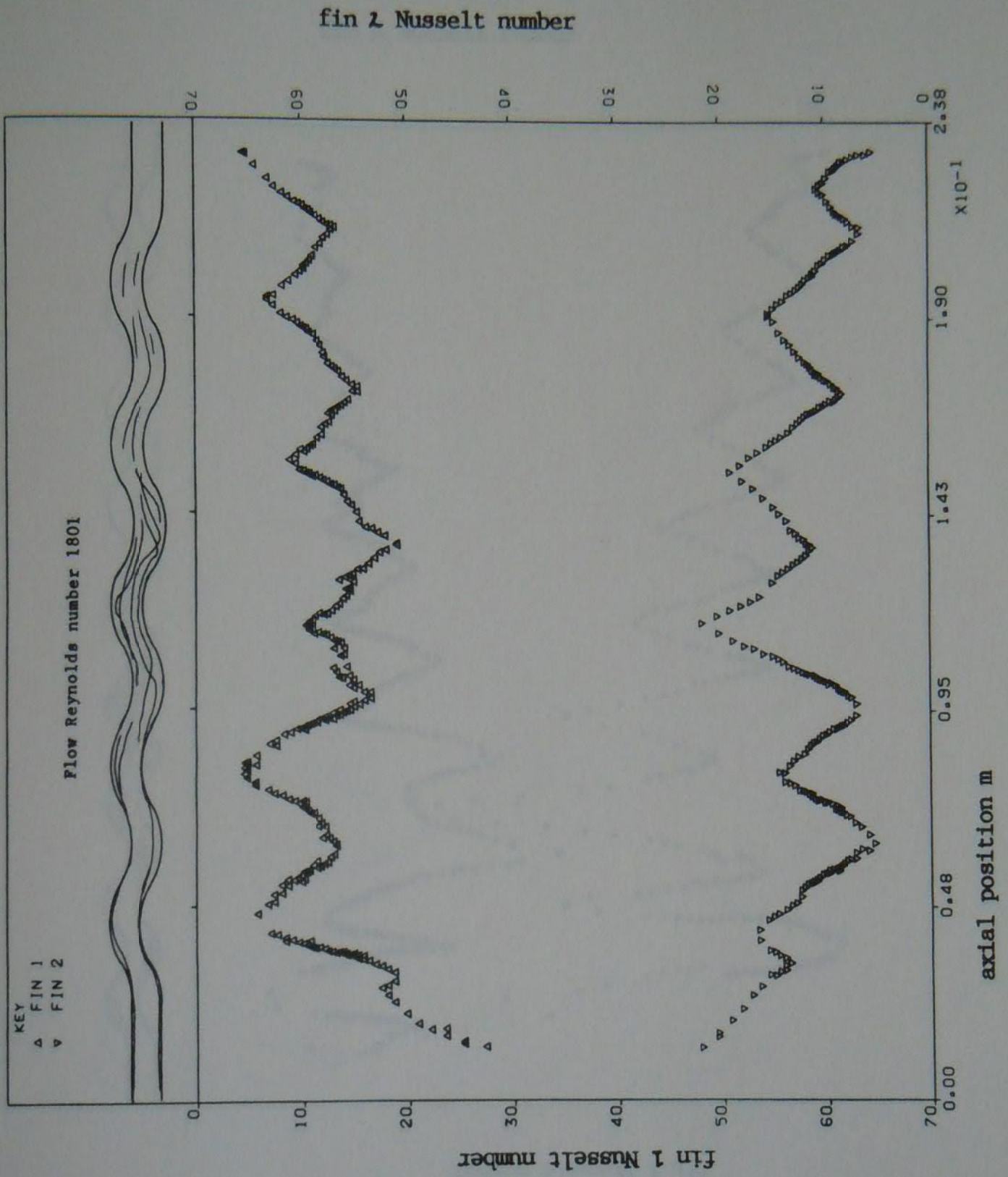
Figure 7.6   Local Nusselt number against axial coordinate, profile 2
Dh = 0.0142 m, Re = 2040

324

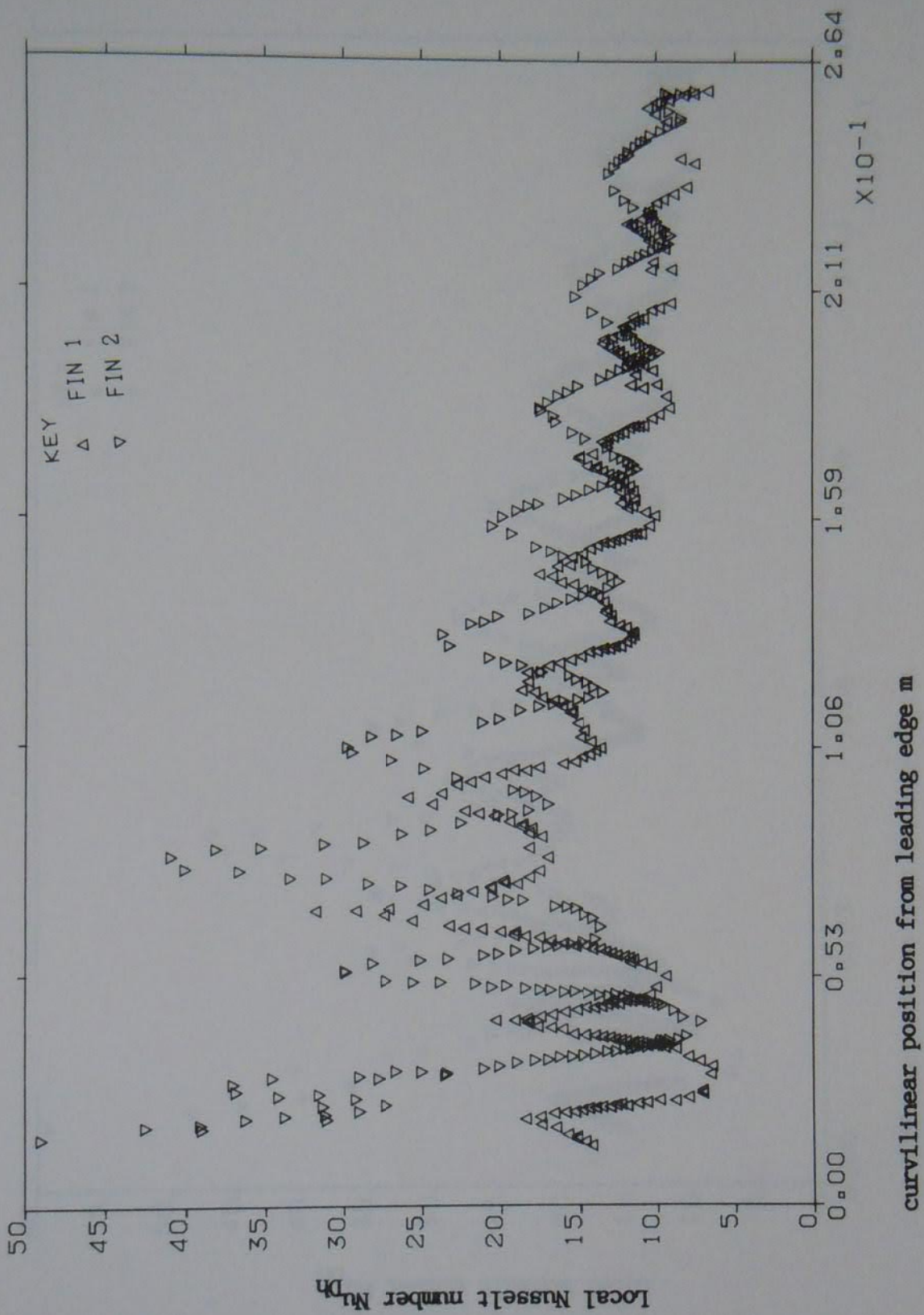fin 2 Nusselt number
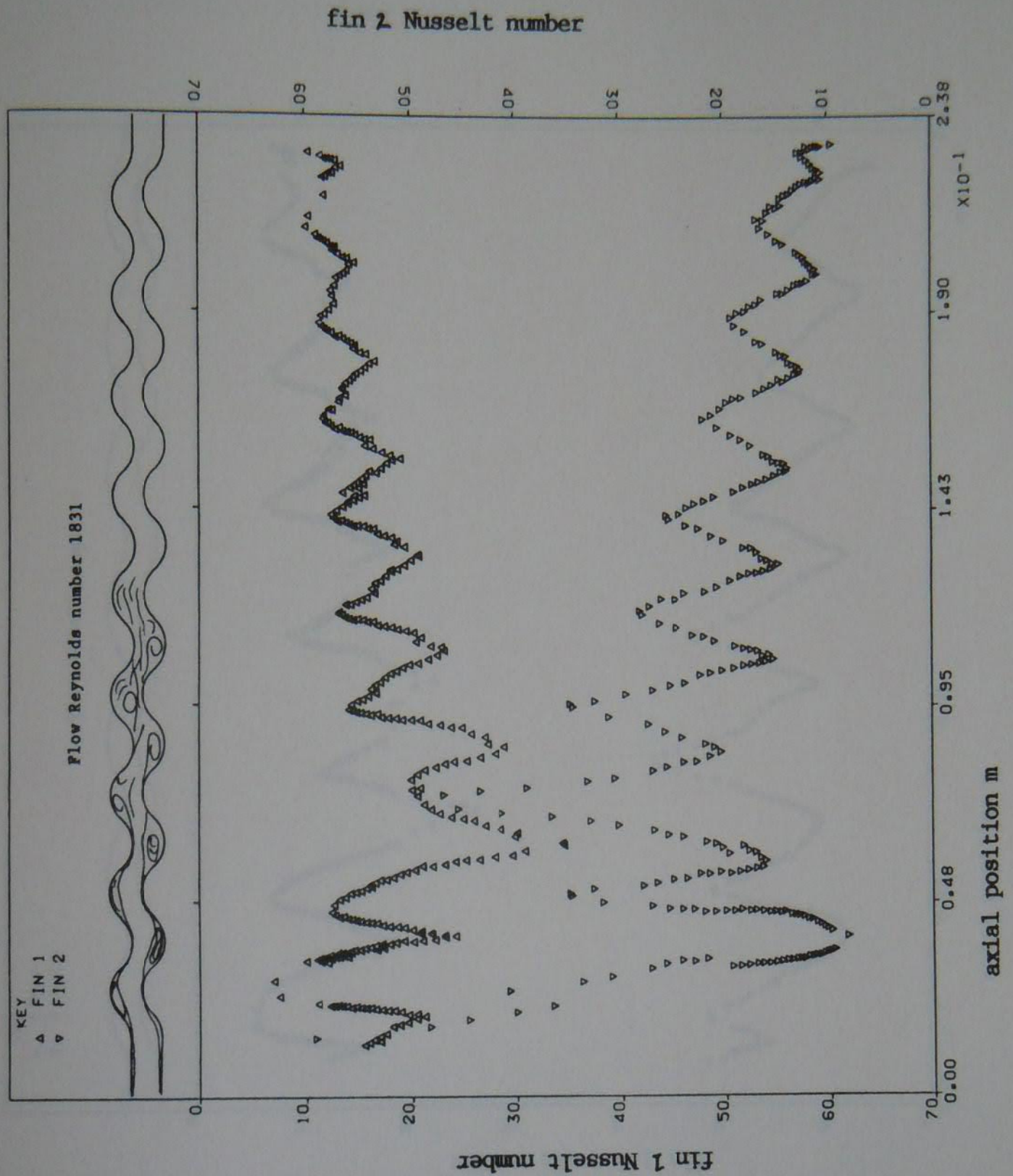
Figure 7.7 Local Nusselt number against axial coordinate, profile 3
Dh = 0.0142 m, Re = 2023

fin 2 Nusselt number

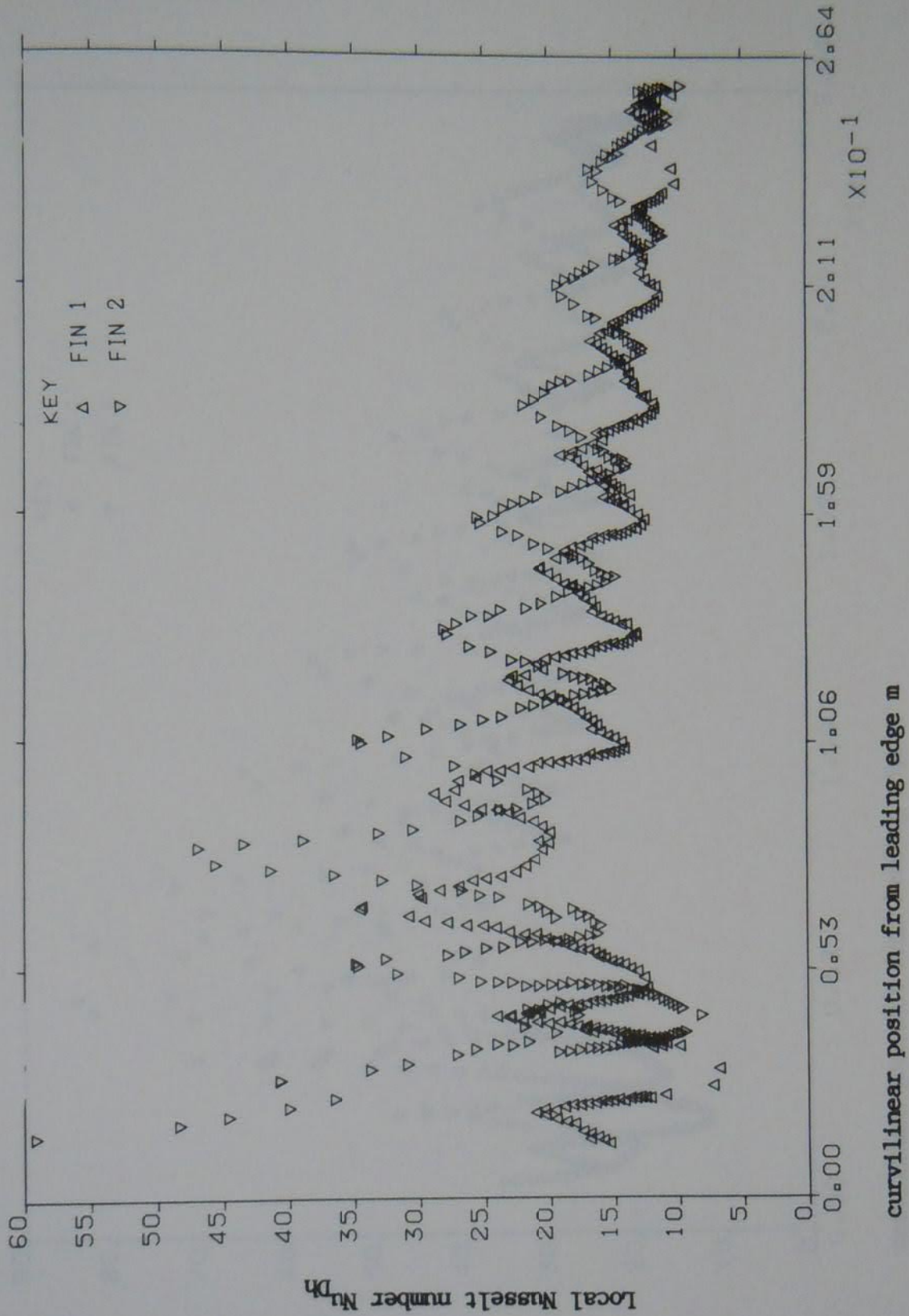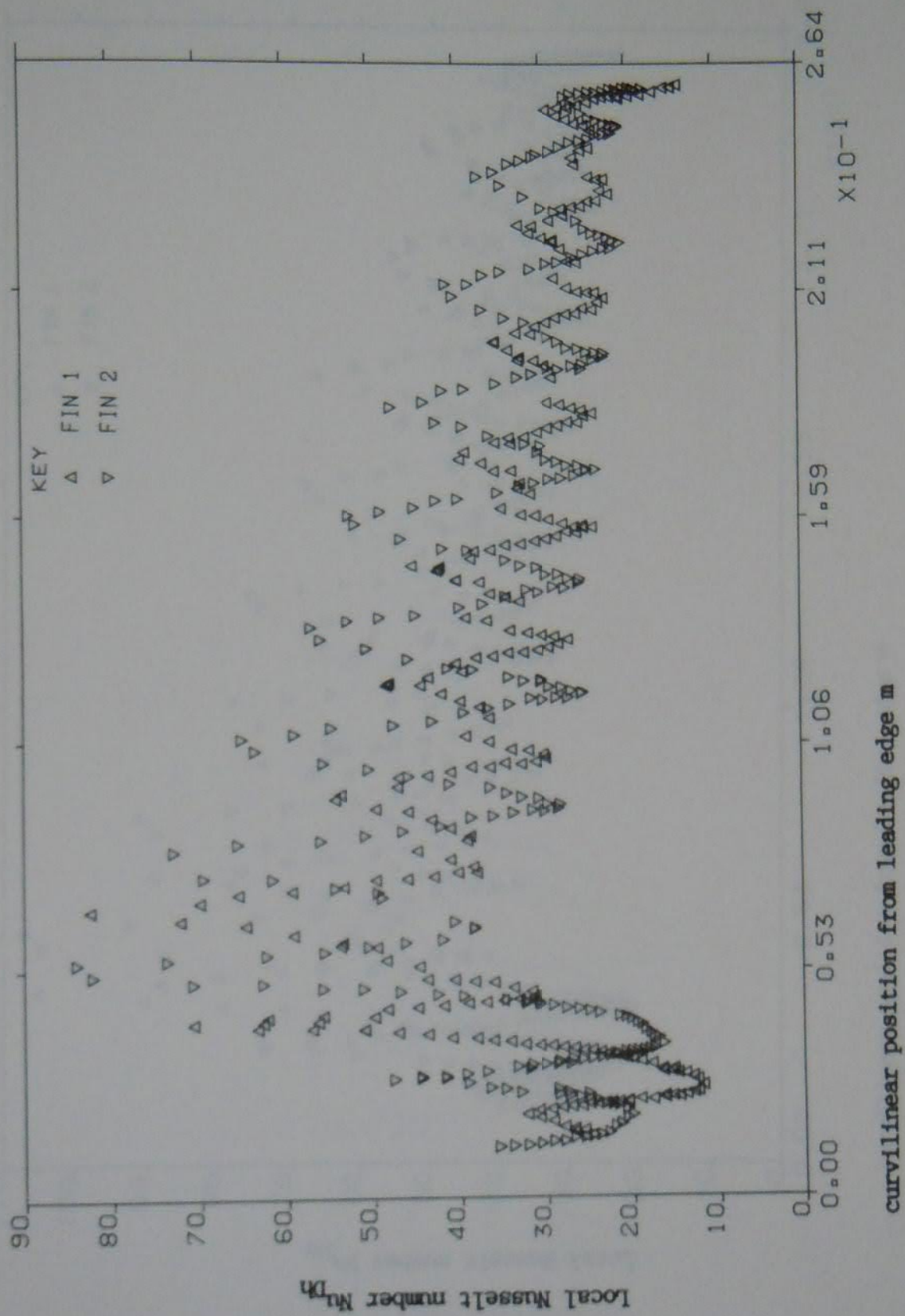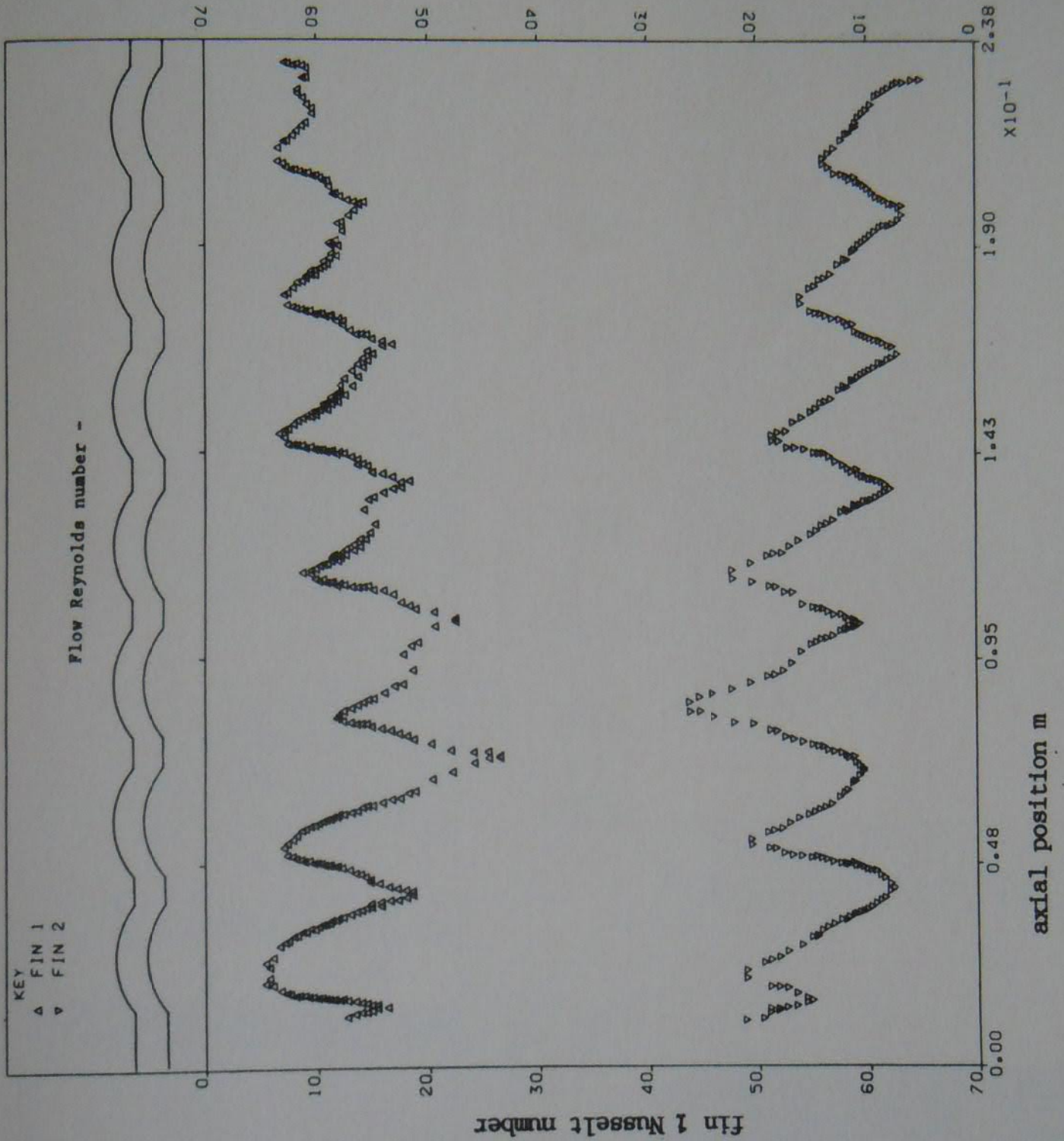

Figure 7.8 Local Nusselt number against axial coordinate, profile 4
Dh = 0.0142 m, Re = 1999
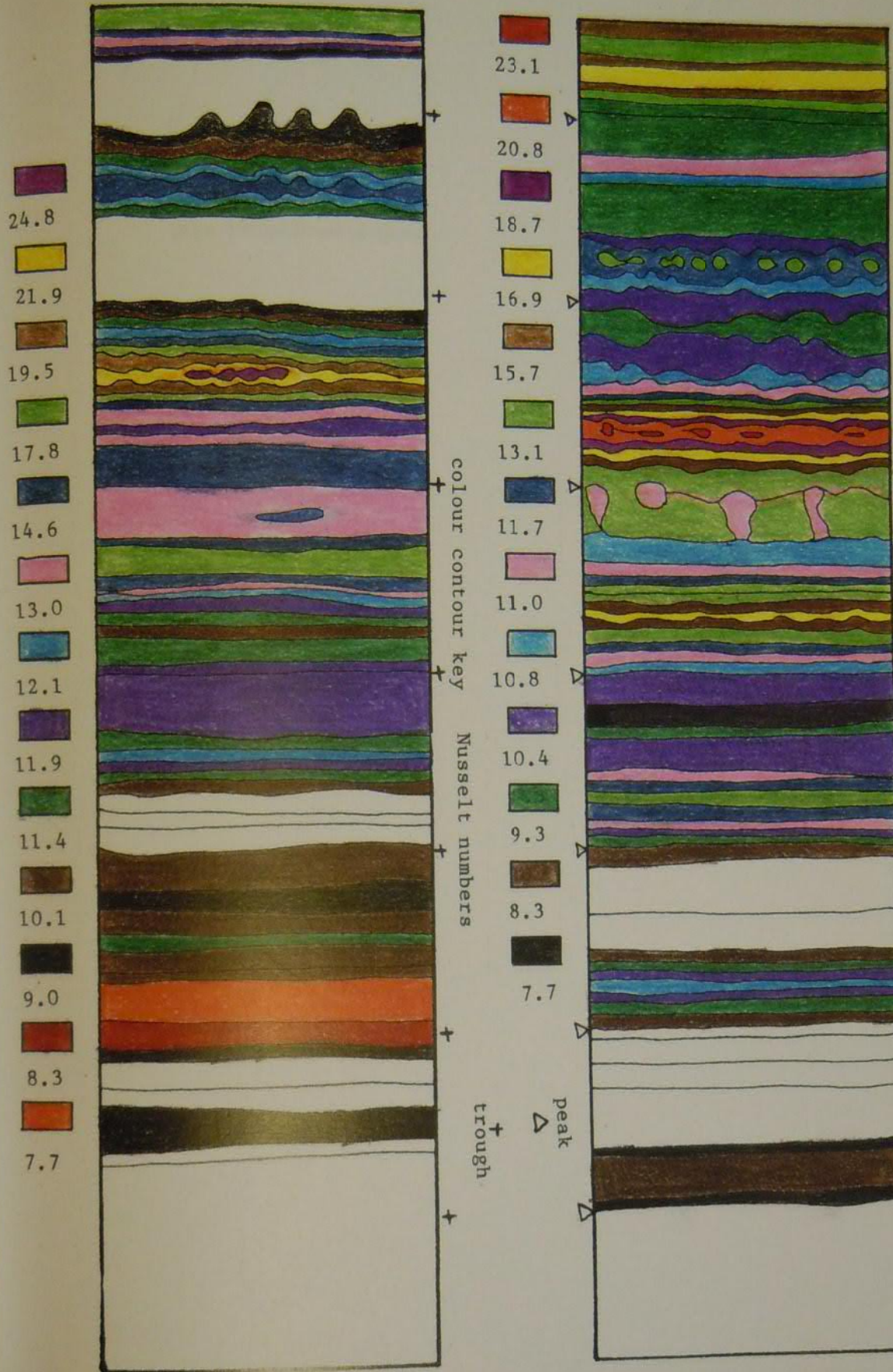
Figure 7.9 Local Nusselt number against axial coordinate, profile 1
Dh = 0.0098 m, Re = 1590

Flow Reynolds number 1459

fin 1

fin 2

colour contour key Nusselt numbers

17.6	14.4
15.8	13.0
14.7	12.3
14.0	11.7
13.3	11.1
12.6	10.6
12.1	10.2
10.7	9.1
9.6	8.1
8.5	7.2
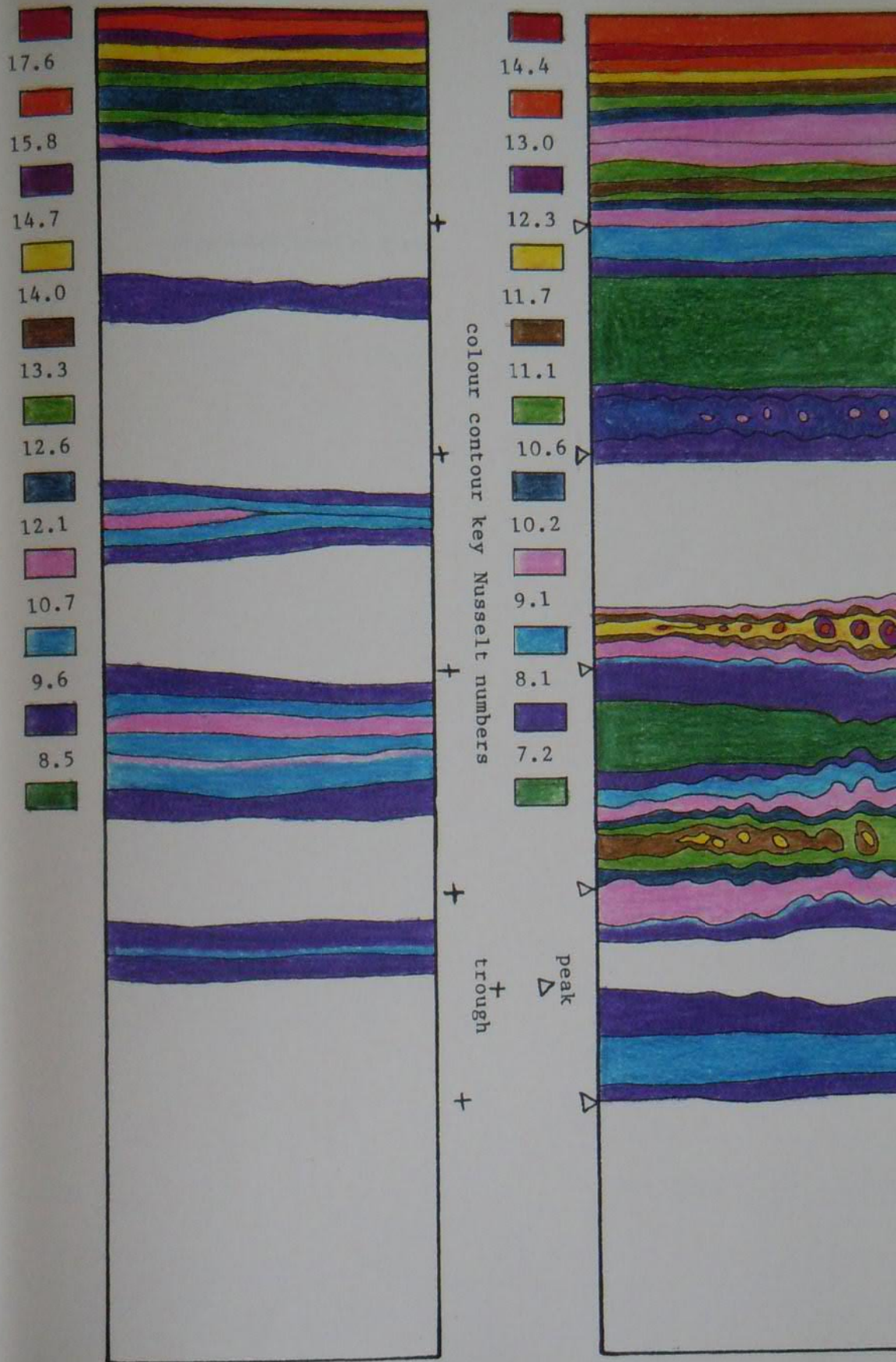
peak △

trough +

Flow Reynolds number 1576

Figure 7.10 Local Nusselt number against axial coordinate, profile 2
Dh = 0.0098 m, Re = 1579
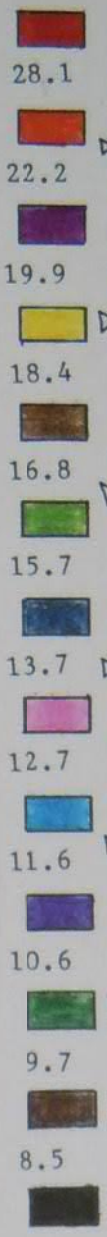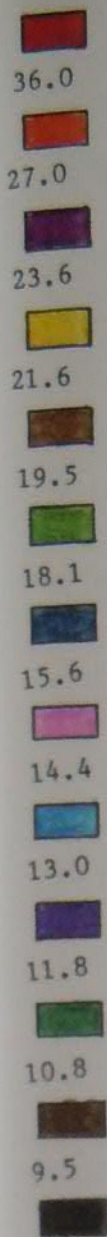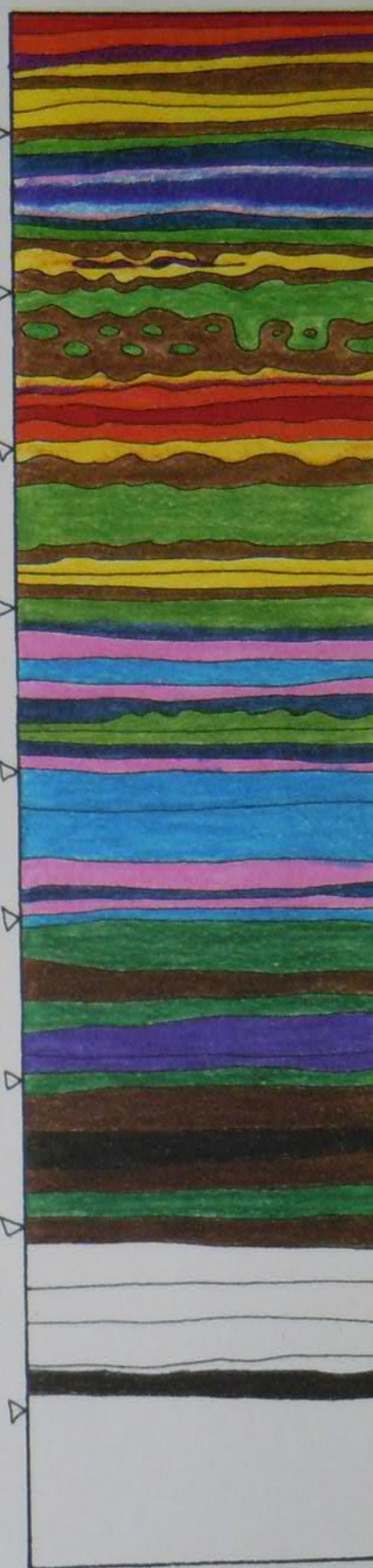
Figure 7.11 Local Nusselt number against axial coordinate, profile 3
Dh = 0.0098 m, Re = 1573

Flow Reynolds number 1395

fin 1

fin 2

colour contour key Nusselt numbers

peak △
trough +

36.0	28.1
27.0	22.2
23.6	19.9
21.6	18.4
19.5	16.8
18.1	15.7
15.6	13.7
14.4	12.7
13.0	11.6
11.8	10.6
10.8	9.7
9.5	8.5

fin 1

fin 2

colour contour key Nusselt numbers

19.4

18.5

17.5

16.9

14.7

14.4

13.3

13.1

12.6

12.5

11.2

11.2

10.1

10.2

9.1

9.2

8.3

8.4

7.6

7.7

7.0

7.1

6.2

6.3
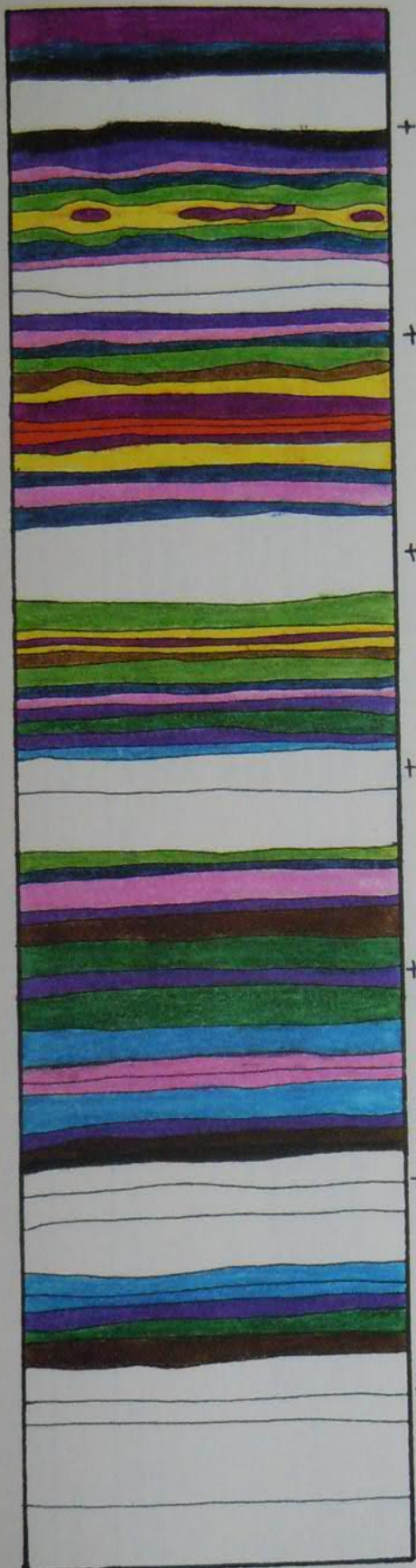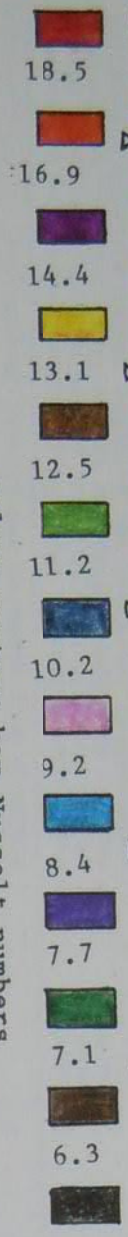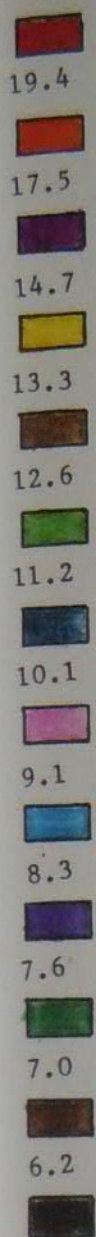
peak

trough
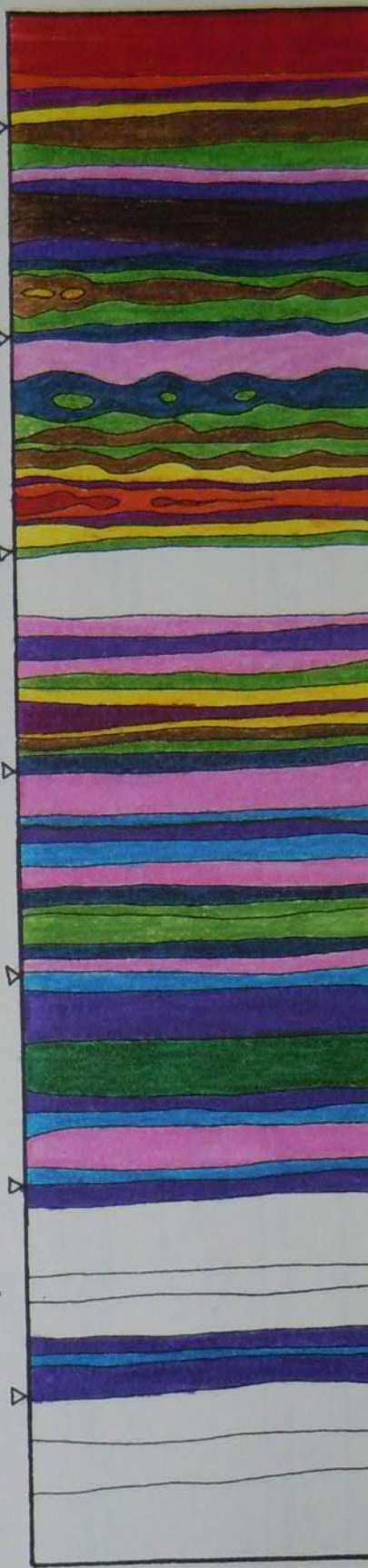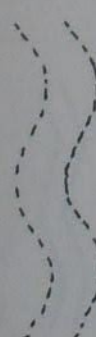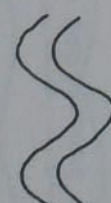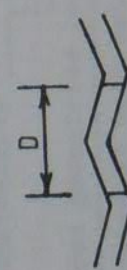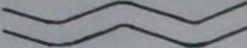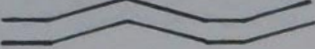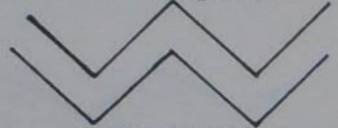
Flow Reynolds number –

Figure 7.12 Local Nusselt number against axial coordinate, profile 4
Dh = 0.0098 m, Re = 1593

Table 2.1 Literature Survey and Review : Condensed Notes

Reference	Geometry	Nondimensional Number Range	Comments
Beloborodov V.G. Volgin B.P. 1971	Wavy walled channels profile not defined. Other geometries tested.	ReDh=5000-45000 RH=0.5 RI=0.25 Pr=water	Heat transfer and flow friction characteristics measured for a range of heat exchanger channel geometries, though mainly for plate heat exchangers. Results presented in regression equation form. For the wavy rippled duct the result was; $$Nu = 0.097\ ReDh^{0.73} \cdot Pr^n\ (Pr/Prw)^{0.25}$$ where n = 0.3 cooling and 0.43 heating Straight channel heat transfer equation gave good comparison with turbulent pipe flow equations (Dittus-Boelter, Colburn).
Okada K. Ono M. Tomimura T. Okuma T. Konno H. Ohtani S. 1972	Wavy walled channel used in plate heat exchangers	ReDh=400-15000, RH=0.294,0.429, 0.588 RI=0.5 RN=20 Pr=water	Mean heat transfer coefficients over inlet and fully developed regions reported in form $$Nu = C \cdot ReDh^m \cdot Pr^{0.4}$$ Dh C m 6.2 0.3 0.63 8.8 0.27 0.66 11.8 0.29 0.67 Pressure drop measured and plotted graphically
Chow J.C.F. Soda K. 1973	Wavy wall channels	Re2H=<140. RH=0.2 RI=0.08	Analytical solutions for flow and mass transfer in various wavy walled channels with adjacent plates mounted at various phase angles. Work had application to the flow of blood. As the channel constriction increased the Reynolds number at which separation occurred decreased.
Goldstein L.Jr. Sparrow E.M. 1976	Flat sided corrugated tube with circular tube	ReDh=135-1200 RH=0.178 RI=0.3584 RN=2 Sc=2.5 H/D=0.193 S/D=2.50 L/D=2.17 THETA=21°	Local and average mass transfer coefficients by naphthalene sublimation. No pressure drop measurements. Complex fluid flow phenomena around the tube were noted. No mass transfer from tube wall surfaces.
Goldstein L.Jr. Sparrow E.M. 1976	Flat sided corrugated duct		Shorter communication which discussed the complex fluid flow mechanisms which exist in flat sided ducts.

Author / Year	Geometry	Parameters	Description
Goldstein L.Jr. Sparrow E.M. 1977	Flat sided corrugated duct	Re2H=140-8000 RH=0.178 RI=0.3584 RN=2 Sc=2.5 THETA=21°	Local and average mass transfer coefficients by the naphthalene sublimation technique. No pressure drop measurements. Entrance region, not periodically fully developed. Presence of secondary flow vortices noted.
Hosoda T. 1977	Flat sided corrugated duct	Re=unknown RI=0.268 RN=4 RH=0.191 RJ=0.198 THETA=15°	Flow visualisation used water and tracer particles, illuminated. Sheet metal bent at corners formed the duct. Flow pattern showed boundary layer growth and separation.
Mandel S.W. Townsend M.A. Parrish T.F. 1979	Flat sided corrugated duct corrugations joined by flat sections	Re2H=100-1200 THETA=10-30° RN=0-3	Numerical scheme developed to optimize the design of heat exchangers using rippled (corrugated) fins. The work was limited to the laminar flow regime, but serious deficiencies were present in the numerical model.
Vajravelu K. 1980	Wavy sinusoidal channels	Re=laminar	Theoretical solution using linearised equations solving for the flow in two parts, mean and perturbed. Mean part poiseuille flow between parallel plates. Flow only mildly affected by the wavy walls due to long wavelength approximation.
Faas S.E. McEligot D.M. 1980	Flat sided corrugated duct	Re=10-250 THETA=45 RI=0.5 RH=1.0, 0.667, 0.5 RJ=0.707, 0.4714, 0.3556	Used computer program TEACH to model the laminar flow and heat transfer in corrugated ducts and rib roughened channels. The work was limited to the periodical fully developed region.
Izumi R. Yamashita H. Oyakawa K. 1981	Flat channel bent twice perpendicularly Various geometries tested	Re2H=0-2400 Pr=0.71, 1.0	Numerical investigation used the finite difference method, for laminar flow and constant heat flux boundary condition. Flow solutions presented as streamline plots, with local Nusselt number and pressure drop also given.
Izumi R. Oyakawa K. Kaga S. Yamashita H. 1981	Flat channel bent twice perpendicularly Various geometries tested	Re2H=300-10000 Pr=0.71	Experimental investigation into the characteristics of the duct bent twice. Flow visualisation and pressure drop measurements were made using water whilst heat transfer used air with a constant heat flux thermal boundary condition. Results compared against the earlier numerical work and showed reasonable for flow streaklines, but local heat transfer coefficient did not.

Sobey I.J.   Wavy wall channels asymmetric geometries

1982

Numerical analysis of oscillatory flows in wavy walled channels and comparison with flow visualisation of particle tracers in water. The walls were sinusoidal (cosine function) and different geometries using out of phase walls investigated.

1982
Izumi R.
Yamashita H.
Kaga S.
Miyajima N.

Flat sided corrugated duct

Re2H=600-20000
THETA=45°
RJ*=0.3536
RI=0.5
RH=0.5
Pr=0.71

Heat transfer experiments used air, heated by steam and modelled constant wall temperature. Pressure drop measurements reported. Amano, Bagherlee, Smith and Niess used the data to compare against numerical solutions, and some of this data obtained from their paper.

1982   in Japanese
O'Brien J.E.
Sparrow E.M.

Flat sided corrugated duct

ReDh=1500-25000
RN=10
Pr=4.-8.
RI=0.289

RH=0.289
RJ=0.250
THETA=30°

Heat transfer measurements used water at various temperatures, by electrically heated copper plates. Flow friction and visualisation studies used air. Results were limited to the periodically fully developed region. Regression equation correlated results to give

$Nu = 0.409 . ReDh^{0.614} . Pr^{0.34}$

Flow friction results presented in tabular form, but was found to be almost independent on the Reynolds number, and equal to 0.57 Flow visualisation by oil and lampblack revealed flow separation and reattachment points.

$Dh=2JW/(J+W)$

1982
Sparrow E.M.
Comb J.W.

Flat sided corrugated duct

ReDh=2000-27000
RN=10
Pr=4.-12.
RI=0.289
RH=0.419
RJ=0.363
THETA=30°

Heat transfer, flow friction and flow visualisation by the same methods as O'Brien and Sparrow. Flow visualisation showed that the increase in interwall spacing gave rise to more of the duct being blanketed by recirculation zones. The separation occurred at the corrugation peaks. The effect of conduction in the side wall was taken into account and for the comparison with the earlier work of O'Brien the data was reworked. Two regression equations were generated as follows;

$Nu = 0.412 . ReDh^{0.614} . Pr^{0.332}$ for O'Brien's data and

$Nu = 0.491 . ReDh^{0.632} . Pr^{0.3}$ for Comb's data

Table of fully developed friction factors show a slight increase with increasing Reynolds number.

$Dh=2JW/(J+W)$

1983
Izumi R.
Yamashita H.
Oyakawa K.
Mori N.
1983

Flat sided channel bent twice various bending angles

Re2H=600-40000
Pr=0.71

Experimental and analytical methods used to study the heat transfer and pressure drop characteristics. Heat transfer boundary condition was constant heat flux. Bends had sharp corners. Pressure drops reported for numerical results only, which were in the laminar flow region.

Year / Author	Geometry	Parameters	Description
Izumi R Yamashita H. Oyakawa K.	Flat sided corrugated channel	ReDh=0-40000 Pr=0.71 THETA=0-45°	Heat transfer and flow friction were examined by numerical study using K-KL turbulence model. Heat transfer boundary condition was constant heat flux, and the flow periodically fully developed. Local and mean Nusselt numbers and friction factor presented graphically. Grids used were 17 by 81 to 33 by 131 for a cycle.
1983 Sparrow E.M. Hossfeld L.M.	Flat sided corrugated duct with rounded protruding edges.	ReDh=2000-33000 RN=10 Pr=4., 7., 11. RH=0.419 RJ=0.363 RI=0.289, 0.281, 0.274 THETA=30°	Heat transfer measurements in the periodically fully developed region, by electric heated copper plates. Flow visualisation by oil and lampblack. Rounding reduced both heat transfer and flow friction. The rounded ducts exhibited smaller separation zones and reduced disturbance levels. Results reported by graph of Nusselt numbers and a table of friction factors. A simple performance evaluation indicated that the Nusselt number was insensitive to corrugation rounding. Heat transfer used water, oil and air.
1984 Amano R.S.	Dh=2JW/(J+W) Channel with two bends	Re2H=200-2000	The laminar flow, heat transfer and flow friction behaviour of a channel with two right angled bends was studied numerically.
1984 Amano R.S.	Different step ratio geometries Channel with two bends	Re2H=3000-10000 Pr=unknown	Numerical study of flow and heat transfer for turbulent flow in a channel with two right angled bends. Fully developed channel flow at inlet. Local heat transfer coefficients from either RSM or K-E models did not agree very well with data.
1985a Amano R.S.	Different step ratio geometries Flat sided corrugated channel	ReDh=10-25000 Dh=2J RH=0.5, 0.333, 0.250 RJ=0.354, 0.236, 0.177 RI=0.5 Pr=unknown THETA=45°	Numerical study of laminar and turbulent flows in periodically fully developed regime. K-E turbulent model with near wall refinement used. Local and average heat transfer and friction factor presented graphically. Equation fitted to heat transfer coefficient was; $$Nu = 0.307 \cdot ReDh^{0.642} \cdot (1.404 \cdot H/J)^{-0.592}$$ For constant heat flux boundary condition. Apparently no Prandtl number variation and equation appears Prandtl number independent. Relatively coarse two dimensional grid. Meshes used 27 by 32 to 57 by 52.
1985b Nakayama A. Koyama H.	Wavy sinusoidal wall channel		Numerical investigation used K-E turbulence model in the three dimensionally modelled duct. Vector plots show spanwise and streamwise vortex systems. Written in Japanese but it appears that geometric parameters were systematically varied.
1985			

	Wavy sinusoidal wall channel		
Focke W.W. Zachariades J. Oliver I. 1985	Wavy sinusoidal wall channel for plate heat exchangers.	Re2H=200–16000 RH=0.5 RI=0.5 RN=40 Sc=2500(approx.)	Mass transfer measurements used the diffusion limited mass transfer technique, (effectively constant wall temperature) Results presented graphically and regression equations were fitted to the data, for both j factor and friction factor. Work mainly relates to plate heat exchangers having Herringbone profile patterns at various crossing angles.
Nishimura T. Ohori Y. Kajimoto Y. Kawamura Y. 1985	Wavy sinusoidal wall channel Symmetric wavy walls	ReDh=100–10000 RI=0.25 Sc=unknown	Mass transfer characteristics of symmetric channel was studied by theoretical and experimental methods. Local Sherwood number measured by electro chemical method in a diffusion controlled process in the periodically fully developed region. No pressure drop measurements made.
Nishimura T. Kajimoto Y. Kawamura Y. 1986	Wavy sinusoidal wall channel Dh=H	ReDh=100–10000 Sc=1170 RI=0.25 RH=0.464 RN=10	Mass transfer and flow friction characteristics of three wavy channels was reported. The phase angle only was varied. The wavy asymmetric channel showed the lowest flow friction, whilst the symmetric channel highest. All channels exhibited similar mass transfer characteristics, indicating that asymmetric channel had best performance. Periodically fully developed region studied. Flow visualisation study revealed that stable recirculation regions within the channel troughs become unsteady at ReDh=350.
Nishimura T. Kajimoto Y. Tarumoto A. Kawamura Y. 1986	Wavy sinusoidal wall channel Dh=H	ReDh=100–10000 Sc=1570 RI=0.25 RH=0.464 RN=10	Investigated the flow structure and transfer characteristics of a wavy channel in the periodically fully developed region.Flow visualisation photographs were presented using illuminated hydrogen bubbles.The following results obtained; ReDh>240 Steady 2D flow with spanwise recirculating vortices. ReDh>350 Separated shear layer becomes unstable, 3D vorticular flow pattern ensues at reattachment point. ReDh>560 Onset of turbulent flow. ReDh>1230 Vortex shedding from just behind a ripple peak. Local sherwood number presented for fully developed cycle integrated with fluid flow study.
Focke W.W. Knibbe P.G. 1986	Wavy sinusoidal wall channel	Re2H=10–1000 RI=0.5 RH=0.5 RN=40	Flow visualisation in periodically fully developed region. Re2H>20 flow separation occurs Re2H>260 shear layers became unstable and transition to turbulent flow began.

Molki M. Yuen C.M.	Flat sided corrugated ducts	Sc=2.5 ReDh=4000-45000 RH=0.289, 0.419, 0.577 RJ=0.25, 0.363, 0.5 RN=20 RI=0.289 THETA=30°	Mass transfer measurements used the thick film naphthalene technique, flow visualisation by oil and lampblack and pressure drop measurements. Results presented for half cycle averaged mass transfer in the entrance region and periodically developed regions. Flow visualisation was only performed at ReDh=30000. The results were presented graphically for both Sherwood number and friction factor. For ReDh>10000 equations fitted to the data of the form;

$$Shfd = C . ReDh^m$$

J/L	C	m
0.250	0.159	0.724
0.363	0.213	0.719
0.5	0.261	0.717

1986   Dh=4JW/2(J+W)

Molki M.	Flat sided corrugated ducts	ReDh=4000-30000 Sc=2.5 THETA=0, 10, 20, 30° RP=0.250 RH=0, 0.254, 0.266, 0.289 RI=0, 0.0882, 0.182, 0.289 RN=20	Mass transfer measurements investigated effect of corrugation inclination angle at constant wall spacing for both periodically fully developed and entrance regions. Results plotted in graphs for local and fully developed Sherwood number and friction factor. Regression equations fitted to the mass transfer data;
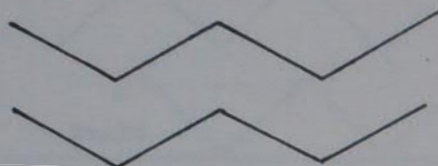
$$Shfd = C . ReDH^m$$

THETA	C	m
0	0.023	0.84
10	0.046	0.80
20	0.076	0.77
30	0.191	0.71

1986
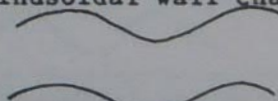
Hasegawa E. Nagashima F. 1986	Wavy sinusoidal wall channel Dh=H	ReDh=0-100 Pr=1., 2.	Theoretical analysis of the transfer characteristics of wavy channels. The effect of the plates being out of phase was investigated. Small amplitude approximation

---

Asako Y. Faghri M.	Flat sided corrugated ducts	ReDh=100-1500 Pr=.7, 4., 8. THETA=15, 30, 45° RI=0.134, 0.289, 0.5 RH=0.0670, 0.134, 0.268 (15) RH=0.144, 0.289, 0.419, 0.577 (30) RH=0.25, 0.333, 0.50, 1.0 (45) RJ=0.0647, 0.1229, 0.259 (15) RJ=0.125, 0.250, 0.363, 0.5 (30) RJ=0.168, 0.236, 0.354, 0.707 (45)	Numerical solutions for periodically fully developed laminar flow, for three corrugation angles and several plate spacings. Uniform wall temperature, but coarse grid (18 by 34). Model used coordinate transformation within finite volume technique. Graphs of Nusselt number and friction factor given.

1987   Dh=2J

Authors / Year	Geometry	Parameters	Description
Faghri M. Asako Y. 1987	Flat sided corrugated channel converging-diverging	THETA=5, 10, 15°	Numerical analysis for heat transfer and pressure drop characteristics in laminar flow. Streamline patterns presented show flow separation. Only the periodically fully developed region was modelled.
Nishimura T. Yoshino T. Kawamura Y. 1987	Wavy channel with sinusoidal walls	Re2H=200-500 ReH=100-250 RH=0.143 RI=0.25 RN=10	Dye streakline flow visualisation in the periodically fully developed region. ReH<100 streaklines follow surface profiles. 100<ReH<160 three dimensional Gortler vortices appeared. 160<ReH<250 streamwise Gortler vortices became unsteady and spiralled.
Amano R.S. Bagherlee A. Smith R.J. Niess T.G. 1987	Flat sided corrugated channel with additional fins. Dh=2J	ReDh=1000-20000 RI=0.5 RH=0.5, 0.80, 0.668 RJ=0.354, 0.471 0.566 Pr=unknown THETA=45°	Numerical model for turbulent flow in corrugated channels used the Reynolds stress model. The computer code was validated by comparison against backward facing step experimental results. Flow exhibited marked separation in the troughs and the addition of fins increased the recirculation. Heat transfer, flow friction and turbulence quantities were reported graphically. The Reynolds stress turbulence model was preferred for this type of flow.
Motamed-Ektesabi M.R. Sako M. Chiba T 1987	Wavy sinusoidal channels	ReDh=300-40000	Measurements of flow friction and flow visualisation were reported. Paper written in Japanese. Friction factors given in graphs and regression equation forms. Flow visualisation photographs show complex fluid flow patterns.
Asako Y. Nakamura H. Faghri M. 1988	Wavy sinusoidal channels (cosine function)	Re2H=100-1000 Pr=0.7 THETA=15, 30, 45° RI=0.067, 0.144, 0.25 RH=0.067, 0.134, 0.268 (15) RH=0.144, 0.289, 0.419 (30) RH=0.250, 0.333, 0.500 (45)	Numerical study of the heat transfer and pressure drop characteristics in the periodically fully developed region, using constant wall temperature boundary condition. Streamline plots show flow separation in the curved troughs in comparison with the flow in a channel with sharp corners. Graphs of Nusselt number and flow friction presented. The numerical method used involved coordinate transformation within the finite difference technique.

x=(1-(2/PI)cos(2PIy/L))(P/4)tan(THETA)

Xin Tao	Wavy channel	Re2H=100-1000 Pr=0.707 RI=0.333, 0.250 0.167 RH=0.133, 0.233, 0.333, 0.4 RI=0.333 RH=0.10, 0.175 0.25, 0.30 RI=0.250 RH=0.067, 0.117, 0.167, 0.20 RI=0.167	Numerical model of the laminar flow in the periodically fully developed region of a wavy channel. Flow friction and heat transfer for the constant wall temperature boundary condition were reported. Streamline and velocity vector plots show the flow separation zone and recirculation.
1988			
Garg V.K. Maji P.K.	Wavy sinusoidal duct	Re2H=100-500 Pr=1.0 RH=0.5 RI=0.1, 0.2	Laminar flow in the inlet region of a sinusoidal wavy walled channel was numerically modelled. Flow vectors, pressure drops and Nusselt number distributions presented. Wavy geometry was transformed onto a rectangular mesh. Very small number of nodes used to solve the problem making fluid flow characteristics in the inlet region difficult to track.
1988			
Xiao Q. Xin R.C. Tao W.Q.	Asymmetric Wavy Channel Various wave profiles	Re2H=100-1000 Pr=0.7 RI=0.250, 0.167	
1989			

Table 3.1, Four row heat exchanger geometry data

Surface	4	5
Geometry Details		
Fins/inch	7.52	6.83
Fins/m	296	269
Hydraulic diameter mm	5.274	5.622
A_c/A_{fr}	0.8317	0.8200
β m2/m3	655.1	606.3
A_{fi}/A_{ht}	0.7922	0.7786
Profile	B	B
Tubes/m	263	263
L_{1f} mm	77.6	77.6
Depth mm	76.2	76.2

Table 3.2, Performance data for the four row surfaces

<u>Surface 4</u>

Re	j	f
500	0.0187	0.125
750	0.0167	0.102
1000	0.0155	0.092
1250	0.0147	0.087
1500	0.0141	0.085
2000	0.0128	0.081
2500	0.0119	0.0765
3000	0.0112	0.075
3500	0.0112	0.0745
4000	0.0102	0.075
5000	0.0094	0.072
6000	0.0088	0.069
6500	0.0084	0.068

<u>Surface 5</u>

Re	j	f
1000	0.0159	0.0832
1250	0.0149	0.082
1500	0.01425	0.081
2000	0.0132	0.0776
2500	0.0123	0.0746
3000	0.0116	0.072
3500	0.0110	0.0712
4000	0.0106	0.071
5000	0.00965	0.0695
6000	0.0092	0.068
7000	0.0087	0.0655

Table 3.3 Comparison of geometry details of the Kays and London heat exchangers.

Geometry Detail	Surface Designation					
	11.44-3/8W	11.5-3/8W	17.8-3/8W	9.29-.737-SR	9.1-.737-S	11.32-0.737-SR
Fin Pitch fins/m	450	453	701	366	258	446
Fin length in flow direction L_{1f} mm	19.05	19.05	19.05	60.2	60.2	60.2
Heat transfer area A_{ht} m^2	18.14	17.61	26.55	45.46	44.42	53.51
Fin area A_{fi} m^2	14.91	14.48	23.68	37.15	36.10	45.23
Hydraulic diameter mm	3.23	3.02	2.12	4.12	4.21	3.51
Double wave amplitude mm	1.97	1.98	1.97	0.635	0.635	0.635
Wave pitch mm	9.525	9.525	9.525	6.35	6.35	6.35
Tube pitch tubes/m per row	79	85	79	72	72	72

Table 5.1 Comparison of mass flow rates measured by both orifice plates and velocity traverse.

Mass flowrates kg/s

velocity traverse	orifice plate	% difference
orifice plate diameter 0.02255 m		
orifice pipe diameter 0.05096 m		
1.241E-2	1.229E-2	1.0
1.432E-2	1.424E-2	0.6
1.009E-2	1.009E-2	0.0
orifice plate diameter 0.01253 m		
orifice pipe diameter 0.05096 m		
8.783E-3	8.787E-3	0.05
8.257E-3	8.235E-3	0.3
6.894E-3	6.845E-3	0.8
orifice plate diameter 0.00623 m		
orifice pipe diameter 0.02614 m		
2.416E-3	2.327E-3	3.9
2.271E-3	2.197E-3	3.4
2.365E-3	2.252E-3	5.0

Table 5.2 Rippled duct geometry details

Profile ripple numbers and double amplitudes, all experimental tests

Profile	1	2	3	4
RN	7	5	9	7
RI	0.164	0.136	0.222	0.141

Flow visualisation nondimensional wall spacings

RH	0.430	0.356	0.580
RH	0.330	0.273	0.445
RH	0.266	0.220	0.359
RH	0.227	0.189	0.306
RH	0.203	0.168	0.274
RH	0.153	0.127	0.207

(six fin spacings 13.75, 10.55, 8.50, 7.25, 6.50 and 4.90 mm, giving hydraulic diameters of 0.0275, 0.0211, 0.0170, 0.0145, 0.0130 and 0.0098 m)

Flow friction and heat transfer (local and overall) nondimensional wall spacings

RH	0.350	0.290	0.473	0.350
RH	0.272	0.225	0.367	0.272
RH	0.222	0.184	0.300	0.222

(three fin spacings 11.2, 8.7 and 7.1 mm, giving hydraulic diameters of 0.0224, 0.0174 and 0.0142 m)

Table 5.3 Flow visualisation classification and results

The following flow visualisation pictures illustrate fluid flows from right to left.

1   Steady, laminar flow with no separation or recirculation.

2   Steady, laminar flow with separation and recirculation vortex regions

3   Steady, laminar flow with streamwise secondary flow vortex system. Vortices are generally known as Taylor-Goertler vortices.

4   Marginally unsteady flow. The streamline bounding a separated region became an unstable shear layer.

5   Vortex shedding phenomena, similar in appearance to the Karman vortex shedding that occurs behind circular cylinders. There were other forms of the phenomena that occurred at different Reynolds numbers;

6   Synchronised vortex shedding occurred at low Reynolds number. The vortices tended to be large almost spanning the channel.

7   Independent vortex shedding occurred at high Reynolds number. The vortices were small, had a high shedding frequency and were ejected into the main channel from just behind a ripple peak.

8   Secondary flow vortex system became unsteady and formed a highly complex flow phenomenon. The vortices rotated by spiralling. The unsteady nature exhibited periodic phases of growth and destruction of the vortex system.

9   Central streaklines mixed in an unsteady flow which ensued downstream of vortex shedding flows.
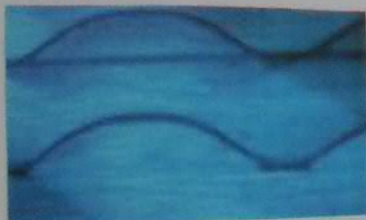
10   Fully turbulent flow where the dye streaklines were dispersed.

<u>Hydraulic Diameter = 0.0275m</u>

PROFILE 1 RH = 0.430
Re position

Re	1	2	3	4	5	6	7
432	2	2	2	2	2	2	2
534	2	2	2	2	2	2	2
961	2	2	2	2	2	2	5
1372	2	4	4	4	5	9	9
1846	2	4	4	5	5	9	9

PROFILE 2 RH = 0.356
Re Position

Re	1	2	3	4	5
561	1	2	2	2	2
872	1	2	2	2	2
1162	2	2	2	4	4
1277	2	2	2	4	4
1779	2	4	4	5	5
2329	2	4	4	5	9

PROFILE 3 RH = 0.580
Re Position

Re	1	2	3	4	5	6	7	8	9
524	2	2	2	2	2	2	2	2	2
669	2	2	4	4	4	4	4	4	4
848	2	4	4	4	4	4	4	4	4
1081	4	4	4	5	5	5	5	5	5
1241	4	4	4	5	5	5	5	5	5
1594	4	4	4	5	5	5	5	9	9
1937	4	4	5	5	5	9	9	9	9

Hydraulic Diameter = 0.0211 m

PROFILE 1 RH = 0.330
Re   position

Re	1	2	3	4	5	6	7
273	1	2	2	2	2	2	2
386	1	2	2	2	2	2	2
527	2	2	2	2	2	2	2
536	2	2	2	2	2	2	2
659	2	2	4	4	4	5	5
855	2	2	4	4	5	5	9
1120	2	4	5	5	5	9	9
1432	2	4	5	5	9	9	10
1876	2	4	5	9	9	10	10
1882	2	5	5	9	9	10	10

PROFILE 2 RH = 0.273
Re   Position

Re	1	2	3	4	5
324	1	1	1	1	1
606	2	2	2	2	2
880	2	2	2	4	4
1125	2	2	4	5	5
1294	2	4	5	5	9
1624	2	4	5	9	9
1826	2	4	5	9	9
1993	2	4	5	9	10

PROFILE 3 RH = 0.445
Re   Position

Re	1	2	3	4	5	6	7	8	9
367	2	2	2	2	2	2	2	2	2
472	2	2	2	2	2	2	2	2	2
635	4	4	4	4	4	4	4	4	4
912	4	4	4	4	4	4	4	4	5
1127	4	4	4	4	4	4	5	9	9
1371	4	4	4	5	5	9	9	10	10
1601	4	4	4	5	9	9	9	10	10
1847	4	4	5	5	9	9	10	10	10
1878	4	4	5	5	9	9	10	10	10
2505	4	5	9	9	10	10	10	10	10

Hydraulic Diameter = 0.0170 m

PROFILE 1 RH = 0.266

Re	position						
	1	2	3	4	5	6	7
182	1	1	1	1	1	1	1
317	1	1	1	1	1	1	1
489	1	2	2	2	2	2	4
629	1	2	4	4	5	5	5
946	2	4	4	5	5	9	9
1217	2	4	5	5	9	9	10

PROFILE 2 RH = 0.220

Re	Position				
	1	2	3	4	5
246	1	1	1	1	1
511	1	1	1	2	2
733	2	2	2	2	4
898	2	2	4	4	9
1030	2	2	4	4	5
1124	2	4	5	5	9
1358	2	4	5	9	9
1770	2	4	5	9	10
2163	2	7	9	10	10

PROFILE 3 RH = 0.359

Re	Position								
	1	2	3	4	5	6	7	8	9
426	1	2	2	2	2	2	2	2	2
474	1	2	2	2	2	2	2	2	2
537	1	2	2	2	4	4	4	4	9
577	2	2	2	4	4	4	4	9	9
845	2	2	4	4	5	5	9	9	9
1044	2	4	4	5	5	5	9	9	9
1322	2	4	5	5	5	9	9	9	9
1449	2	4	5	5	9	9	9	10	10
1700	4	4	5	9	10	10	10	10	10
2234	4	7	7	10	10	10	10	10	10

Hydraulic Diameter = 0.0145 m

PROFILE 1 RH = 0.227

Re	position						
	1	2	3	4	5	6	7
257	1	1	1	1	1	1	1
307	1	1	1	2	2	2	2
432	1	2	2	2	2	2	2
586	1	2	2	2	2	2	4
726	2	2	4	4	4	5	5
872	2	4	4	5	5	9	9
1103	2	4	5	9	9	10	10
1656	4	4	9	9	10	10	10
1826	4	5	9	10	10	10	10
2303	4	5	9	10	10	10	10

PROFILE 2 RH = 0.189

Re	Position				
	1	2	3	4	5
270	1	1	1	1	1
317	1	1	1	1	1
455	1	1	1	1	1
626	1	2	2	2	2
818	2	2	3	3	3
922	2	2	3	8	9
1053	2	3	3	8	9
1220	2	3	8	8	9
1408	2	8	8	9	9
1779	2	8	8	9	10
1801	2	8	8	9	10
2332	2	8	9	10	10

PROFILE 3 RH = 0.306

Re	Position							
	1	2	3	4	5	6	7	8	9
267	1	2	2	2	2	2	2	2	2
323	2	2	2	2	2	2	2	2	2
465	2	2	2	2	4	4	6	6	6
623	2	2	2	4	4	6	6	9	9
764	2	2	4	4	8	8	9	9	10
899	2	4	7	8	8	9	9	10	10
1056	2	4	7	8	9	10	10	10	10
1215	2	4	7	9	9	10	10	10	10
1388	4	4	8	9	9	10	10	10	10
1743	4	4	8	9	10	10	10	10	10
1831	4	5	8	9	10	10	10	10	10
2375	4	7	9	10	10	10	10	10	10

<u>Hydraulic Diameter = 0.013 m</u>

PROFILE 1 RH = 0.203
Re   position

Re	1	2	3	4	5	6	7
306	1	1	1	1	1	1	1
431	1	1	1	3	3	3	3
532	1	2	2	3	3	3	8
637	1	2	3	3	3	9	9
797	1	4	3	8	9	9	10
983	4	8	8	9	9	10	10
1210	4	5	9	9	10	10	10
1848	4	8	9	10	10	10	10

PROFILE 2 RH = 0.168
Re   Position

Re	1	2	3	4	5
313	1	1	1	1	1
373	1	1	1	1	2
448	1	1	1	1	2
544	1	1	1	3	3
619	1	2	2	3	3
775	1	2	2	3	8
909	2	2	3	8	8
1006	2	3	8	8	9
1194	2	3	8	9	9
1815	3	8	9	9	10
2155	4	8	9	10	10

PROFILE 3 RH = 0.274
Re   Position

Re	1	2	3	4	5	6	7	8	9
291	2	2	2	2	2	2	2	2	2
362	2	2	2	4	4	4	6	9	9
436	2	2	2	4	6	6	9	9	9
589	2	2	2	4	6	6	9	9	10
773	2	4	4	6	6	9	10	10	10
882	4	4	7	8	9	10	10	10	10
1233	4	7	8	8	9	10	10	10	10
1657	4	7	8	9	10	10	10	10	10
2536	7	7	9	10	10	10	10	10	10

<u>Hydraulic Diameter = 0.0098 m</u>

PROFILE 1 RH = 0.153

Re	position						
	1	2	3	4	5	6	7
169	1	1	1	1	1	1	1
301	1	2	1	1	1	3	3
406	1	2	2	3	3	3	3
551	2	2	3	3	3	3	3
696	2	2	3	3	8	8	8
845	2	2	3	3	8	8	8
951	2	3	3	8	8	9	9
1191	2	8	8	9	10	10	10
1459	2	8	9	10	10	10	10
1938	4	8,9	8,9	10	10	10	10

PROFILE 2 RH = 0.127

Re	Position				
	1	2	3	4	5
401	1	1	1	1	1
493	1	1	1	1	1
565	1	1	1	1	3
646	1	1	3	3	3
1236	1	3	3	8	8
1576	1	3	8	9	9

PROFILE 3 RH = 0.207

Re	Position								
	1	2	3	4	5	6	7	8	9
222	1	1	1	1	1	1	1	1	1
300	1	2	2	2	3	3	3	3	3
418	2	2	2	3	3	8	8	8	9
566	2	2	4	3	8	8	8	9	9
725	2	2	4	5	8	9	9	10	10
827	2	4	7	8	8	9	10	10	10
959	2	4	7	7	9	10	10	10	10
1127	4	8	8	9	10	10	10	10	10
1395	4	8	9	10	10	10	10	10	10
2002	4	7	9	10	10	10	10	10	10

Table 5.4 Temperatures forming the boundary conditions to the transient heat transfer tests

Flat plate data Dha = 0.0224 m

Test	Re	Tinitial	T fluid	Temp ratio
1	7832	24.3	52.9	0.599
2	7953	22.3	52.7	0.628
3	4973	23.1	53.1	0.611
4	6424	22.5	53.2	0.616
5	2049	20.1	52.1	0.666
6	2948	23.1	52.1	0.631

Rippled duct data

Dha = 0.0224 m
profile 1

3	2000	23.8	53.0	0.603
2	5000	22.7	52.8	0.621
1	8000	22.4	52.8	0.625

profile 2

4	2000	23.4	52.2	0.624
6	5000	22.1	52.2	0.642
5	8000	18.9	51.5	0.689

profile 3

9	2000	21.4	52.9	0.635
7	5000	21.5	53.0	0.632
8	8000	21.4	53.0	0.633

profile 4

10	2000	23.1	52.9	0.615
12	5000	22.6	53.1	0.617
11	8000	21.6	53.0	0.630

Dha = .0174 m
profile 1

18	2000	22.3	52.5	0.634
13	5000	20.5	52.0	0.663
23	8000	22.9	53.1	0.613

profile 2

19	2000	20.0	51.6	0.677
14	5000	19.7	51.6	0.679
24	8000	19.4	51.6	0.683

profile 3

20	2000	22.4	52.5	0.632
15	5000	20.2	52.3	0.661
21	8000	22.6	52.9	0.620

profile 4

17	2000	19.9	52.4	0.662
16	5000	22.4	52.4	0.633
22	8000	22.9	53.0	0.616

Dha = .0142 m

Test	Re	Tinitial	T fluid	Temp ratio
profile 1				
25	1600	21.7	52.5	0.638
30	2000	23.0	52.7	0.620
35	5000	21.1	52.0	0.656
40	8000	21.5	51.7	0.659
profile 2				
26	1600	23.1	52.2	0.628
31	2000	20.9	52.0	0.660
36	5000	20.1	52.1	0.666
37	8000	20.5	51.7	0.670
profile 3				
27	1600	24.0	52.7	0.607
32	2000	22.8	52.7	0.622
33	5000	22.0	52.1	0.644
38	8000	21.2	51.7	0.662
profile 4				
28	1600	23.2	52.7	0.617
29	2000	22.1	52.7	0.632
34	5000	20.6	52.0	0.664
39	8000	22.3	51.8	0.648

Table 5.5 Performance data for the rippled ducts

Re	j	f	Tu$_{heat}$	Tu$_{friction}$

$\underline{Dh = 0.0224}$ m

profile 1

Re	j	f	Tu$_{heat}$	Tu$_{friction}$
2000.0	1.0114E-2	0.14335	0.063	0.078
5000.0	8.8522E-3	0.11703	0.025	0.031
8000.0	8.3774E-3	0.10291	0.016	0.019

profile 2

Re	j	f
2000.0	9.2138E-3	0.080518
5000.0	7.5278E-3	0.061845
8000.0	6.8304E-3	0.051164

profile 3

Re	j	f
2000.0	1.1500E-2	0.170313
5000.0	9.8090E-3	0.168375
8000.0	9.6917E-3	0.16595

profile 4

Re	j	f
2000.0	8.0770E-3	0.095364
5000.0	8.0709E-3	0.079993
8000.0	7.8605E-3	0.068761

$\underline{Dh=0.0174}$ m

profile 1

Re	j	f	Tu$_{heat}$	Tu$_{friction}$
2000.0	9.8702E-3	0.12680	0.048	0.060
5000.0	8.0262E-3	0.10088	0.019	0.024
8000.0	7.6696E-3	0.08562	0.012	0.015

profile 2

Re	j	f
2000.0	7.0369E-3	0.051405
5000.0	6.3525E-3	0.049160
8000.0	6.1684E-3	0.040165

profile 3

Re	j	f
2000.0	1.2088E-2	0.19629
5000.0	9.9080E-3	0.17309
8000.0	8.2536E-3	0.15130

profile 4

Re	j	f
2000.0	8.4790E-3	0.078141
5000.0	7.4963E-3	0.068096
8000.0	6.8738E-3	0.057305

Re	j	f	Tu$_{heat}$	Tu$_{friction}$

Dh = 0.0142 m

profile 1

1600.0	8.8416E-3	0.096924	0.050	0.062
2000.0	9.0093E-3	0.10727	0.040	0.049
5000.0	7.2197E-3	0.083791	0.016	0.020
8000.0	6.4715E-3	0.070689	0.010	0.012

profile 2

1600.0	7.9940E-3	0.039508		
2000.0	6.8851E-3	0.041540		
5000.0	5.4093E-3	0.041878		
8000.0	5.2442E-3	0.036852		

profile 3

1600.0	1.1106E-2	0.14866		
2000.0	1.0695E-2	0.15481		
5000.0	8.3538E-3	0.13484		
8000.0	7.0812E-3	0.11740		

profile 4

1600.0	7.6635E-3	0.056185		
2000.0	7.4719E-3	0.066304		
5000.0	6.5896E-3	0.057952		
8000.0	6.0181E-3	0.049543		

Table 5.6 Tolerances for the measured parameters used for the uncertainty analysis of the Reynolds number and friction factor

Atmospheric pressure	± 40.0 N/m^2
Length of fin	± 0.5 mm
Orifice diameter	± 0.05 mm
Orifice pipe diameter	± 0.1 mm
Orifice upstream pressure[1]	
Airflow Developments manometer	± 10.0 N/m^2
Pressure drop (duct)	
Airflow Developments manometer	
range 0 – 5000 N/m^2	± 2.0 N/m^2
Combustion Instruments manometer	
range 0 – 3000 N/m^2	± 0.2 N/m^2
Relative humidity	± 20.0 %
Temperature of air[2] (isothermal test)	
thermocouple output (mV)	negligible
Wall (duct) spacing	± 0.2 mm
Water head in manometer[3]	± 0.1 mm

[1] The uncertainty in the atmospheric pressure was added to this measurement.

[2] The uncertainty was taken to be the measured variation over the test period.

[3] Manometer used to measure the pressure drop across the orifice plate

Table 5.7 Rippled Duct Heat Exchanger Geometry

Frontal area 1 m by 1 m

Heat exchanger flow length 0.0595 m

3 tube rows in line (all 12 heat exchangers)

65 tubes/row 195 tubes in total

Tube pitch (spanwise) 0.0152 m

Tube Dimensions 0.019 m by 0.0022 m

Fin thickness 0.076 mm copper

Tube wall thickness 0.20mm brass

Internal surface area of tubes 7.655 m^2

Fin efficiency fin length 0.0065 m

Table 5.8 Table of rippled duct heat exchanger detail

heat ex.	1	2	3	4	5	6	7	8	9	10	11	12
Profile	1	2	3	4	1	2	3	4	1	2	3	4
Dh_{test} mm	22.4	22.4	22.4	22.4	17.4	17.4	17.4	17.4	14.2	14.2	14.2	14.2
Dh_{real} mm	5.6	5.6	5.6	5.6	4.35	4.35	4.35	4.35	3.55	3.55	3.55	3.55
Fin Pitch mm	2.876	2.876	2.876	2.876	2.251	2.251	2.251	2.251	1.851	1.851	1.851	1.851
fins/m	348	348	348	348	444	444	444	444	540	540	540	540
fin length mm	63.46	61.86	66.05	63.15	63.46	61.86	66.05	63.15	63.46	61.86	66.05	63.15
A_c/A_{fr}	.8305	.8305	.8305	.8305	.8243	.8243	.8243	.8243	.8181	.8181	.8181	.8181
A_{fi}/A_{ht}	.8330	.8293	.8385	.8323	.8651	.8620	.8697	.8645	.8871	.8845	.8911	.8866
A_{ht}/vol m^2/m^3	773.9	757.4	800.5	770.7	950.7	929.8	984.7	946.7	1128.	1102.	1169.	1123.

Table 6.1 Geometries and flows modelled with PHOENICS

Ripple pitch = 31 mm for all profiles

Dha=0.0112 m, RH=0.361, RN=7

profiles	1	2	3	4
RI	0.161	0.148	0.161	0.161

Reynolds numbers 536, 8000, 10000, 12000

Dha 0.0087 m, RH=0.281, RI=0.148, RN=7

profile 2

Reynolds numbers 6213, 8000, 10000

Table 6.2 Table of PHOENICS generated rippled duct solutions.

		Bulk parameter calculated		
Profile	inlet pressure	exit enthalpy		
		Prandtl number		
		0.707	1.0	6.09
	N/m2	J/kg		

Comparitive investigation

Reynolds number 536, laminar flow, RH=0.361

Profile	inlet pressure	0.707	1.0	6.09
1	2.195			100540.
2	2.052			99622.
3	2.253			100860.
4	2.301			100430.

Reynolds number 8000, K-E model, RH=0.361

Profile	inlet pressure	0.707	1.0	6.09
1	595.1			92775.
2	611.2			92687.
3	648.0			92852.
4	659.7			92872.

Reynolds number 10000, K-E model, RH=0.361

Profile	inlet pressure	0.707	1.0	6.09
1	921.0	105490.	102390.	91495.
2	951.8	105420.	102300	91436.
3	1008.1	105630.	102500.	91566.
3	1007.3			
3	1007.7			
4	1025.2	105660.	102540.	91579.

Reynolds number 12000, K-E model, RH=0.361

Profile	inlet pressure	0.707	1.0	6.09
1	1303.5	103540.	100610.	90571.
2	1352.8	103470.	100520.	90525.
3	1431.6	103650.	100710.	90634.
4	1456.1	103690.	100750.	90646.
4	1456.5			

Additional runs

Reynolds number 8000, K-E model LOGIC(92)=.FALSE., RH=0.361

Profile	inlet pressure	0.707	1.0	6.09
2	210.93	104890.	101870.	91675.

Reynolds number 12000, K-E model LOGIC(92)=.FALSE., RH=0.361

Profile	inlet pressure	0.707	1.0	6.09
2	414.4		98442.	

Reynolds number 12000, constant eddy viscosity model. Turbulent viscosity = 100. laminar viscosity. LOGIC(92)=.TRUE., RH=0.361

Profile	inlet pressure	0.707	1.0	6.09
2	1488.0		103630.	

Reynolds number 12000, constant eddy viscosity model. Turbulent viscosity = 100. laminar viscosity. LOGIC(92)=.FALSE., RH=0.361

Profile	inlet pressure	0.707	1.0	6.09
2	709.0		103860.	

Reynolds number 6213, K-E model LOGIC(92)=.FALSE., RH=0.281

Profile	inlet pressure	0.707	1.0	6.09
2	275.4	109890.	106830.	94913.

Reynolds number 8000, K-E model LOGIC(92)=.FASLE., RH=0.281

Profile	inlet pressure	0.707	1.0	6.09
2	414.3	107330.	104380.	93281.

Reynolds number 10000, K-E model LOGIC(92)=.FALSE., RH=0.281

Profile	inlet pressure	0.707	1.0	6.09
2	598.04	105090.	102530.	91971.

Table 6.3 PHOENICS results reduced to nondimensional numbers.

Profile	friction factor	Colburn j factor		
		nondimensional number		
		Prandtl number		
		0.707	1.0	6.09

Comparitive investigation
Reynolds number 536, laminar flow, RH=0.361

Profile	friction factor	0.707	1.0	6.09
1	0.1656			3.983E-2
2	0.1548			3.702E-2
3	0.1700			4.084E-2
4	0.1736			3.949E-2

Reynolds number 8000, K-E model, RH=0.361

1	0.2018			1.873E-2
2	0.2073			1.852E-2
3	0.2197			1.891E-2
4	0.2237			1.896E-2

Reynolds number 10000, K-E model, RH=0.361

1	0.1998	1.357E-2	1.374E-2	1.573E-2
2	0.2065	1.351E-2	1.365E-2	1.560E-2
3	0.2187	1.370E-2	1.385E-2	1.590E-2
3	0.2185			
3	0.2186			
4	0.2224	1.373E-2	1.389E-2	1.593E-2

Reynolds number 12000, K-E model, RH=0.361

1	0.1964	1.185E-2	1.201E-2	1.364E-2
2	0.2038	1.179E-2	1.193E-2	1.354E-2
3	0.2157	1.194E-2	1.210E-2	1.378E-2
4	0.2194	1.198E-2	1.214E-2	1.381E-2
4	0.2195			

Additional runs
Reynolds number 8000, K-E model LOGIC(92)=.FALSE., RH=0.361

2	0.07153	1.302E-2	1.322E-2	1.615E-2

Reynolds number 12000, K-E model LOGIC(92)=.FALSE., RH=0.361

2	0.06244		1.006E-2	

Reynolds number 12000, constant eddy viscosity model. Turbulent viscosity = 100. laminar viscosity. LOGIC(92)=.FALSE., RH=0.361

2	0.1068		1.527E-2	

Reynolds number 12000, constant eddy viscosity model. Turbulent viscosity = 100. laminar viscosity. LOGIC(92)=.TRUE., RH=0.361

2	0.2242		1.503E-2	

Reynolds number 6213, K-E model LOGIC(92)=.FALSE., RH=0.281

2	0.07254	1.410E-2	1.454E-2	1.864E-2

Reynolds number 8000, K-E model LOGIC(92)=.FASLE., RH=0.281

2	0.06583	1.193E-2	1.231E-2	1.549E-2

Reynolds number 10000, K-E model LOGIC(92)=.FALSE., RH=0.281

2	0.06081	1.026E-2	1.078E-2	1.308E-2

Table 6.4 Table of performance criteria data (Pr=6.09)

Profile	pumping power W	heat transfer rate kW	Ratio Rqp –

Comparitive investigation
Reynolds number 536, laminar flow, RH=0.361

Profile	pumping power W	heat transfer rate kW	Ratio Rqp
1	6.146E-4	4.650	7.566E+6
2	5.746E-4	4.393	7.646E+6
3	6.308E-4	4.739	7.513E+6
4	6.444E-4	4.619	7.168E+6

Reynolds number 8000, K-E model, RH=0.361

Profile	pumping power W	heat transfer rate kW	Ratio Rqp
1	2.485	36.99	14884
2	2.553	36.63	14348
3	2.706	37.31	13787
4	2.755	37.40	13572

Reynolds number 10000, K-E model, RH=0.361

Profile	pumping power W	heat transfer rate kW	Ratio Rqp
1	4.809	39.58	8230
2	4.970	39.27	7902
3	5.264	39.95	7589
4	5.353	40.02	7475

Reynolds number 12000, K-E model, RH=0.361

Profile	pumping power W	heat transfer rate kW	Ratio Rqp
1	8.167	41.71	5107
2	8.476	41.42	4887
3	8.969	42.11	4694
4	9.123	42.18	4623

Additional runs
Reynolds number 8000, K-E model LOGIC(92)=.FALSE., RH=0.361

Profile	pumping power W	heat transfer rate kW	Ratio Rqp
2	.8809	32.41	36790

Reynolds number 6213, K-E model LOGIC(92)=.FALSE., RH=0.281

Profile	pumping power W	heat transfer rate kW	Ratio Rqp
2	0.8935	35.66	39910

Reynolds number 8000, K-E model LOGIC(92)=.FASLE., RH=0.281

Profile	pumping power W	heat transfer rate kW	Ratio Rqp
2	1.731	39.11	22600

Reynolds number 10000, K-E model LOGIG(92)=.FALSE., RH=0.281

Profile	pumping power W	heat transfer rate kW	Ratio Rqp
2	3.123	42.06	13470

Appendix 1, Published work

Maltson J D, Wilcock D and Davenport C J, (1989).

J. D. Maltson
Research Student,

D. Wilcock

Department of Mechanical Engineering,
Coventry Polytechnic,
West Midlands, United Kingdom

C. J. Davenport[1]
Covrad Heat Transfer,
Canley, Coventry,
West Midlands, United Kingdom

Comparative Performance of Rippled Fin Plate Fin and Tube Heat Exchangers

Continuous rippled fins are preferred to interrupted fins in applications where fouling by fibrous matter or insects is a problem. The performance characteristics of three rippled fin heat exchangers have been measured in a thermal wind tunnel. The results of these measurements are reported and comparisons are made with published data on similar surfaces. The performance evaluation criteria used as the basis for the comparisons were those recommended by Shah (1978). The tested rippled fin surfaces were found to have a higher performance than a similar surface reported in Kays and London (1984). The heat transfer enhancement was found to be dependent upon the profile of the fin.

Some materials have been removed due to 3rd party copyright. The unabridged version can be viewed in Lancester Library - Coventry University.

Some materials have been removed due to 3rd party copyright. The unabridged version can be viewed in Lancester Library - Coventry University.

APPENDIX 2
A PROBLEM WITH THE TRANSIENT THERMAL HEAT TRANSFER TESTING TECHNIQUE

The problem is best described by considering the transient thermal boundary layer on a flat plate as follows;

When a flat plate is inserted into a hot airstream the local surface temperature of the plate changes relative to its position on the plate. Consider a point on the surface some distance down the plate. The wall temperature upstream of this point increases, due to heat energy transfer from the air entering the plate and the temperature also increases at a faster rate due to the higher heat transfer coefficient nearer the leading edge. As time progresses the rate of heat transfer from the air to the plate upstream of the point decreases with the reduced temperature difference. Therefore the temperature of the air close to the plate at the considered point is hotter than it would otherwise be had the plate remained at constant temperature upstream of the point. As the air temperature is now hotter, the local heat transfer rate at the point is greater resulting in an increased heat transfer coefficient. This effect has occurred because of the transient thermal behaviour of the boundary layer flow.

This heat transfer problem may be considered as being similar, but not quite as severe to the analogous mass transfer "bare patch" effect, analysed and measured by Brakell and Cowell (1986). Significant errors were noted by neglecting the effect in a laminar boundary layer.

To investigate this thermal problem the transient temperature variation in a thin skinned flat plate was numerically simulated. The analysis was performed for both laminar and turbulent boundary layers for which the local heat transfer coefficient for a plate with an arbitrary temperature was known. Using the Theory of Superposition, Kays and Crawford (Convective Heat and Mass Transfer, McGraw Hill, 2nd ed., 1983), for the arbitrary wall temperature variation the local heat flux is found from the following equation;

$$q_0'' = \int_0^x h(\xi, x) \cdot \left(\frac{dt_0}{d\xi}\right) \cdot d\xi + \sum_{i=1}^k h(\xi_i, x) \cdot \Delta t_{0,i} \qquad (A2.1)$$

(See Kays and Crawford for an explanation of the symbols and the figure in the text below).

For the laminar boundary layer the step function for the laminar boundary layer is;

$$h(\xi, x) = \frac{0.332 \cdot k}{x} \cdot Pr^{1/3} \cdot Re_x^{1/2} \cdot \left| 1 - \left(\frac{\xi}{x}\right)^{3/4} \right|^{-1/3} \qquad (A2.2)$$

and for the turbulent boundary layer the equation is;

$$h(\xi, x) = \frac{0.0296 \cdot Re_x^{-0.2} \cdot \rho \cdot v \cdot cp}{Pr^{0.4}} \cdot \left| 1 - \left(\frac{\xi}{x}\right)^{9/10} \right|^{-1/9} \qquad (A2.3)$$

Equations A2.1 and A2.2 were substituted in turn in equation A2.1. For the case considered here, that of either a laminar or wholely turbulent boundary layer on a flat plate in a transient heat

transfer test, the term in the summation reduces as there is only one step in temperature at the leading edge. The step in the summation term is the leading edge wall temperature minus the fluid stream temperature. The two equations for the heat flux for the arbitrary wall temperature case for laminar and turbulent boundary layers are;

$$q_o'' = \frac{0.332 \cdot k}{x} \, Re_x^{1/2} \, Pr^{1/3} \left\langle \int_o^x \left| 1 - \left(\frac{\xi}{x} \right)^{3/4} \right|^{-1/3} \cdot \frac{dt_o}{d\xi} \cdot d\,\xi + a \right\rangle$$

$$q_o'' = \frac{0.0296 \cdot \rho \cdot v \cdot cp}{Re_x^{0.2} \cdot Pr^{0.4}} \left\langle \int_o^x \left| 1 - \left(\frac{\xi}{x} \right)^{9/10} \right|^{-1/9} \cdot \frac{dt_o}{d\xi} \cdot d\,\xi + a \right\rangle$$
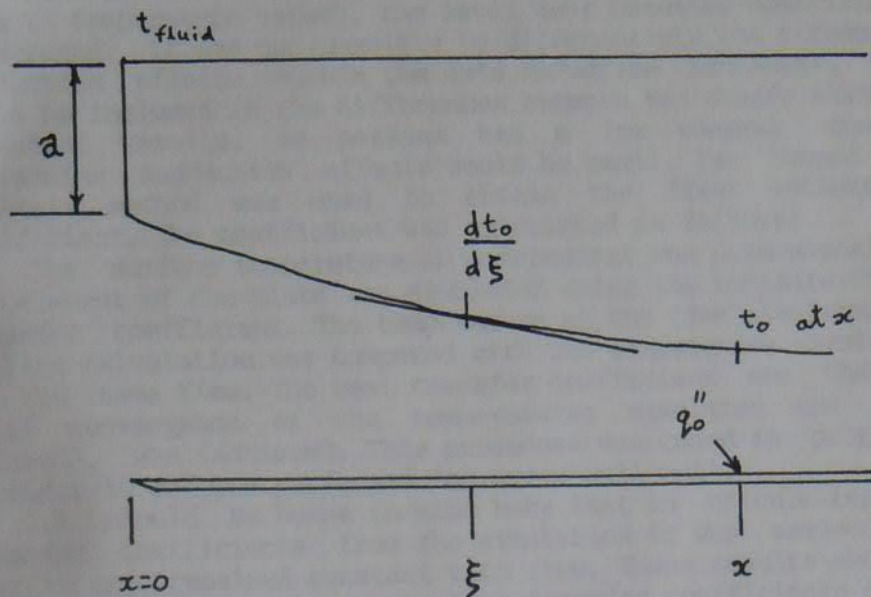
Figure to describe the symbols used in the simulation

Within the plate the temperatures were calculated from;

$$\frac{dT}{dt} = \frac{k_p}{\rho_p \cdot cp_p} \cdot \left| \frac{d^2T}{dx^2} + \frac{d^2T}{dy^2} \right|$$

The perspex plate modelled was 2.0 mm thick and the other side of the plate was specified to have a heat transfer coefficient of 4.0 w/m^{2}K and an ambient temperature of 20.ºC, being similar to a typical test. The fluid stream velocity was 2.5 and 25.0 m/s for the laminar and turbulent cases respectively and had a temperature of 60.0^{o}C. The initial plate temperature was 20.0^{o}C.

372

The transient simulation of a thin skin transient heat transfer test was performed. Initially the plate was isothermal, hence in the heat flux equation the temperature gradient is zero and the heat flux reverts to the isothermal flat plate solution.

The method described below was then applied to the results to obtain the heat transfer coefficients. The properties of the wall were those for perspex. The plate surface temperature was monitored with time at a temperature of 40.0°C. When the temperature in a surface wall cell reached the temperature specified, the time at this position was stored. This "storing" process was equivalent to taking photographs of the plate in a transient test with either phase change paint or liquid crystals sprayed onto the surface. At the end of the simulation when the whole plate temperature was above 40.0°C, the stored times were written to a file.

From the data file containing the coordinates and the associated time to temperature values, the local heat transfer coefficients were calculated. It was not possible to differentiate the streamwise heat conduction effects within the data reduction procedure, but these would be included in the differences between the steady state and the transient results. As perspex has a low thermal conductivity, streamwise conduction effects would be small. The lumped parameter analysis method was used to obtain the first estimate of the coefficient. The coefficient was calculated as follows;

The surface temperature in a transient one dimensional model of an element of the plate was simulated using the estimate of the heat transfer coefficient. The temperature at the time simulated in the earlier calculation was compared with the temperature simulated here at the same time. The heat transfer coefficient was then adjusted until convergence of the temperatures simulated and "measured" (stored), was achieved. This procedure was coded in program T1HTA, Appendix 10 and was performed for every wall cell.

It should be borne in mind here that in calculating the heat transfer coefficients from the simulation it was assumed that the coefficient remained constant with time. These results show that for the laminar boundary layer the heat transfer coefficients do vary with a temperature variation in the wall and hence with time. This variation shown as higher coefficients in Fig. A2.1 was expected due to the reasons given above. In the case of a turbulent boundary layer Fig. A2.2 the agreement is excellent between the two curves showing that the heat transfer coefficient is only mildly sensitive to an arbitrary wall temperature variation.

In conclusion, the investigation reported in this appendix has shown that transient effects are negligible for turbulent flows and therefore in this case the transient heat transfer test technique is an accurate measurement method. For laminar flows however there are latent transient effects in the technique which cannot be included in the data reduction procedure of the experiment. In a laminar boundary layer flow the simulation of a transient test showed the heat transfer coefficients to increase above the isothermal wall values as described.
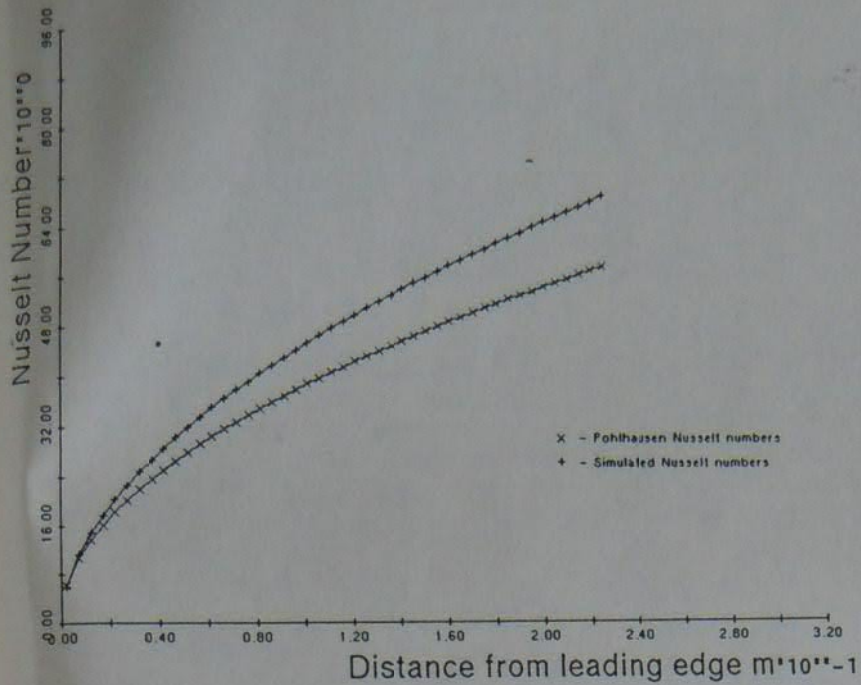
Figure A2.1 Comparison of the simulated Nusselt numbers for a laminar flat plate boundary layer against the laminar flat plate solution of Pohlhausen.
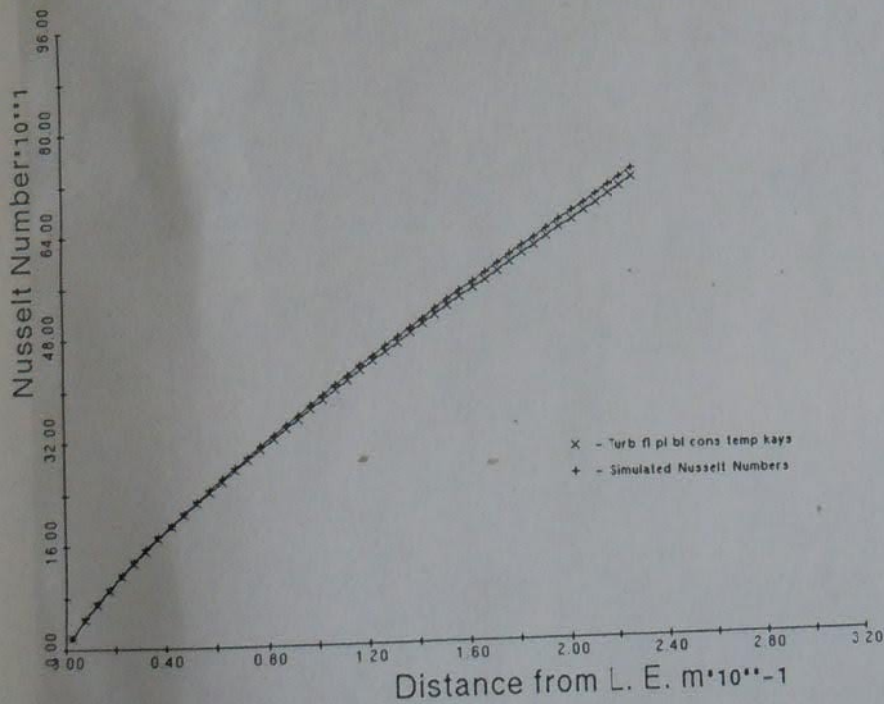
Figure A2.2 Comparison of the simulated Nusselt numbers for a turbulent boundary layer against the isothermal Nusselt numbers of Kays and Crawford.

374

INVESTIGATION INTO THE STREAMWISE CONDUCTION EFFECTS IN THE TRANSIENT
HEAT TRANSFER TECHNIQUE WITH THIN SKINNED BODIES

The reason for this investigation was that it was not possible
to calculate the local heat transfer coefficient distribution allowing
for the streamwise heat conduction effects from the temperature time
history of an actual heat transfer test. The problem is impossible to
solve as the distribution must be solved for as well as the
coefficient at a particular slab. A program was attempted, but the
iterative method of updating the local heat transfer coefficient
induced instabilities into the solution which subsequently diverged.
Another problem was that from the digitisation process of the fin
(described in Chapter 5), the longitudinal node spacing was arbitrary
and may have been extremely small. This very small longitudinal
spacing would have been the limiting criteria for the time step. The
problem of streamwise heat conduction may be very important in highly
complex geometries such as corrugated ducts where the heat transfer
coefficient distribution varies drastically due to the flow being
highly turbulent and regions of separation and reattachment are known
to exist.

In this investigation the streamwise conduction effects were
considered, this was a purely numerical exercise and was carried out
under the assumption that the heat transfer coefficient was steady
with time. The method of analysis was that a transient simulation was
performed to model a transient heat transfer test on a plate, with a
prescribed heat transfer distribution. No heat transfer was permitted
from the rear of the plate. The transient simulation was performed
using a two dimensional model of the plate, which allowed for the
streamwise heat conduction. Two temperatures were monitored in the
simulation, 30.0 and 41.43 $^{\circ}$C. The simulated temperature time history
for the model was then used to calculate back the local heat transfer
coefficient, by the iterative numerical procedure. The local heat
transfer coefficient was then calculated using a one dimensional model
and hence the effect of the conduction could then be obtained from the
difference between the prescribed and the calculated coefficients. The
initial plate temperature was 20.0 $^{\circ}$C and the fluid temperature was 52
$^{\circ}$C. By monitoring two surface temperatures the the effect of the
following temperature ratio could be found;

$$\frac{(T_j - T_{s,i})}{(T_f - T_{s,i})}$$

The analysis was performed for five cases of varying severity for
the conduction effects to exist and these will be described below. In
all cases the plate modelled was 0.7 mm thick and 11 nodes were placed
across this thickness with a spacing of 0.07 mm. The properties of the
material were those of perspex. The node spacing in the streamwise
direction was 1.0 mm. There were 28 nodes in the streamwise direction
making 27.0 mm in length, which was chosen as a similar length to the
ripple pitch in the main investigation. Program T2DEMD used to
generate the temperature time history for the plate. Program T1HTA was
used to calculate the heat transfer coefficients based on an iterative
numerical procedure.

The prescribed heat transfer distributions are given in the
following tables and the forms of the distributions were as follows;

1   Step

2   Ramp
3   Two ramps
4   Two ramps similar to case 3
5   Ramp similar to 2
6   Developing flow over a flat plate

The results to the investigation are given both graphically and in tabular form in Figs. A3.1 to A3.6 and Tables A3.1 to A3.6. These results show that the calculated heat transfer coefficient is affected the most in regions where there is a marked change in the prescribed coefficient profile. The effect is for a section having a high coefficient to conduct heat energy to a section having a low coefficient. This in turn increases and decreases the time-to-temperature for a high and low coefficient sections respectively. In the ramp and developing flow cases the heat energy was conducted into and also out of a section reducing the effect of the change of heat transfer coefficient.

In conclusion the following points were noted;

1   A reduction in the temperature ratio defined above reduced the effect that streamwise heat conduction has upon the results.

2   The calculated heat transfer coefficient is most affected where there is a change in the gradient of the prescribed heat transfer coefficient. The steepest gradient change was the step function which caused large differences near the step which decreased very quickly with position away from the step. A similar trend was noted for the ramp cases where a change of the coefficient gradient occurred at a particular point. Provided that either gradients or values do not change abruptly, this work has shown that the streamwise heat conduction effects can be neglected.

376

Table A3.1 Table of results for case 1

position mm	prescribed h W/m²K	simulated 41.43°C W/m²K	simulated 30.0°C W/m²K
0.0	20.0	19.982	20.041
1.0	20.0	19.982	20.041
2.0	20.0	19.985	20.041
3.0	20.0	19.993	20.041
4.0	20.0	20.008	20.041
5.0	20.0	20.043	20.041
6.0	20.0	20.107	20.041
7.0	20.0	20.227	20.049
8.0	20.0	20.439	20.067
9.0	20.0	21.807	20.144
10.0	20.0	21.395	20.372
11.0	20.0	22.348	20.946
12.0	20.0	23.891	22.290
13.0	20.0	26.482	25.365
14.0	20.0	31.841	34.869
15.0	40.0	35.579	38.636
16.0	40.0	37.855	39.747
17.0	40.0	39.039	40.017
18.0	40.0	39.585	40.052
19.0	40.0	39.829	40.086
20.0	40.0	39.921	40.086
21.0	40.0	39.956	40.086
22.0	40.0	39.967	40.086
23.0	40.0	39.979	40.086
24.0	40.0	39.979	40.086
25.0	40.0	39.979	40.086
26.0	40.0	39.979	40.086
27.0	40.0	39.979	40.086

Figure A3.1 Graph of the heat transfer coefficients, prescribed and simulated for Case 1 against position showing the effect of longitudinal conduction in the wall.

Table A3.2 Table of results for case 2

position mm	prescribed h W/m2K	simulated 41.43°C W/m2K	simulated 30.0°C W/m2K
0.0	20.0	21.247	20.345
1.0	20.0	21.412	20.497
2.0	20.0	21.938	21.040
3.0	22.0	22.968	22.386
4.0	24.0	24.358	24.126
5.0	26.0	26.009	26.041
6.0	28.0	27.845	28.033
7.0	30.0	29.780	30.029
8.0	32.0	31.768	32.038
9.0	34.0	33.774	34.035
10.0	36.0	35.791	36.046
11.0	38.0	37.803	38.042
12.0	40.0	39.829	40.042
13.0	42.0	41.838	42.057
14.0	44.0	43.850	44.066
15.0	46.0	45.867	46.094
16.0	48.0	47.863	48.096
17.0	50.0	49.860	50.089
18.0	52.0	51.856	52.081
19.0	54.0	53.829	54.112
20.0	56.0	55.710	56.105
21.0	58.0	57.465	58.035
22.0	60.0	58.880	59.694
23.0	60.0	59.511	60.073
24.0	60.0	59.793	60.073
25.0	60.0	59.897	60.149
26.0	60.0	59.948	60.149
27.0	60.0	59.948	60.149

key
△ htc set
▽ 41.43 stm
+ 30.0 stm

Figure A3.2 Graph of the heat transfer coefficients, prescribed and simulated for Case 2 against position showing the effect of longitudinal conduction in the wall.

Table A3.3 Table of results for case 3

position mm	prescribed h W/m²K	simulated 41.43°C W/m²K	simulated 30.0°C W/m²K
0.0	20.0	21.247	20.345
1.0	20.0	21.412	20.497
2.0	20.0	21.938	21.040
3.0	22.0	22.968	22.386
4.0	24.0	24.353	24.126
5.0	26.0	26.009	26.041
6.0	28.0	27.834	28.033
7.0	30.0	29.761	30.029
8.0	32.0	31.724	32.038
9.0	34.0	33.684	34.035
10.0	36.0	35.588	36.046
11.0	38.0	37.374	38.011
12.0	40.0	38.885	39.848
13.0	42.0	39.910	41.318
14.0	42.0	39.910	41.318
15.0	40.0	38.885	39.848
16.0	38.0	37.374	38.011
17.0	36.0	35.588	36.046
18.0	34.0	33.684	34.035
19.0	32.0	31.724	32.038
20.0	30.0	29.761	30.029
21.0	28.0	27.834	28.033
22.0	26.0	26.009	26.041
23.0	24.0	24.353	24.126
24.0	22.0	22.968	22.386
25.0	20.0	21.938	21.040
26.0	20.0	21.412	20.497
27.0	20.0	21.247	20.345

Figure A3.3 Graph of the heat transfer coefficients, prescribed and simulated for Case 3 against position showing the effect of longitudinal conduction in the wall.

Table A3.4 Table of results for case 4

position mm	prescribed h W/m2K	simulated 41.43°C W/m·K	simulated 30.0°C W/m·K
0.0	20.0	22.262	20.623
1.0	20.0	22.556	20.917
2.0	20.0	23.518	21.956
3.0	24.0	25.497	24.607
4.0	28.0	28.278	28.117
5.0	32.0	31.666	31.994
6.0	36.0	35.452	35.991
7.0	40.0	39.428	40.017
8.0	44.0	43.497	44.025
9.0	48.0	47.502	48.047
10.0	52.0	51.452	52.081
11.0	56.0	55.222	56.039
12.0	60.0	58.581	59.921
13.0	64.0	60.923	63.118
14.0	64.0	60.923	63.118
15.0	60.0	58.581	59.921
16.0	56.0	55.222	56.039
17.0	52.0	51.452	52.081
18.0	48.0	47.502	48.047
19.0	44.0	43.479	44.025
20.0	40.0	39.428	40.017
21.0	36.0	35.452	35.991
22.0	32.0	31.666	31.994
23.0	28.0	28.278	28.117
24.0	24.0	25.479	24.607
25.0	20.0	23.518	21.956
26.0	20.0	22.556	20.917
27.0	20.0	22.262	20.623
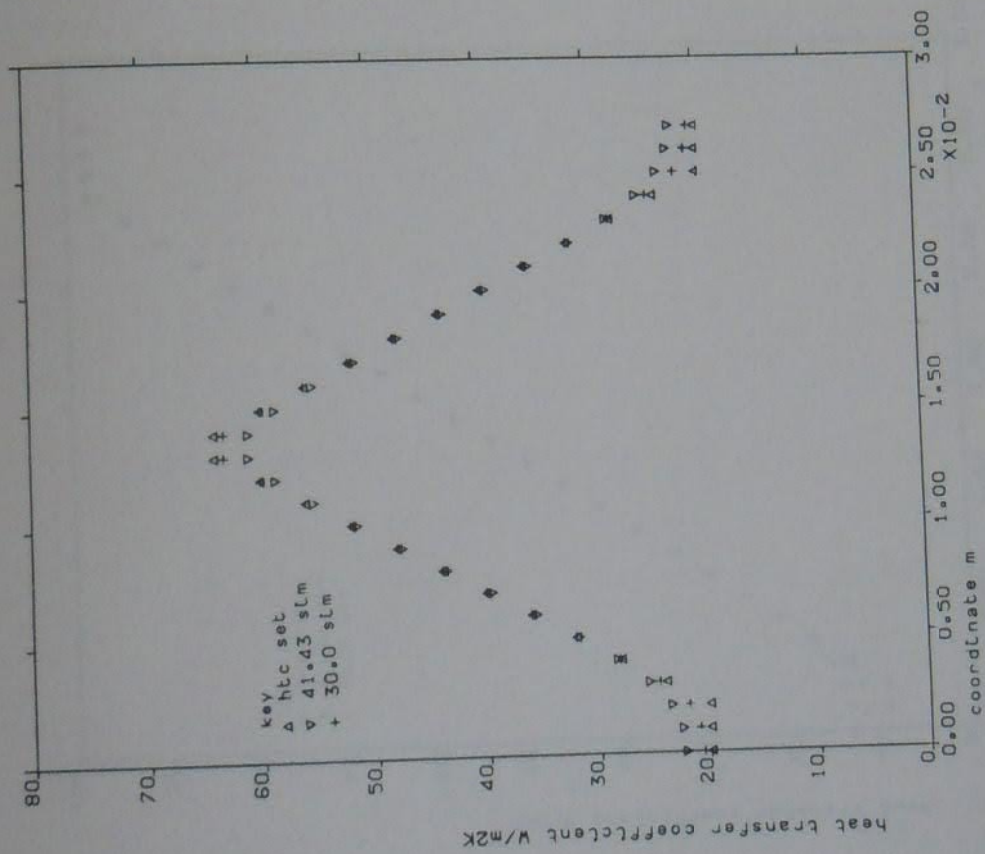
Figure A3.4 Graph of the heat transfer coefficients, prescribed and simulated for Case 4 against position showing the effect of longitudinal conduction in the wall.

380

Table A3.5 Table of results for case 5

position mm	prescribed h W/m²K	simulated 41.43°C W/m²K	simulated 30.0°C W/m²K
0.0	10.0	13.492	11.413
1.0	10.0	13.717	11.713
2.0	10.0	14.454	12.714
3.0	14.0	15.991	14.976
4.0	18.0	18.314	18.168
5.0	22.0	21.408	21.936
6.0	26.0	25.077	25.912
7.0	30.0	29.073	29.933
8.0	34.0	33.184	33.986
9.0	38.0	37.314	38.011
10.0	42.0	41.450	42.020
11.0	46.0	45.536	46.049
12.0	50.0	49.593	50.036
13.0	54.0	53.641	54.112
14.0	58.0	57.680	58.107
15.0	62.0	61.709	62.124
16.0	66.0	65.743	66.114
17.0	70.0	69.776	70.123
18.0	74.0	73.780	74.140
19.0	78.0	77.789	78.160
20.0	82.0	81.820	82.205
21.0	86.0	85.777	86.214
22.0	90.0	89.652	90.283
23.0	94.0	93.326	94.141
24.0	98.0	96.367	97.785
25.0	98.0	97.448	98.184
26.0	98.0	97.791	98.184
27.0	98.0	97.859	98.184
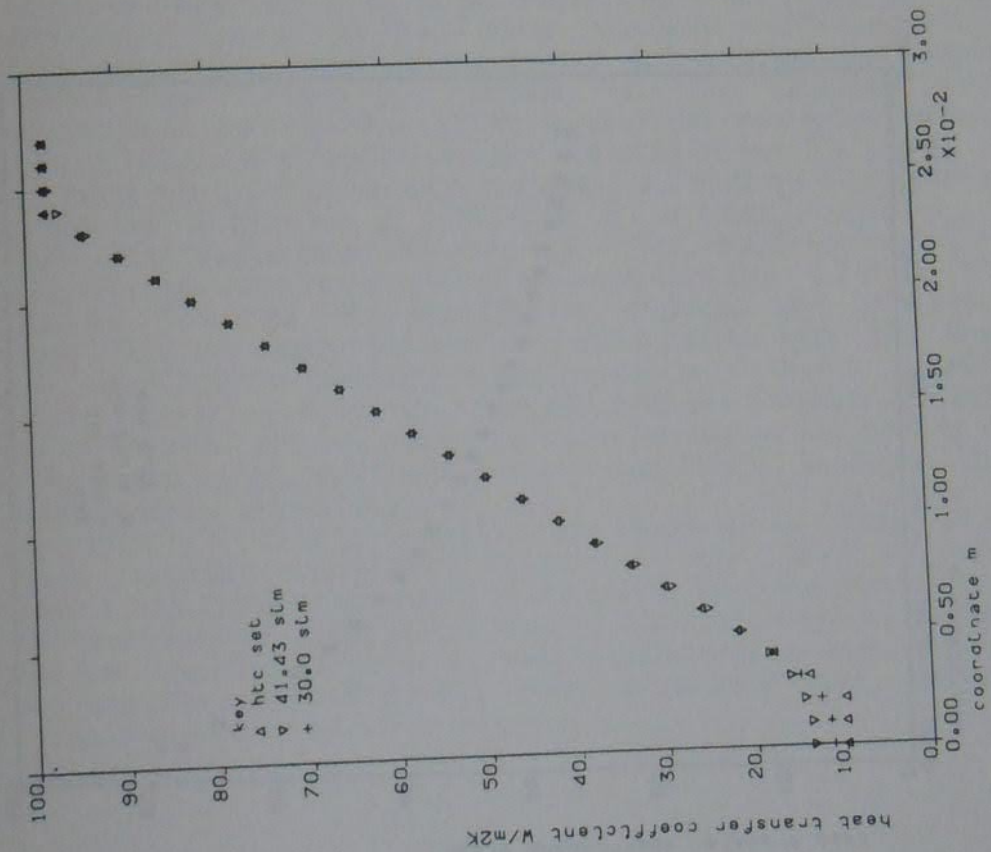
Figure A3.5 Graph of the heat transfer coefficients, prescribed and simulated for Case 5 against position showing the effect of longitudinal conduction in the wall.

Table A3.6 Table of results for case 6

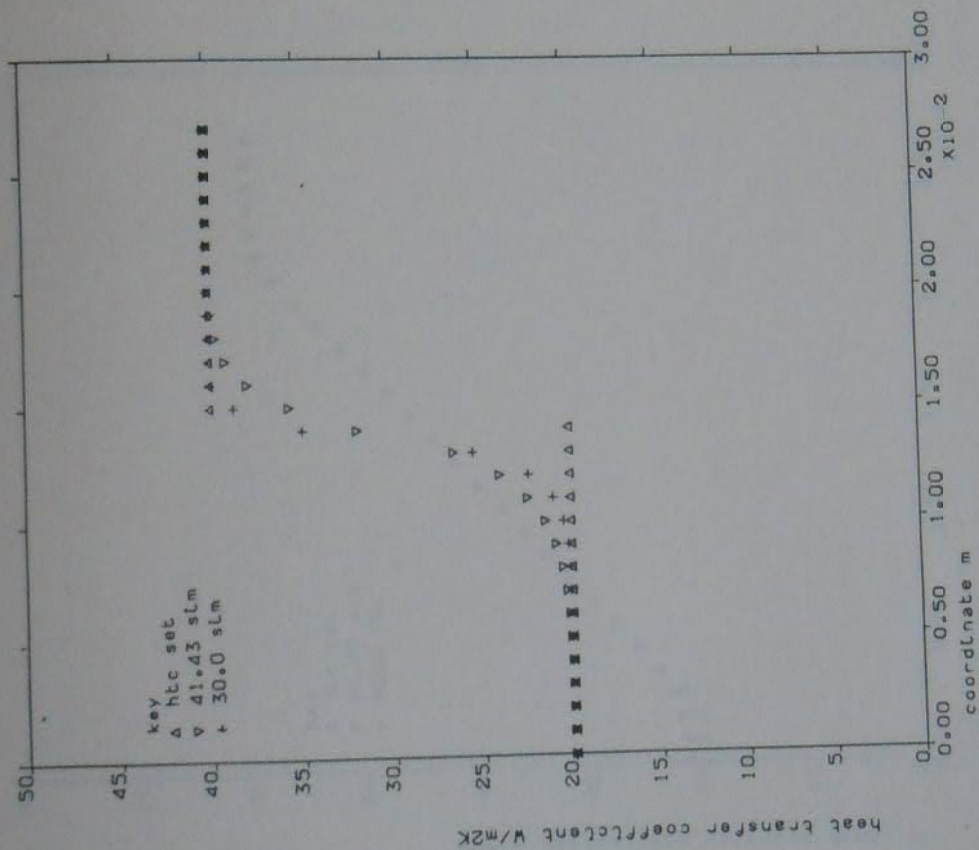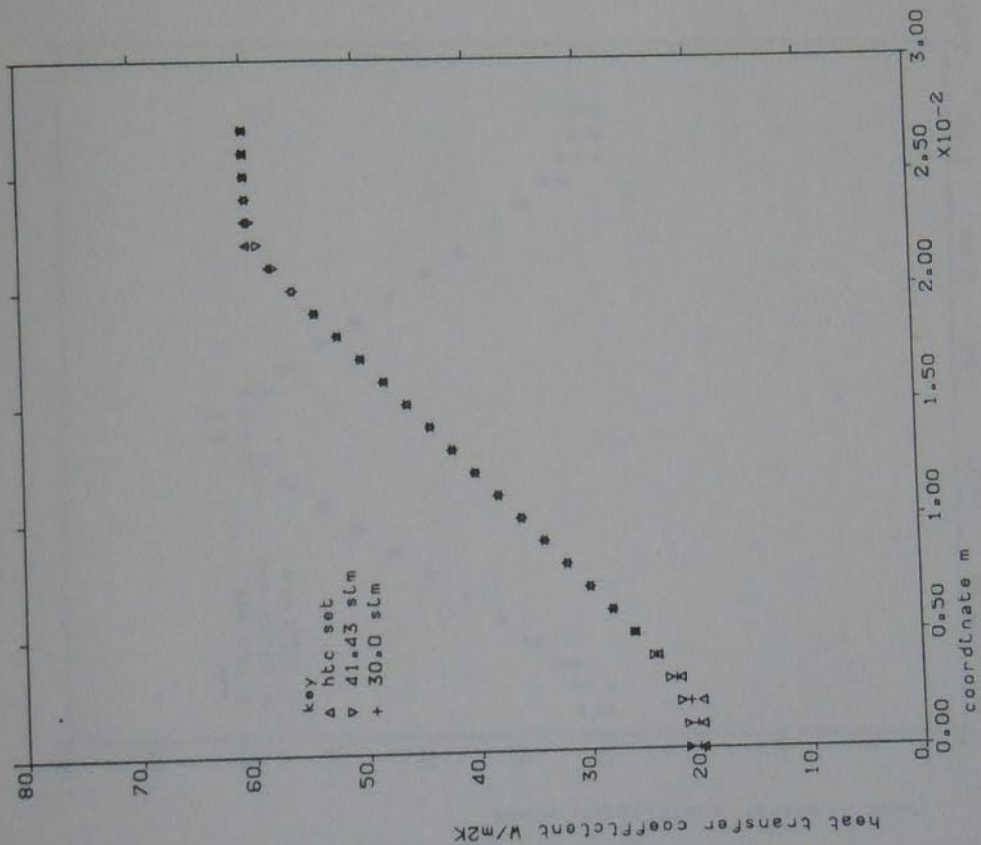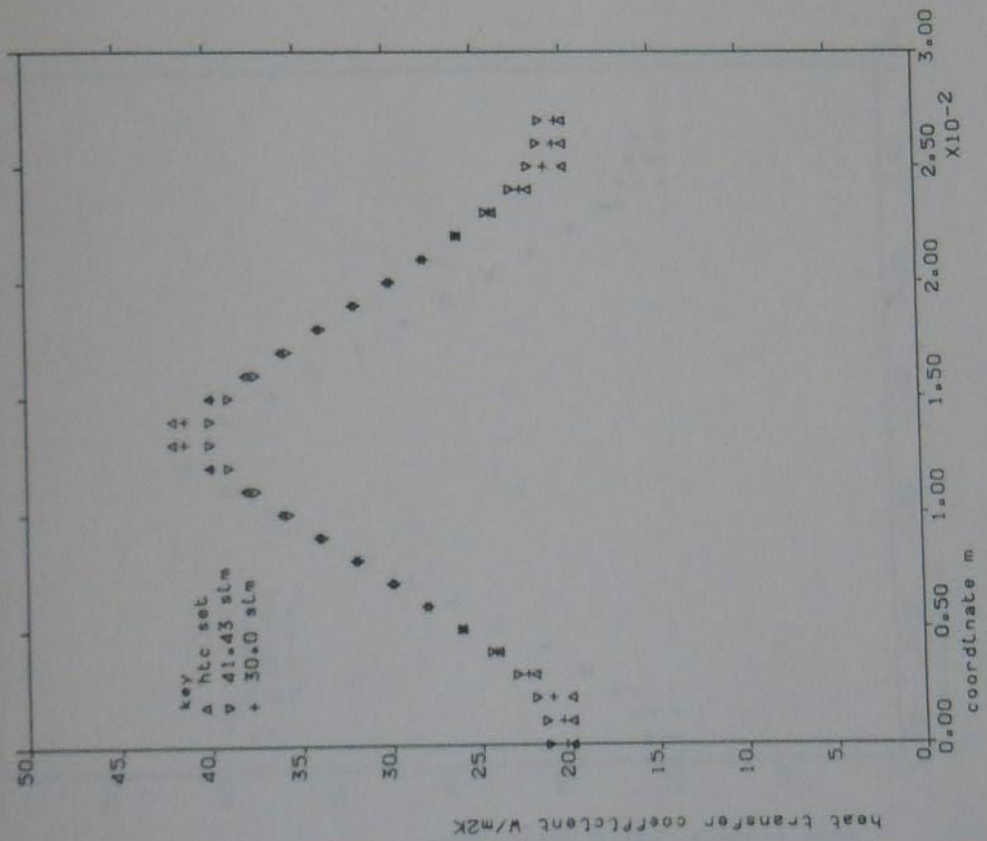| position m	prescribed h W/m^{2}K	siml. 41.43^{o}C W/m^{2}K	siml. 30.0^{o}C W/m^{2}K
0.0005	64.799	59.384	62.700
0.0015	59.153	57.489	59.124
0.0025	54.765	54.527	55.058
0.0035	51.228	51.471	51.512
0.0045	48.298	48.653	48.541
0.0055	45.819	46.173	46.049
0.0065	43.687	44.003	43.901
0.0075	41.827	42.105	42.020
0.0085	40.186	40.422	40.361
0.0095	38.725	38.907	38.860
0.0105	37.411	37.567	37.556
0.0115	36.223	36.354	36.353
0.0125	35.142	35.262	35.261
0.0135	34.152	34.250	34.258
0.0145	33.241	33.327	33.358
0.0155	32.399	32.475	32.504
0.0165	31.618	31.688	31.713
0.0175	30.891	30.951	30.981
0.0185	30.212	30.268	30.301
0.0195	29.576	29.627	29.650
0.0205	28.979	29.024	29.044
0.0215	28.416	28.464	28.493
0.0225	27.885	27.947	27.967
0.0235	27.382	27.464	27.459
0.0245	26.906	27.046	26.985
0.0255	26.454	26.697	26.557
0.0265	26.024	26.447	26.216
0.0275	25.614	26.336	26.027

key
△ htc set
▽ 41.43 stm
+ 30.0 stm
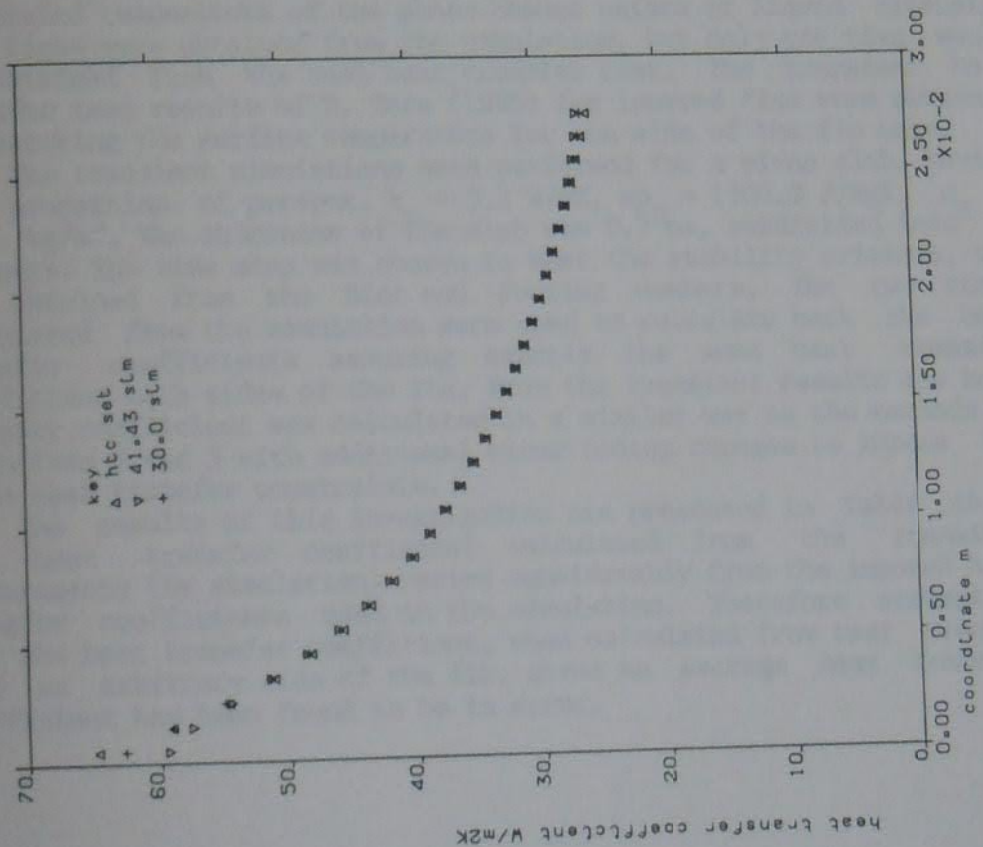
Figure A3.6 Graph of the heat transfer coefficients, prescribed and simulated for Case 6 against position showing the effect of longitudinal conduction in the wall.

APPENDIX 4

NUMERICAL INVESTIGATION INTO THE EFFECTS OF ASSUMING A HEAT TRANSFER COEFFICIENT EQUAL ON BOTH SIDES OF A BODY IN A THIN SKIN TRANSIENT TEST

This work was necessary to evaluate the effects of heat conduction through the wall of a thin skinned body of asymmetrical geometry in a transient heat transfer test. Such cases arise in rippled or louvred fin geometries when the temperature of one side only of the fin is measured, but both sides are exposed to the main flow. In rippled or louvred geometries the flow can separate from the surface leaving a recirculation region underneath the fin when the upper surface is under the action of an attached flow. When the fin is inserted into a heated fluid stream and both sides of the fin are exposed to the hot fluid the temperature profile through an element of the fin is affected by the heat transfer coefficients on both sides of the element.

By imposing fixed heat transfer coefficients on an element and performing a transient simulation it was possible to monitor the temperature time history of both sides of the element. The simulation involved the explicit solution of the finite difference form of the heat conduction equation. The temperature time history was calculated using program TEMD. Using a typical temperature which would be the calibrated temperature of the phase change paints or liquid crystals, two times were obtained from the simulation, but only one time would be obtained from the real heat transfer test. The transient heat transfer test results of R. Tura (1986) for louvred fins were obtained by measuring the surface temperature for one side of the fin only.

The transient simulations were performed for a plane slab having the properties of perspex. k_p = 0.2 W/mK, cp_p = 1500.0 J/kgK, ρ_p = 1190 kg/m^3. The thickness of the slab was 0.7 mm, subdivided into 15 segments. The time step was chosen to meet the stability criteria, and was obtained from the Biot and Fourier numbers. The two times calculated from the simulation were used to calculate back the heat transfer coefficients assuming exactly the same heat transfer coefficient both sides of the fin. From the transient results the heat transfer coefficient was calculated in a similar way to the methods of Appendices 2 and 3 with additional minor coding changes to impose the above heat transfer constraints.

The results of this investigation are presented in Table A4.1. The heat transfer coefficient calculated from the transient measurements (by simulation) varies considerably from the imposed heat transfer coefficients used in the simulation. Therefore assumption that the heat transfer coefficient, when calculated from test results from an arbitrary side of the fin, gives an average heat transfer coefficient has been found to be in error.

Table A4.1 Comparison of heat transfer coefficients : Imposed against those calculated from a transient simulation emulating a transient heat transfer test.

imposed heat transfer coefficients		monitored times		calculated heat transfer coefficients	
W/m^2K		sec	sec	W/m^2K	
20.0	20.0	34.636	34.636	19.999	19.999
40.0	20.0	22.866	23.586	30.307	29.381
60.0	20.0	17.068	18.154	40.614	38.185
80.0	20.0	13.612	14.924	50.948	46.462
100.0	20.0	11.312	12.784	61.325	54.253
100.0	40.0	9.646	10.564	71.935	65.674
100.0	60.0	8.4766	9.002	81.881	77.089
100.0	80.0	7.6100	7.842	91.212	88.510
100.0	100.0	6.944	6.944	99.971	99.971
60.0	20.0	7.476	9.238	92.849	75.117
160.0	10.0	7.998	10.044	86.782	69.080
50.0	5.0	25.072	25.588	27.638	25.769
30.0	5.0	39.396	40.966	17.581	16.907
10.0	5.0	92.078	92.804	7.519	7.460

PRESSURE LOSS TEST 23   DATE 26/2/88

ATMOSPHERIC PRESSURE.
  READING 102320. N/m² TEMP 19 °C CORRECTION 250 N/m²

VALUE 102070 N/m²

DUCT MASS FLOW RATE

ORIFICE PLATE ∅12 , PIPE ∅50

UPSTREAM PRESSURE AT ORIFICE PLATE 122 N/m²

UPSTREAM TEMPERATURE AT ORIFICE PLATE IMV 4 , TMVO·843 mV
                                     AFTER TEST 0·859

PRESSURE DIFFERENCE ACROSS ORIFICE PLATE
AS HEAD MEASURED OF WATER h 0·6615 m H₂O.
                           AFTER TEST 0·6553

DUCT PRESSURES   TMV13 767 mV   AFTER 0·775 mV
MANOMETER

WALL SPACING 9·7 mm WALL MOUNT SPACING 57 mm

PROFILE SHAPE 4

            MANCHESTER COMBIST

APPROX REYNOLDS NUMBER 5000

ZERO START 0·226 mbar, END 0·225 mbar. BIT-ATMOS, START 0·767 mbar, END 0·760 mbar.

UPPER		POSITION							
1	2	3	4	5	6	7	8	9	10
0·806	0·6057	0·5845	0·535	0·474	0·420	0·361	0·342		1

LOWER									
1	2	3	4	5	6	7	8	9	10
0·5575	0·7165	0·7015	0·670	0·607	0·5545	0·492	0·4245		

Appendix 5 Typical pressure drop measurement records

385

INSTRUMENT or DEVICE CALIBRATED

Make: RS   Type: 258-192   Serial No: 02431

Description: Digital Electronic Thermometer with probe

1) Test Procedure: The instrument was calibrated by comparison with a standard resistance thermometer in various controlled environments. The standard resistance thermometer was used in conjunction with a Tinsley bridge to determine the true temperature of the test environment. The instrument was switched on for 15 minutes prior to any readings. All standards and devices used have known and traceable values.

2) Test Results: To IPTS 1968.

Standard Temp °C	Instrument Indication °C	Rear Socket Output mV
0.00	0.8	0.345
9.99	10.8	10.349
19.99	20.7	20.354
29.98	30.7	30.381
49.95	50.7	50.398
69.98	70.8	70.490
100.07	100.9	100.602

3) Uncertainty of Values:

on instrument indication: ± 1 least significant digit

on standard temperature: ± 0.01°C at 0°C
± 0.05°C above 0°C

on rear socket output: ± 0.05% of value ± 10μV

Customer: Coventry Polytechnic
Order No: LR8172000

Calibrated by: Edward Davis
Date of Calibration: 23rd October 1985
Harwell Ref: 61609

Certified: D D Scargill

Previous Calibration Certificate:

Approval No:

Certificate No:

Date of issue:

The uncertainties are based on arithmetic summation of the contributions

Appendix 6 Platinum resistance thermometer Harwell Calibration

HEAT TRANSFER TEST   16.   DATE   10/3/88

FIN PROFILE 4   PLATE SPACING   8.7mm

ATMOSPHERIC PRESSURE   READING   N/m² , CORRECTION   TEMP   °C
VALUE 98600   N/m²

APPROX REYNOLDS NUMBER   5000   DUCT MASS FLOW RATE   Kg/s
                                                    0.009803 Kg/s

ACTUAL MASS FLOW RATE MEASUREMENTS
ORIFICE PLATE Ø 2 ORIFICE PIPE Ø 50   2, 2
MANOMETER AM   BEFORE 0.8161   m
    "   AFTER 0.8200 m
UPSTREAM ORIFICE PLATE PRESSURE 174   N/m²

CONTROLLER   SET TEMPERATURE 62 °C
INLET VENTURI ΔP   N/m²
INLET TEMPERATURE   IMV 3   TMV
EXIT TEMPERATURE   ITDW1   TMV 2.230

TEMPERATURES IMMEDIATELY BEFORE INSERTION
11   12   13   14   15   16   TIME
867   969   818   883   855   967   4.55
870   BEFORE |
TUNNEL TEMP   IMV 50   TMV   2.154 | 2 1 5 8
ORIFICE TEMP IMV 4   TMV   0.418 | 1.252
                                     | AFTER

TEMPERATURES AFTER TEST
11   12   13   14   15   16   TIME
817   1140   817   974   984   1130   4.58

OBC FILE NAMES ZT16
HARRIS FILE NAMES ZT16
OUTPUT HARRIS NAMES ZT16 OUT

Appendix 7 Typical heat transfer measurement records

387

APPENDIX 8

HEAT TRANSFER DATA REDUCTION PROCEDURE

The data reduction procedure for calculating the local heat transfer coefficients from the experimental transient heat transfer tests is described below.

The experimental data was taken in two parts;

A8.1 The boundary conditions for the transience

These were the measurements of temperature at the various locations within the rig. These were fully described in Chapter 5 section 5.3.2.4.

A8.2 Location of the heat transfer coefficient

The locations of the heat transfer coefficient (surface temperature isotherm locations) at a particular time during the test. The photographs of the transient phenomenon were taken with (positive) slide film (Kodak Kodachrome 36 exposure Tungsten 160 ASA film). The camera was set up in exactly the same position relative to the duct for all tests on a specially made frame. This ensured that the datum points for the digitising process were always in view. The developed slides were then projected onto a digitising tablet, connected to a BBC computer which received the coordinates of cursor locations from the digitiser and transferred the information to data files. The digitiser and computer used are shown in Plate A.1. The slide projector did not accurately position the slide and the datum points of the duct were digitised with every photograph. The BBC files containing the coordinates were then transferred to the Harris (1000) mainframe computer in order to process the data. Since there were many transient simulations to perform the speed of this mainframe was required.

A8.3 Data reduction procedure

The heat transfer coefficient was obtained iteratively from an initial starting point. The first approximation to the coefficient was made using the lumped parameter analysis equation assuming a uniform temperature profile across the fin thickness and no natural convection from the non duct side surface of the fin. The differential equation which described the temperature variation with time of a fin element was

$$ m_p \cdot cp_p \cdot \frac{dT_p}{dt} = h_s \cdot A_{ht} \cdot (T_f - T_p) $$

was integrated to give the approximate heat transfer coefficient

$$ h_s = \frac{\rho_p \cdot cp_p \cdot th_p}{t} \cdot \log_e \left| \frac{(T_f - T_{p,i})}{(T_f - T_{p,c})} \right| $$

The longer the time of the test, the more heat transfer by natural convection, and the poorer the approximation was from the lumped parameter analysis. Poor approximations were also found when temperature gradients existed across the fin thickness. The fin properties were required for the analysis. The plain fins were made of 2. mm thick perspex and the rippled fins from a vacuum formable

material known as Cobex, 0.7mm approx. thick. The properties of these materials are given in Appendix 9.

A subroutine was written, which adopted the procedures of Simonson, (1984), to calculate the transient heat transfer by conduction within the fin. The thermal transience was performed with the latest heat transfer coefficient and the measured time-to-calibration temperature for the measured point was compared with the simulated time-to-temperature data. Adjustment was made to the heat transfer coefficient until the simulated data matched the measurements.

Program T1DHTC was written to perform the calculations, (see Appendix 10), incorporating the subroutine described above and was thoroughly checked by comparing transient temperatures calculated by the program to those from an analytic solution to the surface temperature time history for a semi-infinite plane wall, see Ireland and Jones (1985). Excellant agreement was obtained over a typical range of heat transfer coefficients and temperatures.

The above mentioned procedure assumed that the heat transfer coefficient was steady with time, which was the subject of discussion in Appendix 2. The fin was divided into elements to allow the finite difference equations to be allocated within the fin at node points. The differential equation for the transient temperature in one dimension was:

$$\frac{dT}{dt} = \frac{k_p}{\rho_p \cdot cp_p} \cdot \left| \frac{d^2T_p}{dy^2} \right|$$

and in nodal form:

$$\frac{(T_{0,n} - T_{0,o})}{dt} = \frac{k_p}{\rho_p \cdot cp_p} \cdot \left| \frac{T_{2,o} + T_{1,o} - (2 \cdot T_{0,o})}{a_y^2} \right|$$

The equation for the node at the fin surface was;

$$\frac{(T_{0,n} - T_{0,o})}{dt} = \frac{k_p}{\rho_p \cdot cp_p} \cdot \left| \frac{T_{1,o} - T_{0,o}}{a_y^2} \right| + \frac{h_s \cdot (T_f - T_{0,o})}{\rho_p \cdot cp_p \cdot a_y}$$

The fin (node) temperatures were calculated until the time reached was equal to the measured time at those location when the surface temperature of the surface was represented by the liquid crystals appearing green. The heat transfer coefficient was corrected by a factor, dependent upon the temperature difference between the measured and simulated surface node temperatures. The process was then repeated with the new heat transfer coefficient until convergence was achieved. The fluid (air) temperature used in the data reduction for the heat transfer coefficient was the tunnel air temperature, not the log mean temperature, which could not be defined for the transient tests. The tunnel air temperature and the fin starting temperature were both measured by thermocouples.

Natural convection was permitted from the non duct side surface of the fin and was calculated by the method of Raithby and Hollands (1985). These equations were representative of a rectangular enclosure

with flat confining walls extensive in the horizontal direction. The non duct wall surface was corrugated and this regression equation was an approximation to the actual local natural heat transfer coefficient. The heat transfer by natural convection from a wavy surface is of a different nature than that from a flat surface, in that the critical Rayleigh number does not exist and heat is transferred by convection and conduction for all Rayleigh numbers greater than zero, Kelly and Pal (1978). For the flat surface the critical Rayleigh number is 1707.8, below which heat is transferred by conduction only. The local natural heat transfer coefficient for the corrugated rippled geometries tested within the test section opposite a flat plate were not available. A regression equation was available for a corrugated surface opposite a flat plate having three corrugations formed with flat sides from Chinnappa (1970), however the geometry was thought too severe for the present measurements.

The fins varied in thickness and this variation, brought about by the degree of stretching in the vacuum forming process needed to be considered in the data reduction procedure. There were computational difficulties in iterating on the local heat transfer coefficient for every time and position. To solve this difficulty a mean fin thickness was used to calculate the heat transfer coefficient at every time. This heat transfer coefficient was then multiplied by the actual local thickness divided by the mean thickness to give a better approximation. The local thicknesses were measured at discrete points on the fin centreline by a micrometer screw gauge with ball contacts, and interpolation was carried out to obtain the intermediate thicknesses. A computer file contained the thicknesses of all the fins, THDATA was accessed by the program in the interpolation procedure. The surface length of a digitised point was calculated by firstly calculating the digitised length relative to the datum position and then used that length to calculate the surface length.

The local Nusselt number was calculated as follows;

$$Nu_{Dh} = \frac{h_s \cdot Dh}{k_a} \qquad \text{where } Dh = 2.0 \cdot p_s$$

The thermal conductivity k_a was evaluated at the tunnel exit temperature.

APPENDIX 9

PHYSICAL CONSTANTS AND MATERIAL PROPERTIES

Standard gravity 9.80665 m/s^2

Gravitational acceleration of Coventry 9.8125 m/s^2

Estimated by the British Standard method (B.S. 2520)

Density of Mercury at $0.{}^{\circ}C$ 13595.1 kg/m^3

Properties used for the perspex plain fins

ρ_p $1190. \text{ kg/m}^3$

cp_p $1500. \text{ J/kgK}$

k_p 0.20 W/mK

Properties for the Cobex vacuum formed ripple fins were given by the manufacturer G. H. Bloores, Birmingham.

ρ_p $1430. \text{ kg/m}^3$

cp_p $1050. \text{ J/kgK}$

k_p 0.16 W/mK

Thermal conductivities of heat exchanger materials

copper	385. W/mK
brass	111. W/mK
solder	50. W/mK

PROCEEDINGS OF

2ND INTERNATIONAL

PHOENICS

USER CONFERENCE

23 -25 NOVEMBER 1987

Heathrow Penta Hotel

London England

Appendix 11 Published work, Maltson J. D. and Wilcock D. (1987)

LAMINAR FLOW AND HEAT TRANSFER IN CORRUGATED (RIPPLED) DUCTS

J. D. MALTSON and D. WILCOCK

Department of Mechanical Engineering,
Coventry Polytechnic,
Priory Street,
Coventry,
CV1 5FB.

532

533

534

535

536

542

543

544

545

546

```
CXXXXXXXXXXXXXXXXXXXXXXXXXXXXXXXXXXXXXXXXX USER SECTION 1 STARTS:
        DIMENSION PE(60,1,230),PN(60,1,230),PH(60,1,230),PC(60,1,230)
CXXXXXXXXXXXXXXXXXXXXXXXXXXXXXXXXXXXXXXXXX USER SECTION 1 ENDS.
CXXXXXXXXXXXXXXXXXXXXXXXXXXXXXXXXXXXXXXXXX USER SECTION 3 STARTS:
C---    GROUP 3. X-DIRECTION :
        NX=60;XULAST=0.0120;XFRAC(1)=-60.0;XFRAC(2)=1.0/(REAL(NX)
C---    GROUP 4. Y-DIRECTION :
        NY=1;YVLAST=200.0
C---    GROUP 5. Z-DIRECTION :
        NZ=230;ZWLAST=0.230;ZFRAC(1)=-230.0;ZFRAC(2)=1.0/(REAL(NZ))
C----GROUP 7. BLOCKAGE:
        BLOCK=.TRUE.;IPWRIT=-1
        DO 77 IZ=1,NZ
        DO 78 IY=1,NY
        DO 79 IX=1,NX
        PE(IX,IY,IZ)=1.0;PH(IX,IY,IZ)=1.0
        PN(IX,IY,IZ)=1.0;PC(IX,IY,IZ)=1.0
79      CONTINUE
78      CONTINUE
77      CONTINUE
C CELL POROSITIES 0.0 FOR THE FIN
C INLET CHANNEL
        DO 81 IX=12,15
        DO 82 IZ=1,6
        PC(IX,1,IZ)=0.0
82      CONTINUE
81      CONTINUE
C RIPPLED SECTION
        IZ=7;KSTZ=IZ
        DO 90 K=1,7
        DO 95 IZ=KSTZ,KSTZ+30
        KZ=IZ-KSTZ+1;CALL MARLS(KZ,KX);KSTX=KX+12
        DO 91 IX=KSTX,KSTX+3
        PC(IX,1,IZ)=0.0
91      CONTINUE
95      CONTINUE
        KSTZ=KSTZ+31
90      CONTINUE
C OUTLET CHANNEL
        DO 83 IX=12,15
        DO 84 IZ=224,230
        PC(IX,1,IZ)=0.0
84      CONTINUE
83      CONTINUE
C---    GROUP 8.DEPENDENT VARIABLES TO BE SOLVED FOR OR STORED :
        SOLVAR(PP)=.TRUE.;SOLVAR(P1)=.TRUE.;SOLVAR(U1)=.TRUE.
        SOLVAR(W1)=.TRUE.;SOLVAR(H1)=.TRUE.
C---    GROUP 10 PROPERTIES:
        IRHO1=1;RHO1=998.0
        IEMU1=1;EMULAM=0.0010422;EMU1=EMULAM
        SIGMA(H1)=6.09;SIGMA(24)=6.09
C---    GROUP 13 INITIAL FIELDS :
        FIINIT(W1)=0.025;FIINIT(U1)=0.0
        FIINIT(P1)=2.0;FIINIT(H1)=83900.0
C---    GROUP 14 BOUNDARY/INTERNAL CONDITIONS :
        DO 141 I=7,10
        REGION(I)=.FALSE.
141     CONTINUE
        XCYCLE=.TRUE.
C---    GROUP 15 TO 24; REGIONS 1 TO 10
C INLET PLANE BELOW FIN
                                549
```

410

```
                CALL PLACE(1,LOW,1,11,1,1,1,1)
                CALL COVAL(1,M1,FIXFLU,(0.025*RHO1))
                CALL COVAL(1,W1,ONLYMS,0.025)
                CALL COVAL(1,U1,FIXVAL,0.0)
                CALL COVAL(1,H1,FIXVAL,83900.0)
C INLET PLANE ABOVE FIN
                CALL PLACE(2,LOW,16,60,1,1,1,1)
                CALL COVAL(2,M1,FIXFLU,(0.025*RHO1))
                CALL COVAL(2,W1,ONLYMS,0.025)
                CALL COVAL(2,U1,FIXVAL,0.0)
                CALL COVAL(2,H1,FIXVAL,83900.0)
C OUTLET PLANE BELOW FIN
                CALL PLACE(3,HIGH,1,11,1,1,NZ,NZ)
                CALL COVAL(3,M1,FIXVAL,0.0)
C OUTLET PLANE ABOVE FIN
                CALL PLACE(4,HIGH,16,60,1,1,NZ,NZ)
                CALL COVAL(4,M1,FIXVAL,0.0)
C WALL ABOVE FIN
                CALL PLACE(5,WEST,16,16,1,1,1,1)
                CALL COVAL(5,W1,WALL,0.0)
                CALL COVAL(5,U1,WALL,0.0)
                CALL COVAL(5,H1,FIXVAL,125700.0)
C WALL BELOW FIN
                CALL PLACE(6,EAST,11,11,1,1,1,1)
                CALL COVAL(6,W1,WALL,0.0)
                CALL COVAL(6,U1,WALL,0.0)
                CALL COVAL(6,H1,FIXVAL,125700.0)
C---     GROUP 26 SOLUTION TYPE AND RELATED PARAMETERS :
                WHOLEP=.TRUE.
C---     GROUP 27 SWEEP AND ITERATION NUMBERS :
                LITER(PP)=125;LITER(W1)=25;LITER(U1)=25;LITER(H1)=10
C---     GROUP 29 RELAXATION   :
                RLXP=1.00;DTFALS(W1)=0.08;DTFALS(U1)=0.08
C---     GROUP 39 ERROR AND RESIDUAL PRINT-OUT :
C MEAN VELOCITY 0.025 M/S
                RESREF(1)=0.025*XULAST*YVLAST
CXXXXXXXXXXXXXXXXXXXXXXXXXXXXXXXXXXXXXXXXXX USER SECTION 3 ENDS.
C
C
                SUBROUTINE MARLS(JZ,JX)
                INTEGER JDMX(31),JZ,JX
C PROFILE 1
                DATA JDMX/0,1,2,4,7,10,13,16,18,20,21,22,23,24,25,25,25,24,23,22,
           & 21,20,18,16,13,10,7,4,2,1,0/
C PROFILE 2
C          DATA JDMX/0,0,0,2,5,8,11,13,15,17,19,20,21,22,23,23,23,22,21,20,
C          & 19,17,15,13,11,8,5,2,0,0,0/
C PROFILE 3
C          DATA JDMX/0,1,2,4,6,8,11,13,16,19,21,23,24,25,25,25,25,24,23,21,
C          & 19,16,13,11,8,6,4,2,1,0,0/
C PROFILE 4
C          DATA JDMX/0,0,1,2,3,4,5,7,9,12,15,18,21,24,25,25,25,24,23,22,21,
C          & 20,18,16,13,10,7,4,1,0,0/
                JX=JDMX(JZ)
                RETURN
                END
```

GROUND 1

```
C SET F-ARRAY DIMENSION AS NEEDED, & SET NFMAX ACCORDINGLY.
      COMMON F(450700);NFMAX=450700
C
C     CHAPTER 3: CALLED AT THE START OF EACH SLAB;
  300 CONTINUE
      IF (IZED.GE.7) GO TO 230
C INLET CHANNEL
      REGION(5)=.TRUE.;REGION(6)=.TRUE.
      LOC5(1)=16;LOC5(2)=16;LOC5(3)=1
      LOC5(4)=1;LOC5(5)=IZED;LOC5(6)=IZED
      LOC6(1)=11;LOC6(2)=11;LOC6(3)=1
      LOC6(4)=1;LOC6(5)=IZED;LOC6(6)=IZED
      GO TO 250
  230     CONTINUE
      IF (IZED.GE.224) GO TO 240
C SET RIPPLE Z COUNTERS
      IF (IZED.EQ.7) JZ=1
      IF (IZED.EQ.38) JZ=1
      IF (IZED.EQ.69) JZ=1
      IF (IZED.EQ.100) JZ=1
      IF (IZED.EQ.131) JZ=1
      IF (IZED.EQ.162) JZ=1
      IF (IZED.EQ.193) JZ=1
C RIPPLED SECTION
      REGION(5)=.TRUE.;REGION(6)=.TRUE.
      CALL MARLS (JZ,JX);JX=JX+12;JZ=JZ+1
      LOC5(1)=JX+4;LOC5(2)=JX+4;LOC5(3)=1
      LOC5(4)=1;LOC5(5)=IZED;LOC5(6)=IZED
      LOC6(1)=JX-1;LOC6(2)=JX-1;LOC6(3)=1
      LOC6(4)=1;LOC6(5)=IZED;LOC6(6)=IZED
      GO TO 250
  240     CONTINUE
C OUTLET CHANNEL
      REGION(5)=.TRUE.;REGION(6)=.TRUE.
      LOC5(1)=16;LOC5(2)=16;LOC5(3)=1
      LOC5(4)=1;LOC5(5)=IZED;LOC5(6)=IZED
      LOC6(1)=11;LOC6(2)=11;LOC6(3)=1
      LOC6(4)=1;LOC6(5)=IZED;LOC6(6)=IZED
  250     CONTINUE
      RETURN
```

SATELLITE 2

```
CXXXXXXXXXXXXXXXXXXXXXXXXXXXXXXXXXXXXXXXX USER SECTION 1 STARTS:
          DIMENSION PE(60,1,242),PN(60,1,242),PH(60,1,242),PC(60,1,242)
CXXXXXXXXXXXXXXXXXXXXXXXXXXXXXXXXXXXXXXXXXXXXXX USER SECTION 1 ENDS.
C---     GROUP 3. X-DIRECTION :
         NX=60;XULAST=0.0120;XFRAC(1)=-60.0;XFRAC(2)=1.0/(REAL(NX))
C---     GROUP 4. Y-DIRECTION :
         NY=1;YVLAST=200.0
C---     GROUP 5. Z-DIRECTION :
         NZ=242;ZWLAST=0.242;ZFRAC(1)=-242.0;ZFRAC(2)=1.0/(REAL(NZ))
C---     GROUP 7. BLOCKAGE: BLOCK<.F.>,IPLANE,IPWRIT
         BLOCK=.TRUE.;IPWRIT=-1
         DO 77 IZ=1,NZ
         DO 78 IY=1,NY
         DO 79 IX=1,NX
         PE(IX,IY,IZ)=1.0;PH(IX,IY,IZ)=1.0
         PN(IX,IY,IZ)=1.0;PC(IX,IY,IZ)=1.0
77       CONTINUE
78       CONTINUE
77       CONTINUE
C INLET CHANNEL
         DO 81 IX=12,15
         DO 82 IZ=7,12
         PC(IX,1,IZ)=0.0
82       CONTINUE
81       CONTINUE
C RIPPLED SECTION
         IZ=13;KSTZ=IZ
         DO 90 K=1,7
         DO 95 IZ=KSTZ,KSTZ+30
         KZ=IZ-KSTZ+1;CALL MARLS(KZ,KX);KSTX=KX+12
         DO 91 IX=KSTX,KSTX+3
         PC(IX,1,IZ)=0.0
91       CONTINUE
95       CONTINUE
         KSTZ=KSTZ+31
90       CONTINUE
C OUTLET CHANNEL
         DO 83 IX=12,15
         DO 84 IZ=230,236
         PC(IX,1,IZ)=0.0
84       CONTINUE
83       CONTINUE
C---     GROUP 8.DEPENDENT VARIABLES TO BE SOLVED FOR OR STORED :
         SOLVAR(PP)=.TRUE.;SOLVAR(P1)=.TRUE.;SOLVAR(U1)=.TRUE.
         SOLVAR(W1)=.TRUE.;SOLVAR(H1)=.TRUE.
C---     GROUP 10 PROPERTIES:
         IRHO1=1;RHO1=1.177
         IEMU1=1;EMULAM=0.00001846;EMU1=EMULAM
         SIGMA(H1)=0.707;SIGMA(24)=0.707
C---     GROUP 13 INITIAL FIELDS :
         FIINIT(W1)=0.3755;GVEL=(56.0/60.0)*0.3755
         FIINIT(U1)=0.0;FIINIT(P1)=0.0;FIINIT(H1)=0.0
C---     GROUP 14 BOUNDARY/INTERNAL CONDITIONS :
         DO 141 I=7,10
         REGION(I)=.FALSE.
141      CONTINUE
         XCYCLE=.TRUE.
C---     GROUP 15 TO 24; REGIONS 1 TO 10
         WALLH=80392.0
```

554

```
C INLET PLANE
      CALL PLACE(1,LOW,1,15,1,1,1,1)
      CALL COVAL(1,M1,FIXFLU,(GVEL*RHO1))
      CALL COVAL(1,W1,ONLYMS,GVEL)
      CALL COVAL(1,U1,FIXVAL,0.0)
      CALL COVAL(1,H1,FIXVAL,0.0)
C INLET PLANE
      CALL PLACE(2,LOW,16,60,1,1,1,1)
      CALL COVAL(2,M1,FIXFLU,(GVEL*RHO1))
      CALL COVAL(2,W1,ONLYMS,GVEL)
      CALL COVAL(2,U1,FIXVAL,0.0)
      CALL COVAL(2,H1,FIXVAL,0.0)
C OUTLET PLANE
      CALL PLACE(3,HIGH,1,15,1,1,NZ,NZ)
      CALL COVAL(3,M1,FIXVAL,0.0)
C OUTLET PLANE
      CALL PLACE(4,HIGH,16,60,1,1,NZ,NZ)
      CALL COVAL(4,M1,FIXVAL,0.0)
C WALL ABOVE FIN
      CALL PLACE(5,WEST,16,16,1,1,7,7)
      CALL COVAL(5,W1,WALL,0.0)
      CALL COVAL(5,U1,WALL,0.0)
      CALL COVAL(5,H1,FIXVAL,WALLH)
C WALL BELOW FIN
      CALL PLACE(6,EAST,11,11,1,1,7,7)
      CALL COVAL(6,W1,WALL,0.0)
      CALL COVAL(6,U1,WALL,0.0)
      CALL COVAL(6,H1,FIXVAL,WALLH)
C---   GROUP 26 SOLUTION TYPE AND RELATED PARAMETERS :
      WHOLEP=.TRUE.
C---   GROUP 27 SWEEP AND ITERATION NUMBERS :
      LITER(PP)=125;LITER(P1)=10
      LITER(W1)=25;LITER(U1)=25;LITER(H1)=10
C---   GROUP 29 RELAXATION   :
      DTFALS(W1)=0.0004;DTFALS(U1)=0.0004;RLXP=1.0
C---   GROUP 39 ERROR AND RESIDUAL PRINT-OUT :
C MEAN VELOCITY GVEL M/S
      RESREF(1)=GVEL*XULAST*YVLAST
CXXXXXXXXXXXXXXXXXXXXXXXXXXXXXXXXXXXXXXXXX USER SECTION 3 ENDS.
```

555

416

APPENDIX 1

```
C SET F-ARRAY DIMENSION AS NEEDED, & SET NFMAX ACCORDINGLY.
      COMMON F(468200);NFMAX=468200
C
C      CHAPTER 3:CALLED AT THE START OF EACH SLAB;
  300 CONTINUE
      IF (IZED.LE.6) GO TO 250
      IF (IZED.GE.13) GO TO 230
C INLET CHANNEL
      REGION(5)=.TRUE.;REGION(6)=.TRUE.
      LOC5(1)=16;LOC5(2)=16;LOC5(3)=1
      LOC5(4)=1;LOC5(5)=IZED;LOC5(6)=IZED
      LOC6(1)=11;LOC6(2)=11;LOC6(3)=1
      LOC6(4)=1;LOC6(5)=IZED;LOC6(6)=IZED
      GO TO 250
  230 CONTINUE
      IF (IZED.GE.230) GO TO 240
C SET RIPPLE COUNTERS
      IF (IZED.EQ.13)  JZ=1
      IF (IZED.EQ.44)  JZ=1
      IF (IZED.EQ.75)  JZ=1
      IF (IZED.EQ.106) JZ=1
      IF (IZED.EQ.137) JZ=1
      IF (IZED.EQ.168) JZ=1
      IF (IZED.EQ.199) JZ=1
C RIPPLED SECTION
      REGION(5)=.TRUE.;REGION(6)=.TRUE.
      CALL MARLS (JZ,JX);JX=JX+12;JZ=JZ+1
      LOC5(1)=JX+4;LOC5(2)=JX+4;LOC5(3)=1
      LOC5(4)=1;LOC5(5)=IZED;LOC5(6)=IZED
      LOC6(1)=JX-1;LOC6(2)=JX-1;LOC6(3)=1
      LOC6(4)=1;LOC6(5)=IZED;LOC6(6)=IZED
      GO TO 250
  240 CONTINUE
      IF (IZED.GE.237) GO TO 250
C OUTLET CHANNEL
      REGION(5)=.TRUE.;REGION(6)=.TRUE.
      LOC5(1)=16;LOC5(2)=16;LOC5(3)=1
      LOC5(4)=1;LOC5(5)=IZED;LOC5(6)=IZED
      LOC6(1)=11;LOC6(2)=11;LOC6(3)=1
      LOC6(4)=1;LOC6(5)=IZED;LOC6(6)=IZED
  250 CONTINUE
      RETURN
```

557

FIGURES 6.M.1 to 6.M.19

COM
DOCUMENT FILMING
OPTICAL DISK SYSTEMS
READERS
READER PRINTERS
STORAGE DEVICES
CONSUMABLES

MICROSCRIBE
BUSINESS SYSTEMS PLC

LONDON 01-375-0505
ANDOVER 0264-65060
SWINDON 0793-783360

MILTON KEYNES 0908-261252
NORTHWICH 0606-49414
HULL   0482-212170